



**FRIEDRICH-SCHILLER-
UNIVERSITÄT
JENA**

**The delivery of biologicals across endosomal
membranes by pH-responsive polymers**

Dissertation

(kumulativ)

zur Erlangung des akademischen Grades

doctor rerum naturalium (Dr. rer. nat.)

vorgelegt dem Rat der Chemisch-Geowissenschaftlichen Fakultät

der Friedrich-Schiller-Universität Jena

von Franziska Hausig-Punke, M. Sc.

geboren am 02.04.1990 in Gera

Gutachter:

- | | |
|---------------------------------|-------------------------------------|
| 1. Dr. Johannes C. Brendel | Friedrich-Schiller-Universität Jena |
| 2. Prof. Dr. Ulrich S. Schubert | Friedrich-Schiller-Universität Jena |

Tag der öffentlichen Verteidigung: 30.06.2023

Table of contents

Table of contents	1
Documentation of authorship	2
1. Delivery of biologically active substances by polymers	7
2. Exploring endosomal release	11
2.1. Calcein as a sensor molecule to study endosomal release	11
2.2. Endosomal release of macromolecules	14
3. Motivation and aims	17
4. Evaluating pH-adjustable polypiperazines as release agents	19
4.1. Polypiperazines as a new class of polymers in biomedical applications	19
4.2. Probing endosomal release of polypiperazines	21
5. Polypiperazines in gene delivery	27
5.1. Complexation of genetic material by near-neutral polypiperazines	27
5.2. Endosomal escape and gene expression of polypiperazine polyplexes	311
6. Alternative polymer systems in the field of endosomal release	35
6.1. A pH-responsive polymer micelle	35
6.2. Integrating hydrophobicity in copolymers	38
6.3. A cationic, pH-independent polymer	41
7. Summary	45
8. Zusammenfassung	49
8. References	55
List of abbreviations	59
Publication list	61
Acknowledgements/Danksagung	63
Declaration of authorship/Selbstständigkeitserklärung	65
Publications Pub1 to Pub6	67

Documentation of authorship

This section contains a list of individual authors' contributions to the publications reprinted in this thesis.

Pub1 “Tracking the Endosomal Escape: A Closer Look at Calcein and Related Reporters” <u>Franziska Hausig-Punke</u> , ^{1,‡} Friederike Richter, ^{2,‡} Maria Hoernke, ³ Johannes C. Brendel, ⁴ Anja Traeger, ⁵ <i>Macromol. Biosci.</i> , 2022 , 2200167.					
Author	1	2	3	4	5
Development of the concept	×	×			
Preparation of the manuscript	×	×	×	×	×
Correction of the manuscript	×	×	×	×	×
Supervision of F. Hausig-Punke				×	
Proposed publication equivalent	0.5				

[‡] Authors contributed equally.

Pub2 “Correlation between Protonation of Tailor-Made Polypiperazines and Endosomal Escape for Cytosolic Protein Delivery” <u>Franziska Hausig</u> , ¹ Fabian H. Sobotta, ² Friederike Richter, ³ Dominic O. Harz, ⁴ Anja Traeger, ⁵ Johannes C. Brendel, ⁶ <i>ACS Appl. Mater. Interfaces</i> , 2021 , 13, 35233-35247.						
Author	1	2	3	4	5	6
Development of the concept	×					×
Monomer and polymer synthesis		×		×		
Chemical characterization	×	×		×		
Biological investigation	×					
Method development	×		×			
Preparation of the manuscript	×					
Correction of the manuscript	×	×	×		×	×
Supervision of F. Hausig						×
Proposed publication equivalent	1.0					

<p>“Efficient transfection <i>via</i> an unexpected mechanism by near-neutral polypiperazines with tailored response to endosomal pH”</p> <p>Pub3 <u>Franziska Hausig-Punke</u>,¹ Gregor Dekevic,² Fabian H. Sobotta,³ Jana I. Solomun,⁴ Friederike Richter,⁵ Denise Salzig,⁶ Anja Traeger,⁷ Johannes C. Brendel,⁸ <i>submitted</i>.</p>								
Author	1	2	3	4	5	6	7	8
Development of the concept	×						×	×
Polymer synthesis		×						
Polyplex characterization	×							
Biological investigation	×							
DoE		×						
Method development	×			×	×		×	
Preparation of the manuscript	×							
Correction of the manuscript		×	×	×	×	×	×	×
Supervision of F. Hausig								×
Proposed publication equivalent	1.0							

<p>“Improved gene delivery to K-562 leukemia cells by lipoic acid modified block copolymer micelles”</p> <p>Pub4 Friederike Richter,^{1, ‡} Prosper Mapfumo,^{2, ‡} Liam Martin,³ Jana I. Solomun,⁴ <u>Franziska Hausig</u>,⁵ Jochen J. Frietsch,⁶ Thomas Ernst,⁷ Stephanie Hoeppener,⁸ Johannes C. Brendel,⁹ Anja Traeger,¹⁰ <i>J. Nanobiotechnol.</i>, 2021, 19, 70.</p>										
Author	1	2	3	4	5	6	7	8	9	10
Development of the concept	×									×
Polymer synthesis		×	×							
Micelle characterization		×								
TEM investigation								×		
Biological investigation	×									
Method development	×			×	×	×	×			
Providing cells						×	×			
Preparation of the manuscript	×									
Correction of the manuscript		×	×	×	×	×	×	×	×	×
Supervision of F. Hausig									×	
Proposed publication equivalent	0.5									

[‡] Authors contributed equally.

Documentation of authorship

<p>“Solely aqueous formulation of hydrophobic cationic polymers for efficient gene delivery”</p> <p>Pub5 Jana I. Solomun,¹ Gizem Cinar,² Prosper Mapfumo,³ Friederike Richter,⁴ Elisabeth Moek,⁵ <u>Franziska Hausig</u>,⁶ Liam Martin,⁷ Stephanie Hoeppener,⁸ Ivo Nischang,⁹ Anja Traeger,¹⁰ <i>Int J. Pharm.</i>, 2021, 593, 120080.</p>										
Author	1	2	3	4	5	6	7	8	9	10
Development of the concept	×									×
Polymer synthesis			×				×			
Polymer/particle characterization	×		×			×	×			
TEM investigation								×		
AUC investigation		×							×	
Biological investigation	×				×					
Method development	×			×		×				
Preparation of the manuscript	×									
Correction of the manuscript		×	×	×	×	×	×	×	×	×
Proposed publication equivalent	0.5									

“Tuning of endosomal escape and gene expression by functional groups, molecular weight and transfection medium: a structure–activity relationship study”							
Pub6	Friederike Richter, ¹ Liam Martin, ² Katharina Leer, ³ Elisabeth Moek, ⁴ <u>Franziska Hausig</u> , ⁵ Johannes C. Brendel, ⁶ Anja Traeger, ⁷ <i>J. Mater. Chem. B</i> , 2020 , 8, 5026-5041.						
Author	1	2	3	4	5	6	7
Development of the concept	×						
Polymer synthesis			×				×
Particle characterization	×						
TEM investigation							
AUC investigation		×					
Biological investigation	×				×		
Method development	×			×		×	
Preparation of the manuscript	×						
Correction of the manuscript		×	×	×	×	×	×
Supervision of F. Hausig						×	
Proposed publication equivalent					0.5		

Erklärung zu den Eigenanteilen der Promovendin/des Promovenden sowie der weiteren Doktorandinnen/Doktoranden als Co-Autorinnen/-Autoren an den Publikationen und Zweitpublikationsrechten bei einer kumulativen Dissertation

Für alle in dieser kumulativen Dissertation verwendeten Manuskripte liegen die notwendigen Genehmigungen der Verlage („Reprint permissions“) für die Zweitpublikation vor.

Die Co-Autorinnen/-Autoren der in dieser kumulativen Dissertation verwendeten Manuskripte sind sowohl über die Nutzung, als auch über die oben angegebenen Eigenanteile der weiteren Doktorandinnen/Doktoranden als Co-Autorinnen/-Autoren an den Publikationen und Zweitpublikationsrechten bei einer kumulativen Dissertation informiert und stimmen dem zu.

Die Anteile der Promovendin/des Promovenden sowie der weiteren Doktorandinnen/Doktoranden als Co-Autorinnen/Co-Autoren an den Publikationen und Zweitpublikationsrechten bei einer kumulativen Dissertation sind in der Anlage aufgeführt.

Franziska Hausig-Punke	04.10.2022	Jena	_____
Name des Promovenden	Datum	Ort	Unterschrift des Promovenden

Ich bin mit der Abfassung der Dissertation als publikationsbasierte Dissertation, d.h. kumulativ, einverstanden und bestätige die vorstehenden Angaben.

Dr. Johannes Brendel	04.10.2022	Jena	_____
Name des Betreuers	Datum	Ort	Unterschrift des Betreuers

1. Delivery of biologically active substances by polymers

The delivery of biologically active compounds has received particularly intense public interest in recent years during the SARS-CoV-2 pandemic, when first nucleic acid-based and later protein-based systems were introduced for immunization against the infectious disease. In the last decade, the development of systems for efficient delivery of biologically active agents has accelerated. However, despite continuous improvements in delivery systems, the development of materials for efficient and safe delivery of biologic agents for therapeutic treatments remains a challenge. Genetic engineering is not only of interest for the development of new therapies for genetic diseases and in cancer treatment, but also represents a fundamental area of biotechnology, for example in the production of enzymes. Classically, bio technologically modified viruses are used for the transfer of genetic material. In particular, adeno-associated and lentiviruses are employed, which have already been applied *ex vivo* and *in vivo* in drugs approved by the U.S. Food and Drug Administration (FDA). Polymers are becoming increasingly important as delivery vehicles because they are simple and inexpensive to produce on a large scale, have a long shelf life, and offer selective design options through the introduction of chemical variations.^[1] Although historically inferior in efficiency to viral vectors, polymers are becoming more efficient and thus more interesting through the increased efforts of growing global research groups of chemists, biologists, and materials scientists. Polymer-based delivery systems are also of particular interest because they can mimic viral delivery vectors while offering additional safety aspects such as reduced pathogenicity and immunogenicity.^[2] Relevant cargoes include complex macromolecular substances such as genetic material and proteins, as well as small molecules with pharmacological activity. In addition to enzymes, various nucleic acids such as plasmid DNA (pDNA), messenger RNA (mRNA), or regulatory short interfering RNA (siRNA) are therapeutically relevant. Interestingly, so far only non-viral systems offer the possibility to transfer siRNA. Crucial to the delivery of these sensitive biological materials is their protection from the defensive biological environment, *e.g.*, nucleases in the bloodstream. In polymer-based gene delivery systems, the group of cationic polymers can complex nucleic acids due to electrostatic interactions, thus packaging and protecting the sensitive cargo.

At the cellular level, nanoscale transport systems must overcome a variety of extracellular and intracellular barriers to deliver the biologically relevant substance to the site of action. In general, the cell membrane and endosomal entrapment present major obstacles at the cellular

level.^[3-5] Therefore, researchers in the fields of biology, materials science, and chemistry have developed a variety of nanoscale strategies to overcome these obstacles.

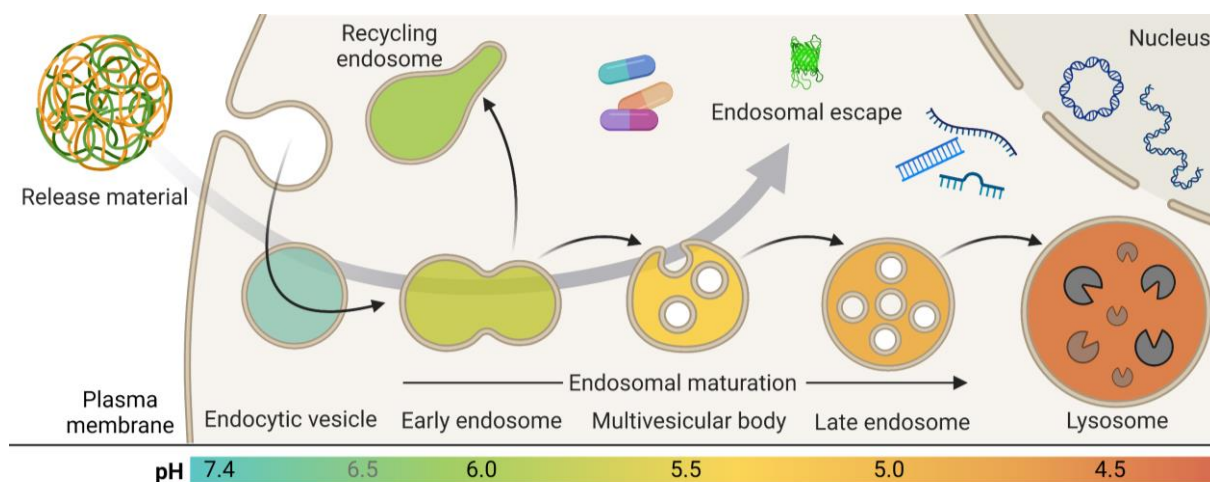


Figure 1.1. Release of biologically active compounds during endosomal maturation. During endocytosis, the endocytic vesicle transports the internalized cargo to the early endosome, where it is either recycled or transported to the lysosome *via* the endolysosomal pathway and degraded. In addition to membrane invagination and fusion of different vesicles, this is accompanied by a change in intraluminal pH. To avoid enzymatic degradation within the lysosome, the releasing material (polymers, liposomes, nanoparticles) accompanied by drugs or biologicals must escape this process at an earlier stage. Adopted from ^[6].

Particles, as well as fluids, solutes, macromolecules, or plasma membrane components, are taken up by the cell through endocytosis, in which the plasma membrane is first invaginated and then separated, allowing the formation of intracellular vesicles. In addition to their role in nutrient uptake, endosomes are also involved in the regulation and fine-tuning of numerous signalling pathways in the cell, such as receptor recycling. After vesicle formation, they fuse to form early endosomes and become connected to the microtubule network.^[7] In this way, vesicles and their cargoes can move along microtubules toward the perinuclear region and gradually mature into late endosomes, where hydrolases and membrane components of the secretory pathway are recruited. Subsequently, they enlarge, form more intraluminal vesicles, and eventually fuse with the lysosome to form the endolysosomes.^[7] During endosomal maturation, the size of endocytic vesicles increases from ≈ 100 nm (early endosome) to ≈ 1000 μ m (lysosome).^[7-10] Inside the endolysosomes, various digestive processes take place that degrade most compounds of biological origin, creating a dead end for the released substances that should be avoided. During endosomal maturation, not only the size and structure of organelles change, but more importantly the intravesicular pH and the composition of the

membrane, both in terms of proteins and lipids, change (see Figure 1.1).^[7, 11] In early endosomes, the membrane is composed mainly of neutral lipids (including sphingolipids and sterols), similar to the cytoplasmic membrane. As vesicles acidify (from 7.4 to 4.5), the proportion of sterols decreases, leading to an increase in membrane fluidity. In addition, the proportion of anionic lipids (e.g., lysobisphosphatidic acid, also called bis(monoacylglycerol) phosphate) (BMP) increases.^[6, 12-14]

This complex process of endocytosis is abused by viruses that hijack this pathway. Viruses overcome the endosomal membrane by a pH-dependent change in conformation or hydrophobicity of their surface peptides, resulting in vesicle membrane penetration. The development of cell-penetrating polymers has often been inspired by membrane-permeabilizing or cell-penetrating peptides present in viral proteins.^[15-16] The changes in pH and lipid composition of the endosomal membrane during maturation can be used to design targeted polymers with suitable physicochemical properties for endosomal escape. Smart cationic polymers that respond to pH are of interest because they can be tuned to respond to pH changes in the endosomal pathway (e.g., with protonation), which may help overcome endosomal entrapment. To circumvent endosomal digestion, pH-dependent cationic amines have often been used for polymers or lipids. This results in more amines being protonated, and the cationic polymers can facilitate interaction with anionic lipids due to electrostatic interactions and hydrogen bonding between the amino groups of the nanocarrier and the phosphate groups of the lipids. Thus, it is an endosomal escape concept based on destabilization of the negatively charged endosomal membrane by progressive interaction with increasingly cationic polymers.^[17-19] In particular, the inherent decrease in pH during the internalization process from the extracellular space (pH 7.4) through the early (pH 5.9-6.5) and late endosome (pH 5.9-4.9) to the lysosome (pH 4.9-4.0) has attracted much attention in the development of such polymers. Many known polymers are already protonated at a physiological pH of 7.4, which is related to their main application, the transport of genetic material. Cationic charges have the potential to interact with serum proteins and disrupt the plasma membrane under physiological conditions.^[20-21] Therefore, many successful cationic pH-dependent materials face an efficacy-toxicity dilemma, as they allow efficient endosomal release of therapeutics but often cause severe cytotoxic side effects.^[21-22] On the other hand, endosomal release of uncharged, hydrophilic nanocarriers unfortunately does not succeed, so many are either excreted (exocytosis) or degraded (lysosome). Since endosomal release is such an important factor in the efficiency of a carrier system,^[4-5, 23] it is very interesting to adjust the degree of protonation

of the carrier according to the pH shift along the endosomal pathway. Thus, the polymer can interact locally with the endosomal membrane to destabilize it and promote the release of the nanocarrier into the cytoplasm. However, fine-tuning the response of pH-responsive polymers presents a challenge on the chemical side.

Cationic charges are particularly well suited for the delivery of genetic material for reasons other than their ability to cross the endosome, as they shield the negative charges of nucleic acids beforehand to enhance cellular uptake.^[24] For genetic material to be transported into the nucleus, nuclear import is required after successful endosomal release, which is regulated by cellular proteins and their interactions with the cellular transport machinery. Nuclear import can be assisted by polymers, although the precise mechanisms have not yet been described in detail.^[25] Over the last decade, correlations have been observed between the properties of cationic polymers and transfection efficiency in terms of the nature of the cationic moieties as well as molar mass and polymer architecture.^[26-27] A correlation has been observed between higher molar masses of polymers and increased transfection efficiency, but this is often also associated with increased cytotoxicity.^[28-31] However, cationic polymers can also be integrated into more complex polymer architectures (hydrogel, micelles, particles) or combined with additional anionic polymers to circumvent the activity-toxicity dilemma.^[32] Although these trends can be considered as guidelines, the ideal properties of efficient transfection polymers are difficult to specify because various interacting parameters must be considered. For example, the nature of the cationic moiety is a crucial factor, as it is critical for pDNA binding, cellular uptake, endosomal escape, and pDNA release.^[33-38]

2. Exploring endosomal release

2.1. Calcein as a sensor molecule to study endosomal release

In order to study endosomal escape as an important adjusting screw for delivery system design, it is essential first of all to have methods for studying endosomal escape and evaluating the efficiency of release materials. Thus, several *in vitro* tests have been introduced to investigate release materials and their performance at this barrier. Among these, the release of the small membrane-impermeable dye calcein from vesicles or within cells has become a very popular and straightforward method because it is accessible to most laboratories worldwide, allows rapid and simple conclusions to be drawn about release potential, and enables the study of release mechanisms. In particular, the straightforward detection of escape events from endo-/lysosomal compartments after cellular uptake renders this simple molecule a powerful tool in the study of various release materials such as cell entry vectors or membrane destabilizing agents. Its unique properties (a high charge density due to its multiple carboxylic acid groups, low toxicity, high extinction coefficient and quantum yield, self-quenching at higher concentrations, and low sensitivity to pH changes) prevent undesirable membrane penetrations, enable detection even at low concentrations, and allow broad applicability in relevant physiological settings, thus facilitating release detection. Its application appears straightforward, as no additional chemical modifications to the dye are required and simple co-incubation with the release agent is sufficient to monitor intracellular release events *in vitro*.

As a general procedure, the dye (encapsulated or not) is first taken up by cells *via* endocytotic pathways. At this stage, a punctate pattern is often seen in fluorescence microscopy because the fluorescence of the dye is often only partially quenched at the given concentrations. If appropriate experimental conditions are chosen in terms of calcein concentration, self-quenching in combination with an acidic pH is sufficient to reduce the fluorescence intensity of calcein in endosomes. In the next phase, *i.e.*, upon the occurrence of an endosomal leakage event, calcein rapidly diffuses and dilutes into the neutral cytosol, which microscopically not only causes a more diffuse fluorescence signal but can also lead to a significant increase in intensity if appropriate conditions are initially chosen.^[39] In this manner, calcein was used to evaluate the endosomal escape efficiency of different release materials. Escape was examined in a number of different cell lines, with experimental conditions varying in terms of media composition, calcein concentration, incubation time, type of calcein addition, and cell analyses.

The type of calcein addition can be divided into encapsulated and non-encapsulated or simultaneous and sequential addition. The calcein assay is thereby influenced by the type of material released and the way it is performed, particularly with respect to the simultaneous presence and concentrations of the two compounds (calcein and material) in the endosome. Calcein, being a small molecule, is rapidly taken up by cells, whereas the release materials take longer to accumulate in the endosome, depending on its size and charge. Often, the release material and calcein are added to the cells at the same time without mixing the two components beforehand. Calcein concentrations ranging from 10 μM to 3.21 mM have been reported for non-encapsulated calcein,^[40-42] with most studies using concentrations between 161 and 322 μM ^[43-54] and incubation times from 30 min to 2 days. For encapsulated calcein, higher concentrations are often used to exploit its ability to self-quench. In general, incubation times varied from 10 min to 4 days for this type of calcein addition, which could be attributed to the different endocytosis kinetics of the various release materials. For example, long incubation times could be related to the incorporation of molecules such as poly(ethylenglycol) (PEG) chains, which could shield the surface of the release material and hinder rapid endosomal escape.^[55-56]

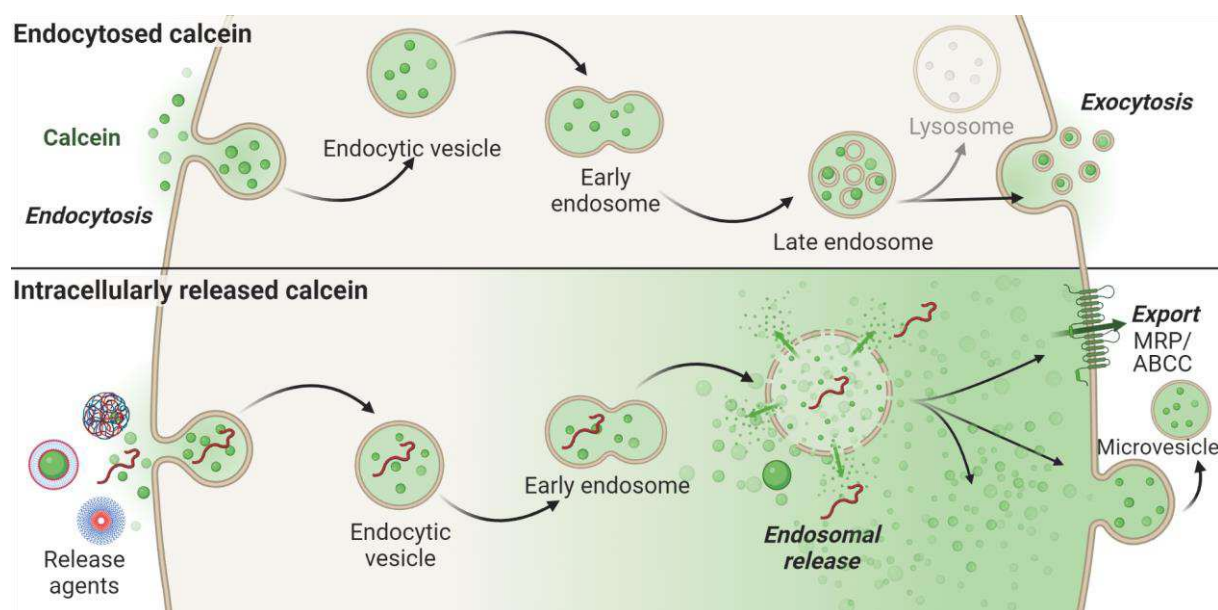


Figure 2.1. Cellular fate of endocytosed and intracellularly released calcein. Calcein is taken up *via* endocytosis and remains trapped within the endosomal pathway without the addition of any endosomolytic agents. Upon endosomal release calcein can be either exported by specific exporters, secreted by microvesicles or undergo the autophagosomal pathway.

Analysis of the calcein release assay can be performed in a variety of approaches depending on the research question. Assay analysis requirements range from attention to detail (accurate

spatial and/or temporal resolution of the intracellular signal) to statistical significance of the data. In most studies, confocal microscopy has proven to be a very powerful tool, even more useful than epifluorescence microscopy because the subcellular distribution of calcein can be elucidated.^[35] Z-stacks can also be created for this purpose.^[43, 46-47] Primarily, live cell microscopy is used, which also allows for kinetic studies.^[51, 57] Less commonly, cells are analyzed after fixation.^[47, 53] In addition, the subcellular distribution and fluorescence intensity of the calcein signal have been quantitatively analyzed.^[43-45, 55, 58-61] It is possible to manually count the cells with punctate and diffuse calcein signal,^[62-63] but a more effective approach relies on the use of various image analysis software where areas of interest and/or thresholds are defined for automated analysis.^[35, 41, 64] Acquisition of many cells, *e.g.*, using montages, is also desirable for statistical power. Colocalization studies with acidic compartments can also be performed (mainly Mander's coefficient)^[49] and may provide further information on the efficacy of calcein release, with lower colocalization indicating more efficient escape.^[47] In addition, high-throughput methods based on flow cytometry are also used to quantify calcein release, with higher cellular fluorescence intensities generally indicating released calcein compared with control cells with punctate fluorescence.^[8, 51, 65-71] Again, appropriate thresholds for fluorescence intensity of escape-positive cells need to be established. Microscopic and flow cytometric methods can also be combined, providing greater insight into endosomal escape.^[40, 51] Because microscopic studies provide spatial (and in the case of live cell microscopy, temporal) resolution of the calcein signal, release events can be measured unambiguously, although the degree of detail varies. Microscopy remains the most commonly used technique, but is comparatively time consuming and can only provide statistical information when large numbers of cells are analyzed. For statistically reliable results, flow cytometry is a faster complementary method, but it cannot spatially resolve the calcein signal within a cell. Although both analytical methods ideally match in the number of release-positive cells to provide reliable results, discrepancies can still occur, for example, due differences in the applied thresholds.^[57]

Overall, successful endosomal escape can be detected using a variety of assay parameters and analytical strategies optimized for each release material, medium, and cell type examined. The wide variety of these parameters hardly allows deriving specific trends from the experiments found in the literature. In fact, a screening of the data published in the literature raised the question of whether significantly different experimental procedures for studying endosomal release efficiency may even lead to different conclusions for similar systems.

2.2. Endosomal release of macromolecules

Nanocarriers are loaded with different drug molecules that may have properties other than calcein, such as size, charge, and hydrophilicity. Therefore, the release of calcein from endosomes may not reflect the drug delivery potential of the nanocarrier. Ultimately, the calcein release experiment should be complemented by studies on the release of other model substances and drug molecules (Figure 2.2). In addition to calcein, other dyes are commonly used for dequenching assays, e.g., 6-carboxyfluorescein and sulforhodamine B. More specific indicators such as pHrodo and acridine orange, which change their fluorescence in response to pH, provide further insight into the endosomal release process. The release of such small marker dyes can only provide information about the presence of small pores. However, when evaluating release materials for biomedical applications, it is of interest whether larger compounds or macromolecules can be released. Therefore, other methods can be combined with the release of the small molecule calcein to evaluate the escape mechanism and release efficiency of a drug for biomedical applications. When calcein release is studied in comparison to the escape of macromolecules of different sizes, conclusions can be drawn about the size of the membrane defect that has occurred.^[47] For such studies, polysaccharides such as dextrans can be used, which exhibit a relatively fast diffusion rate through the cytosol despite their different sizes. This favors a temporal determination of the release event.^[58] Ogris and colleagues used a fluorescein isothiocyanate (FITC)-labeled dextran (10 kDa) that allowed them to study the release of melittin-modified poly(ethylenimine) (PEI) polyplexes. In this case, the fluorescence of the FITC upon release is enhanced by the increase in pH.^[72] In another example, Zhan and colleagues^[47] measured the release of various dextrans by blend particles containing a poly[2-(dimethylamino)ethyl methacrylate] (PDMAEMA) domain compared with calcein. They incubated DC2.4 dendritic cells simultaneously with calcein and dextrans of different sizes (4 - 2000 kDa).^[47] Their study showed that endosomal release of compounds does not depend on the blend composition but on the size of the sensor molecule, with the smaller molecules being released more readily.

In addition to polysaccharides, peptides and proteins can also be used as markers to study endosomal release and place even greater demand on the release material when if their 3D structure has to remain intact.^[57] Fluorescent proteins such as R-phycoerythrin (R-PE, 240 kDa) or enhanced green fluorescent protein (EGFP) (27 kDa) can also be used to study endosomal release. Although endosomal uptake of these proteins is low without additional treatment with an uptake-inducing material, the mechanism of endosomal release of the same material can be

studied in more detail with fluorescent proteins. Because these proteins undergo a loss of fluorescence on the endolysosomal pathway due to denaturation, a release of the fluorescent signal clearly indicates escape from the early endosome. Labeled proteins can also be used to study endosomal escape, but unlike intrinsically fluorescent proteins, the timing of endosomal escape cannot be studied with labeled proteins because denaturation of the protein might not affect the fluorescence intensity of the dye. Again, a combination with other methods is useful. Nevertheless, labeled bovine serum albumin (BSA) is a suitable and readily available candidate because it is efficiently taken up *via* endocytosis and can be detected more rapidly than other complex proteins due to its moderate diffusion rate after the escape event. Diffusion in the cytosol is slower than for a small molecule such as calcein because the higher molar mass and more complex structure of the protein result in comparatively slower diffusion.^[57-58]

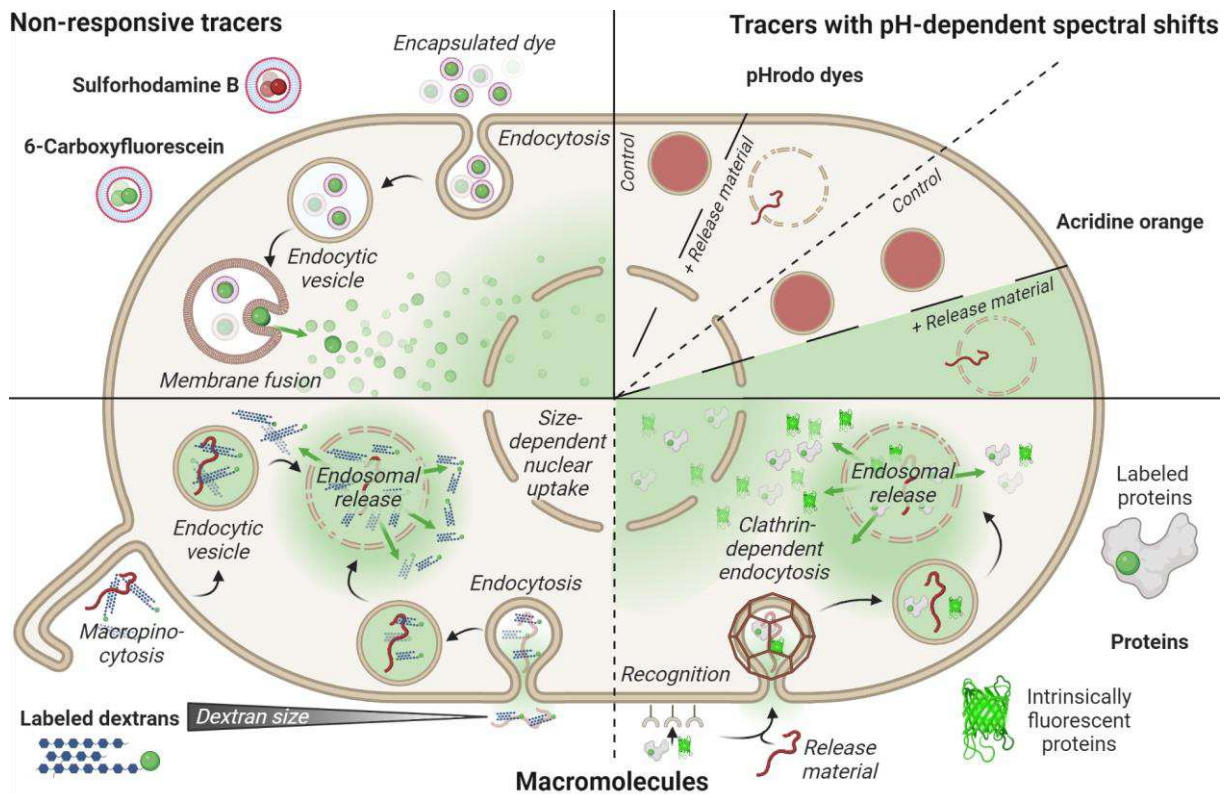


Figure 2.2. Complementary methods to the calcein release assay. In addition to calcein, other tracers such as sulforhodamine B or 6-carboxyfluorescein can be encapsulated in vesicles to determine their release capabilities in cells. pH-dependent tracers such as pHrodo or acridine orange can also be of interest, as they indicate the pH in their environment through changes in fluorescence. Besides small molecules, macromolecules such as dextrans or proteins are intriguing, as their size and complexity provide additional information about the escape.

Actual transfection, *i.e.*, delivery of genetic material to its site of action, can also serve as evidence for endosomal release. Depending on the type of genetic cargo, different measurements are used. In the case of pDNA transfection, protein expression provides very clear evidence that endosomal release of the plasmid must have been successful. In the case of successful release of RNAs, either protein expression (mRNA) or silencing (*e.g.*, siRNA) may indicate successful release, depending on the particular cargo. In either case, successful transfer (measurable as expression or knockdown) is a global indicator that demonstrates the functionality of the genetic load. Calcein release is often studied in the context of transfection of nucleic acids with cationic polymers. Frequently, calcein escape efficiency is correlated with pDNA transfection, regardless of the release material used.^[35, 44, 60, 64, 70-71] However, this correlation does not hold true in all cases. Rather, protein expression indicates the successful overcoming of various hurdles, of which endosomal release is only one step. For example, Vermeulen and coworkers studied the endosomal escape mechanism of JetPEI polyplexes, a linear PEI derivative,^[8] and attempted to correlate calcein or labeled oligonucleotide release with transfection efficiency according to a previously published procedure.^[73] Interestingly, calcein release was observed in far more cells than transfection and therefore does not correlate, but oligonucleotide release appeared to be a more reliable indicator of efficient transfection. The authors conclude that endosomal leakage for small molecules may be caused by destabilization of the membrane due to interaction with cationic polyplexes, which prevents effective buildup of osmotic pressure due to ion influx across this disrupted membrane, thus preventing endosomal escape and macromolecule leakage. Therefore, the study of calcein release may provide further evidence of the mechanism of endosomal escape in addition to its efficacy.

Despite the alternative methods for studying endosomal release, the calcein assay remains a simple but effective method that provides a straightforward entry point for analyzing potential release events and may not yet have reached its full potential.

3. Motivation and aims

The aim of this work is to understand the influence of physicochemical properties of polymers on their ability to overcome endosomal entrapment and thus provide materials for the delivery of biologically derived pharmaceuticals. An important aspect herein is the influence of the basicity of pH-responsive cationic polymers. The basicity of a cationic polymer determines its charge density as a function of the prevailing pH. The charge, in turn, is crucial for the endosomal release ability of the material. Despite knowledge of this dependence and its influence on endosomal release, it is difficult to derive clear structure-property relationships for directed polymer design from the reported studies and materials. First, most of the reported polymers were designed for gene delivery and are required to perform several tasks, including complexation of the genetic material. In this regard, several studies have examined correlations between the pH response of the polymer, often referred to as buffering capacity, in the range of interest (pH 5-7.4) and its effectiveness in gene delivery. For example, the type of amine (primary, secondary, or tertiary) was found to have a critical effect on pDNA release.^[33-35] An interesting study was conducted by Du *et al.*^[74] who examined the effects of the acid dissociation constant (pK_a) - a measure of the basicity of a material that correlates with the buffer range - of various copolymers on the efficacy of siRNA release. While pK_a values between 5.8 and 6.2 were identified as most effective, the polymers studied also undergo a phase transition with the change in pH, which is related to their inherent hydrophobic structure. Indeed, most pH-responsive polymers with pK_a values in the interesting range of 6-7 are hydrophobic in the neutral state, which affects their membrane interaction and complicates the evaluation of independent factors.^[75-76] Purely hydrophilic polymers with pK_a values close to 6 are based on imidazole units, as also found in histidine.^[77] While no clear conclusions on structure-property correlations can be drawn from the reported materials, incorporation of imidazole or histidine moieties clearly improved the efficacy of the delivery systems, which was attributed to the favorable pK_a value.^[64, 78-79] Moreover, the second protonation of ethylenediamino groups (a subunit of PEI) was found to occur at pH 6 and to be critical for efficient gene delivery,^[80] whereas similar units with a slightly lower second pK_a value (≈ 5.5) did not improve it.^[81] Therefore, it is crucial to investigate the fundamental effects of basicity (pK_a value) or buffer capacity in the crucial range (pH 5-7.4) for endosomal escape, regardless of the release of complexed biologicals or the inherent hydrophobic structure of the release materials.^[82] The main challenge is to find suitable materials that allow fine tuning of the pK_a value without major structural changes and provide good solubility in aqueous media over a

wide pH range. Polypiperazines are a new class of polymers that have not previously been employed in biomedical applications and enable an easy adjustment of their basicity by modification of the substituents on the amino group.^[83-84] A detailed analysis of their structure-property relationships and their initial application in the delivery of biologicals is presented in *Chapters 4 and 5*.

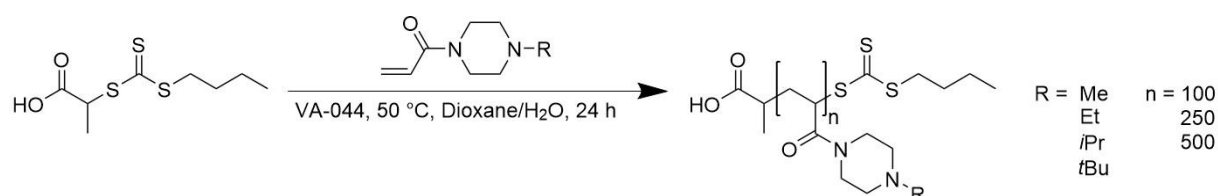
In addition to the basicity or degree of charge of the delivery system, the balance between hydrophilicity and hydrophobicity is also critical for release from the endosome. While the intrinsic hydrophilicity of the system is critical for use in aqueous environments in biomedical applications, hydrophobic moieties enhance interactions with cellular membranes. In addition to release potency, the incorporation of hydrophobic monomers also matters in polymer assembly, which in turn affects the charge density of a system. Alternative polymer systems for the delivery of genetic material are presented in *Chapter 6*.

In this first set of studies, cell lines were used for *in vitro* studies only. Common to all of the studies presented is the employment of HEK 293T cells, as they have been widely used for many years as a cell line that is comparatively easy to handle and transfect. HEK 293T is a human cell line that can be readily cultured in serum-free media and whose cells grow adherently. Because it was artificially transformed, the cell line, like any simple model, has limited applicability and the results are of limited value. However, since HEK 293T (or variants) are widely used in the development of viral vaccines, chemotherapeutics, and in the production of recombinant adenovirus vectors, basic conclusions can be drawn, especially for biotechnological applications.

4. Evaluating pH-adjustable polypiperazines as release agents

4.1. Polypiperazines as a new class of polymers in biomedical applications

Inspired by the structure of commonly used biological buffers (*e.g.*, 4-(2-hydroxyethyl)-1-piperazineethanesulfonic acid (HEPES) buffers), the interesting class of pH-responsive polypiperazines were considered for biomedical applications in this study for the first time. Nevertheless, previous reports indicate favorable pK_a values that can be tuned by the respective substituents by an enhanced inductive effect of methyl (Me) to ethyl (Et), isopropyl (*i*Pr) and finally tert-butyl (*t*Bu) groups.^[83-84] The easy and straightforward accessibility of the monomers and their acrylamide structure allow controlled polymerization *via* reversible addition-fragmentation chain transfer (RAFT). In agreement with similar acrylamides,^[85] the chosen RAFT polymerization facilitated access to well-defined polymers with variable degrees of polymerization (DP). Typical of the free radical polymerization of acrylamide monomers in water, the rate of polymerization was very high, such that quantitative conversions (> 99%) were achieved within a few hours. Consequently, a set of different homopolymers poly(*N*-acryloyl-*N'*-methylpiperazine) (PNAMP), poly(*N*-acryloyl-*N'*-ethylpiperazine) (PNAEP), poly(*N*-acryloyl-*N'*-*iso*-propylpiperazine) (PNA*i*PP), and poly(*N*-acryloyl-*N'*-*tert*-butylpiperazine) (PNA*t*BP) with DPs ranging from 100 up to 500 (16-99 kDa) were prepared.



Scheme 4.1. Syntheses of polypiperazines. The piperazine based vinyl monomers were polymerized *via* RAFT polymerization.

The described polypiperazines represent an exciting new set of materials, where protonation occurs exactly in physiologically interesting range and the basicity of the amino group can gradually be increased with subtle modifications on the substituent without notably affecting its solubility. This fine-tuning of buffer capacity and pK_a in this region renders these materials ideal for investigating the impact of basicity on endosomal release. Indeed, the tested polypiperazines exhibited a wide buffer range in the desired pH range. Moreover, in agreement with the original hypothesis, the systematic modifications of the side group resulted in a gradual

shift of this buffering capacity to higher pH values with increasing substituent size. Similarly, calculations revealed a gradual increase in the respective pK_a^{app} values in the range of 6.2 to 7.1 (Figure 4.1.b), covering the most interesting pH region from the extracellular environment to early and late endosome.^[86-87] Based on theoretical considerations derived from titration of the polymers the degree of charge at physiological pH value of 7.4 was determined, ranging from 9% for the less basic PNAMP to a maximum of 36% for the more basic PNA ι BP (Figure 4.1.c). Along the endo/lysosomal pathway, all materials become fully protonated and thus fully charged. Interestingly, the sharpest increase in charge level for all materials is expected during the transition from the extracellular space to the early endosome.

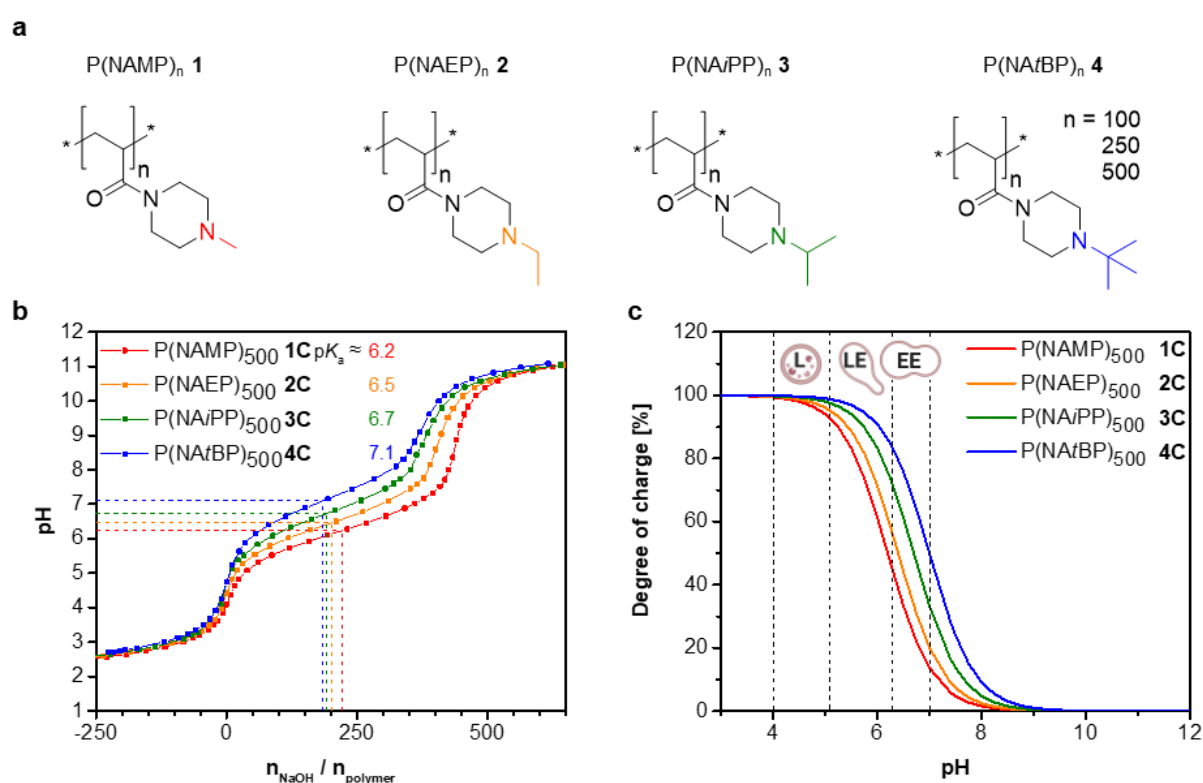


Figure 4.1. pH-Responsiveness of polypiperazines depending on substituent. **a** The polypiperazines of the investigated library differ in their DP and pendant group. **b** The titration curves of the polypiperazines were obtained from potentiometric titrations of acidified polymer solutions against sodium hydroxide in water with 150 mM sodium chloride. The red, orange, green and blue squares represent PNAMP₅₀₀, PNAEP₅₀₀, PNAiPP₅₀₀ and PNA ι BP₅₀₀, respectively. The pK_a is indicated for each material. **c** The degree of charge at different pH values was calculated from the titration data (symbols) and according to the Henderson-Hasselbalch equation (1) (lines) for PNAMP₅₀₀ (red), PNAEP₅₀₀ (orange), PNAiPP₅₀₀ (green) and PNA ι BP₅₀₀ (blue). The pH range within the compartments of the endo-lysosomal pathway, early endosomes, late endosomes and lysosomes are indicated according to Maxfield & Yamashiro^[86] and Huotari & Helenius^[87]. EE - early endosome, LE - late endosome, L - lysosome.

The necessity of such a fine-tuning becomes already apparent when testing their biocompatibility. Significant cytotoxic effects were only observed for the most basic PNA/BP_n and elevated concentrations of PNAiPP_n with the highest DP, while all other polymers revealed no toxicity. The results corroborate a previous study about the impact of charge density and molar mass of polycations on cytotoxicity and even allow a more distinct differentiation.^[88] The biocompatibility of the materials was also evident in the high blood compatibility of the non-hemolytic materials, of which only the most basic PNA/BP with highest DP induced aggregation of erythrocytes. The plasma membrane of HEK 293T cells was also not permeabilized by the materials except, again, PNA/BP₅₀₀ or in the absence of serum in a basicity-dependent manner. Microscopic studies of cellular uptake of the labelled polymers showed fluorescence signals in small enclosed compartments of the cell, indicating endocytotic uptake. Flow cytometric studies revealed that the uptake of polypiperazine depends on the degree of charge and also on the cell culture medium used, with cytotoxic effects collapsing the uptake trend in the case of PNA/BP₅₀₀ under serum free conditions.

4.2. Probing endosomal release of polypiperazines

The key element of this study is to establish correlations between the basicity/ pK_a of the materials and their ability to facilitate endosomal escape. Therefore, various fluorescent model probes, ranging from the small molecule calcein to the biomacromolecule dextran (70 kDa) or the protein bovine serum albumin (BSA, 66.4 kDa), were co-incubated with the respective polymers to allow monitoring of size-dependent endosomal escape. In initial tests, nor calcein, dextran or BSA were found to form any complex with the tested polymers. First, the subcellular distribution of the model probes and the fate of the polymer were imaged by confocal laser scanning microscopy (CLSM). PNAiPP₅₀₀ was initially investigated for its pH response in the physiologically relevant pH range, sufficient uptake, and membrane activity at endosomal pH values, while exhibiting good bloodcompatibility and cell viability at physiological conditions. A fluorescent version was synthesized to localize the polymer and the probe simultaneously. Control cells treated with calcein alone displayed a punctate pattern,^[17, 82, 89] while cells additionally treated with PNAiPP indicated diffuse green fluorescence in the cytoplasm and nucleus, indicating the release of calcein from the endosome (Figure 4.2.d). Interestingly, a similar effect was also observed for the larger BSA (66.4 kDa). In both cases, the rate of endosomal release by the labeled PNAiPP is moderate, as a strong punctate fluorescent signal is still detectable in the included compartments.

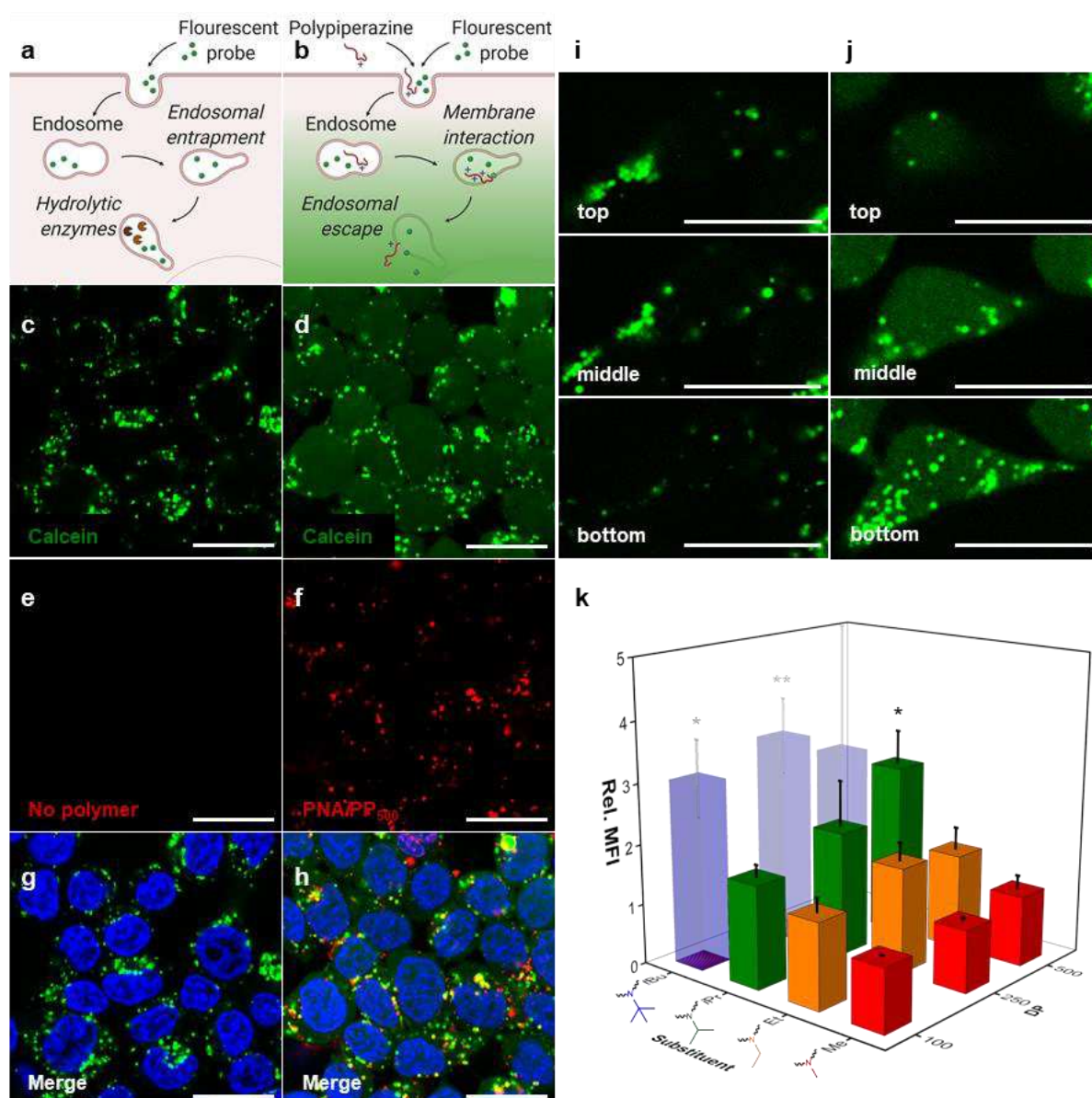


Figure 4.2. Endosomal escape of calcein. **a** Schematic presentation of the endosomal entrapment of calcein in cells and **b** of the cytosolic delivery facilitated by the polypiperazines. **c**, **e**, **g** Confocal images of HEK 293T cells treated with the non-membrane permeable dye calcein as control. **d**, **f**, **h** Cellular uptake and endosomal release of calcein were imaged using HEK 293T cells that were treated with the same concentration of calcein as the control cells and labeled PNAiPP₅₀₀. The calcein channel (**c**, **d**) and the corresponding image of the red channel (polymer, **e**, **f**) as well as the merge of the calcein, polymer and Hoechst channel (**g**, **h**) are shown. **i**, **j** Example images of a z-stack acquisition from the lower, middle and upper part of a cell treated either with calcein alone as control (**i**) or with PNAiPP₅₀₀ and calcein (**j**). **c-j** Scale bar 20 μ m. **k** High-throughput analysis of fluorescence intensities of HEK 293T cells treated with calcein and polypiperazines. The means \pm SD of three independent experiments relative to control cells treated with calcein only (rel. MFI = 1) are shown. *, **: significant difference ($p < 0.05$, $p < 0.01$) compared to control cells. Transparency of bars indicates gated cell populations below 70% (slight transparency) or 50% (distinct transparency) according to reduced viability of the samples. rel. MFI - relative mean fluorescence intensity.

By flow cytometry, two cumulative trends were observed when examining all polymers for their potential to facilitate endosomal escape using calcein as a probe (Figure 4.2.k). Both DP and basicity correlate with MFI, indicating more efficient endosomal escape induced by the respective polymers. Similar to the uptake studies, the trend collapses as the cytotoxicity of the materials increases. A similar trend was observed for other types of cationic polymers before,^[70, 90-92] and considering the minor impact on cytotoxicity in case of the highly charged polymers such as PNA β BP, the tuning of polymer size might represent an interesting lever to optimize release with insignificant loss of viability. Among the nontoxic materials, the best calcein release was observed for PNA β PP with a DP of 500, which showed a significant increase in MFI compared with cells treated with calcein alone (relative mean fluorescence intensity (rel. MFI)). However, the screening revealed that the basicity and pK_a value of the polymers have a greater effect on the efficiency of endosomal escape than DP. Interestingly, the release studies on various compounds ranging from small dyes (calcein) to macromolecules (proteins or dextran) depict similar correlations. While the differences in calcein release may be due in part to an increased uptake rate for the more basic polymers, the key to efficient release of larger molecules appears to be the basicity or pK_a of the polymers (Figure 4.3.b). In a direct comparison of BSA release, PNA β PP or PNA β BP proved to be the most efficient release polymers, which were comparable in efficiency with l-PEI 25 kDa despite the very different basicity and buffer capacity. While PNA β PP caused a considerable release in Opti-MEM® without signs of toxicity in the tested range, almost no effect is found if serum-containing medium is applied. On the contrary, the more alkaline PNA β BP suffers from increased toxicity in the first case but facilitates a concentration-dependent escape despite the presence of serum. These findings emphasize the peculiarities of media such as Opti-MEM® which is optimized for transfection, and demonstrate potential difficulties induced by serum proteins narrowing the window for efficient release without causing severe toxicity. Interestingly, the release was dependent on the type of polymer rather than their concentration (Figure 4.3.a).

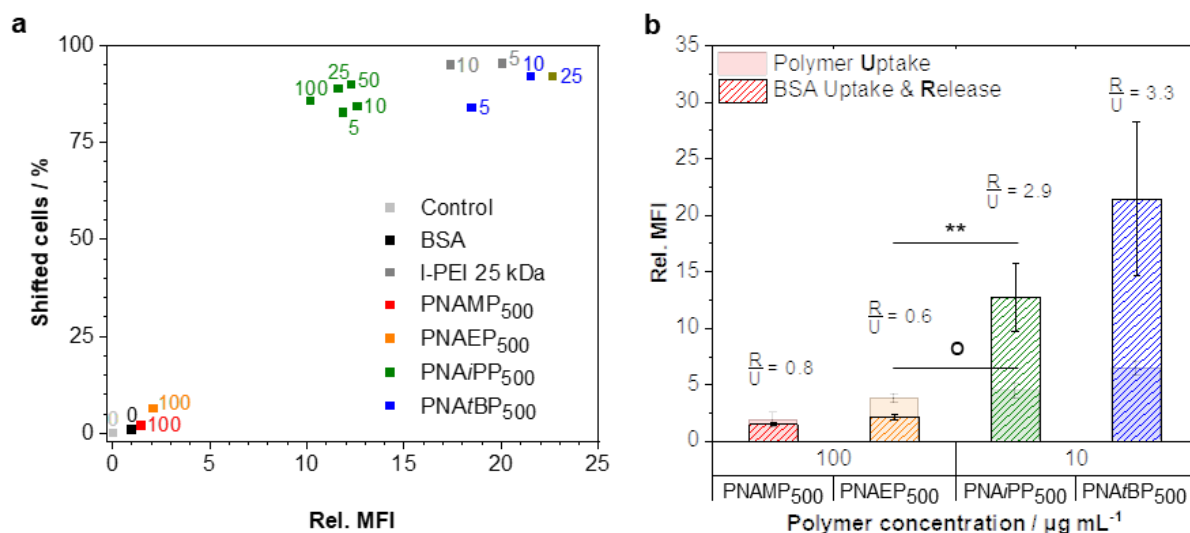


Figure 4.3. Basicity-dependent endosomal escape of labeled BSA. **a** Exemplary, the endosomal escape facilitated by the polypiperazines in comparison to commercial l-PEI 25 kDa in Opti-MEM® is plotted to show correlations between the polymers' basicity and concentration. The polymer concentration is given near the corresponding data point. Means of three independent experiments are shown. **b** The cellular uptake of Oregon Green-labelled polymers (DP: 500) as well as the endosomal escape of labelled BSA in HEK 293T cells was assessed by flow cytometry. For the uptake studies, the obtained MFI values were corrected by the labelling efficiency of the polymers and are given in relation to the untreated control. Regarding the endosomal escape studies, the relative MFI values are given in relation to cells treated without polymers. Mean \pm SD of three independent experiments is shown. The ratio of BSA release to polymer uptake (R/U) is given for the respective polymers at the concentration shown. o: no significant difference, **: significant difference ($p < 0.01$), rel. MFI - relative mean fluorescence intensity.

A crucial factor for the efficient delivery of biological therapeutics is the preservation of their structure during this process. Usually, the decrease in pH and the presence of hydrolases following the endolysosomal pathway lead to degradation of biological material such as proteins. Therefore, escape from the early endosome is key to bypassing this degradation and ensuring an intact delivery of proteins, antibodies, or genetic material. Following previous reports,^[93] RNase A was incubated with the promising polymers PNAiPP₅₀₀ and PNAiBP₅₀₀ in different media. While the pure enzyme does not exert toxic activity on cells, release into the cytosol results in cell death due to degradation of cytosolic RNA, which can be monitored by a concentration-dependent cell viability assay. In agreement with previous experiments, a clear difference was observed between Opti-MEM® and serum-containing medium (Figure 4.4.a vs. b). To visually confirm the previous results, PNAiPP₅₀₀ and PNAiBP₅₀₀ were further tested for delivery of EGFP monitored by CLSM. However, it is important to note that HEK 293T cells

generally exhibit limited EGFP uptake (Figure 4.4.c,e), which reduces the probability of congregation with the polymer in the same compartments. In serum-containing medium, PNA β BP resulted in increased uptake and cytosolic release of fluorescent EGFP (Figure 4.4.d), which was similarly observed with PNA β PP in the absence of serum (Figure 4.4.f). In both cases, the number of affected cells examined by flow cytometry appears to be lower compared with the results obtained with BSA administration, which again may be due to the limited uptake of this protein. Despite these challenges in the delivery itself, the final RNase A and EGFP delivery assays confirmed that intact transport of sensitive biological molecules can be achieved with these polymers and that protein activity is maintained in the cytosol. Therefore, it can be assumed that the release is triggered at least to some extent in the early endosomes, since the fluorescence of EGFP in particular would certainly be affected by conditions in the late endosome or in the lysosome.^[94-95]

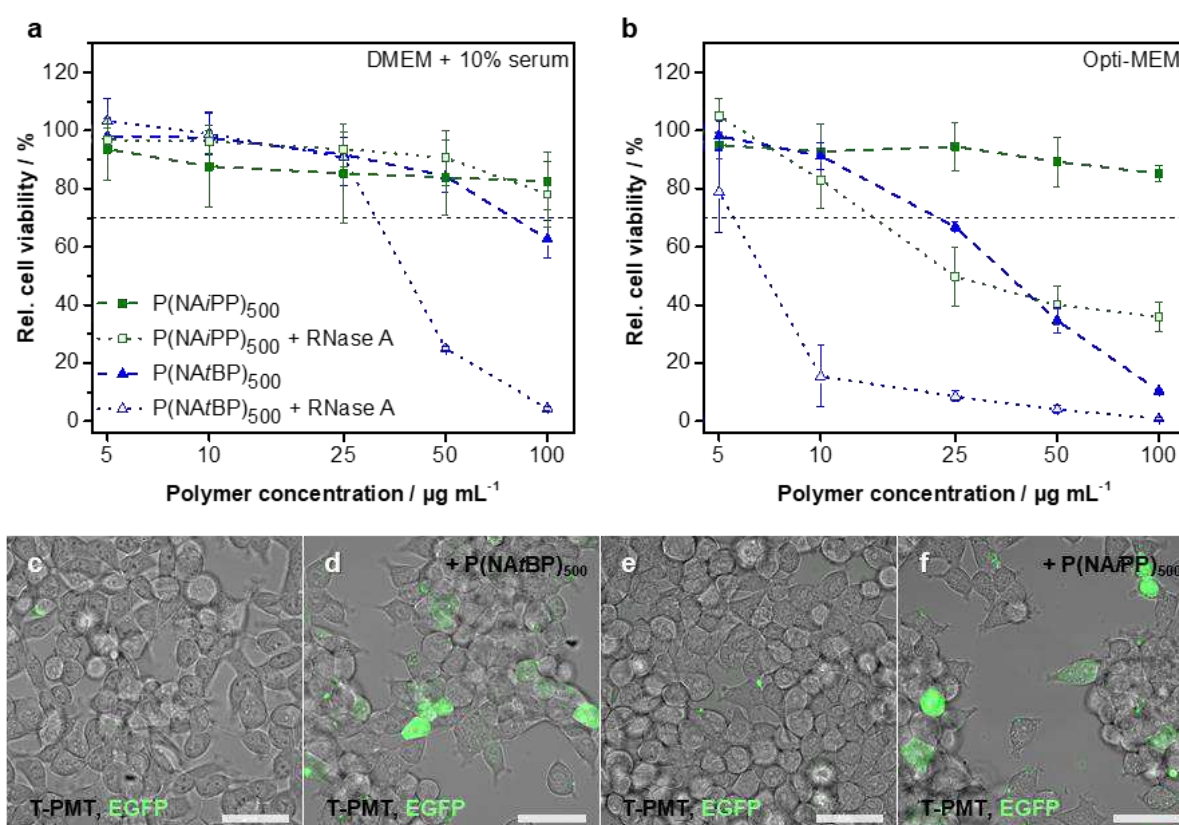


Figure 4.4. Cell culture medium-dependent delivery efficiency of functioning proteins. **a,b** The relative viability of HEK 293T cells **a** in the presence of serum or **b** in Opti-MEM® treated with indicated concentrations of the polymers PNA β PP₅₀₀ (green, solid squares) and PNA β BP₅₀₀ (blue, solid triangles) or with additional 500 $\mu\text{g mL}^{-1}$ RNase A (respective color, open symbols) were measured *via* the alamarBlue assay. Means \pm SD of three independent experiments are shown. **c,e** HEK 293T cells **c** in serum-containing medium or **e** in Opti-MEM® were treated with EGFP for 16 h and analysed *via*

CLSM as a control. The overlay of the T-PMT and EGFP channel are shown. **d** HEK 293T cells in serum-containing medium were treated with the same concentration of EGFP as control cells but with additional $50 \mu\text{g mL}^{-1}$ PNA/BP₅₀₀ at the same time and analysed as described in **c**. **f** HEK 293T cells in Opti-MEM® were treated with the same concentration of EGFP as control cells but with additional $50 \mu\text{g mL}^{-1}$ PNA/PP₅₀₀ at the same time and analysed as described in **c**. Scale bar 25 μm . EGFP - enhanced green fluorescent protein, T-PMT - transmitted light detector.

From the studies on release from the small molecule calcein to functioning proteins, it can be concluded that the pK_a values and thus maximum buffer capacities of release polymers must be closer to 7 for efficient endosomal escape, which is in good agreement with the research on ionizable lipids, where a substantial increase in delivery efficiency was identified at a pK_a value of 6.8, while pK_a values of 6.8-7 were described as most effective.^[96-99] Consequently, the often-considered range of 5-7.4^[64, 100-101] for polymeric vectors should be narrowed down, which might explain previously observed discrepancies concerning the importance of buffer capacities in this range.^[80-81]

5. Polypiperazines in gene delivery

Following the demonstration that the endosomal hurdle can be overcome with polypiperazines, the question arose whether this property can be used to create synergies in the field of gene delivery. However, the most important question is whether the almost neutral polypiperazines are able to bind genetic material at physiological pH and to stimulate all cellular processes from the endocytotic uptake of the polyplexes to the transcription in the nucleus.

5.1. Complexation of genetic material by near-neutral polypiperazines

Due to their low protonation and thus limited positive charge at physiological pH values, the polypiperazines were not expected to interact strongly with genetic material. While initial complexation studies based on an EtBr assay (Figure 5.1.) indicated only a weak binding ability of these polymers at the physiological pH value of 7.4, more detailed investigations based on gel retardation revealed indeed a stable polyplex formation, which however differs in terms of pDNA condensation from common transfection polymers such as l-PEI (Figure 5.2.b).

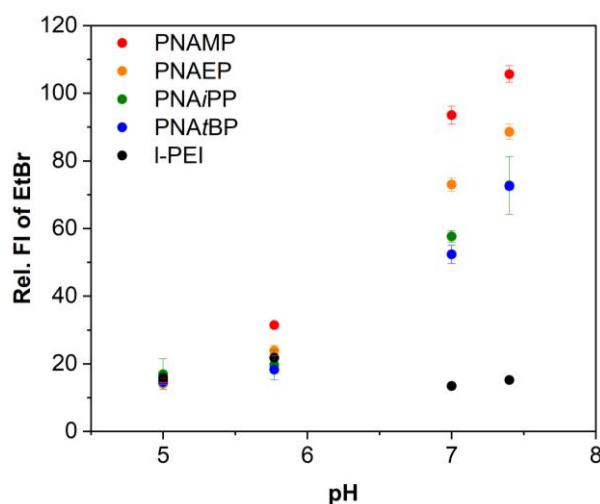


Figure 5.1. pH-dependent pDNA binding of polypiperazines. The pH-dependent pDNA binding of the polypiperazines was studied at N*/P 30 by an EtBr quenching assay using different buffers in a pH range from 5 to 7.4, representing the physiologically relevant pH range during transfection experiments. Data are presented as the mean \pm SD (n = 3). l-PEI was investigated for comparison.

As expected, PNAMP did not complex pDNA at any of the ratios of protonatable amines to phosphates (N*/P ratios) examined, confirming that its low charge density was not sufficient for stable polyplex formation (Figure 5.2.b). However, PNAEP displayed an unexpected N*/P-

dependent retardation of pDNA. More astonishingly, PNA*i*PP and PNA*t*BP retained pDNA even at a low N*/P of 3, which suggested polyplex formation contradictory to the initial EtBr assay. Interestingly, PNA*i*PP, PNA*t*BP and l-PEI showed the same pattern for pDNA binding despite their substantially different charge density at pH 7. Thus, the polypiperazines were able to efficiently bind pDNA and inhibited its gel migration, although they resulted in only a modest EtBr displacement. For comparison, commercial l-PEI leads to a displacement of nearly 90%, which reflects the effective pDNA condensation known for this type of polymer. These data support that PNA*i*PP and l-PEI polyplexes may differ in their pDNA binding mode and may be packaged differently. A different binding mode in PNA*i*PP and PNA*t*BP is also supported by the hydrophobicity of the *i*-Pr and *t*-Bu side chains, which may interact with the solvophobic portions of the DNA chains. To better understand the interaction of polypiperazines with genetic material, the polyplexes were studied in more detail in terms of their hydrodynamic diameter, polydispersity index (PDI) and surface charge. Accordingly, polyplexes ≤ 200 nm were formed with PNAEP, PNA*i*PP, and PNA*t*BP. PNAMP formed larger aggregates, confirming the less intense packing mentioned earlier. The PDI for all polyplexes was in a desirable range < 0.250 . The zeta potential correlated with the charge density of the polymers, with the l-PEI polyplexes exhibiting the strongest positive surface charge.

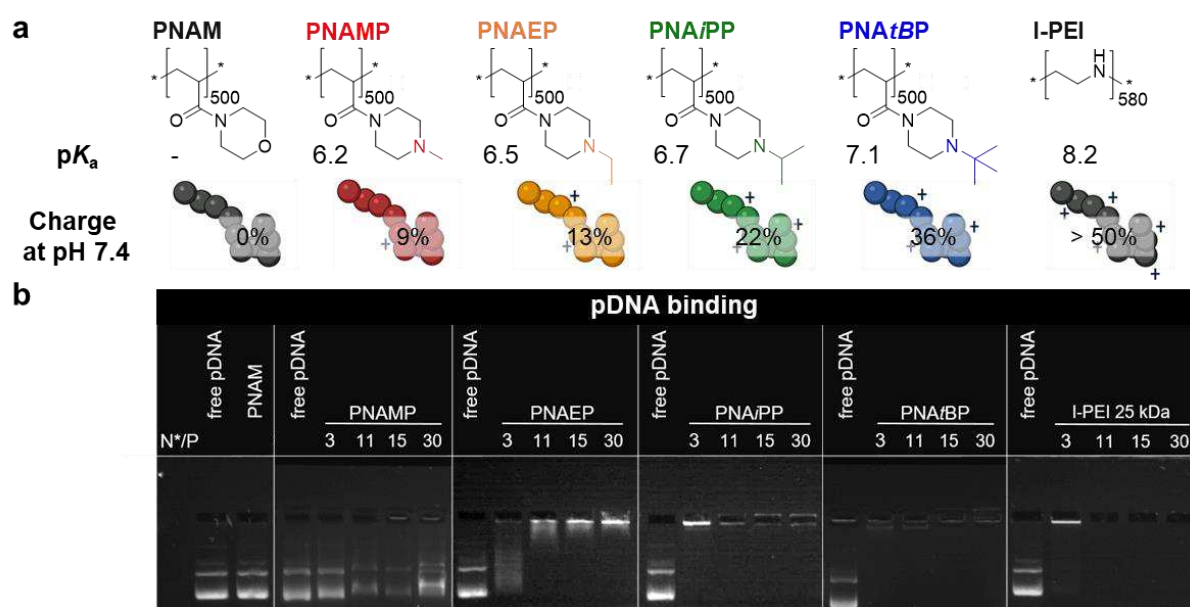


Figure 5.2. Charge-dependent pDNA binding of polypiperazines. **a** Chemical structure of polypiperazines and the controls l-PEI and poly(*N*-acryloylmorpholine) (PNAM) and charge density of the polymers at pH 7.4.^[57] **b** The pDNA binding ability of the polymers was studied at various N*/P ratios by gel electrophoresis ($n \geq 1$). Free pDNA was investigated as control.

In contrast to conventional cationic transfection agents and polymers, almost no pDNA release was observed in polyplexes based on PNA ι PP and PNA ι BP when treated with the competitive polyanion heparin (Figure 5.3.a). Among the polypiperazines a trend towards increased stability with increased basicity was found. At the investigated N*/P ratios, pDNA can be released from the PNAEP polyplexes at all investigated heparin concentrations, whereas only a negligible pDNA release was observed for PNA ι PP polyplexes at any of the tested conditions. Finally, no pDNA release was observed for PNA ι BP. On the contrary, l-PEI fully releases pDNA in each of the tested conditions, indicating a different mode of pDNA binding of polypiperazines and l-PEI. We hypothesize that the increasing hydrophobicity of the alkyl side chains could cause local secondary interactions that stabilize the polypiperazine polyplexes even in the presence of heparin. In the case of PNAEP (lowest hydrophobicity), the secondary interactions might not be sufficient to prevent dissociation of the polyplex with addition of the polyanion. On the other hand, in case of low PNAEP excess, the packing density of the polymer chains at the pDNA could be much higher, favoring the proximity of the molecules and possibility of formation of local secondary interactions. Unpacking of pDNA was described as a critical factor in transfection and sophisticated systems were developed for pDNA release.^[1, 102-103] However, the heparin release experiment performed suggests that the release mechanism of polypiperazines differs from the well-known l-PEI and does not involve complete release of pDNA.

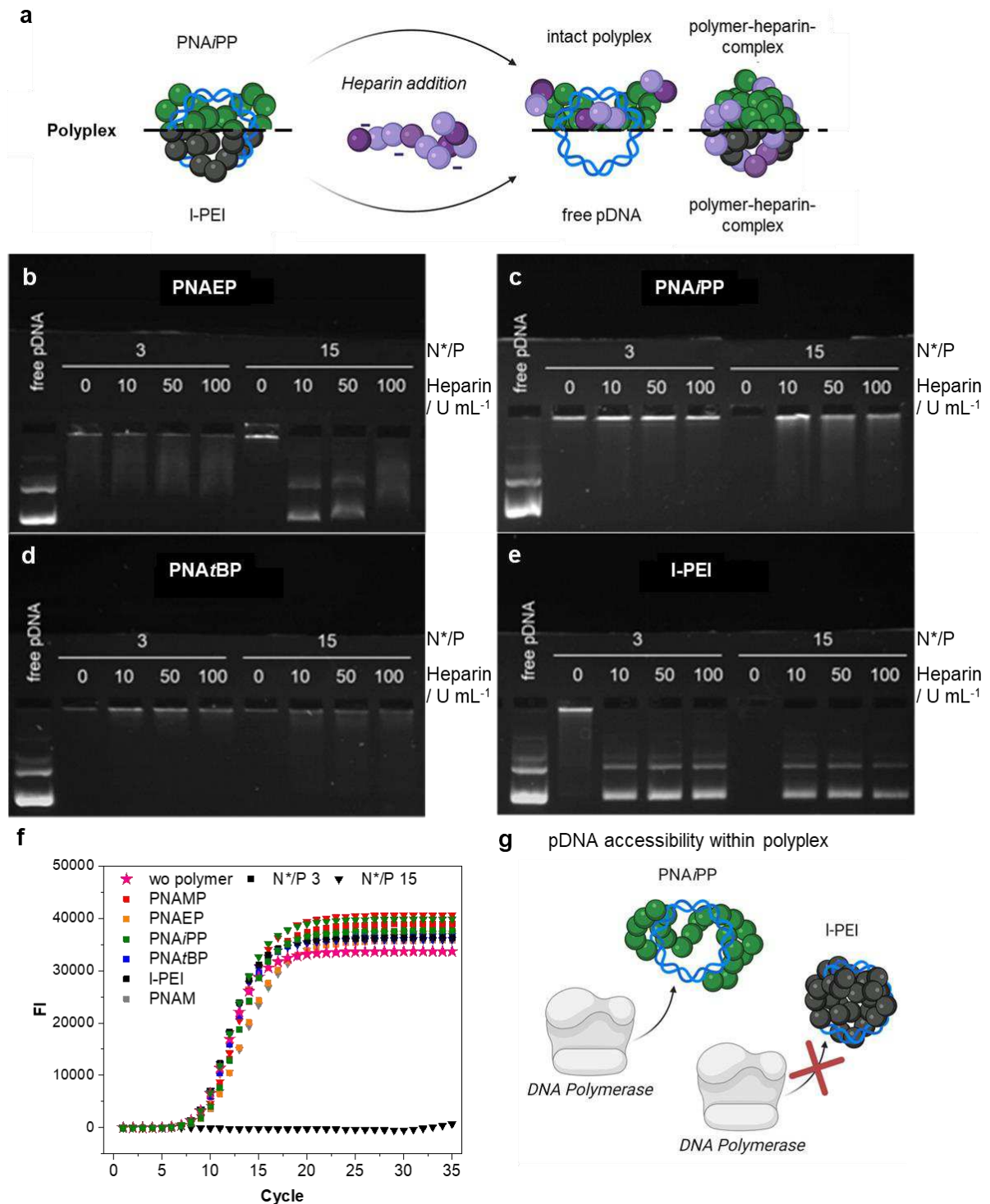


Figure 5.3. Stability and pDNA accessibility of polypiperazine polyplexes. **a** PNAiPP (green, upper) and I-PEI (black, lower) polyplexes differ in their pDNA release behavior upon heparin treatment. **b-e** Agarose gel electrophoresis was conducted to investigate pDNA release. Polyplexes were prepared at N*/P 3 and 15 and incubated with different concentrations of heparin as a competitive polyanion. For comparison, free pDNA was investigated as well. A representative image (n = 2) for **b** PNAEP, **c** PNAiPP, **d** PNAiBP and **e** I-PEI is shown. **f** pDNA accessibility of polyplexes was investigated *via* qPCR in comparison to free pDNA. Representative amplification curves (n = 2) are shown for PNAMP (red), PNAEP (orange), PNAiPP (green), PNAiBP (blue), I-PEI (black) as well as uncharged PNAM

(grey) and free pDNA (pink). **g** A schematic representation of PNAiPP (green) and l-PEI (black) polyplexes illustrates differences in their pDNA accessibility.

Nevertheless, the successful amplification (quantitative polymerase chain reaction (qPCR)) of the pDNA bound in a polyplex with the polypiperazines indicated that a release is not necessary for an efficient transcription in the case of the polypiperazines (Figure 5.2.f). The condensation of the pDNA by the polypiperazines differs significantly from previously described polyplexes, for example l-PEI, which is also indicated by the differences in EtBr displacement. The polypiperazines provide the opportunity for pDNA to remain accessible within the polyplex for transfection, thus circumventing the need for release of genetic material (Figure 5.2.g). Assumably, the comparably loose binding of the polypiperazines enables an unhindered transcription of the pDNA even if complexed by the polymers. The significantly lower charge density of polypiperazines compared to l-PEI could explain the differences in polyplex packaging, pDNA binding, and accessibility.

5.2. Endosomal escape and gene expression of polypiperazine polyplexes

In the calcein release data presented previously, the endosomal escape efficiencies of the free polypiperazines were evaluated. These indicated an increase in relative fluorescence intensity for PNAiPP, PNAiBP, and l-PEI (see *Chapter 4.2.*). The question arises whether endosomal release is also successful in the presence of pDNA. Based on the presented assay with the free polypiperazines, which demonstrated clear correlations between microscopy and flow cytometry (see *Chapter 4.2.*), we performed only flow cytometric analyses in this study. The results revealed that PNAiPP, PNAiBP and l-PEI caused an increase in the fluorescence intensity of the calcein signal even in the presence of pDNA. Interestingly, at lower pDNA concentrations, PNAiPP showed comparable endosomal release efficiency to l-PEI despite their significantly different basicity, whereas at higher pDNA and correspondingly higher polymer concentrations, the endosomal release capacity of l-PEI significantly exceeded that of PNAiPP. As shown previously, the increased amount of free l-PEI has a pivotal role in endosomal escape and is also crucial for the transfection mechanism.^[104-105] Previous endosomal escape studies also showed very low endosomal release efficiency for PNAEP, which was too low for efficient calcein release and protein delivery (see *Chapter 4*). In the context of nucleic acid transfection, however, a rather low endosomal escape rate may be sufficient because a plasmid can be repeatedly transcribed for subsequent protein production.^[73] However, the results are generally consistent with the previously published study on cytosolic delivery of proteins (see *Chapter*

4).^[57] Although showing superior calcein release, the plasma membrane activity of the higher charged PNA α BP has a particularly unfavorable effect in the context of transfection with nucleic acids, as limitations in cell viability impede protein biosynthesis.

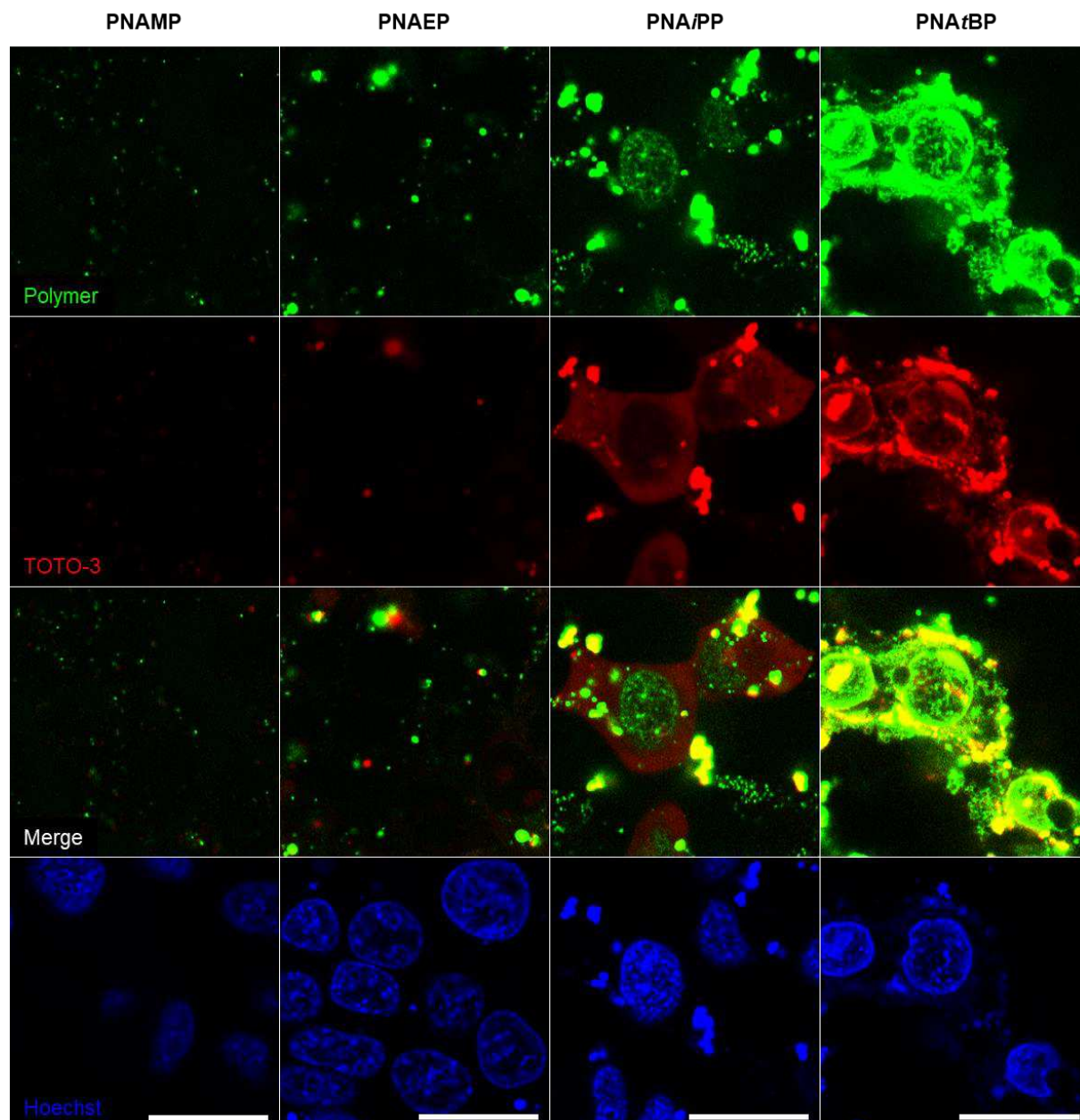


Figure 5.4. Intracellular trafficking of piperazine-based polyplexes. HEK 293T cells were treated with polyplexes of Oregon Green-labeled polypiperazines (green channel) and TOTO-3 iodide-stained pKMyC pDNA (red channel, P conc = 12 $\mu\text{mol L}^{-1}$) at N*/P 15 for 4 h. The cells were stained with Hoechst 33342 (blue channel) to visualize the nuclei in live-cell confocal microscopy. Representative images of two independent experiments are shown. Scale bar 20 μm .

To further investigate the uptake of polyplexes and their interaction with different cell membranes, CLSM was employed using live cells and polyplexes of Oregon Green labelled

polypiperazines and TOTO-3 stained pDNA.^[57] For PNAMP, negligible polymer uptake was observed in small isolated compartments, but no pDNA uptake was found (Figure 5.4). For PNAEP, negligible uptake was measured, and PNAiBP caused toxic effects despite the onset of a decreased polymer concentration. PNAiPP induced efficient polymer and pDNA uptake. The TOTO-3 signal was distributed throughout the cytoplasm in approximately 10% of cells, indicating endosomal escape of polyplexes. Interestingly, the PNAiPP (Oregon Green) signal did not distribute throughout the cytosol after release but was assimilated in the nucleus (Figure 5.4). We hypothesize that the entry of PNAiPP into the nucleus may also support the uptake of pDNA into the nucleus.^[25] In the case of PNAiBP, we also observed Oregon Green signals in the nucleus, but here we assume toxic effects such as membrane disruption as causative.

After confirming that the polypiperazines, especially PNAiPP, induce effective endosomal escape even in association with pDNA, and also discovering that PNAiPP enters the nucleus, we investigated the transfection efficiency of the pDNA-binding polypiperazines in comparison to l-PEI 25 kDa. In order to find optimal conditions for this new class of polymers, a design of experiments (DoE) approach was applied to screen a broad design space in terms of concentrations of pDNA and polymer. The optimization of the transfection efficiency with a DoE approach enabled the creation of statistically valid models regarding the optimal settings for polypiperazines and l-PEI while saving enormous amounts of material and time. These experiments revealed that even the slightly charged polypiperazines PNAEP (13% charge density) and PNAiPP (22%) can transfect as efficiently as the highly charged l-PEI (> 50%, Figure 5.5). Although the overall activity of the polypiperazines correlated with their charge density, the upward trend collapsed in the case of PNAiBP, which is due to toxic effects induced by this polymer in serum free conditions. In the case of PNAiPP, the moderate charge density seems to represent a fine balance for achieving efficient transfection, without causing toxic side-effects, yet. Interestingly, PNAiPP appears to transfect very effectively over a very wide range of concentrations and N*/P ratios and outperforms l-PEI in terms of the latter ratios as it still achieves excellent transfection efficiencies at a N*/P ratio of 3 (Figure 5.5.f vs. h). In contrast, the transfection efficiency of l-PEI decreased with decreasing N* and increasing P concentrations, confirming the importance of high N*/P ratios for l-PEI. Surprisingly, even PNAEP was effective at higher polymer concentrations, although its ability to induce endosomal escape was limited compared to the more basic polymers (PNAiPP, PNAiBP, and PEI). The less basic PNAEP was most efficient at comparatively high polymer concentrations and low pDNA concentrations, *i.e.*, at higher N*/P ratios. PNAEP achieved the same efficiency

as PNAiPP at higher polymer concentrations and N^*/P ratios, probably due to its lower charge density. A concentration-dependent endosomal escape may explain as to why transfection efficiencies comparable to PNAiPP were obtained for the less basic PNAEP, although higher polymer concentrations had to be applied. Thus, PNAEP, which showed no toxicity up to concentrations of 1 mg mL^{-1} (corresponds to $6 \text{ mmol L}^{-1} N^*$) according to ISO10993-5, is a positive example that the efficiency-toxicity dilemma can also be overcome by simple homopolymers, if the pH-response and the charge density is finely tuned.

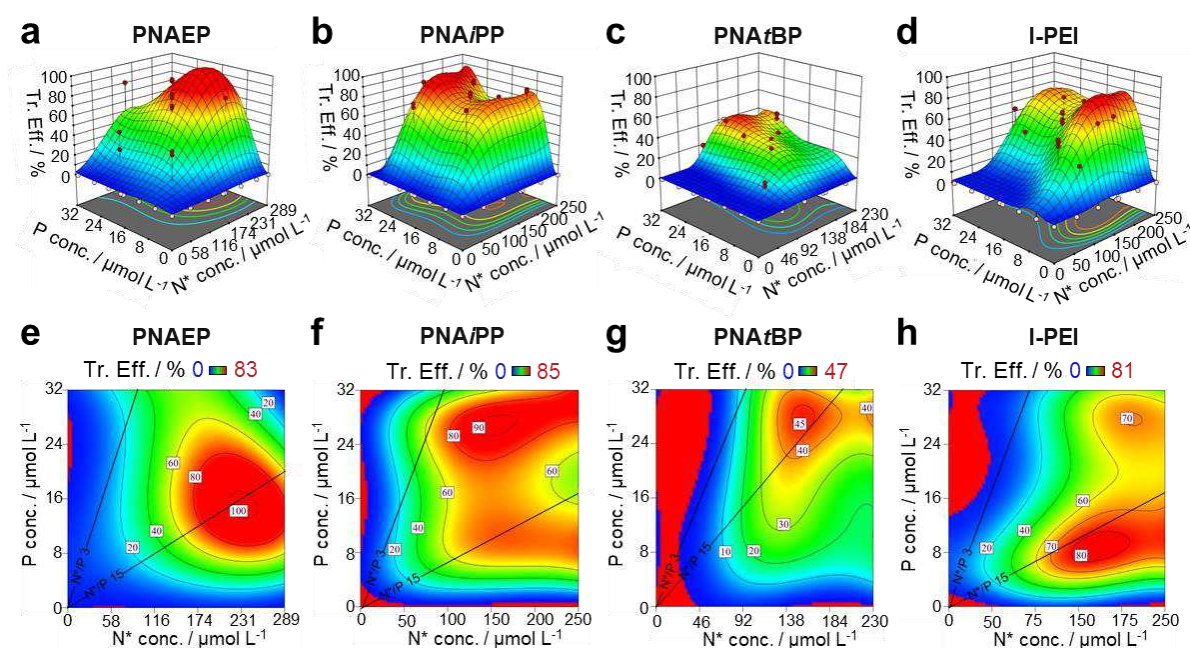


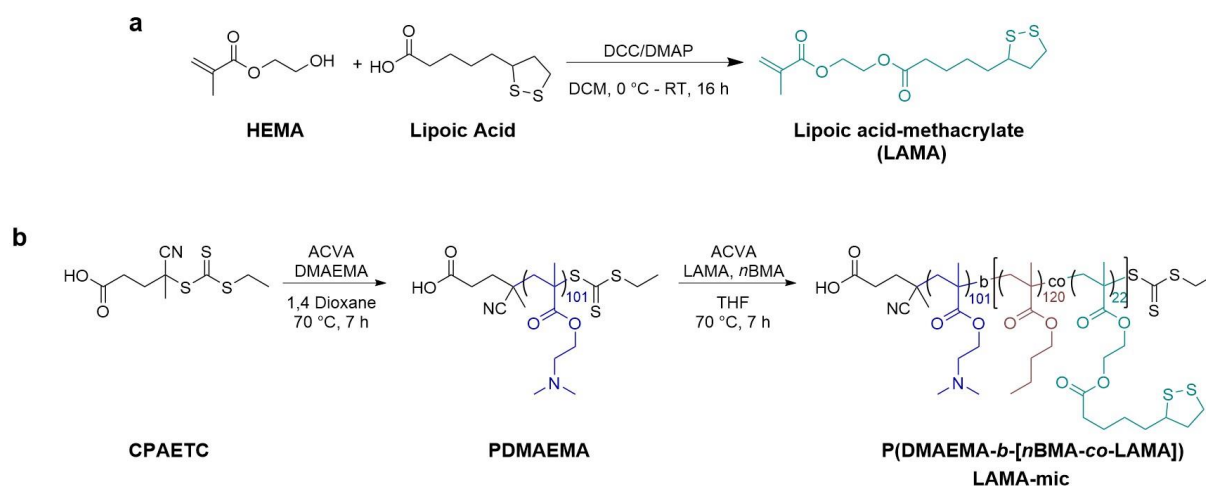
Figure 5.5. Optimization of the transfection efficiency of polypiperazines in HEK 293T cells *via* DoE. **a-d** Augmented 3D surface models and **e-h** augmented contour plots of the response surface predicting the transfection efficiency (percentage of viable green fluorescent protein (GFP)-fluorescent cells) of **a, e** PNAEP, **b, f** PNAiPP, **c, g** PNAiBP, and **d, h** I-PEI show transfection maxima at different conditions. In the 3D plots, the measurement points located in front of the model are indicated with red dots. Constant N^*/P -ratios were plotted along the guidance lines drawn in the contour plots. **a-h** HEK 293T cells were treated with various polyplex formulations. Transfection efficiency was investigated by flow cytometry. N^* conc – concentration of protonatable amines, P conc – concentration of phosphates, Tr.Eff. – transfection efficiency.

6. Alternative polymer systems in the field of endosomal release

While the fine-tuning of cationic charges was central in the study of polypiperazines, the following studies examined alternative polymer systems for delivery of biologicals (in this case, nucleic acids) and evaluated the impact of polymer assembly (*Chapter 6.1.*), integration of hydrophobic moieties and adjustments of the hydrophobic-hydrophilic balance (*Chapter 6.2.*), as well as the effect of permanent cationic charge (*Chapter 6.3.*).

6.1. A pH-responsive polymer micelle

Although significant progress has been made in the field of gene delivery, there are still some challenges, such as difficult-to-transfect cell types like primary or suspension cells.^[106-108] One strategy to overcome this obstacle is to combine cationic polymers with other monomers that introduce additionally beneficial biological and chemical properties. By incorporating hydrophobic monomers, particularly in the form of block copolymers, cationic micelles can be formed that have a better chance of transfection in otherwise difficult-to-transfect cells.^[109-110] The assembly of homopolymers into a micelle leads to a denser packing of cationic charges. In this study, the antioxidant biomolecule lipoic acid, which can also be used as a crosslinker, was additionally incorporated into the hydrophobic block of a diblock copolymer, poly{[2-(dimethylamino)ethyl methacrylate]₁₀₁-*b*-[*n*-(butyl methacrylate)₁₂₄-*co*-(lipoic acid methacrylate)₂₂]} (P(DMAEMA₁₀₁-*b*-[*n*BMA₁₂₄-*co*-LAMA₂₂]), which was synthesized by RAFT polymerization and assembled into micelles (LAMA-mic) (Scheme 6. 1.). These micelles were evaluated for their pDNA binding, cytotoxicity mechanisms, and transfection efficiency in HEK 293T and K-562 cells, a difficult-to-transfect suspension leukemia cell line.



Scheme 6.1. Synthetic routes of LAMA-mic. **a** Synthesis of the lipoic acid-methacrylate (LAMA) monomer *via* N,N'-dicyclohexylcarbodiimide (DCC) /4- (dimethylamino)pyridine (DMAP) esterification coupling reaction. **b** A chain transfer agent, (4-cyano pentanoic acid)yl ethyl trithiocarbonate (CPAETC), was used to synthesize a macro chain transfer agent (macroCTA), PDMAEMA, *via* RAFT polymerization. The macroCTA was then used to synthesize the block copolymer under the same conditions.

The LAMA-mic was able to bind genetic material (Figure 6.1.a) and partially release it after treatment with a competitive polyanion (heparin, Figure 6.1.b). The incomplete quenching of EtBr upon binding of pDNA might indicate a synergism of electrostatic and hydrophobic interactions, which could also explain the incomplete dequenching of EtBr upon heparin addition.

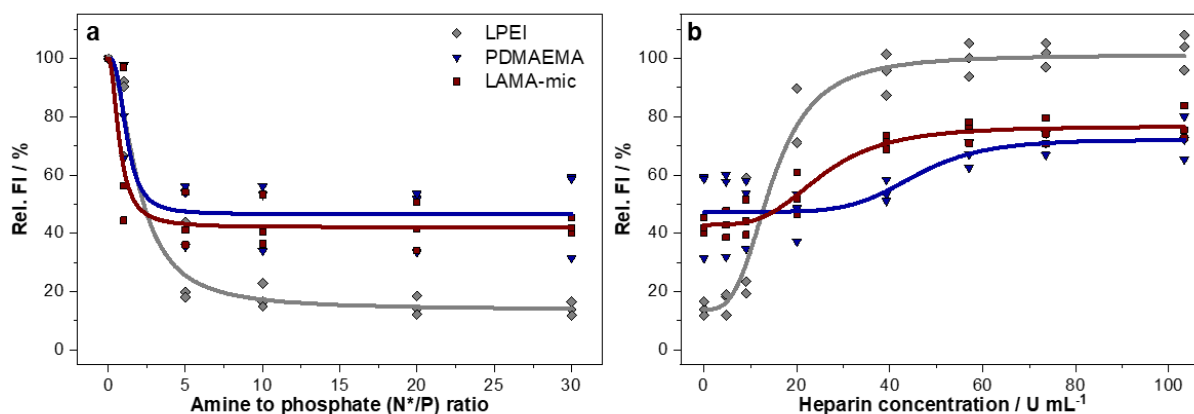


Figure 6.1. Polyplex formation and pDNA release of LAMA-mic. **a** EtBr assay at different N*/P ratios. **b** Heparin release assay of polyplexes at N*/P 30. **a,b** Values represent mean (line) and individual data points (symbols) of $n = 3$.

The LAMA-mic was only mildly toxic at the low concentrations used (Figure 6.2.a) and transfected HEK 293T cells comparable to the commercial control l-PEI 25 kDa (Figure 6.2.b

left bar row). Remarkably, while l-PEI showed almost no transfection in K-562 suspension cells, LAMA-mic caused an increase in EGFP-positive cells by more than sevenfold (Figure 6.2.b right set of bars).

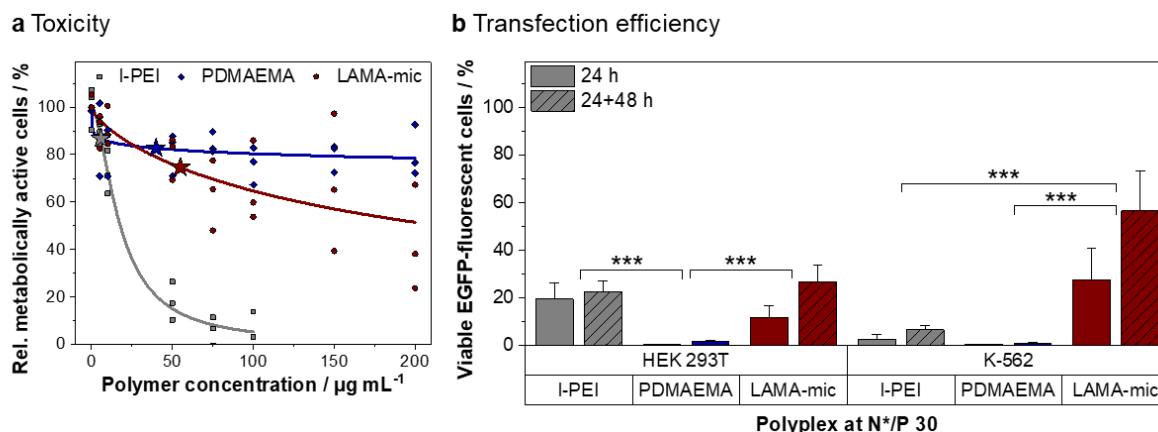


Figure 6.2. Toxicity and transfection efficiency of LAMA-mic in different cell lines. **a** PrestoBlue™ assay in L929 cells following incubation with respective polymers at indicated concentrations for 24 h. Dots represent values of single repetitions and lines represent logistic fit functions ($n = 3$). Stars indicate polymer concentrations used for N*/P 30 in transfection assays. **b** EGFP expression of viable cells was analyzed *via* flow cytometry following incubation of cells with polyplexes of mEGFP-N1 pDNA and polymers at N*/P 30 in respective growth medium (D10 or R10 with 10 mM HEPES) for 24 h or for 24 h followed by splitting of cells and medium and further incubation for 48 h. Values represent mean \pm SD ($n \geq 3$). Significant differences identified only main effects of the polymers, as there were no significant interactions between incubation time and treatment. ***: significant difference ($p < 0.001$)

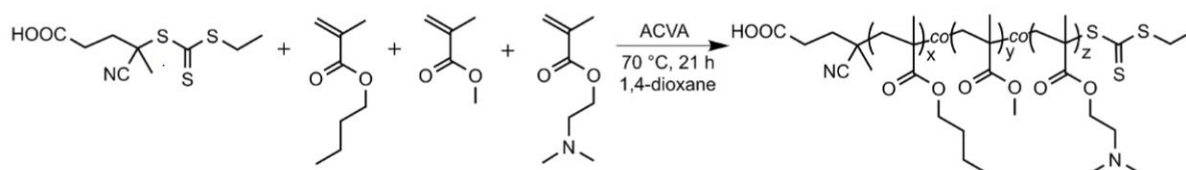
Additional mechanistic studies were performed on the kinetics of polyplex uptake, but these did not correlate with polymer performance, as different substitutions of the polymers showed no effect on cellular uptake in different cell lines. Although transfection efficiency was independent of the cellular uptake of the polymer-pDNA complexes, it did correlate with the endosomal release of the LAMA-mic. Strikingly, endosomal release was particularly high within a short time after treatment. In contrast to l-PEI, the LAMA-mic showed good endosomal release in both cell lines, possibly indicating different release mechanisms.

To investigate the role of lipoic acid in the improved transfection efficiency of the LAMA-mic in detail, an additional set of polymers without lipoic acid was prepared, P(DMAEMA₈₉-*b*-nBMA₆₈) and poly[2-(dimethylamino)ethyl methacrylate]₈₉-*b*-[*n*-(butyl methacrylate)₉₂-*co*-(hydroxyethyl methacrylate)₁₇] (P(DMAEMA₈₉-*b*-[nBMA₉₂-*co*-HEMA₁₇])). The first resembled an amphiphilic block copolymer lacking the LAMA moiety, while the second was

synthesized to mimic a hydrolysed and cleaved lipoic acid from the original LAMA copolymer. Comparison of the different micelles revealed that the micelles lacking lipoic acid also transfected HEK 293T cells, albeit to a slightly lesser extent. In K-562 cells, the transfection efficiency of LAMA-mic polyplexes at N*/P 15 was significantly higher than that of the polyplexes of the other micelles at N*/P 30, suggesting an increase in efficiency due to the incorporation of lipoic acid into micelles. However, for HEK 293T cells, the increase in efficiency was less pronounced. In conclusion, all three micelle systems are promising candidates for efficient gene transfer into K-562 cells, with the higher transfection efficiency of LAMA-mic suggesting a synergistic effect of lipoic acid and architecture. Therefore, incorporation of lipoic acid into the core of hydrophobic cationic micelles represents a promising tailored transfer strategy that could be useful for other difficult-to-transfect cell types.

6.2. Integrating hydrophobicity in copolymers

Introducing hydrophobic moieties into cationic polymers can further improve the efficiency of the system,^[111-115] but common formulation techniques of hydrophobic polymers require the use of organic solvents, which might compromise the integrity and loading efficiency of the genetic material.^[116] In this study, a mild aqueous formulation method for encapsulating large amounts of genetic material into cationic polymer nanoparticles could be established. For this purpose, a polymer corresponding to the commercially used polymer Eudargit® was developed. Thanks to its different solubility in different media, Eudragit® E(PO/100) serves as a matrix excipient for sustained-release pharmaceutical tablets. The insolubility of the polymer in water under neutral pH conditions and its solubility under acidic pH conditions was used in this study as the most important requirement for successful encapsulation of nucleic acids. For the development of the pH-dependent formulation method, a well-defined pH-responsive hydrophobic copolymer, *i.e.*, poly((*n*-butyl methacrylate)-*co*-(methyl methacrylate)-*co*-(2-(dimethylamino) ethyl methacrylate)) (PBMD), was synthesized by RAFT polymerization.



Scheme 6.2. Synthesis of P(*n*BMA-*co*-MMA-*co*-DMAEMA) (PBMD). Polymerization synthesis scheme of P(*n*BMA-*co*-MMA-*co*-DMAEMA) (PBMD) *via* statistical RAFT polymerization.

Dissolution of the PBMD polymer in acidic buffer facilitated pDNA binding, while pH was shifted to neutral values during formulation. This enhanced the hydrophobic interactions that stabilized the formed nanoparticles, particularly under physiological conditions in the presence of proteins and salts.^[111, 117-118] The aqueous pH-controlled formulation of cationic hydrophobic polymers showed high pDNA encapsulation efficiency and desired stability under physiological conditions. In-depth characterization by AUC, cryo-TEM and DLS/ELS showed complete complexation of the genetic material. The PBMD polymer exhibited the desired pH-dependent solubility and pDNA binding behavior in physiological solution. These physiological solution conditions are essential for the assembly of pDNA-polymer complexes in a fully aqueous scenario. The polyplex formation study at neutral pH value revealed stable polyplex formation (Figure 6.3.a.), but only a slight quenching of EtBr (Figure 6.3.b), which may indicate a high contribution of hydrophobic interactions. However, the fact that the nature of pDNA binding can be shifted in a pH-dependent manner was demonstrated when pDNA was displaced from the complex by the competitive polyanion heparin under acidic conditions (Figure 6.3.c). Evident from the increase in EtBr signal dependent on heparin concentration, indicating displacement of pDNA upon addition of the competitive polyanion heparin, electrostatic interactions likely predominate at acidic pH. In contrast, at neutral pH, no displacement of pDNA was observed after addition of heparin, indicating predominantly hydrophobic interactions under physiological conditions.

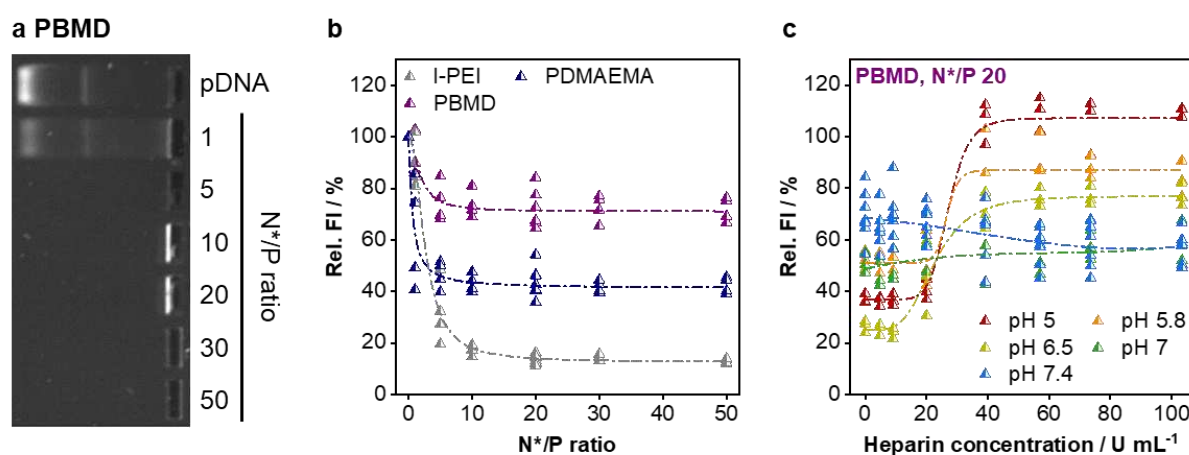


Figure 6.3. pDNA binding and release behaviour of the PBMD polymer. pDNA binding ability of the polymers was studied by **a** agarose gel electrophoresis and **b** EtBr assay in comparison to PDMAEMA and I-PEI at different N^*/P ratios (1–50). **c** To investigate the influence of pH on polyplex stability upon addition of a competitive polyanion, the release of pDNA upon heparin addition was examined. For this purpose, complexes were formed at N^*/P 20 and treated with heparin at pH 5 - 7.4, the physiologically relevant pH range in transfection experiments.

The PBMD polymer showed higher toxicity than l-PEI 25 kDa, which was time and concentration dependent. Shorter incubation times and lower concentrations resulted in higher cell viability and decreasing half maximal inhibitory concentrations (IC_{50}) values (Figure 6.4.a). The novel formulation approach resulted in high transfection efficiencies in HEK 293T cells, while requiring 5- to 10-fold less pDNA compared to l-PEI 25 kDa and was superior at short incubation times and in serum-containing media (Figure 6.4.b). The new formulation resulted also in improved transfection efficiency at lower pDNA concentrations compared to commercial control Viromer® RED and was successful with the commercially approved Eudragit® E(PO/100) and various types of genetic material, such as siRNA and mRNA. The formulation approach showed high versatility and promising potential for further optimization and application to other classes of hydrophobic cationic copolymers for a general vehicle design for genetic material.

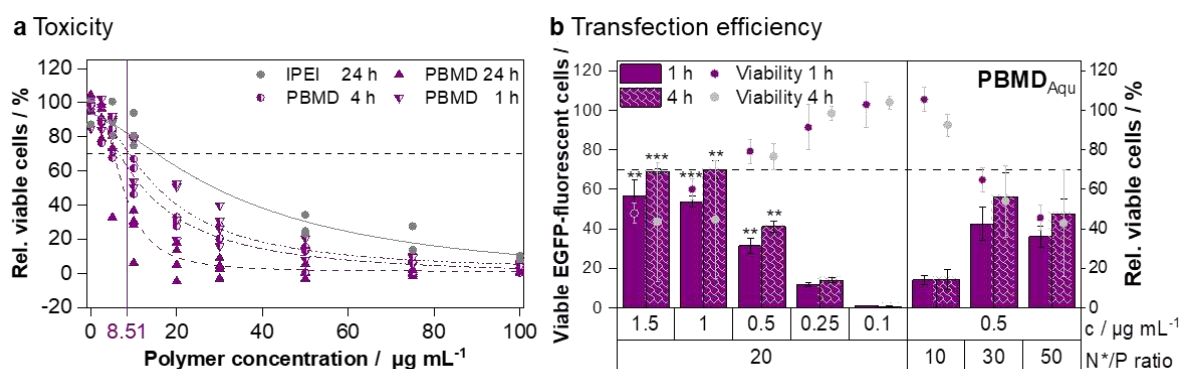
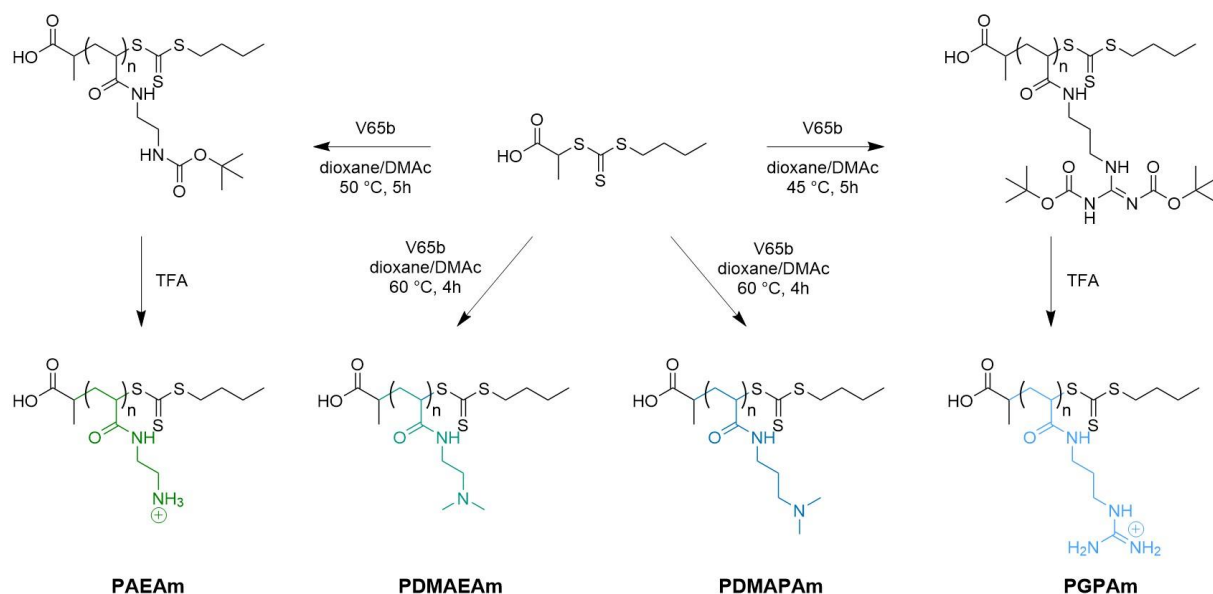


Figure 6.4. Toxicity and transfection efficiency of PBMD. **a** Evaluation of the cytotoxicity of the PBMD polymer dissolved in acetate buffer in L929 cells. Cells were treated with the polymer for 1, 4 and 24 h and cytotoxicity was determined by the PrestoBlue™ assay after 24 h. The dashed line indicates 70% cell viability and the concentration of PBMD polymer under optimized transfection conditions is indicated by the blue line. **b** N*/P ratio and pDNA concentrations were optimized to achieve high efficiencies (high number of viable fluorescent cells) while maintaining low cytotoxicity. The expression of EGFP in HEK 293T cells after transfection (columns) was measured *via* flow cytometry (mean of $n = 3 \pm \text{SD}$). Cytotoxicity of the PBMD_{Aqu} complexes (dots) was determined under conditions used for transfection by the PrestoBlue™ assay (mean of $n = 3 \pm \text{SD}$).

6.3. A cationic, pH-independent polymer

Another interesting cationic moiety is the guanidinium group, which is not pH-dependent in the physiological context ($pK_a > 12$). Guanidine is found in many different biomolecules and contributes to protein denaturation, inhibition of DNA synthesis, or in the amino acid arginine at active sites of enzymes.^[119] Many cell-penetrating peptides, such as the trans-activating transcriptional activator (TAT) peptide, are rich in arginine residues.^[120] While their potential for intracellular transport is established, the mechanism of their entry into the cell, *i.e.*, *via* transduction or endocytosis, remains controversial.^[121-126] Assuming endocytosis, the mechanism of endosomal escape of guanidinium-containing cell-penetrating peptides (CPPs) must be considered. In studies with membrane lipids of the endolysosomal pathway, arginine-containing CPPs have been shown to bind BMP, a lipid present on the inner surface of the membrane of intra late endosomal vesicles (ILEVs, see *Chapter 1*), and to destroy BMP-containing liposomes, suggesting a possible mechanism of endosomal escape.^[127-128] Because this is an important property, the guanidinium group is often used for the development of synthetic vectors.^[126, 129-133] Funhoff *et al.* reported promising transfection and uptake of poly(3-guanidinopropyl methacrylate) (PGPMA) homopolymers in COS-7 cells prepared by radical polymerization.^[81] However, well-defined homopolymers of guanidinium-functional polyacrylates have not been systematically studied as vectors for gene delivery before. However, they are crucial for the potential exploitation of nature-inspired specific cation-lipid interactions. In this study, the structure-property relationship of polyacrylamides with guanidinopropylacrylamide groups was investigated in comparison with other cationic moieties using well-defined polymers, focusing on the influence of molar mass and cationic content on complex formation with pDNA, cytotoxicity, and transfection. Well-defined polymers with narrow dispersity and molar mass distributions were obtained by RAFT polymerization (Scheme 6.3.), whereas the pH-independent polymer poly(3-guanidinopropylacrylamide) (PGPAm) exhibited a very high degree of protonation even at physiological pH.



Scheme 6.3. Synthetic route towards cationic polyacrylamide library.

Binding of genetic material was detected by the EtBr displacement assay described earlier. The highly charged PGAm was able to efficiently condense pDNA and displace EtBr (Figure 6.5.a) and release it almost completely upon treatment with the competitive polyanion heparin (Figure 6.5.b), suggesting electrostatic interactions to stabilize the polyplex. The release exhibited slight DP-dependent effects in this regard.

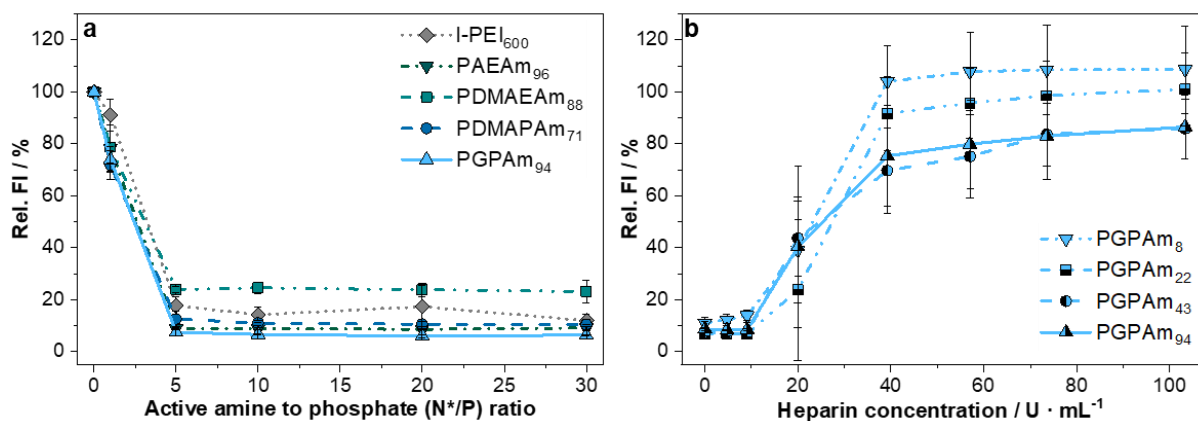


Figure 6.5. pDNA binding and release of PGAm in comparison to polyacrylamide library. **a** EtBr displacement assay of polymers with highest DP at different N*/P ratios showing strong pDNA binding of all polymers. Values represent mean \pm SD ($n \geq 3$). **b** Heparin release assay of polyplexes formed with PGPAm polymers at N*/P 30 using heparin as a competing polyanion showing the reversible pDNA binding. Values represent mean \pm SD ($n \geq 3$).

Besides complexation of genetic material, toxicity and efficiency are the most important properties of transfection polymers. PGAm proved to be less cytotoxic than l-PEI in L929 cells

(Figure 6.6.a), but more toxic than polypiperazines (*Chapters 4 and 5*) or the pH-responsive micelle (*Chapter 6.1.*). However, PGAm achieved the same transfection efficiency as l-PEI despite its lower toxicity (Figure 6.6.b). To better understand the transfection mechanism of the polymers, further studies were performed in detail: Polyplex uptake, membrane interaction, and endosomal release. The results showed that an increase in molecular mass and the presence of guanidinium groups affected the transfection-related aspects. Interestingly, PGAm exhibited very efficient endosomal release properties, outperforming polypiperazines, although it did not respond to pH. On the contrary, there was a strong correlation with enhanced lysis of cytoplasmic membranes (erythrocytes, HEK 293T) and efficient endosomal release, which may be attributed to the lack of a pH response. The permanently highly charged polymer can cause a membrane permeability not only in the endosome, but also attack the plasma membrane at physiological pH in a pH-independent manner. Because PGPAm is not further protonated in endosomes, current escape theories did not appear to be applicable. Therefore, the interaction with BMP, a lipid specific for ILEV, was investigated. In a lipid-polymer binding assay, binding to BMP was tested and demonstrated that all polymers tested were able to bind BMP, with PGAm being the most efficient. A possible explanation could be the different lipid composition of natural ILEV composed of more than one lipid or a more effective mechanism of guanidinium polymers to leave the endolysosome once the polymers passed the ILEV. Nevertheless, the strong interaction of the polymer with the endolysosomal membrane was identified as the most promising mechanism for explaining the observed endosomal release. With transfection efficiency as high as that of l-PEI and superior calcein release properties, the polyacrylates with guanidinium function represent a promising class of polymers for gene delivery.

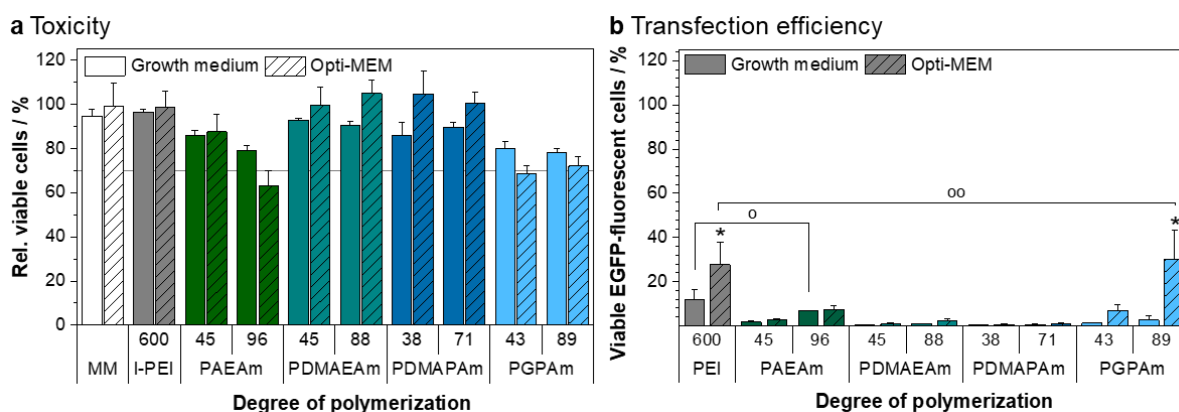


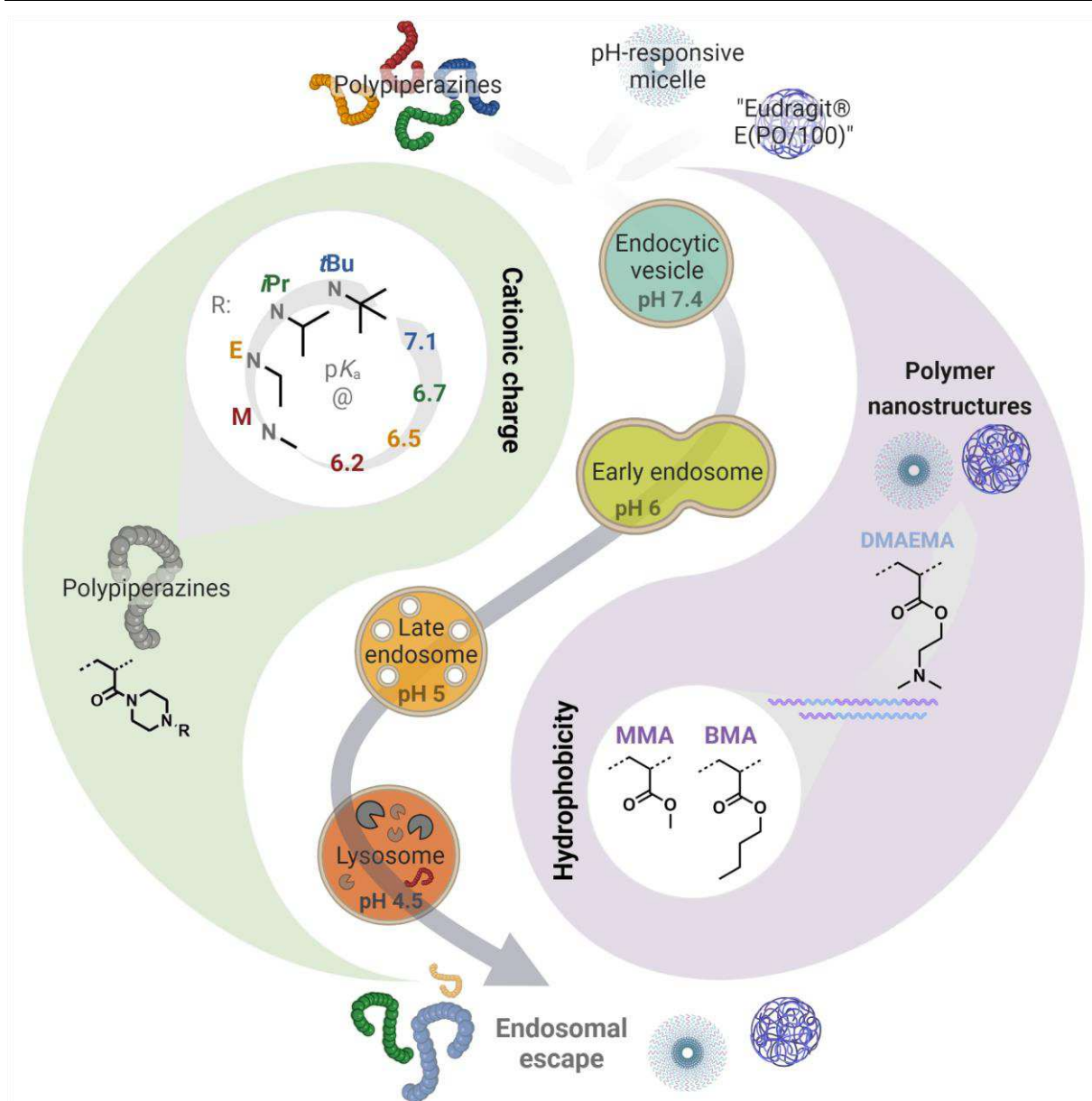
Figure 6.6. Transfection efficiency and toxicity of polyacrylates in HEK 293T cells. a Metabolic activity of HEK 293T cells was measured using the alamarBlue™ assay following incubation with indicated polymers at equal amine concentrations (\triangleq N*/P 30) for 4 h. Values represent mean \pm SD (n

= 3). **b** Cells were incubated with polyplexes of pEGFP-N1 pDNA and polymers at N*/P 30. EGFP expression of viable cells was analyzed *via* flow cytometry. Two different transfection protocols were applied; either 24 h in growth medium (DMEM + 10% FCS + 10 mM HEPES) or 4 h in serum-reduced Opti-MEM® followed by medium change to growth medium and further incubation for 20 h. Values represent mean \pm SD ($n \geq 3$). o: no significant difference ($p > 0.05$) to l-PEI in growth medium, oo: no significant difference ($p > 0.05$) to l-PEI in Opti-MEM®, ***: significant difference ($p < 0.001$) to same polymer in growth medium.

7. Summary

The efficient and safe delivery of complex biological agents offers great potential for the challenges of our time. Polymers offer considerable advantages in this regard, not only because of their low risk for immunogenic reactions, their comparatively inexpensive large-scale production and their long shelf life. In particular, their chemical versatility enables manifold options for a goal-oriented design according to the structure-activity principle. An understanding of fundamental relationships between the physicochemical properties of polymers and their biological effects is however essential in this regard.

The biological properties of organisms, organs, tissues and cells determine the design of safe and efficient delivery systems and should be considered as inspiration for new attempts to create effective materials. In addition to the balance between hydrophobicity and hydrophilicity, the degree of charge of a nanocarrier is also critical for efficient delivery and overcoming the endosome. Cationic charges do not only enhance cellular uptake but can also mediate a crossing of the endosomal barrier due to membrane interactions. The introduction of hydrophobic or even lipophilic components can further significantly increase membrane interactions. Besides the interaction with the cell membrane, it is important to consider that both the degree of charge and the hydrophobic-hydrophilic balance also affect the packaging and protection of sensitive biological cargo such as genetic material. However, cationic charges and hydrophobic components introduce some disadvantages, as electrostatic and hydrophobic interactions may disrupt the integrity of other cellular membranes, triggering toxic effects. Fine adjustment of the degree of charge and the hydrophobic-hydrophilic balance offer the possibility of balancing the requirements for a safe, yet efficient delivery process. In the present dissertation, various polymer systems with adjustable charge density and hydrophobic-hydrophilic balance were investigated with respect to their delivery efficiencies. A particular focus was set on the key step in delivery, the endosomal release (Scheme 7.1).



Scheme 7.1. Overview of the relevant factors of polymer design. The overview illustrates the relevant factors cationic charge and hydrophobic-hydrophilic balance, which were investigated in this dissertation with the aim of efficient delivery of sensitive biopharmaceuticals.

Fine-tuning, in particular the influence of cationic charge density on release efficiency, has been underrepresented and poorly understood in the literature, as in most reports to date it has been accompanied by a concomitant drastic change in the hydrophobicity of the releasing polymers. The class of polypiperazines, not previously used in biomedicine, opened a new opportunity to study this aspect individually. Already during the basic biological characterization (cytotoxicity, hemocompatibility), the relevance of a fine-tuning of charge densities became apparent. The endosomal release capacity was demonstrated to be primarily determined by the basicity or degree of charge of the polymers, although molar mass, polymer

concentrations and incubation times also had an influence. The pK_a range around 6.7 was identified as the most efficient in this work. The application of the hydrophilic, adjustable polypiperazines was essential for obtaining these findings. Our results are in good agreement with research on ionizable lipids, where a significant increase in delivery efficiency was found at a pK_a value of 6.8, while pK_a values of 6.8-7 were described as most effective.^[96-99] Interestingly, cell culture media composition also had a significant effect on the central properties of the polymers. The calcein release assay was crucial to the assessment of endosomal release efficiencies, in which the release of the non-membranepерmeable dye from the endosome by the release polymers was quantified using CLSM and flow cytometry. In addition to the small molecule, the release of more complex macromolecules such as dextrans (70 kDa) and BSA could further be achieved. In this regard, even sensitive proteins such as RNase A or EGFP were successfully and functionally delivered to the cytosol.

Despite their moderate charge density, the polypiperazines were able to bind genetic material and efficiently transfect cells *in vitro*, which unexpectedly renders them an interesting class of materials for use in gene delivery. The mode of binding and the density of packing of the genetic material differed significantly from highly charged cationic polymers such as commercial l-PEI 25 kDa. PNAiPP appeared to transport genetic material into the nucleus, a critical hurdle in pDNA transfection, but nevertheless showed little or no evidence of toxicity. In contrast to common cationic transfection agents and polymers such as l-PEI, almost no pDNA release was observed in polyplexes based on PNAiPP and PNAiBP when treated with the competitive polyanion heparin. However, successful amplification (qPCR) of pDNA bound in a polyplex with the polypiperazines suggested that release is not necessary for efficient transcription in these cases and that the underlying mechanism must be different from that of other commonly used cationic polymers, where release is essential for efficient transcription.^[134-135] As mentioned previously, condensation of pDNA by the polypiperazines differs markedly from previously described polyplexes, *e.g.*, l-PEI. We assume that the comparatively loose binding of the polypiperazines allows unhindered transcription of the pDNA, even when complexed by the polymers.

Besides the tuning of charge density on the polypiperazine homopolymers, more complex polymer systems for overcoming the endosomal barrier were evaluated in this thesis. These materials were designed keeping different critical aspects for safe and efficient delivery in mind. On one hand, pH-responsive micelles were assembled from block copolymers of hydrophilic

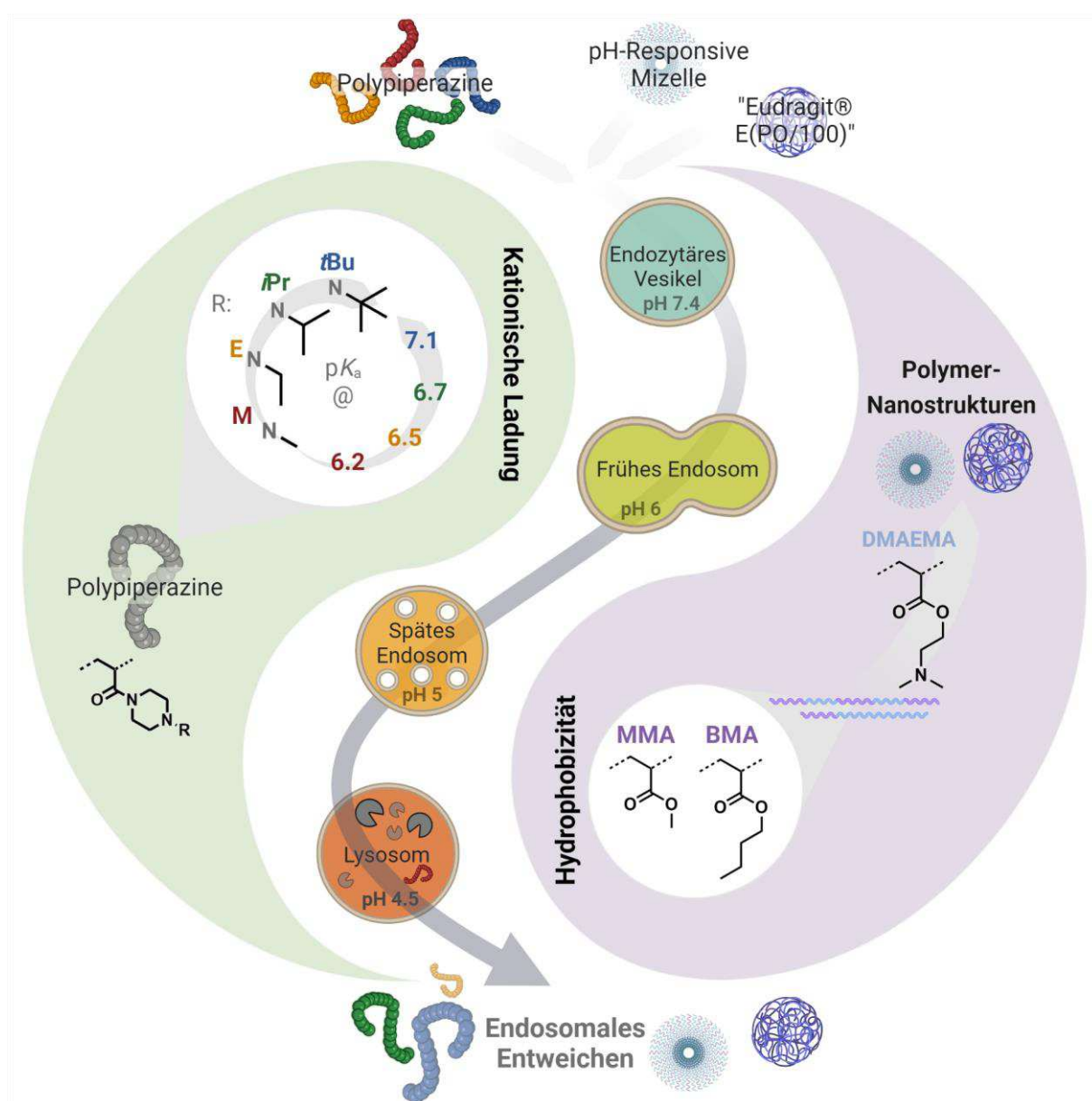
DMAEMA and hydrophobic *n*-BMA. This polymer assembly and the associated higher local concentration of cationic charge aided the overcoming of the endosomal entrapment in difficult-to-transfect leukemia suspension cells. The superior endosomal release capacity compared to l-PEI 25 kDa was identified as a crucial mechanism. In another alternative system, hydrophobic moieties MMA and *n*-BMA were statistically incorporated into a copolymer based on the pH-sensitive DMAEMA. In combination with a novel "green" formulation approach for genetic material, these polymers achieved transfection efficiencies that exceeded commercial l-PEI 25 kDa. The formulation approach was based on the pH-responsiveness of the solubility behavior of the copolymer, and the copolymer exhibited some similarities to polypiperazines in terms of its pH-dependent mode of binding the genetic material. Finally, a pH-independent polyacrylamide with guanidinium moieties was presented that could transfect more efficiently than l-PEI 25 kDa while being less toxic. Again, the significantly higher endosomal release capacity was identified as the cause. Since the polymer is not further protonated in endosomes, the current escape theories appeared unsuitable. Therefore, the interaction with BMP, a lipid specific for endosomal vesicles, was investigated. Our studies suggested that the interactions between amines and lipids may be of greater importance than previously thought. However, the significantly higher toxicity of the promising homopolymer compared to polypiperazines might be related to the pH-independent permanent charge and the resulting damage to membranes and organelles at a physiological pH of 7.4.

The study of the different polymer systems revealed that cationic charges, pH responsiveness and a fine-tuned hydrophilicity-hydrophobicity balance have a favorable effect on the transfer of biologically active compounds. Cationic charges are essential for binding and thus protection of sensitive genetic material, although even low charge densities might be sufficient for complexation. Endosomal release is clearly promoted by increased cationic charges, but a fine balance has to be maintained not to induce exceeding toxic effects. An intelligent design of pH-dependent materials may therefore be a key for endosomal release while maintaining the integrity of the plasma membrane at physiological pH. Although hydrophobic interactions with the membrane may be beneficial, they must be fine-tuned due to their strong toxic potential, and not to impede complexation of genetic material in sufficient concentrations. The fundamental aspects evaluated in this thesis hopefully provide a better understanding of the interplay of cationic charges, pH responsiveness, and hydrophobic properties, as well as polymer assembly capabilities and set the basis for the development of novel, non-toxic polymer designs that enable efficient delivery.

8. Zusammenfassung

Die effiziente und sichere Verabreichung komplexer biologischer Wirkstoffe bietet ein großes Potenzial für die Herausforderungen unserer Zeit. Polymere bieten hier erhebliche Vorteile, nicht nur wegen ihres geringen Risikos für immunogene Reaktionen, ihrer vergleichsweise kostengünstigen großtechnischen Herstellung und ihrer langen Lagerfähigkeit. Insbesondere ihre chemische Vielseitigkeit ermöglicht vielfältige Möglichkeiten für ein zielgerichtetes Design nach dem Struktur-Wirkungs-Prinzip. Ein Verständnis der grundlegenden Zusammenhänge zwischen den physikochemischen Eigenschaften von Polymeren und ihren biologischen Wirkungen ist dabei jedoch unerlässlich.

Die biologischen Eigenschaften von Organismen, Organen, Geweben und Zellen sind ausschlaggebend für die Gestaltung sicherer und effizienter Liefersysteme und sollten als Inspiration für neue Ansätze zur Schaffung wirksamer Materialien dienen. Neben dem Gleichgewicht zwischen Hydrophobie und Hydrophilie ist auch der Ladungsgrad eines Nanoträgers entscheidend für eine effiziente Lieferung und die Überwindung des Endosoms. Kationische Ladungen verbessern nicht nur die zelluläre Aufnahme, sondern können aufgrund von Membraninteraktionen auch die Überwindung der endosomalen Barriere bewirken. Die Einführung von hydrophoben oder sogar lipophilen Komponenten kann die Membranwechselwirkungen noch erheblich verstärken. Neben der Wechselwirkung mit der Zellmembran ist es wichtig zu bedenken, dass sowohl der Ladungsgrad als auch das hydrophob-hydrophile Gleichgewicht die Verpackung und den Schutz empfindlicher biologischer Fracht, wie z. B. genetischen Materials, ebenfalls beeinflussen. Kationische Ladungen und hydrophobe Komponenten bringen jedoch einige Nachteile mit sich, da elektrostatische und hydrophobe Wechselwirkungen die Integrität anderer Zellmembranen stören und toxische Wirkungen auslösen können. Die Feineinstellung des Ladungsgrads und des hydrophob-hydrophilen Gleichgewichts bietet die Möglichkeit, die Anforderungen an einen sicheren und gleichzeitig effizienten Lieferprozess auszugleichen. In der vorliegenden Dissertation wurden verschiedene Polymersysteme mit einstellbarer Ladungsdichte und hydrophob-hydrophilem Gleichgewicht auf ihre Effizienz bei der Wirkstoffabgabe hin untersucht. Ein besonderer Schwerpunkt lag dabei auf dem Schlüsselschritt der Freisetzung, der endosomalen Freisetzung (Schema 7.1).



Schema 7.1. Überblick über die relevanten Faktoren des Polymerdesigns. Die Übersicht zeigt die relevanten Faktoren kationische Ladung und hydrophob-hydrophiles Gleichgewicht, die in dieser Dissertation mit dem Ziel der effizienten Lieferung von empfindlichen Biopharmazeutika untersucht wurden.

Die Feinabstimmung, insbesondere der Einfluss der kationischen Ladungsdichte auf die Freisetzungseffizienz, ist in der Literatur unterrepräsentiert und schlecht verstanden, da sie in den meisten bisherigen Berichten mit einer gleichzeitigen drastischen Veränderung der Hydrophobizität der freisetzenden Polymere einhergeht. Die Klasse der Polypiperazine, die bisher in der Biomedizin nicht verwendet wurde, eröffnete eine neue Möglichkeit, diesen Aspekt individuell zu untersuchen. Bereits bei der grundlegenden biologischen Charakterisierung (Zytotoxizität, Hämokompatibilität) wurde die Bedeutung einer genauen Einstellung der Ladungsdichten deutlich. Es zeigte sich, dass die endosomale

Freisetzungskapazität in erster Linie durch die Basizität bzw. den Ladungsgrad der Polymere bestimmt wird, obwohl auch die molare Masse, die Polymerkonzentrationen und die Inkubationszeiten einen Einfluss haben. Der pK_a -Bereich um 6,7 wurde in dieser Arbeit als der effizienteste identifiziert. Die Verwendung der hydrophilen, einstellbaren Polypiperazine war für die Gewinnung dieser Erkenntnisse entscheidend. Unsere Ergebnisse stimmen gut mit Forschungsergebnissen über ionisierbare Lipide überein, bei denen ein signifikanter Anstieg der Freisetzungseffizienz bei einem pK_a -Wert von 6,8 festgestellt wurde, während pK_a -Werte von 6,8-7 als am effektivsten beschrieben wurden.^[96-99] Interessanterweise hatte auch die Zusammensetzung der Zellkulturmedien einen signifikanten Einfluss auf die zentralen Eigenschaften der Polymere. Der Calcein-Freisetzungstest war entscheidend für die Bewertung der endosomalen Freisetzungseffizienz, bei der die Freisetzung des nicht-membranpermeablen Farbstoffs aus dem Endosom durch die Freisetzungspolymere mittels CLSM und Durchflusszytometrie quantifiziert wurde. Neben dem kleinen Molekül konnte auch die Freisetzung von komplexeren Makromolekülen wie Dextranen (70 kDa) und BSA erreicht werden. Selbst empfindliche Proteine wie RNase A oder EGFP wurden erfolgreich und funktionell an das Zytosol abgegeben.

Trotz ihrer moderaten Ladungsdichte waren die Polypiperazine in der Lage, genetisches Material zu binden und Zellen *in vitro* effizient zu transfizieren, was sie überraschenderweise zu einer interessanten Materialklasse für den Gentransport macht. Die Art der Bindung und die Packungsdichte des genetischen Materials unterschieden sich deutlich von hochgeladenen kationischen Polymeren wie dem kommerziellen l-PEI 25 kDa. PNAiPP schien genetisches Material in den Zellkern zu transportieren, eine kritische Hürde bei der pDNA-Transfektion, zeigte aber dennoch wenig oder keine Hinweise auf Toxizität. Im Gegensatz zu gängigen kationischen Transfektionsmitteln und Polymeren wie l-PEI wurde in Polyplexen auf der Basis von PNAiPP und PNAiBP bei Behandlung mit dem kompetitiven Polyanion Heparin fast keine pDNA-Freisetzung beobachtet. Die erfolgreiche Amplifikation (qPCR) von pDNA, die in einem Polyplex mit den Polypiperazinen gebunden war, deutete jedoch darauf hin, dass die Freisetzung in diesen Fällen für eine effiziente Transkription nicht notwendig ist und dass der zugrunde liegende Mechanismus ein anderer sein muss als bei anderen üblicherweise verwendeten kationischen Polymeren, bei denen die Freisetzung für eine effiziente Transkription unerlässlich ist.^[134-135] Wie bereits erwähnt, unterscheidet sich die Kondensation von pDNA durch die Polypiperazine deutlich von zuvor beschriebenen Polyplexen, z. B. l-PEI. Wir gehen davon aus, dass die vergleichsweise lockere Bindung der Polypiperazine eine

ungehinderte Transkription der pDNA ermöglicht, auch wenn diese durch die Polymere komplexiert ist.

Neben der Einstellung der Ladungsdichte an den Polypiperazin-Homopolymeren wurden in dieser Arbeit auch komplexere Polymersysteme zur Überwindung der endosomalen Barriere untersucht. Diese Materialien wurden unter Berücksichtigung verschiedener kritischer Aspekte für eine sichere und effiziente Lieferung entwickelt. Einerseits wurden pH-empfindliche Mizellen aus Blockcopolymeren von hydrophilem DMAEMA und hydrophobem *n*-BMA aufgebaut. Dieser Polymeraufbau und die damit verbundene höhere lokale Konzentration der kationischen Ladung halfen bei der Überwindung des endosomalen Einschlusses in schwer zu transfizierenden Leukämie-Suspensionszellen. Die überlegene endosomale Freisetzungskapazität im Vergleich zu l-PEI 25 kDa wurde als ein entscheidender Mechanismus identifiziert. In einem anderen alternativen System wurden hydrophobe Einheiten MMA und *n*-BMA statistisch in ein Copolymer auf der Basis des pH-sensitiven DMAEMA eingebaut. In Kombination mit einem neuartigen "grünen" Formulierungsansatz für genetisches Material erreichten diese Polymere Transfektionseffizienzen, die die von kommerziellem l-PEI 25 kDa übertrafen. Der Formulierungsansatz basierte auf der pH-Empfindlichkeit des Löslichkeitsverhaltens des Copolymers, und das Copolymer zeigte einige Ähnlichkeiten mit den Polypiperazinen in Bezug auf seine pH-abhängige Art der Bindung des genetischen Materials. Schließlich wurde ein pH-unabhängiges Polyacrylamid mit Guanidinium-Anteilen vorgestellt, das effizienter transfizieren konnte als l-PEI 25 kDa und gleichzeitig weniger toxisch war. Auch hier wurde die deutlich höhere endosomale Freisetzungskapazität als Ursache ausgemacht. Da das Polymer in Endosomen nicht weiter protoniert wird, erschienen die gängigen Escape-Theorien ungeeignet. Daher wurde die Wechselwirkung mit BMP, einem für endosomale Vesikel spezifischen Lipid, untersucht. Unsere Untersuchungen legten nahe, dass die Wechselwirkungen zwischen Aminen und Lipiden von größerer Bedeutung sein könnten als bisher angenommen. Die deutlich höhere Toxizität des vielversprechenden Homopolymers im Vergleich zu Polypiperazinen könnte jedoch mit der pH-unabhängigen permanenten Ladung und der daraus resultierenden Schädigung von Membranen und Organellen bei einem physiologischen pH-Wert von 7,4 zusammenhängen.

Die Untersuchung der verschiedenen Polymersysteme ergab, dass sich kationische Ladungen, pH-Responsivität und ein fein abgestimmtes Hydrophilie-Hydrophobie-Gleichgewicht günstig

auf den Transfer biologisch aktiver Verbindungen auswirken. Kationische Ladungen sind für die Bindung und damit für den Schutz von empfindlichem genetischem Material unerlässlich, obwohl auch geringe Ladungsdichten für die Komplexierung ausreichen können. Die endosomale Freisetzung wird durch erhöhte kationische Ladungen eindeutig gefördert, doch muss ein feines Gleichgewicht gewahrt werden, um keine übermäßigen toxischen Wirkungen hervorzurufen. Ein intelligentes Design von pH-abhängigen Materialien könnte daher ein Schlüssel für die endosomale Freisetzung sein, wobei die Integrität der Plasmamembran bei physiologischem pH-Wert erhalten bleibt. Obwohl hydrophobe Wechselwirkungen mit der Membran vorteilhaft sein können, müssen sie aufgrund ihres starken toxischen Potenzials fein abgestimmt werden, um die Komplexierung von genetischem Material in ausreichenden Konzentrationen nicht zu behindern. Die in dieser Arbeit untersuchten grundlegenden Aspekte werden hoffentlich zu einem besseren Verständnis des Zusammenspiels von kationischen Ladungen, pH-Responsivität und hydrophoben Eigenschaften sowie der Möglichkeiten der Polymerassemblierung führen und die Grundlage für die Entwicklung neuartiger, nicht-toxischer Polymerkonzepte bilden, die eine effiziente Lieferung ermöglichen.

8. References

- [1] D. W. Pack, A. S. Hoffman, S. Pun, P. S. Stayton, *Nat. Rev. Drug Discov.* **2005**, *4*, 581-593.
- [2] J. W. Schott, M. Morgan, M. Galla, A. Schambach, *Mol. Ther.* **2016**, *24*, 1513-1527.
- [3] M. J. Mitchell, M. M. Billingsley, R. M. Haley, M. E. Wechsler, N. A. Peppas, R. Langer, *Nat. Rev. Drug Discov.* **2021**, *20*, 101-124.
- [4] V. Sanna, M. Sechi, *ACS Med. Chem. Lett.* **2020**, *11*, 1069-1073.
- [5] P. Foroozandeh, A. A. Aziz, *Nanoscale Res. Lett.* **2018**, *13*, 339.
- [6] F. Hullin-Matsuda, T. Taguchi, P. Greimel, T. Kobayashi, *Semin. Cell Dev. Biol.* **2014**, *31*, 48-56.
- [7] S. Pfeffer, *Nat. Cell Biol.* **2005**, *7*, 856-857.
- [8] L. M. P. Vermeulen, T. Brans, S. K. Samal, P. Dubruel, J. Demeester, S. C. De Smedt, K. Remaut, K. Braeckmans, *ACS Nano* **2018**, *12*, 2332-2345.
- [9] M. E. G. de Araujo, G. Liebscher, M. W. Hess, L. A. Huber, *Traffic* **2020**, *21*, 60-75.
- [10] A. El-Sayed, H. Harashima, *Mol. Ther.* **2013**, *21*, 1118-1130.
- [11] H. D. Gallala, B. Breiden, K. Sandhoff, *J. Neurochem.* **2011**, *116*, 702-707.
- [12] J. Gruenberg, *Traffic* **2020**, *21*, 76-93.
- [13] T. Kobayashi, M. H. Beuchat, J. Chevallier, A. Makino, N. Mayran, J. M. Escola, C. Lebrand, P. Cosson, T. Kobayashi, J. Gruenberg, *J. Biol. Chem.* **2002**, *277*, 32157-32164.
- [14] H. Schulze, K. Sandhoff, *Cold Spring Harb. Perspect. Biol.* **2011**, *3*, No. a004804.
- [15] M. P. Stewart, A. Lorenz, J. Dahlman, G. Sahay, *Wiley Interdiscip. Rev. Nanomed. Nanobiotechnol.* **2016**, *8*, 465-478.
- [16] A. Ahmad, J. M. Khan, S. Haque, *Biochimie* **2019**, *160*, 61-75.
- [17] S. A. Smith, L. I. Selby, A. P. R. Johnston, G. K. Such, *Bioconjugate Chem.* **2019**, *30*, 263-272.
- [18] S. Vaidyanathan, B. G. Orr, M. M. Banaszak Holl, *Acc. Chem. Res.* **2016**, *49*, 1486-1493.
- [19] T. Bus, A. Traeger, U. S. Schubert, *J. Mater. Chem. B* **2018**, *6*, 6904-6918.
- [20] Y. Wang, M. Ye, R. Xie, S. Gong, *Bioconjugate Chem.* **2019**, *30*, 325-337.
- [21] H. Lv, S. Zhang, B. Wang, S. Cui, J. Yan, *J. Control. Release* **2006**, *114*, 100-109.
- [22] A. Kargaard, J. P. G. Sluijter, B. Klumperman, *J. Control. Release* **2019**, *316*, 263-291.
- [23] S. Behzadi, V. Serpooshan, W. Tao, M. A. Hamaly, M. Y. Alkawareek, E. C. Dreaden, D. Brown, A. M. Alkilany, O. C. Farokhzad, M. Mahmoudi, *Chem. Soc. Rev.* **2017**, *46*, 4218-4244.
- [24] I. M. S. Degors, C. Wang, Z. U. Rehman, I. S. Zuhorn, *Acc. Chem. Res.* **2019**, *52*, 1750-1760.
- [25] A. P. Lam, D. A. Dean, *Gene Ther.* **2010**, *17*, 439-447.
- [26] X. Sun, N. Zhang, *Mini-Rev. Med. Chem.* **2010**, *10*, 108-125.
- [27] A. C. Rinkenauer, S. Schubert, A. Traeger, U. S. Schubert, *J. Mater. Chem. B* **2015**, *3*, 7477-7493.
- [28] A. Aied, U. Greiser, A. Pandit, W. Wang, *Drug Discov. Today* **2013**, *18*, 1090-1098.
- [29] J. Cai, Y. Yue, D. Rui, Y. Zhang, S. Liu, C. Wu, *Macromolecules* **2011**, *44*, 2050-2057.
- [30] M. Wagner, A. C. Rinkenauer, A. Schallon, U. S. Schubert, *RSC Adv.* **2013**, *3*, 12774-12785.
- [31] C. V. Synatschke, A. Schallon, V. Jérôme, R. Freitag, A. H. Müller, *Biomacromolecules* **2011**, *12*, 4247-4255.
- [32] F. Richter, K. Leer, L. Martin, P. Mapfumo, J. I. Solomun, M. T. Kuchenbrod, S. Hoepfner, J. C. Brendel, A. Traeger, *J. Nanobiotechnol.* **2021**, *19*, 292.
- [33] D. Sprouse, T. Reineke, *Biomacromolecules* **2014**, *15*, 2616-2628.
- [34] H. Li, M. A. Cortez, H. R. Phillips, Y. Wu, T. M. Reineke, *ACS Macro Lett.* **2013**, *2*, 230-235.
- [35] A. K. Trützschler, T. Bus, M. Reifarh, J. C. Brendel, S. Hoepfner, A. Traeger, U. S. Schubert, *Bioconjugate Chem.* **2018**, *29*, 2181-2194.
- [36] S. T. Hemp, M. H. Allen, M. D. Green, T. E. Long, *Biomacromolecules* **2012**, *13*, 231-238.
- [37] V. Loczenski Rose, F. Mastrotto, G. Mantovani, *Polym. Chem.* **2017**, *8*, 353-360.
- [38] D. Zhu, H. Yan, X. Liu, J. Xiang, Z. Zhou, J. Tang, X. Liu, Y. Shen, *Adv. Funct. Mater.* **2017**, *27*, 1606826.
- [39] D. F. Wallach, T. L. Steck, *Anal. Biochem.* **1963**, *6*, 176-180.
- [40] R. A. Jones, C. Y. Cheung, F. E. Black, J. K. Zia, P. S. Stayton, A. S. Hoffman, M. R. Wilson, *Biochem. J.* **2003**, *372*, 65-75.
- [41] R. A. Jones, M. H. Poniris, M. R. Wilson, *J. Control. Release* **2004**, *96*, 379-391.

- [42] G. Rong, C. Wang, L. Chen, Y. Yan, Y. Cheng, *Sci. Adv.* **2020**, *6*, eaaz1774.
- [43] S. Deshpande, S. Patil, N. Singh, *ACS Omega* **2018**, *3*, 8042-8049.
- [44] D. K. Bonner, X. Zhao, H. Buss, R. Langer, P. T. Hammond, *J. Control. Release* **2013**, *167*, 101-107.
- [45] Y. Hu, T. Litwin, A. R. Nagaraja, B. Kwong, J. Katz, N. Watson, D. J. Irvine, *Nano Lett.* **2007**, *7*, 3056-3064.
- [46] K. K. Tran, X. Zhan, H. Shen, *Adv. Healthc. Mater.* **2014**, *3*, 690-702.
- [47] X. Zhan, K. K. Tran, L. Wang, H. Shen, *Pharm. Res.* **2015**, *32*, 2280-2291.
- [48] X. Su, J. Fricke, D. G. Kavanagh, D. J. Irvine, *Mol. Pharm.* **2011**, *8*, 774-787.
- [49] S. Wannasarit, S. Q. Wang, P. Figueiredo, C. Trujillo, F. Eburnea, L. Simon-Gracia, A. Correia, Y. P. Ding, T. Teesalu, D. F. Liu, R. Wiwattanapatapee, H. A. Santos, W. Li, *Adv. Funct. Mater.* **2019**, *29*, 1905352.
- [50] J. Chen, J. Li, J. Zhou, Z. Lin, F. Cavalieri, E. Czuba-Wojnilowicz, Y. Hu, A. Glab, Y. Ju, J. J. Richardson, F. Caruso, *ACS Nano* **2019**, *13*, 11653-11664.
- [51] F. Salomone, F. Cardarelli, M. Di Luca, C. Boccardi, R. Nifosi, G. Bardi, L. Di Bari, M. Serresi, F. Beltram, *J. Control. Release* **2012**, *163*, 293-303.
- [52] J. R. Clegg, J. A. Sun, J. Gu, A. K. Venkataraman, N. A. Peppas, *J. Control. Release* **2021**, *329*, 1162-1171.
- [53] J. S. Kim, D. K. Choi, J. Y. Shin, S. M. Shin, S. W. Park, H. S. Cho, Y. S. Kim, *J. Control. Release* **2016**, *235*, 165-175.
- [54] D. Adams, A. Gonzalez-Duarte, W. D. O'Riordan, C. C. Yang, M. Ueda, A. V. Kristen, I. Tournev, H. H. Schmidt, T. Coelho, J. L. Berk, K. P. Lin, G. Vita, S. Attarian, V. Plante-Bordeneuve, M. M. Mezei, J. M. Campistol, J. Buades, T. H. Brannagan, 3rd, B. J. Kim, J. Oh, Y. Parman, Y. Sekijima, P. N. Hawkins, S. D. Solomon, M. Polydefkis, P. J. Dyck, P. J. Gandhi, S. Goyal, J. Chen, A. L. Strahs, S. V. Nochur, M. T. Sweetser, P. P. Garg, A. K. Vaishnav, J. A. Gollob, O. B. Suhr, *N. Engl. J. Med.* **2018**, *379*, 11-21.
- [55] B. Illes, P. Hirschle, S. Barnert, V. Cauda, S. Wuttke, H. Engelke, *Chem. Mater.* **2017**, *29*, 8042-8046.
- [56] S. Niedermayer, V. Weiss, A. Herrmann, A. Schmidt, S. Datz, K. Müller, E. Wagner, T. Bein, C. Bräuchle, *Nanoscale* **2015**, *7*, 7953-7964.
- [57] F. Hausig, F. H. Sobotta, F. Richter, D. O. Harz, A. Traeger, J. C. Brendel, *ACS Appl. Mater. Interfaces* **2021**, *13*, 35233-35247.
- [58] N. Brkovic, L. Zhang, J. N. Peters, S. Kleine-Doepke, W. J. Parak, D. Zhu, *Small* **2020**, *16*, e2003639.
- [59] J. Connor, L. Huang, *J. Cell Biol.* **1985**, *101*, 582-589.
- [60] D. K. Bonner, C. Leung, J. Chen-Liang, L. Chingozha, R. Langer, P. T. Hammond, *Bioconjugate Chem.* **2011**, *22*, 1519-1525.
- [61] A. S. Wong, S. K. Mann, E. Czuba, A. Sahut, H. Liu, T. C. Suekama, T. Bickerton, A. P. Johnston, G. K. Such, *Soft Matter* **2015**, *11*, 2993-3002.
- [62] N. Kongkatigumjorn, C. Cortez-Jugo, E. Czuba, A. S. Wong, R. Y. Hodgetts, A. P. Johnston, G. K. Such, *Macromol. Biosci.* **2017**, *17*.
- [63] N. Kongkatigumjorn, S. A. Smith, M. Chen, K. Fang, S. Yang, E. R. Gillies, A. P. R. Johnston, G. K. Such, *ACS Appl. Nano Mater.* **2018**, *1*, 3164-3173.
- [64] U. Lächelt, P. Kos, F. M. Mickler, A. Herrmann, E. E. Salcher, W. Rödl, N. Badgajar, C. Bräuchle, E. Wagner, *Nanomedicine* **2014**, *10*, 35-44.
- [65] E. Ducat, J. Deprez, A. Gillet, A. Noël, B. Evrard, O. Peulen, G. Piel, *Int. J. Pharm.* **2011**, *420*, 319-332.
- [66] V. A. Slepishkin, S. Simões, P. Dazin, M. S. Newman, L. S. Guo, M. C. Pedroso de Lima, N. Düzgüneş, *J. Biol. Chem.* **1997**, *272*, 2382-2388.
- [67] S. Simões, V. Slepishkin, N. Düzgüneş, M. C. Pedroso de Lima, *Biochim. Biophys. Acta* **2001**, *1515*, 23-37.
- [68] H. Xu, W. Zhang, Y. Li, F. F. Ye, P. P. Yin, X. Yu, M. N. Hu, Y. S. Fu, C. Wang, J. Shang de, *Pharm. Res.* **2014**, *31*, 3038-3050.
- [69] Z. Li, B. li, M. Wang, M. Xie, H. Shen, S. Shen, X. Wang, X. Guo, M. Yao, Y. Jin, *J. Mater. Chem. B* **2013**, *1*, 1466-1474.

References

- [70] F. Richter, L. Martin, K. Leer, E. Moek, F. Hausig, J. C. Brendel, A. Traeger, *J. Mater. Chem. B* **2020**, 8, 5026-5041.
- [71] F. Richter, P. Mapfumo, L. Martin, J. I. Solomun, F. Hausig, J. J. Frietsch, T. Ernst, S. Hoepfener, J. C. Brendel, A. Traeger, *J. Nanobiotechnol.* **2021**, 19, 70.
- [72] M. Ogris, R. C. Carlisle, T. Bettinger, L. W. Seymour, *J. Biol. Chem.* **2001**, 276, 47550-47555.
- [73] Z. u. Rehman, D. Hoekstra, I. S. Zuhorn, *ACS Nano* **2013**, 7, 3767-3777.
- [74] L. Du, C. Wang, L. Meng, Q. Cheng, J. Zhou, X. Wang, D. Zhao, J. Zhang, L. Deng, Z. Liang, A. Dong, H. Cao, *Biomaterials* **2018**, 176, 84-93.
- [75] G. Kocak, C. Tuncer, V. Bütün, *Polym. Chem.* **2017**, 8, 144-176.
- [76] T. Thavanesan, C. Herbert, F. A. Plamper, *Langmuir* **2014**, 30, 5609-5619.
- [77] D. Velasco, G. Réthoré, B. Newland, J. Parra, C. Elvira, A. Pandit, L. Rojo, J. San Román, *Eur. J. Pharm. Biopharm.* **2012**, 82, 465-474.
- [78] N. P. Truong, W. Gu, I. Prasad, Z. Jia, R. Crawford, Y. Xiao, M. J. Monteiro, *Nat. Commun.* **2013**, 4, 1902.
- [79] E. Gallon, T. Matini, L. Sasso, G. Mantovani, A. Armiñan de Benito, J. Sanchis, P. Caliceti, C. Alexander, M. J. Vicent, S. Salmaso, *Biomacromolecules* **2015**, 16, 1924-1937.
- [80] N. Kanayama, S. Fukushima, N. Nishiyama, K. Itaka, W.-D. Jang, K. Miyata, Y. Yamasaki, U.-i. Chung, K. Kataoka, *ChemMedChem* **2006**, 1, 439-444.
- [81] A. M. Funhoff, C. F. van Nostrum, G. A. Koning, N. M. Schuurmans-Nieuwenbroek, D. J. Crommelin, W. E. Hennink, *Biomacromolecules* **2004**, 5, 32-39.
- [82] L. I. Selby, C. M. Cortez-Jugo, G. K. Such, A. P. R. Johnston, *Wiley Interdiscip. Rev. Nanomed. Nanobiotechnol.* **2017**, 9, e1452.
- [83] L. H. Gan, Y. Y. Gan, G. R. Deen, *Macromolecules* **2000**, 33, 7893-7897.
- [84] G. Roshan Deen, L. H. Gan, *J. Appl. Polym. Sci.* **2008**, 107, 1449-1458.
- [85] F. H. Sobotta, F. Hausig, D. O. Harz, S. Hoepfener, U. S. Schubert, J. C. Brendel, *Polym. Chem.* **2018**, 9, 1593-1602.
- [86] F. R. Maxfield, D. J. Yamashiro, *Adv. Exp. Med. Biol.* **1987**, 225, 189-198.
- [87] J. Huotari, A. Helenius, *Embo J.* **2011**, 30, 3481-3500.
- [88] D. Fischer, Y. Li, B. Ahlemeyer, J. Krieglstein, T. Kissel, *Biomaterials* **2003**, 24, 1121-1131.
- [89] T. F. Martens, K. Remaut, J. Demeester, S. C. De Smedt, K. Braeckmans, *Nano Today* **2014**, 9, 344-364.
- [90] K. Kunath, A. von Harpe, D. Fischer, H. Petersen, U. Bickel, K. Voigt, T. Kissel, *J. Control. Release* **2003**, 89, 113-125.
- [91] C.-H. Ahn, S. Y. Chae, Y. H. Bae, S. W. Kim, *J. Control. Release* **2002**, 80, 273-282.
- [92] M. Breunig, U. Lungwitz, R. Liebl, A. Goepferich, *Proc. Natl. Acad. Sci. U S A* **2007**, 104, 14454-14459.
- [93] J. L. N. Dubois, N. Lavignac, *J. Mater. Chem. B* **2015**, 3, 6501-6508.
- [94] G. H. Patterson, S. M. Knobel, W. D. Sharif, S. R. Kain, D. W. Piston, *Biophys. J.* **1997**, 73, 2782-2790.
- [95] P. J. Cranfill, B. R. Sell, M. A. Baird, J. R. Allen, Z. Lavagnino, H. M. de Gruiter, G. J. Kremers, M. W. Davidson, A. Ustione, D. W. Piston, *Nat. Methods* **2016**, 13, 557-562.
- [96] S. C. Semple, A. Akinc, J. Chen, A. P. Sandhu, B. L. Mui, C. K. Cho, D. W. Sah, D. Stebbing, E. J. Crosley, E. Yaworski, I. M. Hafez, J. R. Dorkin, J. Qin, K. Lam, K. G. Rajeev, K. F. Wong, L. B. Jeffs, L. Nechev, M. L. Eisenhardt, M. Jayaraman, M. Kazem, M. A. Maier, M. Srinivasulu, M. J. Weinstein, Q. Chen, R. Alvarez, S. A. Barros, S. De, S. K. Klimuk, T. Borland, V. Kosovrasti, W. L. Cantley, Y. K. Tam, M. Manoharan, M. A. Ciufolini, M. A. Tracy, A. de Fougerolles, I. MacLachlan, P. R. Cullis, T. D. Madden, M. J. Hope, *Nat. Biotechnol.* **2010**, 28, 172-176.
- [97] C. A. Alabi, K. T. Love, G. Sahay, H. Yin, K. M. Luly, R. Langer, D. G. Anderson, *Proc. Natl. Acad. Sci. U S A* **2013**, 110, 12881-12886.
- [98] M. Jayaraman, S. M. Ansell, B. L. Mui, Y. K. Tam, J. Chen, X. Du, D. Butler, L. Eltepu, S. Matsuda, J. K. Narayanannair, K. G. Rajeev, I. M. Hafez, A. Akinc, M. A. Maier, M. A. Tracy, P. R. Cullis, T. D. Madden, M. Manoharan, M. J. Hope, *Angew. Chem. Int. Ed.* **2012**, 51, 8529-8533.

References

-
- [99] K. A. Whitehead, J. R. Dorkin, A. J. Vegas, P. H. Chang, O. Veiseh, J. Matthews, O. S. Fenton, Y. Zhang, K. T. Olejnik, V. Yesilyurt, D. Chen, S. Barros, B. Klebanov, T. Novobrantseva, R. Langer, D. G. Anderson, *Nat. Commun.* **2014**, *5*, 4277.
 - [100] A. K. Varkouhi, M. Scholte, G. Storm, H. J. Haisma, *J. Control. Release* **2011**, *151*, 220-228.
 - [101] J.-P. Behr, *Chimia (Aarau)* **1997**, *51*, 34-36.
 - [102] K. Modra, S. Dai, H. Zhang, B. Shi, J. Bi, *Eng. Life Sci.* **2015**, *15*, 489-498.
 - [103] Z. Shen, B. Shi, H. Zhang, J. Bi, S. Dai, *Soft Matter* **2012**, *8*, 1385-1394.
 - [104] S. Vaidyanathan, J. Chen, B. G. Orr, M. M. Banaszak Holl, *Mol. Pharm.* **2016**, *13*, 1967-1978.
 - [105] S. Boeckle, K. von Gersdorff, S. van der Piepen, C. Culmsee, E. Wagner, M. Ogris, *J. Gene Med.* **2004**, *6*, 1102-1111.
 - [106] B. R. Olden, Y. Cheng, J. L. Yu, S. H. Pun, *J. Control. Release* **2018**, *282*, 140-147.
 - [107] O. Gresch, F. B. Engel, D. Nesic, T. T. Tran, H. M. England, E. S. Hickman, I. Körner, L. Gan, S. Chen, S. Castro-Obregon, R. Hammermann, J. Wolf, H. Müller-Hartmann, M. Nix, G. Siebenkotten, G. Kraus, K. Lun, *Methods* **2004**, *33*, 151-163.
 - [108] S. Basiouni, H. Fuhrmann, J. Schumann, *BioTechniques* **2012**, *53*, 1-4.
 - [109] Y. Mai, A. Eisenberg, *Chem. Soc. Rev.* **2012**, *41*, 5969-5985.
 - [110] D. Sprouse, Y. Jiang, J. E. Laaser, T. P. Lodge, T. M. Reineke, *Biomacromolecules* **2016**, *17*, 2849-2859.
 - [111] E. J. Adolph, C. E. Nelson, T. A. Werfel, R. Guo, J. M. Davidson, S. A. Guelcher, C. L. Duvall, *J. Mater. Chem. B* **2014**, *2*, 8154-8164.
 - [112] A. J. Convertine, D. S. W. Benoit, C. L. Duvall, A. S. Hoffman, P. S. Stayton, *J. Control. Release* **2009**, *133*, 221-229.
 - [113] V. Incani, A. Lavasanifar, H. Uludağ, *Soft Matter* **2010**, *6*, 2124-2138.
 - [114] Z. Liu, Z. Zhang, C. Zhou, Y. Jiao, *Prog. Polym. Sci.* **2010**, *35*, 1144-1162.
 - [115] D. H. Wakefield, J. J. Klein, J. A. Wolff, D. B. Rozema, *Bioconjugate Chem.* **2005**, *16*, 1204-1208.
 - [116] C. S. Lengsfeld, T. J. Anchordoquy, *J. Pharm. Sci.* **2002**, *91*, 1581-1589.
 - [117] A. A. Eltoukhy, D. Chen, C. A. Alabi, R. Langer, D. G. Anderson, *Adv. Mater* **2013**, *25*, 1487-1493.
 - [118] A. C. Rinkenauer, A. T. Press, M. Raasch, C. Pietsch, S. Schweizer, S. Schwörer, K. L. Rudolph, A. Mosig, M. Bauer, A. Traeger, U. S. Schubert, *J. Control. Release* **2015**, *216*, 158-168.
 - [119] E. D. Raczyńska, M. K. Cyrański, M. Gutowski, J. Rak, J.-F. Gal, P.-C. Maria, M. Darowska, K. Duczmal, *J. Phys. Org. Chem.* **2003**, *16*, 91-106.
 - [120] C. Bechara, S. Sagan, *FEBS Lett.* **2013**, *587*, 1693-1702.
 - [121] J. K. Allen, D. J. Brock, H. M. Kondow-McConaghy, J. P. Pellois, *Biomolecules* **2018**, *8*.
 - [122] F. Madani, S. Lindberg, U. Langel, S. Futaki, A. Gräslund, *J. Biophys.* **2011**, *2011*, 414729.
 - [123] A. Pantos, I. Tsogas, C. M. Paleos, *Biochim. Biophys. Acta Biomembr.* **2008**, *1778*, 811-823.
 - [124] M. Silhol, M. Tyagi, M. Giacca, B. Lebleu, E. Vivès, *Eur. J. Biochem.* **2002**, *269*, 494-501.
 - [125] S. Futaki, I. Nakase, *Acc. Chem. Res.* **2017**, *50*, 2449-2456.
 - [126] J. D. Ramsey, N. H. Flynn, *Pharmacol. Ther.* **2015**, *154*, 78-86.
 - [127] A. Erazo-Oliveras, K. Najjar, D. Truong, T. Y. Wang, D. J. Brock, A. R. Prater, J. P. Pellois, *Cell Chem. Biol* **2016**, *23*, 598-607.
 - [128] E. Zaitseva, S.-T. Yang, K. Melikov, S. Pourmal, L. V. Chernomordik, *PLoS Pathog.* **2010**, *6*, e1001131.
 - [129] Y. Kim, S. Binauld, M. H. Stenzel, *Biomacromolecules* **2012**, *13*, 3418-3426.
 - [130] N. Schmidt, A. Mishra, G. H. Lai, G. C. Wong, *FEBS Lett.* **2010**, *584*, 1806-1813.
 - [131] M. Ahmed, *Biomater. Sci.* **2017**, *5*, 2188-2211.
 - [132] K. J. Abd Karim, R. H. Utama, H. Lu, M. H. Stenzel, *Polym. Chem.* **2014**, *5*, 6600-6610.
 - [133] C. Cokca, L. Zartner, I. Tabujew, D. Fischer, K. Peneva, *Macromol. Rapid Commun.* **2020**, e1900668.
 - [134] R. N. Cohen, M. A. E. M. van der Aa, N. Macaraeg, A. P. Lee, F. C. Szoka, *J. Control. Release* **2009**, *135*, 166-174.
 - [135] D. J. Glover, D. L. Leyton, G. W. Moseley, D. A. Jans, *J. Gene Med.* **2010**, *12*, 77-85.

List of abbreviations

ABL	Abelson murine leukemia viral oncogene homolog
ACVA	4,4'-azobis(4-cyanovaleric acid)
AML	acute myeloid leukemia
BCR	breakpoint cluster region
BMP	bis(monoacryloylglycerol) phosphate
BSA	bovine serum albumin
CML	chronic myelogenous leukemia
conc	concentration
COS-7 cells	CV-1 in Origin, carrying SV40
CPAETC	(4-cyano pentanoic acid)yl ethyl trithiocarbonate
CPPs	cell-penetrating peptides
DCC	N,N'-dicyclo hexyl carbodiimide
DCM	dichloromethane
DMAEMA	2-(dimethylamino)ethyl methacrylate
DMAP	4-(dimethylamino)pyridine
DoE	design of experiments
DP	degree of polymerization
EE	early endosome
EGFP	enhanced green fluorescent protein
FDA	Food and Drug Administration
FITC	fluorescein isothiocyanate
GFP	green fluorescent protein
HEK	human embryonic kidney
HEMA	hydroxyethyl methacrylate
HEPES	4-(2-hydroxyethyl)-1-piperazineethanesulfonic acid
IC ₅₀	half maximal inhibitory concentration
ILEV	intra late endosomal vesicles
L	lysosome
LAMA	lipoic acid-methacrylate
LAMA-mic	P(DMAEMA ₁₀₁ - <i>b</i> -[nBMA ₁₂₄ - <i>co</i> -LAMA ₂₂])
LE	late endosome
macroCTA	macro chain transfer agent

List of abbreviations

mRNA	messenger RNA
N*	protonatable amines
N*/P ratio	ratio of protonatable amines to phosphates
<i>n</i> BMA	<i>n</i> -butyl methacrylate
P	phosphates
PBMD	poly((<i>n</i> -butyl methacrylate)- <i>co</i> -(methyl methacrylate)- <i>co</i> -(2-(dimethylamino) ethyl methacrylate))
PBMD _{Aqu}	aqueous formulation of poly((<i>n</i> -butyl methacrylate)- <i>co</i> -(methyl methacrylate)- <i>co</i> -(2-(dimethylamino) ethyl methacrylate))
PDI	polydispersity index
PDMAEMA	poly[2(dimethylamino)ethyl methacrylate]
pDNA	plasmid DNA
PEG	poly(ethyleneglycol)
PEI	poly(ethylenimine)
PGPAm	poly(3-guanidinopropylacrylamide)
PGPMA	poly(3-guanidinopropyl methacrylate)
p <i>K</i> _a	acid dissociation constant
PNAEP	poly(<i>N</i> -acryloyl- <i>N'</i> -ethylpiperazine)
PNAiPP	poly(<i>N</i> -acryloyl- <i>N'</i> - <i>iso</i> -propylpiperazine)
PNAM	poly(<i>N</i> -acryloylmorpholine)
PNAMP	poly(<i>N</i> -acryloyl- <i>N'</i> -methylpiperazine)
PNAiBP	poly(<i>N</i> -acryloyl- <i>N'</i> - <i>tert</i> -butylpiperazine)
qPCR	quantitative polymerase chain reaction
RAFT	reversible addition-fragmentation chain transfer
rel. MFI	relative mean fluorescence intensity
R-PE	R-phycoerythrin
SARS-CoV-2	severe acute respiratory syndrome coronavirus 2
siRNA	short interfering RNA
TAT	trans-activating transcriptional activator
THF	tetrahydrofuran
Tr.Eff.	transfection efficiency

Publication list

‡ Authors contributed equally.

Peer reviewed publications

- [1] N. Urban,[‡] D. Tsitsipatis,[‡] F. Hausig, K. Kreuzer, K. Erler, V. Stein, M. Ristow, H. Steinbrenner, L. O. Klotz, Non-linear impact of glutathione depletion on *C. elegans* life span and stress resistance, *Redox Biol.*, **2017**, *11*, 502-515.
- [2] F. H. Sobotta, F. Hausig, D. O. Harz, S. Hoepfener, U. S. Schubert, J. C. Brendel, Oxidation-responsive micelles by a one-pot polymerization-induced self-assembly approach, *Polym. Chem.*, **2018**, *9*, 1593-1602.
- [3] F. Richter, L. Martin, K. Leer, E. Moek, F. Hausig, J. C. Brendel, A. Traeger, Tuning of endosomal escape and gene expression by functional groups, molecular weight and transfection medium: a structure-activity relationship study, *J. Mater. Chem. B*, **2020**, *8*, 5026-5041.
- [4] F. Richter,[‡] P. Mapfumo,[‡] L. Martin, J. I. Solomun, F. Hausig, J. J. Frietsch, T. Ernst, S. Hoepfener, J. C. Brendel, A. Traeger, Improved gene delivery to K-562 leukemia cells by lipic acid modified block copolymer micelles, *J. Nanobiotechnology*, **2021**, *19*, 70.
- [5] J. I. Solomun, G. Cinar, P. Mapfumo, F. Richter, E. Moek, F. Hausig, L. Martin, S. Hoepfener, I. Nischang, A. Traeger, Solely aqueous formulation of hydrophobic cationic polymers for efficient gene delivery, *Int J. Pharm.*, **2021**, *25*, 120080.
- [6] F. Hausig, F. H. Sobotta, F. Richter, D. O. Harz, A. Traeger, J. C. Brendel, Correlation between Protonation of Tailor-Made Polypiperazines and Endosomal Escape for Cytosolic Protein Delivery, *ACS Appl. Mater. Interfaces*, **2021**, *13*, 35233-35247.
- [7] F. Gruschwitz, F. Hausig, P. Schüler, J. Kimmig, S. Hoepfener, D. Pretzel, U. S. Schubert, S. Catrouillet, J. C. Brendel, Shear-thinning and rapidly recovering hydrogels of polymeric nanofibers formed by supramolecular self-assembly, *Chem. Mater.*, **2022**, *34*, 2206-2217.

- [8] F. Hausig-Punke,[‡] F. Richter,[‡] M. Hoernke, J. C. Brendel, A. Traeger, Tracking the Endosomal Escape: A Closer Look at Calcein and Related Reporters, *Macromol. Biosci.*, 2022, 2200167.

Submitted Manuscript

- [9] F. Hausig-Punke, G. Dekevic, F. H. Sobotta, J. I. Solomun, F. Richter, D. Salzig, A. Traeger, J. C. Brendel, Efficient transfection *via* an unexpected mechanism by near-neutral polypiperazines with tailored response to endosomal pH, *submitted*.

Poster presentations

- [1] F. Hausig, V. Stein, K. Kreuzer, D. Tsitsipatis, N. Urban, L. O. Klotz, Regulation des insulinresponsiven Transkriptionsfaktors DAF-16 durch Glutathiondepletion führt zur Modulation von Lebensspanne und Stressresistenz von *C. elegans*, *Annual conference of the national society in nutrition (DGE) 2016*, Fulda, Germany.
- [2] F. Hausig, F. H. Sobotta, A. Traeger, J. C. Brendel, Novel non-toxic polymers for overcoming the endosomal barrier, *ESGCT/SETGYC Collaborative Congress 2019*, Barcelona, Spain.

Acknowledgements/Danksagung

An der ersten Stelle danke ich Dr. Johannes C. Brendel, der mich immer unterstützt und an mich geglaubt hat. Ich danke ihm für das entgegengebrachte Vertrauen in unsere interdisziplinäre Zusammenarbeit. Neben den interessanten wissenschaftlichen Diskussionen, fachlichen und experimentellen Anregungen bin ich besonders für seine stetige Ermutigung und seine Geduld dankbar. Ich hätte mir keinen besseren Betreuer für meine Promotion vorstellen können.

Ich möchte mich bei Prof. Dr. Ulrich S. Schubert dafür bedanken, dass ich unter besten Bedingungen forschen und wissenschaftlich arbeiten durfte. Ich bin sehr dankbar für die Möglichkeit, in seiner interdisziplinären Gruppe mit Chemikern, Biologen, Physikern und Materialwissenschaftlern mit hervorragender Ausstattung forschen zu dürfen. Es ist ein Privileg, in einem so hochwertigen Umfeld zu arbeiten und die Möglichkeit zu haben, sich mit anderen Wissenschaftlern zu vernetzen.

Ein besonderer Dank gilt auch Dr. Anja Träger, die mich in das Netzwerk von Biologen am Lehrstuhl eingebunden und mich in ihre Arbeitsgruppe "adoptiert" hat. Ich bin dankbar, wie ihre Kreativität und ihre Schaffenskraft meine Arbeit bereichert haben.

Ich danke der DFG für die Förderung im Rahmen des Emmy-Noether-Programms. Eine Doktorarbeit kann man ohne tatkräftig unterstützende Kollegen nicht gut bewältigen, denen ich hiermit meinen herzlichen Dank aussprechen möchte.

Beginnen möchte ich mit den Kollegen, die schon vor meiner Zeit in der Schubert-Gruppe arbeiteten und mich in den ersten Monaten meiner Arbeit in deren Kosmos eintauchen ließen. Ich danke Dr. Tanja Bùs und Dr. Meike Leiske, Dr. Fabian Sobotta und Anne-Kristin Trützschler dafür, dass sie so verständnisvoll waren, sich trotz der hohen Anforderungen, die an sie gestellt wurden, auch der Neuen anzunehmen.

Mein Dank gilt den ersten Minions der APS-Gruppe, die sich zu Beginn meiner Promotion formte. Ich danke Dr. Fabian Sobotta, Dr. Tobias Klein und Dr. Franka Gruschwitz dafür, dass sie mich besonders in chemischen Kontexten immer unterstützt haben, sei es von Verständnisfragen bei Reaktionen bis hin zur Synthese für gemeinsame Projekte. An dieser Stelle gilt mein besonderer Dank Dr. Fabian Sobotta, der die Polymere herstellte, die für meine Arbeit am entscheidendsten werden sollten, auch wenn wir das damals noch nicht geahnt hätten!

Ich danke auch den nachrückenden Minions der APS-Gruppe Nicole Ziegenbalg, Hans F. Ulrich und Juliane Eberhardt.

Mein Dank gilt allen Bio-Doktorandinnen der Nanocarrier-Gruppe, mit denen ich zusammenarbeiten durfte: Jana I. Solomun, Liên S. Reichelt und Friederike Richter. Ein besonderer Dank gilt Friederike Richter für die enge Zusammenarbeit, ihre Leidenschaft für die Wissenschaft und ihren unermüdlichen Antrieb. Jana I. Solomun möchte ich für das gegenseitige Verständnis danken. Ich bin sehr froh, dass wir uns unterstützen konnten.

Ein unendlich wichtiger Dank geht an das technische Personal der Bio-Abteilung und der Leitung von Dr. David Pretzel. Ich danke Bärbel Behringer-Siemers, Carolin Kellner, Elisabeth Moek, Elisabeth Preußger und Karina Rost.

Eine motivierende Arbeitsumgebung ist für eine erfolgreiche Doktorarbeit, die auch noch Spaß macht, unerlässlich. Hier gilt mein besonderer Dank den tollen Menschen, mit denen ich das Büro teilen durfte. Dr. Marcel Enke verdanke ich ganz nebenbei noch eine fundierte Altersvorsorge und ohne Renzo Paulus wäre so manches IT-Problem eine Hürde geworden.

Ich danke allen tollen Kollegen im CEEC und im ZAF: Franziska Adermann, Julien Alex, Aman Anand, Mira Behnke, Dr. Justyna Czaplewska, Dr. Michael Dirauf, Lada Elbinger, Nora Engel, Dr. Grit Festag, Nicole Fritz, Gauri Gangapurwala, Dr. Michael Gottschaldt, Natalie Göppert, PD Dr. Stephanie Höppner, Paul Klemm, Dr. Uwe Köhn, Alexander Meier, Dr. Simon Münch, Irina Muljajew, PD Dr. Ivo Nischang (auch für das gelungene Praktikum), Adrian Saal, Leanne Stafast, Kristin Schreyer, Dr. Stephanie Schubert, Dr. Christian Stolze, Dr. Jürgen Vitz, Dr. Antje Vollrath (auch für den Büroplatz), Ivan Volodin, Dr. Christin Weber, Thomas Wloka ... sowie allem administrativem Personal: Sylvia Braunsdorf, Franka Frister, Katja Gattung, Mandy Necke, Ulrike Kaiser und Doreen Küchler.

Ich danke meinen Co-Autoren Prof. Dr. Sylvain Catroulliet, Gizem Cinar, Dr. Franka Gruschwitz, Dominic O. Harz, PD Dr. Stephanie Höppner, Dr. Thomas Ernst, Dr. Jochen J. Frietsch, Katharina Leer, Julian Kimming, Prosper Mapfumo, Dr. Liam Martin, Elisabeth Moek, PD Dr. Ivo Nischang, Dr. David Pretzel, Friederike Richter, Dr. Fabian Sobotta, Philipp Schüler, Prof. Dr. Ulrich S. Schubert und Jana I. Solomun für die erfolgreiche Zusammenarbeit.

Ich bin dankbar für meine Kooperationspartner unter der Leitung von Prof. Dr. Christian Eggeling: Dr. Pablo Carravilla, Anindita Dasgupta und Dr. Ziliang Zhao.

Mein finaler Dank gilt meinen Eltern Kathrin und Burkhard Hausig, meinen Großeltern, meiner Schwester Stefanie Hausig mit Familie und meiner Cousine Sophie Hausig. Danke, dass ihr mich so unterstützt habt.

Mein größter Dank gilt meiner Ehefrau Sarah S. Punke. Dein Rückhalt, deine Liebe und deine Zuversicht machen es mir möglich, meine Ziele zu erreichen.

Declaration of authorship/Selbstständigkeitserklärung

Ich erkläre, dass ich die vorliegende Arbeit selbstständig und unter Verwendung der angegebenen Hilfsmittel, persönlichen Mitteilungen und Quellen angefertigt habe.

Jena, 04. 10. 2022

Franziska Hausig-Punke

Publications Pub1 to Pub6

Pub1 Reprinted with permission from Pub1. Copyright 2022 Wiley.

Pub2 Reprinted with permission from Pub2. Copyright 2021 American Chemical Society.

Pub3 Reprinted with permission from Pub3.

Pub4 Reprinted with permission from Pub4. Copyright 2021 BioMed Central.

Pub5 Reprinted with permission from Pub5. Copyright 2021 Elsevier.

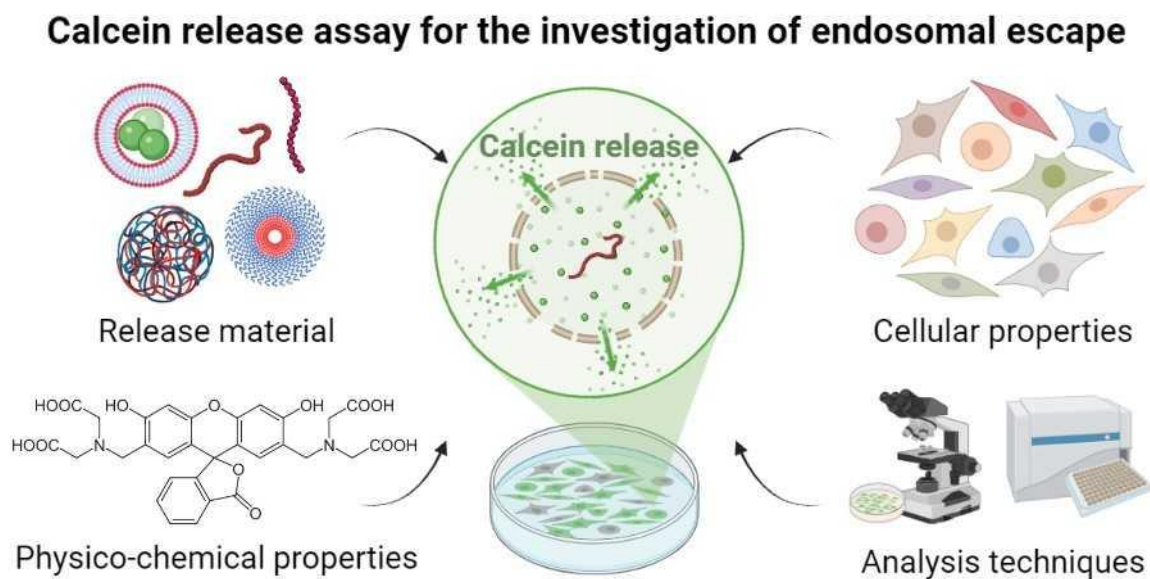
Pub6 Reprinted with permission from Pub6. Copyright 2020 Royal Society of Chemistry.

Publication Pub1

Tracking the Endosomal Escape: A Closer Look at Calcein and Related Reporters

F. Hausig-Punke,[‡] F. Richter,[‡] M. Hoernke, J. C. Brendel, A. Traeger,⁵
Macromol. Biosci., 2022, 2200167.

[‡] Authors contributed equally.



Tracking the Endosomal Escape: A Closer Look at Calcein and Related Reporters

Franziska Hausig-Punke, Friederike Richter, Maria Hoernke, Johannes C. Brendel,* and Anja Traeger*

Crossing the cellular membrane and delivering active pharmaceuticals or biologicals into the cytosol of cells is an essential step in the development of nanomedicines. One of the most important intracellular processes regarding the cellular uptake of biologicals is the endolysosomal pathway. Sophisticated nanocarriers are developed to overcome a major hurdle, the endosomal entrapment, and delivering their cargo to the required site of action. In parallel, *in vitro* assays are established analyzing the performance of these nanocarriers. Among them, the release of the membrane-impermeable dye calcein has become a popular and straightforward method. It is accessible for most researchers worldwide, allows for rapid conclusions about the release potential, and enables the study of release mechanisms. This review is intended to provide an overview and guidance for scientists applying the calcein release assay. It comprises a survey of several applications in the study of endosomal escape, considerations of potential pitfalls, challenges, and limitations of the assay, and a brief summary of complementary methods. Based on this review, it is hoped to encourage further research groups to take advantage of the calcein release assay for their own purposes and help to create a database for more efficient cross-correlations between nanocarriers.

In particular the nucleic acid-based systems, such as the SARS-CoV-2 vaccines or novel cancer therapies underline the enormous potential of this technology. Despite the current success of lipid-based gene carriers, the number of papers on polymer-based gene carriers is also constantly increasing due to their impressive versatility and stability. For the successful delivery of nucleic acids, several challenges need to be addressed, including nanoparticle formulation, targeting, intracellular release, and transport to its destination. Especially, the intracellular processes represent a key aspect, which surprisingly are still not well understood. Therefore, no consistent theory can be applied to the various nanocarrier systems, but two aspects predominate among the cellular barriers, cellular uptake, and endosomal release. Further hurdles may also play a role such as the transfer of genetic material into the cell nucleus, which can be neglected in mRNA/siRNA applications, because their site of action is inside

1. Introduction

The field of nonviral nanocarriers for the delivery of nucleic acids into cells has made great progress in the last decades.


the cytosol. Cellular uptake is obviously fundamental and depends on the physicochemical parameters of the nanocarrier or the introduction of active target components, which is well reviewed elsewhere.^[1–4] However, successful uptake into cells does not necessarily correlate with efficient gene expression. Therefore, escape from the endo-lysosomal compartment is considered as a critical cellular step for the successful carrier-dependent delivery of sensitive cargos, such as genetic material or proteins.^[5] The main reasons are, on the one hand, the risk of enzymatic degradation and, on the other hand, the fact that genetic material can only exert its effect outside the endosomes. Unfortunately, several nanocarriers fail in this regard, as they are either excreted (exocytosis) or degraded (lysosome), which means that endosomal release can be considered an important lever for improving cellular gene delivery.^[6–8] In this review, we refer to the general term nanocarrier, although not all mentioned materials may contain a cargo as it is implied for carriers. The term comprises all compounds that promote endosomal release and include lipid-based materials (liposomes, lipid nanoparticles), polymer-based materials (linear or branched polymers, polymersomes, micelles, nanoparticles and peptides), as well as peptide-based materials.

In order to optimize the design of nanocarriers, the biological processes must be considered in more detail, because they determine the conditions the nanocarriers have to deal with.

F. Hausig-Punke, F. Richter, J. C. Brendel, A. Traeger
Laboratory of Organic and Macromolecular Chemistry (IOMC)
Friedrich Schiller University Jena
Humboldtstrasse 10, 07743 Jena, Germany
E-mail: johannes.brendel@uni-jena.de; anja.traeger@uni-jena.de

F. Hausig-Punke, F. Richter, J. C. Brendel, A. Traeger
Jena Center for Soft Matter (JCSM)
Friedrich Schiller University Jena
Philosophenweg 7, 07743 Jena, Germany

M. Hoernke
Chemistry and Pharmacy
Albert-Ludwigs-Universität Freiburg
Hermann-Herder-Str. 9, 79104 Freiburg i.Br., Germany

 The ORCID identification number(s) for the author(s) of this article can be found under <https://doi.org/10.1002/mabi.202200167>

© 2022 The Authors. Macromolecular Bioscience published by Wiley-VCH GmbH. This is an open access article under the terms of the Creative Commons Attribution-NonCommercial License, which permits use, distribution and reproduction in any medium, provided the original work is properly cited and is not used for commercial purposes.

DOI: 10.1002/mabi.202200167

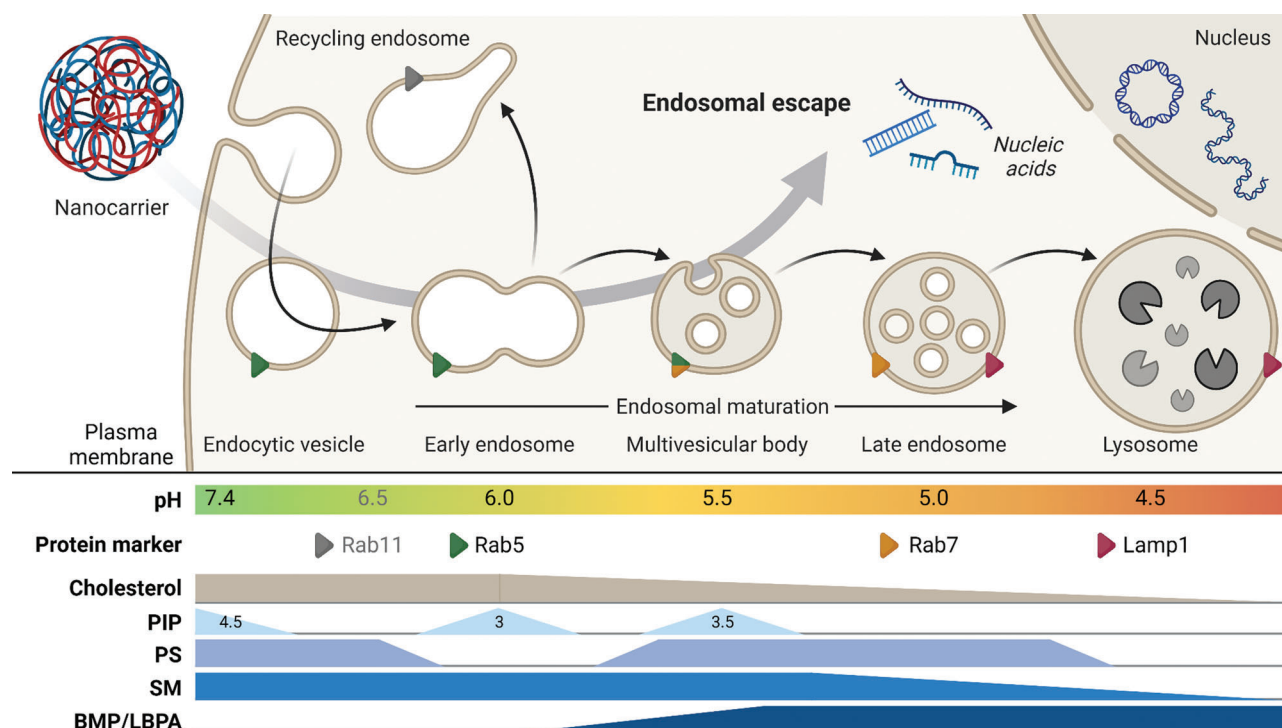


Figure 1. Endosome maturation. Following endocytosis, the endocytic vesicle delivers the internalized cargo to the early endosome, where it is either recycled through the recycling endosome or evolves further along the endolysosomal pathway to be degraded. Beside the fusion of different vesicles and membrane invagination, this is accompanied by changes in the intravesicular pH value, membrane lipid composition, and important protein markers. To avoid the enzymatic degradation within the lysosome, the nanocarrier (representative for polymers, liposomes, nanoparticles) delivering drugs or nucleic acids, thus, must escape this process at an earlier stage. PIP—phosphoinositides (numbers indicate phosphate positions on the inositol ring), PS—phosphatidylserine, SM—sphingomyelin, BMP/LBPA—bis(monoacylglycerol)phosphate/lysobisphosphatidic acid. Adapted with permission.^[16] Copyright 2014, Elsevier.

Particles as well as liquids, solutes, macromolecules, or plasma membrane components are taken up by the cell through endocytosis, in which the plasma membrane is first invaginated and then segregated, allowing for the formation of intracellular vesicles.^[4,9] Besides their role in nutrient uptake, endosomes are involved in the regulation and fine-tuning of numerous signaling pathways in the cell, e.g., the recycling of receptors. After vesicle formation, they fuse to form early endosomes and become linked to the microtubule network.^[10] In this way, the vesicles and their cargos are able to move alongside the microtubules toward the perinuclear region and gradually transform into late endosomes, where hydrolases and membrane components of the secretory pathway are recruited. Subsequently, they enlarge in size, form more intraluminal vesicles and finally fuse with the lysosome to form the endolysosomes.^[9] During endosomal maturation, the size of endocytic vesicles increases from ≈ 100 nm (early endosome) to ≈ 1000 nm (lysosome).^[9,11–13] Inside the endolysosomes a variety of digestive processes take place, which degrade most compounds of biological origin and, thus, represent a dead end for the nanocarriers which should be avoided. During endosomal maturation, not only the size and structure of the organelles change, but more importantly the intravesicular pH value and the composition of the membrane, both, in terms of proteins and lipids (see **Figure 1**).^[9,14] In early endosomes, the membrane consists mainly of neutral lipids (including sphingolipids, sterols), similar to the cytoplasmic

membrane. Along with the acidification of the vesicles (from 7.4 to 4.5), the proportion of sterols decreases leading to an increase in membrane fluidity. Furthermore, the proportion of anionic lipids (e.g., lysobisphosphatidic acid (LBPA), also termed bis(monoacylglycerol)phosphate (BMP)) increases.^[15–18] This increase in LBPA during endosomal maturation was identified as critical for the mode of endosomal escape.^[19,20]

This complex process is exploited by viruses, which can thus enter the cell in an optimized way and reprogram it without destroying it. Viruses cross the endosomal membrane by a pH-dependent change of conformation or hydrophobicity of their surface peptides leading to penetration of the vesicular membrane. This inspired material designers to mimic the efficiency of viral systems and optimize them with a lower risk potential, e.g., in the form of cell-penetrating peptides (CPPs), liposomes, synthetic polymers, and nanoparticles.^[21,22] To circumvent lysosomal digestion, pH-dependent cationic amines were commonly included in polymers or lipids. Along the endosomal pathway, the amines become increasingly protonated and enable electrostatic interactions with anionic lipids or facilitate hydrogen bonding between the amino groups of the nanocarrier and the phosphate groups of the lipids. Hence, the nanocarriers can interact locally with the membrane destabilizing it and, thereby, promoting the escape of the nanocarriers and their cargos into the cytoplasm.^[23] Furthermore, the “proton-sponge” hypothesis remains an accepted explanation for the endosomal

release of some polymers. The buffering capacity of polycations is considered to cause a change in vesicular pH and an influx of ions, which increases the osmotic pressure and eventually causes a rupture of the lipid membrane.^[24] However, this hypothesis is under debate in the community.^[25] Comparison of polymers with different buffer capacities revealed that a reduction in buffer capacity toward the early endosomal pH range was often associated with higher transfection efficiencies,^[26–28] although high buffer capacities at low pH values along the endolysosomal pathway were identified as not beneficial.^[29] However, it should be noted that any modifications to the polymers may have affected the performance of the carrier at the level of intracellular barriers upstream or downstream of the endosomal exit (vector packing and unpacking, endocytosis rates, changes in hydrophobicity). In addition, the read-out of the transfection may not be the best approach to evaluate the proton sponge effect. Others have questioned the validity of the proton sponge hypothesis by considering endosomal acidification. While some studies have demonstrated the necessity of acidification for the escape of poly(ethylenimine) (PEI) polyplexes,^[8,26,30–32] other researchers investigated the effect of buffer polymers on the actual pH in endosomes. Several reports showed that endosomal acidification was slowed down after administration of buffer polymers, while the pH of endosomes containing a nonbuffering polymer decreased more rapidly.^[28,30] However, these observations have been questioned by other authors because buffering polymers are not able to increase endolysosomal pH, which could refute the proton sponge effect.^[25,33] In addition, there is a debate about the lack of colocalization with LysoTracker in microscopy images, as the buffering effect of the polymer inhibits staining with acidotropic dyes such as LysoTracker,^[34,35] because even if the polymers have a buffering effect in endosomes, this is no guarantee that the pH of the vesicle will remain elevated.^[25,36]

For the detailed investigation of the cellular fate of nanoparticles and in particular the endosomal release, different techniques can be applied. Predominantly, the integrity of the endosomal membrane is evaluated for endosomal escape. Related experiments can be performed in cells, isolated cell organelles and artificial or model vesicles. The latter represents a more controlled and reproducible environment since endosomes can be modeled by liposomes with membranes of known phospholipid composition. The variety of applied methods can be found elsewhere.^[37,38] However, the potency and limitations of each approach should be kept in mind. In the case of gene delivery, the expression or functionality of the genetic material (e.g., expression or knock down) is one possible test, representing a global read-out and functionality. Fluorescent dyes/proteins or reporter systems can be used additionally to study endosomal release in more detail.^[5,39–44] Although they might not exactly match the intended cargos of the investigated nanocarrier with regard to size, charge or hydrophilicity and, hence, might not reflect its real cargo delivery potential, they can be used as well-available and less expensive model molecules for the investigation of the release mechanism. The most popular sensor molecule is calcein, which is straightforward to apply, affordable, and easily accessible. Therefore, it is used to study a variety of different nanocarriers.

However, different experimental settings, conditions, and analytical methods are used for this purpose, which makes it difficult to evaluate/compare different materials. In this review, we eluci-

date the key application of calcein as a powerful yet simple tool to investigate the endosomal escape. Various conditions have been reported, which reflects the complexity of the calcein release assay and sometimes might even cause contradictory outcomes. In Sections 2–5, calcein is first introduced regarding its basic chemistry and historical development, followed by overviews of the different applied methods in models or cells, and a section reflecting on pitfalls, challenges, and limitations of the calcein release assay within the cellular environment. A few complementary methods are described in Section 6, which certainly does not represent a comprehensive overview, but provides some guidance to alternatives overcoming the previously mentioned issues.

2. Chemical Background of Calcein

Calcein, also known as bis[*N,N*-bis(carboxymethyl)aminomethyl]fluorescein, fluorescein complexone, and fluorexon, was first described by Diehl and Ellingboe in 1956 as an indicator for the complexometric titration of calcium^[45,46] followed by several Ph.D. theses at the Iowa State University with detailed descriptions regarding its synthesis, characterization and applications (Figure 2).^[47–50] It is synthesized via a Mannich-type condensation of fluorescein, formaldehyde, and iminodiacetic acid and can, thus, be considered as a derivative of fluorescein belonging to the substance class of xanthenes.^[45,48,51] Due to the condensation reaction, calcein combines two features within one molecule: the fluorescence of fluorescein and the chelation property of iminodiacetic acid, which is also part of the well-known chelator ethylenediaminetetraacetic acid (EDTA).^[48] Comparable to fluorescein, calcein absorbs light in the cyan spectrum range and fluoresces in the green range with absorption and emission maxima at $\lambda_{\text{Ex/Em}} = 495/515 \text{ nm}$.^[47,52] The self-quenching of fluorescein at high concentrations, known since 1888,^[53–55] also characterizes calcein and other derivatives, such as 6-carboxyfluorescein (Figure 3A, 1). This property has been exploited since the late 1970s to investigate the stability of liposomes encapsulating 6-carboxyfluorescein^[56,57] or calcein,^[58,59] as a damage of the liposomal membrane would result in dilution of the dye and an increase in its fluorescence intensity. Regarding calcein, a self-quenching concentration of 70 mM is often utilized,^[60,61] but there are also studies showing different values which could be attributed to different buffer systems and fluorescence measurement methods (Table 1).

Another factor influencing the fluorescence of calcein is the pH value (Figure 3A, 2). However, with the six carboxy groups available for protonation, the fluorescence of calcein is less pH dependent than that of fluorescein and exhibits high intensities between pH 4.5 and 10.^[47,50,69] Therefore, it remains fluorescent within the biologically relevant pH range including endolysosomal pH values important for the analysis of endosomal escape. Additionally, the carboxy moieties lead to a higher polarity and increased hydrophilicity of calcein compared to fluorescein (for TPSA and logP values refer to Figure 2A) and, thus, make it less membrane permeable at low pH values.^[57,70,71] The pH value also affects the solubility in water of calcein with higher pH values leading to a better solubility.^[50]

In addition, the calcein fluorescence is influenced by various di- or multivalent metal ions, more precisely by their chelation which has been used for the determination of the cations in

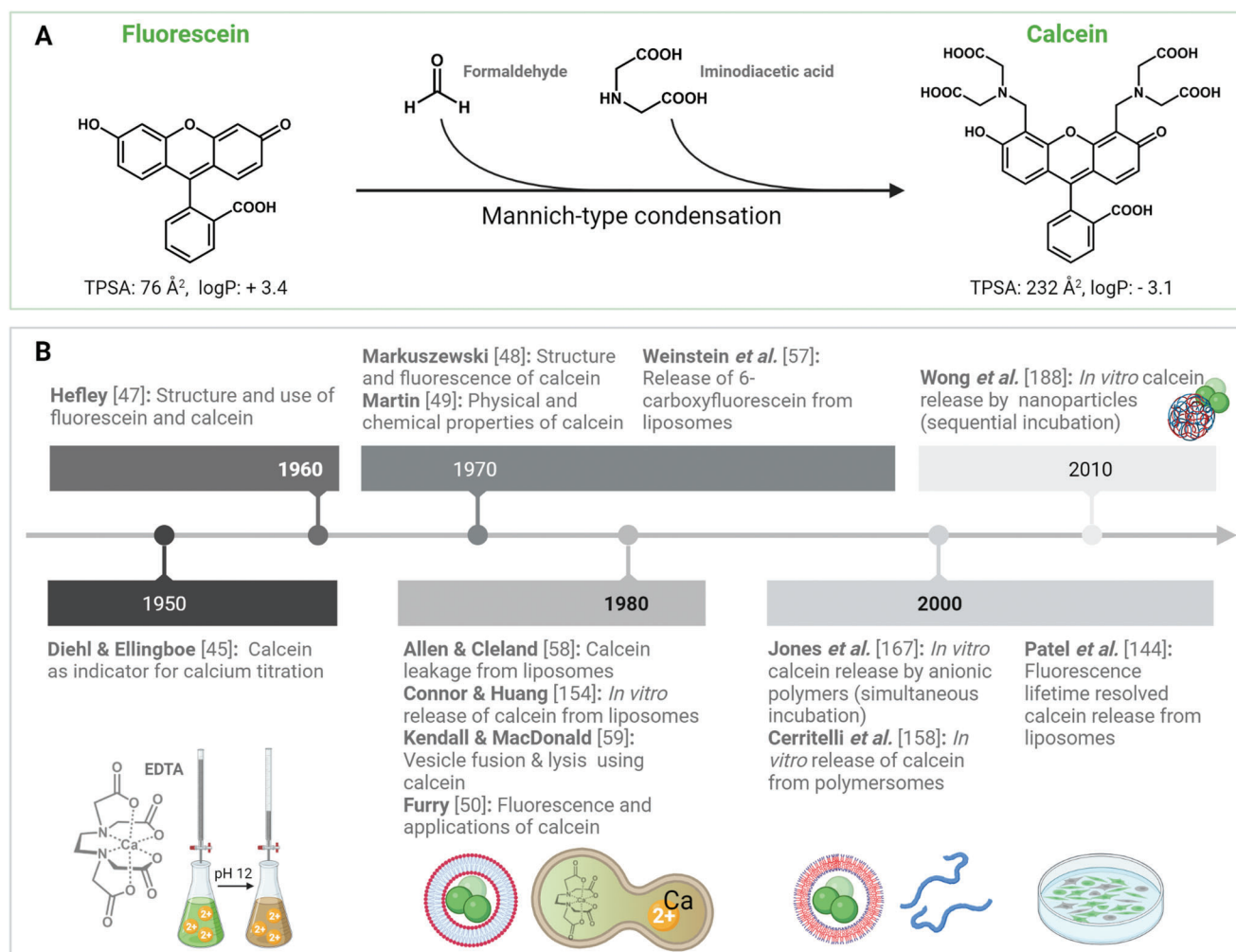


Figure 2. Synthesis and utilization of calcein. A) The synthesis route of calcein starting from fluorescein with indicated polarity (TPSA: topological polar surface area) and hydrophobicity measures for both molecules. B) Historical overview on the development of calcein as a fluorescent molecule and its utilization to investigate endosomal escape.

various tissues and fluids (Figure 3A, 3). The complexation of the cations has two different effects, which in turn are pH and concentration dependent.^[52] Under the tested conditions, the ions of the alkaline earth metals magnesium, calcium, barium, and strontium enhance the calcein fluorescence at alkaline pH values when calcein would otherwise be quenched.^[49,50,69] At neutral pH values and metal:calcein ratios of 4 or 10:1, however, these ions only influence the absorption spectrum in the UV range but not the fluorescence of the brightly emitting calcein.^[69] By contrast, ions of the transition metals manganese, cobalt, nickel, copper,^[49,69,72,73] and iron^[50,74–76] have been shown to quench the fluorescence in liposomes at neutral pH values. Furthermore, ions with higher valencies are able to increase the fluorescence intensity of calcein, such as aluminum ions at low pH values.^[49,69,77] On the other side, the addition of sodium can enhance fluorescence at high pH values. Interestingly, potassium or lithium ions, however, do not affect the fluorescence, favoring KOH solutions over NaOH solutions to dissolve the calcein.^[52,78] Besides calcein, there are also other combinations of the iminodiacetic acid and various dyes that can be used to

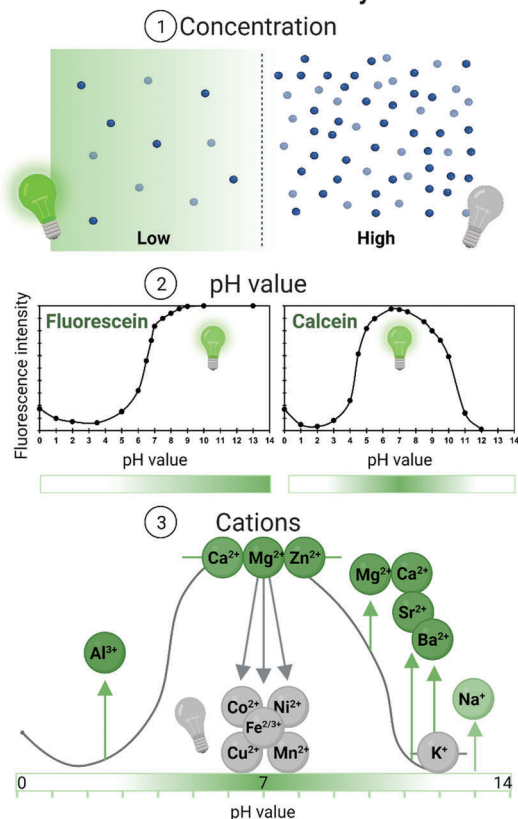
chelate cations, such as calcein blue (umbellikomplexon),^[79–83] or Calcium Green, Calcium Orange, and Fluo-3 (Figure 3B).^[84–86]

Besides the determination of cations, calcein, or more precisely its acetoxymethyl ester (calcein AM) is also used to identify viable cells. In contrast to calcein, the hydrophobic and nonfluorescent calcein AM is membrane permeable (Figure 3C). Upon entering the cells, the esters of calcein AM are hydrolyzed by non-specific intracellular esterases active only in living cells resulting in the fluorescent calcein that cannot easily permeate the cellular membrane and is retained within the cells.^[87–90] Similarly, this method is also used to determine the membrane integrity of cells by preloading the cells with calcein AM/calcein and measuring the release of calcein upon membrane destruction by various substances.^[91–93]

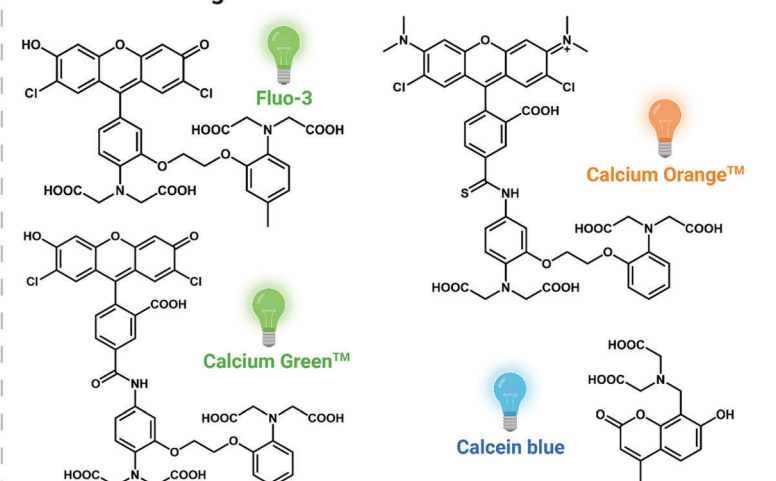
3. Calcein Leakage from Artificial Model Vesicles

Early experiments to investigate interactions of potential nanocarriers with lipid membranes include release studies with artificial liposomes, also called lipid vesicles. The

A Fluorescence is influenced by ...



B Similar chelating alternatives



C Membrane permeating derivatives

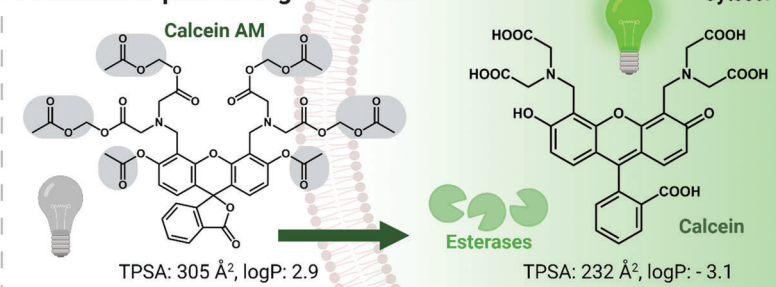


Figure 3. Physico-chemical properties and derivatives of calcein. A) Factors influencing the fluorescence intensity of calcein: Concentration, pH value and different cations. Arrows in 3 indicate an increase or decrease in fluorescence intensity through the respective cation. B) Further cation chelating molecules with structures similar to calcein. C) Principle for the identification of viable cells using calcein AM.

Table 1. Overview of quenching concentrations (conc.) and pH values in different studies.

Ref.	Buffer [mM]	pH value	Conc. at Flmax [mM]	Conc. at 50% Flmax [mM]	Conc. at 10% Flmax [mM]
Hamann 2002 ^[62]	119 Na ⁺ , 5 K ⁺ , 0.8 Mg ²⁺ , 1.8 Ca ²⁺ , 114 Cl ⁻ , 0.8 SO ₄ ²⁻ , 25 HEPES, 5.6 glucose, 44 mannitol	7.4	4.000	8.400 ^{a)}	> 30.00 ^{a)}
Roberts 2003 ^[63]	PBS (350 mOs mol L ⁻¹)	7.4	0.019	0.055	0.20 ^{a)}
Andersson 2007 ^[64]	50 PBS + POPC	7.0	0.032 ^{a)}	0.100 ^{a)}	> 0.10 ^{a)}
Imamura 2017 ^[65]	PBS	7.4	2.000	9.000 ^{a)}	25.00 ^{a)}
Dorrington 2018 ^[66]	0.1 EDTA, 10 Tris, 100 NaCl	7.8	0.970	N/A	> 6.40 ^{a)}
Brkovic 2020 ^[67]	0.2 Na ₂ HPO ₄ -NaH ₂ PO ₄	7.5	0.002 ^{a)}	0.005 ^{a)}	0.01 ^{a)}
Bae 2021 ^[68]	50 HEPES, 100 Na ⁺ , 100 Cl ⁻ , 5 % glycerol	7.4	0.001	0.002 ^{a)}	> 0.20 ^{a)}
Own data ^{b)}	20 HEPES, 5% glucose	5, 6, 7	0.080	1.120	> 3.20 ^{a)}

^{a)} Values were read from the graph. ^{b)} Not published.

strong self-quenching properties of calcein and the related 6-carboxyfluorescein at high concentrations had already been exploited in these experiments, i.e., for the investigation of endosomal escape. These dyes still represent prominent reporters to monitor the release from lipid vesicles by different nanocarriers or vectors. As liposomes have been used as artificial cell models since the 1970s, numerous reviews and protocols with^[94–96] and without^[97,98] calcein are available, which we like to refer to. In

this section, only studies with calcein as a reporter and directly related to endosomal escape will be discussed to illustrate the liposomal features that can be exploited for the investigation of the specific characteristics of endosomal escape (Table 2).

In general, typical leakage experiments with encapsulated calcein involve the addition of the investigated nanocarrier to a dispersion of vesicles (Figure 4). Upon permeabilization of the lipid bilayer, the released calcein is diluted in the outer buffer. In the

Table 2. Investigation of calcein release from model vesicles.

Nanocarrier	Vesicle type ^{a)}	Lipids ^{b)}	Calcein concentr. mM	Incubation conditions buffer, pH, temperature, time	Ref.
Polymer	SUV	DHP, PC, Chol	40	• 10 mM phosphate, pH 7.4, 25 °C or 65 °C, 20 min	[101]
	LUV	PC, PG	80	• 10 mM HEPES + glucose, pH 5.8–7.6, up to 60 min	[102]
		PC	200	• 10 mM Tris-HCl, 100 mM NaCl, pH 10, 25 °C, up to 60 min	[103]
Peptide	LUV	PC, PE, BMP, Chol	60	• in: 10 mM NaH ₂ PO ₄ , 100 mM NaCl, pH 7.4 out: 10 mM NaH ₂ PO ₄ , 100 mM NaCl, pH 5.5, (or pH 7.4) RT, 60 min	[104–106]
				• 5 mM NaH ₂ PO ₄ , 100 mM KCl, pH 7.4, RT, 60 min	[107]
		PC, PE, BMP, PG	70	• 10 mM phosphate, 100 mM NaCl, pH 7.4, RT, up to 20 min, 60 min	[108]
		PC, PE, BMP, Chol, PA, PG	60	• 10 mM NaH ₂ PO ₄ , 100 mM NaCl, pH 5.5, RT, 60 min	[109]
	GUV	PC, PE, BMP, PI	70	• PBS, pH 7.4, up to 30 min	[110]
		PC, Chol	100	• in: 375 mM NaOH, 50 mM NaCl, pH 7.4 out: 200 mM NaCl, 20 mM citrate, pH 7.4/5, up to 60 min	[111]
		PC, PE, BMP, PG	70	• 10 mM phosphate, 100 mM NaCl, pH 7.4, RT, up to 20 min, 60 min	[108]
		PC, PG, Chol	50	• in: 130 mM NaCl, 20 mM Na ₃ PO ₄ out: 130 mM KCl, 20 mM K ₃ PO ₄ , pH 7, 4 h	[112]
Peptide/polymer	LUV	PC	40	• 10 mM NaH ₂ PO ₄ , pH 7.4, 5 min	[113]
		PC, Chol	90	• in: 137 mM HEPES, pH 7.4 out: 137 mM HEPES, pH 7.4 or 137 mM sodium citrate buffer, pH 5.0; 37 °C, 60 min	[29]
Peptide/liposome	LUV	PC, Chol	90	• 5 mM HEPES, 150 mM NaCl, pH 7.4, RT, 60 min	[114]
		PC, PS, Chol	40	• in: 1 mM EDTA, out: PBS or citrate/phosphate, pH 7.4/5.5, 37 °C 30 min	[115, 116]

^{a)} SUV—small unilamellar vesicle (30–100 nm), LUV—large unilamellar vesicle (100 nm–1 µm), GUV—giant unilamellar vesicle (1–200 µm) ^{b)} In different ratios. Only types of phospholipids are distinguished, fatty acids can vary. DHP—dihexadecyl phosphate, PC—phosphatidylcholine, Chol—cholesterol, PE—phosphatidylethanolamine, BMP—bis(monoacylglycerol)phosphate, PG—phosphatidylglycerol, PA—phosphatidic acid, PI—phosphatidylinositol, PS—phosphatidylserine.

case of a gradual leakage, also calcein that remains entrapped is diluted. Thereby, self-quenching is reduced, and the fluorescence increases. There are two calcein release assays in artificial vesicles: The reduced self-quenching can be monitored via the fluorescence intensity and normalized to the maximal fluorescence reached by lysis of the remaining liposomes. Alternatively, the fluorescence lifetime and amount of free and entrapped dye can be determined. Typically, leakage is examined after 1 h incubation time. However, studying the time course of leakage over several hours can indicate certain leakage mechanisms.^[99,100]

The model vesicles can roughly be classified according to their size into small unilamellar vesicles (SUV, 0.02–0.1 µm), large unilamellar vesicles (LUV, 0.1–1 µm) and giant unilamellar vesicles (GUV, 1–200 µm).^[117] However, the size of the lipid vesicles only matters for comparison purposes. In the surveyed studies, mostly LUVs and GUVs have been investigated, which have too small membrane curvature to result in packing defects. More importantly, identical leakage mechanisms can appear different in vesicles of different sizes.^[118] LUVs are commonly prepared by solvent-free self-assembly (Figure 4). For this, thin lipid films are obtained from organic solutions containing all lipid components. The films are rehydrated with an aqueous calcein buffer, followed by multiple freeze-thaw cycles,^[102,105,108,110] and repeated extrusion through polycarbonate membranes with pore sizes of 100 nm,^[101,102,104–106,108,109,113] or larger.^[110,115] The outer buffer with free dye is exchanged via size exclusion chromatography (SEC) or centrifugation protocols.^[114] GUVs can be obtained

by swelling of the dried lipid film in the desired buffer,^[119,120] sometimes involving a polymer gel.^[108] Electroformation can also be utilized, but GUVs obtained this way might suffer from artefacts when using charged lipids and calcein might also interfere.^[121,122]

Not only the size, but more importantly the membrane composition is known to change during endolysosomal maturation (see as well Introduction).^[9] These changes in composition inspired investigations of different lipid compositions containing BMP.^[104–110] For instance, the group of J. P. Pellois tested different variants of the CPP TAT with liposomes containing BMP and/or other lipids and found that liposomal leakage occurred only in presence of BMP, but not if other anionic phospholipids such as phosphatidylglycerol (PG) or phosphatidic acid (PA) were incorporated.^[104–106,108,109] Their further investigations included the simple binding between TAT variants and lipid and the endosomal escape in HeLa cells by analyzing the fluorescence distribution pattern (punctate vesicular or broad cytosolic) of the tetramethylrhodamine (TMR) the TAT variants were labeled with.^[105,109] In these assays, the liposomal leakage/endosomal escape was concentration dependent and showed similar optimal concentrations for the respective TAT variant indicating that the results of the methods correlate well. Moreover, Pellois and co-workers also demonstrated that the incubation with anti-BMP antibodies inhibits the leakage/escape, both in liposomes and in cells.^[108,109] The influence of the changing cholesterol content on the leakage of further peptides

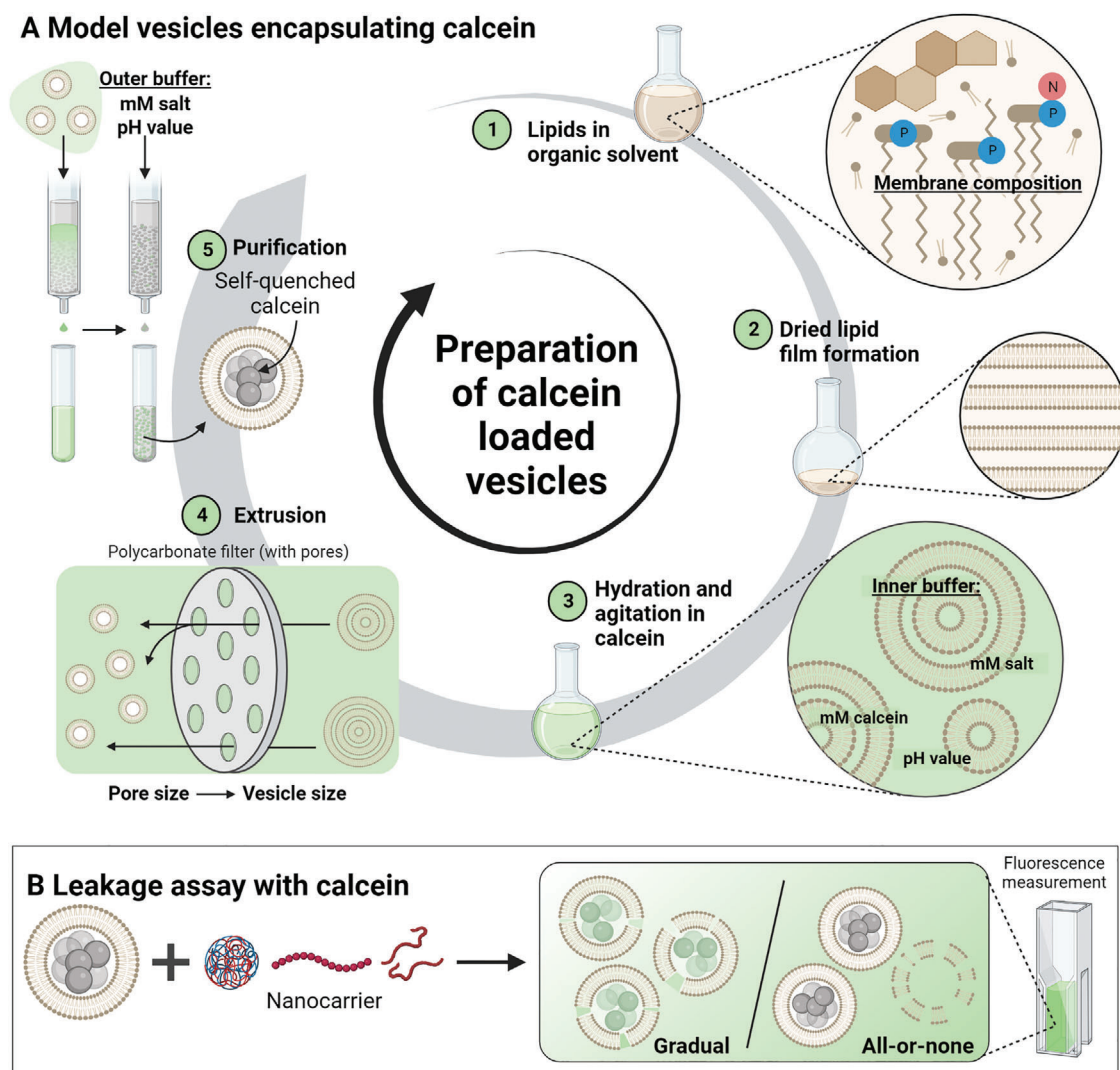


Figure 4. Preparation and calcein leakage from model vesicles. A) The model liposomes (LUVs) can be modified at different steps to mimic different properties of the endolysosomal pathway. B) Upon mixing of the liposomes with different nanocarriers, the release of calcein can be determined and characterized regarding the release mechanism (for example, gradual or all-or-none, transient or continuous). Adapted from “Liposome Preparation via Thin Film Hydration” (2022) by BioRender.com. Retrieved from <https://app.biorender.com/biorender-templates>.

was studied similarly,^[111] demonstrating the potential of experiments with model liposomes to address specific questions more precisely.

Another aspect relevant for the design of leakage experiments in LUVs is the endolysosomal acidification process that can be mimicked by the appropriate pH value of the buffers. Changes in pH can lead to a change in the degree of charge not only of the tested nanocarrier but also of the anionic phospholipids, which can be exploited to design pH-responsive nanocarriers and lipidic drug delivery systems.^[16,29,111,115,116] To correctly reflect the role of the endolysosomal acidification, the appropriate, isosmotic buffers, and salts have to be used for vesicle preparation, purification, and incubation. In most cases, phosphate buffers are employed, although concentrations and the type of added salt can vary significantly. For instance, Pellois and co-workers used an intra-liposomal pH of 7.4 to mimic the cytosol and an extra-liposomal pH of 5.5 to mimic the endolysosomal lumen.^[104–106,109]

By contrast, Sarkar et al. used HEPES buffer (4-(2-hydroxyethyl)-1-piperazineethanesulfonic acid) to investigate calcein leakage of triblock copolymer micelles by varying the pH range from 5.8 to 7.6 outside the liposomes.^[102] Furthermore, glucose was added to balance the different osmotic pressures inside and outside the liposomes, whereas other studies mostly used NaCl or KCl for compensation. If very high calcein concentrations (>70 mM) are required, also the weak solubility of calcein at low pH values has to be considered which requires the use of basic buffers (e.g., Tris-HCl pH 10)^[103] for the hydration of the lipid film. Additionally, also a Na⁺/K⁺ gradient can be applied to liposomes to mimic conditions present in nascent endosomes,^[123] as Rangasamy et al. have shown with LUVs composed of PC, PG, and Chol with a sodium inside-buffer and a potassium outside-buffer mimicking high intra-liposomal Na⁺-concentrations and high cytosolic K⁺-concentrations, respectively.^[112]

Despite the large variations in the experimental procedures limiting comparability of results, the calcein release from model vesicles represents a straightforward method to mimic selected aspects of endosomal escape in a controlled environment independent of the complex cellular processes. Nevertheless, membrane models, other conditions and procedures as well as theoretical concepts are still being advanced to further optimize the transferability of the results to experiments in cells.^[61,124] For example, some studies chose an incubation temperature of 37 °C instead of room temperature.^[115,116] This corresponds to the cellular environment and, together with the choice of fatty acid chains, may have an impact on the membrane fluidity of liposomes.^[117,125] Furthermore, mimicking the exact membrane composition of endolysosomal organelles including different fatty acids and associated proteins is very complex and can only gradually be approached. To increase the similarity to natural lipid compositions, also naturally derived vesicles can be utilized. They can be obtained either via chemically induced cell blebbing followed by harvesting of the resulting GUVs, or by the rehydration of total lipid extracts from different cells/tissues.^[126] The advantages and relevance of natural lipid compositions are limited by the uncertainty of their lipid composition, which is rather similar to the plasma membrane, or by missing asymmetry in the lipid distribution over the membrane. Nevertheless, these improvements are invaluable in filling the gap between mechanistic conclusions from simplified model studies to the biological behavior in cells.

To investigate vesicle compositions more comparable to endolysosomes, exosomes can be isolated from the cell culture supernatant since they originate from the multivesicular endosome (see also Figure 9) and also comprise the characteristics of different cell types.^[127,128] While they are difficult to load with hydrophilic molecules such as calcein directly,^[129] the nonfluorescent derivative calcein AM can be used instead. Calcein AM can diffuse into the exosomes and is subsequently converted to calcein by the esterases contained therein.^[130] One minor limitation is that the high calcein concentrations required for the full information range encoded in self-quenching behavior cannot be reached. A similar approach is also utilized to examine the leakage of calcein AM from red blood cells upon perturbation of their plasma membrane by different nanocarriers.^[88,131,132] Another aspect which has rarely been considered so far, is that nanocarriers in cellular endolysosomal organelles escape from the inside to the outside of the organelles, whereas they have to take the opposite way in assays using model vesicles. This could have an impact on the apparent leakage since the concentration gradient of the entrapped nanocarrier is reversed and the asymmetric membrane composition is not reproduced correctly. Furthermore, osmotic swelling as hypothesized for the proton-sponge mechanism cannot be modeled.

Strikingly, the calcein-based methods can be slightly modified in various ways, to not only examine the occurrence of calcein release from these model vesicles, but also the mechanism of the release. Here, we will only summarize assays using calcein, even though they might be based on calcein-free variants and there are calcein-free alternatives mentioned elsewhere.^[96]

There are many postulated release mechanisms that can be classified in different aspects. One way is to distinguish transient leakage from continuous leakage.^[133] Transient leakage occurs

fast upon interaction of the nanocarrier and the membrane and stops thereafter. Most commonly, this behavior is explained by the asymmetry stress mechanism,^[134–136] or an involvement of membrane fusion in leakage (see below).^[108,137] Continuous leakage, on the other hand, will happen through stochastically reoccurring leakage events or pores, thus slowly continues and affects the sample over several hours.^[99,133,138] These types of pore formation kinetics can be distinguished for example by visualizing GUVs by confocal microscopy and acquiring time-resolved images, which allows for a direct optical monitoring of the leakage process in individual vesicles.^[108,112,139–141] The large number of LUVs in a sample cuvette can also be exploited, when leakage is monitored over time. This allows for the same distinction of transient or reoccurring leakage.^[99,142]

Release mechanisms can also be classified according to the number of pores or other leakage events affecting a given artificial vesicle.^[118,143] In all-or-none leakage, rare leakage events are distributed heterogeneously over the artificial vesicle population. While the entire dye has been released through these strong events from some vesicles, others are not affected at all. In contrast, many weak pores or defects need to occur much more often in an individual artificial vesicle to cause detectable leakage. These events are distributed homogeneously over all vesicles and cause gradual or graded leakage. In artificial model vesicles, this behavior can be distinguished indirectly by measuring the concentration of entrapped dye, for example. In all-or-none behavior, the dye that is still entrapped was not diluted, while in gradual leakage, the entrapped dye dilutes gradually. For determining this, the relation of the calcein concentration to the extent of its self-quenching and hence the fluorescence-lifetime can be exploited.^[60,118,144,145]

Furthermore, release mechanisms might involve additional effects such as membrane fusion of vesicles in models or intracellular endosomal vesicles in cells. For example, an interesting approach relies on the chelation property of calcein with divalent cations such as Co^{2+} or Cu^{2+} , which allows to investigate if calcein release occurs via the fusion of vesicles. Different vesicles are combined, some being loaded with EDTA (or divalent ions) and the others loaded with a mix of calcein and divalent ions (or calcein alone). Upon fusion of these vesicles, the fluorescence intensity increases (or decreases) due to the fluorescence (de)quenching.^[101,114,146] If transferred to endolysosomal vesicles, these methods could provide valuable information on the endosomal escape mechanism.

4. Calcein Release Studied within Cells

In Section 4, we revise calcein as a marker for studying endosomal escape. As a general procedure of all considered experiments, the dye (encapsulated or not) is first taken up by cells via endocytotic pathways. In this stage, a dotted pattern is often found in fluorescence microscopy since the fluorescence of the dye is often only partially quenched at the given concentrations. If appropriate experimental conditions are chosen with respect to calcein concentration, self-quenching in combination with the acidic pH is sufficient to reduce the fluorescence intensity of calcein in endosomes. In the next stage, i.e., with occurrence of an endosomal leakage event, calcein rapidly diffuses and dilutes into the neutral cytosol, which microscopically causes not only

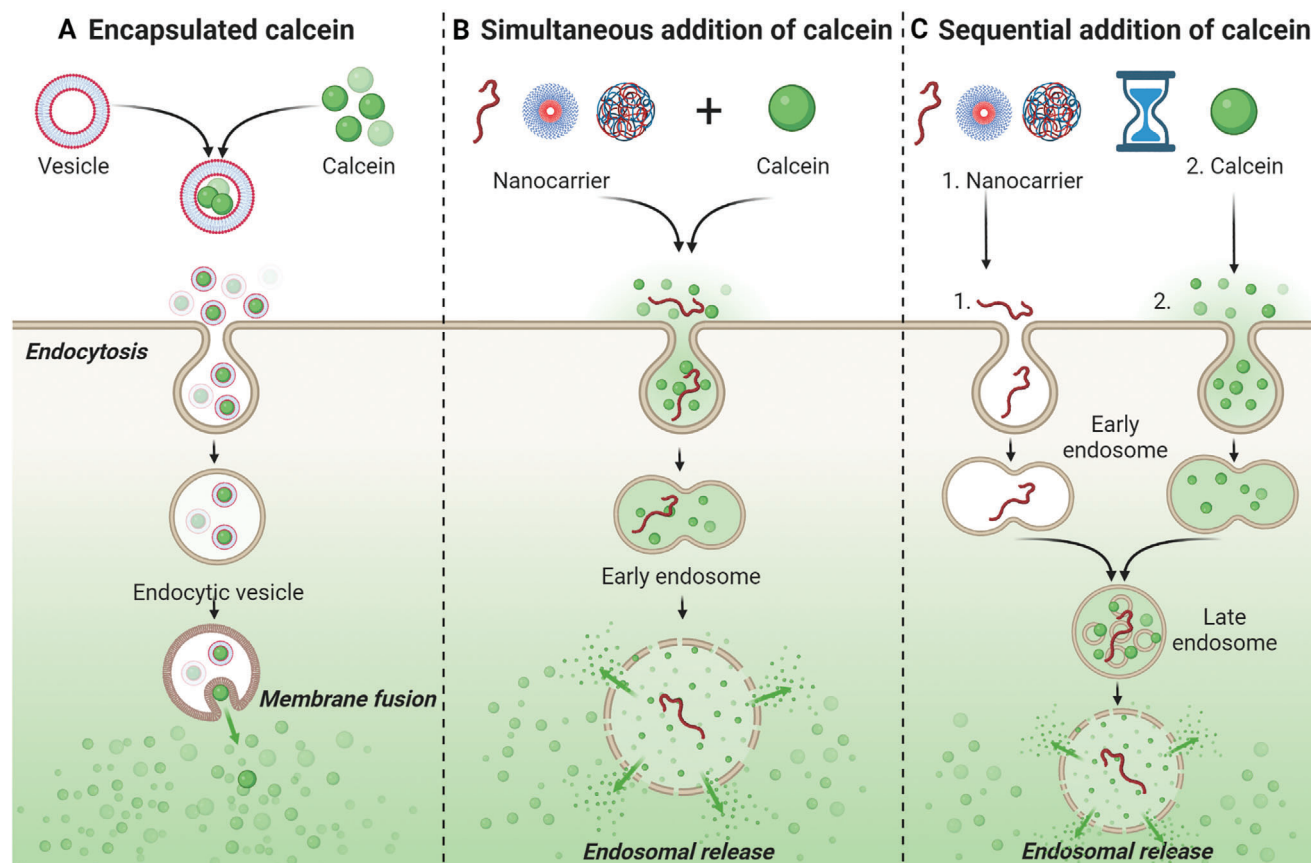


Figure 5. Types of calcein addition. The type of calcein addition is primarily determined by the type of nanocarrier (peptides/polymers, dendrimers, or nanoparticles). In the case of simultaneous addition, calcein can either be A) encapsulated in the nanostructure (often using self-quenching concentrations) or B) added to the cell culture medium at the same time as the agents. C) Sequential addition is also possible. In most cases, the cells are preincubated with the nanocarrier and calcein is added afterward.

a more diffuse fluorescent signal, but may also lead to a significant increase in intensity, if appropriate conditions are chosen initially.^[147]

In this way, calcein has been used to evaluate the endosomal escape efficiency of various nanocarriers. Thereby, the escape has been investigated in a range of different cell lines, with experimental settings varying in terms of media composition, calcein concentration, incubation time, type of calcein addition as well as cell analyses. The type of calcein addition can be categorized into encapsulated and nonencapsulated or simultaneous and sequential addition and is described in Section 4.1-4.2 (Figure 5).

4.1. Release of Encapsulated Calcein within Cells

In this approach, the investigated nanocarriers are able to encapsulate calcein at self-quenching concentrations within their hydrophilic interior. These nanostructures often consist of amphiphilic lipids forming liposomes similar to the model vesicles described above (Table 3). To facilitate drug delivery via endosomal release, modified lipids or lipids with advantageous properties are included, e.g., phosphatidylethanolamine (PE), cholesteryl hemisuccinate (CHEMS), or 1,2-dioleoyl-3-trimethylammonium propane (DOTAP).^[148–154] Thereby, ioniz-

able lipids can facilitate endosomal escape via membrane fusion due to the formation of nonbilayer structures (hexagonal H_{II} phase) with (naturally present) anionic phospholipids. Neutral fusogenic helper lipids such as unsaturated PE can further enhance the endosomal escape by their cone-like shape also favoring the membrane lysis via formation of nonlamellar intermediates.^[155–157] Furthermore, synthetic variants of liposomes, polymersomes, formed by amphiphilic block copolymers have been investigated regarding their endosomal escape.^[158–160] Combinations of lipids and polymers,^[161–163] peptides, and liposomes^[164] or completely different nanostructures, such as hollow capsules^[67] have also been studied.

In general, the incubation times varied within a wide range, from 10 min to 4 days which could be related to varying kinetics between the different nanocarriers regarding endocytosis, material-cell interactions and endosomal escape. Long incubation times, e.g., could be related to the incorporation of molecules, such as polyethylene glycol (PEG)-chains that shield the surface of the nanocarrier and may interfere with a fast and efficient endosomal escape.^[129,165]

The applied calcein concentrations in the nanostructures exhibited greater variation than those reported for the model liposomes, which may be attributed to the different preparation methods. Most of the polymer- and/or lipid-containing

Table 3. Investigation of calcein release from vesicles inside cells.

Nanocarrier	Polymers/lipids ^{a)}	Lipid composition mol%	Calcein concentr. ^{b)} mM	Cells ^{c)}	Incubation time	Analysis ^{d)}	Ref.
Liposome	PE:PHC, PC	8:2	60 (0.3)	L929 in PBS + 16 mM D-glucose	1.5 + 2 h	Quant.	[154]
	CHEMS:PE/PC	4:6	50	RAW264.7 in D10	1 h	Qual., stabil.	[148]
	CHEMS:PE:PEG:PC:Chol	21:43:6:30	40	HS578t in D10, HG	15 min	Qual., stabil., FC	[149]
	PEG-PE:PC:Chol	6:47:47				Qual., stabil., FC	
	CHEMS:PE (:PEG-PE/PC)	4:6 (:0.06)	80	Differentiated THP-1 in R10	4 h	Qual., stabil., FC	[150]
Polymersome	CHEMS:PE (:PEG-PE/PC/PS/PG)	4:6 (:0.3/6/4/4)				Qual., FC	[151]
	CHEMS:PE:PEG-PE/PEG-Hz-CHEMS:PC:Chol	2:4:0.5:2:2	80	Mia-Paca 2	1, 2 h	Qual.	[152]
	DOTAP:PEG-PE:PC:Chol	1:0.25:4.8:2.3	60	HeLa in D10, HG	4 h	Qual., stabil.	[153]
	DOTAP:PEG-PE:PC:Chol: PE	1:1.3:1.9:9.6:1.8				Qual., stabil.	
	PEG-SS-PPS	—	100	J774A in D10	10, 60, 120 min	Qual.	[158]
Polymer/lipid	PEG- <i>b</i> -PPS	—	200	mouse dendritic cells in D	6, 12, 24 h	qual.	[159]
	PEG- <i>b</i> -PPS	—	30	RAW264.7 in D	2 h	Qual., stabil.	[160]
	Suc-poly(glycidol) + PC	—	200	CV-1 in D10	3 h	Qual.	[161]
	PEOX-CHMC + Chol, PC	—	60	HeLa in D10	1, 4 h	Qual., stabil., FC, LC	[162]
	DOX-PLGA + DMAB + PC	—	0.008*	MCF-7, HL-60 in R	15, 60, 240 min	Qual., FC	[163]
Peptide/liposome	(GALA-His-Z _{HER2} -BNC + PC, Chol, PG	—	105	SKBR3 in R10	1 + 5–47 h	Qual.	[164]
Other	Gold NP + PSS, PAH	—	4.8**	MCF-7 in D10, HG	over night	Quant., LC	[67]
	Exosome coated MOF-NP	—	1**	HeLa in D	2, 3, 4 d	Quant. stabil., LC	[129]
	MSN-PVP-PEG	—	1**	HeLa or KB in D10-F12	18 h	Qual., LC	[165]

^{a)} Types of phospholipids by headgroup are mentioned. Fatty acids can be different, for PC and PE they were mostly dioleoyl or distearoyl. **BNC**—bio-nanoparticle, **CHEMS**—cholesterol hemisuccinate, **CHMC**—cholesterol hemisuccinate, **Chol**—cholesterol, **DMAB**—dimethyldidodecylammonium bromide, **DOTAP**—1,2-dioleoyl-3-trimethylammonium propane, **DOX**—doxorubicin, **H_z**—hydrozone, **MOF**—metal-organic framework, **MSN**—mesoporous silica nanoparticles, **NP**—nanoparticle, **PAH**—poly(allylamine), **PC**—phosphatidylcholine, **PE**—phosphatidylethanolamine, **PEG**—poly(ethylene glycol), **PEOX**—poly(2-ethyl-oxazoline), **PG**—phosphatidylglycerol, **PHC**—palmitoyl homocysteine, **PLGA**—poly(lactic-co-glycolic acid) **PPS**—poly(propylene sulfide), **PS**—phosphatidylserine, **PSS**—poly(styrenesulfonate), **PVP**—poly(2-vinylpyridine), **Suc**—succinylated. ^{b)} Gray shade indicates capsule preparation other than thin film rehydration or reverse phase evaporation. *—converted based on information from the original publications. **—concentration of capsule loading solution. ^{c)} D—DMEM, D10—DMEM + 10% FCS, F12—Ham's F12 medium, HG—high glucose (4.5 g L⁻¹), R—RPMI, R10—RPMI + 10% FCS. ^{d)} FC—flow cytometry, LC—loading capacity/encapsulation efficiency, qual.—qualitative microscopy, quant.—quantitative image analyses, stabil.—stability against changes in environment.

structures were assembled via the already mentioned thin film hydration^[148–154,158–162,164] usually resulting in high encapsulation efficiencies.^[94] Thus, the calcein concentration within the polymersomes/liposomes is assumed to be similar to that used to rehydrate the thin film. However, some vesicles were prepared by more complex procedures and the actual amount of calcein within the nanocapsules was determined afterward.^[67,129,165] Nevertheless, endosomal escape can still be detected with low (non-quenching) calcein concentrations as a change from a punctate fluorescence pattern to diffuse cytosolic fluorescence. Illes and co-workers described another interesting approach using metal-organic frameworks (MOF) to encapsulate calcein first in nanoparticles and then coating these with exosomal membranes derived from HeLa cells. This resulted in a strong shielding from the immune system and high calcein release from both, the exosome coated MOF and the endosome following 4 days of incubation in HeLa cells.^[129]

Moreover, high (quenching) calcein concentrations inside the nanocarrier can be used to determine the stability of the nanocarrier similar to the method for the calcein release from artificial liposomes, by changing the ambient conditions, such as temperature,^[148,149,153] serum content,^[148,153] or pH-value.^[129,149,150,162] In case of low calcein concentrations, also a calcein diffusion method (Franz cell diffusion) was used. The released calcein diffuses into a buffer without the nanocarrier which is separated by a dialysis membrane allowing for the discrimination between fluorescence originating from inside the nanocarrier and from released calcein in the solution.^[94,129] Therefore, encapsulating nanocarriers allow for both, a general investigation within the natural environment (cells), and a detailed investigation of one specific feature of the endosomal escape within only one approach (stability of the nanocarrier).

4.2. Simultaneous and Sequential Addition of Nanocarrier and Calcein as Sensor

The calcein assay is influenced by the nature of the nanocarriers and how it is performed, particularly with respect to the simultaneous presence and concentrations of the two substances (calcein and material) in the endosome. Calcein, as a small molecule, is rapidly taken up by cells, while nanocarriers may take longer to accumulate in the endosome, depending on their size and charge. Often, the nanocarrier and calcein are added simultaneously to the cells (Table 4), without mixing the two components beforehand.

Cationic polymers are often considered as synthetic gene transporters and nanocarriers to facilitate endosomal escape. The most studied polymeric gene transporters include PEI and poly(2-(dimethylamino)-ethylmethacrylate (PDMAEMA), whose endosomal release has also been investigated in several studies with calcein. PEI represents the commercial gold standard and is particularly interesting for the study of calcein release not only because of the controversial proton-sponge hypothesis. Bonner et al. tested different PEI architectures (crosslinked, linear, branched) and found endosomal escape in 75% of cells using the calcein assay if a crosslinked PEI variant was applied, which showed no toxic effects at this concentration and incubation time.^[173] Vermeulen et al. investigated the endosomal escape

mechanism of linear PEI (JetPEI) and performed the calcein release assay in cell lines differing in endosomal size. They conclude that endosomal release can be promoted by smaller endosomes and an undisturbed buildup of osmotic potential. (Table 5).^[111] Another well-known polymer is PDMAEMA as it is easily applied for a variety of nanocarriers and enables endosomal release of calcein.^[169,175] This was demonstrated in fibroblasts and dendritic cells with different nanoparticle compositions, where calcein was added sequentially (after treatment with the polymer) or simultaneously with the polymer.^[178,185–188] By inhibiting endosomal escape with bafilomycin A1, Wong et al. showed that acidification of the endosomes is crucial for release of calcein.^[188] However, the large number of studies on vinyl polymers such as PDMAEMA do not yield clear correlations, which can also be attributed to the different investigation methods. Therefore, no final conclusion can be drawn about the release mechanism.

Due to its wide application and good availability, it is not surprising that different calcein concentrations and incubation times were used to study the endosomal escape of nanocarriers (Figure 6). Concentrations from 10 μM to 3.21 mM were reported to study systems codelivering calcein,^[167,170,191] with the majority of studies applying concentrations between 161 and 322 μM .^[168,173,177–186,190,192]

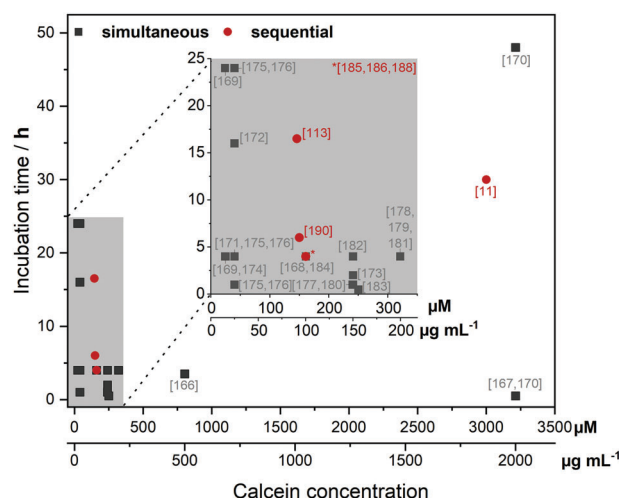
Using a calcein concentration of 161 μM , Deshpande et al. have shown that poly(*N*-isopropylacrylamide nanogels with poly- ϵ -lysine can release calcein in cervical cancer cells.^[168] Similar concentrations were used to study nanoparticles with hydrophobic components. Su and co-workers showed that pH-responsive polyaminoester nanoparticles with lipid shells induce highly efficient endosomal escape in dendritic cells at a calcein concentration of 240 μM .^[180] Wannasari and colleagues were able to induce a poly(lauryl methacrylate-co-methacrylic acid)-mediated calcein release in three different colorectal adenocarcinoma cell lines using a calcein concentration of 322 μM .^[181] Calcein concentrations in a similar range have also been shown to be useful for studying CPPs.^[184] As an example, Salomone and colleagues showed that a fusion peptide from the arginine-rich TAT motif with additional residues of cecropin-A and melittin can efficiently release calcein within 30 min with a calcein concentration of 250 μM .^[183] However, endosomal escape could also be detected with significantly lower calcein doses of 40 μM or less. In HEK cells, calcein release was detectable with concentrations $\leq 40 \mu\text{M}$ applying differently structured polyvinyl polymers and culture conditions.^[169,171,175,176] Calcein concentrations in this lower range were also successfully used in leukemia cells and human prostate cancer cells to show escape induced by polyamidoamides and a PDMAEMA-containing micelle.^[174,175] Jones et al. showed that PAA (poly(2-alkylacrylic acid) can deliver calcein to the cytosol by disrupting endosomes.^[167] For this purpose, they coin-cubated human myelomonocytic cells in complete medium with the polymers and calcein concentration of 3.21 mM for 30 min. In contrast to this, Ren et al. investigated receptor-mediated endosomal escape in human lymphoblastic leukemia cells in serum-containing medium by incubating the cells with 25 μM calcein for 6 h.^[193] As can be seen from the experimental set-up in these two studies, the calcein concentration and incubation time for efficient release detection are mutually dependent. The two studies also differed in the type of microscopy conducted (confocal or

Table 4. Investigation of calcein release with simultaneous addition of vector and calcein in vitro.

Type of carrier ^{a)}	Nanocarrier ^{b)}	Delivery of ^{c)}	Cell line	Calcein concentr. μM	Incubation conditions	Analysis ^{d)}	Ref.
Oligomers Linear polymers	Oligo(ethanamine) amides	pDNA	DUI45	803	Growth medium + 10% serum, 3.5 h	Quant.	[166]
	Poly(2-alkylacrylic acid)s	pDNA	U937 (Jurkat)	3214	Growth medium + 5% serum, 30 min	Quant. + FC	[167]
	Poly(N-isopropylacrylamide)	siRNA	Hela, MG-63	161	Growth medium + 10% serum, 4 h	Quant.	[168]
	Poly(aminoethyl-methacrylate)s	pDNA	HEK	25	Opti-MEM, 4 or 4 + 20 h	Quant.	[169]
	PDMAEMA	—	U937, (Jurkat)	3214	Growth medium + 5% serum, 30 min, 48 h	Quant.	[170]
Dendritic polymers Micelles	Polyacrylamides, I-PEI	pDNA	HEK 293T	40	Growth medium + 10% serum + HEPES, Opti-MEM, 4 h	FC	[171]
	Polypiperazines, I-PEI	Dextran, BSA, RNase A, EGFP	HEK 293T	40	Opti-MEM, 16 h	Quant. + kinetics, FC	[172]
	(crosslinked) PEI	pDNA	KB	241	Opti-MEM, 2 h	Quant.	[173]
	Poly(amidoamine)	pDNA	DUI45	25	Opti-MEM, 4 h	Quant.	[174]
	PDMAEMA-containing shell, PEI	pDNA	HEK 293T, K562	40	Growth medium + 10% serum + HEPES, 1, 4, 24 h	FC	[175]
Nanoparticles	PDMAEMA-containing shell, I-PEI	pDNA	HEK 293T	40	Growth medium + 10% serum + HEPES, 1, 4, 24 h	Quant.	[176]
	Core: PDEAMA, shell: poly(aminomethyl-methacrylate)	Proteins	Dendritic cells	241	Growth medium + 10% serum, 1 h	Quant.	[177]
	PLCA/PDMAEMA-co-PAA-BMA blend particles	—	DC2.4	321	Growth medium + 10% serum + HEPES, 4 h	Fixed, qual.	[178]
	Polyaminoester particles with lipid shell	Dextran mRNA	DC2.4	240	Growth medium + 10% serum + HEPES, 1 h	Fixed, quant.	[179]
	Graft of poly(lauryl methacrylate-co-methacrylic acid) on acetylated dextran	—	CT-26	321	Growth medium (+ 10% serum), 1 + 3 h	Qual., FC	[180]
CPPs	Org./inorg. Nanoparticles with poly(phenol tannic acid) and metal ions	—	MDA-MB-231	241	Growth medium + 10% serum, 4 h	LTR, qual.	[181]
	Arginine-rich TAT with residues of cecropin-A and melittin	EGFP-TAT fusion protein, dextran, pDNA	Hela, CHO-K1, HUVEC	250	According to cell manufacturer's instructions, 30 min	Baf, qual.	[182]
	Poly(acrylamide-co-methacrylic acid) nanogels with peptides	NPs	SW-48	161	Growth medium + 2% serum, 4 h	Quant. + kinetics, FC with threshold	[183]
	—	—	—	—	—	Quant.	[184]
	—	—	—	—	—	Quant.	[185]

^{a)} **CPPs**—cell-penetrating peptides. ^{b)} **BMA**—butylmethacrylate, **PAA**—2-propylacrylic acid, **PDEAEMA**—poly[2-(diethylamino)ethyl methacrylate], **PDMAEMA**—poly[2-(dimethylamino)-ethylmethacrylate], **PEI**—poly(ethyleneimine), **PLGA**—poly(lactic-co-glycolic acid), **RNase A**—ribo-nuclease A, **TAT**—trans-activator of transcription, ^{c)} **BSA**—bovine serum albumin, **EGFP**—enhanced green fluorescent protein, **mRNA**—messenger RNA, **NPs**—nanoparticles, **PDNA**—plasmid DNA, **siRNA**—small interfering RNA, **TAT**—trans-activator of transcription. ^{d)} **baf**—bafilomycin-A1, **FC**—flow cytometry, **LTR**—LysoTracker Red, **Qual.**—qualitative microscopy, **Quant.**—quantitative image analyses.

Type of carrier	Nanocarrier ^{a)}	Delivery of ^{b)}	Cell line	Calcein concentr. μM	Incubation conditions	Analysis ^{c)}	Ref.
Linear polymers	JetPEI	pDNA	Hela, ARPE-19, A549, H1299	3000	Growth medium + 10% serum, 15 + 15 min	Quant. + FC	[11]
Nanoparticles	PDMAEMA- <i>b</i> -PEG	—	3T3 MEFs WT	161	Growth medium + 10% serum, 2 + 2 h	Quant.	[188]
	PEG- <i>b</i> -PDEAEMA	Ovalbumin	NIH/3T3	161	Growth medium + 10% serum, 2 + 2 h	Quant.	[185, 186]
Peptides	Crosslinked PLGA/PEI particles	BSA, SOD	NIH-3T3	50 μg/dish	Growth medium + 10% serum, 2 h + 30 min	Qual.	[189]
	Cytotransmab, TAT	—	Hela	150	Serum-free medium, 4 + 2 h	Inhibitors, fixated, quant.	[190]
	Polymer/cyclic peptide conjugate	—	HEK 293	146	Growth medium + 10% serum, 16 h + 30 min	Quant.	[113]



Overall, a successful endosomal escape can be detected with different assay parameters optimized for each investigated carrier material, medium, and cell type (Figure 6). The broad varieties in these settings hardly allow to derive any specific trends from the yet given set of experiments found in literature. Indeed, our screening of literature reported data further raised the question, whether significantly different experimental procedures to studying endosomal release efficiency may even lead to different conclusions for similar systems. In this regard, we also like to refer to Section 5 and our final conclusions at this point.

The analysis of the calcein release assay can be performed in a variety of ways, depending on the problem to be addressed. The requirements for the analysis of the assay vary from attention to detail (accurate spatial and/or temporal resolution of the intracellular signal) to statistical significance of the data. To address the diverse requirements, the different analytical methods and their applications and limitations are discussed in the following (Figure 7).

In most studies, confocal microscopy has been shown to be a very powerful tool, even more useful than epifluorescence microscopy as the subcellular distribution of calcein can be elucidated.^[169] For this purpose, also z-stacks can be prepared.^[168,178,179] Primarily, live cell microscopy is used, also allowing kinetic studies.^[172,183] Less commonly, cells are studied after fixation.^[178,190] Fixation with subsequent permeabilization may complicate the interpretation of the calcein assay due to false positive results as a result of fixation artifacts. Besides, the subcellular distribution and fluorescence intensity of the calcein signal have been analyzed quantitatively.^[67,129,154,168,173,174,177,188]

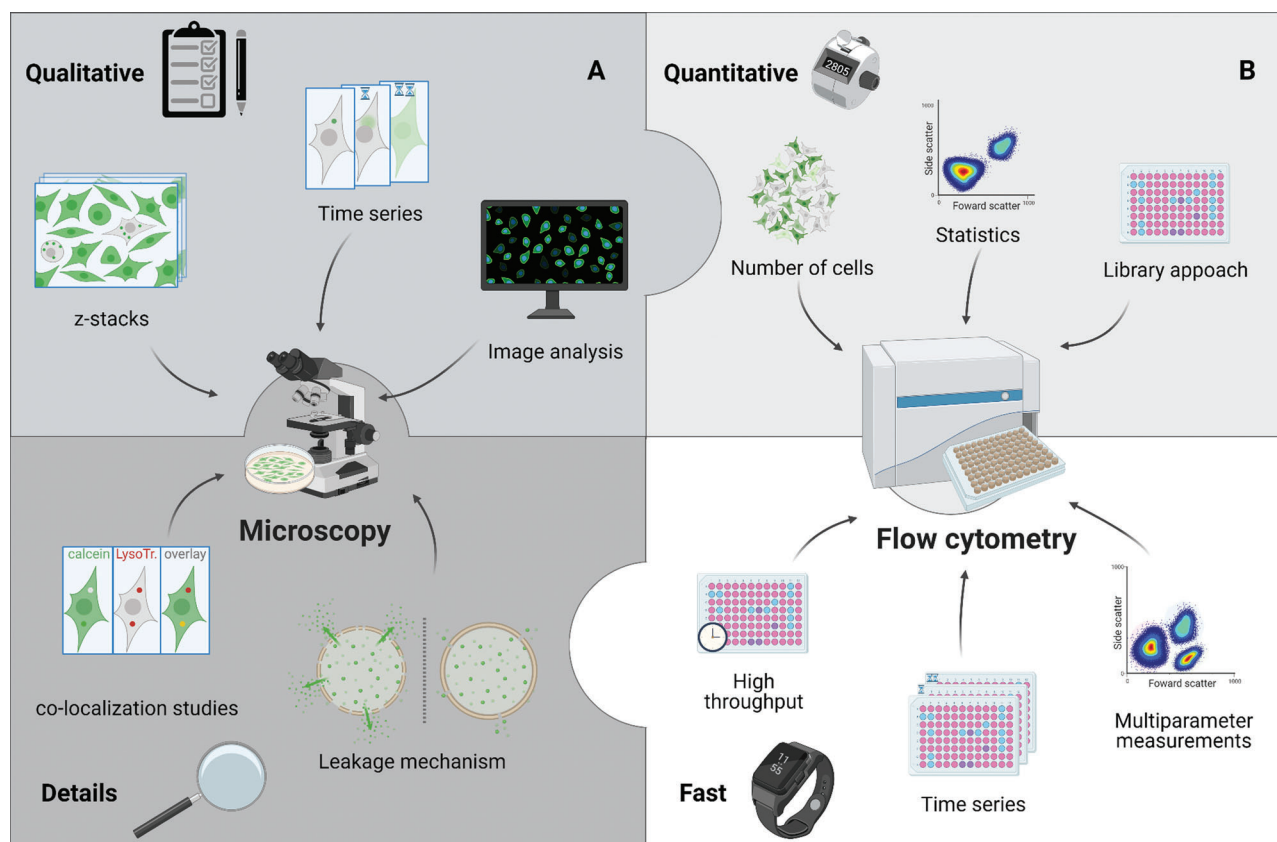


Figure 7. Analysis techniques of the calcein release assay. The predominant analytical technique for the calcein release assay is microscopy, as it provides spatial (and in the case of live cell microscopy, temporal) resolution of the fluorescence signal. The primarily qualitative conclusions can also be supplemented by statistically more robust conclusions through the use of image analysis techniques. For rapid quantitative measurements, flow cytometry can also be used to increase the statistical power of the data.

It is possible to count the cells with punctate and diffused calcein signal manually,^[185,186] but a more effective approach relies on the use of various image analysis software, where regions of interest and/or thresholds are defined for an automated analysis.^[166,169,170] The acquisition of many cells, e.g., with the help of montages, is also desirable for statistical significance. Colocalization studies with acidic compartments by acidotropic dyes can be conducted and may provide further information about the efficacy of calcein release, with lower colocalization indicating more efficient escape.^[179] The Manders' coefficient is mainly used for this purpose. It quantifies the degree of colocalization between two fluorophores based on their absolute intensities within a pixel and is rather sensitive to background changes.^[194,195] It should further be kept in mind that these dyes or also the investigated nanocarriers are usually weak bases increasing the pH value in endolysosomal compartments following longer incubation times which could alter the endosomal escape or the colocalization behavior. Furthermore, the fluorescence of calcein can be quenched at very low pH values inside the lysosome. Another very interesting approach was shown by Connor and Huang already in 1985 who established a calibration curve of calcein using a microscope photometer so that the cytosolic concentration of calcein within L929 cells was quantified.^[154]

Furthermore, high-throughput methods based on flow cytometry are also used to quantify the calcein release, with higher cellular fluorescence intensities generally indicating released calcein compared to control cells with punctuate fluorescence.^[11,149–151,162,163,171,175,183] Again, appropriate thresholds must be defined for the fluorescence intensity of escape-positive cells. Microscopic and flow cytometric methods can also be combined, which provides more robust insights about endosomal escape.^[167,183] Because microscopic studies allow spatial (and in the case of live cell microscopy, temporal) resolution of the calcein signal, release events can be measured unambiguously, with varying degrees of attention to detail. Microscopy is still the most commonly used technique but is comparatively time consuming and can only provide statistical information if a large number of cells are analyzed. For statistically robust results, flow cytometry is a faster complementary method, but it cannot spatially resolve the calcein signal within a cell. For fast statistically robust results, flow cytometry is a complementary method, but it cannot spatially resolve the calcein signal within a cell. In the best case, both methods are used in a complementary manner to provide a detailed picture of any potential escape. Although, both analytical techniques ideally coincide in the number of escape-positive cells in order to provide reliable results, deviations nevertheless might occur for example due to the applied thresholding.^[172]

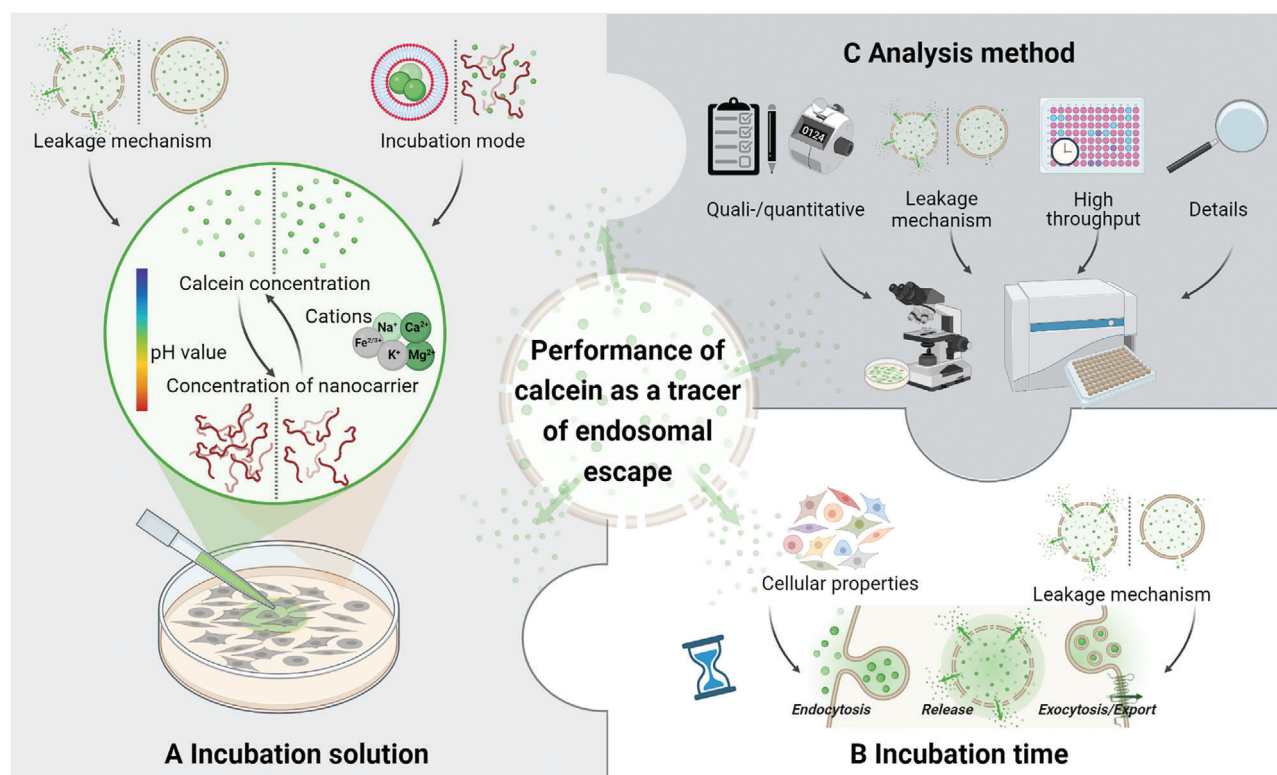


Figure 8. Factors determining the performance of the calcein release assay within cells. When planning the parameters of the assay, i.e., incubation solution, incubation time, and analysis method, the influence of different factors needs to be considered, e.g., the leakage mechanism of the nanocarrier, the incubation mode, cellular properties, and the requirements of the desired readout.

5. Potential Pitfalls of the Calcein Release Assay in Cells

Calcein has been extensively used to investigate endosomal escape of various types of nanocarriers within cells. However, the performed methods show differences in several aspects which demonstrates the complexity as well as the robustness of the assay. In general, it can be concluded that the performance of calcein as an indicator for endosomal escape depends on three main parameters which should be considered when planning a calcein release assay and will be discussed in this section: i) incubation solution, ii) incubation time, and iii) the analysis method (Figure 8). Regarding the calcein leakage assay with model vesicles, experimental parameters affecting liposomal leakiness have recently been reviewed elsewhere, e.g.,^[94,117] and are therefore not considered further.

5.1. Physicochemical Factors Relevant for the Calcein Solution

As described before, three main factors influence the calcein fluorescence and should therefore be considered when thinking about the composition of the calcein solution: pH value, calcein concentration and the presence of cations (Figure 8A). However, the pH value is only of interest for the preparation of the calcein stock solution due to the pH dependent solubility of calcein.

Since the calcein release assay is based on the change in the fluorescence pattern upon endosomal escape (punctate endolysosomal to diffuse cytosolic) which also leads to an increase in the

fluorescence intensity within the cytosol, the calcein concentration is of major importance. A wide range of calcein concentrations has been applied by different research groups, demonstrating the robustness of the calcein release assay. The applied concentrations can roughly be related to the incubation mode of calcein, either encapsulated (self-quenching concentrations) or in simultaneous or sequential incubation with the nanocarrier (<3.5 mM calcein). Higher (self-quenching) concentrations could lead to an increase in the fluorescence intensity difference between endolysosome and cytosol and, hence, an easier detection of endosomal escape. However, dequenching of calcein upon endosomal escape (i.e., nonfluorescent endosomes indicative of quenched calcein fluorescence before the release) has only been observed in one study applying 146 μ M calcein.^[113] In the other studies, mostly diffusion of calcein into the cytosol rather than dequenching was measured. Only in the case of calcein encapsulated at self-quenching concentrations into the nanocarriers, at least a dequenching of calcein released from the nanocarrier within the endolysosomes could be assumed. Nevertheless, higher concentrations of the small molecule calcein can also increase the osmotic pressure inside the endolysosomes promoting endosomal escape of materials using proton sponge mechanisms which might not occur otherwise.^[37] Controls comprising treatment with high concentrations of calcein alone, or high calcein concentrations plus a nonreleasing substance equimolar to the investigated nanocarrier could help preventing false positive results. Furthermore, the chelation of calcium ions at high calcein concentrations could be problematic for the cells. To increase the

difference in the fluorescence intensity between endolysosomes and cytosol, also other factors can be adjusted such as the incubation time of calcein (shorter, subsequent to the nanocarrier) or the measurement settings in microscopy (optimal for the bright cytosolic fluorescence).

When choosing calcein concentrations for in vitro investigations, also the mode of calcein release by the nanocarrier is of importance. Although the reviewed studies often addressed the calcein release but not the mechanism so far, the results can again be influenced by the concentration of the nanocarrier. As an example, the combination of a nanocarrier gradually releasing calcein with too low concentrations of calcein could lead to the observation of no calcein leakage, which would be different at higher calcein concentrations. Therefore, a concentration-dependent calcein release could enable the investigation of gradual calcein release and may provide insights into the endosomal escape mechanism. Moreover, also time-resolved measurements at short intervals using microscopy can indicate the mode of calcein release (transient/continuous, gradual/burst) which has been shown already, e.g., with photoactivatable nanocarriers.^[67,160,165] For this type of nanocarriers it is rather easy due to the rough determination of the release time point by the time of photoactivation, whereas for other nanocarriers some luck is required to image the right cell in the right moment. Nevertheless, we think this effort might improve the assay and provide further mechanistic insights.

Regarding the presence of cations, it should be considered that these may interact differently with calcein at various pH values and concentrations, very well illustrating the mutual dependence of these factors. Although the influence of different ions on the calcein fluorescence was already the topic of the earliest calcein studies, the conditions present in the calcein release assay to study endosomal escape inside cells can be more complex making it difficult to draw conclusions. A calibration curve of calcein in the respective buffer composition and/or cell culture medium as well as the inclusion of a corresponding control without the nanocarrier can help in visualizing the influence of ions in the applied buffers or cell culture media. Since nanocarriers for gene delivery are often cationic, they could interact with the calcein also electrostatically and influence its fluorescence intensity. This fact should further be considered for the design of the experiments, in particular regarding either a premixing of nanocarrier and calcein or their sequential addition. However, studies on potential interactions are seldom reported and the different addition modes of calcein and nanocarrier are rarely compared within a publication.

5.2. Biological Factors Relevant for the Incubation Time

Consideration of various parameters is particularly relevant when choosing the incubation time (Figure 8B). On the one hand, the uptake of the nanocarrier into the cell matters. On the other hand, the intracellular fate of the applied calcein should also be regarded, in particular if longer incubation times are studied. To visualize endosomal escape, calcein and the nanocarrier have to be present in the same compartment. Hu et al. examined this factor in their study and were able to verify the importance of the simultaneous presence of calcein and the delivering core-shell par-

ticles within the endolysosome for the investigated system. When calcein and the core-shell particles were added simultaneously, endosomal escape was successfully reported by calcein release. However, when the cells were first treated with calcein and then, after a washing step, the release particles were added, no endosomal escape was observed, but might have occurred unnoticed,^[187] suggesting a rapid transport of calcein into, though, and out of the cell.

Since there is no evidence that calcein is metabolized within cells, conclusions about the intracellular fate of calcein might be drawn based on the fluorescence and its temporal and spatial changes. Thus, a punctate fluorescence pattern within cells incubated with calcein alone indicates an endocytotic uptake mechanism (Figure 9A). With regard to the calcein release assay, it should be considered that different cell types can exhibit different endocytosis rates for different (macro)molecules,^[196,197] and might therefore require different incubation times to take up similar amounts of calcein or the nanocarrier. Although the details of endocytosis in different cell lines were not investigated for calcein so far, they have been shown for different nanocarriers.^[11,175,198,199] Considering more quantitative measurements (flow cytometry), the normalization of the calcein release induced by any nanocarrier to a control sample (cells treated with calcein only) can be used to attenuate cell type dependent endocytosis rates of calcein.^[11,171,172,175] In addition to the different endocytosis rates of the nanocarrier, the nanocarrier itself can have an impact on the endocytosis rate of calcein which is however not as easy to determine and therefore difficult to take into account. Nevertheless, one way to compensate for at least different endocytosis rates of the various nanocarriers is to report the calcein release in relation to the uptake of the nanocarrier.^[150,151,172,176]

Interestingly, a decrease of the overall calcein fluorescence intensity in the cytosol was observed upon increasing incubation times with different polymers and cell lines.^[169,175] Such observations hint toward a calcein excretion mechanism from the cytosol (Figure 9B). Since calcein AM is intracellularly converted into calcein upon esterase activity in viable cells, conclusions can be drawn from studies with multidrug resistant (MDR) cells and calcein AM. In these studies, calcein has been shown to be ATP-dependently exported from the cytosol by the multidrug resistance protein (MRP) belonging to the ATP binding cassette transport proteins,^[200,201] whereas the calcein AM itself has been shown to be exported via the multidrug transporter 1 (MDR1) encoded P-glycoprotein.^[202,203] Furthermore, cytosolic calcein can be exported within exosomes, microvesicles, or via gap junctions to other cells, which can be derived from studies utilizing calcein AM as a tracking label, e.g., for extracellular vesicles derived from calcein AM loaded cells.^[204–206] Regarding the calcein efflux via gap junctions, a cell type dependency was observed when measuring the inward diffusion of calcein within spheroids of different cell lines which were preloaded with calcein AM.^[207] The influence of the cell type on calcein efflux was further demonstrated using different prostate cancer cells and bone marrow endothelial cells. The results revealed a halving of intracellular calcein fluorescence already 6 h after calcein AM loading of the cells.^[208]

Additionally, the calcein which is not released from endolysosomes can be expected to either end up in the lysosome, where its fluorescence might for example be quenched due to the

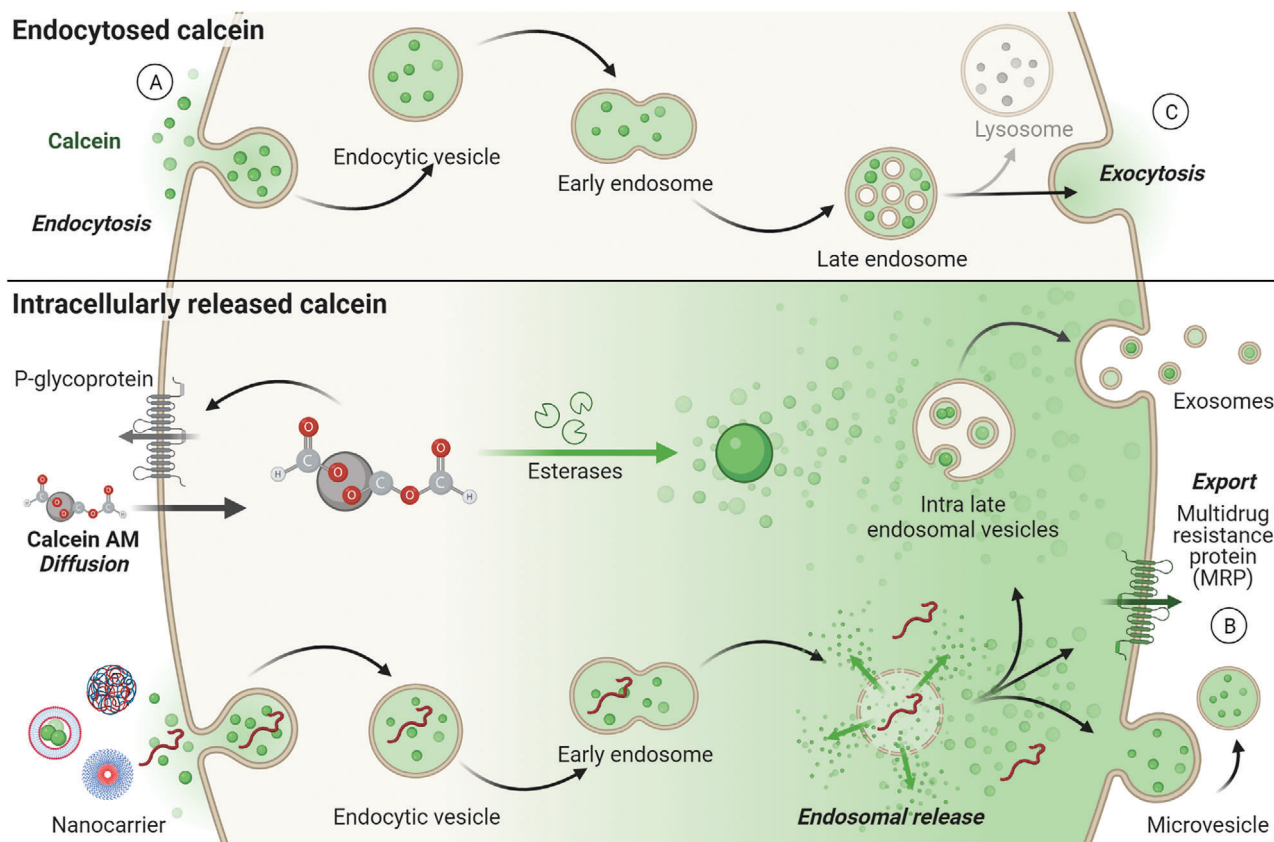


Figure 9. Intracellular pathways of calcein. A) Punctate fluorescence patterns within cells point toward an endocytotic uptake mechanism of calcein. B) Cytosolic/released calcein can be exported via the multidrug resistance protein, within microvesicles as shown in studies of cells loaded with calcein AM or in exosomes via the uptake into intra late endosomal vesicles. C) Regarding the excretion of endocytosed calcein, exocytosis is a hypothesis for calcein not released from endolysosomes. Adapted from “Endocytic Pathway Comparison (Layout)” and “Endocytic Pathway with Macropinocytosis and Phagocytosis” (2022) by BioRender.com. Retrieved from <https://app.biorender.com/biorender-templates>.

decreased pH value, or to be exported via exocytosis, since cells are known to dispose redundant, nondigestible molecules (Figure 9C).^[127] Over time, this can also lead to a decreased intracellular calcein concentration ready to be released from endosomes which in turn can vary between different cell types. However, the accuracy of this assumption remains an open question, since the intracellular pathway of calcein, more importantly its kinetics and cell line dependencies, have not been investigated in detail so far. Nevertheless, this information could provide more insights into the calcein release assay including hints on how the assay should be planned and should therefore be thoroughly investigated.

A delayed addition of calcein (sequential incubation) might circumvent potential interferences of excretion mechanisms with nanocarriers requiring longer incubation times due to low endocytosis rates,^[113] which could possibly result in misleading conclusions. If calcein is initially encapsulated within the nanocarrier (e.g., in liposomes), at least the degradation and/or exocytosis of calcein seem to be of limited importance, as the nanocarrier might disturb the endolysosomal maturation process and might protect the encapsulated calcein. Hence, the incubation time mainly depends on the time required for the nanocarrier to escape the endolysosome. In some studies, calcein release was observed following four days of incubation,^[129] or even following

incubation with the nanocarrier encapsulating calcein for 1 h and medium for further 47 h.^[164] This points toward slow uptake or endosomal escape kinetics.

All in all, the incubation time should be chosen long enough to allow i) a sufficient amount of calcein and nanocarrier inside the endolysosomes and ii) intracellular fusion of the organelles along the endolysosomal pathway, in case calcein and the nanocarrier were taken up by different organelles. In case of nanocarriers encapsulating calcein, the incubation time only has to be adapted to the former one. For comparison purposes, not only the uptake and excretion rates of calcein and the nanocarrier should be considered, but also the differences between cell types.

5.3. Factors Influencing the Accuracy of the Measurement

As described in the preceding section, different analytical methods have been utilized to characterize the calcein release within cells qualitatively or even quantitatively with different degrees of detail. When deciding which method to perform, (confocal) microscopy is preferred, due to a straightforward (and more reliable) discrimination of endocytosed and released calcein. Continuous advancement in technology allows images to also be quantified and processed using high-throughput analysis. Moreover, kinetic

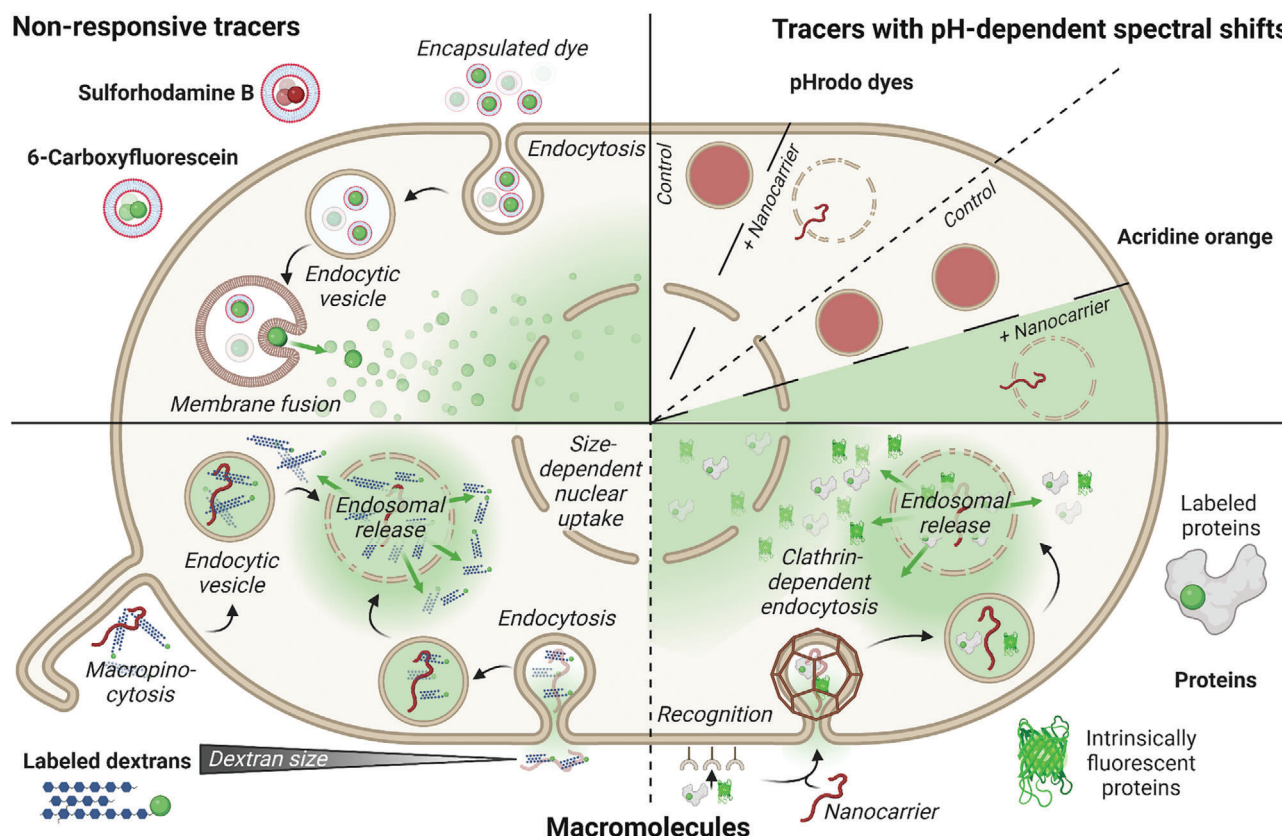


Figure 10. Complementary methods to the calcein release assay. In addition to calcein, other tracers, such as sulforhodamine B or 6-carboxyfluorescein can be encapsulated in vesicles to determine their release capabilities in cells. Tracers with pH-dependent spectral shifts, such as pHrodo or acridine orange can also be of interest, as they indicate the pH in their environment through changes in fluorescence. Besides small molecules, macromolecules such as dextrans or proteins are intriguing, as their size and complexity provide additional information about the escape.

investigations can be performed, which can lead to conclusions regarding the escape mechanism. Nevertheless, flow cytometry is the method of choice if more reliable statistics (fast analysis of >10 000 cells possible) are required, which would still be very tedious using confocal microscopy even if advanced image analysis software is used. However, there are certain pitfalls to be aware of and, in some cases, it should be considered more as a screening method that requires verification by microscopy. The latter becomes particularly important if the nanocarrier might alter the endocytosis rate of the cells leading to variations in fluorescence intensity within the endosomes, but not the cytosol. As only the overall fluorescence intensity per cell is detected in flow cytometry, this analysis alone would result in a false positive outcome compared to a control without the nanocarrier. On the contrary, a nanocarrier which induces only limited calcein release from endosomes can also hardly be detected but could suffice for transfection in the actual application. Therefore, it would lead to a false negative result due to the limited overall increase of fluorescence intensity within the cytosol which is overlaid by that of the endosomes. This issue has to be kept in mind in microscopy as well. In particular, acquisition settings which are optimized for the rather bright endosomes might not allow an identification of a graded or weak release. In general, it is advisable to combine several methods for determining calcein release, to enable quantitative as well as qualitative analysis.

6. Complementary Methods

The calcein release assay is a model for studying the release of cargo from nanocarriers. However, the carriers are loaded with different drug molecules that may have properties other than calcein, such as size, charge, and hydrophilicity. Therefore, the release of calcein from endosomes may not reflect the drug delivery potential of the nanocarrier. Ultimately, the calcein release experiment should be complemented by studies on the release of other model substances and drug molecules (Figure 10). In these cases, release from the carrier and endosomal permeabilization should also allow passage and release into the cytosol.

Besides calcein, other dyes are frequently used for dequenching assays in artificial vesicles, such as 6-carboxyfluorescein and sulforhodamine B. The recent review by Nasr and colleagues provides information on the use of these fluorophores for the study of liposomal membrane integrity.^[94] These dyes are also inexpensive and easily accessible but have drawbacks as well. For example, the fluorescence of 6-carboxyfluorescein is strongly pH-dependent in the physiologically interesting pH range from the extracellular space to early endosome, whereas calcein is less sensitive in this regard.^[58,94,209] Although the fluorescence intensity of sulforhodamine B is entirely pH-independent in the physiological relevant pH range,^[210] its higher self-quenching concentration is rather disadvantageous.

The review by Martens et al. provides more information on other methods for studying endosomal escape in cells, as well as an overview of escape mechanisms.^[37,96] This section focuses on methods that can be used complementary and provides comparisons to the calcein release assay. Sulforhodamine B can also be used inside cells as calcein analog to study endosomal escape.^[210] However, it has been suggested that sulforhodamine B distributes less rapidly within the cell than calcein,^[67] which may delay accurate timing of the endosomal escape event and could be disadvantageous in live cell microscopy.

In addition to the above mentioned chromophores, more specific indicators can be used which change their fluorescence in dependence of pH and, thus, provide further insight into the endosomal escape process.^[5] Both, dyes that are quenched in a pH-dependent manner and those that shift in their excitation/emission wavelength are of interest. An interesting example are the commercially available, pH-sensitive pHrodo dyes (rhodamine derivatives), which show little to no fluorescent signal at neutral pH but are highly fluorescent in acidic environments.^[211,212] These properties render the uncharged, membrane-permeable dyes ideal candidates for use as pH indicators in endosomal escape investigations when covalently bound to an endocytosed macromolecule. Consequently, a limited or impeded acidification of endosomes can be monitored by the absence of fluorescence in comparison to a control experiment, which allows to evaluate for example the pore formation in treatment with a nanocarrier by microscopy or cytometry.^[113] Another interesting alternative is the membrane-penetrating, acidotropic, and metachromatic dye acridine orange. When cells are treated with acridine orange, the dye penetrates the membrane and distributes within the cell entering also any present endolysosomes. In the acidic endosomal milieu, acridine orange becomes protonated and is then no longer able to penetrate the cell membranes, which eventually leads to an accumulation in lysosomes. At the resulting higher concentrations in the lysosomes, acridine orange forms red fluorescent dimers, trimers, and oligomers,^[213] which can be observed as red fluorescence, if the endo/lysosomes remain intact. Release of protonated acridine orange, e.g., by permeabilization of endosomes in the presence of any nanocarrier, results in deprotonation of the dye in the cytosol and thus in strong green cytosolic fluorescence of the homogeneously distributed monomer, which can be analyzed microscopically or by flow cytometry.^[167,214] The strong concentration-dependent difference in the spectra of the dye, therefore, allows a clear distinction between cytosolic and endosomal fluorescence, i.e., differentiation between uptake and endosomal escape. To remove diffusing acridine orange, cells must be washed thoroughly both immediately after addition of acridine orange as well as before each analysis. It represents an elegant method in addition to investigations with calcein. However, acidotropic dyes such as LysoTracker or acridine orange might delay the lowering of pH in the endosome because they accumulate to high concentrations in acidic endosomes where they scavenge protons. Depending on the basicity of the nanocarriers relative to the acidotropic dyes used, protonation of the nanocarriers may also be delayed.

All complementary methods for calcein release discussed so far provide information on the occurrence of small pores, because of the size of the marker dye. However, in the evaluation of nanocarriers for biomedical applications, it is also of interest

if larger compounds or macromolecules can be released. Thus, other methods can be combined with the release of the small molecule calcein to evaluate the escape mechanism and delivery efficiency of a drug regarding biomedical applications. Calcein release is frequently studied in the context of nucleic acid transfection with cationic polymers. Often, calcein escape efficiency is correlated with pDNA transfection, independent of the used nanocarrier.^[166,169,171,173–175] However, this correlation does not hold true in all cases. For example, Vermeulen and coworkers investigated the endosomal escape mechanism of JetPEI polyplexes, a linear PEI derivative,^[11] and tried to correlate the release of calcein or labeled oligonucleotide according to a previously published procedure with the transfection efficiency.^[6] Interestingly, a calcein release was observed in far more cells than the transfection and therefore does not correlate well, but the oligonucleotide release appeared to be a more reliable indicator for efficient transfection. The authors conclude that endosomal leakiness for small molecules can be induced by membrane destabilization due to the interaction with cationic polyplexes, hindering an effective buildup of osmotic pressure due to ion flux across this disturbed membrane and thus preventing the endosomal burst and escape of any macromolecules. Thus, investigations of calcein release may provide further indications about the mechanism of endosomal escape in addition to its efficacy.

If calcein release is studied in comparison to the escape of macromolecules of different sizes, a conclusion can be drawn about the size of the membrane defect that has occurred. For such studies, polysaccharides can be used such as dextrans, which have a rather rapid diffusion rate through the cytosol despite their different sizes. This favors a temporal determination of the escape event.^[67] Ogris and colleagues used a FITC-labeled dextran (10 kDa), which allowed them to study the release of melittin-modified PEI polyplexes. In this case, the fluorescence of the FITC is enhanced upon release due to the increase in pH.^[215] In another example, Zhan and colleagues^[179] measured the release of various dextrans by blend particles featuring a PDMAEMA domain in comparison to calcein. They incubated dendritic DC2.4 cells simultaneously with calcein and dextrans of different sizes (4–2000 kDa), respectively.^[179] Their study showed that endosomal release of compounds was not depending on the composition of the blend but on the size of the sensor molecule, whereas the smaller ones are released more easily. In addition to calcein release, Salomone et al. also investigated the release of different sized dextrans (3–40 kDa) by CPPs and found endosomal release.^[183]

In addition to polysaccharides, peptides, and proteins can also be used as markers to study endosomal escape and place even greater demands on the nanocarrier due to their 3D structure.^[172] Fluorescent proteins such as R-phycoerythrin (R-PE, 240 kDa) or EGFP (27 kDa) can also be used to study endosomal release. Although the endosomal uptake of these proteins without additional treatment with an uptake-inducing material is low, the mechanism of endosomal escape of the same material can be studied in more detail with fluorescent proteins. Since these proteins undergo a loss of fluorescence along the endolysosomal pathway due to denaturation, the presence of fluorescent signal inside the cytosol indicates an escape from the early endosome very robustly. Kopp and colleagues delivered R-PE into four different cell lines using calcium phosphate nanoparticles as

delivery materials.^[216] Labeled proteins can also be used to investigate endosomal escape, but unlike intrinsically fluorescent proteins, the timing of the endosomal escape event cannot be investigated with labeled proteins since denaturation of the protein has no influence on the fluorescence intensity of the dye. Also, a positive signal does not necessarily indicate a complete release of the entire protein with its intact 3D structure. Here, too, a combination with other methods is meaningful. Nevertheless, labeled bovine serum albumin (BSA) is a suitable and easily available candidate, since it is efficiently taken up by endocytosis and can be detected more quickly than other complex proteins after the escape event due to its moderate diffusion speed. Diffusion in the cytosol is slower than for a small molecule like calcein, because the higher molar mass and the more complex structure of the protein result in comparatively slower diffusion.^[67,172]

Actual transfection, i.e., the delivery of genetic material to its site of action, can also serve as evidence of endosomal release. Depending on the type of genetic cargo, different read-outs are used. In the case of pDNA transfection, protein expression provides very clear evidence that endosomal release of the plasmid must have been successful. However, the intensity of protein expression does not necessarily correlate with the rate of release. Rather, protein expression in this case indicates a successful overcoming of the nuclear barrier in addition to various other aspects. In the case of successful delivery of RNAs, either protein expression (mRNA) or silencing (e.g., siRNA) may indicate successful delivery, depending on the cargo. In either case, successful delivery (measurable as expression or knockdown) represents a global read-out that demonstrates the functionality of the genetic cargo.

7. Conclusion and Perspectives

Initially being developed for the detection of multivalent ions, calcein has without doubt become a working horse in the analysis of lipid membrane leakage in cells as well as in artificial liposomes. In particular, the detection of escape events from endo-/lysosomal compartments after cellular uptake renders this simple molecule a powerful tool in the investigation of diverse nanocarriers such as cell entry vectors or membrane destabilization agents. Its unique set of properties (i.e., a high charge density due to the multiple carboxylic acid groups, a low toxicity, a high extinction coefficient, and quantum yield, the self-quenching at increased concentrations, and a low sensitivity toward changes in pH) hinders undesired membrane penetrations, allows its detection in even low concentrations, enables a broad applicability in relevant physiological environments, and most importantly facilitates the detection of release events, respectively. On top, calcein is affordable for most researchers worldwide, since the straightforward synthetic access keeps costs low compared to many other complex sensor dyes used in biology or pharmacy. Its application further appears straightforward, since no additional chemical modifications are required, and simple cocultivation is sufficient to monitor intracellular release events.

Nevertheless, various aspects should be kept in mind when planning experiments with calcein as reporter, since several pitfalls might deteriorate sensitivity, affect outcomes, or entirely lead to false interpretations of the data. The presence of multivalent ions or unintended interactions with nanocarriers (e.g., cationic polymers) can, among other factors, impact fluorescence

intensities, and have to be assessed prior to the experiments. Further down the road, additional difficulties may arise from the incubation conditions, the incubation time, or most of all the analysis of a potential escape. In particular, individual methods, such as microscopy or flow cytometry measurements, may underestimate or overrate escape events, respectively, if not carefully analyzed and compared to suitable controls. Due to all these different parameters affecting the outcome of the calcein release assay, it is hardly possible to suggest one specific protocol valid for different nanocarriers and cell lines. Generally, it can be recommended to start with testing different calcein concentrations and incubation times for each nanocarrier and cell line individually, not only for finding the appropriate concentrations and times but also for obtaining more information on the release mechanism. It is also overall advisable to combine several methods to investigate the calcein release assay, in order to facilitate not only a qualitative but also a quantitative analysis. For example, a combination of fluorescence-activated cell sorting and downstream microscopy or fluorescence correlation spectroscopy could be interesting to confirm the correlation between the different fluorescence intensities of the cells and the subcellular distribution of the fluorescent dye but has not yet been reported for calcein. Furthermore, live cell imaging is favorable due to the possibility to acquire more detailed information on the release mechanism (gradual/burst, transient/continuous).

Besides this individual optimization of experiments, a more global challenge resides in the comparability of datasets across various studies and particularly across different research groups. Of course, each nanocarrier or vector might require a specific set of conditions to effectively induce endosomal escape, which is further related to different analysis methods or assay parameters optimized for the respective system. Differences arise from the employed cell lines, the applied medium, or the potency and toxicity of the nanocarrier. The application of significantly different conditions might ultimately lead to different conclusions for similar or even the same nanocarriers. Fundamental understanding of key factors influencing endosomal escape however require that experimental setups allow a certain degree of comparison between results obtained in different laboratories worldwide. A minimum step toward a better comparability is in our opinion a comprehensive and detailed description of the experimental conditions including the initial preparation of the calcein solution, the incubation times with calcein and/or the applied nanocarrier, the incubation conditions and media, as well as the analytical methods. Moreover, also the not-optimal concentrations and incubation times measured during the assay establishment could be indicated in supplementary materials or made accessible on open data platforms. Ideally, any future study on this matter should maintain reasonable ranges of concentration for calcein,^[5] which avoids the appearance of artifacts in the measurements, and include control experiments with established and commercial nanocarriers for comparability.^[217] We are convinced that all research groups would benefit from such measures.

In a long-term perspective, certainly more advanced sensors will gain growing interest and complement the calcein release assay. Interesting candidates include among others pH-sensitive dyes, which allow for an additional readout of the increasing acidification during endosome maturation. Dye modified macromolecules or proteins of various sizes further allow more

detailed conclusions on the release process, since far larger pores or a burst of the compartments are required to release these molecules. The application of specific proteins or attached ligands might even facilitate to select specific uptake routes and gain information on the influence of different entry pathways. In addition, the application of fluorescent proteins represents a promising approach to verify a release prior to any degradation processes along the endo-/lysosomal pathway, which is crucial if the delivery of active enzymes is for example considered. Dyes that react in the presence of certain enzymes may also be of interest.^[218] Combined with knowledge of the processes along the uptake pathway, a timing of release could become accessible.

The calcein assay nonetheless remains a basic, but potent method, which represents a straightforward entry into the analysis of potential release events, and it might not yet have revealed its full potential. If the nanocarrier is investigated with different calcein concentrations and at different incubation times, conclusions could be drawn about the release mechanism. For instance, distinguishing continuous release over time from more concerted, transient release, or distinguishing the individual release events as gradual or all-or-none. Furthermore, the excretion of released calcein from the cytosol might be detected. However, for such detailed conclusions, a more thorough understanding of the intracellular processing/trafficking/transport (rate) of calcein (in different cell lines) are required. Also, the combination with complementary sensor molecules or dyes promises to reveal a deeper understanding of the responsible processes for release or a more quantitative evaluation of efficacies. The continuous developments in fluorescence imaging, might provide additional insight into the cellular release mechanism (graded leakage vs. all-or-none leakage mechanism) based on the increasing knowledge derived from artificial liposomes. Furthermore, the model liposomes allow for the detailed investigation of the nanocarrier's performance in response to a specific feature of endosome maturation (change in pH or membrane composition), which certainly does not reflect the complex cellular environment but can give at least a hint on the release mechanism.

Overall, we are convinced that the calcein assay, if planned carefully and ideally combined with additional methods, will remain an essential tool in the characterization of release from lipid compartments in cells and a key toward a more fundamental understanding of the mode of action of many nanocarriers. The presented review hopefully inspires further groups to apply this assay and provides a sufficient database for efficient cross-correlations, which holds the potential to reveal key features relevant for the design of future nanocarriers.

Acknowledgements

F.H-P. and F.R. contributed equally to this work. The authors gratefully acknowledge the Bundesministerium für Bildung und Forschung (BMBF, Germany, No. 13XP5034A PolyBioMik); the German Research Foundation (DFG) for generous funding within the Emmy-Noether Programme (Projekt ID: 358263073); German Research Foundation (DFG, ID: 415894560); and the support by the DFG-funded Collaborative Research Centre PolyTarget (SFB 1278, Project A05, B01, Z01, Project ID: 316213987). The figures were created with BioRender.com, which was also provided by the SFB 1278.

Open access funding enabled and organized by Projekt DEAL.

Conflict of Interest

The authors declare no conflict of interest.

Keywords

calcein release, endosomal escape, leakage, method comparison, polymer-membrane interactions, pore formation

Received: April 27, 2022

Revised: July 19, 2022

Published online: August 17, 2022

- [1] M. J. Mitchell, M. M. Billingsley, R. M. Haley, M. E. Wechsler, N. A. Peppas, R. Langer, *Nat. Rev. Drug Discovery* **2021**, *20*, 101.
- [2] V. Sanna, M. Sechi, *ACS Med. Chem. Lett.* **2020**, *11*, 1069.
- [3] P. Foroozandeh, A. A. Aziz, *Nanoscale Res. Lett.* **2018**, *13*, 339.
- [4] S. Behzadi, V. Serpooshan, W. Tao, M. A. Hamaly, M. Y. Alkawarek, E. C. Dreaden, D. Brown, A. M. Alkilany, O. C. Farokhzad, M. Mahmoudi, *Chem. Soc. Rev.* **2017**, *46*, 4218.
- [5] K. Deprey, L. Becker, J. Kritzer, A. Pluckthun, *Bioconjugate Chem.* **2019**, *30*, 1006.
- [6] Z. ur Rehman, D. Hoekstra, I. S. Zuhorn, *ACS Nano* **2013**, *7*, 3767.
- [7] A. T. Dinh, C. Pangarkar, T. Theofanous, S. Mitragotri, *Biophys. J.* **2007**, *92*, 831.
- [8] T. Merdan, K. Kunath, D. Fischer, J. Kopecek, T. Kissel, *Pharm. Res.* **2002**, *19*, 140.
- [9] J. Huotari, A. Helenius, *EMBO J.* **2011**, *30*, 3481.
- [10] S. R. Pfeffer, *Nat. Cell Biol.* **1999**, *1*, E145.
- [11] L. M. P. Vermeulen, T. Brans, S. K. Samal, P. Dubruel, J. Demeester, S. C. De Smedt, K. Remaut, K. Braeckmans, *ACS Nano* **2018**, *12*, 2332.
- [12] M. E. G. de Araujo, G. Liebscher, M. W. Hess, L. A. Huber, *Traffic* **2020**, *21*, 60.
- [13] A. El-Sayed, H. Harashima, *Mol. Ther.* **2013**, *21*, 1118.
- [14] H. D. Gallala, B. Breiden, K. Sandhoff, *J. Neurochem.* **2011**, *116*, 702.
- [15] J. Gruenberg, *Traffic* **2020**, *21*, 76.
- [16] F. Hullin-Matsuda, T. Taguchi, P. Greimel, T. Kobayashi, *Semin. Cell Dev. Biol.* **2014**, *31*, 48.
- [17] T. Kobayashi, M. H. Beuchat, J. Chevallier, A. Makino, N. Mayran, J. M. Escola, C. Lebrand, P. Cosson, T. Kobayashi, J. Gruenberg, *J. Biol. Chem.* **2002**, *277*, 32157.
- [18] H. Schulze, K. Sandhoff, *Cold Spring Harbor Perspect. Biol.* **2011**, *3*, a004804.
- [19] I. M. S. Degors, C. Wang, Z. U. Rehman, I. S. Zuhorn, *Acc. Chem. Res.* **2019**, *52*, 1750.
- [20] M. Durymanov, J. Reineke, *Front. Pharmacol.* **2018**, *9*, 971.
- [21] M. P. Stewart, A. Lorenz, J. Dahlman, G. Sahay, *Wiley Interdiscip. Rev. Nanomed. Nanobiotechnol.* **2016**, *8*, 465.
- [22] A. Ahmad, J. M. Khan, S. Haque, *Biochimie* **2019**, *160*, 61.
- [23] T. Bus, A. Traeger, U. S. Schubert, *J. Mater. Chem. B* **2018**, *6*, 6904.
- [24] O. Boussif, F. Lezoualc'h, M. A. Zanta, M. D. Mergny, D. Scherman, B. Demeneix, J. P. Behr, *Proc. Natl. Acad. Sci. USA* **1995**, *92*, 7297.
- [25] R. V. Benjaminsen, M. A. Matthebjerg, J. R. Henriksen, S. M. Moghimi, T. L. Andresen, *Mol. Ther.* **2013**, *21*, 149.
- [26] P. Midoux, M. Monsigny, *Bioconjugate Chem.* **1999**, *10*, 406.
- [27] B. Singh, S. Maharjan, T.-E. Park, T. Jiang, S.-K. Kang, Y.-J. Choi, C.-S. Cho, *Macromol. Biosci.* **2015**, *15*, 622.
- [28] N. D. Sonawane, F. C. Szoka, A. S. Verkman, *J. Biol. Chem.* **2003**, *278*, 44826.
- [29] A. M. Funhoff, C. F. van Nostrum, M. C. Lok, J. A. Kruijtz, D. J. Crommelin, W. E. Hennink, *J. Controlled Release* **2005**, *101*, 233.

- [30] A. Akinc, M. Thomas, A. M. Klivanov, R. Langer, *J. Gene Med.* **2005**, 7, 657.
- [31] A. Kichler, C. Leborgne, E. Coeytaux, O. Danos, *J. Gene Med.* **2001**, 3, 135.
- [32] Z. ur Rehman, D. Hoekstra, I. S. Zuhorn, *ACS Nano* **2013**, 7, 3767.
- [33] M. L. Forrest, D. W. Pack, *Mol. Ther.* **2002**, 6, 57.
- [34] T. Bieber, W. Meissner, S. Kostin, A. Niemann, H.-P. Elsasser, *J. Controlled Release* **2002**, 82, 441.
- [35] R. Mo, Q. Sun, N. Li, C. Zhang, *Biomaterials* **2013**, 34, 2773.
- [36] I. Richard, M. Thibault, G. De Crescenzo, M. D. Buschmann, M. Lavertu, *Biomacromolecules* **2013**, 14, 1732.
- [37] T. F. Martens, K. Remaut, J. Demeester, S. C. De Smedt, K. Braeckmans, *Nano Today* **2014**, 9, 344.
- [38] E. Xu, W. M. Saltzman, A. S. Piotrowski-Daspi, *J. Controlled Release* **2021**, 335, 465.
- [39] S. L. Y. Teo, J. J. Rennick, D. Yuen, H. Al-Wassiti, A. P. R. Johnston, C. W. Pouton, *Nat. Commun.* **2021**, 12, 3721.
- [40] N. I. Zahaf, A. E. Lang, L. Kaiser, C. D. Fichter, S. Lassmann, A. McCluskey, A. Augspach, K. Aktories, G. Schmidt, *Sci. Rep.* **2017**, 7, 41252.
- [41] S. Schmidt, M. J. Adjobo-Hermans, R. Wallbrecher, W. P. Verdurmen, P. H. Bovee-Geurts, J. van Oostrum, F. Milletti, T. Enderle, R. Brock, *Angew. Chem., Int. Ed. Engl.* **2015**, 54, 15105.
- [42] N. Milech, B. A. Longville, P. T. Cunningham, M. N. Scobie, H. M. Bogdawa, S. Winslow, M. Anastasas, T. Connor, F. Ong, S. R. Stone, M. Kerfoot, T. Heinrich, K. M. Kroeger, Y. F. Tan, K. Hoffmann, W. R. Thomas, P. M. Watt, R. M. Hopkins, *Sci. Rep.* **2015**, 5, 18329.
- [43] B. C. Evans, R. B. Fletcher, K. V. Kilchrist, E. A. Dailing, A. J. Mukalel, J. M. Colazo, M. Oliver, J. Cheung-Flynn, C. M. Brophy, J. W. Tierney, J. S. Isenberg, K. D. Hankenson, K. Ghimire, C. Lander, C. A. Gersbach, C. L. Duvall, *Nat. Commun.* **2019**, 10, 5012.
- [44] H. Du Rietz, H. Hedlund, S. Wilhelmson, P. Nordenfelt, A. Wittrup, *Nat. Commun.* **2020**, 11, 1809.
- [45] H. Diehl, J. L. Ellingboe, *Anal. Chem.* **1956**, 28, 882.
- [46] H. Diehl, *Anal. Chem.* **1967**, 39, A30.
- [47] A. J. Hefley, *Ph.D. Thesis*, Iowa State University **1967**.
- [48] Richard Markuszewski, *Ph.D. Thesis*, Iowa State University **1976**.
- [49] D. B. Martin, *Ph.D. Thesis*, Iowa State University **1977**.
- [50] J. W. Furry, *Ph.D. Thesis*, Iowa State University **1985**.
- [51] R. W. Sabnis, in *Handbook of Biological Dyes and Stains*, John Wiley & Sons, Inc., Hoboken, NJ **2010**, p. 71.
- [52] H. Diehl, *Calcein, Calmagite and o, o'-Dihydroxyazobenzene. Titrimetric, Colorimetric, and Fluorometric Reagents for Calcium and Magnesium*, G. Frederick Smith Chemical Company, Columbus, OH **1964**.
- [53] B. Walter, *Ann. Phys.* **1888**, 270, 316.
- [54] B. Walter, *Ann. Phys.* **1889**, 272, 502.
- [55] B. Walter, *Ann. Phys.* **1889**, 272, 518.
- [56] R. F. Chen, J. R. Knutson, *Anal. Biochem.* **1988**, 172, 61.
- [57] J. N. Weinstein, S. Yoshikami, P. Henkart, R. Blumenthal, W. A. Hagens, *Science* **1977**, 195, 489.
- [58] T. M. Allen, L. G. Cleland, *Biochim. Biophys. Acta* **1980**, 597, 418.
- [59] D. A. Kendall, R. C. MacDonald, *Anal. Biochem.* **1983**, 134, 26.
- [60] H. Patel, C. Tscheka, K. Edwards, G. Karlsson, H. Heerklotz, *Biochim. Biophys. Acta* **2011**, 1808, 2000.
- [61] S. Salassi, F. Simonelli, A. Bartocci, G. Rossi, *J. Phys. D: Appl. Phys.* **2018**, 51, 384002.
- [62] S. Hamann, J. F. Kiilgaard, T. Litman, F. J. Alvarez-Leefmans, B. R. Winther, T. Zeuthen, *J. Fluoresc.* **2002**, 12, 139.
- [63] K. E. Roberts, A. K. O'Keeffe, C. J. Lloyd, D. J. Clarke, *J. Fluoresc.* **2003**, 13, 513.
- [64] A. Andersson, J. Danielsson, A. Graslund, L. Maler, *Eur. Biophys. J.* **2007**, 36, 621.
- [65] R. Imamura, N. Murata, T. Shimanouchi, K. Yamashita, M. Fukuzawa, M. Noda, *Sensors* **2017**, 17, 1630.
- [66] G. Dorrington, N. P. Chmel, S. R. Norton, A. M. Wemyss, K. Lloyd, D. Praveen Amarasinghe, A. Rodger, *Biophys. Rev.* **2018**, 10, 1385.
- [67] N. Brkovic, L. Zhang, J. N. Peters, S. Kleine-Doecke, W. J. Parak, D. Zhu, *Small* **2020**, 16, e2003639.
- [68] W. Bae, T. Y. Yoon, C. Jeong, *PLoS One* **2021**, 16, e0247326.
- [69] D. F. H. Wallach, T. L. Steck, *Anal. Chem.* **2002**, 35, 1035.
- [70] R. M. Straubinger, K. Hong, D. S. Friend, D. Papahadjopoulos, *Cell* **1983**, 32, 1069.
- [71] F. C. Szoka, K. Jacobson, D. Papahadjopoulos, *Biochim. Biophys. Acta* **1979**, 551, 295.
- [72] C. B. Billesbolle, C. M. Azumaya, R. C. Kretsch, A. S. Powers, S. Gonen, S. Schneider, T. Arvedson, R. O. Dror, Y. Cheng, A. Manglik, *Nature* **2020**, 586, 807.
- [73] N. Oku, D. A. Kendall, R. C. Macdonald, *Biochim. Biophys. Acta* **1982**, 691, 332.
- [74] A. Ali, Q. Zhang, J. Dai, X. Huang, *BioMetals* **2003**, 16, 285.
- [75] B. B. Hasinoff, *J. Inorg. Biochem.* **2003**, 95, 157.
- [76] F. Thomas, G. Serratrice, C. Beguin, E. S. Aman, J. L. Pierre, M. Fontecave, J. P. Lauthere, *J. Biol. Chem.* **1999**, 274, 13375.
- [77] H. B. Li, F. Chen, *Fresenius' J. Anal. Chem.* **2000**, 368, 501.
- [78] J. Körbl, F. Vydra, R. Pribil, *Talanta* **1958**, 1, 281.
- [79] J. H. Eggers, *Talanta* **1960**, 4, 38.
- [80] A. M. Escarilla, *Talanta* **1966**, 13, 363.
- [81] G. M. Huitink, H. Diehl, *Talanta* **1974**, 21, 1193.
- [82] G. M. Huitink, D. P. Poe, H. Diehl, *Talanta* **1974**, 21, 1221.
- [83] D. H. Wilkins, *Talanta* **1960**, 4, 182.
- [84] I. D. Johnson, in *Molecular Probes Handbook: A Guide to Fluorescent Probes and Labeling Technologies*, 11th ed. (Ed: I. D. Johnson), Life Technologies Corporation, Carlsbad, CA **2010**, p. 833.
- [85] D. Thomas, S. C. Tovey, T. J. Collins, M. D. Bootman, M. J. Berridge, P. Lipp, *Cell Calcium* **2000**, 28, 213.
- [86] A. B. Harkins, N. Kurebayashi, S. M. Baylor, *Biophys. J.* **1993**, 65, 865.
- [87] E. S. Kaneshiro, M. A. Wyder, Y. P. Wu, M. T. Cushion, *J. Microbiol. Methods* **1993**, 17, 1.
- [88] D. Bratosin, L. Mitrofan, C. Palii, J. Estaquier, J. Montreuil, *Cytometry A* **2005**, 66, 78.
- [89] K. I. McConnell, S. Shamsudeen, I. M. Meraz, T. S. Mahadevan, A. Ziemys, P. Rees, H. D. Summers, R. E. Serda, *J. Biomed. Nanotechnol.* **2016**, 12, 154.
- [90] S. Neri, E. Mariani, A. Meneghetti, L. Cattini, A. Facchini, *Clin. Diagn. Lab. Immunol.* **2001**, 8, 1131.
- [91] G. Drin, S. Cottin, E. Blanc, A. R. Rees, J. Temsamani, *J. Biol. Chem.* **2003**, 278, 31192.
- [92] R. Lichtenfels, W. E. Biddison, H. Schulz, A. B. Vogt, R. Martin, *J. Immunol. Methods* **1994**, 172, 227.
- [93] A. Nitsch, L. Haralambiev, R. Eienkel, D. O. Muzzio, M. T. Zygmunt, A. Ekkernkamp, M. Burchardt, M. B. Stope, *In Vivo* **2019**, 33, 1767.
- [94] G. Nasr, H. Greige-Gerges, A. Elaissari, N. Khreich, *Int. J. Pharm.* **2020**, 580, 119198.
- [95] S. Dutta, B. G. Watson, S. Mattoo, J. C. Rochet, *Bio-Protoc.* **2020**, 10, e3690.
- [96] S. Guha, J. Ghimire, E. Wu, W. C. Wimley, *Chem. Rev.* **2019**, 119, 6040.
- [97] A. Akbarzadeh, R. Rezaei-Sadabady, S. Davaran, S. W. Joo, N. Zarghami, Y. Hanifepour, M. Samiei, M. Kouhi, K. Nejati-Koshki, *Nanoscale Res. Lett.* **2013**, 8, 102.
- [98] S. Chatterjee, D. K. Banerjee, in *Liposome Methods and Protocols* (Eds: S. C. Basu, M. Basu), Humana Press, Totowa, NJ **2002**, p. 3.
- [99] A. Stulz, A. Vogt, J. S. Saar, L. Akil, K. Lienkamp, M. Hoernke, *Langmuir* **2019**, 35, 16366.
- [100] W. C. Wimley, K. Hristova, *Aust. J. Chem.* **2019**, 73, 96.
- [101] I. Tsogas, D. Tsiourvas, G. Nounesis, C. M. Paleos, *Langmuir* **2006**, 22, 11322.

- [102] Y. Sarkar, S. Roy, R. Majumder, S. Das, D. V. Bhalani, A. Ray, S. K. Jewrajka, P. P. Parui, *Soft Matter* **2020**, *16*, 798.
- [103] J. L. Thomas, H. You, D. A. Tirrell, *J. Am. Chem. Soc.* **1995**, *117*, 2949.
- [104] J. Allen, K. Najjar, A. Erazo-Oliveras, H. M. Kondow-McConaghy, D. J. Brock, K. Graham, E. C. Hager, A. L. J. Marschall, S. Dubel, R. L. Juliano, J. P. Pellois, *ACS Chem. Biol.* **2019**, *14*, 2641.
- [105] D. J. Brock, L. Kustigian, M. Jiang, K. Graham, T. Y. Wang, A. Erazo-Oliveras, K. Najjar, J. Zhang, H. Rye, J. P. Pellois, *Traffic* **2018**, *19*, 421.
- [106] K. Najjar, A. Erazo-Oliveras, D. J. Brock, T. Y. Wang, J. P. Pellois, *J. Biol. Chem.* **2017**, *292*, 847.
- [107] K. Sudo, K. Niihara, K. Iwaki, S. Kohyama, K. Fujiwara, N. Doi, *J. Controlled Release* **2017**, *255*, 28385674.
- [108] D. J. Brock, H. Kondow-McConaghy, J. Allen, Z. Brkljaca, L. Kustigian, M. Jiang, J. Zhang, H. Rye, M. Vazdar, J. P. Pellois, *Cell Chem. Biol.* **2020**, *27*, 1296.
- [109] A. Erazo-Oliveras, K. Najjar, D. Truong, T. Y. Wang, D. J. Brock, A. R. Prater, J. P. Pellois, *Cell Chem. Biol.* **2016**, *23*, 598.
- [110] Z. Qian, A. Martyna, R. L. Hard, J. Wang, G. Appiah-Kubi, C. Coss, M. A. Phelps, J. S. Rossman, D. Pei, *Biochemistry* **2016**, *55*, 2601.
- [111] S. M. Van Rossenberg, K. M. Sliedregt-Bol, N. J. Meeuwenoord, T. J. Van Berkel, J. H. Van Boom, G. A. Van Der Marel, E. A. Biessen, *J. Biol. Chem.* **2002**, *277*, 45803.
- [112] L. Rangasamy, V. Chelvam, A. K. Kanduluru, M. Srinivasarao, N. A. Bandara, F. You, E. A. Orellana, A. L. Kasinski, P. S. Low, *Bioconjugate Chem.* **2018**, *29*, 1047.
- [113] J. C. Brendel, J. Sanchis, S. Catrouillet, E. Czuba, M. Z. Chen, B. M. Long, C. Nowell, A. Johnston, K. A. Jolliffe, S. Perrier, *Angew. Chem., Int. Ed. Engl.* **2018**, *57*, 16678.
- [114] E. Mastrobattista, G. A. Koning, L. van Bloois, A. C. Filipe, W. Jiskoot, G. Storm, *J. Biol. Chem.* **2002**, *277*, 27135.
- [115] A. El-Sayed, I. A. Khalil, K. Kogure, S. Futaki, H. Harashima, *J. Biol. Chem.* **2008**, *283*, 23450.
- [116] A. El-Sayed, T. Masuda, I. Khalil, H. Akita, H. Harashima, *J. Controlled Release* **2009**, *138*, 160.
- [117] E. Rideau, R. Dimova, P. Schwillie, F. R. Wurm, K. Landfester, *Chem. Soc. Rev.* **2018**, *47*, 8572.
- [118] S. Braun, S. Pokorna, R. Sachl, M. Hof, H. Heerklotz, M. Hoernke, *ACS Nano* **2018**, *12*, 813.
- [119] A. Jesorka, O. Orwar, *Annu. Rev. Anal. Chem.* **2008**, *1*, 801.
- [120] P. Walde, K. Cosentino, H. Engel, P. Stano, *ChemBioChem* **2010**, *11*, 848.
- [121] H. Stein, S. Spindler, N. Bonakdar, C. Wang, V. Sandoghdar, *Front. Physiol.* **2017**, *8*, 63.
- [122] J. Steinkuhler, P. De Tillieux, R. L. Knorr, R. Lipowsky, R. Dimova, *Sci. Rep.* **2018**, *8*, 11838.
- [123] C. C. Scott, J. Gruenberg, *BioEssays* **2011**, *33*, 103.
- [124] T. Shimanouchi, H. Ishii, N. Yoshimoto, H. Umakoshi, R. Kuboi, *Colloids Surf., B* **2009**, *73*, 156.
- [125] N. Wang, M. Chen, T. Wang, *J. Controlled Release* **2019**, *303*, 130.
- [126] L. Wang, N. Hartel, K. Ren, N. A. Graham, N. Malmstadt, *Environ. Sci.: Nano* **2020**, *7*, 963.
- [127] G. Raposo, W. Stoorvogel, *J. Cell Biol.* **2013**, *200*, 373.
- [128] C. Zivko, G. Fuhrmann, P. Luciani, *Biochim. Biophys. Acta, Gen. Subj.* **2021**, *1865*, 129559.
- [129] B. Illes, P. Hirschle, S. Barnert, V. Cauda, S. Wuttke, H. Engelke, *Chem. Mater.* **2017**, *29*, 8042.
- [130] W. D. Gray, A. J. Mitchell, C. D. Searles, *MethodsX* **2015**, *2*, 360.
- [131] I. Sovadinova, E. F. Palermo, R. Huang, L. M. Thoma, K. Kuroda, *Biomacromolecules* **2011**, *12*, 260.
- [132] S. K. Zhang, L. Gong, X. Zhang, Z. M. Yun, S. B. Li, H. W. Gao, C. J. Dai, J. J. Yuan, J. M. Chen, F. Gong, Y. X. Tan, S. P. Ji, *J. Gene Med.* **2020**, *22*, e3259.
- [133] W. C. Wimley, K. Hristova, *Aust. J. Chem.* **2020**, *73*, 96.
- [134] S. Esteban-Martin, H. J. Risselada, J. Salgado, S. J. Marrink, *J. Am. Chem. Soc.* **2009**, *131*, 15194.
- [135] H. Heerklotz, *Biophys. J.* **2001**, *81*, 184.
- [136] S. Shi, A. M. Markl, Z. Lu, R. Liu, M. Hoernke, *Langmuir* **2022**, *38*, 2379.
- [137] S. T. Yang, E. Zaitseva, L. V. Chernomordik, K. Melikov, *Biophys. J.* **2010**, *99*, 2525.
- [138] C. Mazzuca, B. Orioni, M. Coletta, F. Formaggio, C. Toniolo, G. Maulucci, M. De Spirito, B. Pispisa, M. Venanzi, L. Stella, *Biophys. J.* **2010**, *99*, 1791.
- [139] I. Plaza-Ga, V. Manzaneda-Gonzalez, M. Kisovec, V. Almendro-Vedia, M. Munoz-Ubeda, G. Anderluh, A. Guerrero-Martinez, P. Natale, I. Lopez Montero, *J. Nanobiotechnol.* **2019**, *17*, 108.
- [140] Y. Tamba, M. Yamazaki, *Biochemistry* **2005**, *44*, 15823.
- [141] G. Fuertes, A. J. Garcia-Saez, S. Esteban-Martin, D. Gimenez, O. L. Sanchez-Munoz, P. Schwillie, J. Salgado, *Biophys. J.* **2010**, *99*, 2917.
- [142] S. G. Hovakeemian, R. Liu, S. H. Gellman, H. Heerklotz, *Soft Matter* **2015**, *11*, 6840.
- [143] A. S. Ladokhin, W. C. Wimley, S. H. White, *Biophys. J.* **1995**, *69*, 1964.
- [144] H. Patel, C. Tscheka, H. Heerklotz, *Soft Matter* **2009**, *5*, 2849.
- [145] B. Apellaniz, J. L. Nieva, P. Schwillie, A. J. Garcia-Saez, *Biophys. J.* **2010**, *99*, 3619.
- [146] D. A. Kendall, R. C. MacDonald, *J. Biol. Chem.* **1982**, *257*, 13892.
- [147] D. F. Wallach, T. L. Steck, *Anal. Biochem.* **1963**, *6*, 176.
- [148] C. J. Chu, J. Dijkstra, M. Z. Lai, K. Hong, F. C. Szoka, *Pharm. Res.* **1990**, *7*, 824.
- [149] E. Ducat, J. Deprez, A. Gillet, A. Noel, B. Evrard, O. Peulen, G. Piel, *Int. J. Pharm.* **2011**, *420*, 319.
- [150] V. A. Slepishkin, S. Simoes, P. Dazin, M. S. Newman, L. S. Guo, M. C. Pedrosa de Lima, N. Duzgunes, *J. Biol. Chem.* **1997**, *272*, 2382.
- [151] S. Simoes, V. Slepishkin, N. Duzgunes, M. C. P. de Lima, *Biochim. Biophys. Acta, Biomembr.* **2001**, *1515*, 23.
- [152] M. Kanamala, B. D. Palmer, H. Ghandehari, W. R. Wilson, Z. Wu, *Pharm. Res.* **2018**, *35*, 154.
- [153] P. Enzian, C. Schell, A. Link, C. Malich, R. Pries, B. Wollenberg, R. Rahmzadeh, *Mol. Pharmaceutics* **2020**, *17*, 2779.
- [154] J. Connor, L. Huang, *J. Cell. Biol.* **1985**, *101*, 582.
- [155] C.-J. Chu, F. C. Szoka, *J. Liposome Res.* **1994**, *4*, 361.
- [156] X. Cheng, R. J. Lee, *Adv. Drug Delivery Rev.* **2016**, *99*, 129.
- [157] P. R. Cullis, M. J. Hope, *Mol. Ther.* **2017**, *25*, 1467.
- [158] S. Cerritelli, D. Velluto, J. A. Hubbell, *Biomacromolecules* **2007**, *8*, 1966.
- [159] E. A. Scott, A. Stano, M. Gillard, A. C. Maio-Liu, M. A. Swartz, J. A. Hubbell, *Biomaterials* **2012**, *33*, 6211.
- [160] A. E. Vasdekis, E. A. Scott, C. P. O'Neil, D. Psaltis, J. A. Hubbell, *ACS Nano* **2012**, *6*, 7850.
- [161] K. Kono, T. Igawa, T. Takagishi, *Biochim. Biophys. Acta* **1997**, *1325*, 143.
- [162] H. Xu, W. Zhang, Y. Li, F. F. Ye, P. P. Yin, X. Yu, M. N. Hu, Y. S. Fu, C. Wang, J. Shang de, *Pharm. Res.* **2014**, *31*, 3038.
- [163] Z. Li, B. Li, M. Wang, M. Xie, H. Shen, S. Shen, X. Wang, X. Guo, M. Yao, Y. Jin, *J. Mater. Chem. B* **2013**, *1*, 1466.
- [164] Y. Nishimura, K. Takeda, R. Ezawa, J. Ishii, C. Ogino, A. Kondo, *J. Nanobiotechnol.* **2014**, *12*, 11.
- [165] S. Niedermayer, V. Weiss, A. Herrmann, A. Schmidt, S. Datz, K. Muller, E. Wagner, T. Bein, C. Brauchle, *Nanoscale* **2015**, *7*, 7953.
- [166] U. Lachelt, P. Kos, F. M. Mickler, A. Herrmann, E. E. Salcher, W. Rodl, N. Badgujar, C. Brauchle, E. Wagner, *Nanomedicine* **2014**, *10*, 35.
- [167] R. A. Jones, C. Y. Cheung, F. E. Black, J. K. Zia, P. S. Stayton, A. S. Hoffman, M. R. Wilson, *Biochem. J.* **2003**, *372*, 65.
- [168] S. Deshpande, S. Patil, N. Singh, *ACS Omega* **2018**, *3*, 8042.

- [169] A. K. Trutzschler, T. Bus, M. Reifarth, J. C. Brendel, S. Hoepfner, A. Traeger, U. S. Schubert, *Bioconjugate Chem.* **2018**, *29*, 2181.
- [170] R. A. Jones, M. H. Poniris, M. R. Wilson, *J. Controlled Release* **2004**, *96*, 379.
- [171] F. Richter, L. Martin, K. Leer, E. Moek, F. Hausig, J. C. Brendel, A. Traeger, *J. Mater. Chem. B* **2020**, *8*, 5026.
- [172] F. Hausig, F. H. Sobotta, F. Richter, D. O. Harz, A. Traeger, J. C. Brendel, *ACS Appl. Mater. Interfaces* **2021**, *13*, 35233.
- [173] D. K. Bonner, X. Zhao, H. Buss, R. Langer, P. T. Hammond, *J. Controlled Release* **2013**, *167*, 101.
- [174] D. K. Bonner, C. Leung, J. Chen-Liang, L. Chingozha, R. Langer, P. T. Hammond, *Bioconjugate Chem.* **2011**, *22*, 1519.
- [175] F. Richter, P. Mapfumo, L. Martin, J. I. Solomun, F. Hausig, J. J. Frietsch, T. Ernst, S. Hoepfner, J. C. Brendel, A. Traeger, *J. Nanobiotechnol.* **2021**, *19*, 70.
- [176] F. Richter, K. Leer, L. Martin, P. Mapfumo, J. I. Solomun, M. T. Kuchenbrod, S. Hoepfner, J. C. Brendel, A. Traeger, *J. Nanobiotechnol.* **2021**, *19*, 292.
- [177] Y. Hu, T. Litwin, A. R. Nagaraja, B. Kwong, J. Katz, N. Watson, D. J. Irvine, *Nano Lett.* **2007**, *7*, 3056.
- [178] K. K. Tran, X. Zhan, H. Shen, *Adv. Healthcare Mater.* **2014**, *3*, 690.
- [179] X. Zhan, K. K. Tran, L. Wang, H. Shen, *Pharm. Res.* **2015**, *32*, 2280.
- [180] X. Su, J. Fricke, D. G. Kavanagh, D. J. Irvine, *Mol. Pharmaceutics* **2011**, *8*, 774.
- [181] S. Wannasari, S. Q. Wang, P. Figueiredo, C. Trujillo, F. Eburnea, L. Simon-Gracia, A. Correia, Y. P. Ding, T. Teesalu, D. F. Liu, R. Wattanapatapee, H. A. Santos, W. Li, *Adv. Funct. Mater.* **2019**, *29*, 1905352.
- [182] J. Chen, J. Li, J. Zhou, Z. Lin, F. Cavalieri, E. Czuba-Wojnilowicz, Y. Hu, A. Glab, Y. Ju, J. J. Richardson, F. Caruso, *ACS Nano* **2019**, *13*, 11653.
- [183] F. Salomone, F. Cardarelli, M. Di Luca, C. Boccardi, R. Nifosi, G. Bardi, L. Di Bari, M. Serresi, F. Beltram, *J. Controlled Release* **2012**, *163*, 293.
- [184] J. R. Clegg, J. A. Sun, J. Gu, A. K. Venkataraman, N. A. Peppas, *J. Controlled Release* **2021**, *329*, 1162.
- [185] N. Kongkatigumjorn, S. A. Smith, M. Chen, K. T. Fang, S. L. Yang, E. R. Gillies, A. P. R. Johnston, G. K. Such, *ACS Appl. Nano Mater.* **2018**, *1*, 3164.
- [186] N. Kongkatigumjorn, C. Cortez-Jugo, E. Czuba, A. S. Wong, R. Y. Hodgetts, A. P. Johnston, G. K. Such, *Macromol. Biosci.* **2017**, *17*, 1600248.
- [187] Y. Hu, P. U. Atukorale, J. J. Lu, J. J. Moon, S. H. Um, E. C. Cho, Y. Wang, J. Chen, D. J. Irvine, *Biomacromolecules* **2009**, *10*, 756.
- [188] A. S. Wong, S. K. Mann, E. Czuba, A. Sahut, H. Liu, T. C. Suekama, T. Bickerton, A. P. Johnston, G. K. Such, *Soft Matter* **2015**, *11*, 2993.
- [189] M. Galliani, C. Tremolanti, G. Signore, *Nanomaterials* **2019**, *9*, 652.
- [190] J. S. Kim, D. K. Choi, J. Y. Shin, S. M. Shin, S. W. Park, H. S. Cho, Y. S. Kim, *J. Controlled Release* **2016**, *235*, 165.
- [191] G. Rong, C. Wang, L. Chen, Y. Yan, Y. Cheng, *Sci. Adv.* **2020**, *6*, eaaz1774.
- [192] D. Adams, A. Gonzalez-Duarte, W. D. O'Riordan, C. C. Yang, M. Ueda, A. V. Kristen, I. Tournev, H. H. Schmidt, T. Coelho, J. L. Berk, K. P. Lin, G. Vita, S. Attarian, V. Plante-Bordeneuve, M. M. Mezei, J. M. Campistol, J. Buades, T. H. Brannagan, 3rd, B. J. Kim, J. Oh, Y. Parman, Y. Sekijima, P. N. Hawkins, S. D. Solomon, M. Polydefkis, P. J. Dyck, P. J. Gandhi, S. Goyal, J. Chen, A. L. Strahs, S. V. Nochur, M. T. Sweetser, P. P. Garg, A. K. Vaishnav, J. A. Gollob, O. B. Suhr, *N. Engl. J. Med.* **2018**, *379*, 11.
- [193] K. Ren, Y. Liu, J. Wu, Y. Zhang, J. Zhu, M. Yang, H. Ju, *Nat. Commun.* **2016**, *7*, 13580.
- [194] E. M. M. Manders, F. J. Verbeek, J. A. Aten, *J. Microsc.* **1993**, *169*, 375.
- [195] K. W. Dunn, M. M. Kamocka, J. H. McDonald, *Am. J. Physiol.: Cell Physiol.* **2011**, *300*, C723.
- [196] B. Alberts, A. Johnson, J. Lewis, P. Walter, M. Raff, K. Roberts, *Molecular Biology of the Cell*, 4th ed., International Student Edition, Routledge, England **2002**.
- [197] S. Kumari, S. Mg, S. Mayor, *Cell Res.* **2010**, *20*, 256.
- [198] Q. Xia, J. Huang, Q. Feng, X. Chen, X. Liu, X. Li, T. Zhang, S. Xiao, H. Li, Z. Zhong, K. Xiao, *Int. J. Nanomed.* **2019**, *14*, 6957.
- [199] H. Shin, M. Kwak, T. G. Lee, J. Y. Lee, *Nanoscale* **2020**, *12*, 15743.
- [200] M. Essodaigui, H. J. Broxterman, A. Garnier-Suillerot, *Biochemistry* **1998**, *37*, 2243.
- [201] N. Feller, H. J. Broxterman, D. C. R. Wahrer, H. M. Pinedo, *FEBS Lett.* **1995**, *368*, 385.
- [202] L. Homolya, Z. Hollo, U. A. Germann, I. Pastan, M. M. Gottesman, B. Sarkadi, *J. Biol. Chem.* **1993**, *268*, 21493.
- [203] Z. Hollo, L. Homolya, C. W. Davis, B. Sarkadi, *Biochim. Biophys. Acta, Biomembr.* **1994**, *1191*, 384.
- [204] V. B. Cismasiu, L. M. Popescu, *J. Cell. Mol. Med.* **2015**, *19*, 351.
- [205] K. A. Sinclair, S. T. Yerkovich, P. M. Hopkins, D. C. Chambers, *Stem Cell Res. Ther.* **2016**, *7*, 91.
- [206] S. Strassburg, N. W. Hodson, P. I. Hill, S. M. Richardson, J. A. Hoyland, *PLoS One* **2012**, *7*, e33739.
- [207] T. M. Achilli, S. McCalla, J. Meyer, A. Tripathi, J. R. Morgan, *Mol. Pharmaceutics* **2014**, *11*, 2071.
- [208] F. L. Miles, J. E. Lynch, R. A. Sikes, *J. Biol. Methods* **2015**, *2*, e29.
- [209] S. A. Smith, L. I. Selby, A. P. R. Johnston, G. K. Such, *Bioconjugate Chem.* **2019**, *30*, 263.
- [210] W. Viricel, A. Mbarek, J. Leblond, *Angew. Chem., Int. Ed. Engl.* **2015**, *54*, 12743.
- [211] N. J. Dolman, J. A. Kilgore, M. W. Davidson, *Curr. Protoc. Cytom.* **2013**, *12*, Unit 12.30.
- [212] M. Ogawa, N. Kosaka, C. A. Regino, M. Mitsunaga, P. L. Choyke, H. Kobayashi, *Mol. Biosyst.* **2010**, *6*, 888.
- [213] M. G. Palmgren, *Anal. Biochem.* **1991**, *192*, 316.
- [214] R. Kandil, Y. Xie, R. Heermann, L. Isert, K. Jung, A. Mehta, O. M. Merkel, *Adv. Ther.* **2019**, *2*, 1900047.
- [215] M. Ogris, R. C. Carlisle, T. Bettinger, L. W. Seymour, *J. Biol. Chem.* **2001**, *276*, 47550.
- [216] M. Kopp, O. Rotan, C. Papadopoulos, N. Schulze, H. Meyer, M. Epple, *PLoS One* **2017**, *12*, e0178260.
- [217] N. Bono, F. Ponti, D. Mantovani, G. Candiani, *Pharmaceutics* **2020**, *12*, 183.
- [218] C. R. Drake, D. C. Miller, E. F. Jones, *Curr. Org. Synth.* **2011**, *8*, 498.



Franziska Hausig-Punke studied nutrition sciences (B.Sc.) and molecular nutrition (M.Sc.) at the Friedrich Schiller University Jena. Since 2017, she conducts her Ph.D. in the research group of Dr. Johannes C. Brendel at the Jena Center for Soft Matter (JCSM) at Friedrich Schiller University Jena. She complements the chemically oriented research group with her strong biochemical background and focuses on the biological characterization of polymers for biomedical applications from all sides. Her dissertation explores the overcoming of the endosomal membrane by pH-responsive polymers for intracellular delivery of biopharmaceuticals.



Friederike Richter studied nutrition sciences (B.Sc.) and molecular nutrition (M.Sc.) at the Friedrich Schiller University in Jena. After her graduation in 2017, she started as a Ph.D. student in the junior research group of Dr. Anja Traeger at the Friedrich Schiller University in Jena. Her research focuses on the biological in vitro investigation of tailor-made synthetic polymers and cationic polymer micelles for gene delivery.



Maria Hoernke conducted her Ph.D. research on amyloid formation at the Max-Planck-Institute of Colloids and Interfaces in Potsdam. After receiving her Ph.D. (2012), Maria joined Gothenburg University (Sweden) where she obtained a Marie Curie IEF fellowship for protein structural dynamics investigated by time resolved X-ray scattering and surface-sensitive infrared spectroscopy. Since 2015, she continues her academic activities at Freiburg University (Germany) where she now leads an independent team funded by the German Research Foundation (DFG) and the Daimler and Benz Foundation. She is an expert in biophysical chemistry of lipid membranes in response to peptides, proteins, or polymers.



Johannes C. Brendel studied chemistry at the University of Bayreuth (Germany) and received his Ph.D. in 2013 on his studies of semiconducting polymers. From 2014 to 2016, he worked at the University of Warwick (UK) and the Monash Institute of Pharmaceutical Sciences (Australia) as a postdoctoral researcher funded by the German Research Foundation (DFG). In 2016, he established an independent research group at the Friedrich Schiller University Jena (Germany) which became funded within the Emmy Noether Programme in 2017. His research interests include the design of reactive monomers, the synthesis of well-defined polymer architectures, and their self-assembly into complex nanostructures.

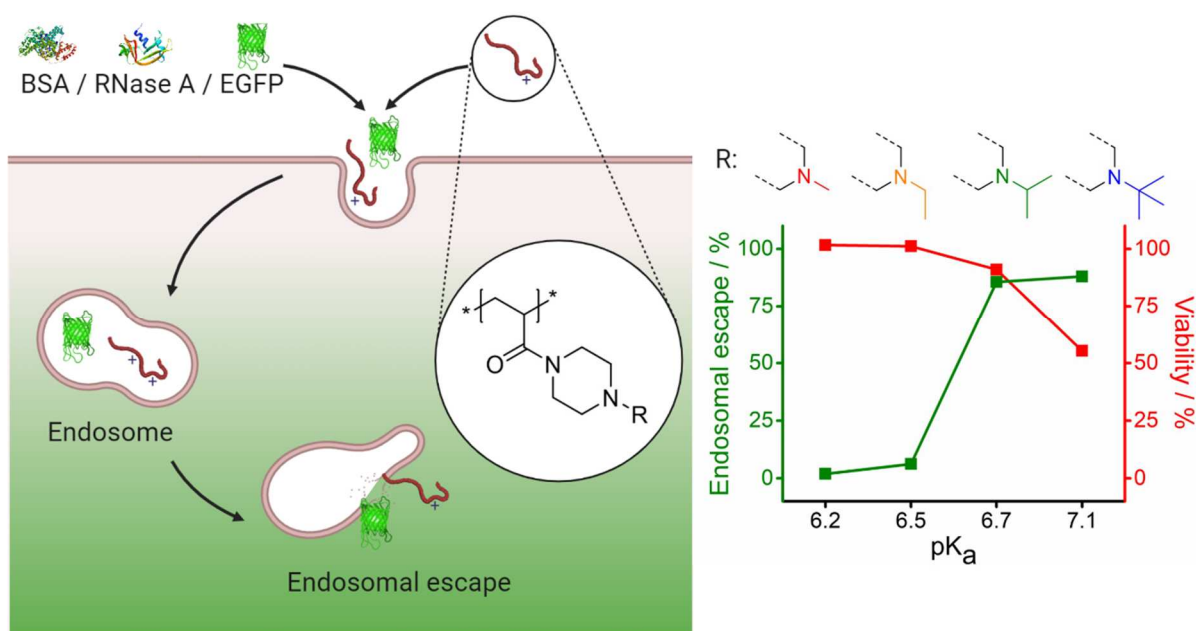


Anja Traeger studied biochemistry with a focus on genetics (Bayreuth, York) and received her Ph.D. in biotechnology (Bayreuth) in 2011, where she investigated polymers for cellular delivery. Afterward, she moved to the Friedrich Schiller University Jena to do her habilitation under the supervision of Prof. U. S. Schubert after a research stay with Prof. K. Kataoka (Tokyo). In 2017, she received funding for her independent research group through the BMBF NanoMatFutur program. Her applied research focused on well-defined copolymers for gene delivery and interaction of polymer-based materials with cellular membranes for endosomal escape.

Publication Pub2

Correlation between Protonation of Tailor-Made Polypiperazines and Endosomal Escape for Cytosolic Protein Delivery

F. Hausig, F. H. Sobotta, F. Richter, D.O. Harz, A. Traeger, J. C. Brendel, *ACS Appl. Mater. Interfaces*, **2021**, 13, 35233-35247.



Correlation between Protonation of Tailor-Made Polypiperazines and Endosomal Escape for Cytosolic Protein Delivery

Franziska Hausig, Fabian H. Sobotta, Friederike Richter, Dominic O. Harz, Anja Traeger, and Johannes C. Brendel*



Cite This: *ACS Appl. Mater. Interfaces* 2021, 13, 35233–35247



Read Online

ACCESS |



Metrics & More



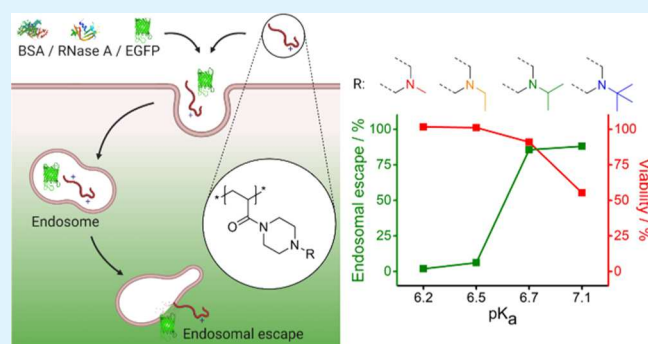
Article Recommendations



Supporting Information

ABSTRACT: Responsive polymers, which become protonated at decreasing pH, are considered a milestone in the development of synthetic cell entry vectors. Exact correlations between their properties and their ability to escape the endosome, however, often remain elusive due to hydrophobic interactions or limitations in the design of water-soluble materials with suitable basicity. Here, we present a series of well-defined, hydrophilic polypiperazines, where systematic variation of the amino moiety facilitates an unprecedented fine-tuning of the basicity or pK_a value within the physiologically relevant range (pH 6–7.4). Coincubation of HEK 293T cells with various probes, including small fluorophores or functioning proteins, revealed a rapid increase of endosomal release for polymers with pK_a values above 6.5 or 7 in serum-free or serum-containing media, respectively. Similarly, cytotoxic effects became severe at increased pK_a values (>7). Although the window for effective transport appears narrow, the discovered correlations offer a principal guideline for the design of effective polymers for endosomal escape.

KEYWORDS: membrane leakage, calcein release, endosomolytic polymers, pH-responsive polymers, basicity



INTRODUCTION

Despite continuous improvements in delivery systems, the development of materials for efficient and safe delivery of biologicals remains challenging for therapeutic treatments such as protein or gene therapy. On a cellular level, the cell membrane and endosomal entrapment represent the most challenging barriers.^{1–3} Crossing the areas of biology to materials science and chemistry, scientists have, therefore, developed a large variety of strategies based on nano-scaled virus capsids,^{4,5} liposomes,^{6,7} peptides,^{8,9} or polymers^{10,11} to overcome these barriers. Because nanocarriers are mainly taken up by endocytotic processes, release from the endosome is essential to bring the therapeutic agents to their site of action and to avoid degradation in the lysosome. Membrane-permeabilizing or cell-penetrating peptides, for example, were often derived from virus proteins and inspired the design of cell-penetrating polymers.^{12–18} Another concept relies on the use of smart polymers, which are able to react to changes in their environment. In particular, the inherent decrease in pH during the internalization process from the bloodstream (pH 7.4) via the early (pH 5.9–6.5) and late endosome (pH 5.9–4.9) to the lysosome (pH 4.9–4.0) attracted considerable attention in the design of such polymers.^{19–22} In comparison to biological carrier systems (e.g., viruses), polymers offer the advantage of scalable synthesis, limited immunogenicity, and

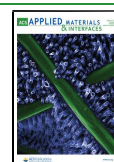
tunable chemistry. Nevertheless, most of these materials face an efficacy–toxicity dilemma, that is, cationic pH-responsive delivery agents can facilitate efficient endosomal escape of therapeutics, but often cause severe cytotoxic side effects.^{23,24} Despite its toxicity, poly(ethylene imine) (PEI) is still considered the “gold standard” for polymer-based nucleic acid delivery, and different theories have been investigated to enlighten the endosomal escape mechanism of this cationic polymer.²⁵ The proton sponge theory has been postulated with the first applications of PEI,²⁶ but it remains heavily debated in the literature.²⁷ Other reports describe an endosomal escape concept based on the destabilization of the endosomal membrane due to the interaction with increasingly cationic polymers.^{11,28,29}

Independent of the endosomal escape mechanism, the effects of all these different materials rely on their reaction to the change of the pH value or the influx of protons into the endosome. Despite the knowledge on this dependency and its

Received: January 13, 2021

Accepted: July 9, 2021

Published: July 20, 2021



influence on the endosomal escape, clear structure–property relationships for the purposeful design of polymers are hard to derive from the reported studies and materials. First, most of the reported polymers were designed for gene delivery and have to fulfill several tasks including the complexation of genetic materials. In this context, several studies identified correlations between the pH response of the polymers, often referred to as buffer capacity, in the interesting range (pH 5–7.4) and their efficacy in gene delivery. For example, the type of amine (primary, secondary, or tertiary) was found to have a crucial influence on plasmid DNA delivery.^{17,30–32} An interesting study was reported by Du et al.,³³ which focused on the impact of the acid dissociation constant (pK_a), a measure of the basicity of a material correlating with the buffer range, of various copolymers on the efficacy of siRNA delivery. While pK_a values between 5.8 and 6.2 were identified as the most effective, the reported polymers also undergo a phase transition with the change of the pH value, which is related to their inherent hydrophobic structure. Indeed, most pH-responsive polymers with pK_a values in the interesting range of 6–7 are hydrophobic in their neutral state, which certainly impacts their membrane interaction and complicates the evaluation of independent factors.^{34,35} Pure hydrophilic polymers with pK_a values close to 6 are based on imidazole units, as also present in histidine.³⁶ While no clear conclusion on structure–property correlations can be drawn from the reported materials, the incorporation of imidazole or histidine moieties clearly enhanced the efficacy of the delivery systems, which was attributed to the beneficial pK_a value.^{37–39} Moreover, the second protonation of diamino ethylene moieties (a subunit of PEI) was also found to occur around pH 6 and is crucial for efficient gene delivery,⁴⁰ while similar units with a slightly lower second pK_a (≈ 5.5) previously resulted in no enhancement.⁴¹ Therefore, we consider it crucial to investigate the fundamental impact of the pK_a or buffer capacity, respectively, in the decisive range (pH 5–7.4) for endosomal escape independently of the delivery of biologicals.⁴² The key challenge remains to find suitable materials, which enable a fine-tuning of the pK_a without major structural changes and good solubility in aqueous media over a broad pH range.

Inspired by the chemical structure of commonly used biological buffers (e.g., HEPES buffer), we envisaged polypiperazines as an interesting class of pH-responsive materials, which have so far not been considered for any biomedical applications. Nevertheless, previous reports indicate favorable pK_a values, which can be tuned by the respective substituents.^{43,44} Moreover, the monomers are accessible with a simple reaction step and the acrylamide structure allows controlled polymerization via the reversible addition–fragmentation chain transfer (RAFT) process. Small but systematic variations of the substituents on the amino group should influence the resulting pK_a value of the polymers by an enhanced inductive effect from methyl (Me) to ethyl (Et), *iso*-propyl (*i*Pr), and finally *tert*-butyl (*t*Bu) groups. The resulting homopolymers of various sizes were tested for cytotoxicity and the ability to induce an endosomal escape in HEK 293T cells. The latter was first investigated by a fluorescence-based assay, which evaluates the release of either the dye calcein, a tetramethylrhodamine (TRITC)-labeled dextran (70 kDa), or the model protein bovine serum albumin [BSA, 66.4 kDa, isoelectric point (pI): 4.7].⁴⁵ In addition, the escape of intact proteins was tested using a pH-sensitivity-

enhanced green fluorescent protein (EGFP, 33 kDa, pI: 6.2),⁴⁶ and RNase A (14 kDa, pI: 8.6),⁴⁵ which induces apoptosis if released into the cytosol. Cytotoxicity and biocompatibility were evaluated by cell viability assays (metabolic rate and integrity of plasma membranes) using HEK 293T cells. In addition, erythrocyte aggregation and hemolysis assays at different pH values were conducted.

MATERIALS AND METHODS

General Procedure for the Homopolymerization of Piperazine Monomers. A typical procedure for the homopolymerization of piperazine monomers was as follows: NAI₂PP (0.5 g, 2.74 mmol, 500 equiv) was dissolved in ultrapure water (2.19 mL) and the pH-value was adjusted to 3–5 by the addition of aqueous hydrochloric acid solution. The mixture was transferred into a microwave vial, 2-(((butylthio)carbonothioyl)thio)propanoic acid (PABTC, 1.0 μ L of a 0.5 M solution in 1,4-dioxane, 5.49 μ mol, 1 equiv), VA-044 solution (9.1 μ L of a 2 wt % aqueous solution, 0.549 μ mol, 0.1 equiv), 1,4-dioxane (547 μ L), and 1,3,5-trioxane (20 mg) as an internal standard were added. To the red-labeled polymer P(NAI₂PP_{499-co}-SR101₁) 3C'', a sulforhodamine monomer (907.9 μ L of a 6 mM solution in dimethylformamide, 5.49 μ mol, 1 equiv) was added additionally. After sealing with a rubber septum, the mixture was deoxygenated by a stream of bubbled nitrogen for 20 min. To start the polymerization, the vial was placed in a preheated oil bath at 50 °C, samples (100 μ L) were successively taken, and the monomer conversion was monitored by ¹H NMR (D₂O). When no monomer could be detected, the mixture was cooled to room temperature and opened to air. For subsequent neutralization, the solution was diluted by ultrapure water (20 mL) and stirred over an excess of basic Amberlyst A21 resin for 24 h. After filtration, the neutralized polymer was obtained after lyophilization and characterized by ¹H NMR and size-exclusion chromatography (SEC). SEC (eluent: DMAc + 0.21% LiCl, PS-standard): M_n : 65 000 g mol⁻¹, M_w : 79 900 g mol⁻¹, \bar{D} = 1.23.

Size-Exclusion Chromatography. SEC of the polymers was performed on a Shimadzu system equipped with a SCL-10A system controller, a LC-10AD pump, a RID-10A refractive index (RI) detector, and a PSS SDV column with *N,N*-dimethylacetamide (DMAc) + 0.21% LiCl as the eluent.

DMAc–SEC was conducted using an Agilent 1200 series instrument (Shimadzu, Japan) equipped with a SCL-10A system controller, a LC-10AD pump, a RID-10A differential RI, and an UV/vis detector (diode array detector). The liquid chromatography system used a 1 \times GRAM 30 Å column (300 \times 0.8 mm, 10 μ m particle size, PSS, Mainz, Germany) and a 1 \times PSS GRAM 1000 Å column (300 \times 0.8 mm, 10 μ m particle size, PSS). The DMAc eluent contained 0.21% (w/w) LiCl as the additive. The column oven was set to 50 °C. Samples were run at 1 mL min⁻¹ at 40 °C. Analyte samples were filtered through a polytetrafluoroethylene membrane with a 0.45 μ m pore size prior to injection. Polystyrene (PS) narrow standards (PSS) were used to calibrate the SEC system.

Potentiometric Titration. The pK_a^{app} values were determined by potentiometric titrations of acidified solutions of the polymers using sodium hydroxide. Approximately 10 mL of solution at 1 mg mL⁻¹ was used for each potentiometric titration experiment. Potentiometric titration was performed at room temperature using automated titration (Metrohm, Herisau, Switzerland). The addition of the titrant (NaOH at 0.1 mol L⁻¹) occurred dynamically at a flow rate of 0.05 mL min⁻¹. The pH of the solution as a function of the volume of the titrant was derived from the raw titration data. From these data, the pK_a^{app} of the polymers was determined as the corresponding pH of the mean value of the volume of the titrant at the two maxima of the first derivative of this function according to the Henderson–Hasselbalch eq 1

$$\text{pH} = \text{p}K_a + \log \frac{[\text{A}^-]}{[\text{HA}]} \quad (1)$$

The degree of charge was calculated and plotted as a function of pH. The data were treated according to the published procedures with some minor modifications to fit for poly(base)s instead of poly(acid)s.⁴⁷ The buffer capacity was calculated as reported^{27,32,48} according to eq 2

$$\beta = \frac{\Delta n(\text{OH}^-)}{\Delta \text{pH}} \quad (2)$$

Cell Culture. HEK 293T cells (ACC 635, DSMZ) were routinely cultured in Dulbecco's modified eagle's medium (DMEM) with 2 mM L-glutamine (Biochrom, Berlin, Germany) supplemented with 10% fetal calf serum (FCS, Capricorn Scientific, Ebersdorfergrund, Germany), 100 U mL⁻¹ penicillin, and 100 $\mu\text{g mL}^{-1}$ streptomycin (Biochrom) at 37 °C under a humidified 5% (v/v) CO₂ atmosphere.

Cellular Uptake Studies. To investigate the uptake of the polypiperazines into cells, the homopolymers with the highest degrees of polymerization (DP) (DP: 500) were labeled with Oregon Green postpolymerization. HEK 293T cells were seeded with 10⁵ cells mL⁻¹ in 24-well plates (VWR, Radnor, US) and cultured for 32 h. The medium was changed to a fresh cell culture medium 1 h prior to treatment. The cells were incubated with Oregon Green-labeled polypiperazines in PBS (Biochrom) at 37 °C under a humidified 5% (v/v) CO₂ atmosphere. The control cells were incubated with fresh culture medium containing the same amount of PBS as the treated cells. The cells were harvested by trypsin treatment and diluted in Hank's buffered salt solution (HBSS, Sigma-Aldrich, St. Louis, US) supplemented with 2% FCS and 20 mM 4-(2-hydroxyethyl)-1-piperazineethanesulfonic acid (HEPES, Biochrom) after 16 h. To quench the outer fluorescence of the cells, a 0.4% trypan blue solution (Sigma-Aldrich, filtered through a cellulose-mixed ester membrane with a 0.22 μm pore size) was added to obtain a final concentration of 0.04%. To determine the relative uptake of the labeled homopolymers, 10,000 events were measured via flow cytometry (Cytoflex S, Beckman Coulter, Brea, US) using gates of forward and side scatters to exclude the debris and cell aggregates.

Calcein and Labeled BSA Release Assays. The cell membrane-impermeable dye calcein and the labeled protein BSA were used to determine the endosomal escape properties of the homopolymers. Calcein (Sigma-Aldrich) was dissolved in 1 M NaOH at a concentration of 50 mg mL⁻¹ to create a stock solution, which was diluted with water to generate solutions of desired concentrations for the experiments. BSA, Alexa Fluor 488 conjugate (Thermo Fisher, Waltham, US, catalogue number A13100), was dissolved in PBS at 2 mg mL⁻¹. Investigations were carried out at dimmed light. HEK 293T cells were seeded with 2 \times 10⁵ cells mL⁻¹ in cell culture dishes with a glass bottom (Cellview, Greiner Bio-One, Kremsmünster, Austria) or with 10⁵ cells mL⁻¹ in 24-well plates and cultured for 32 h. The medium was changed to fresh cell culture medium 1 h prior to treatment. The incubation solutions were prepared in PBS and diluted 1:10 into the medium. The cells were incubated at 100 $\mu\text{g mL}^{-1}$ of the respective polymer solutions in PBS and 25 $\mu\text{g mL}^{-1}$ calcein or 5 $\mu\text{g mL}^{-1}$ labeled BSA at 37 °C under a humidified 5% (v/v) CO₂ atmosphere for 16 h. The control cells were incubated with fresh culture medium containing the same concentration of calcein or labeled BSA as well as the same amount of PBS as the treated cells. Endosomal escape was evaluated either via confocal laser scanning microscopy (CLSM) or flow cytometry.

For microscopic investigations, cells were either treated with sulforhodamine 101-labeled or nonlabeled homopolymers. In any case, cells were washed twice with PBS. To image the intracellular distribution in living cells, Hoechst 33342 (Thermo Fisher) was added at a final concentration of 10 $\mu\text{g mL}^{-1}$ for 10 min to stain cell nuclei. For microscopic evaluation of endosomal escape, cells were imaged in HBSS supplemented with 2% FCS and 20 mM HEPES. Confocal live cell imaging was performed using a LSM880, Elyra PS.1 system (Zeiss, Oberkochen, Germany) applying an argon laser for excitation at 405 nm (1%) and 488 nm (5%) as well as emission filters for Hoechst (410–450 nm) and green fluorescence (490–570 nm) with gains of 800 and 700, respectively. In the case of imaging

sulforhodamine 101-labeled polymers, a laser for excitation at 561 nm (3%) and an emission filter for sulforhodamine 101 (610–700 nm) with a gain of 800 were utilized. For three-dimensional (3D) investigations, confocal live cell imaging was conducted acquiring z-stack images. HEK 293T cells in Opti-MEM were treated with the same concentrations of the compounds as described before, but were incubated for 24 h before washing. For measurements, the aforementioned LSM880, Elyra PS.1 system was used applying an argon laser for excitation at 405 nm (0.2%) and 488 nm (0.5%) as well as emission filters for Hoechst (410–450 nm) and calcein fluorescence (500–570 nm) with gains of 700 and 800, respectively. The step width for the z-steps was set to optimal (0.31 μm) with adapted pin holes. For the time series investigations of the calcein release, HEK 293T cells were seeded and treated with calcein and 100 $\mu\text{g mL}^{-1}$ P(NAiPP)₅₀₀ 3C" as described above. The LSM880, Elyra PS.1 system was used to apply an argon laser for excitation at 488 nm (0.5%) and 561 nm (2%) as well as emission filters for calcein (499–570 nm) and SR101 fluorescence (571–710 nm) with gains of 800 for both channels. Cells were incubated at 37 °C under a 5 (v/v)% CO₂ atmosphere within the microscope, while measurements were conducted every 15 min. For magnification, a 40 \times 1.4 NA plan apochromatic oil objective was applied for all the microscopy conducted. All images of all experiments were acquired (ZEN, black edition, version 2.3 SP1, Zeiss) and processed (ImageJ, Java 8) consistently across polymer-treated cells with cells serving as control.

For high-throughput analysis, cells grown in 24-well plates were harvested by trypsin treatment and resuspended in HBSS supplemented with 2% FCS and 20 mM HEPES following the washing step. 10,000 events were measured via flow cytometry using gates of forward and side scatters to exclude the debris and cell aggregates. The sides of viable cells showing a higher Alexa Fluor 488 signal than the control cells treated with the labeled BSA solely were gated.

Cytosolic RNase A Delivery. RNase A (Merck, Darmstadt, Germany, catalogue number 10109169001) was suspended in sterile ultrapure water at 10 mg mL⁻¹. RNase A delivery studies were performed using HEK 293T cells that were either treated with RNase A only or coinubated with the same RNase A concentration and various concentrations of the polypiperazines. The incubation solutions were prepared in PBS and diluted 1:10 into the medium. In order to assess the efficiency of the RNase A delivery, the alamarBlue assay was conducted. In detail, HEK 293T cells were seeded at 10³ cells mL⁻¹ (10⁴ cells per well) in a 96-well plate (VWR) and incubated for 32 h. No cells were seeded in the outer wells. The medium was changed to fresh cell culture medium 1 h prior to treatment. The cells were incubated with (i) the solvent PBS only, and they serve as control cells, (ii) RNase A at a final concentration of 500 $\mu\text{g mL}^{-1}$, (iii) the polymer solutions in PBS at the indicated concentrations (from 5 to 100 $\mu\text{g mL}^{-1}$), or (iv) both RNase A and the polymers. The control cells were incubated with fresh culture medium containing the same amount of PBS as the treated cells. After 16 h of incubation, the medium was changed to DMEM containing 10% FCS and cells were incubated for an additional 24 h. Subsequently, the medium was replaced by a mixture of fresh culture medium and the resazurin-based solution alamarBlue (Thermo Fisher). The relative cell viability relative to untreated cells (i) was analyzed as described in the Methods section for the determination of cytotoxicity (see Supporting Information).

EGFP Release Assay. Lyophilized EGFP (BioVision Inc., Milpitas, US) was reconstituted to 1 mg mL⁻¹ with sterile PBS according to the manufacturer's instructions. HEK 293T cells were seeded with 10⁵ cells mL⁻¹ in cell culture dishes with glass bottom and treated analogously to calcein and BSA release assays, but employing 50 $\mu\text{g mL}^{-1}$ EGFP and P(NAiPP)_{499-co-SR101} 3C". CLSM studies were conducted as described for the calcein and BSA release assays, but applying an argon laser for excitation at 405 nm (1%), 488 nm (5%), and 561 nm (3%) as well as emission filters for Hoechst (410–450 nm), EGFP (490–570 nm), and sulforhodamine 101 fluorescence (610–700 nm) with gains of 800, 850, and 800. Flow cytometry analysis was conducted immediately following CLSM

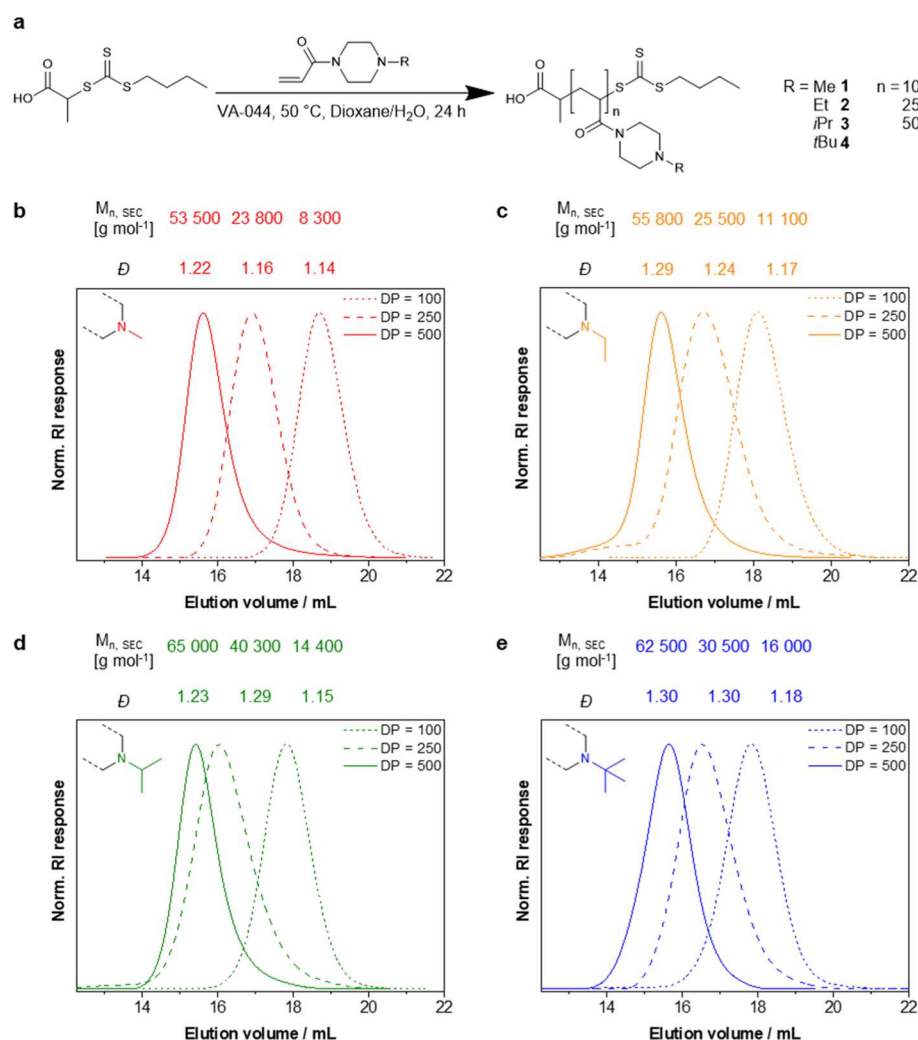


Figure 1. Synthesis and SEC traces of polypiperazines. (a) Piperazine-based vinyl monomers were polymerized via RAFT polymerization. (b–e) SEC traces of P(NAMP)_n (b), P(NAEP)_n (c), P(NAiPP)_n (d), and P(NAtBP)_n (e). SEC: DMAc + 0.21 wt % LiCl, RI detection, and PS calibration.

studies. Therefore, cells were washed with prewarmed PBS once and harvested by trypsin treatment in HBSS supplemented with 2% FCS and 20 mM HEPES. 10,000 events were measured via flow cytometry using gates of forward and side scatters to exclude the debris and cell aggregates.

Statistical Analysis. Statistical analysis was performed using SPSS Statistics (IBM, Armonk, US) version 26. Homogeneity of variances was assessed with Levene's test. In the case of homogeneity of variances, the one-way analysis of variance (ANOVA) was used, followed by Dunnett's multiple comparison test. In the case of heterogeneity of variances, Welch-ANOVA, followed by Dunnett's T3 test was conducted. For comparisons between two means (Figure 7b), the unpaired two-tailed Student's *t*-test was applied. Differences with *P* > 0.05 were considered statistically significant. The results are presented as the mean value ± standard deviation (mean ± SD) of at least three independent determinations.

RESULTS

Synthesis of pH-Responsive Polypiperazines. The initial monomers were prepared from acryloylchloride and the respective monofunctionalized (Me, Et, *i*Pr, or *t*Bu) piperazine (Figure S2). Straightforward reaction and purification by distillation enable reasonable yields and access to sufficient quantities (>20 g). In accordance with our experience on similar acrylamides,⁴⁹ the chosen RAFT

polymerization facilitates access to well-defined polymers with variable DP. The polymerization can conveniently be conducted in deionized water, which was slightly acidified to prevent hydrolysis of the trithiocarbonate chain transfer agent (CTA). Typical for the radical polymerization of acrylamide monomers in water, the polymerization rate was very high, and therefore quantitative conversions (>99%) were reached within a few hours. Consequently, a library of different homopolymers poly(*N*-acryloyl-*N'*-methylpiperazine) (P(NAMP)_n), poly(*N*-acryloyl-*N'*-ethylpiperazine) (P(NAEP)_n), poly(*N*-acryloyl-*N'*-iso-propylpiperazine) (P(NAiPP)_n), and poly(*N*-acryloyl-*N'*-tert-butylpiperazine) (P(NAtBP)_n) with DPs ranging from 100 to high values of 500 were prepared (Figures 1a and S3) while retaining good to moderate dispersities (Đ ≤ 1.3) as determined by size exclusion chromatography (SEC, Figure 1b–e). Although no purification of the residual monomer was required, the polymers were neutralized and deionized to remove the present chloride ions prior to further investigations.

All resulting polymers (Figure 2a) were fully water-soluble even in their neutralized state and at temperatures of up to 50 °C (data not shown), which is crucial for the following studies. In contrast to the lower critical solution temperatures

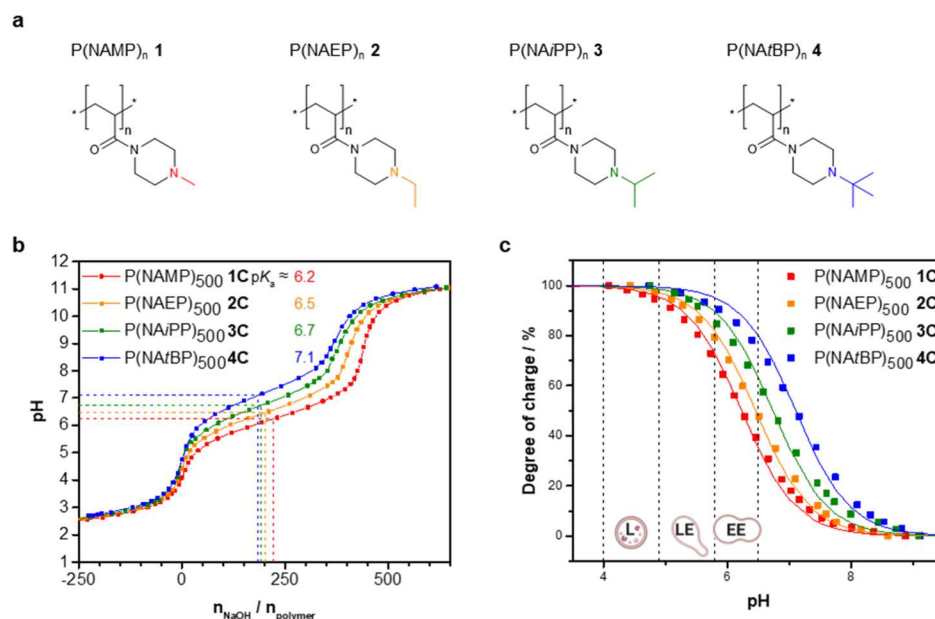


Figure 2. pH-responsiveness of polypiperazines depending on substituents. (a) Polypiperazines of the investigated library differ in their DP and pendant group. (b) Titration curves of the polypiperazines were obtained from potentiometric titrations of acidified polymer solutions against sodium hydroxide in water with 150 mM sodium chloride. The red, orange, green, and blue squares represent $P(NAMP)_{500}$, $P(NAEP)_{500}$, $P(NAiPP)_{500}$, and $P(NAfBP)_{500}$, respectively. The pK_a is indicated for each material. (c) Degree of charge at different pH values was calculated from the titration data (symbols) and according to the Henderson–Hasselbalch eq 1 (lines) for $P(NAMP)_{500}$ (red), $P(NAEP)_{500}$ (orange), $P(NAiPP)_{500}$ (green), and $P(NAfBP)_{500}$ (blue). The pH ranges within the compartments of the endolysosomal pathway, early endosomes, late endosomes, and lysosomes, are indicated according to Maxfield and Yamashiro¹⁹ and Huotari and Helenius.⁵¹ EE: Early endosome; LE: late endosome; and L: lysosome.

for previously reported poly(*N*-acryloyl-*N'*-propylpiperazine) (*n*Pr substituent),⁴³ the compact structure of our *i*Pr and *t*Bu renders the respective polymers more hydrophilic. To determine the pK_a values of the materials, acidified polymer solutions (excess of HCl) in water were titrated potentiometrically using sodium hydroxide solution. In contrast to previous titrations,⁴⁴ we added 150 mM sodium chloride to resemble physiological salt concentrations. As clearly visible in the titration profile (Figure 2b), the tested polypiperazines exhibit a broad buffer range in the desired pH range. Moreover, the systematic modifications of the pendant group resulted in a gradual shift of this buffer capacity toward higher pH values with increasing size of the substituent and in accordance with our initial hypothesis (Figure S4). To the same extent, our calculations revealed a stepwise increase of the respective pK_a^{app} values ranging from 6.2 to 7.1 (Figure 2b). A comparable titration of commercial I-PEI of 25 kDa gave a pK_a^{app} of 8.2 (Figure S5a), with a steeper increase of the pH value in the buffer region spanning a wide range of pH values (6–10, Figure S5b). This is considered a key factor for the efficacy of PEI and related to the close proximity of the reactive amino groups in PEI.^{27,50}

From the titration data, a degree of charge (ratio between the amounts of protonated units to the total amount of units) can be estimated for each pH value (Figure 2c). At the physiological pH value of blood and within the extracellular space, all polymers are partially cationic, whereas $P(NAMP)_{500}$ 1C is approximately 9%, $P(NAEP)_{500}$ 2C 13%, $P(NAiPP)_{500}$ 3C 22%, and $P(NAfBP)_{500}$ 4C 36% protonated. Along the endolysosomal pathway, all the materials become completely protonated and thus fully charged, considering the respective pH values as indicated in the Introduction section. Interestingly, the steepest increase in the degree of charge

for all materials can be expected during the transition from the extracellular space to the early endosome (Figure 2c). Within the late endosome (pH 4.9–6.0),⁵¹ the different materials become highly charged (70–90% depending on the substituent).

Cytotoxicity and Cellular Uptake of Polypiperazines.

Following the determination of basicity, the degree of charge, and buffer capacity of the polymers, we focused on their fundamental in vitro properties. Therefore, all materials were analyzed concerning their concentration-dependent cytotoxicity (tested according to ISO 10993-5) using the resazurin-based alamarBlue cell viability reagent. Despite the present cationic charges at pH 7.4, no indication of cytotoxicity was observed for $P(NAMP)_n$ 1A–C, $P(NAEP)_n$ 2A–C, and $P(NAiPP)_n$ 3A, and B (A: DP 100, B: DP 250, and C: 500) up to a final concentration of 1 mg mL^{−1} (Figure S6). $P(NAiPP)_{500}$ 3C with a high DP of 500 showed slight toxicity at concentrations above 100 μg mL^{−1} (cell viability of 70.0 ± 5.4% at 200 μg mL^{−1}). In contrast to the polymers 1–3, $P(NAfBP)_n$ 4 induced cytotoxic effects at concentrations above 50 μg mL^{−1} independent of the DP (Figure S6). This result indicates a rather sharp transition from nontoxic to harmful materials with only minor changes in terms of pK_a or charge density on the linear polymers.

For further evaluation of the cell interaction of these materials, their uptake was studied. Therefore, the polymers with highest DP were functionalized with Oregon Green (see Supporting Information for details, Figure S1a). The uptake of the labeled polymers (1C', 2C', 3C', and 4C') in HEK 293T cells was investigated via flow cytometry using different cell culture media. The obtained mean fluorescence intensities (MFI) were corrected with the respective degree of labeling. Concentration-dependent uptake studies revealed a negligible

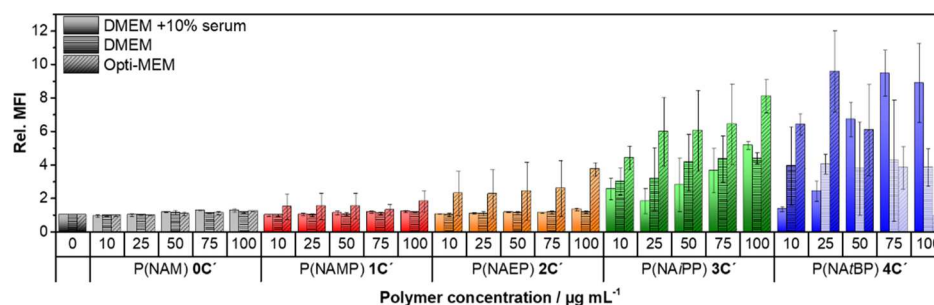


Figure 3. Cellular uptake of Oregon Green-labeled polypiperazines investigated by flow cytometry. The cellular uptake of Oregon Green-labeled polymers (DP: 500) at different concentrations was assessed by flow cytometry after 16 h. The obtained MFI values were corrected by the labeling efficiency of the polymers and are given in relation to the untreated control (see Figure S7 for the raw data and their correction). Mean \pm SD of three independent experiments is shown. Transparency of bars indicates reduced viability of the samples.

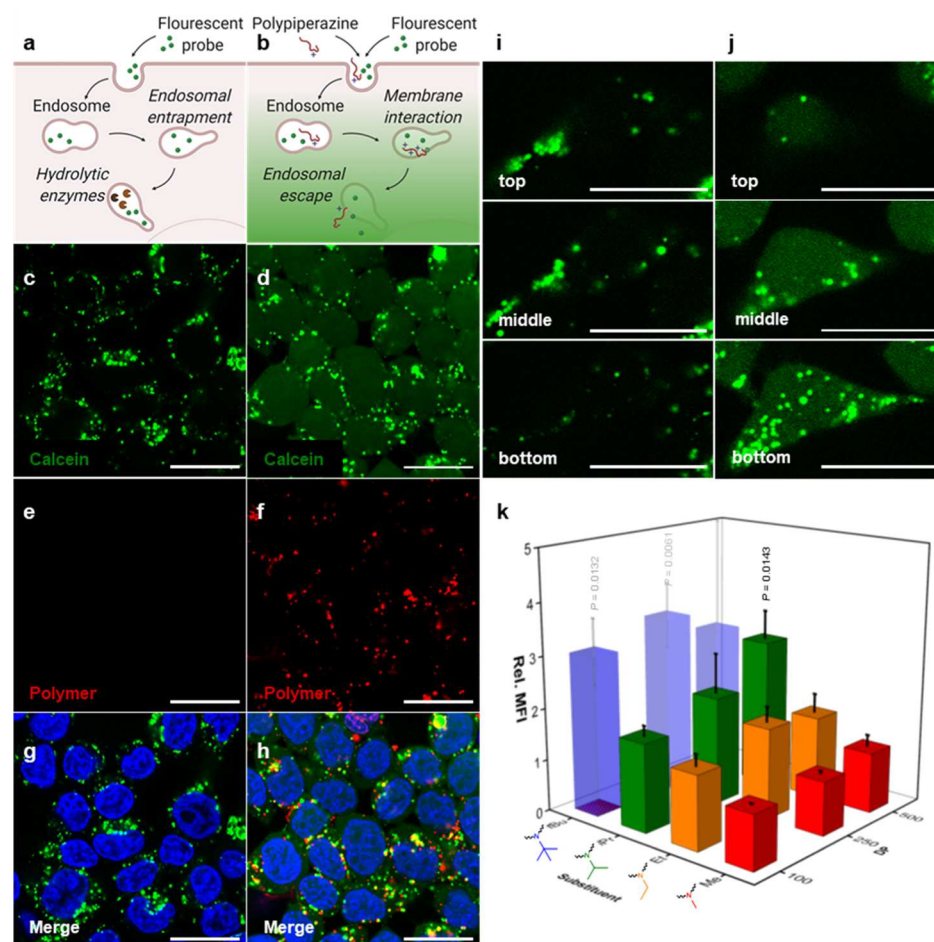


Figure 4. Endosomal escape of calcein. (a) Schematic presentation of the endocytosis and endosomal entrapment of fluorescent probes in cells not treated with endosomolytic polymers and (b) of the cytosolic and nuclear delivery of fluorescent probes facilitated by the polypiperazines. (c,e,g) Confocal images of HEK 293T cells in Opti-MEM treated with the nonmembrane permeable dye calcein as control. (d,f,h) Cellular uptake and endosomal release of calcein were imaged using HEK 293T cells that were treated with the same concentration of calcein as the control cells and additional $100 \mu\text{g mL}^{-1}$ labeled $\text{P(NAiPP)}_{500} \text{ 3C''}$ for 16 h. The calcein channel (c,d) and the corresponding image of the red channel (polymer, e,f) as well as the merge of the calcein, polymer, and Hoechst channel (g,h) are shown. (i,j) Example images of a z-stack acquisition from the lower, middle, and upper parts of a cell treated either with calcein alone as control (i) or with $\text{P(NAiPP)}_{500} \text{ 3C''}$ and calcein (j, also see S12 for images showing a co-staining with Hoechst). (c–j) Scale bar $20 \mu\text{m}$. All corresponding images comparing the calcein control with the polymer-treated samples were acquired and processed with the same settings. (k) High-throughput analysis of fluorescence intensities of HEK 293T cells in Opti-MEM treated with calcein and $100 \mu\text{g mL}^{-1}$ polypiperazines. The means \pm SD of three independent experiments relative to control cells treated with calcein only (rel. MFI = 1) are shown. For comparison, an analogous treatment with $25 \mu\text{g mL}^{-1}$ l-PEI resulted in a rel. MFI of 2.7 ± 0.3 (mean \pm SD of three independent experiments), although only 62% of the cells were considered viable in this case. Significant differences between the means were calculated with Dunnett's T3 test. Transparency of bars indicates gated cell populations below 70% (slight transparency) or 50% (distinct transparency) according to reduced viability of the samples. (a,b) Created with biorender.com. rel. MFI—relative mean fluorescence intensity.

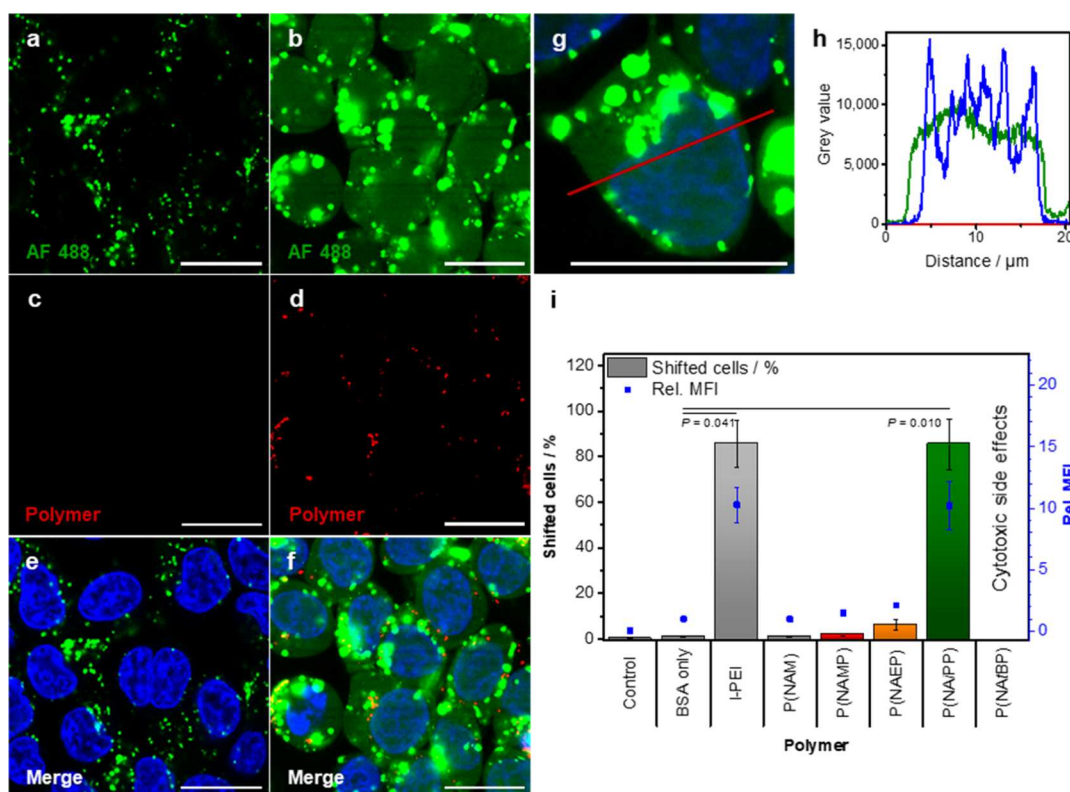


Figure 5. Endosomal escape of labeled BSA. (a) Confocal images of HEK 293T cells in Opti-MEM show cellular uptake and endosomal entrapment of AF 488-labeled BSA. (b) Diffuse fluorescence signals in the cytosol and nuclei were observed in HEK 293T cells treated with the same concentration of AF 488-labeled BSA as control cells but with additional 100 $\mu\text{g mL}^{-1}$ labeled P(NAiPP)₅₀₀ 3C'' for 16 h. (a,b) AF 488 channel (BSA) and (c,d) corresponding images of the polymer channel as well as (e,f) merged images with the Hoechst channel are shown. (a–f) All images comparing control and treated sample were acquired and processed with the same settings. (g) A merged image of the Hoechst and the BSA channel of a HEK 293T cell treated as described for (b), and (h) the corresponding plot profile of the AF 488 signal in comparison to the Hoechst signal are shown (refer to S14 for the corresponding image of the control). (a–g) Scale bar 20 μm . (i) Endosomal escape was quantified via flow cytometry in HEK 293T cells treated with labeled BSA and polymers at comparable reactive amine contents. Means \pm SD of three independent experiments are shown. Significant differences between the means of the percentages of shifted cells were calculated with Dunnett's T3 test. AF 488—Alexa Fluor 488, and rel. MFI—relative mean fluorescence intensity.

cellular uptake of labeled P(NAMP)₅₀₀ 1C' and P(NAEP)₅₀₀ 2C' into HEK 293T cells in DMEM with 10% or without serum (Figure 3). P(NAiPP)₅₀₀ 3C' and P(NAiBP)₅₀₀ 4C', the more cationic polymers, are taken up to a greater extent, with the increase for P(NAiBP)₅₀₀ 4C' being superior. In Opti-MEM, a modified DMEM with reconciled ingredients including buffers, polypiperazine uptake is generally increased compared to DMEM with or without serum. However, a similar trend was found for the basicity of the material (Figure S7). Differences observed for P(NAiBP)₅₀₀ 4C' in nonserum media may probably be due to increased membrane interaction and cytotoxic side effects. All in all, the uptake of polymers seems to be rather low, particularly for P(NAMP)₅₀₀ 1C' and P(NAEP)₅₀₀ 2C' according to the flow cytometry data, which is surprising for cationic polymers. A reduced uptake could be explained with the polymers' moderate degree of charge at pH 7.4 and their high structural similarities to P(NAM), which is considered to suppress unspecific interactions similar to polyethylene oxide (PEO) or polyoxazolines.^{52–55}

Hemocompatibility and Interaction with Plasma Membranes. To assess the biocompatibility of the materials, their influence on human red blood cells was investigated. At the physiological pH of blood, no hemoglobin release above 2% was found (Figure S8c) classifying all the materials as nonhemolytic up to a concentration of 100 $\mu\text{g mL}^{-1}$. An

aggregation of erythrocytes at pH 7.4 was only observed for P(NAiBP)₅₀₀ 4C that induced severe aggregation (Figure S8a). From this, we conclude that there are no noteworthy interactions between the polymers [except P(NAiBP)₅₀₀ 4C] and the plasma membrane of human erythrocytes, indicating high biocompatibility of the materials. In addition, similar tests were performed at pH 6 to obtain an insight into the interaction of the polymer with cellular membranes at endosomal pH. Interestingly, the behavior of some of the polymers differs considerably from their behavior at pH 7.4. Proportionally to the pK_a^{APP} and to a smaller extent to the DP of the polymers, the aggregation of erythrocytes increases considerably (Figure S8b). However, no hemolytic activity was observed at pH 6, thus indicating that the interactions between the polypiperazines and the plasma membrane are insufficient to induce leakage of hemoglobin (Figure S8d).

To investigate the interactions between the materials and plasma membranes of HEK 293T cells, the CytoTox-ONE homogenous membrane integrity assay was employed. Here, the release of the cytosolic enzyme lactate dehydrogenase (LDH) from cells with damaged plasma membranes is measured in relation to cells lysed with Triton X-100. Besides the polypiperazines 1C, 2C, 3C, and 4C with the highest DP, the commercial I-PEI (25 kDa, equal to DP \approx 580) was included in this study (Figure S9). To ensure similar

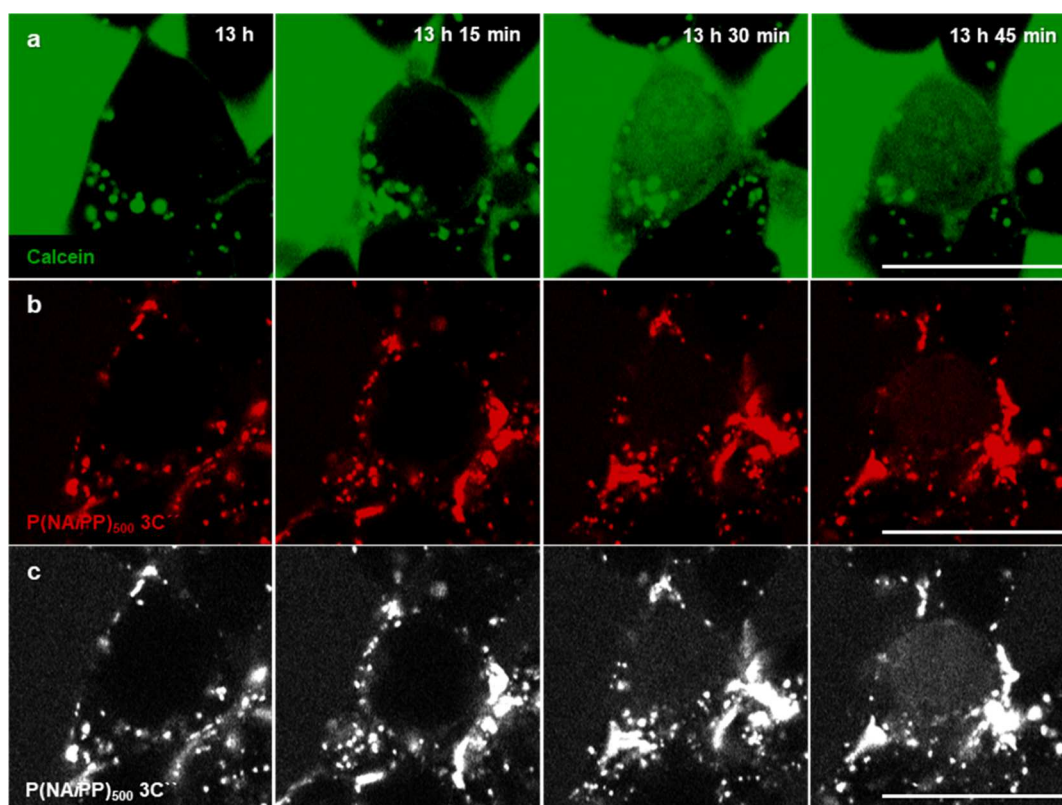


Figure 6. Timescale of endosomal calcein release by P(NAiPP)₅₀₀ 3C''. The endosomal escape of calcein in HEK 293T cells in Opti-MEM treated with 25 $\mu\text{g mL}^{-1}$ calcein and 100 $\mu\text{g mL}^{-1}$ P(NAiPP)₅₀₀ 3C'' was monitored over time. (a) Calcein channel and (b) polymer channel are shown. (c) Latter channel was added in the enhanced grayscale to improve the visibility of the faint signal in the cytosol.

concentrations of reactive amino groups, the concentrations were set to 100 $\mu\text{g mL}^{-1}$ for the polypiperazines and 25 $\mu\text{g mL}^{-1}$ for I-PEI. No significant LDH release was detected except for P(NAiBP)₅₀₀ 4C and I-PEI, both of which caused a slight LDH release of 4.3 ± 3.7 and $6.1 \pm 0.7\%$, respectively. In Opti-MEM, on the other hand, LDH release increases considerably and correlates with the increasing activity and basicity previously observed for the materials.

Endosomal Escape Efficiency Depending on Basicity, Molar Mass, and Biocompatibility. Although the experiments conducted so far are essential investigations and have already revealed interesting trends in terms of cytotoxicity as well as membrane interaction, a key element of this study is to identify correlations between the basicity/ pK_a of the materials and their capability to facilitate endosomal escape. Therefore, different fluorescent model probes, ranging from the small molecule calcein to the biomacromolecule dextran (70 kDa) or the protein BSA (66.4 kDa), were coincubated with the respective polymers to enable monitoring of a size-dependent endosomal escape. In preliminary tests, calcein, dextran, and BSA were not found to form any complexes with the tested polymers (Figure S10). Besides, the concentrations of the various compounds, polymers and buffers were kept within the isotonic range to ensure that no osmotic stress for the cells is to be expected. The pure probes were also tested as control. Initially, the subcellular distribution of the model probes and the fate of the polymers were imaged using a confocal laser scanning microscope. A punctate fluorescence pattern was observed for probes entrapped in organelles (Figure 4a,c), while more diffuse fluorescence signals indicated a cytosolic localization (Figure 4b,d).^{11,42,56} P(NAiPP)₅₀₀ 3C was

investigated first due to its pH response in the physiologically relevant pH range, sufficient uptake, and membrane activity at endosomal pH values, while it displays good biocompatibility and cell viability under physiological conditions. In order to simultaneously localize the polymer and the probe, a red fluorescent version (3C'') was synthesized (see Supporting Information for details, Figure S1b). Figure 4c–d displays HEK 293T cells treated with either calcein (control) or calcein and 3C''. The control reflects a punctated pattern, while a diffuse green fluorescence within the cytoplasm can be observed for 3C'' indicating the release of calcein from the endosome (also see Figure S19e for a lower magnification image showing a larger number of cells). The red fluorescence is visible within closed compartments, which indicates that the polymer remains mostly within the endolysosomes (Figure 4e,f). To further assess the subcellular distribution of the released calcein, confocal live cell imaging in z-stacks was conducted to image the cells in 3D. A uniform calcein signal through the entire cell interior including the nucleus was observed (Figures 4i–j and S12).

Interestingly, a similar effect was also monitored for the larger BSA (66.4 kDa, Figure 5b,f, also see Figure S13). Confocal measurements confirmed the cytosolic and nuclear localization of the AF 488 signal (Figure 5g–h, also see Figure S22e for a lower magnification image), which is surprising considering the large size of BSA in comparison to the nuclear pore size. In some cases, even small quantities of the polymer were observed in the nuclei of cells (see Figure S16b), which may be an indication that the polymer is further able to assist a nuclear entry of BSA. Due to the extended incubation time of 16 h, it is also possible that BSA could be distributed

throughout the cell during mitosis when the nuclear envelope disintegrates. During a few measurements (data not shown), the AF 488 signal appeared diminished in the nucleus compared to the cytosol, which may hint at such a mechanism, but clearly further studies are required to prove the underlying process, which was beyond the scope of this work. In both cases, calcein and BSA, the rate of endosomal escape facilitated by the labeled $P(\text{NAiPP})_{500}$ 3C'' is moderate because a strong punctate fluorescence signal is still detectable within enclosed compartments. It is worth mentioning that coincubation of TRITC-labeled dextran (70 kDa) and $P(\text{NAiPP})_{500}$ 3C revealed cytosolic, but no nuclear distribution of the fluorescence signal in contrast to calcein and BSA (Figure S15). The latter difference might be attributed to a different uptake pathway of the dextran requiring an extended time frame for a possible nuclear entry in the course of mitosis, which, however, was not further pursued here. In contrast to BSA, the used dextran might further not pass the nuclear membrane due to its more random conformation and thus larger hydrodynamic size.⁵⁷

In an attempt to investigate the time dependency of this process, confocal microscopy images of the treated cells were recorded every 15 min over a period of 14 h. Interestingly, $P(\text{NAiPP})_{500}$ 3C'' showed a very clear accumulation at the plasma membrane immediately after the addition of the polymer (see Figure S16a). In our studies, the cells began to take up this polymer within the first 30 min. Cytosolic release of calcein was first observed in just over 13 h (see exemplarily chosen cell in Figure 6a). In contrast to the occurrence of a clear calcein signal throughout the cell, the amount of released polymer in the cytosol remained low, although still a very faint signal could be observed in the examined cell (see Figure 6b and gray scale image in Figure 6c for a more visible contrast, third and fourth images at 13 h 30 min and 13 h 45 min, respectively). In accordance with previous studies on PEI, only a small amount of polymer may be released, which quickly dilutes in the cytosol.⁵⁸ Considering the strong affinity of the polymers with the cell membrane, a further attachment to the remaining endolysosomal membrane is feasible, which is in accordance with the mostly punctual concentration of the SR101 signal (see Figure 6b). Following calcein release, we also could in part detect a fluorescence signal of the polymer in the nuclei (see Figure S16b, third image). However, the nuclear signal was low compared to the intensities of the remaining endolysosomes. The rather slow delivery is likely owing to the coincidence that calcein and polymer have to be present in one endosome in sufficient amounts, as they do not form any complex (see Figure S10b).

In order to investigate the endosomal escape of the polymer library, flow cytometry was used because it provides a rapid high-throughput quantification of fluorescence intensities of cells. The applied method is based on the difference of the fluorescence intensities of cells with entrapped fluorescent probes (lower relative fluorescence signal) compared to cells, where the labeled probe is released from the endolysosome (higher relative fluorescence signal).⁵⁹ When examining all polymers with regard to their endosomal escape in Opti-MEM using calcein as the probe, two accumulative trends were observed (Figure 4k, see Figure S17 for the serum-containing medium). Both DP and basicity correlate with the MFI indicating more efficient endosomal escape of the respective polymers. Similar to the uptake studies (Figure 3), the trend collapses with increasing cytotoxicity of the materials.

Cytotoxic effects, identified prior to flow cytometry by changes in the cell morphology (data not shown, also see Figure S18), occurred in particular for $P(\text{NAiBP})_{500}$ 4 (Figure 4k) and the data should, therefore, be considered with care. In the case of the nontoxic materials, the best calcein release was observed for $P(\text{NAiPP})_{500}$ 3C showing a significant increase in MFI compared to cells treated with calcein only (Figure S18h rel. MFI, $P = 0.014$). An evaluation of the ratio of positive cells was not attempted in this case due to a rather broad scattering of the data resulting in a limited accuracy in gating the appropriate cells (Figure S18d–f). As an alternative approach to determine the number of affected cells in Opti-MEM, the release was exemplarily quantified for $P(\text{NAiPP})_{500}$ 3C'' analyzing large area microscopy images (see example in Figure S19), which should further verify that this increase is due to the additional cytosolic fluorescence. For this purpose, binary images of the Hoechst and the calcein channels were generated based on a minimal threshold, which was determined in the control experiment. All cells with a significant overlap of the calcein signal and nucleus were counted as positive for a successful endosomal escape (see Supporting Information for further details). An average value of $87.7 \pm 16.5\%$ positive cells is obtained for $P(\text{NAiPP})_{500}$ 3C'' (three images compared to two control images with $0.3 \pm 0.4\%$ positive cells), which is in good agreement with the increased MFI from the flow cytometry measurements.

Because the basicity and pK_a of the polymers had a higher influence on the endosomal escape efficiency than the DP, only the polypiperazines with the highest DP were considered in following experiments and further compared to commercial l-PEI. In contrast to calcein, a more distinct pattern was observed for the release of labeled BSA (Figure S21), which facilitated a more accurate gating into positive cells compared to the control. In particular, coincubation with $P(\text{NAiPP})_{500}$ 3C resulted in a drastic increase of fluorescence intensities and the number of positive cells ($86 \pm 11\%$, $P = 0.010$), while all other polypiperazines only led to insignificant release (Figure S1). This result, however, might be because of an increased uptake of BSA in the presence of the polymers, which is why larger microscopy images as described for the calcein release were again analyzed (five different areas were evaluated, see exemplarily shown images in Figure S22). A value of $89.4 \pm 9.6\%$ positive cells was determined, which is in excellent agreement with the data from flow cytometry. In contrast to the calcein study, this drastic increase cannot only be related to the enhanced uptake (Figure 3) of $P(\text{NAiPP})_{500}$ 3C compared to the less-basic polymers. Despite its very different basicity and buffer capacity, this efficiency is only comparable to l-PEI 25 kDa ($86 \pm 10\%$, $P = 0.041$). $P(\text{NAiBP})_{500}$ 4C was not investigated as cytotoxic effects in Opti-MEM were observed, although its pK_a and degree of protonation are lower compared to those of l-PEI under the same conditions (see Figure S20 for the serum-containing medium). Of course, the different concentrations ($100 \mu\text{g mL}^{-1}$ for $P(\text{NAiBP})_{500}$ vs $25 \mu\text{g mL}^{-1}$ for l-PEI) have to be considered in this comparison, but this adjustment results in a similar amount of protonatable amino groups.

Due to the promising results, the influence of cell culture medium and polymer concentration was examined in more detail for the most promising candidates $P(\text{NAiPP})_{500}$ 3C and $P(\text{NAiBP})_{500}$ 4C as well as for the commercial l-PEI. Co-staining of endolysosomes using LysoTracker Red first of all confirmed the localization of $P(\text{NAiPP})_{500}$ 3C' and P-

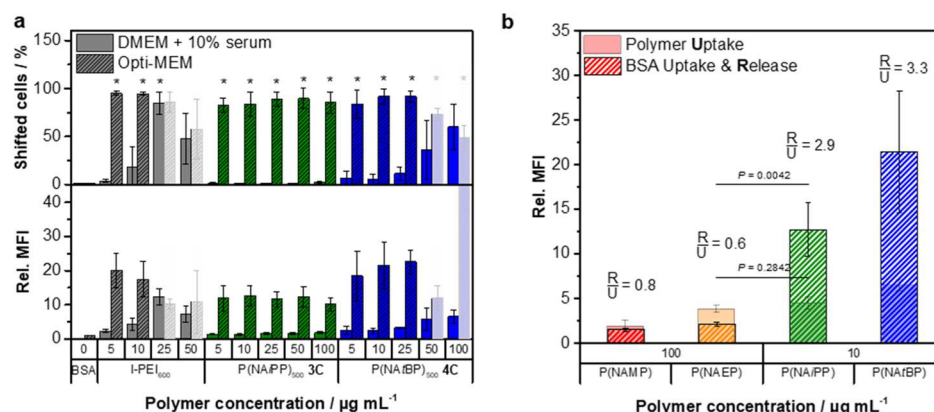


Figure 7. Polymer concentration-dependent endosomal escape of labeled BSA by novel polypiperazines. (a) Endosomal escape in HEK 293T cells treated with $5 \mu\text{g mL}^{-1}$ Alexa Fluor 488-labeled BSA, and the respective polymer concentration was quantified via flow cytometry. Means \pm SD of three independent experiments are shown. Significant differences between the means were calculated with Dunnett's T3 test ($*P < 0.001$ vs BSA). (b) Cellular uptake of Oregon Green-labeled polymers (DP: 500) as well as the endosomal escape of labeled BSA in HEK 293T cells in Opti-MEM was assessed by flow cytometry after 16 h. For the uptake studies, the obtained MFI values were corrected by the labeling efficiency of the polymers and are given in relation to the untreated control. Regarding the endosomal escape studies, the relative MFI values are given in relation to cells treated without polymers. Mean \pm SD of three independent experiments is shown. The ratio of BSA release to polymer uptake (R/U) is given for the respective polymers at the concentration shown. Significant differences between the means of rel. MFI were calculated with unpaired two-tailed student's *t*-test. rel. MFI—relative mean fluorescence intensity.

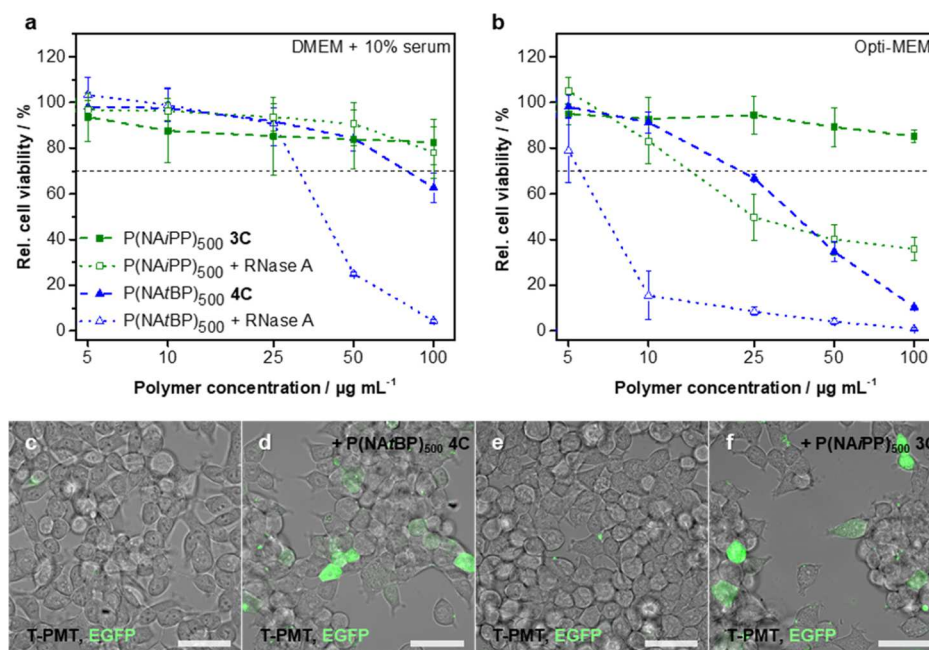


Figure 8. Cytosolic and nuclear delivery of functioning proteins. (a) Relative viability of HEK 293T cells in the presence of serum treated with indicated concentrations of the polymers P(NAiPP)₅₀₀ 3C (green, solid squares) and P(NAiBP)₅₀₀ 4C (blue, solid triangles) or with additional $500 \mu\text{g mL}^{-1}$ RNase A (respective color, open symbols) measured via the alamarBlue assay. (b) Relative viability of HEK 293T cells in Opti-MEM treated with different concentrations of P(NAiPP)₅₀₀ 3C (green, solid squares), P(NAiBP)₅₀₀ 4C (blue, solid triangles), or with additional $500 \mu\text{g mL}^{-1}$ RNase A (respective color, open symbols) measured via the alamarBlue assay. (a,b) Means \pm SD of three independent experiments are shown. (c) HEK 293T cells in the serum-containing medium were treated with EGFP for 16 h and analyzed via CLSM as a control. The overlay of the T-PMT and EGFP channel is shown. (d) HEK 293T cells in the serum-containing medium were treated with the same concentration of EGFP as control cells but with additional $50 \mu\text{g mL}^{-1}$ P(NAiBP)₅₀₀ 4C at the same time and analyzed as described in (c). (e) HEK 293T cells in Opti-MEM were treated with EGFP for 16 h and analyzed as described in (c). (f) HEK 293T cells in Opti-MEM were treated with the same concentration of EGFP as control cells but with additional $50 \mu\text{g mL}^{-1}$ P(NAiPP)₅₀₀ 3C at the same time and analyzed as described in (c). Scale bar $25 \mu\text{m}$. EGFP—enhanced green fluorescent protein and T-PMT—transmitted light detector.

(NAiBP)₅₀₀ 4C' in endolysosomes (Figure S23). The most pronounced difference is caused by the type of medium (Figure 7a). In accordance with the results above, superior endosomal escape of BSA was found for these polymers in Opti-MEM. The endosomal escape efficiency regarding the

number of positive cells in Opti-MEM appears to be largely independent of the concentration for P(NAiPP)₅₀₀ 3C and P(NAiBP)₅₀₀ 4C. A further evaluation of the impact of uptake rates on the release efficiency was made based on the data obtained for different applied concentrations of the polymers

(Figure 7b). Comparing the uptake rates of P(NAMP)₅₀₀ 1C and P(NAEP)₅₀₀ 2C at the highest tested concentration (100 $\mu\text{g mL}^{-1}$) with P(NAiPP)₅₀₀ 3C and P(NAfBP)₅₀₀ 4C at low concentrations of 10 $\mu\text{g mL}^{-1}$, similar amounts of taken up polymer are found in particular for the samples (P(NAEP)₅₀₀ 2C and P(NAiPP)₅₀₀ 3C, $P = 0.2842$). However, significantly more BSA is released into the cytosol for the latter ($P = 0.0042$, see Figure 7b). To further correlate the amount of taken up polymer with the release, we also calculated the ratio of BSA release to polymer uptake (R/U) for the above-mentioned samples. A considerable increase in this ratio is observed from P(NAEP)₅₀₀ 2C to P(NAiPP)₅₀₀ 3C. Overall, the relative MFI values for P(NAiPP)₅₀₀ 3C remained below the ones for P(NAfBP)₅₀₀ 4C or l-PEI, implying that the overall amount of released BSA from the endosome may be lower in the first case. The coincubation of HEK 293T cells with labeled BSA and various concentrations of P(NAiPP)₅₀₀ 3C in growth medium revealed no significant increase of the fluorescent signal and the number of affected cells compared to the control. Only P(NAfBP)₅₀₀ 4C and l-PEI resulted in a polymer concentration-dependent increase of the fluorescence signal and number of shifted cells.

Transport of Functioning Proteins. A crucial factor for the efficient delivery of any biological therapeutic is the preservation of its structure during this process. Commonly, the decrease of pH and the presence of hydrolases following the endolysosomal pathway trigger a degradation of biological material such as proteins. Therefore, an escape from the early endosome is the key to bypass this degradation and ensure an intact delivery of proteins, antibodies, or genetic material. Following previous reports,⁶⁰ RNase A was coincubated with our most promising polymers P(NAiPP)₅₀₀ 3C and P(NAfBP)₅₀₀ 4C in different media to investigate their capability for intact release of this protein. Also in this case, no aggregation of polymer and protein was detected (Figure S10a) and no osmotic stress is to be expected at the chosen experimentation settings. Although the pure enzyme displays no toxic activity on the cells (Figure S24), a release into the cytosol induces cell death due to the degradation of cytosolic RNA, which can be monitored by a concentration-dependent cell viability assay (Figure 8a–b). In accordance with previous experiments, a distinct difference for Opti-MEM and the serum-containing medium was observed. In the presence of serum proteins, P(NAiPP)₅₀₀ 3C induced no effect for concentrations up to 100 $\mu\text{g mL}^{-1}$. In contrast, P(NAfBP)₅₀₀ 4C was found to efficiently induce endosomal escape at 50 $\mu\text{g mL}^{-1}$ as the viability was reduced to $25.0 \pm 0.7\%$ in the presence of RNase A compared to the pure polymer causing no cytotoxic effects. The further increase of the polymer content enhanced the effect indicating a concentration-dependent release by P(NAfBP)₅₀₀ 4C, although an increased cytotoxicity of the polymer at these concentrations has to be considered. In Opti-MEM, coincubation of RNase A with both P(NAiPP)₅₀₀ 3C as well as P(NAfBP)₅₀₀ 4C affected the cell viability in a concentration-dependent manner. In particular, the coincubation of RNase A and P(NAiPP)₅₀₀ 3C, which itself caused no adverse effects on cell viability, resulted in declining cell viabilities by $50.2 \pm 0.7\%$ starting at a polymer concentration of 25 $\mu\text{g mL}^{-1}$. However, the most significant decrease (by $84.5 \pm 10.5\%$) was found for P(NAfBP)₅₀₀ 4C at a concentration of 10 $\mu\text{g mL}^{-1}$. While the pure polymer displayed no adverse effect in this case, the cell viability was reduced to approx. 10% relative to the untreated controls by

coincubation of P(NAfBP)₅₀₀ 4C and RNase A. A further increase in the polymer concentration affected cytotoxicity more than it increased endosomal escape efficiency.

In order to visually confirm the previous results, P(NAiPP)₅₀₀ 3C and P(NAfBP)₅₀₀ 4C were further tested for the delivery of EGFP monitored by CLSM. It has to be mentioned, however, that HEK 293T cells in general display a limited EGFP uptake (Figure 8c,e), which reduces the probability of concurrent presence with the polymer in the same compartments. Interestingly, coincubation with 50 $\mu\text{g mL}^{-1}$ P(NAfBP)₅₀₀ 4C in the presence of serum caused a more distinct punctate fluorescence pattern and several cells showed a diffuse EGFP fluorescence signal throughout the cytosol with varying intensities (Figure 8d). A similar result was found in the case of P(NAiPP)₅₀₀ 3C in Opti-MEM (Figure 8f). In both cases, the numbers of affected cells investigated by flow cytometry appear small compared to the results from BSA delivery (Figure S25), which again might be a result of the limited uptake of this protein.

DISCUSSION

Endosomal escape is crucial for the delivery of many therapeutics and can be facilitated by pH-responsive cationic polymeric vectors. Thereby, the pK_a or basicity of the polymers is considered as an important factor. Previous studies on correlations between pK_a and escape, however, often focused on the delivery of genetic materials, where complexation is an additional key factor,^{17,32} or comprise transitions from hydrophilic to hydrophobic at the pK_a of the materials, which alter their solubility and interactions with membranes.³³ A limiting factor is certainly the scarce number of hydrophilic polymers with pK_a values and buffer capacities between 5 and 7.4. The described polypiperazines, therefore, represent an exciting new set of materials, where protonation occurs exactly in this range and the basicity of the amino group can gradually be increased with subtle modifications on the substituent without notably affecting its solubility. This fine-tuning of buffer capacity and pK_a in this region is to our knowledge unprecedented and renders these materials ideal for investigating the impact of basicity on endosomal release and cytotoxicity. As a controlled polymerization (RAFT process) appeared feasible, we were able to create a library of different polypiperazines with DPs ranging from 100 up to 500 and pK_a values of 6.2, 6.5, 6.7, or 7.1, respectively, covering the most interesting pH region from the extracellular environment to early and late endosomes.^{19,51} The necessity of such a fine-tuning becomes already apparent from the biocompatibility tests, where significant cytotoxic effects were only observed for the most basic P(NAfBP)_n and elevated concentrations of P(NAiPP)_n with the highest DP, while all other polymers revealed no toxicity. The results corroborate a previous study about the impact of charge density and molar mass of poly(cation)s on cytotoxicity and even allow a more distinct differentiation.⁶¹ Interestingly, our release studies on various compounds ranging from small dyes (calcein) to macromolecules (proteins or dextran) depict similar correlations. A closer look, however, reveals a greater impact of the molar mass of the polymers, as only the highest DPs caused a significant release in the case of calcein. A similar trend was observed for other types of cationic polymers before,^{17,62–64} and considering the minor impact on cytotoxicity in the case of the highly charged polymers such as P(NAfBP)_n, the tuning of the polymer size might represent an interesting step to

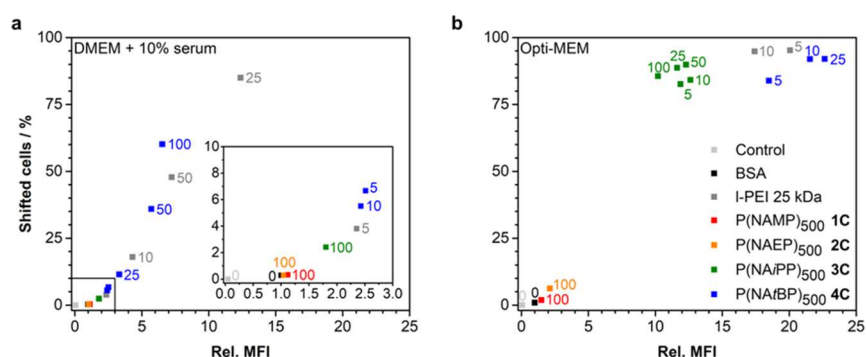


Figure 9. Influence of the cell culture medium, basicity, and concentration of the polypiperazines on endosomal escape. Exemplarily, the endosomal escape facilitated by the polypiperazines in comparison to commercial I-PEI 25 kDa is plotted to show correlations between the polymers' basicity and concentration depending on the media composition. Endosomal escape of labeled BSA in HEK 293T cells was quantified via flow cytometry in (a) serum-containing medium and (b) Opti-MEM (see Figure 5). The polymer concentration is given near the corresponding data point, including the highest investigated concentration only in the case of P(NAiPP)₅₀₀ 3C in the serum-containing medium to support clarity. Means of three independent experiments are shown. rel. MFI - relative mean fluorescence intensity.

optimize release with insignificant loss of viability. Differences in the release of BSA are on first sight accounted for an increased uptake rate for the more basic polymers. Nevertheless, a direct comparison of P(NAiPP)_n and P(NAiBP)_n at concentrations, where a similar uptake is given (Figure 7b), revealed that an important factor for efficient release of larger molecules seems to be the pK_a of the polymers. More significantly, the most basic polymers P(NAiBP)_n and P(NAiPP)_n appeared to be effective at any tested concentration (Figure 9), which was as low as 5 $\mu\text{g mL}^{-1}$, which corroborates our assumption that a key factor is the basicity of the polymers. However, a clear distinction has to be made between the applied conditions. Although P(NAiPP)_n can cause a considerable release in Opti-MEM without signs of toxicity in the tested range, almost no effect is found in the serum-containing medium (DMEM). On the contrary, the more alkaline P(NAiBP)_n suffers from increased toxicity in the first case but facilitates a concentration-dependent escape despite the presence of serum, which is comparable to the commercial I-PEI. Despite the lack of an interaction with BSA according to DLS measurements, we assume that the polypiperazines interact with other proteins or components of the serum-containing medium, resulting in a partial shielding of the charges. This aspect is also reflected in the influence of the medium on plasma membrane integrity in the presence of these polymers (Figure S9). The release efficiency in the serum-containing medium is consequently only enhanced at higher pK_a values compensating for the shielding effect of the charges by serum components, while they also mitigate toxic effects. These findings emphasize the peculiarities of media such as Opti-MEM, and demonstrate potential difficulties induced by serum proteins narrowing the window for efficient release without causing severe toxicity. Despite these challenges in the delivery itself, our final tests on RNase A and EGFP confirm that an intact transport of sensitive biological molecules can be achieved with these polymers and the activity of the proteins in the cytosol is preserved. As mentioned for the potential release mechanisms of PEI in the introduction, either a proton sponge effect or a membrane destabilization can be responsible for the release. In both cases, the protonation of the polypiperazines during the pH decrease along the endosomal maturation is crucial. The rather fast nature of the release as well as the effectivity in delivering molecules of different sizes indicate a proton sponge

effect, although similar effects would be expected for a severe destabilization of the endosomal membrane and the formation of large pores. Further detailed studies are certainly required to unequivocally determine the nature of the endosomal escape mechanism. In addition, investigations on other cell types are certainly of interest to evaluate the potential of these polypiperazines because the present study was performed exclusively using HEK 293T cells, which are considered easy-to-transfect and not very sensitive to high transfection efficiencies. However, still the presented results support that pK_a values and thus maximum buffer capacities need to be close to 7 for efficient endosomal escape, which is in good agreement with the research on ionizable lipids, where a substantial increase in delivery efficiency was identified at a pK_a value of 6.8, while pK_a values of 6.8–7 were described as the most effective.^{65–68} Consequently, the often considered range of 5–7.4^{21,69,70} for polymeric vectors should be narrowed down, which might explain previously observed discrepancies concerning the importance of buffer capacities in this range.^{40,41}

CONCLUSIONS

In summary, our study reveals a fine balance between efficiency and cytotoxicity of cationic polymers for endosomal escape and further highlights the influence by the media used. As we initially hypothesized, the fine-tuning of basicity and pK_a is pivotal for pH-responsive polymers and a clear correlation between the proportion of cationic moieties at endosomal pH and the endosomal escape efficiency was observed. The most significant response is observed if the greatest change in the degree of protonation or the maximum buffer capacity occurs in a narrow window between 7.4 and around 6.5. Further aspects can certainly be addressed in future studies, but we are convinced that the presented findings further inspire the design of tailor-made pH-responsive polymers for enhanced endosomal release. The newly discovered polypiperazines may also play a key role in this development and further studies are already ongoing in our group.

ASSOCIATED CONTENT

Supporting Information

The Supporting Information is available free of charge at <https://pubs.acs.org/doi/10.1021/acsami.1c00829>.

Polymer labeling strategies; ^1H NMR traces; potentiometric titration data; biocompatibility studies; polymer uptake data; investigations of possible polymer–protein interactions; microscopic investigations of endosomal escape of calcein, dextran, BSA, and EGFP; and image analyses and flow cytometry gating strategies (PDF)

AUTHOR INFORMATION

Corresponding Author

Johannes C. Brendel – Laboratory of Organic and Macromolecular Chemistry (IOMC), Friedrich Schiller University Jena, 07743 Jena, Germany; Jena Center for Soft Matter (JCSM), Friedrich Schiller University Jena, 07743 Jena, Germany; orcid.org/0000-0002-1206-1375; Email: johannes.brendel@uni-jena.de

Authors

Franziska Hausig – Laboratory of Organic and Macromolecular Chemistry (IOMC), Friedrich Schiller University Jena, 07743 Jena, Germany

Fabian H. Sobotta – Laboratory of Organic and Macromolecular Chemistry (IOMC), Friedrich Schiller University Jena, 07743 Jena, Germany

Friederike Richter – Laboratory of Organic and Macromolecular Chemistry (IOMC), Friedrich Schiller University Jena, 07743 Jena, Germany

Dominic O. Harz – Laboratory of Organic and Macromolecular Chemistry (IOMC), Friedrich Schiller University Jena, 07743 Jena, Germany

Anja Traeger – Laboratory of Organic and Macromolecular Chemistry (IOMC), Friedrich Schiller University Jena, 07743 Jena, Germany; Jena Center for Soft Matter (JCSM), Friedrich Schiller University Jena, 07743 Jena, Germany; orcid.org/0000-0001-7734-2293

Complete contact information is available at: <https://pubs.acs.org/10.1021/acsami.1c00829>

Author Contributions

This manuscript was written through contributions of all authors. All authors have given approval to the final version of the manuscript. J.C.B. and F.H. conceived the study. F.S. and D.O.H. synthesized the polymers. F.S., D.O.H., and F.H. characterized the polymers. F.H. and J.C.B. planned the biological experiments in consultation with A.T. and F.R. F.H. conducted the biological characterization and analyzed the data. A.T. and J.C.B. contributed to the interpretation of the results. F.H. and J.C.B. took the lead in writing the manuscript. All authors provided critical feedback and helped shape the research, analysis, and manuscript.

Notes

The authors declare no competing financial interest.

ACKNOWLEDGMENTS

This work was supported by the German Science Foundation (DFG) within the Emmy-Noether Program (project-ID: 358263073), the Collaborative Research Center PolyTarget, project A05 and B01 (project-ID: 316213987—SFB 1278), the Federal Ministry of Education and Research (BMBF, #13XP5034A PolyBioMik), and the Fonds der Chemischen Industrie (FCI). The authors thankfully acknowledge Bärbel Beringer-Siemers, Dr. Grit Festag, Lena Jesse, Carolin Kellner, Elisabeth Preußger, and Karina Rost for technical assistance as

well as Elisabeth Moek, Dr. David Pretzel, and Jana Solomun for discussions. The LSM880 ELYRA PS.1 was funded with a grant from the DFG. Furthermore, Prof. U. S. Schubert is acknowledged for his continuous support and providing access to excellent research facilities. Finally, the authors acknowledge the reviewers for their expert opinions and the resulting improvement of this work.

ABBREVIATIONS

AF 488, Alexa Fluor 488
ANOVA, analysis of variance
BSA, bovine serum albumin
CLSM, confocal laser scanning microscopy
CTA, chain transfer agent
DAD, diode array detector
DMac, *N,N*-dimethylacetamide
DMEM, Dulbecco's modified Eagle's medium
DRI, differential refractive index
EE, early endosome
EGFP, enhanced green fluorescent protein
FCS, fetal calf serum
L, lysosome
LE, late endosome
LCST, lower critical solution temperature
LDH, lactate dehydrogenase
MFI, mean fluorescence intensity
PABTC, 2-(((butylthio)carbonothioyl)thio)propanoic acid
PEI, poly(ethylenimine)
pI, isoelectric point
 pK_a , acid dissociation constant
 pK_a^{app} , apparent acid dissociation constant
P(NAEP), poly(*N*-acryloyl-*N'*-ethylpiperazine)
P(NAiPP), poly(*N*-acryloyl-*N'*-iso-propylpiperazine)
P(NAM), poly(*N*-acryloyl-*N'*-morpholine)
P(NAMP), poly(*N*-acryloyl-*N'*-methylpiperazine)
P(NA_tBP), poly(*N*-acryloyl-*N'*-*tert*-butylpiperazine)
PS, polystyrene
PTFE, polytetrafluoroethylene
RAFT, reversible addition–fragmentation chain transfer
rel. MFI, relative mean fluorescence intensity
SEC, size exclusion chromatography
SR 101, sulforhodamine 101
T-PMT, transmitted light detector

REFERENCES

- (1) Blanco, E.; Shen, H.; Ferrari, M. Principles of Nanoparticle Design for Overcoming Biological Barriers to Drug Delivery. *Nat. Biotechnol.* **2015**, *33*, 941.
- (2) Zhao, J.; Stenzel, M. H. Entry of Nanoparticles into Cells: The Importance of Nanoparticle Properties. *Polym. Chem.* **2018**, *9*, 259–272.
- (3) Pei, D.; Buyanova, M. Overcoming Endosomal Entrapment in Drug Delivery. *Bioconjugate Chem.* **2019**, *30*, 273–283.
- (4) Chailertvanitkul, V. A.; Pouton, C. W. Adenovirus: A Blueprint for Non-Viral Gene Delivery. *Curr. Opin. Biotechnol.* **2010**, *21*, 627–632.
- (5) Suwan, K.; Yata, T.; Waramit, S.; Przystal, J. M.; Stoneham, C. A.; Bentayebi, K.; Asavarut, P.; Chongchai, A.; Pothachareon, P.; Lee, K.-Y.; Topanurak, S.; Smith, T. L.; Gelovani, J. G.; Sidman, R. L.; Pasqualini, R.; Arap, W.; Hajitou, A. Next-Generation of Targeted Aavp Vectors for Systemic Transgene Delivery against Cancer. *Proc. Natl. Acad. Sci. U.S.A.* **2019**, *116*, 18571–18577.
- (6) Zhen, S.; Li, X. Liposomal Delivery of Crispr/Cas9. *Cancer Gene Ther.* **2020**, *27*, 515–527.

- (7) Ichimizu, S.; Watanabe, H.; Maeda, H.; Hamasaki, K.; Ikegami, K.; Chuang, V. T. G.; Kinoshita, R.; Nishida, K.; Shimizu, T.; Ishima, Y.; Ishida, T.; Seki, T.; Katsuki, H.; Futaki, S.; Otagiri, M.; Maruyama, T. Cell-Penetrating Mechanism of Intracellular Targeting Albumin: Contribution of Macropinocytosis Induction and Endosomal Escape. *J. Controlled Release* **2019**, *304*, 156–163.
- (8) LeCher, J. C.; Nowak, S. J.; McMurry, J. L. Breaking in and Busting Out: Cell-Penetrating Peptides and the Endosomal Escape Problem. *Biomol. Concepts* **2017**, *8*, 131–141.
- (9) Allen, J.; Brock, D.; Kondow-McConaghy, H.; Pellois, J.-P. Efficient Delivery of Macromolecules into Human Cells by Improving the Endosomal Escape Activity of Cell-Penetrating Peptides: Lessons Learned from Dftat and Its Analogs. *Biomolecules* **2018**, *8*, 50.
- (10) Evans, B. C.; Fletcher, R. B.; Kilchrist, K. V.; Dailing, E. A.; Mukalel, A. J.; Colazo, J. M.; Oliver, M.; Cheung-Flynn, J.; Brophy, C. M.; Tierney, J. W.; Isenberg, J. S.; Hankenson, K. D.; Ghimire, K.; Lander, C.; Gersbach, C. A.; Duvall, C. L. An Anionic, Endosome-Escaping Polymer to Potentiate Intracellular Delivery of Cationic Peptides, Biomacromolecules, and Nanoparticles. *Nat. Commun.* **2019**, *10*, 5012.
- (11) Smith, S. A.; Selby, L. I.; Johnston, A. P. R.; Such, G. K. The Endosomal Escape of Nanoparticles: Toward More Efficient Cellular Delivery. *Bioconjugate Chem.* **2019**, *30*, 263–272.
- (12) Prchla, E.; Plank, C.; Wagner, E.; Blaas, D.; Fuchs, R. Virus-Mediated Release of Endosomal Content in Vitro: Different Behavior of Adenovirus and Rhinovirus Serotype 2. *J. Cell Biol.* **1995**, *131*, 111–123.
- (13) Li, W.; Nicol, F.; Szoka, F. C. Gala: A Designed Synthetic Ph-Responsive Amphipathic Peptide with Applications in Drug and Gene Delivery. *Adv. Drug Delivery Rev.* **2004**, *56*, 967–985.
- (14) Stewart, M. P.; Langer, R.; Jensen, K. F. Intracellular Delivery by Membrane Disruption: Mechanisms, Strategies, and Concepts. *Chem. Rev.* **2018**, *118*, 7409.
- (15) Erazo-Oliveras, A.; Najjar, K.; Dayani, L.; Wang, T.-Y.; Johnson, G. A.; Pellois, J.-P. Protein Delivery into Live Cells by Incubation with an Endosomolytic Agent. *Nat. Methods* **2014**, *11*, 861.
- (16) Tabujew, I.; Freidel, C.; Krieg, B.; Helm, M.; Koynov, K.; Müllen, K.; Peneva, K. The Guanidinium Group as a Key Part of Water-Soluble Polymer Carriers for SiRNA Complexation and Protection against Degradation. *Macromol. Rapid Commun.* **2014**, *35*, 1191–1197.
- (17) Richter, F.; Martin, L.; Leer, K.; Moek, E.; Hausig, F.; Brendel, J. C.; Traeger, A. Tuning of Endosomal Escape and Gene Expression by Functional Groups, Molecular Weight and Transfection Medium: A Structure-Activity Relationship Study. *J. Mater. Chem. B* **2020**, *8*, 5026–5041.
- (18) Cokca, C.; Zartner, L.; Tabujew, I.; Fischer, D.; Peneva, K. Incorporation of Indole Significantly Improves the Transfection Efficiency of Guanidinium-Containing Poly(Methacrylamide)s. *Macromol. Rapid Commun.* **2020**, *41*, 1900668.
- (19) Maxfield, F. R.; Yamashiro, D. J. Endosome Acidification and the Pathways of Receptor-Mediated Endocytosis. In *Immunobiology of Proteins and Peptides IV: T-Cell Recognition and Antigen Presentation*; Atassi, M. Z., Ed.; Springer US: Boston, MA, 1987; pp 189–198.
- (20) Wagner, E. Polymers for Nucleic Acid Transfer—an Overview. In *Advances in Genetics*; Huang, L.; Liu, D.; Wagner, E., Eds.; Academic Press, 2014; Vol. 88, Chapter 8, pp 231–261.
- (21) Lächelt, U.; Wagner, E. Nucleic Acid Therapeutics Using Polyplexes: A Journey of 50 Years (and Beyond). *Chem. Rev.* **2015**, *115*, 11043–11078.
- (22) Peng, L.; Wagner, E. Polymeric Carriers for Nucleic Acid Delivery: Current Designs and Future Directions. *Biomacromolecules* **2019**, *20*, 3613–3626.
- (23) Lv, H.; Zhang, S.; Wang, B.; Cui, S.; Yan, J. Toxicity of Cationic Lipids and Cationic Polymers in Gene Delivery. *J. Controlled Release* **2006**, *114*, 100–109.
- (24) Kargaard, A.; Sluijter, J. P. G.; Klumperman, B. Polymeric SiRNA Gene Delivery — Transfection Efficiency Versus Cytotoxicity. *J. Controlled Release* **2019**, *316*, 263–291.
- (25) Lungwitz, U.; Breunig, M.; Blunk, T.; Göpferich, A. Polyethylenimine-Based Non-Viral Gene Delivery Systems. *Eur. J. Pharm. Biopharm.* **2005**, *60*, 247–266.
- (26) Boussif, O.; Lezoualc'h, F.; Zanta, M. A.; Mergny, M. D.; Scherman, D.; Demeneix, B.; Behr, J. P. A Versatile Vector for Gene and Oligonucleotide Transfer into Cells in Culture and in Vivo: Polyethylenimine. *Proc. Natl. Acad. Sci. U.S.A.* **1995**, *92*, 7297–7301.
- (27) Benjaminsen, R. V.; Mattheij, M. A.; Henriksen, J. R.; Moghimi, S. M.; Andresen, T. L. The Possible “Proton Sponge” Effect of Polyethylenimine (Pei) Does Not Include Change in Lysosomal Ph. *Mol. Ther.* **2013**, *21*, 149–157.
- (28) Vaidyanathan, S.; Orr, B. G.; Banaszak Holl, M. M. Role of Cell Membrane–Vector Interactions in Successful Gene Delivery. *Acc. Chem. Res.* **2016**, *49*, 1486–1493.
- (29) Bus, T.; Traeger, A.; Schubert, U. S. The Great Escape: How Cationic Polyplexes Overcome the Endosomal Barrier. *J. Mater. Chem. B* **2018**, *6*, 6904–6918.
- (30) Li, H.; Cortez, M. A.; Phillips, H. R.; Wu, Y.; Reineke, T. M. Poly(2-Deoxy-2-Methacrylamido Glucopyranose)-B-Poly-(Methacrylate Amine)s: Optimization of Diblock Glycopolyplexations for Nucleic Acid Delivery. *ACS Macro Lett.* **2013**, *2*, 230–235.
- (31) Sprouse, D.; Reineke, T. M. Investigating the Effects of Block Versus Statistical Glycopolyplexations Containing Primary and Tertiary Amines for Plasmid DNA Delivery. *Biomacromolecules* **2014**, *15*, 2616–2628.
- (32) Trützschler, A.-K.; Bus, T.; Reifarth, M.; Brendel, J. C.; Hoeppener, S.; Traeger, A.; Schubert, U. S. Beyond Gene Transfection with Methacrylate-Based Polyplexes—the Influence of the Amino Substitution Pattern. *Bioconjugate Chem.* **2018**, *29*, 2181–2194.
- (33) Du, L.; Wang, C.; Meng, L.; Cheng, Q.; Zhou, J.; Wang, X.; Zhao, D.; Zhang, J.; Deng, L.; Liang, Z.; Dong, A.; Cao, H. The Study of Relationships between Pka Value and SiRNA Delivery Efficiency Based on Tri-Block Copolymers. *Biomaterials* **2018**, *176*, 84–93.
- (34) Kocak, G.; Tuncer, C.; Bütün, V. Ph-Responsive Polymers. *Polym. Chem.* **2017**, *8*, 144–176.
- (35) Thavanesan, T.; Herbert, C.; Plamper, F. A. Insight in the Phase Separation Peculiarities of Poly(Dialkylaminoethyl Methacrylate)s. *Langmuir* **2014**, *30*, 5609–5619.
- (36) Velasco, D.; Réthoré, G.; Newland, B.; Parra, J.; Elvira, C.; Pandit, A.; Rojo, L.; Román, J. S. Low Polydispersity (N-Ethyl Pyrrolidine Methacrylamide-Co-1-Vinylimidazole) Linear Oligomers for Gene Therapy Applications. *Eur. J. Pharm. Biopharm.* **2012**, *82*, 465–474.
- (37) Truong, N. P.; Gu, W.; Prasad, I.; Jia, Z.; Crawford, R.; Xiao, Y.; Monteiro, M. J. An Influenza Virus-Inspired Polymer System for the Timed Release of SiRNA. *Nat. Commun.* **2013**, *4*, 1902.
- (38) Lächelt, U.; Kos, P.; Mickler, F. M.; Herrmann, A.; Salcher, E. E.; Rödl, W.; Badgular, N.; Bräuchle, C.; Wagner, E. Fine-Tuning of Proton Sponges by Precise Diaminoethanes and Histidines in Pdna Polyplexes. *Nanomedicine* **2014**, *10*, 35–44.
- (39) Gallon, E.; Matini, T.; Sasso, L.; Mantovani, G.; Armiñan de Benito, A.; Sanchis, J.; Caliceti, P.; Alexander, C.; Vicent, M. J.; Salmaso, S. Triblock Copolymer Nanovesicles for Ph-Responsive Targeted Delivery and Controlled Release of SiRNA to Cancer Cells. *Biomacromolecules* **2015**, *16*, 1924–1937.
- (40) Kanayama, N.; Fukushima, S.; Nishiyama, N.; Itaka, K.; Jang, W.-D.; Miyata, K.; Yamasaki, Y.; Chung, U.-i.; Kataoka, K. A Peg-Based Biocompatible Block Cationic Micelles Showing Efficient Gene Transfer toward Primary Cells. *ChemMedChem* **2006**, *1*, 439–444.
- (41) Funhoff, A. M.; van Nostrum, C. F.; Koning, G. A.; Schuurmans-Nieuwenbroek, N. M. E.; Crommelin, D. J. A.; Hennink, W. E. Endosomal Escape of Polymeric Gene Delivery Complexes Is Not Always Enhanced by Polymers Buffering at Low Ph. *Biomacromolecules* **2004**, *5*, 32–39.

- (42) Selby, L. I.; Cortez-Jugo, C. M.; Such, G. K.; Johnston, A. P. R. Nanocapsulation: Progress toward Understanding the Endosomal Escape of Polymeric Nanoparticles. *WIREs Nanomed. Nanobi.* **2017**, *9*, No. e1452.
- (43) Gan, L. H.; Gan, Y. Y.; Deen, G. R. Poly(N-Acryloyl-N'-Propylpiperazine): A New Stimuli-Responsive Polymer. *Macromolecules* **2000**, *33*, 7893–7897.
- (44) Roshan Deen, G.; Gan, L. H. Influence of Amino Group Pka on the Properties of Stimuli-Responsive Piperazine-Based Polymers and Hydrogels. *J. Appl. Polym. Sci.* **2008**, *107*, 1449–1458.
- (45) Liu, C.; Wan, T.; Wang, H.; Zhang, S.; Ping, Y.; Cheng, Y. A Boronic Acid-Rich Dendrimer with Robust and Unprecedented Efficiency for Cytosolic Protein Delivery and Crispr-Cas9 Gene Editing. *Sci. Adv.* **2019**, *5*, No. eaaw8922.
- (46) Gurunathan, S.; Woong Han, J.; Kim, E.; Kwon, D.-N.; Park, J.-K.; Kim, J.-H. Enhanced Green Fluorescent Protein-Mediated Synthesis of Biocompatible Graphene. *J. Nanobiotechnol.* **2014**, *12*, 41.
- (47) Colombani, O.; Lejeune, E.; Charbonneau, C.; Chassenieux, C.; Nicolai, T. Ionization of Amphiphilic Acidic Block Copolymers. *J. Phys. Chem. B* **2012**, *116*, 7560–7565.
- (48) Chiriac, V.; Balea, G. Buffer Index and Buffer Capacity for a Simple Buffer Solution. *J. Chem. Educ.* **1997**, *74*, 937.
- (49) Sobotta, F. H.; Kuchenbrod, M. T.; Grune, C.; Fischer, D.; Hoepfner, S.; Brendel, J. C. Elucidating Preparation-Structure Relationships for the Morphology Evolution During the Raft Dispersion Polymerization of N-Acryloyl Thiomorpholine. *Polym. Chem.* **2021**, *12*, 1668–1680.
- (50) Ziebarth, J. D.; Wang, Y. Understanding the Protonation Behavior of Linear Polyethylenimine in Solutions through Monte Carlo Simulations. *Biomacromolecules* **2010**, *11*, 29–38.
- (51) Huotari, J.; Helenius, A. Endosome Maturation. *EMBO J.* **2011**, *30*, 3481–3500.
- (52) Knop, K.; Hoogenboom, R.; Fischer, D.; Schubert, U. S. Poly(Ethylene Glycol) in Drug Delivery: Pros and Cons as Well as Potential Alternatives. *Angew. Chem., Int. Ed.* **2010**, *49*, 6288–6308.
- (53) Mochizuki, A.; Kimura, M.; Ina, A.; Tomono, Y.; Tanaka, M. Study on the Water Structure and Blood Compatibility of Poly(Acryloylmorpholine-R-Butyl Methacrylate). *J. Biomater. Sci. Polym. Ed.* **2010**, *21*, 1895–1910.
- (54) Gorman, M.; Chim, Y. H.; Hart, A.; Riehle, M. O.; Urquhart, A. J. Poly(N-Acryloylmorpholine): A Simple Hydrogel System for Temporal and Spatial Control over Cell Adhesion. *J. Biomed. Mater. Res.* **2014**, *102*, 1809–1815.
- (55) Gardey, E.; Sobotta, F. H.; Hoepfner, S.; Bruns, T.; Stallmach, A.; Brendel, J. C. Influence of Core Cross-Linking and Shell Composition of Polymeric Micelles on Immune Response and Their Interaction with Human Monocytes. *Biomacromolecules* **2020**, *21*, 1393–1406.
- (56) Martens, T. F.; Remaut, K.; Demeester, J.; De Smedt, S. C.; Braeckmans, K. Intracellular Delivery of Nanomaterials: How to Catch Endosomal Escape in the Act. *Nano Today* **2014**, *9*, 344–364.
- (57) Ribbeck, K.; Görlich, D. Kinetic Analysis of Translocation through Nuclear Pore Complexes. *EMBO J.* **2001**, *20*, 1320–1330.
- (58) Rehman, Z. u.; Hoekstra, D.; Zuhorn, I. S. Mechanism of Polyplex- and Lipoplex-Mediated Delivery of Nucleic Acids: Real-Time Visualization of Transient Membrane Destabilization without Endosomal Lysis. *ACS Nano* **2013**, *7*, 3767–3777.
- (59) Salomone, F.; Cardarelli, F.; Di Luca, M.; Boccardi, C.; Nifosi, R.; Bardi, G.; Di Bari, L.; Serresi, M.; Beltram, F. A Novel Chimeric Cell-Penetrating Peptide with Membrane-Disruptive Properties for Efficient Endosomal Escape. *J. Controlled Release* **2012**, *163*, 293–303.
- (60) Dubois, J. L. N.; Lavignac, N. Cationic Poly(Amidoamine) Promotes Cytosolic Delivery of Bovine Rnase a in Melanoma Cells, While Maintaining Its Cellular Toxicity. *J. Mater. Chem. B* **2015**, *3*, 6501–6508.
- (61) Fischer, D.; Li, Y.; Ahlemeyer, B.; Krieglstein, J.; Kissel, T. In vitro cytotoxicity testing of polycations: influence of polymer structure on cell viability and hemolysis. *Biomaterials* **2003**, *24*, 1121–1131.
- (62) Kunath, K.; von Harpe, A.; Fischer, D.; Petersen, H.; Bickel, U.; Voigt, K.; Kissel, T. Low-Molecular-Weight Polyethylenimine as a Non-Viral Vector for DNA Delivery: Comparison of Physicochemical Properties, Transfection Efficiency and in Vivo Distribution with High-Molecular-Weight Polyethylenimine. *J. Controlled Release* **2003**, *89*, 113–125.
- (63) Ahn, C.-H.; Chae, S. Y.; Bae, Y. H.; Kim, S. W. Biodegradable Poly(Ethylenimine) for Plasmid DNA Delivery. *J. Controlled Release* **2002**, *80*, 273–282.
- (64) Breunig, M.; Lungwitz, U.; Liebl, R.; Goepferich, A. Breaking up the Correlation between Efficacy and Toxicity for Nonviral Gene Delivery. *Proc. Natl. Acad. Sci. U.S.A.* **2007**, *104*, 14454–14459.
- (65) Semple, S. C.; Akinc, A.; Chen, J.; Sandhu, A. P.; Mui, B. L.; Cho, C. K.; Sah, D. W. Y.; Stebbing, D.; Crosley, E. J.; Yaworski, E.; Hafez, I. M.; Dorkin, J. R.; Qin, J.; Lam, K.; Rajeev, K. G.; Wong, K. F.; Jeffs, L. B.; Nechev, L.; Eisenhardt, M. L.; Jayaraman, M.; Kazem, M.; Maier, M. A.; Srinivasulu, M.; Weinstein, M. J.; Chen, Q.; Alvarez, R.; Barros, S. A.; De, S.; Klimuk, S. K.; Borland, T.; Kosovrasti, V.; Cantley, W. L.; Tam, Y. K.; Manoharan, M.; Ciufolini, M. A.; Tracy, M. A.; de Fougères, A.; MacLachlan, I.; Cullis, P. R.; Madden, T. D.; Hope, M. J. Rational Design of Cationic Lipids for siRNA Delivery. *Nat. Biotechnol.* **2010**, *28*, 172–176.
- (66) Alabi, C. A.; Love, K. T.; Sahay, G.; Yin, H.; Luly, K. M.; Langer, R.; Anderson, D. G. Multiparametric Approach for the Evaluation of Lipid Nanoparticles for siRNA Delivery. *Proc. Natl. Acad. Sci. U.S.A.* **2013**, *110*, 12881–12886.
- (67) Jayaraman, M.; Ansell, S. M.; Mui, B. L.; Tam, Y. K.; Chen, J.; Du, X.; Butler, D.; Eltepu, L.; Matsuda, S.; Narayanannair, J. K.; Rajeev, K. G.; Hafez, I. M.; Akinc, A.; Maier, M. A.; Tracy, M. A.; Cullis, P. R.; Madden, T. D.; Manoharan, M.; Hope, M. J. Maximizing the Potency of siRNA Lipid Nanoparticles for Hepatic Gene Silencing in Vivo. *Angew. Chem., Int. Ed.* **2012**, *51*, 8529–8533.
- (68) Whitehead, K. A.; Dorkin, J. R.; Vegas, A. J.; Chang, P. H.; Veis, O.; Matthews, J.; Fenton, O. S.; Zhang, Y.; Olejnik, K. T.; Yesilyurt, V.; Chen, D.; Barros, S.; Klebanov, B.; Novobrantseva, T.; Langer, R.; Anderson, D. G. Degradable Lipid Nanoparticles with Predictable in Vivo siRNA Delivery Activity. *Nat. Commun.* **2014**, *5*, 4277.
- (69) Varkouhi, A. K.; Scholte, M.; Storm, G.; Haisma, H. J. Endosomal Escape Pathways for Delivery of Biologicals. *J. Controlled Release* **2011**, *151*, 220–228.
- (70) Behr, J.-P. The Proton Sponge: A Trick to Enter Cells the Viruses Did Not Exploit. *Chimia* **1997**, *51*, 34–36.

Supporting Information

Correlation between Protonation of Tailor-Made Polypiperazines and Endosomal Escape for Cytosolic Protein Delivery

*Franziska Hausig¹, Fabian H. Sobotta¹, Friederike Richter¹, Dominic O. Harz¹, Anja Traeger^{1,2},
Johannes C. Brendel^{1,2*}*

¹Laboratory of Organic and Macromolecular Chemistry (IOMC), Friedrich Schiller University
Jena, Jena, Germany

²Jena Center for Soft Matter (JCSM), Friedrich Schiller University Jena, Jena, Germany

(*) corresponding author (johannes.brendel@uni-jena.de)

Tables

Table S1 Summary of polypiperazines used in this study.	13
--	----

Figures

Figure S1 Polymer labeling strategies.....	10
Figure S2 ¹ H NMR traces of piperazine-based monomers.	11
Figure S3 ¹ H NMR traces of polypiperazines.	12
Figure S4 Relative buffer capacity of polypiperazines at different pH values.	14
Figure S5 Potentiometric titration of commercial l-PEI.	14
Figure S6 Cytotoxicity of polypiperazines.....	15
Figure S7 Evaluation of polymer uptake by flow cytometry and data correction	16
Figure S8 Hemolysis and erythrocyte aggregation at different pH values.	17
Figure S9 Interaction of polypiperazines with the plasma membrane of HEK 293T cells.....	18
Figure S10 Investigations of possible interactions between polymer and tested model compounds.	19
Figure S11 T-PMT images visualizing endosomal escape of calcein.....	20
Figure S12 3D-Images of calcein release.....	20
Figure S13 T-PMT images visualizing endosomal escape of BSA.	21
Figure S14 Plot profile of BSA treated control cell.	21
Figure S15 Endosomal escape of labeled dextran investigated by CLSM.	22
Figure S16 Polymer and calcein localization at different time points.	23
Figure S17 Quantification of endosomal escape of calcein by flow cytometry.....	24
Figure S18 Evaluation of endosomal escape of calcein via flow cytometry.....	23
Figure S19 Quantification of nuclear calcein delivery (image analysis).	26
Figure S20 Quantification of endosomal escape of labeled BSA by flow cytometry.....	27
Figure S21 Evaluation of endosomal escape of labeled BSA via flow cytometry.	28
Figure S22 Quantification of nuclear BSA delivery (image analysis).....	29
Figure S23 Colocalisation of polypiperazines and endolysosomes in HEK 293T cells.	30
Figure S24 Cytotoxicity studies of RNase A without polymer addition.....	31
Figure S25 Evaluation of endosomal escape of EGFP via flow cytometry.	32

Further methods

Chemicals

All chemicals and solvents were purchased from Sigma-Aldrich, Carl Roth, Acros Organics, ThermoFisher Scientific, and Iris Biotech and used without further purification, if not stated otherwise. 2-(Butylthiocarbonothioylthio)propanoic acid (PABTC) was prepared as previously reported[1]. 1,4-dioxane was treated with inhibitor remover resin for 24 h prior to use.

General procedure for the synthesis of piperazine monomers

A typical procedure for the synthesis of piperazine monomers was as follows: 1-*Iso*-propylpiperazine (10 g, 77.97 mmol, 1 eq.) was dissolved in distilled dichlormethane (40 mL) and 4-methoxyphenol (20 mg) was added as inhibitor. Subsequently, the solution was placed in an ice-bath and a solution of acryloylchloride (9.5 mL, 116.96 mmol, 1.5 eq.) in 10 mL distilled dichlormethane was added dropwise under stirring. As the addition was finished, the mixture was allowed to warm to room temperature and stirred overnight. The color of the solution changed from yellowish to brown-red during the reaction. Afterward, 25 mL saturated NaOH solution was added, the organic phase separated and the aqueous phase washed with dichlormethane (3 × 20 mL). Next, the combined organic phase were washed with saturated NaHCO₃ solution, dried over Na₂SO₄, and filtrated. Subsequent to evaporation of the solvent, the crude product was purified by vacuum distillation (130 °C, 6 mbar) to obtain the pure product as colorless oil.

NAMP:

Yield: 45%. ¹H NMR (MeOH-d₄, 300 MHz): δ = 2.30-2.38 (s, 3H, -CH₃), 2.40-2.56 (m, 4H, -CH₂-N-), 3.62-3.78 (m, 4H, -CO-N-CH₂-), 3.56-3.80 (m, 4H, -CO-N-CH₂-), 5.73-5.79 (d, 1H, 3J = 9.0, -CH=CH₂), 6.19-6.25 (d, 1H, 3J = 18.0, -CH=CH₂), 6.73-6.82 (dd, 1H, 3J = 9.0, 3J = 18.0, -CH=CH₂).

NAEP:

Yield: 57%. ¹H NMR (MeOH-d₄, 300 MHz): δ = 1.12-1.16 (t, 3H, 3J = 6.0, -CH₃), 2.40-2.65 (m, 6H, -CH₂-N-, -N-CH₂-), 3.69 (m, 4H, -CO-N-CH₂-), 5.74-5.78 (d, 1H, 3J = 9.0, -CH=CH₂), 6.19-6.25 (d, 1H, 3J = 18.0, -CH=CH₂), 6.73-6.82 (dd, 1H, 3J = 9.0, 3J = 18.0, -CH=CH₂).

NAiPP:

Yield: 76%. ^1H NMR (MeOH- d_4 , 300 MHz): δ = 1.09-1.11 (d, 6H, $3J$ = 6.0, -CH $_3$), 2.58 (m, 4H, -CH $_2$ -N-), 2.68-2.81 (sept, 1H, $3J$ = 6.0, -CH-), 3.67 (m, 4H, -CO-N-CH $_2$ -), 5.74-5.78 (d, 1H, $3J$ = 9.0, -CH=CH $_2$), 6.18-6.25 (d, 1H, $3J$ = 18.0, -CH=CH $_2$), 6.73-6.82 (dd, 1H, $3J$ = 9.0, $3J$ = 18.0, -CH=CH $_2$).

NAiBP:

Yield: 79%. ^1H NMR (CDCl $_3$, 300 MHz): δ = 1.06 (s, 9H, -(CH $_3$) $_3$), 2.54-2.57 (t, 4H, $3J$ = 6.0, -CH $_2$ -N-), 3.54-3.67 (m, 4H, -CO-N-CH $_2$ -), 5.65-5.69 (d, 1H, $3J$ = 9.0, -CH=CH $_2$), 6.24-6.30 (d, 1H, $3J$ = 18.0, -CH=CH $_2$), 6.52-6.61 (dd, 1H, $3J$ = 9.0, $3J$ = 18.0, -CH=CH $_2$).

Fluorescence labeling of piperazine polymers

The fluorescence labeling of piperazine polymers was proceeded as follows: PNAiPP $_{500}$ (150 mg, 1.64 μmol , 1 eq.) was dissolved in anhydrous dimethylformamide (DMF, 2 mL). Afterwards, triethylamine (0.455 μL , 3.28 μmol , 2 eq.), Oregon Green cadaverine isomer 5 (164 μL of a 5 mM solution in DMF, 0.821 μmol , 0.5 eq.) and PyBOP (1.23 mg, 3.28 μmol , 2 eq.) were added under stirring. The mixture was stirred for 7 days at room temperature and a labeling efficiency of 78% was monitored by SEC (eluent: DMAc + 0.21% LiCl, UV/Vis: 480-513 nm). Afterward, the polymers were purified from free dye by dialysis of DMF solutions against deionized water for several days (MWCO: 10-12 kDa) until no more free dye could be detected.

Nuclear magnetic resonance (NMR)

^1H NMR were performed at room temperature on a AC 300 MHz spectrometer (Bruker, US). Chemical shifts (δ) are reported in ppm.

Determination of cytotoxicity

Cytotoxicity studies were performed using the mouse fibroblast cell line L929 (400620, CLS), as recommended by ISO10993-5. In detail, cells were seeded at 10^3 cells mL^{-1} (10^4 cells per well) in a 96-well plate (VWR, Germany) and incubated for 24 h. No cells were seeded in the outer wells. The medium was changed to the fresh cell culture medium 1 h prior to treatment. Afterward, the polymer solutions in phosphate buffered saline (PBS) were added to the cells at the indicated concentrations (from 5 to 1000 $\mu\text{g mL}^{-1}$), and the plates were incubated for an additional 24 h. The control cells were incubated with fresh culture medium containing the same amount of PBS as the treated cells. Subsequently, the medium was replaced by a mixture of a fresh culture medium and the resazurin-based solution alamarBlue (Thermo Fisher, Germany, prepared according to the manufacturer's instructions). After further incubation for 4 h at 37 °C under a humidified 5% (V/V) CO₂ atmosphere, the fluorescence was measured at $\lambda_{\text{ex}} = 570 \text{ nm}/\lambda_{\text{em}} = 610 \text{ nm}$, with untreated cells on the same well plate serving as negative controls. The negative control was standardized as 0% of metabolism inhibition and referred to as 100% viability. Cell viability below 70% was considered to be indicative of cytotoxicity. Experiments were conducted in five technical replicates. All experiments were conducted including Blanks, negative controls and cells treated with l-PEI (25 kDa) serving as positive control.

Lactate dehydrogenase (LDH) release assay

To investigate the polymers influence on the integrity of the cell membrane of HEK 293T cells the leakage of LDH from the cytosol to the surrounding cell culture medium was investigated utilizing the CytoTox-ONE™ Homogeneous Membrane Integrity Assay (Promega, Germany) according to the manufacturer's instructions. Briefly, cells were seeded, incubated and treated as described for uptake studies. Following incubation for 16 h the supernatant was transferred into a 96 well plate in triplicates and allowed to equilibrate to room temperature. Subsequently, the assay buffer including the resaruzin-based substrate was added to the supernatant 1:1 and incubated at room temperature for 10 min. After the addition of a stop solution included in the kit the fluorescence intensity was measured at $\lambda_{\text{Ex}}=560 \text{ nm}/\lambda_{\text{Em}}=590 \text{ nm}$. Cells treated with 0.9% (w/V) Triton X-100 30 min prior to harvest of the supernatant served as positive control (100 % LDH release). Cells

incubated solely with the same amount of PBS were used as negative control (0% LDH release). The LDH release of the polymers was calculated as follows (3):

$$\text{LDH-release} / \% = \frac{\text{FI}(\text{sample}) - \text{FI}(\text{Blank})}{\text{FI}(\text{Triton X-100}) - \text{FI}(\text{Blank})} \cdot 100 \quad (\text{S1})$$

Where FI(sample), FI(Blank), and FI(Triton X-100) represent the fluorescence intensity of a given sample, respective cell culture medium without cells, and Triton X-100 treated cells, respectively.

Hemolysis assay

The membrane damaging properties of the polymers were quantified by analyzing the release of hemoglobin from erythrocytes. Human blood was provided by the Department of Transfusion Medicine, Jena University Hospital. Briefly, human blood was centrifuged at 4 500g for 5 min. The pellet was washed three times with PBS (pH 7.4) by centrifugation at 4 500g for 5 min. Human erythrocytes were suspended in PBS at pH 7.4 to resemble physiological conditions in blood/cytoplasm or in PBS at pH 6 to mimic the slightly acidic environment in the early endosome. Polymer suspensions of different concentrations, also prepared in the respective PBS buffer, were mixed 1:1 with erythrocyte suspensions and were incubated at 37°C for 1 h. Erythrocyte suspensions were centrifuged at 2 400g for 5 min. The release of hemoglobin in the supernatant was determined at 544 nm. The absorbance was measured using a plate reader (Tecan, Germany). Concurrently, determinations were conducted with washed erythrocytes either lysed with 1% Triton X-100 or suspended in PBS at the respective pH as a reference. The hemolytic activity of the homopolymers was calculated as follows (4):

$$\text{Hemolysis} / \% = \frac{\text{A}(\text{sample}) - \text{A}(\text{PBS})}{\text{A}(\text{Triton X-100})} \quad (\text{S2})$$

Here, A(sample), A(PBS), and A(Triton X-100) are the absorbance of erythrocytes incubated with a respective sample, suspended in PBS, and erythrocytes lysed with Triton X-100, respectively. The analysis was repeated with blood from three different donors.

Erythrocyte aggregation

To investigate the behaviour of the pH-sensitive homopolymers towards cellular membranes at different pH values, human erythrocytes were treated with homopolymers under physiological

conditions in human blood (pH 7.4) and in slightly acidic environment representing the pH of the early endosome (pH 6). Erythrocyte suspensions in PBS at different pH values were prepared as described above and mixed 1:1 with polymer solutions leading to final concentrations of 100 $\mu\text{g mL}^{-1}$. After incubation at 37 °C for 2 h, erythrocyte aggregation was measured at 645 nm (Tecan, Switzerland). In addition, erythrocyte aggregation was evaluated by microscopic evaluation (100x magnification). As positive and negative assay controls erythrocytes were treated with 50 $\mu\text{g mL}^{-1}$ 25 kDa branched poly(ethylene imine) (bPEI) solution (Polysciences Inc., Warrington, US) or PBS buffer at respective pH. The aggregation activity of the homopolymers is given as an aggregation rate calculated as follows (5):

$$\text{Aggregation rate} = \frac{1}{A(\text{sample})} \quad (\text{S3})$$

Here, A(sample) is the mean absorbance of a given sample.

Dynamic light scattering (DLS)

Hydrodynamic diameter of polypiperazines with and without addition of BSA (Sigma, catalogue number 05470) or RNase A (Merck, catalogue number 10109169001) were determined by using dynamic light scattering (DLS, Zetasizer Nano-ZS, Malvern Instruments, U.K.). The polymers and BSA were diluted in PBS (pH 7.4) for size determinations. RNase A was suspended in water at a concentration of 10 mg mL^{-1} . The instrument was operated with a 633 nm He-Ne Laser and intensity fluctuations at a backscattering angle of 173° at a temperature of 25 °C were measured in three runs (each an average of 3 x 30 s). A cumulants fit was used to calculate the Z-average. The derived hydrodynamic radii are presented as mean \pm SD.

Agarose gel electrophoresis

Potential interactions between the polymers and calcein were investigated by agarose gel electrophoresis. Polymers (DP: 500, final concentration of 1 mg mL^{-1}) mixed with calcein (final concentration of 250 $\mu\text{g mL}^{-1}$) in PBS as well as Oregon Green-labeled polymers (10 mg mL^{-1}) were diluted 1:6 with green gel loading buffer (Jena Biosciences, Jena, Germany) and applied to an agarose gel (1% in TBE buffer). Electrophoresis was run in TBE buffer at 80 V for 60 min

followed by analysis with a gel documentation system (RED, Alpha Innotech, Germany, UV excitation).

Aqueous size exclusion chromatography (SEC)

Aqueous SEC was conducted using a Jasco instrument equipped with DRI and UV detector. The liquid chromatography system used PSS NOVEMA-MAX columns (guard/30/1 000/1 000 Å, 5 µm particle size). The aqueous eluent contained 0.3% (v/v) trifluoroacetic acid + 0.1 mol L⁻¹ NaCl as additive. Samples were run at 1 mL min⁻¹ at 30 °C. Aqueous SEC was measured for a 1+1 mixture of P(NA/PP)₅₀₀ **3C** (concentration: 2.1 mg mL⁻¹) and TRITC-Dex ((Tetramethylrhodamine-labeled dextran, 70 kDa, 20 mg mL⁻¹) as well as both solutions individually, using 100 µL injection volume each.

Dextran release assay

A tetramethylrhodamine functionalized dextran (70 kDa, Thermo Fisher, catalogue number D1818) was dissolved in sterile PBS at 20 mg mL⁻¹. HEK 293T cells were seeded and treated analogous to the calcein and BSA release assays but with a final concentration of 1 mg mL⁻¹ labeled dextran. CLSM analysis was conducted analogously to calcein and BSA release assays, but applying an argon laser for excitation at 405 nm (1%) and 561 nm (2%) as well as emission filters for Hoechst (410-450 nm) and TRITC fluorescence (610-670 nm) with gains of 700 and 800.

Polymer uptake with endolysosomal co-staining.

To study the uptake and fate of the polypiperazines in cells, the homopolymers with the highest DP (DP: 500) were labeled with Oregon Green after polymerization. The labeling efficiency was determined spectrometrically. To obtain equal labeling efficiencies for the microscopic studies, the labeled polymers were adjusted with unlabeled ones. HEK 293T cells (ACC 635, DSMZ) were seeded at 2 x 10⁵ cells mL⁻¹ in glass-bottomed cell culture dishes (Cellview, Greiner Bio-One, Austria) and allowed to grow for 32 h. The medium was replaced with fresh Opti-MEM 1 h before treatment. Cells were incubated with 100 µg mL⁻¹ of the respective polymer solutions at 37 °C

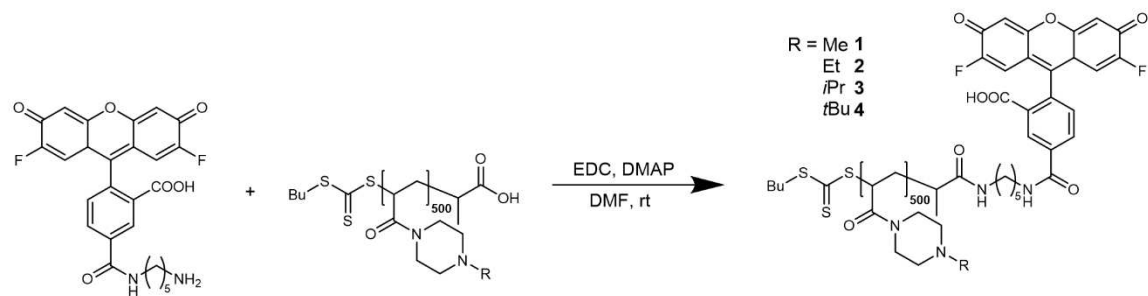
under a humidified 5% (v/v) CO₂ atmosphere for 16 h. To image intracellular distribution in live cells, Hoechst 33342 (Thermo Fisher, USA) was added at a final concentration of 5 µg mL⁻¹ for 10 min to stain cell nuclei. Five minutes before imaging, 50 nM LysoTracker Red DND-99 was added to the cells. Live cell imaging was performed with an LSM880, Elyra PS.1 system (Zeiss, Germany) using an argon laser for excitation at 405 nm (1%), 488 nm (1.2%), and 561 nm (2%), and emission filters for Hoechst (410-451 nm), Oregon green (508-544 nm), and LysoTracker Red (644-722 nm) with gains of 700, 850, and 800, respectively. An apochromatic 40 × 1.4 NA plan oil immersion objective was used for magnification. All images of all experiments were acquired (ZEN, black edition, version 2.3 SP1, Zeiss, Germany) and processed (ImageJ, Java 8[2]) consistently for polymer-treated cells and cells that served as controls. The colocalization image was created with the Image Calculator following background subtraction showing all pixels with green and red signal.

Image analysis for the quantification of endosomal escape

To check for a correlation between the microscopic data and the flow cytometry studies, endosomal release was quantified in the microscopic images. HEK 293T cells were treated as described in the main section. For this purpose, control and polymer images were acquired and processed (ImageJ, Java 8[2]) in the same way. To obtain binary images of the Hoechst and respective green channels (calcein or AF 488 for BSA), the Auto Threshold function of ImageJ was used with Huang's method. Using the Analysis Particles function, the cell nuclei were counted (corresponding to 100% of the cells). To count all nuclei with a green signal, an image was generated using the Image Calculator, showing all nuclei with a green signal. Lastly, these were also counted and related to the total number of nuclei.

Polymer synthesis

a



b

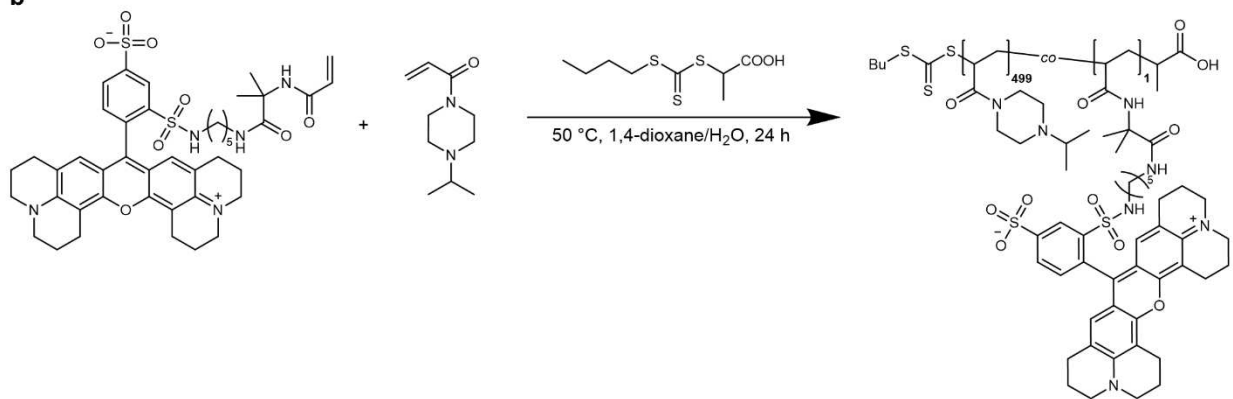


Figure S1 Polymer labeling strategies. **a** The materials with DP 500 were labeled with Oregon Green following a post-polymerization strategy. **b** NAiPP was co-polymerized with a monomer which comprised the fluorescent dye sulfurhodamine 101 to obtain a labeled version of the polymer (**3C''**) complementary to the dyes used in the study.

Polymer characterization

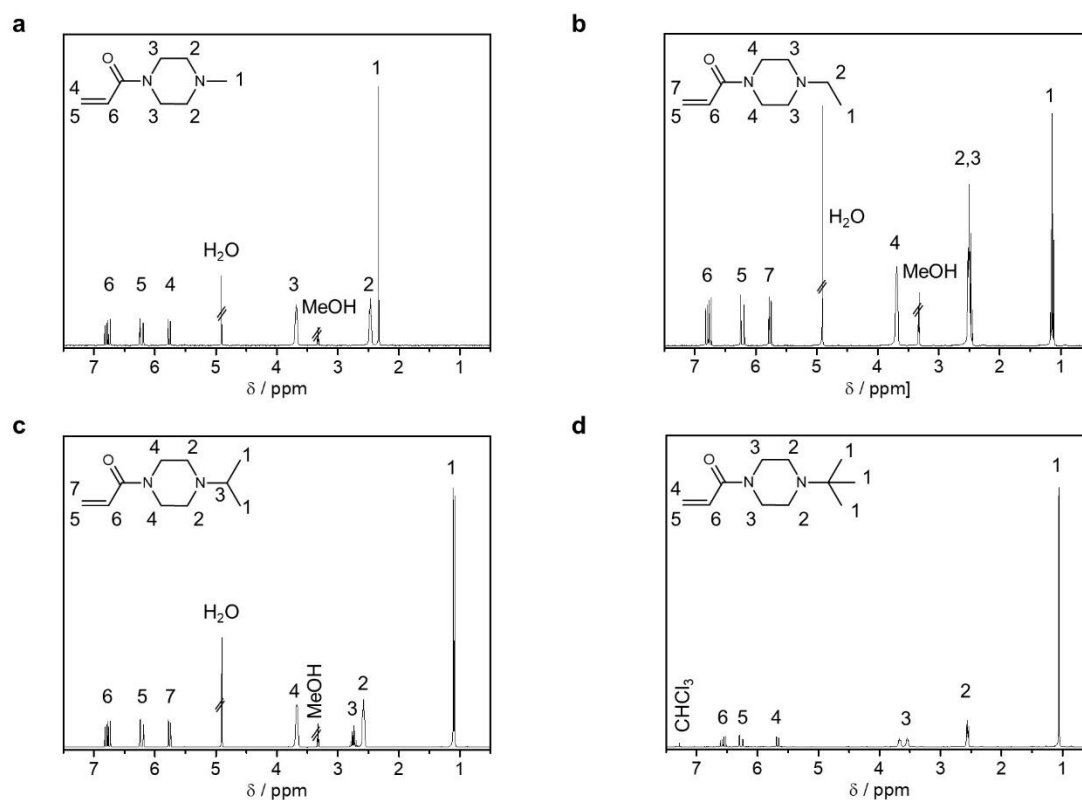


Figure S2 ^1H NMR traces of piperazine-based monomers. ^1H NMR traces of **a** NAMP, **b** NAEP, **c** NAtPP and **d** NAtBP.

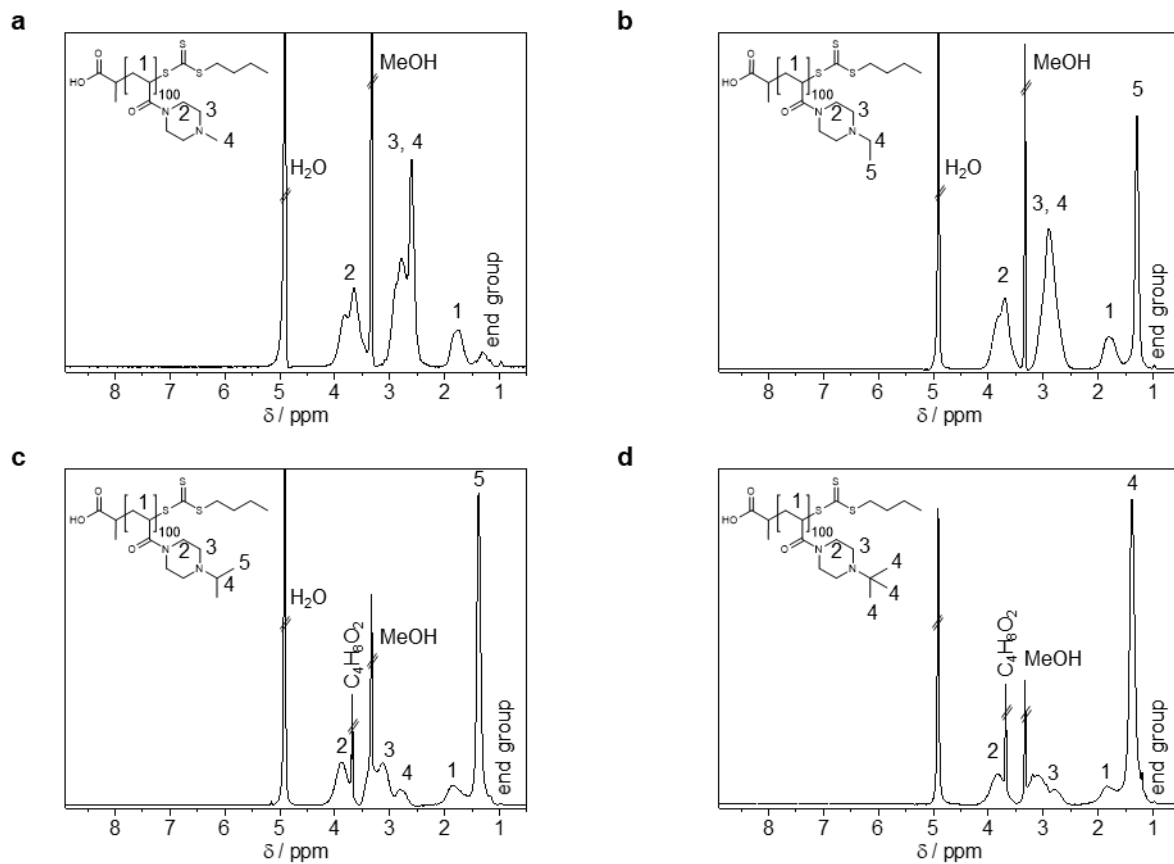


Figure S3 ^1H NMR traces of polypiperazines. ^1H NMR traces of **a** P(NAMP)₁₀₀, **b** P(NAEP)₁₀₀, **c** P(NAiPP)₁₀₀ and **d** P(NAiBP)₁₀₀.

Table S1 Summary of polypiperazines used in this study.

Polymer ID	Polymer abbreviation	$M_{n, th}^a / g\ molL^{-1}$	$M_{n, SEC}^b / g\ molL^{-1}$	\bar{D}^b
0A	P(NAM) ₁₀₀	14 400	13 100	1.06
0B	P(NAM) ₂₅₀	35 500	24 800	1.20
0C	P(NAM) ₅₀₀	70 800	47 200	1.30
0C'	P(NAM) ₅₀₀ -OG	71 300	52 600	1.32
1A	P(NAMP) ₁₀₀	15 700	8 300	1.14
1B	P(NAMP) ₂₅₀	38 800	23 800	1.16
1C	P(NAMP) ₅₀₀	77 300	53 500	1.22
1C'	P(NAMP) ₅₀₀ -OG	77 800	62 000	1.31
2A	P(NAEP) ₁₀₀	17 100	11 100	1.17
2B	P(NAEP) ₂₅₀	42 300	25 500	1.24
2C	P(NAEP) ₅₀₀	84 400	55 800	1.29
2C'	P(NAEP) ₅₀₀ -OG	84 900	68 200	1.45
3A	P(NAiPP) ₁₀₀	18 500	14 400	1.15
3B	P(NAiPP) ₂₅₀	45 800	40 300	1.29
3C	P(NAiPP) ₅₀₀	91 400	65 000	1.23
3C'	P(NAiPP) ₅₀₀ -OG	91 900	67 600	1.30
3C''	P(NAiPP _{499-co} -SR101 ₁)	92 000	52 900	1.29
4A	P(NAiBP) ₁₀₀	19 900	16 000	1.18
4B	P(NAiBP) ₂₅₀	49 300	30 500	1.30
4C	P(NAiBP) ₅₀₀	98 400	62 500	1.30
4C'	P(NAiBP) ₅₀₀ -OG	98 900	59 000	1.33

a Calculated based on $[M]_0/[CTA]_0 \times$ monomer conversion. b Determined by SEC (Eluent: DMAc + 0.21 wt% LiCl, polystyrene calibration). OG: Oregon green cadavarine 5-isomer, SR101: Sulforhodamine 101 cadavarine.

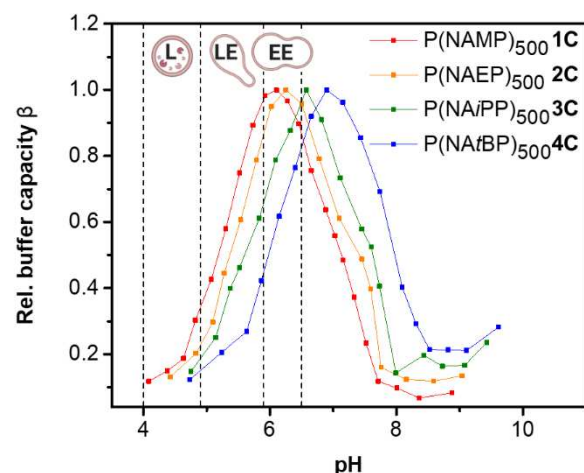


Figure S4 Relative buffer capacity of polypiperazines at different pH values. The relative buffer capacity β was calculated from the titration data according to equation (2) (see methods section) for P(NAMP)₅₀₀ (red), P(NAEP)₅₀₀ (orange), P(NAiPP)₅₀₀ (green) and P(NAiBP)₅₀₀ (blue). According to Maxfield & Yamashiro et al.[3] the pH ranges within the compartments of the endolysosomal pathway, early endosomes, late endosomes and lysosomes are indicated. EE - early endosome, LE - late endosome, L - lysosome.

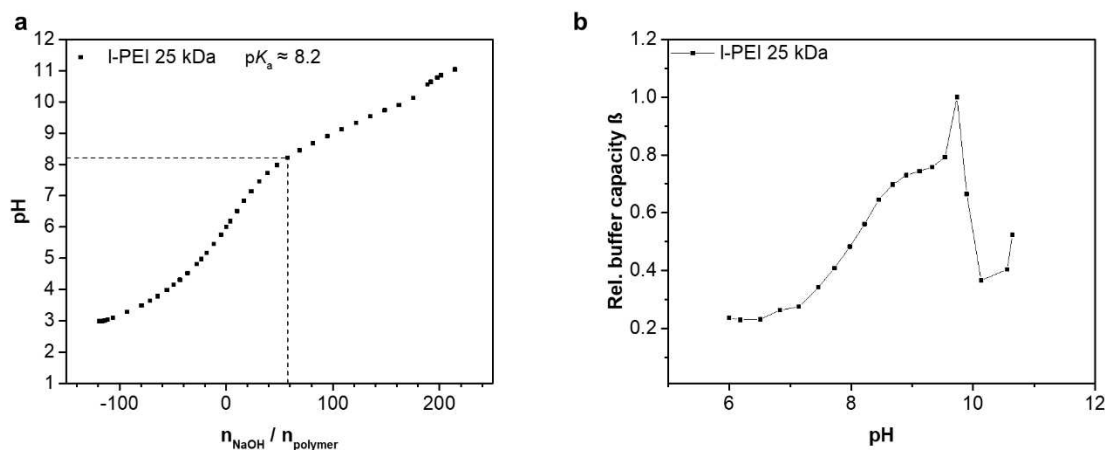


Figure S5 Potentiometric titration of commercial l-PEI. **a** The titration curve of commercial l-PEI (25 kDa) was obtained from potentiometric titration of the acidified polymer solution against sodium hydroxide in water with 150 mM sodium chloride. The pK_a is indicated. **b** The relative buffer capacity β was calculated from the titration data according to equation (2).

Biological studies

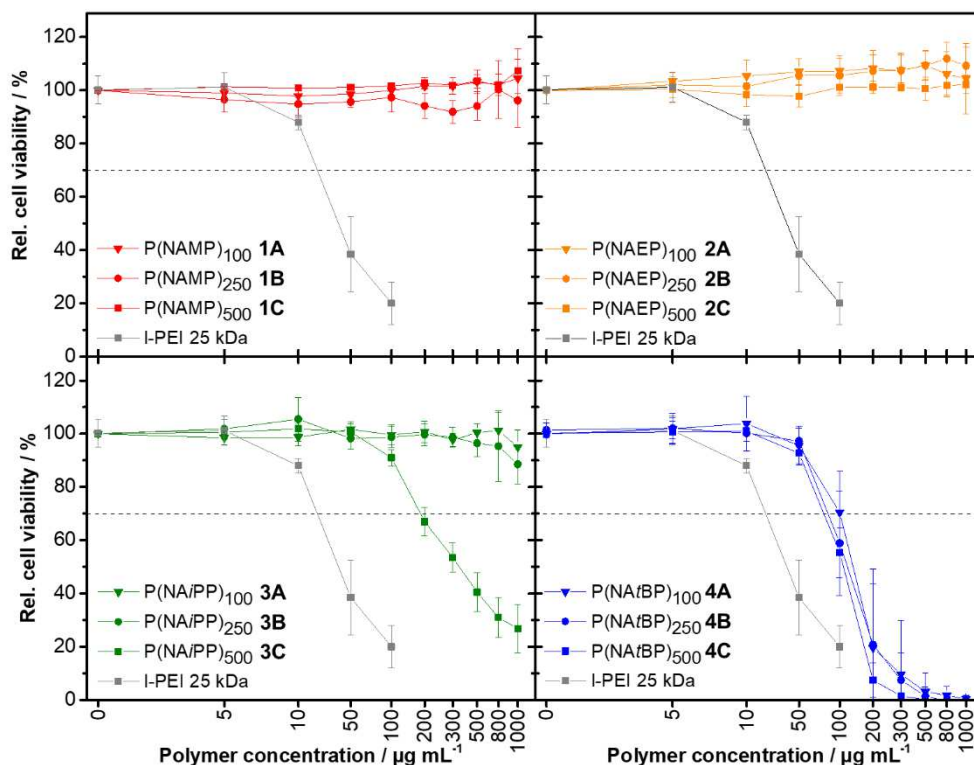


Figure S6 Cytotoxicity of polypiperazines. Polymer concentration-dependent viability of murine fibroblasts L929 was assed according to ISO10993-5 for P(NAMP)_n (red), P(NAEP)_n (orange), P(NAiPP)_n (green) and P(NAiBP)_n (blue) with DP: 100 (triangle), DP: 250 (circle) and DP: 500 (square). Mean ± SD of at least three independent experiments is shown. The viability of L929 cells treated with commercial l-PEI (25 kDa, grey squares) is given for comparison. Connecting lines do not represent actual data points; for visual support.

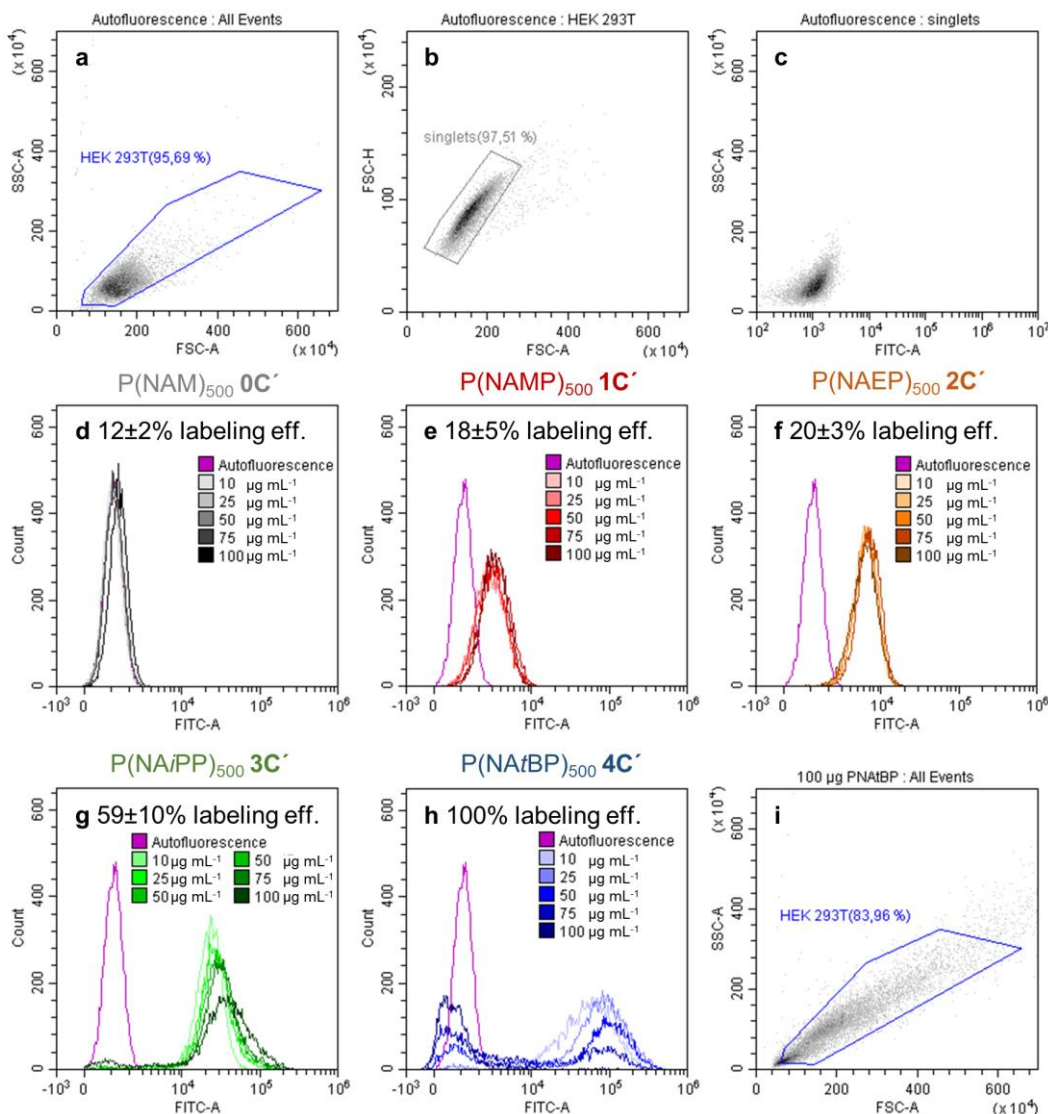


Figure S7 Evaluation of polymer uptake by flow cytometry and data correction. The cellular uptake of Oregon Green-labeled polymers (DP: 500) was assessed by flow cytometry after 16 h. Here, the gating strategy of flow cytometry analysis including forward/sideward scatter (a) to exclude debris, doublet discrimination (b) and the sideward scatter/Oregon Green signal (c) are shown. Histograms of HEK 293T cells in Opti-MEM incubated with $100 \mu\text{g mL}^{-1}$ of the respective polypiperazines (e-h) or P(NAM)₅₀₀ 0C' (d) are displayed. The corresponding labeling efficiency of the polymer in relation to P(NAiBP)₅₀₀ 4C' is given with each histogram. For further data analyses, a correction factor was applied to the obtained data to account for the different labeling efficiencies. i It should be noted that the viability of the P(NAiBP)₅₀₀ 4C' treated cells was reduced.

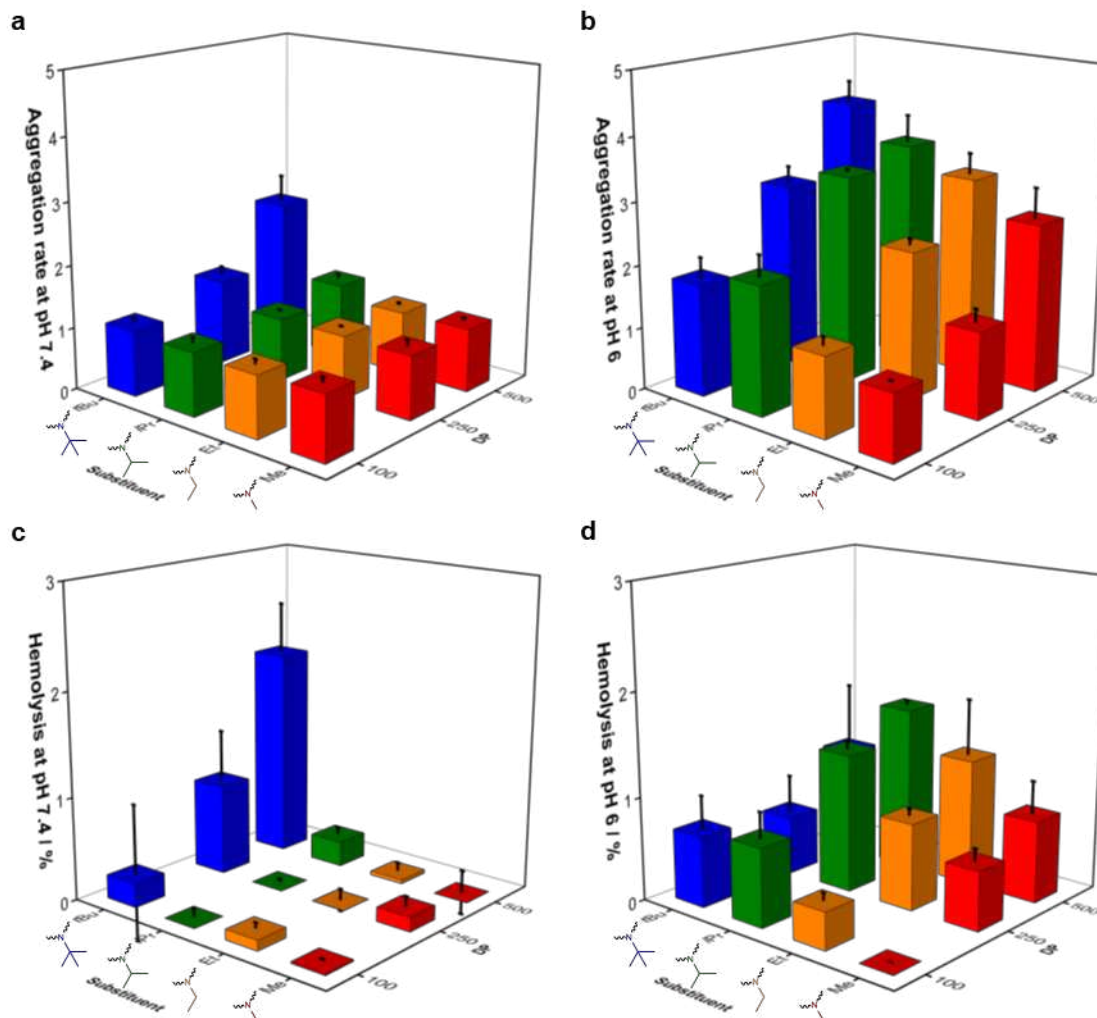


Figure S8 Hemolysis and erythrocyte aggregation at different pH values. Human blood was collected from three different donors. The containing erythrocytes were washed separately and re-suspended in PBS buffers with pH 7.4 (a, c) and pH 6 (b, d), respectively. Red blood cells a in PBS (pH 7.4) or b in PBS (pH 6) were incubated with the respective polymers at a polymer concentration of $100 \mu\text{g mL}^{-1}$ at 37°C for 1 h. The absorbance was measured via a microplate reader (Tecan) and the aggregation rate was calculated according to equation (S3). The erythrocyte aggregation was also evaluated microscopically (data not shown.) Erythrocytes c in PBS (pH 7.4) and d in PBS (pH 6) were incubated with the polymers at a concentration of $100 \mu\text{g mL}^{-1}$ at 37°C for 2 h and centrifuged. The absorbance of the supernatant was determined using a microplate reader (Tecan). Hemolysis was calculated in relation to Triton-X according to equation (S3). a - d A hemoglobin release below 2% classifies the polymers as non-hemolytic according to the ASTM standard F756-00. Mean \pm SD of experiments with blood from three different donors is given.

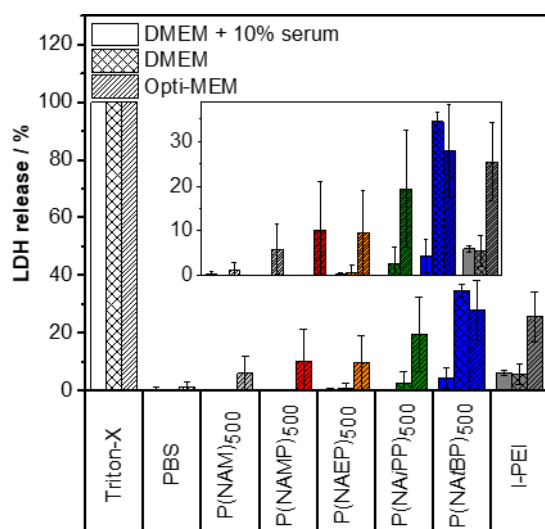


Figure S9 Interaction of polypiperazines with the plasma membrane of HEK 293T cells. The amount of released lactate dehydrogenase (LDH) in the supernatant of HEK 293T cells incubated with Oregon Green-labeled polypiperazines was measured (CytoTox-ONETM Homogeneous Membrane Integrity Assay, Promega, Germany). Cells lysed with Triton X-100 and treated with the buffer PBS only served as assay-internal positive and negative controls, respectively. Labeled P(NAM)₅₀₀ (light grey) served as a non-pH-responsive control. Commercial l-PEI (25 kDa, dark grey) was included for comparison. Mean \pm SD of three independent experiments is shown.

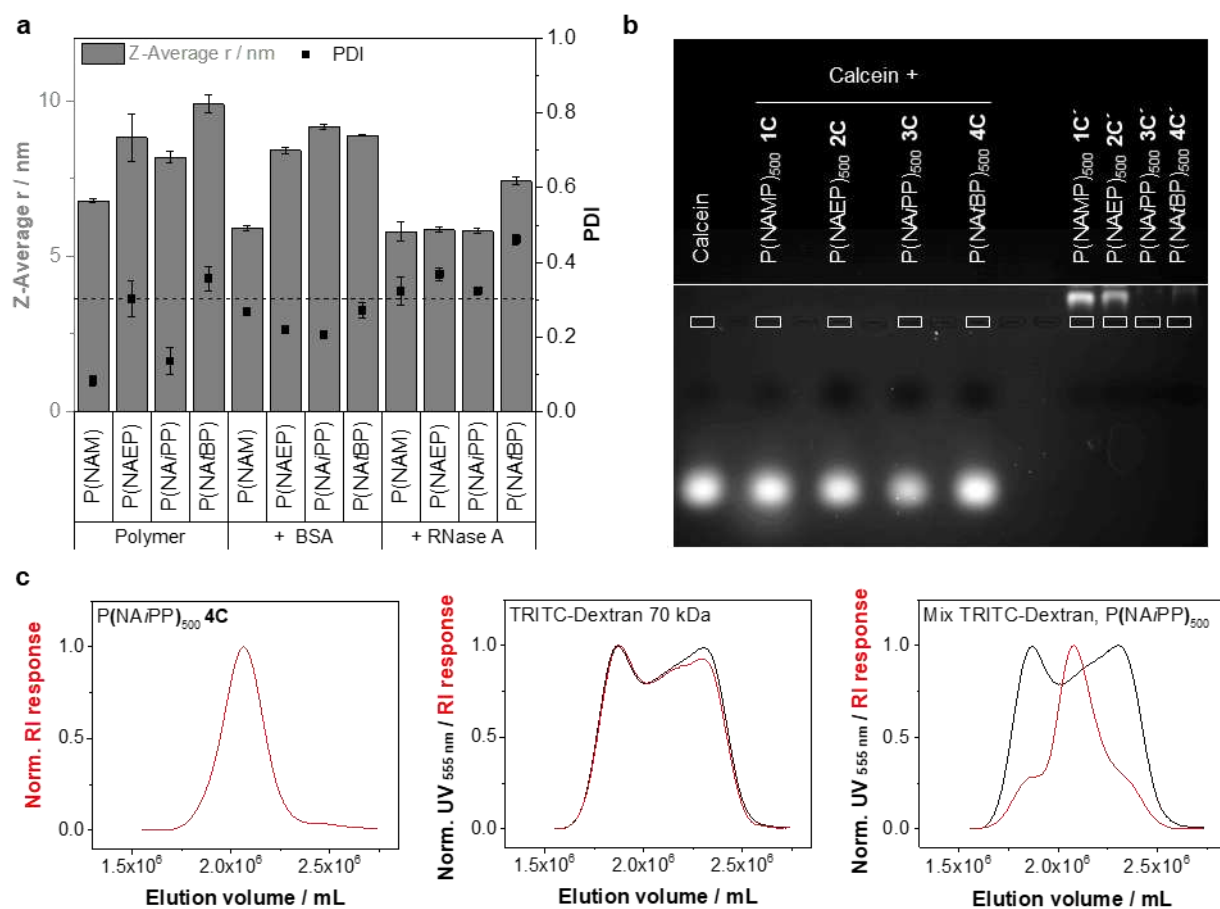


Figure S10 Investigations of possible interactions between polymer and tested model compounds. **a** Pure polymers (DP: 500) or polymers mixed with proteins were suspended in PBS at a final concentration of 5 mg mL⁻¹ and investigated via DLS (°173), mean \pm SD of three runs is shown. **b** Unlabeled polymers (left, DP: 500, 1 mg mL⁻¹) mixed with calcein (250 μ g mL⁻¹) in PBS or labeled polymers (right, 10 mg mL⁻¹) were applied to an agarose gel (1% in TBE buffer) and run in the TBE buffer at 80 V for 60 min followed by analysis with a gel documentation system (RED, Alpha Innotech, UV excitation). Pockets of agarose gel are marked with white boxes. **c** Pure PNAiPP₅₀₀ 3C, pure TRITC-Dex (Tetramethylrhodamine-labeled dextran, 70 kDa) or a 1+1 mixture of both were measured by SEC (Jasco, Eluent: 0.3% (v/v) trifluoroacetic acid + 0.1 M NaCl in water) at 1 mL min⁻¹ at 30 °C (Columns: PSS NOVEMA-MAX 30/1000/1000 Å) equipped with UV (555 nm) and RI detection.

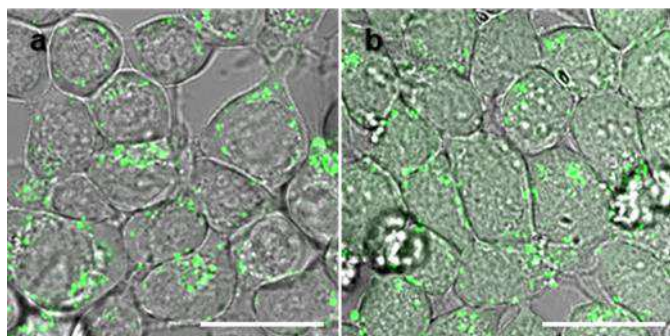


Figure S11 T-PMT images visualizing endosomal escape of calcein. The merge of the calcein channel and T-PMT of HEK 293T in Opti-MEM treated **a** with $25 \mu\text{g mL}^{-1}$ calcein or **b** with additional $100 \mu\text{g mL}^{-1}$ P(NAiPP) **3C''** for 16 h are shown. See Figure 3 for further channels. **a-b** Scale bar 20 μm . T-PMT - transmitted light detector.

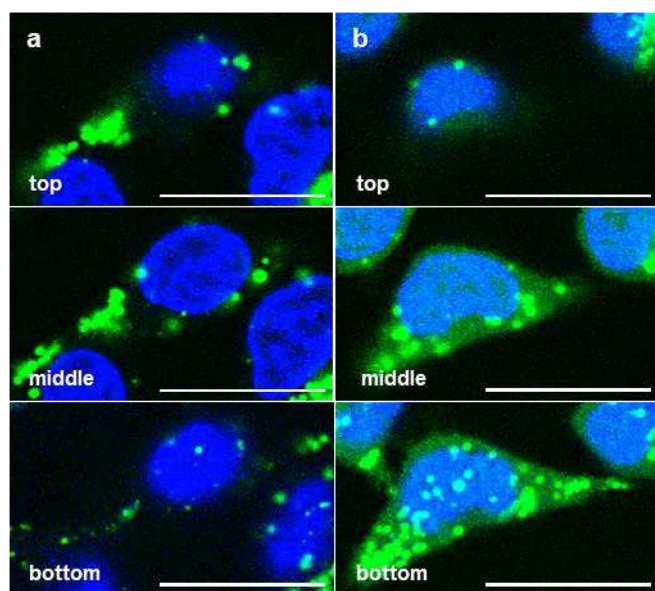


Figure S12 3D-Images of calcein release. **a** Example images from a z-stack acquisition from the lower, middle and upper part of a cell treated with calcein are given as a merge with the Hoechst channel visualizing the nuclei. **b** Corresponding images from the z-stack of a cell additionally treated with P(NAiPP)₅₀₀ **3C''** reveal endosomal release and cytosolic as well as nuclear delivery of calcein (also see Figure 3j for images showing the calcein channel only). **a-b** Scale bar 20 μm .

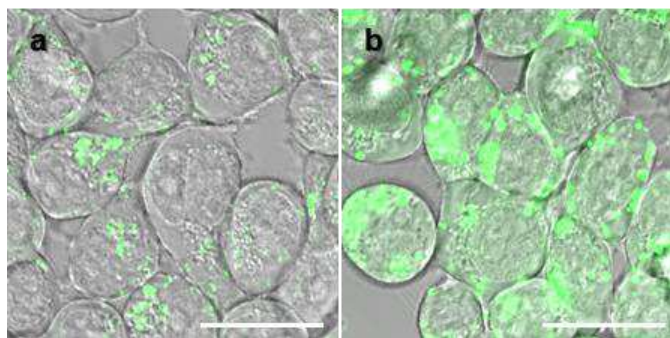


Figure S13 T-PMT images visualizing endosomal escape of BSA. The merged image of the AF488 channel (BSA) and T-PMT of HEK 293T in Opti-MEM treated **a** with 5 $\mu\text{g mL}^{-1}$ labeled BSA or **b** with additional 100 $\mu\text{g mL}^{-1}$ P(NAiPP) 3C'' for 16 h are shown. See Figure 4b, d and f in the main manuscript for further channels. **a-b** Scale bar 20 μm . T-PMT - transmitted light detector.

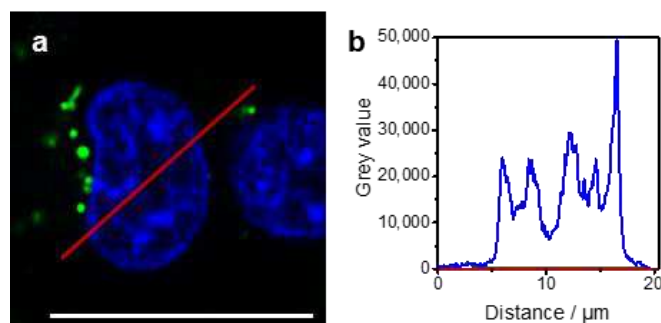


Figure S14 Plot profile of BSA treated control cell. **a** The merged image of the Hoechst and the BSA channel of a HEK 293T cell treated with 5 $\mu\text{g mL}^{-1}$ labeled BSA as a control and **b** the corresponding plot profile is shown, indicating no AF488 signal within the cytosol and nucleus for cells that were not treated with endosomolytic polymers. See Figure 4g-h for the polymer treated cell. **a** Scale bar 20 μm .

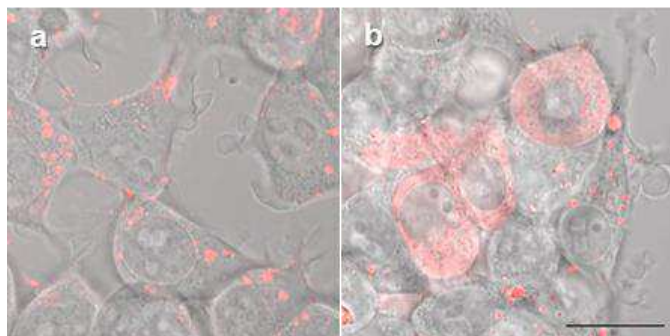


Figure S15 Endosomal escape of labeled dextran investigated by CLSM. **a** HEK 293T cells were treated with 1 mg mL⁻¹ TRITC-labeled dextran (70 kDa) or **b** with additional 100 µg mL⁻¹ P(NAiPP)₅₀₀ **3C**, washed twice and imaged via CLSM. In contrast to the other microscopic studies, unlabeled polymer was used in this experiment because SR 101 and TRITC would not have been indistinguishable due to their similar spectra. Scale bar 20 µm. SR 101 – sulforhodamine 101, TRITC – tetramethylrhodamine.

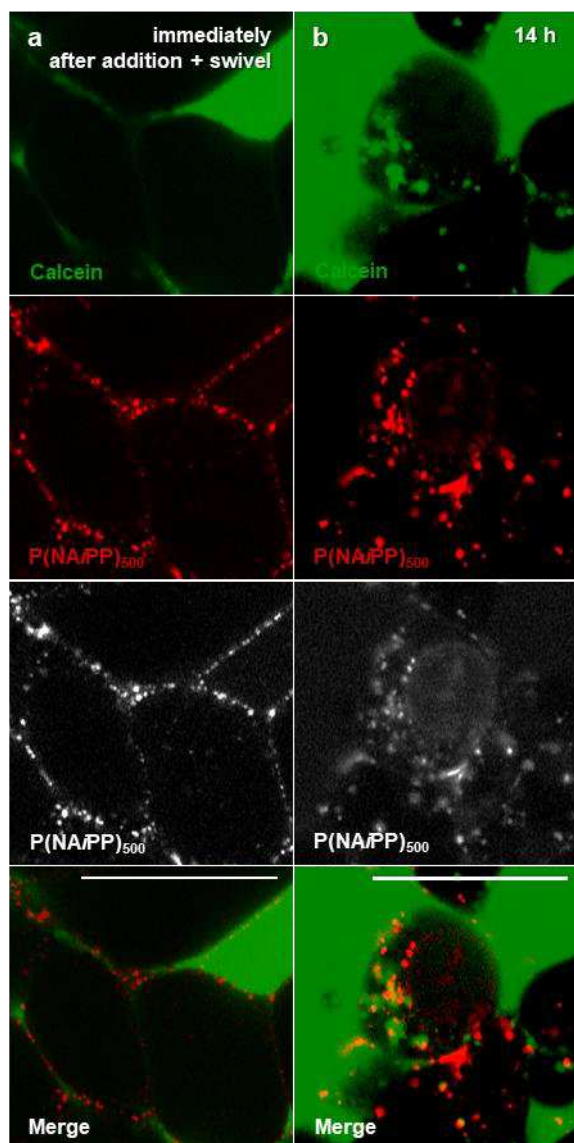


Figure S16 Polymer and calcein localization at different time points. **a** $P(\text{NAiPP})_{500}$ **3C''** interacts with the plasma membrane immediately after polymer and calcein addition and a short swivel. **b** After the calcein release (see Figure 6), partial localization of $P(\text{NAiPP})_{500}$ **3C''** within the nucleus was observed in some HEK 293T cells. **a-b** The calcein channel (first row) and the corresponding image of the red channel in red or gray scale (polymer, second or third rows) as well as the merge of the calcein and polymer channel (fourth row) are shown. Scale bar 20 μm .

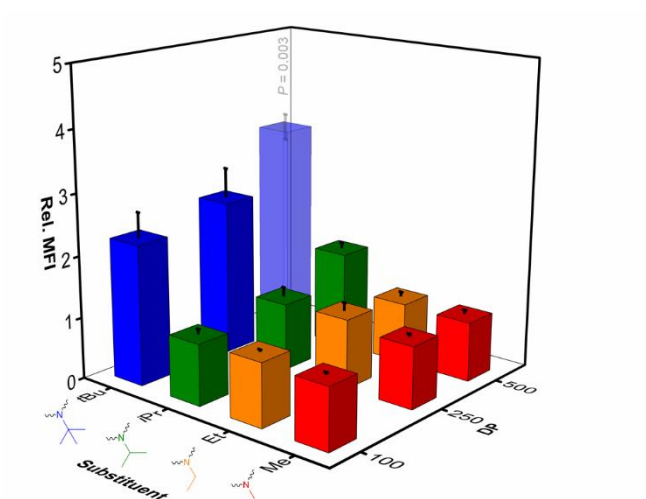


Figure S17 Quantification of endosomal escape of calcein by flow cytometry. HEK 293T cells in DMEM + 10% serum were treated with calcein and 100 $\mu\text{g mL}^{-1}$ polypiperazines, washed twice, trypsinized and analyzed via flow cytometry. The means \pm SD of three independent experiments relative to control cells treated with calcein only (rel. MFI = 1) are shown. Statistical differences between the means were calculated with Dunnett's T3 test. The slight transparency of a bar indicates gated cell populations below 70%. rel. MFI, relative mean fluorescence intensity.

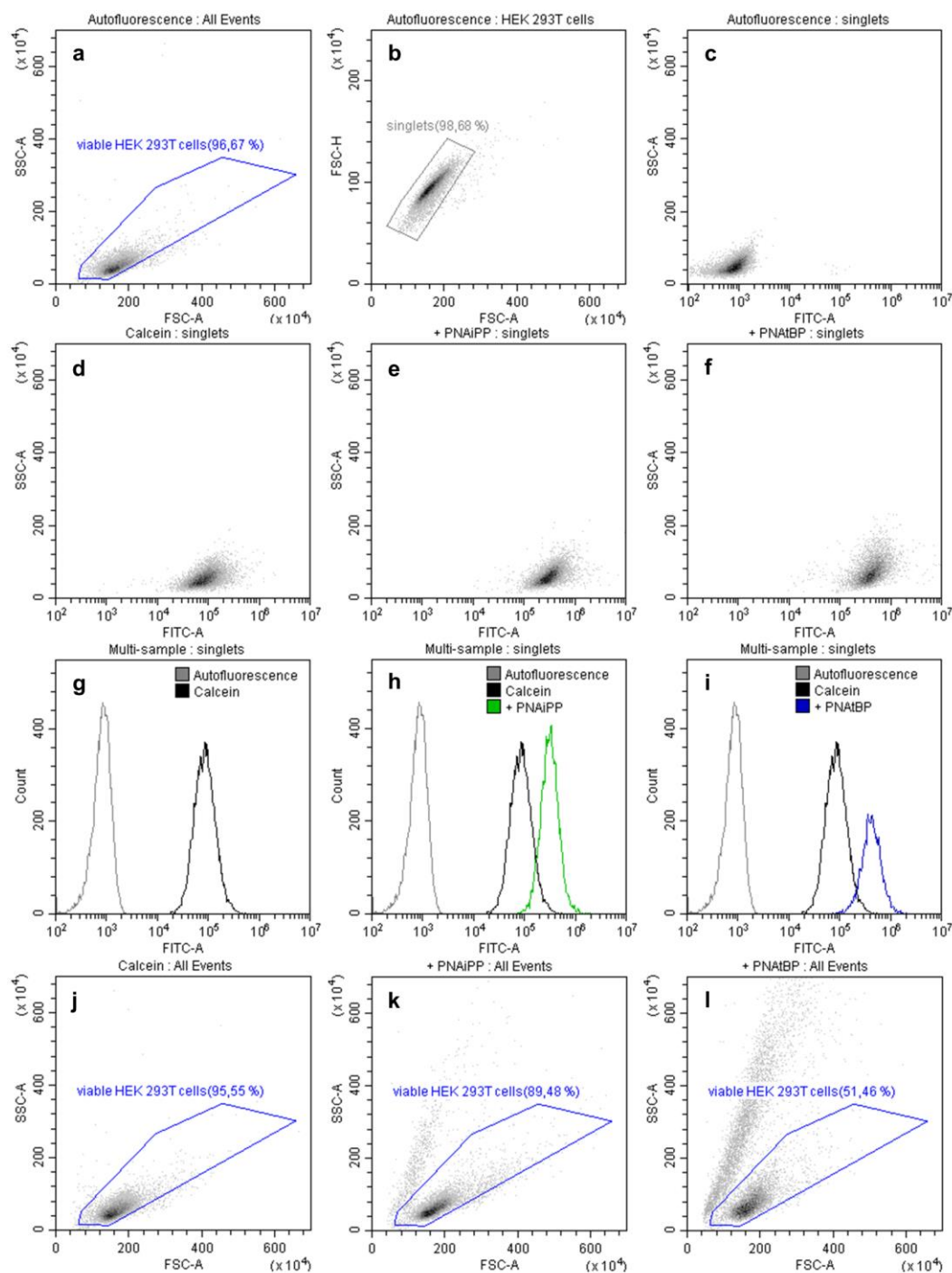


Figure S18 Evaluation of endosomal escape of calcein via flow cytometry. The gating strategy of flow cytometry analysis including forward/sideward scatter (a) to exclude debris, doublet discrimination (b) and the calcein/sideward scatter plot (c) are shown. Scatter plots and histograms of HEK 293T cells in Opti-MEM incubated with $25 \mu\text{g mL}^{-1}$ calcein only (d, g, j), with additional $100 \mu\text{g mL}^{-1}$ P(NAiPP)₅₀₀ 3C (e, h, k) and with additional $100 \mu\text{g mL}^{-1}$ P(NAiBP)₅₀₀ 4C (f, i, l) are shown., indicating changes in the forward/sideward scatter for P(NAiBP)₅₀₀ 4C.

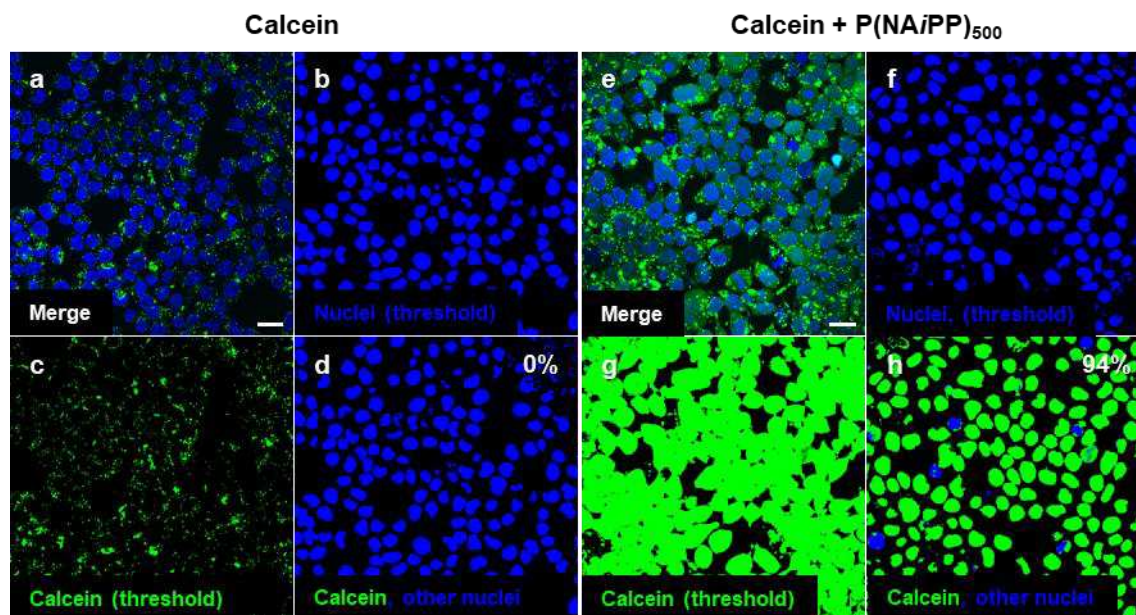


Figure S19 Quantification of nuclear calcein delivery (image analysis). **a-d** Live-cell confocal microscopy was conducted with HEK 293T cells in Opti-MEM either treated with 25 $\mu\text{g mL}^{-1}$ calcein or **e-h** additional 100 $\mu\text{g mL}^{-1}$ P(NAiPP)₅₀₀ **3C** for 16 h. Cells were washed and nuclei stained with Hoechst 33342. **b, f** A binary image of the nuclei was obtained from the Hoechst channel image using thresholding to determine the number of nuclei. **c, g** A binary image of the calcein channel was also obtained using thresholding. **d, h** From the image showing the number of nuclei (**b, f**) and the threshold image of the calcein channel (**c, g**), an image was calculated that outputs all pixels that are simultaneously blue in the nuclei image and green in the calcein image (given in green). These nuclei were counted and specified as a percentage in relation to the number of all nuclei to provide a percentage of cells that show nuclear calcein delivery for this image. For better understanding, the blue nuclei without calcein signal are also indicated (green + blue nuclei correspond to 100%). All images were acquired and processed with the same settings. All image analyses were carried out with ImageJ.[2] Scale bar 20 μm .

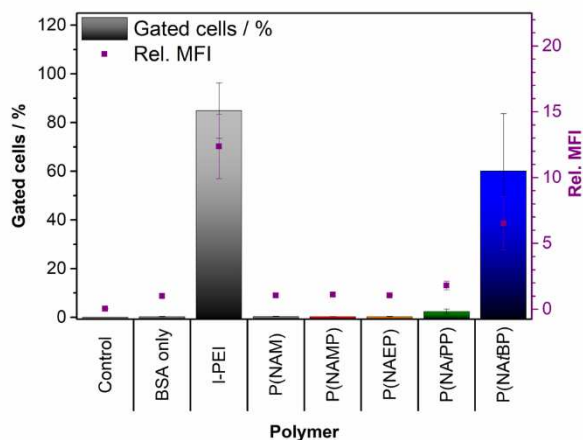


Figure S20 Quantification of endosomal escape of labeled BSA by flow cytometry. HEK 293T cells in DMEM with 10% serum were treated with $5 \mu\text{g mL}^{-1}$ labeled BSA and polymers at comparable reactive amine contents, washed twice, trypsinized and analyzed via flow cytometry. Means \pm SD of three independent experiments are shown. The statistical differences between the means are not significant ($P < 0.05$) according to Dunnett's T3 test. rel. MFI relative mean fluorescence intensity.

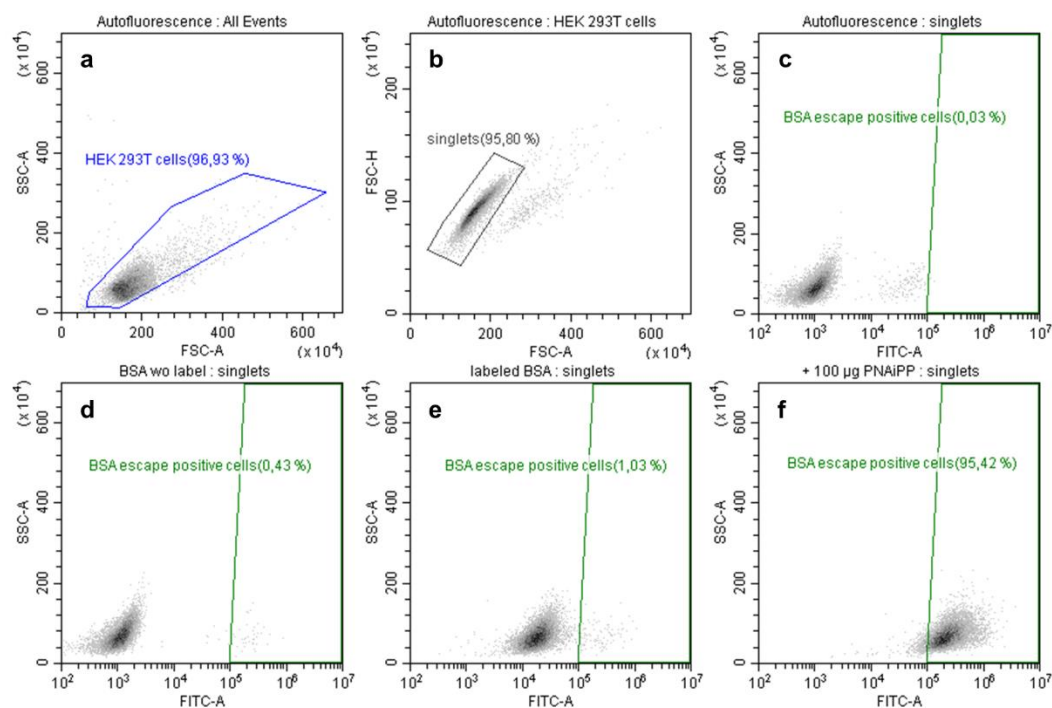


Figure S21 Evaluation of endosomal escape of labeled BSA via flow cytometry. The gating strategy of flow cytometry analysis including forward/sideward scatter (a) to exclude debris, doublet discrimination (b) and the gate for BSA escape positive cells (c) are shown. Scatter plots of HEK 293T cells in Opti-MEM incubated with $5 \mu\text{g mL}^{-1}$ BSA without the Alexa Fluor 488 label only (d), with $5 \mu\text{g mL}^{-1}$ BSA bearing the Alexa Fluor 488 tag (e) and with $5 \mu\text{g mL}^{-1}$ labeled BSA and additional $100 \mu\text{g mL}^{-1}$ P(NAiPP)₅₀₀ 3C (f) are shown.

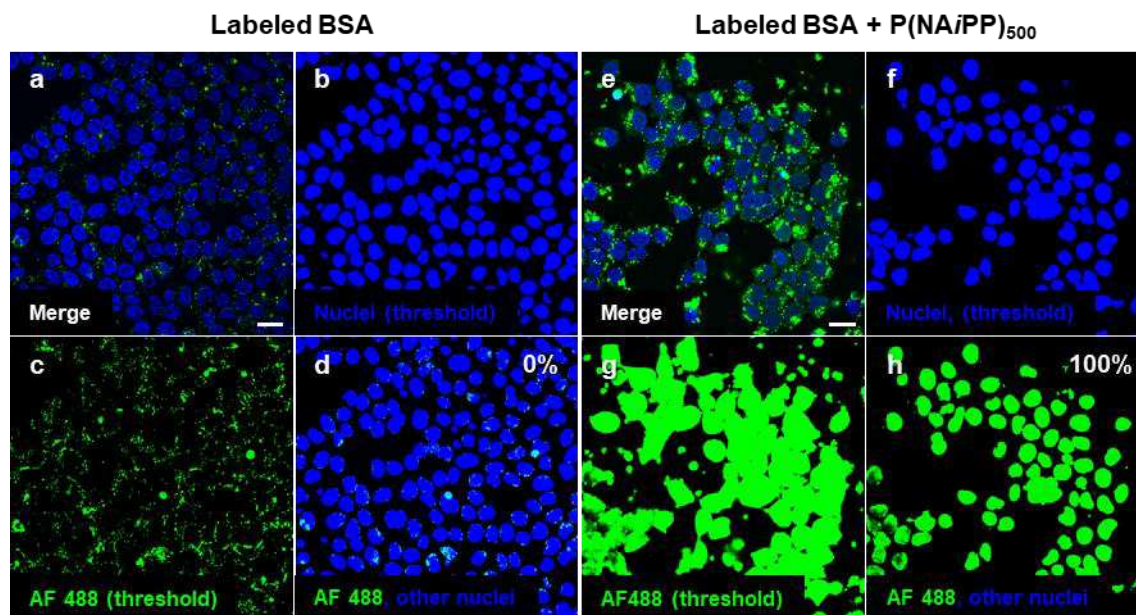


Figure S22 Quantification of nuclear BSA delivery (image analysis). **a-d** Live-cell confocal microscopy was conducted with HEK 293T cells in Opti-MEM either treated with $5 \mu\text{g mL}^{-1}$ AF 488-functionalized BSA or **e-h** additional $100 \mu\text{g mL}^{-1}$ P(NAiPP)₅₀₀ **3C** for 16 h. Cells were washed and nuclei stained with Hoechst 33342. **b, f** A binary image of the nuclei was obtained from the Hoechst channel image using thresholding to determine the number of nuclei. **c, g** A binary image of the AF 488 channel was also obtained using thresholding. **d, h** From the image showing the number of nuclei (**b, f**) and the threshold image of the AF 488 channel (**c, g**), an image was calculated that outputs all pixels that are simultaneously blue in the nuclei image and green in the calcein image (given in green). These nuclei were counted and specified as a percentage in relation to the number of all nuclei to provide a percentage of cells that show nuclear AF 488 delivery for this image. In case of this image all nuclei show AF 488 signal next to the Hoechst signal. All images were acquired and processed with the same settings. All image analyses were carried out with ImageJ.[2] Scale bar 20 μm .

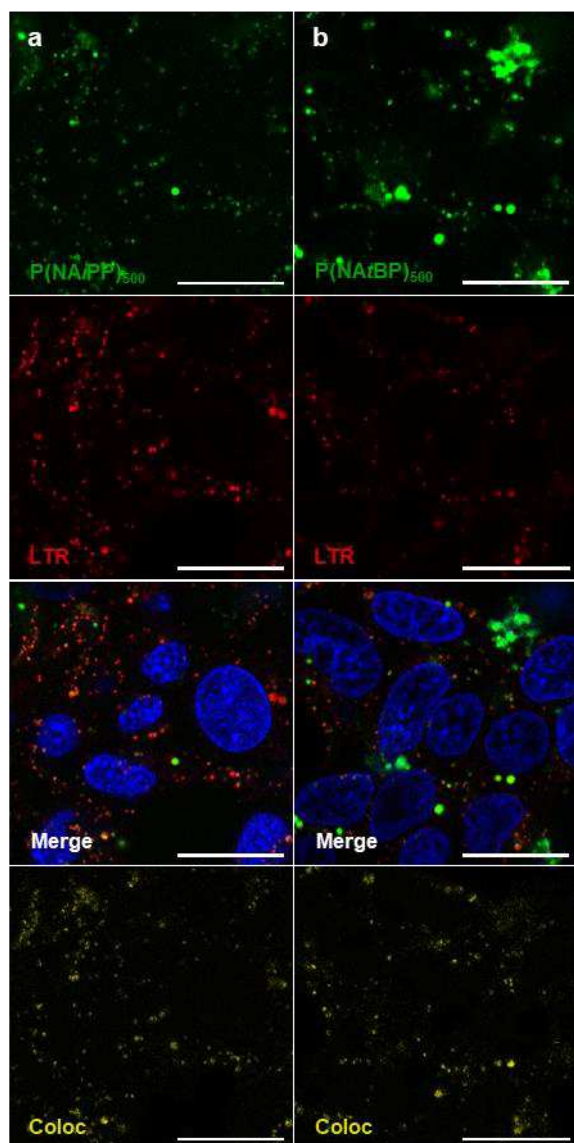


Figure S23 Colocalisation of polypiperazines and endolysosomes in HEK 293T cells. HEK 293T cells in Opti-MEM were treated with 100 ug mL^{-1} Oregon Green-labeled polypiperazines (**a** P(NAiPP)₅₀₀ **3C'**, **b** P(NAiBP)₅₀₀ **4C'**) for 16 h. Cells were stained with Hoechst 33342 and LysoTracker Red. The colocalization image was created with the Image Calculator showing all pixels with green and red signal.[2] Scale bar 20 μm . Coloc – colocalization, LTR – LysoTracker Red.

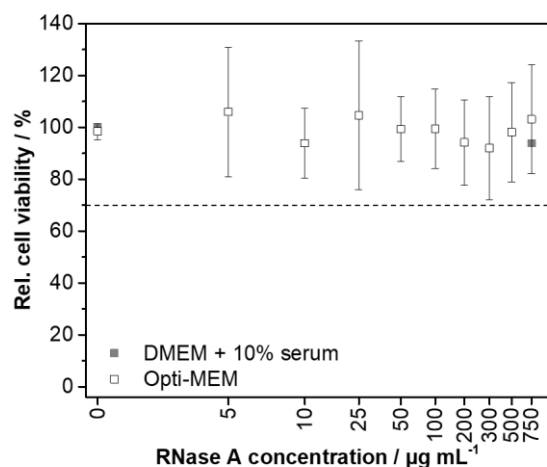


Figure S24 Cytotoxicity studies of RNase A without polymer addition. HEK 293T cells were incubated with RNase A (Roche) at the indicated concentrations (0 – 750 $\mu\text{g mL}^{-1}$) for 24 h, the culture medium was changed to DMEM + 10% serum and the cell viability was determined via the alamarBlue assay (Thermo Fisher). The activity of RNase A was investigated in DMEM + 10% serum (grey solid squares, mean \pm minimum/maximum of two independent experiments is shown) and Opti-MEM (black void squares, mean \pm SD of four independent experiments is shown).

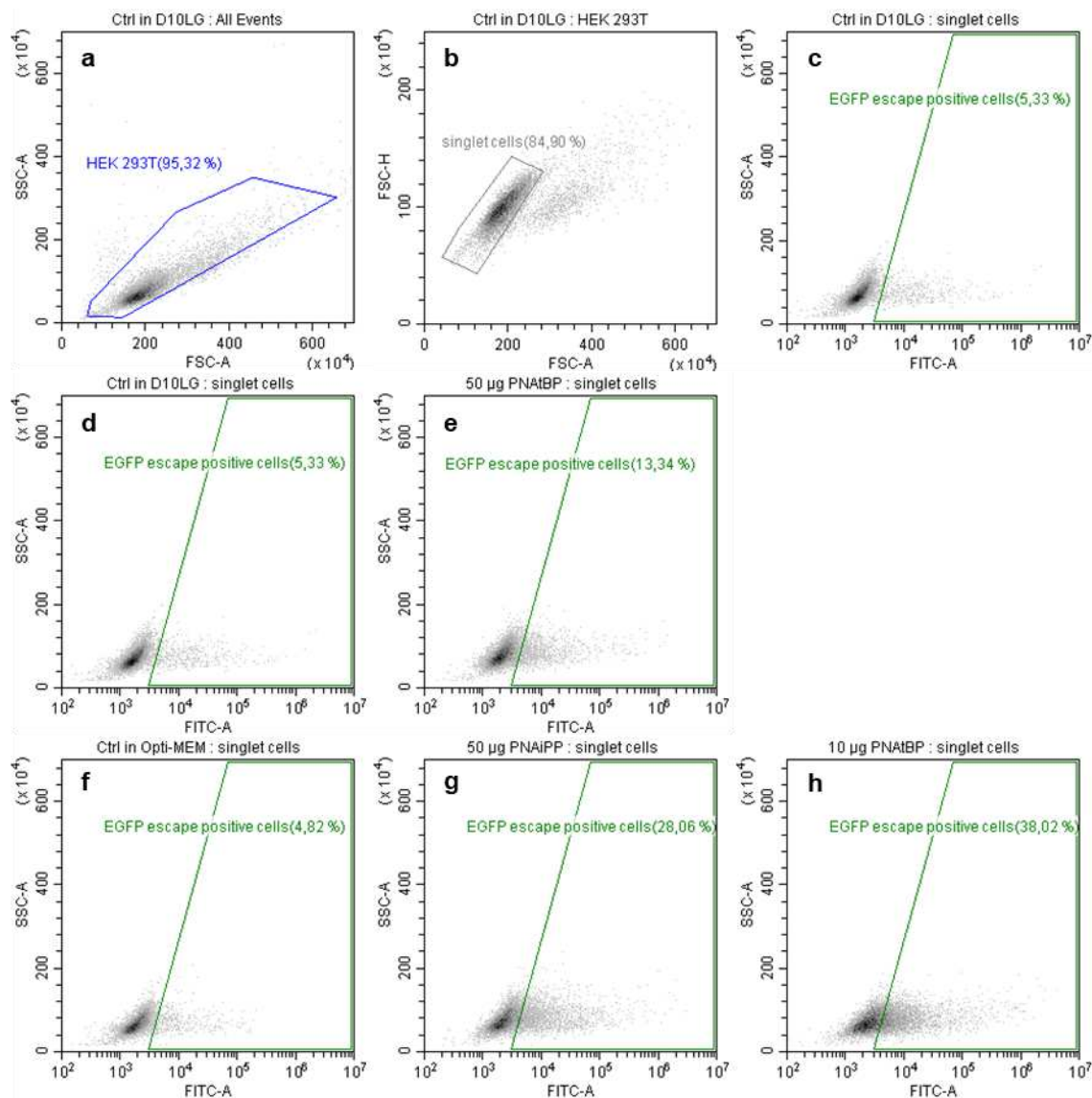


Figure S25 Evaluation of endosomal escape of EGFP via flow cytometry. a, b, c The gating strategy of flow cytometry analysis including forward/sideward scatter (a) to exclude debris, doublet discrimination (b) and the gate for EGFP escape positive cells (c) is shown. Scatter plots of HEK 293T cells in DMEM + 10% serum incubated with 50 µg mL⁻¹ EGFP only (d) and with additional 50 µg mL⁻¹ P(NAiBP)₅₀₀ 4C (e) are shown. Scatter plots of HEK 293T cells in Opti-MEM incubated with 50 µg mL⁻¹ EGFP only (f), with additional 50 µg mL⁻¹ P(NAiPP)₅₀₀ 3C'' (g) and with additional 10 µg mL⁻¹ P(NAiBP)₅₀₀ 4C (h) are shown.

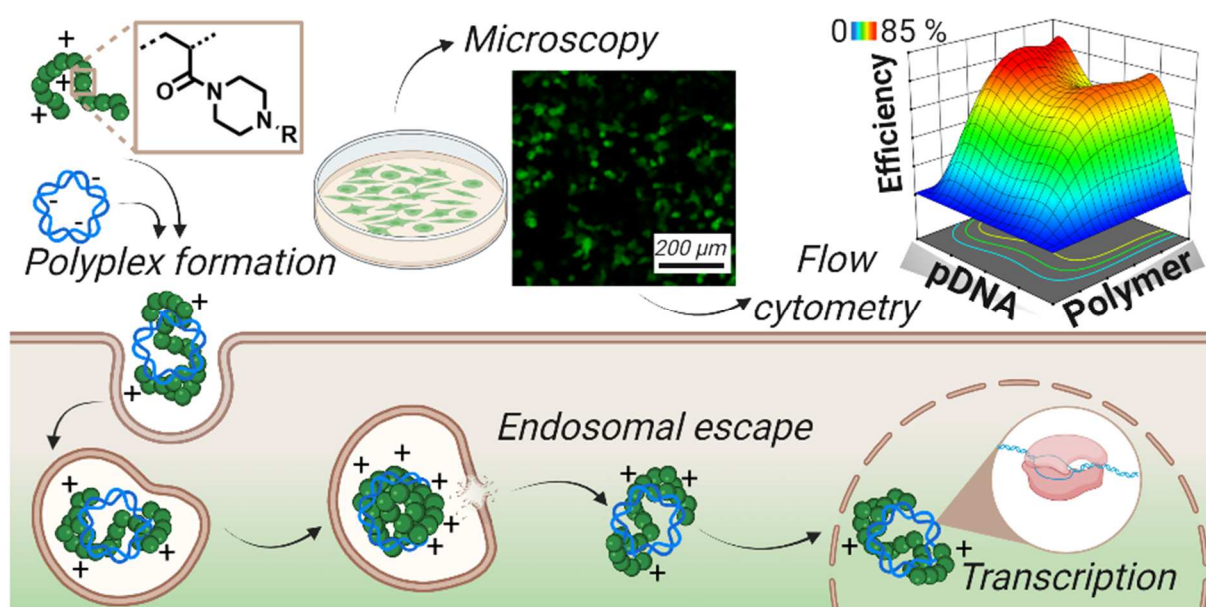
References

- [1] Larnaudie, S. C., Brendel, J. C., Jolliffe, K. A., Perrier, S. Cyclic Peptide–Polymer Conjugates: Grafting-to Vs Grafting-From. *J. Polym. Sci., Part A: Polym. Chem.* 54, 1003-1011 (2016).
- [2] J. Schindelin, I. Arganda-Carreras, E. Frise, V. Kaynig, M. Longair, T. Pietzsch, S. Preibisch, C. Rueden, S. Saalfeld, B. Schmid, J.-Y. Tinevez, D.J. White, V. Hartenstein, K. Eliceiri, P. Tomancak, A. Cardona, Fiji: an open-source platform for biological-image analysis, *Nature Methods* 9(7) (2012) 676-682. 10.1038/nmeth.2019.
- [3] Maxfield, F. R., Yamashiro, D. J. Endosome Acidification and the Pathways of Receptor-Mediated Endocytosis. In: *Immunobiology of Proteins and Peptides IV: T-Cell Recognition and Antigen Presentation* (ed Atassi, M. Z.). Springer US (1987).

Publication Pub3

Efficient transfection *via* an unexpected mechanism by near-neutral polypiperazines with tailored response to endosomal pH

F. Hausig-Punke, G. Dekevic, F. H. Sobotta, J. I. Solomun, F. Richter, D. Salzig, A. Traeger, J. C. Brendel, *submitted*.



Efficient transfection *via* an unexpected mechanism by near-neutral polypiperazines with tailored response to endosomal pH

*Franziska Hausig-Punke,^a Gregor Dekevic,^b Fabian H. Sobotta,^a Jana I. Solomun,^a Friederike Richter,^a Denise Salzig,^b Anja Traeger,^{*a,c} Johannes C. Brendel,^{*a,c}*

^aLaboratory of Organic and Macromolecular Chemistry (IOMC), Friedrich Schiller University
Jena, Humboldtstrasse 10, 07743 Jena, Germany.

^bInstitute of Bioprocess Engineering and Pharmaceutical Technology, University of Applied
Sciences Mittelhessen, Wiesenstrasse 14, 35390 Giessen, Germany.

^cJena Center for Soft Matter (JCSM), Friedrich Schiller University Jena, Philosophenweg 7,
07743 Jena, Germany.

*Correspondence to A. Traeger (anja.traeger@uni-jena.de)
and J. C. Brendel (johannes.brendel@uni-jena.de)

ABSTRACT

Cationic pH-responsive polymers promise to overcome critical challenges in cellular delivery. Ideally the polymers become selectively charged along the endosomal pathway to disturb only the local membrane and avoid unintended serum interactions or cytotoxic side effects at physiological conditions. Polypiperazines represent a novel pH-responsive polymer class whose response can be finely tuned within the relevant pH range (5 - 7.4) by variation of the pendant alkyl unit. Although these materials were initially not considered for gene delivery due to a limited ability to condense DNA, we discovered in the present study that the polypiperazines are still effectively binding plasmid DNA (pDNA) and demonstrate high efficiency in transfection. By design of experiments (DoE), a wide parameter space was evaluated in terms of pDNA and polymer concentrations to identify optimal transfection conditions. Interestingly, the isopropyl modified polypiperazine proved to be highly efficient over a wide range of concentrations outperforming even linear polyethylenimine (l-PEI, 25 kDa) in regions of low N*/P ratios. Intrigued by the high efficiency, we scrutinized the underlying transfection mechanisms. A quantitative polymerase chain reaction (qPCR) surprisingly revealed that the pDNA within the piperazine-based polyplexes can be amplified in contrast to polyplexes based on l-PEI. The pDNA must therefore be highly accessible and bound differently than for other known transfection polymers. Keeping the high efficacy reached by the presented homopolymers in mind, the versatile synthesis promises various opportunities to further optimize the design of these polypiperazines, which makes this class of polymers highly attractive for future gene transfection systems.

KEYWORDS

pH-responsive polymers; gene delivery; structure-activity relationship; pDNA binding; endosomal escape; polyplex characterization, design of experiments

INTRODUCTION

With successful application of RNA-based systems, *e. g.* vaccines to combat the SARS-CoV-2 pandemic or anti-cancer treatments,¹ the developments in the field of genetic material transfer have recently accelerated. Polymer-based gene delivery systems are of special interest because they can mimic viral gene delivery vectors while offering additional safety aspects such as reduced pathogenicity and immunogenicity.² Additionally, polymer-based gene delivery systems provide selective design opportunities through the introduction of chemical variations, can be produced in larger scales, and have an improved long-term stability.³ All gene delivery systems have to overcome a number of extra- and intracellular obstacles to transport, *e. g.* a bulky nucleic acid such as plasmid DNA (pDNA) into the nucleus. Thus, the pDNA must be reversibly packaged and its cellular uptake, endosomal escape, and nuclear transport (even in non-dividing cells) must be facilitated without side effects.³ Within the polymer-based gene delivery systems the group of cationic polymers can complex nucleic acids due to electrostatic interactions and shield their negative charges to enhance cellular uptake and support endosomal escape.⁴ Smart pH-responsive cationic polymers are of interest as they can be tuned to react upon pH changes in the endosomal pathway (*e.g.* with protonation), which may help to overcome endosomal entrapment. Furthermore, pH-responsive protonation can prevent serum interactions and cytotoxic effects induced by cationic charges at physiological conditions.^{5, 6} Following successful endosomal release, nuclear import is required, which is regulated by cellular proteins and their interactions

with the cellular trafficking machinery. Nuclear import can be supported by polymers, although the exact mechanisms have not yet been described in detail.⁷

In the last decade, correlations between the properties of cationic polymers and transfection efficiencies were studied in terms of polymer architecture, molar mass, balance between hydrophobicity and hydrophilicity, and the type of the cationic moieties.^{8, 9} For instance, cationic polymers can be integrated into more complex polymer architectures (hydrogel, micelles, particles) or combined with additional anionic polymers to circumvent the activity-toxicity dilemma.^{10, 11} Another correlation was observed between higher molar masses of the polymers and increased transfection efficiency, but this is often also associated with increased cytotoxicity.¹²⁻¹⁶ Although such trends can be considered as guidelines, ideal characteristics of efficient transfection polymers are hard to specify, since various interacting parameters must be considered. For example, the nature of the cationic moiety represents a crucial factor, since it is a vital feature for pDNA binding, cellular uptake, endosomal escape and pDNA release.¹⁶⁻²² In particular, basicity, and thus the degree of protonation, as well as the size of the gene vehicles have been identified as especially crucial physicochemical properties.²³

Considering the ability to induce endosomal escape, we recently reported a direct correlation of the escape efficiency with the basicity of polymers.²⁴ Therefore, hydrophilic pH-responsive polypiperazines were designed featuring different substituents on the protonatable amino groups. Depending on the electron donating character of the substituent, the protonation or positive charging, respectively, occurs at higher (strong donor) or lower pH values (weak donor). However, all transitions remain in the range of pH 6 - 7 which is particularly interesting for inducing endosomal escape. Since the polymers are barely charged at physiological pH value (pH 7.4) and preliminary tests did not indicate an ability to condense genetic material, we initially did not intent

to test an application in the field of gene delivery. However, recent experiments caused a reconsideration of this decision as these polymers revealed unexpected properties with regard to pDNA complexation and its delivery into cells.

In the present study, we report a detailed investigation of the binding ability of the polypiperazines and the relationships between their basicity and transfection efficiency. Further experiments were performed to shed light on the differences in the transfection mechanism compared to linear polyethylenimine (l-PEI), which is similar in terms of the polymer architecture and well established as non-viral vector.^{25, 26} The investigated set of polypiperazines comprised poly(*N*-acryloyl-*N'*-methylpiperazine) (PNAMP), poly(*N*-acryloyl-*N'*-ethylpiperazine) (PNAEP), poly(*N*-acryloyl-*N'*-*iso*-propylpiperazine) (PNAiPP) and poly(*N*-acryloyl-*N'*-*tert*-butylpiperazine) (PNA_tBP). Since this class of polymers has so far not been applied as gene delivery vectors, the influence of key experimental parameters such as the concentration of nucleic acids or the polymers are unknown and difficult to relate to well-established materials. Finding optimal parameters, however, is pivotal to estimate the potential of such a new class of polymers, but also very tedious if done classically according to the “one-factor-at-a-time” (OFAT) method. Consequently, we have decided to apply a design of experiments (DoE) approach. Although few reports have so far employed DoE methods for transfection optimization, their outcomes already demonstrate its potential for time and resource efficient optimization.²⁷⁻²⁹ The DoE approach analyzes data over a wide range of conditions simultaneously (in our case pDNA and polymer concentration). Overall, the DoE approach enables us to collect model-based data in order to predict transfection efficiencies at any given condition, find the transfection optimum, and identify trends among the polypiperazines. Intrigued by their surprisingly efficient transfection ability, we further investigated potential transfection mechanisms of the polypiperazines. For this purpose,

we utilized quantitative polymerase chain reaction (qPCR) for the first time to investigate pDNA accessibility within the polyplex and discovered differences to l-PEI.

EXPERIMENTAL SECTION

Further methods (size exclusion chromatography (SEC), pH-dependent ethidium bromide (EtBr) displacement assay, microscopic investigation of the transfection efficiency, CC₅₀ calculations) can be found in the Supporting Information (SI).

Materials

The following substances were used to conduct this study: cell culture media and supplements, 4-(2-hydroxyethyl)piperazine-1-ethanesulfonic acid (HEPES), phosphate buffered saline (PBS, Biowest, Nuaille, France), fetal calf serum (FCS, Capricorn Scientific, Ebsdorfergrund, Germany), Opti-MEMTM (Gibco, Thermo Fisher, Waltham, United States), pCMV-GFP pDNA (PlasmidFactory, Bielefeld, Germany), Hoechst 33342, TOTOTM-3 iodide, YOYOTM-1 iodide (Life Technologies, Thermo Fisher), agarose, calcein, glucose, Hanks' balanced salt solution (HBSS), trypsin-ethylenediaminetetraacetic acid (EDTA) solution, Triton X-100, and 0.4 % trypan blue solution (Sigma-Aldrich, St. Louis, United States), green gel loading buffer (Jena Biosciences, Jena, Germany), 1 % ethidium bromide solution (EtBr, Carl Roth, Karlsruhe, Germany), heparin sodium salt from porcine intestinal mucosa (Alfa Aesar, Haverhill, United States), l-PEI ($M_w = 25 \text{ kg mol}^{-1}$, Polysciences, Warrington, United States), SsoAdvanced Universal SYBR Green Supermix (BioRad, Hercules, United States) and the CytoTox-ONETM Homogeneous Membrane Integrity Assay kit (Promega, Madison, United States). As a control plasmid not encoding for any fluorescent protein, pDNA was isolated with the EndoFree® Plasmid Mega Kit (Qiagen, Hilden, Germany) from *E. coli* containing pKMyc (4.8 kb, Addgene #19400,

Watertown, United States). For accessibility studies *via* quantitative polymerase chain reaction (qPCR), pDNA encoding enhanced green fluorescent protein (EGFP) was isolated with the EndoFree[®] Plasmid Mega Kit (Qiagen) from *E. coli* containing pEGFP-N1 (4.7 kb, Clontech, #6085-1, Mountain View, United States).

Cell culture

HEK 293T cells (CLS, Eppelheim, Germany) were routinely cultured in Dulbecco's modified eagle's medium with 2 mM L-glutamine (1 g L⁻¹ glucose, Biochrom, Cambridge, United Kingdom) supplemented with 10 % fetal calf serum, 100 U mL⁻¹ penicillin, and 100 µg mL⁻¹ streptomycin (Biochrom) (growth medium) at 37 °C under a humidified 5 % (v/v) CO₂ atmosphere.

Polyplex preparation

For the preparation of polyplexes resulting in varying pDNA and polymer concentrations as well as N*/P ratios (molar ratio of protonatable nitrogen atoms of polymer to phosphates of pDNA), different amounts of pCMV-GFP pDNA and polymer dissolved in water were mixed in HBG buffer (20 mM HEPES, 5 % (w/v) glucose, pH 7.4), if not stated otherwise. A twofold concentrated pDNA solution was used, which was diluted 1:2 with a twofold concentrated polymer solution. Immediately after combination, the mixtures were vortexed for 10 s at maximum speed (3200 rpm) and incubated at room temperature for 15 min to ensure complex formation. N*/P ratios were calculated as previously published,¹⁶ using different pDNA concentrations in this work.

Transient transfection of adherent cells

For transfection studies, HEK 293T cells were seeded at a density of 0.2×10^6 cells mL⁻¹ in 24-well plates (VWR, Radnor, United States, 10^5 cells per well) and incubated in growth medium at 37 °C

(5 % (v/v) CO₂) for 24 h. One hour prior to transfection, the medium was replaced by 450 μ L serum-free Opti-MEMTM. Polyplexes were prepared as described above with commercial pCMV-GFP pDNA or pKMyC pDNA (not encoding for GFP as negative control). Cells were treated with 50 μ L of the sample solution of the indicated pDNA concentration given as the phosphate concentration (P conc.), polymer concentration given as the protonatable amine concentration (N* conc.) and of the indicated N*/P ratio. Treatment with pure HBG buffer was used as negative control. The supernatant was replaced by fresh growth medium after 4 h and cells were incubated for further 20 h. For analysis *via* flow cytometry, cells were harvested by trypsinization and resuspension in HBSS (Hanks' balanced salt solution) supplemented with 2 % FCS and 20 mM HEPES. Flow cytometry was conducted utilizing a CytoFlex S (Beckman Coulter, Brea, United States). For each experiment, a quantity of 10⁴ events were measured using gates of forward and sideward scatter (FSC/SSC) to exclude debris and cell aggregates. The GFP expression of viable, single cells was analyzed at $\lambda_{\text{Ex}} = 488$ nm combined with a 525/40 nm bandpass filter. The population of cells with higher GFP signal than the control cells was gated as % of cells expressing GFP. A detailed gating strategy is shown in the SI (Figure S5). Also, the mean fluorescence intensity (MFI) of all viable cells is shown. The experiments were performed at least two times and data are expressed as mean \pm SD.

Agarose gel electrophoresis

To investigate the pDNA binding and release abilities of the polypiperazines and l-PEI, agarose gel electrophoresis was conducted. Polyplexes were prepared at varying N*/P ratios (3; 11; 15; 30) as described above at a pCMV-GFP pDNA concentration of 46 $\mu\text{mol L}^{-1}$. In some experiments, heparin was added as a competitive polyanion (final concentrations: 10; 50; 100 U mL^{-1}) after polyplex formation and incubated for further 5 min. The samples were diluted

6:1 with green gel loading buffer and were run on a 1 % (w/v) agarose gel stained with ethidium bromide (EtBr, $0.1 \mu\text{g mL}^{-1}$) in tris(hydroxymethyl)aminomethan (TRIS) borate EDTA (TBE) buffer at 80 V for 1 h. The gels were subsequently imaged using a gel imager (Red Imaging System, Alpha Innotech, Kasendorf, Germany).

Dynamic/electrophoretic light scattering (DLS/ELS)

The hydrodynamic diameter and zeta potential of the polyplexes were investigated by DLS/ELS. The polyplexes were prepared at N*/P 6 (P. conc = $23 \mu\text{mol L}^{-1}$, N* conc. = $138 \mu\text{mol L}^{-1}$) in 50 μL HBG buffer as described above. For zeta potential determinations, the polyplexes were further diluted to 800 μL with ultrapure water. Measurements were conducted on a Zetasizer Nano-ZS (Malvern Instruments, Malvern, United Kingdom) with a He-Ne laser operating at a wavelength of 633 nm. Intensity fluctuations at a backscattering angle of 173° were detected. Each sample was measured with three runs of 30 s at 25°C after an equilibration time of 30 s. The mean particle size was approximated as the effective (Z-average) diameter and the width of the distribution as the polydispersity index (PDI) of the particles obtained by the cumulants fit assuming a spherical shape. Data are expressed as mean \pm SD. Exemplary decay functions and histograms are shown in the SI (Figure S25, S26).

Polyplex uptake

To study the cellular uptake of polyplexes, HEK 293T cells were seeded at a density of $0.2 \times 10^6 \text{ cells mL}^{-1}$ in 24-well plates (VWR, 10^5 cells per well) and cultured for 24 h in growth medium as described for transfection studies. One hour prior to the addition of the polyplexes, the medium was changed to serum-free Opti-MEMTM. Polyplexes were prepared as described above after labeling $1 \mu\text{g}$ pKMyC pDNA with 0.05 nmol YOYOTM-1 iodide. Subsequently, the polyplex suspensions were added to the cells, diluting the polyplexes 1:10 (final P conc. = $46 \mu\text{mol L}^{-1}$).

Following incubation for 4 h, cells were harvested by trypsinization and resuspension in HBSS with 2 % FCS and 20 mM HEPES. Trypan blue solution (0.4 %) was added to a final concentration of 0.04 % to quench fluorescence of polyplexes outside the cells. *Via* flow cytometry, cells were analyzed as described above. The population of viable, single cells with higher YOYOTM-1 iodide signal than the control cells was gated as % of cells that have taken up pDNA. A detailed gating strategy is shown in the SI (Figure S12). Also, the mean fluorescence intensity (MFI) of all viable cells is shown. The experiments were performed three times and data are expressed as mean \pm SD.

For uptake studies *via* confocal laser scanning microscopy (CLSM), polyplexes were prepared with Oregon Green-labeled polymers and TOTOTM-3 iodide stained pKMyC pDNA.²⁴ Here, the labeled polymers were adjusted to the same degree of labeling among the polymers by mixing with unlabeled polymers. TOTOTM-3 iodide (0.25 nmol per 1 μ g pDNA) was used analogously to YOYOTM-1 iodide. HEK 293T cells were seeded and cultured in Opti-MEMTM as described above in glass-bottomed dishes (CellView cell culture dishes with four compartments, Greiner Bio-One, Kremsmuenster, Austria) and analyzed following incubation with polyplexes at N*/P 15 (P conc. = 46 μ mol L⁻¹) for 4 h. To image their intracellular distribution in living cells, Hoechst 33342 (10 μ g mL⁻¹) was added for 10 min to stain cell nuclei. Live cell imaging was performed using a LSM880, Elyra PS.1 system (Zeiss, Oberkochen, Germany) applying the argon laser for excitation at 488 nm (5 %) and 405 nm (1 %) and a He-Ne laser for excitation at 633 nm (2 %), as well as emission filters for Hoechst (410-450 nm), Oregon Green (508-544 nm) and TOTOTM-3 (640-759 nm) with gains of 700, 850 and 750, respectively. For magnification, a 40 \times 1.4 NA plan apochromat oil objective was applied. Images were acquired using the ZEN software, version 2.3 SP1 (Zeiss) and processed with ImageJ (Java 8).³⁰ All images were acquired and processed with the same settings. The experiments were performed twice.

Investigation of plasma membrane integrity

To investigate plasma membrane interactions of the polyplexes with HEK 293T cells, the leakage of lactate dehydrogenase (LDH) from the cytosol to the surrounding cell culture medium was investigated utilizing the CytoTox-ONE™ Homogeneous Membrane Integrity Assay according to the manufacturer's instructions. Briefly, cells were seeded, incubated and treated as described for uptake studies. Following incubation for 1 h and 4 h, respectively, the supernatant was transferred into a 96-well plate in triplicates and allowed to equilibrate to room temperature. Subsequently, the assay buffer including the resazurin-based substrate mixture was added to the supernatant 1:1 and incubated at room temperature for 10 min. After the addition of a stop solution included in the kit, the fluorescence intensity was measured at $\lambda_{\text{Ex}}=560 \text{ nm}$ / $\lambda_{\text{Em}}=590 \text{ nm}$ with gain set to optimal using an Infinite M200 PRO microplate reader (Tecan, Maennedorf, Switzerland). Cells treated with 0.9 % (w/v) Triton X-100 30 min prior to harvest of the supernatant served as positive control (0 % viability). Cells incubated solely with the same amount of HBG buffer were used as negative control (100 % viability). The cell viability was calculated using equation 1:

$$\text{Cell viability} / \% = \frac{\text{FI}(\text{Triton X-100}) - \text{FI}(\text{Blank})}{\text{FI}(\text{sample}) - \text{FI}(\text{Blank})} \cdot 100 \quad (1)$$

Where FI(sample), FI(Blank), and FI(Triton X-100) represent the fluorescence intensity of a given sample, cell culture medium without cells, and Triton X-100 treated cells, respectively.

Calcein release assay

To determine the endosomal escape efficiency of the polyplexes, the membrane-impermeable dye calcein was employed. Following procedures previously reported,^{16, 24, 31, 32} calcein was dissolved in 1 M NaOH at a concentration of 50 mg mL⁻¹ which was diluted with water to generate a working solution at a concentration of 1 mg mL⁻¹. For the experiments, HEK 293T cells were seeded at 2 x 10⁵ cells mL⁻¹ in 24-well plates (VWR, 10⁵ cells per well) and cultured in growth medium at

37 °C (5 % (v/v) CO₂) for 24 h. The medium was changed to fresh Opti-MEM™ 1 h prior to treatment. Cells were treated with polyplexes at N*/P 15 as described for the transfection studies, using pKMyc pDNA. Immediately after the addition of polyplexes, calcein was added to the cells to give a final concentration of 25 µg mL⁻¹. The control cells were incubated with fresh culture medium containing the same concentration of calcein (calcein control) or the same concentrations of calcein and pDNA (pDNA control). For comparison, commercial 1-PEI (25 kDa) was also studied, but at higher concentrations than previously reported.¹⁶ Following incubation for 4 h, cells were carefully washed twice with PBS, harvested by trypsin treatment and resuspended in HBSS supplemented with 2 % FCS and 20 mM HEPES. Investigations were carried out at dimmed light. *Via* flow cytometry, a quantity of 10⁴ events were measured as described before for the transfection studies. The calcein signal of viable, single cells was analyzed at $\lambda_{\text{Ex}} = 488$ nm combined with a 525/40 nm bandpass filter. The rel. MFI of all viable cells was calculated in relation to the calcein control. The scatter plots can be found in the SI (Figure S23). The experiments were performed trice and data are expressed as mean \pm SD.

Quantitative polymerase chain reaction (qPCR)

To investigate the accessibility of pDNA within the polyplex, qPCR was performed. For this purpose, polyplexes were prepared using pEGFP-N1 pDNA and the respective polymers at N*/P 3 and 15 in 20 mM HEPES solution to give a final pDNA concentration of 100 ng mL⁻¹. For qPCR, SsoAdvanced Universal SYBR Green Supermix and a qTOWER³ thermal cycler (Analytik Jena, Jena, Germany) were used according to the manufacturer's instructions. After activation at 98 °C for 3 min, the thermal cycle profile consisted of denaturation at 98 °C for 15 s, annealing at 60 °C for 30 s, and elongation at 60 °C for 30 s with fluorescence data collection for 35 cycles. In these experiments, 1 ng of pDNA per reaction and 250 nM primer were used [forward primer (5'-3'):

AAGTTCATCTGCACCACCG, reverse primer (5'-3'): TCCTTGAAGAAGATGGTGCG].³³

The experiments were conducted twice.

Statistical analysis and DoE approach

To determine the effects of pDNA and polymer concentration and their interactions on transient transfection, the design-of-experiments (DoE) approach was employed. First, historical data were used to define the design space. The focus was set on studying the polymers in the same design space to identify correlations between polymer basicity and transfection. For this purpose, we used a Central Composite Design (CCD) for the Response Surface Methodology (RSM) to create a second or higher degree model using Design-Expert® (StatEase, Minneapolis, United States), version 11. Measurement points in the design space were determined experimentally as described above with key points tested multiple times (see Figure S7 for an exemplarily shown setup). For the DoE approach, a new batch of PNAiPP with comparable molar mass and dispersity was synthesized (Figure S2, table S1). Analysis of variance (ANOVA) was used to determine the significance of the factors studied, their interactions, and the model itself. All other statistical analyses were performed using SPSS Statistics (IBM, Armonk, United States), version 26. To determine the statistical significance among polyplex uptake, membrane integrity and calcein release data, one-way ANOVA was performed. If the ANOVA revealed significant differences ($p < 0.05$), post-hoc analyses with a Bonferroni correction were applied. Statistically significant differences were indicated as follows: $*p < 0.05$, $**p < 0.01$, and $***p < 0.001$. The results are presented as the mean value \pm standard deviation (Mean \pm SD) of at least three independent determinations if not stated otherwise.

RESULTS & DISCUSSION

Charge dependent pDNA binding and transient transfection of adherent cells

Based on our previous study, we did not expect the polypiperazines to exhibit a strong interaction with genetic material, since the polymers revealed only a low protonation and thus only a limited positive charge at physiological pH values, which is also reflected by their low toxicity despite rather high molar masses (71 - 99 kDa, degree of polymerization (DP) = 500, Figure 1, S1, Table S1).²⁴ The tuning of the amino substitution resulted in different charge densities at pH 7.4, ranging from 9 % for the less basic PNAMP to a maximum of 36 % for the more basic PNA ϵ BP, which is based on theoretical considerations derived from the titration of the polymers (Figure 1b).²⁴ Initial pDNA binding experiments relied on an EtBr exclusion assay. Despite the large polymer excess (N*/P 30), only a charge-dependent displacement of EtBr up to 30 % was achieved (Figure S3, pH 7.4). For comparison, commercial l-PEI (25 kDa, DP \approx 580), which has a charge density of more than 50 % at physiological pH value,^{34, 35} leads to a displacement of nearly 90 %, which reflects the effective pDNA condensation known for this type of polymer (Figure S3, black). To further verify the importance of the charge density for pDNA condensation, the EtBr displacement assay with the polypiperazines was additionally performed at lower pH values (pH 5 - 7, Figure S3). Increased pDNA condensation at decreasing pH values confirmed our hypothesis that EtBr can be displaced by protonated polypiperazines, however such conditions cannot be maintained in common cell cultures. Although these results initially prompted us not to consider further investigations, we recently tested the pDNA binding of the polypiperazines at physiological pH using a gel migration assay (Figure 1b,c). As expected, PNAMP did not complex pDNA at any of the N*/P ratios examined (3; 11; 15; 30), confirming that its charge density (9 %) was not sufficient for stable polyplex formation. However, PNAEP displayed an unexpected N*/P-dependent

retardation of pDNA, starting at N*/P 11. More astonishingly, PNA*i*PP and PNA*t*BP retained pDNA even at a low N*/P of 3, which suggested polyplex formation contradictory to the initial EtBr assay. Interestingly, PNA*i*PP, PNA*t*BP and l-PEI showed the same pattern for pDNA binding despite their substantially different charge density at pH 7.4 (22 % and 36 % vs. > 50 %, as previously reported²⁴). Thus, the polypiperazines were able to efficiently bind pDNA and inhibited its gel migration at pH 7.4, although they resulted in only a modest EtBr displacement. We therefore assumed that the polypiperazines bind pDNA differently compared to the highly charged l-PEI at pH 7.4. A different mode of binding in the case of PNA*i*PP and PNA*t*BP is also supported by the hydrophobicity of the *i*-Pr and *t*-Bu side chains, which are able to interact with the solvophobic portions of the DNA chains.

Intrigued by these new results and the high endosomal escape efficiency observed in our previous study, we investigated the transfection efficiency of the polypiperazines. Similar to part of the previous study, serum-free conditions were chosen. Since these polymers have not been utilized for gene transfection before, we tested different pDNA concentrations at a constant polymer concentration (N* conc., Figure 1d) as a starting point for evaluation of their efficiency. These concentrations were subsequently varied in pursuing experiments at fixed N*/P ratios of 15 and 30 (Figure 1e). As anticipated from the pDNA binding experiments, transfection was not detected for PNAMP at any of the conditions examined. In both, the fixed N* conc. and the fixed N*/P ratio studies, the transfection efficiency of investigated polymers PNAEP, PNA*i*PP, PNA*t*BP and l-PEI was significantly determined by the applied pDNA concentration. Moreover, our studies revealed similar transfection patterns for PNA*i*PP and l-PEI of over 90 % and 80 % transfected cells, respectively. Transfection with both polymers resulted in similar percentages of GFP-fluorescent cells whereby the MFI for l-PEI was slightly higher (Figure S4a,c). Both polymers functioned best at medium to high pDNA concentrations (> 12 $\mu\text{mol L}^{-1}$) and medium N*/P ratios

(15), although differences in the polymer/pDNA mass ratios of the polyplexes should be noted (PNAiPP: ~8.4, l-PEI: ~2.0, also see Table S4). Interestingly, PNAiPP and PNAiBP outperformed commercial l-PEI at N*/P 3. It was shown before that the transfection performance of PEI collapses at lower N*/P ratios, whereby the exact ratio is molar mass dependent.³⁶ This reduction in transfection efficiency is associated with the deficiency of excess polymer, which was found to be essential for PEI, as the presence of free polymer chains has a significant impact on the transfection efficiency.³⁷ However, unlike PEI, PNAiPP transfects efficiently at lower N/P ratios, at which free pDNA is no longer detectable. We thus assume that the transfection mechanism of the polypiperazines does not depend on free polymer chains. PNAEP and PNAiBP showed lower transfection efficiencies at the selected conditions, whereby the results for PNAEP showed strong variations, which could so far not be clarified. Cell viability was high in all treatments except for the highest concentration of PNAiBP at N*/P 30 (Figure S4d), where toxic effects were observed (Figure S5i).

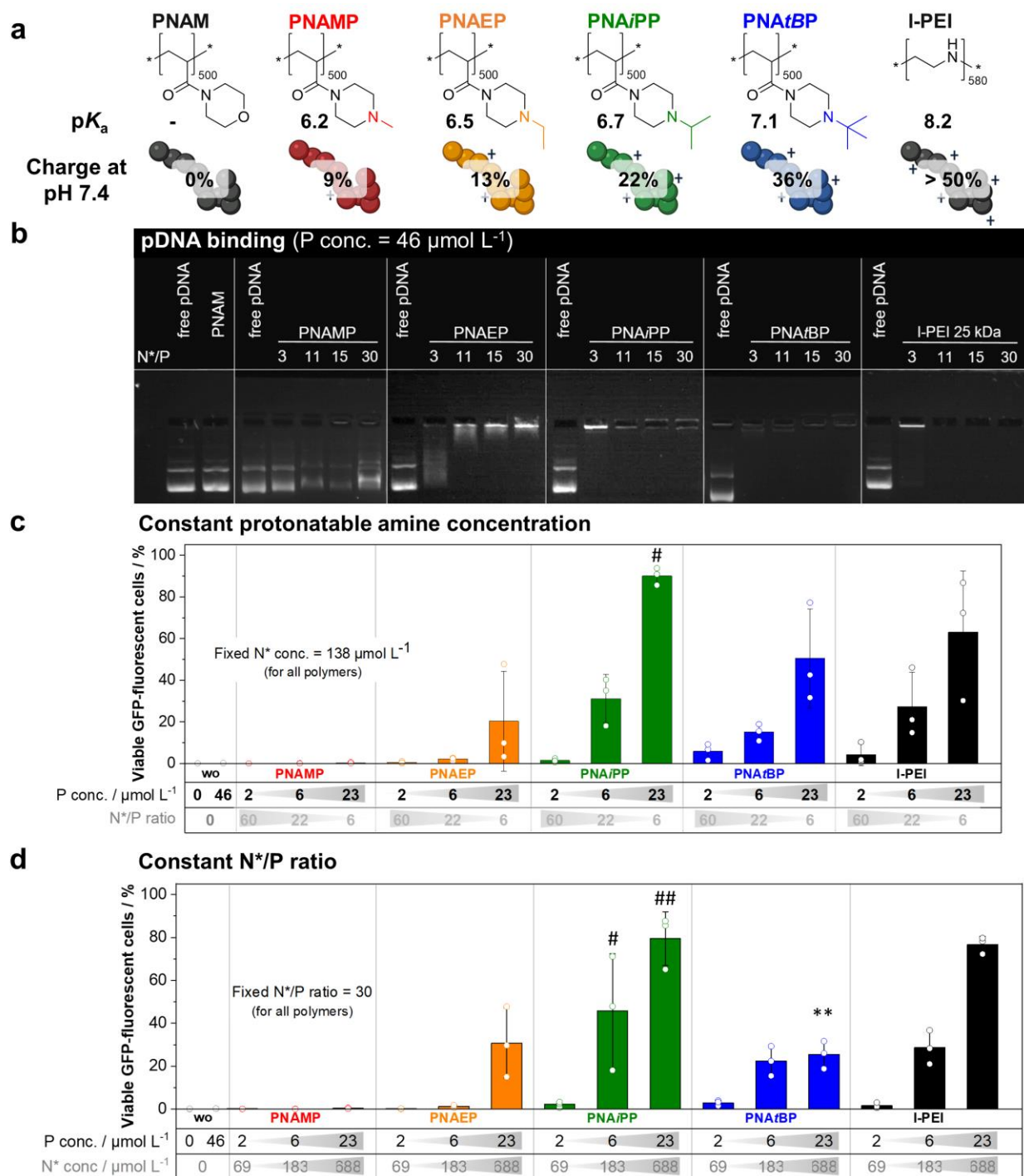


Figure 1. Charge-dependent pDNA binding and transfection efficiency of polypiperazines in HEK 293T cells. **a** Chemical structure of the control poly(*N*-acryloylmorpholine) (PNAM), the polypiperazines, and l-PEI including their pK_a and the corresponding charge density at pH 7.4. **b** The pDNA binding ability of the polymers was studied at various N*/P ratios and an equal P concentration of 46 $\mu\text{mol L}^{-1}$ by gel electrophoresis ($n \geq 1$). Free pDNA was investigated as control. **c** HEK 293T cells were treated with various polyplex formulations at a fixed protonatable amine concentration (N* conc., polymer) resulting in increasing phosphate concentrations (P

conc., pDNA) with decreasing N*/P ratios. **d** HEK 293T cells were treated with various polyplex formulations at a fixed N*/P ratio of 30. **c, d** Transfection efficiency was analyzed by flow cytometry and is shown as mean ($n = 3$) \pm SD and as individual data points (dots). ** Significant difference to the corresponding l-PEI polyplex at respective P concentration ($p < 0.01$), #/### significant difference to the corresponding PNAEP polyplex at respective P concentration ($p < 0.05/0.01$).

Optimization of transfection efficiency

Encouraged by the initial transfection data, a more detailed investigation was conducted. Using DoE methods, the transfection efficiency of the novel polypiperazines was thoroughly investigated over wide concentration ranges. First, the previously generated data were used to define a design space of 7 - 21 $\mu\text{mol L}^{-1}$ P and 67 - 222 $\mu\text{mol L}^{-1}$ N* for the DoE-based optimization of the transfection conditions of the most promising candidate PNAiPP and commercial l-PEI for comparison (also see Figure S6 for PNAEP and PNAiBP). Within this design space, several measurement points were determined experimentally and the results fitted by surface models. The models obtained for PNAiPP and l-PEI are shown in Figure 2. Regardless of the concentration ranges within the design space, PNAiPP formed a plateau where transfection efficiency was predicted to be around 80 %. In contrast, l-PEI showed an optimum at 215 $\mu\text{mol L}^{-1}$ N* and 7 $\mu\text{mol L}^{-1}$ P, and the model decreased with decreasing N* and increasing P concentration. The results correlate very well with the initial measurements and confirm the importance of high N*/P ratios for l-PEI.

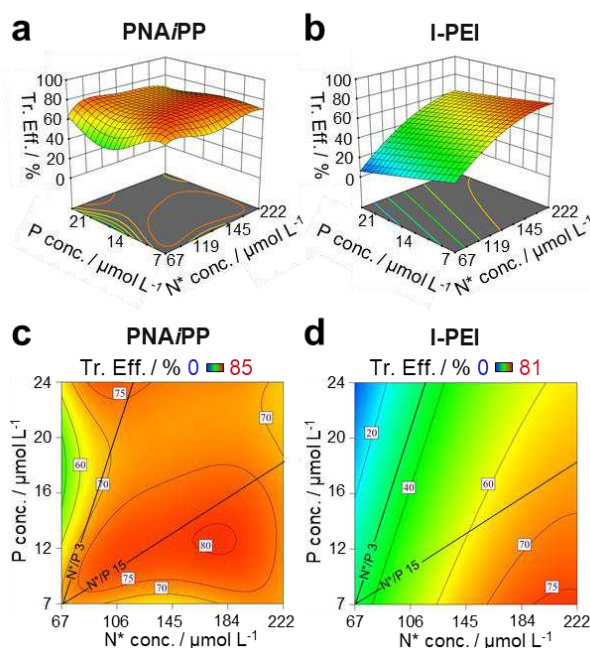


Figure 2. Initial design space for optimization of the transfection efficiency of PNAiPP in comparison to l-PEI in HEK 293T cells via DoE. a,b 3D surface models and c,d contour plots of the response surface predicting the transfection efficiency (percentage of viable GFP-fluorescent cells) in HEK 293T cells under serum-free conditions of a,c PNAiPP and b,d l-PEI show transfection maxima at different conditions.

Subsequently, we augmented the design space to 0 - 32 $\mu\text{mol L}^{-1}$ P and 0 - 250 $\mu\text{mol L}^{-1}$ N* to investigate the transfection efficiency outside the initial design space in order to identify the beginning of the plateau of optimal transfection for PNAiPP at the smallest possible P and N* concentration and compare the pattern with all other polymers (the corresponding measurement points are depicted in Figure S7). The resulting augmented 3D surface models are given in Figure 3. An overlay of the corresponding experimental results and the transparently displayed surface response model is depicted in Figure S8. The augmented models showed that PNAEP and PNAiBP exhibited one optimum, whereas comparable transfection patterns were revealed for PNAiPP and l-PEI. Again, a broader range of conditions for optimal transfection was identified for PNAiPP. The models for PNAEP, PNAiPP and l-PEI predicted transfection efficiency to be > 80 %, whereas PNAiBP had comparatively lower transfection efficiency (~ 40 %) in the range studied.

Interestingly, trends emerged between the basicity of the polypiperazines and the polymer as well as pDNA concentrations for optimal transfection. The less basic PNAEP was most efficient at comparatively high polymer concentrations and low pDNA concentrations, *i.e.*, at higher N*/P ratios. The more basic polypiperazines PNAiPP and PNAiBP revealed optima at lower polymer and higher pDNA concentrations, *i.e.*, at progressively lower N*/P ratios. However, PNAiPP, which has medium basicity, performed best. It was surprising that PNAiBP did not transfect as efficiently, as in comparison to PNAiPP it is highly charged and binds stronger to the pDNA. Previous studies have shown that PNAiBP ($CC_{50} = 105 \mu\text{g mL}^{-1}$, see Figure S9) is more toxic than PNAiPP ($CC_{50} = 386 \mu\text{g mL}^{-1}$),²⁴ suggesting an efficiency-toxicity dilemma. The systematic investigation using DoE surprisingly revealed very high efficiencies for PNAEP, unveiling the optimum for transfection in a concentration range that was not covered in the previous studies (see previous section).³⁸ PNAEP achieved the same efficiency as PNAiPP at higher polymer concentrations and N*/P ratios, probably due to its lower charge density.

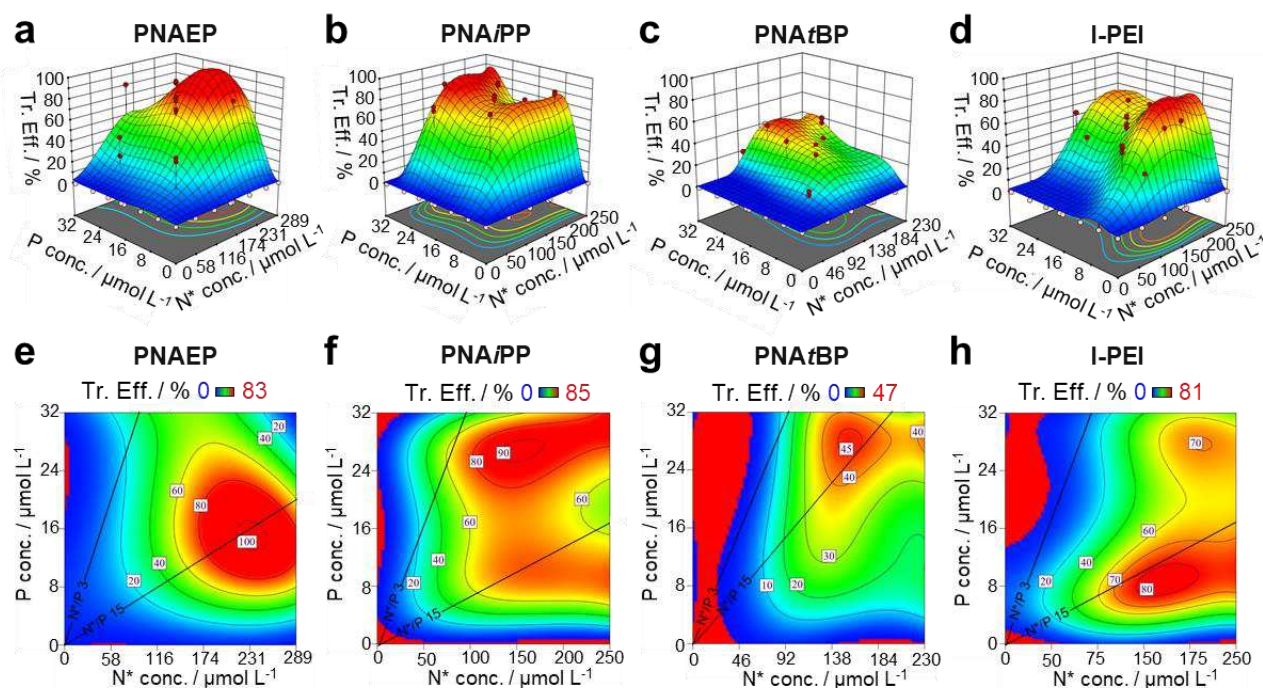


Figure 3. Optimization of the transfection efficiency of polypiperazines in HEK 293T cells under serum-free conditions *via* DoE. **a-d** Augmented 3D surface models and **e-h** augmented contour plots of the response surface predicting the transfection efficiency (percentage of viable GFP-fluorescent cells) of **a, e** PNAEP, **b, f** PNA/PP, **c, g** PNA/BP, and **d, h** I-PEI show transfection maxima at different conditions. In the 3D plots, the measurement points located in front of the model are indicated with red dots. Constant N*/P-ratios were plotted along the guidance lines drawn in the contour plots. **a-h** HEK 293T cells were treated with various polyplex formulations. Transfection efficiency was investigated by flow cytometry (statistics for **b** and **f** are given in Table S2 and S3).

Comparing the initial and the augmented model for PNA/PP, it appeared that especially the boundary regions may be more error-prone in the augmented model and the prediction at these regions may be underestimated. Analysis of variance (ANOVA) revealed an R^2 of 88 - 94 % (Table 1) for the augmented models (Figure 3a-d) indicating that these models were reliable and less than 6 - 12 % of variations remained. The optimal transfection conditions predicted by the models for the four polymers were validated by experimental transfections (Table 1, also see Figure S10, S11 for microscopic images and S12-S18 for scatter plots). Except for PNA/BP, which was validated only in the optimum of the augmented design space, all models were validated at least in the optimum

of the initial and in the optimum of the augmented design space. PNAiPP was also validated at the second optimum (10 $\mu\text{mol L}^{-1}$ P and 165 $\mu\text{mol L}^{-1}$ N*) within the augmented design. In addition, PNAiPP was validated at the plateau boundary (7 $\mu\text{mol L}^{-1}$ P and 67 $\mu\text{mol L}^{-1}$ N*) of the initial design space to save P and N* quantities for the sake of identifying the most economical transfection conditions. For the polypiperazines, the percentage of GFP-fluorescent cells under optimal conditions was predicted to be > 80 % for PNAEP as well as PNAiPP and close to 50 % for PNAiBP (Figure 3). The experimental transfection efficiencies of PNAiPP and l-PEI were close to 100 %, which was higher than predicted (Table 1, also see Table S4 for mass ratios).

Table 1. Regression coefficients for the DoE models and the validation runs.

Polymer	R ² of model	<i>p</i> value of model	Validation runs					
			N* conc.	P conc.	N*/P	Viable GFP-fluorescent cells / %		
			<i>μmol L⁻¹</i>	<i>μmol L⁻¹</i>		Predicted ± SD ^d	Mean ± SD (measured)	
PNAEP	88.6	< 0.0001	a	222	22	10	82.1 ± 22.9	80.14 ± 5.72
			c	243	15	16	100.6 ± 25.6	72.19 ± 17.53
PNAiPP	93.9	< 0.0001	a	176	12	14	76.1 ± 19.4	99.96 ± 0.03
			b	67	7	9	39.4 ± 13.9	99.96 ± 0.01
			c	153	27	6	90.6 ± 21.3	99.99 ± 0.01
			c	165	10	16	76.4 ± 19.6	99.97 ± 0.02
PNAiBP	92.8	< 0.0001	c	155	28	6	45.4 ± 10.5	56.36 ± 17.59
l-PEI	87.4	< 0.0001	a	215	7	29	76.1 ± 25.4	99.83 ± 0.03
			c	171	9	20	82.6 ± 26.2	99.91 ± 0.06

^a predicted experimental conditions from initial design space for high transfection efficiency.

^b factorial point of the initial design space with lowest N* and P concentration.

^c predicted experimental conditions from augmented design space for high transfection efficiency.

^d standard deviation for the predicted values might exceed 100 % for mathematical reasons.

Indeed, values approaching 100 % transfection might appear unusual and are rarely reported, but, to the best of our knowledge, similar systems have so far not been optimized by a DoE approach. A closer look at the experimental flow cytometry measurements of the validation runs further reveals an undeniable shift of the cell population for most experiments (Figures S13-S18) compared to the control. However, it has to be kept in mind that we used adherent HEK 293T cells at high confluency in these experiments, which might for example explain differences to highly optimized suspension cell lines used for technical protein production.³⁹ Considering the augmented model, the exceedance of the predicted values is mainly explained by the possible underestimation of the transfection efficiency in the boundary regions of the design space, which particularly becomes apparent for PNA ι PP at the lowest evaluated concentrations. The predicted optimum for PNA ι BP (45 % GFP-fluorescent cells) was in line with the experimental outcome (56 ± 17 %), which is also the case for the result for PNAEP (80 ± 6 %, predicted: 82 %), if the initial design space is considered. For the augmented design space, the experimental results (72 ± 17 %) at the predicted optimum of PNAEP were however lower than the values obtained from the model (100 %), but still within reasonable range considering the standard deviation of the model (see also Figure S19 for the 95% confidence interval of the model for PNAEP at exemplarily chosen concentrations P of $22 \mu\text{mol L}^{-1}$ and $15 \mu\text{mol L}^{-1}$). Again, we like to emphasize that the discrepancies might arise from the set boundary regions of the augmented design space, but the initial model clearly matches the experimental outcomes.

Overall, the optimization of the transfection efficiency with a DoE enabled the creation of statistically valid models regarding the optimal settings for polypiperazines and l-PEI while saving

enormous amounts of material and time. The highest transfection efficiencies were achieved for PNAiPP and l-PEI (about 100 % in the validation experiments), but PNAEP also reached transfection efficiency of about 80 % in the validation of the optimum. This concentration range would usually not be covered in a classical OFAT approach, which underlines the power of DoE. Thus, PNAEP, which showed no toxicity up to concentrations of 1 mg mL⁻¹ (correspondes to 6 mmol L⁻¹ N*) according to ISO10993-5,²⁴ is a positive example that the efficiency-toxicity dilemma can also be overcome by simple homopolymers, if the pH-response and the charge density is finely tuned. Nevertheless, both the preliminary studies and the systematic optimization of the transfection efficiency revealed PNAiPP to be the best performer of the four polypiperazines. Interestingly, the range of pDNA and polymer concentrations for optimal transfection with PNAiPP is significantly broader than for all other polymers including l-PEI. Although the transfection optimum of PNAiPP is at a higher P conc. (~24 µmol L⁻¹), it also transfects in the optimal range of l-PEI (~8 µmol L⁻¹) with comparably high efficiency and further at lower polymer concentrations (~67 µmol L⁻¹ of N*).

Interactions with cellular membranes and endosomal escape

Due to the low N*/P ratios required for efficient transfection of PNAiPP, interactions with cellular membranes were examined to elucidate the transfection mechanism. To measure polyplex uptake, pDNA was stained with the intercalating dye YOYOTM-1 and polyplexes were formed at N*/P 3 and 15. Simultaneously, plasma membrane integrity was measured by an enzyme-based assay using the cell culture supernatant (LDH assay). The polyplex uptake was found to be dependent on the charge density, the incubation time, the N*/P ratio, and the toxicity of the polymer (Figure 4a, bars). Unlike PNAMP, PNAEP led to substantial uptake at N*/P 15 after 4 h. In general, the more basic PNAiPP and PNAiBP led in general to higher uptake rates with the exception that

PNA*i*PP still gave only a limited uptake at a low N*/P of 3. We did not observe any pDNA uptake for l-PEI at N*/P 3 (Figure 4a, black bars) which correlates with the lack of transfection at these conditions.³⁷ The most efficient uptake in the chosen setup was observed for PNA*i*PP at N*/P 15 after 4 h (also see Figure S20, S21). When the number of cationic charges exceeds a tolerable concentration for the plasma membrane (Figure 4a, dots), the uptake rate collapsed, as it was demonstrated in the case of PNA*t*BP at higher N*/P ratios.

A calcein release assay was performed to investigate a potential perforation of the endosomal membranes by the polyplexes. Although it has to be kept in mind that calcein is much smaller compared to the pDNA, this simple and rapid method often correlates with transfection efficiency.^{16, 40, 41} In a previously published study, a similar assay was used to evaluate the endosomal escape capacities of the free polypiperazines.²⁴ Building on the previous study that showed clear correlations between microscopy and flow cytometry, in this study we performed only flow cytometric analyses to provide an indication of whether endosomal release also is also successful in the presence of pDNA. Under the same conditions as for the polyplex uptake assays, the relative fluorescence intensity of calcein increased for PNA*i*PP, PNA*t*BP, and l-PEI polyplexes, which were most pronounced for l-PEI after 4 h (Figure 4b). Interestingly, at lower pDNA concentration ($12 \mu\text{mol L}^{-1}$, Figure S22), PNA*i*PP showed comparable intensities indicating calcein release as found for l-PEI despite their markedly different basicity, whereas at higher pDNA and correspondingly higher polymer concentrations, the calcein release of l-PEI significantly exceeded that of PNA*i*PP (P conc. = $46 \mu\text{mol L}^{-1}$, Figure 4b). As shown previously, the increased amount of free l-PEI has a pivotal role in endosomal escape and is also crucial for the transfection mechanism.^{42, 43} Our previous studies also showed very low calcein release efficiency for PNAEP.²⁴ In the context of nucleic acid transfection, however, only a few released pDNA strands may be sufficient because a plasmid can be repeatedly transcribed for subsequent

protein production.⁴⁴ This might explain why transfection efficiencies comparable to PNAiPP were obtained for the less basic PNAEP, although higher polymer concentrations had to be applied. In general, our results are consistent with the previously published study on cytosolic delivery of proteins, in which PNAiPP also performed best in Opti-MEM™, considering efficiency and toxicity.²⁴ The increased plasma membrane activity of the more charged PNAiBP has again an unfavorable effect in the context of transfection with nucleic acids, as limitations in cell viability impede protein biosynthesis.

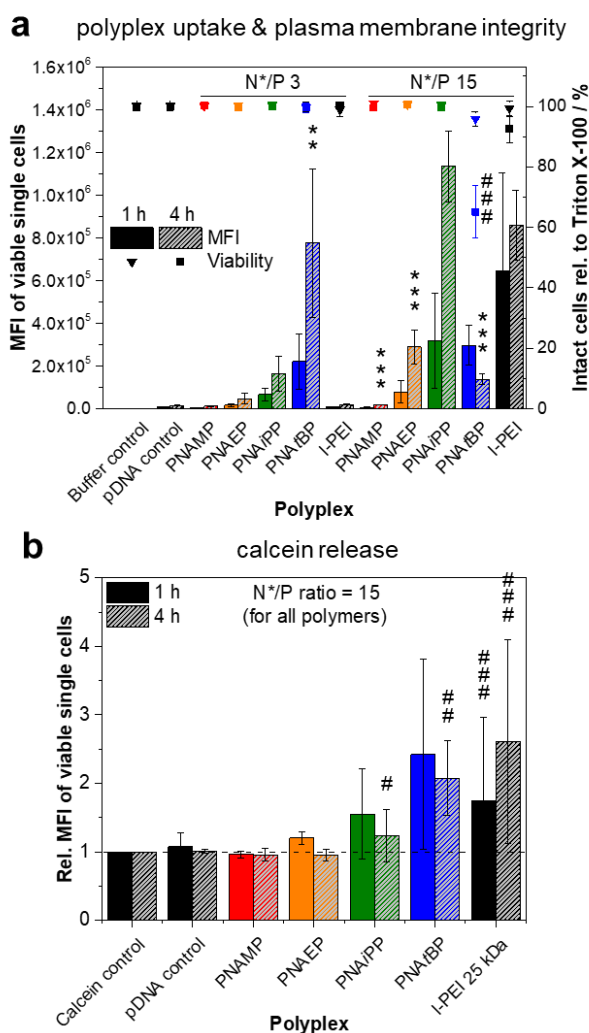


Figure 4. Interactions of polyplexes with plasma and endosomal membranes. **a** Polyplexes were prepared with YOYO™-1 labeled pKMyC pDNA (final P conc. = 46 $\mu\text{mol L}^{-1}$). The polyplex

uptake into HEK 293T cells was investigated *via* flow cytometry, and is represented as the MFI of viable, single cells (bars). Before harvesting the cells for the uptake measurement, their membrane integrity was measured *via* LDH assay, using cells lysed with Triton X-100 as control. Here, the percentage of viable cells with intact membranes is indicated (dots). Data are represented as the mean \pm SD of three independent measurements. **b** The endosomal release of calcein was investigated by flow cytometry, whereby higher intensities relative to the calcein control cells (treated with the same calcein concentration, but without polymers) indicate endosomal escape. HEK 293T cells were treated with polyplexes (final P conc. = 46 $\mu\text{mol L}^{-1}$) and/or 25 $\mu\text{g mL}^{-1}$ calcein. Data are reported as the mean \pm SD of three independent experiments. **a,b** ^{**/**} Significant difference to the corresponding l-PEI polyplex at respective time point ($p < 0.01/0.001$), ^{#/##/###} significant difference to the controls ($p < 0.05/0.01/0.001$).

To investigate uptake and interaction with cellular membranes in more detail, we used live-cell confocal laser scanning microscopy (CLSM) and polyplexes prepared from Oregon Green labeled polypiperazines and TOTOTM-3 stained pDNA.²⁴ Here, a lower polyplex concentration was applied to minimize toxic effects expected for PNA ι BP based on plasma membrane integrity data (final P conc. = 12 $\mu\text{mol L}^{-1}$, also see Figure S22 for calcein release assay data at these conditions). For PNAMP, negligible polymer uptake was observed in small, isolated compartments, but no pDNA uptake was found (Figure 5). A slight uptake was measured for PNAEP, and PNA ι BP showed toxic effects despite the onset of lower polymer concentration (Figure S24). PNA ι PP induced efficient polymer and pDNA uptake. The TOTOTM-3 signal was distributed throughout the cytoplasm in approximately 10 % of cells, indicating endosomal escape of the polyplex and subsequent incorporation of released TOTOTM-3 into cytoplasmic genetic material. Interestingly, when released, the signal of PNA ι PP (Oregon Green) was not distributed throughout the cytosol but assimilated in the nucleus (Figure 5), which confirms the polymers ability to pass the nuclear membrane. In the case of PNA ι BP, we also observed Oregon Green signals in the nucleus, but here we assume toxic effects such as membrane disruption as causative (also see Figure S24).

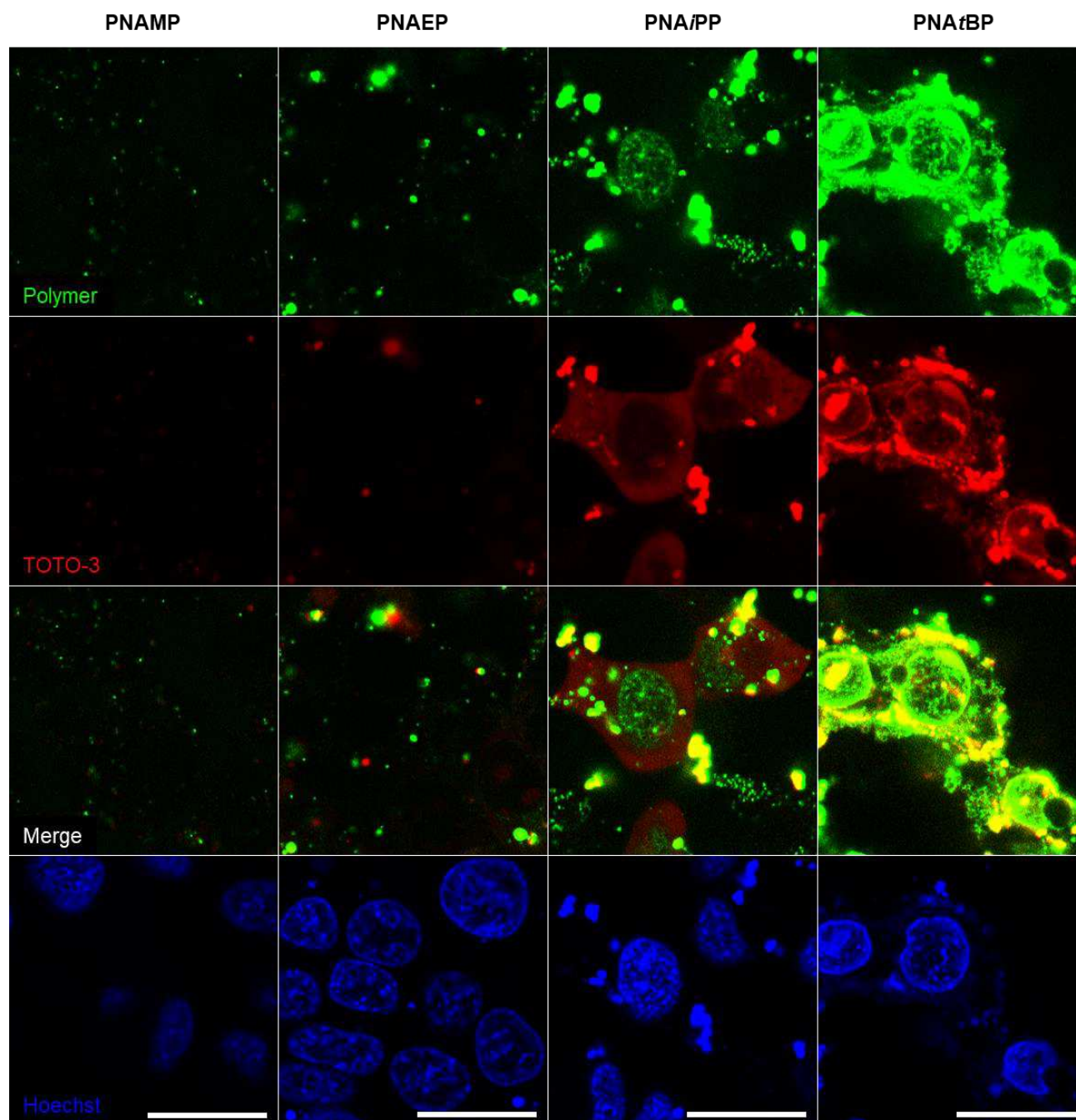


Figure 5. Uptake and intracellular trafficking of piperazine-based polyplexes. HEK 293T cells were treated with polyplexes of Oregon Green-labeled polypiperazines (green channel) and TOTOTM-3 iodide-stained pKMyC pDNA (red channel, P conc = 12 $\mu\text{mol L}^{-1}$) at N*/P 15 for 4 h. The cells were stained with Hoechst 33342 (blue channel) to visualize the nuclei in live-cell confocal microscopy. Representative images of two independent experiments are shown. Scale bar 20 μm . Lower magnification images showing a larger number of cells including bright field images and are provided in the SI (Figure S24).

Polyplex characterization and stability

To better understand the interaction of the polypiperazines with genetic material and to unravel the mystery of why these polymers perform so well despite their lower charge density at pH 7.4, the polyplexes were studied in more detail. The hydrodynamic diameter, polydispersity index (PDI), and surface charge in comparison to free pDNA were investigated by DLS/ELS. Accordingly, polyplexes ≤ 200 nm were formed with PNAEP, PNAiPP and PNAiBP (Figure 6a, S25, S26). PNAMP formed larger aggregates due to less intensive packaging as indicated before. The PDI for all polyplexes was in a desirable range < 0.250 . The zeta potential correlated with the charge density of the polymers, with the l-PEI polyplexes exhibiting the strongest positive surface charge (Figure 6b). In brief, the formation of polyplexes in a favorable size with a desirable surface charge supports the gene delivery potential of PNAEP, PNAiPP and PNAiBP.

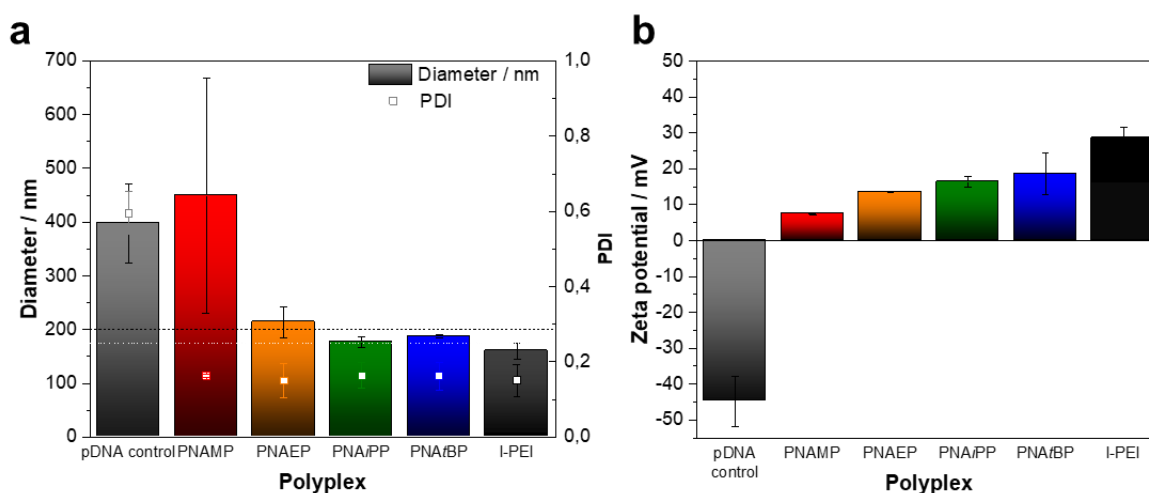


Figure 6. Polyplex characterization Polyplexes at N*/P 6 were characterized in terms of **a** diameter of the intensity weighted maximum peak and PDI by DLS. The black and white dotted lines indicate the desired size (≤ 200 nm) and PDI range (≤ 0.250), respectively. Exemplary decay functions and intensity histograms are shown in the SI (Figure S25, S26). **b** The polyplexes were further characterized in terms of surface charge by ELS. For comparison, free pDNA was investigated as well. **a,b** The values represent the means \pm SD of three technical replicates.

We also investigated the stability of the polyplexes by adding the competitive polyanion heparin to induce the release of pDNA, which can be visualized by a gel migration assay. Among the polypiperazines a trend towards increased stability with increased basicity was found. At N*/P 15, pDNA can be released from the PNAEP polyplexes at all investigated heparin concentrations (Figure 7a), whereas only a negligible pDNA release was observed for PNAiPP polyplexes at any of the tested conditions (Figure 7b). Finally, no pDNA release was observed for PNAiBP (Figure 7c). On the contrary, l-PEI fully releases pDNA in each of the tested conditions, indicating a different mode of pDNA binding of polypiperazines and l-PEI (Figure 7d,e). We hypothesize that the increasing hydrophobicity of the alkyl side chains could form increasing local secondary interactions that stabilize the polypiperazine polyplexes if the competing heparin is added. In the case of PNAEP (lowest hydrophobicity), the secondary interactions might not be sufficient to prevent dissociation of the polyplex under polyanion addition (N*/P 15). On the other hand, in case of low PNAEP excess (N*/P 3), the packing density of the polymer chains at the pDNA could be much higher, favoring the proximity of the molecules and possibility of formation of local secondary interactions. Unpacking of pDNA was described as a critical factor in transfection and sophisticated systems were developed for pDNA release.^{3, 45, 46} However, the conducted heparin release experiment indicated that the delivery mechanism of the polypiperazines differs from well-known l-PEI and may not involve full pDNA release. In consideration of the CLSM studies, even a direct transfer of the still polymer-bound pDNA into the nucleus would be conceivable.

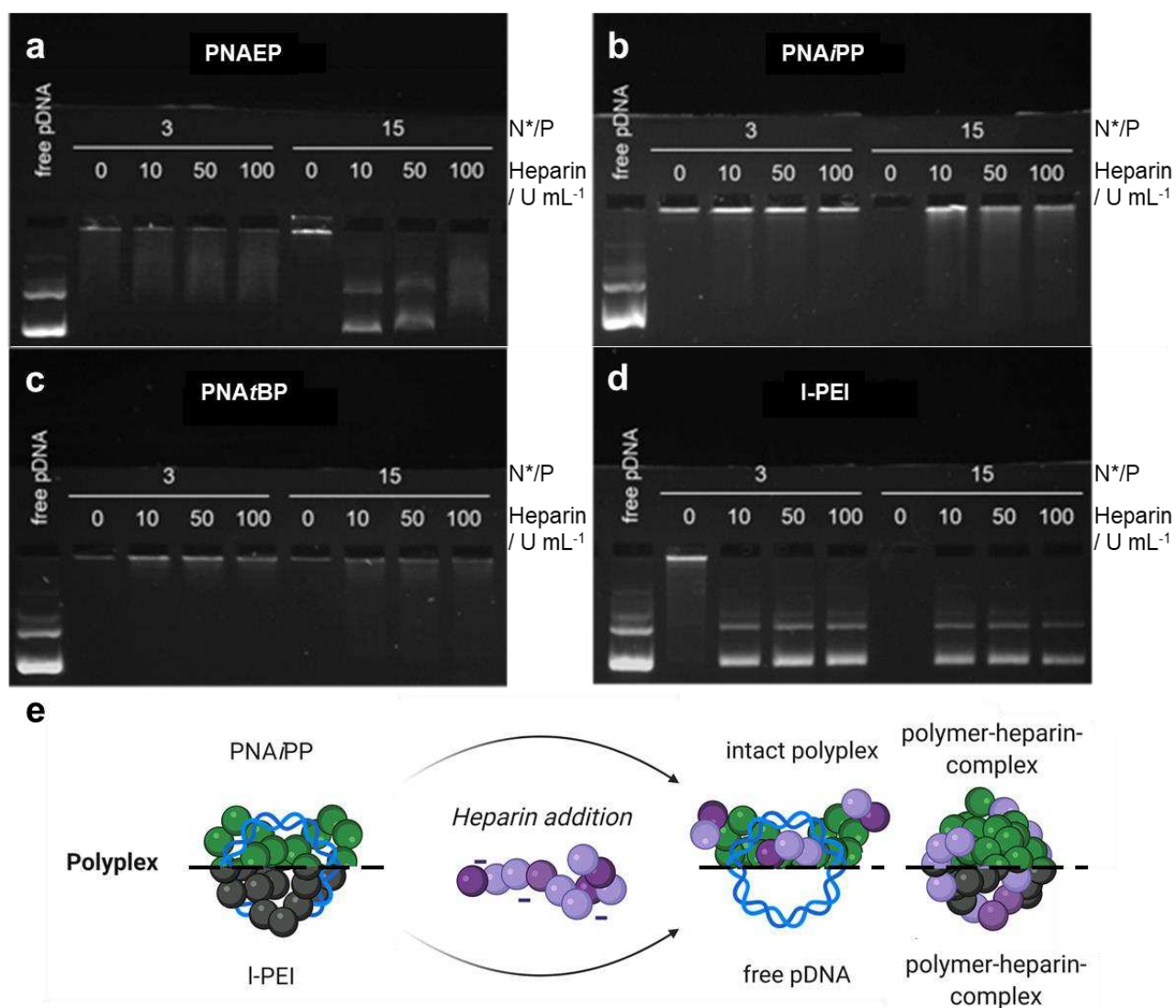


Figure 7. pDNA release behavior of polypiperazines and l-PEI. a-d Agarose gel electrophoresis was conducted to investigate polyplex stability and pDNA release. Polyplexes were prepared at N*/P 3 and 15 and incubated with different concentrations of heparin as a competitive polyanion. For comparison, free pDNA was investigated as well. A representative image (n = 2) for a PNAEP, b PNAiPP, c PNAiBP and d l-PEI is shown. e PNAiPP (green, upper) and l-PEI (black, lower) polyplexes differ in their stability and pDNA release behavior upon heparin treatment. Created with Biorender.com

Accessibility of pDNA within the polyplex and transfection mechanism

These release data raised the question of how polypiperazines, particularly PNAiPP, can effectively transfect cells despite the lack of pDNA release. To test whether the pDNA within the polyplex is accessible for transcription, we used qPCR to model an enzyme complex and examine the accessibility of the pDNA. Interestingly, the presence of the polypiperazines did not inhibit the qPCR under the tested conditions (Figure 8a). l-PEI polyplexes at N*/P 3 (no transfection) also did not disturb qPCR, but in the case of N*/P 15, qPCR was completely inhibited (Figure 8a, black triangles). These data support our hypothesis that PNAiPP and l-PEI polyplexes may differ in their pDNA binding mode and may be packaged differently, which could explain the difference in pDNA accessibility (Figure 8b). The distinctly lower charge density of the polypiperazines compared to l-PEI may explain the differences in polyplex packaging, pDNA binding and accessibility. The polypiperazines provide the opportunity for pDNA to remain freely accessible within the polyplex for transfection, thus circumventing the need for release of genetic material. The transfection mechanism of polypiperazines is thus clearly different from those previously described for other polymers. However, it has also to be mentioned that the different mode of binding and the corresponding accessibility might enhance the degradation of the pDNA by nucleases as well if *in vivo* applications are considered. Corresponding studies on the protective character of these polyplexes will be subject of follow-up investigations, which further include aspects to optimize the system.

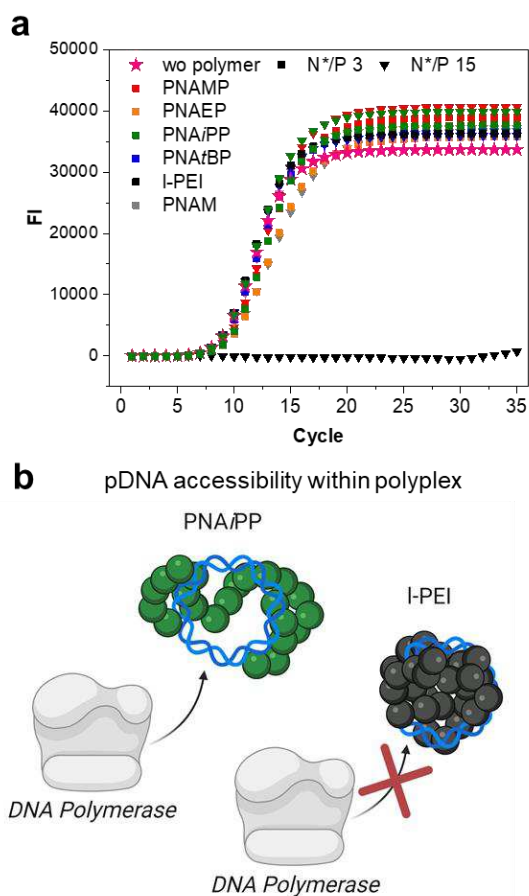


Figure 8. Investigation of pDNA accessibility within polypiperazine and I-PEI polyplexes. a Polyplexes were prepared in 20 mM HEPES buffer at N*/P 3 and 15 to investigate pDNA accessibility *via* qPCR. For comparison, free pDNA in 20 mM HEPES was investigated as well at the same concentration as used for the polyplexes. Representative amplification curves ($n = 2$) are shown for PNAMP (red), PNAEP (orange), PNAiPP (green), PNAiBP (blue), I-PEI (black) as well as uncharged PNAM (grey) and free pDNA (pink). **b** A schematic representation of PNAiPP (green) and I-PEI (black) polyplexes illustrates differences in their pDNA accessibility.

CONCLUSION

The systematic variation of the pendant alkyl unit on the pH-responsive amino group enables a fine tuning of the charge density on a family of piperazine based polymers (charge ratio between 9 % - 36 % at pH 7.4), whereat the polymer featuring an isopropyl group (PNAiPP) and a moderate charge density appears to be an efficient and versatile polymer for pDNA transfection. While initial complexation studies based on an EtBr assay indicated only a weak binding ability of these polymers, more detailed investigations based on gel retardation revealed indeed a stable polyplex formation, which however differs in terms of pDNA condensation from common transfection polymers such as l-PEI. In order to find optimal conditions for this new class of polymers, a DoE approach was applied to screen a broad design space in terms of concentrations of pDNA and polymer. These experiments revealed that even the slightly charged polypiperazines PNAEP (13 % charge density) and PNAiPP (22 %) can transfect as efficiently as the highly charged l-PEI (> 50 %). Although the overall activity of the polypiperazines correlated with their charge density, the upward trend collapsed in the case of PNAiBP, which is due to toxic effects induced by this polymer. In the case of PNAiPP, the limited charge density seems to represent a fine balance for achieving efficient transfection, without causing toxic side-effects, yet. Interestingly, PNAiPP appears to transfect very effectively over a very wide range of concentrations and N*/P ratios and outperforms l-PEI in terms of the latter ratios as it still achieves excellent transfection efficiencies at a N*/P ratio of 3. Surprisingly, even PNAEP was effective at higher polymer concentrations, although its ability to induce endosomal escape was limited compared to the more basic polymers (PNAiPP, PNAiBP, and PEI). More detailed microscopy studies further revealed that the polypiperazines appear to transport genetic material into the nucleus, which is a critical hurdle in pDNA transfection, but still showed no or only limited signs of toxicity. In contrast to common

cationic transfection agents and polymers like l-PEI, almost no pDNA release was observed for polyplexes based on PNAiPP and PNAiBP if treated with the competitive polyanion heparin. However, the successful amplification (qPCR) of the pDNA bound in a polyplex with the polypiperazines indicated that a release is not necessary for an efficient transcription in these cases and the underlying mechanism must differ from that of other commonly applied cationic polymers, where a release is vital for efficient transcription.^{47, 48} As stated above the condensation of the pDNA by the polypiperazines differs significantly from previously described polyplexes, for example l-PEI. We assume that the comparably loose binding of the polypiperazines enables an unhindered transcription of the pDNA even if complexed by the polymers. The unique transfection mechanism we postulate, is further schematically depicted in Figure 9.

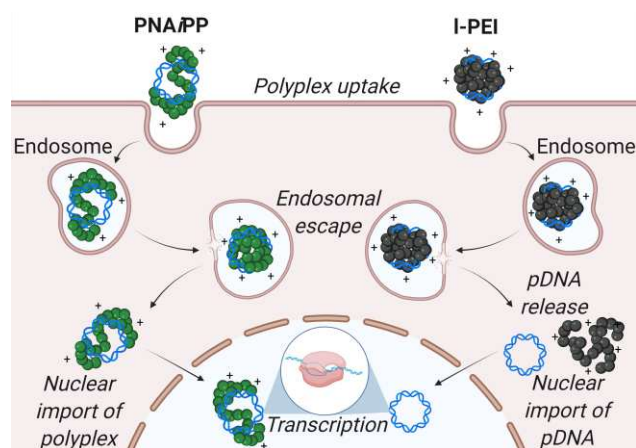


Figure 9. Suggested transfection mechanism of PNAiPP in comparison to l-PEI. PNAiPP and l-PEI polyplexes vary in their transfection mechanism to some extent. The pDNA in PNAiPP polyplexes is more loosely packaged than in the l-PEI polyplexes at physiological pH, but along the endosomal pathway, both polyplexes result in endosomal release. Whereas in the case of PNAiPP, the pDNA enters the nucleus within the polyplex, in the case of l-PEI, the pDNA is released and imported into the nucleus without polymer. The loose packing of PNAiPP polyplexes allows access of the transcribing enzyme complex. Both systems result in efficient transfection under optimal conditions.

Overall, our findings underline that the characteristics of piperazine-based transfection agents might differ significantly from established materials but nevertheless enable highly efficient transfection. Considering the versatile synthesis of the presented polypiperazines, alternative design options arise allowing for example the straightforward integration of targeting moieties, stealth units, or co-delivery of drugs. In particular with regard to tailored gene therapies, these opportunities may open new pathways along the lines of CRISPR/Cas 9 or related editing techniques, and we are convinced that this new class of polymers can play a key role in related developments.

AUTHOR CONTRIBUTIONS

FHP: project administration, conceptualization, methodology, investigation, data management, analysis, visualization, writing – original draft; GD: methodology, analysis, & visualization for DoE; writing – review & editing; FHS: synthesis, writing – review & editing; JIS: methodology, writing – review & editing; FR: methodology, writing – review & editing; DS: funding acquisition, software, supervision of GD, writing – review & editing; AT: funding acquisition, methodology, supervision, writing – review & editing; JCB: conceptualization, funding acquisition, project administration, supervision, writing – review & editing

ASSOCIATED CONTENT

Supporting Information Available: SEC, pH-dependent EtBr displacement assay, microscopic investigation of the transfection efficiency, CC₅₀ calculations

CONFLICT OF INTEREST

The authors declare that they have no competing interests.

ACKNOWLEDGEMENTS

The authors thankfully acknowledge B. Beringer-Siemers, Dr G. Festag, L. Jesse, C. Kellner, E. Moek and E. Preußger for technical assistance and discussions as well as Prof. Dr P. Czermak for his continuous support and the access to research facilities. Furthermore, Prof. Dr U. S. Schubert is acknowledged for his continuous support and providing access to excellent research facilities.

FUNDING

The authors thank the Federal Ministry of Education and Research (BMBF, #13XP5034A PolyBioMik) and the German Science Foundation (DFG) for generous funding within the Emmy-

Noether Program (Project-ID: 358263073). The funding of the collaborative research center PolyTarget, project A05 and B01 (Project-ID: 316213987 – SFB 1278) by the DFG are acknowledged. The authors further acknowledge the Hessen State Ministry of Higher Education, Research and the Arts within the Hessen initiative for scientific and economic excellence (LOEWE-Program and LOEWE Center DRUID, Novel Drug Targets against Poverty-Related and Neglected Tropical Infectious Diseases). The LSM880 ELYRA PS.1 was funded with a grant from the DFG.

DATA AVAILABILITY

The raw/processed data required to reproduce these findings are available on reasonable request.

REFERENCES

1. A. Singh, P. Trivedi and N. K. Jain, *Artif Cells Nanomed Biotechnol*, 2018, **46**, 274-283.
2. J. W. Schott, M. Morgan, M. Galla and A. Schambach, *Mol Ther*, 2016, **24**, 1513-1527.
3. D. W. Pack, A. S. Hoffman, S. Pun and P. S. Stayton, *Nat Rev Drug Discov*, 2005, **4**, 581-593.
4. I. M. S. Degors, C. Wang, Z. U. Rehman and I. S. Zuhorn, *Accounts Chem Res*, 2019, **52**, 1750-1760.
5. Y. Wang, M. Ye, R. Xie and S. Gong, *Bioconjugate Chem*, 2019, **30**, 325-337.
6. H. Lv, S. Zhang, B. Wang, S. Cui and J. Yan, *J Control Release*, 2006, **114**, 100-109.
7. A. P. Lam and D. A. Dean, *Gene Ther*, 2010, **17**, 439-447.
8. X. Sun and N. Zhang, *Mini Rev Med Chem*, 2010, **10**, 108-125.
9. A. C. Rinkenauer, S. Schubert, A. Traeger and U. S. Schubert, *J Mater Chem B*, 2015, **3**, 7477-7493.
10. M. Ahmed and R. Narain, *Biomaterials*, 2013, **34**, 4368-4376.
11. F. Richter, K. Leer, L. Martin, P. Mapfumo, J. I. Solomun, M. T. Kuchenbrod, S. Hoeppener, J. C. Brendel and A. Traeger, *J Nanobiotechnology*, 2021, **19**, 292.
12. A. Aied, U. Greiser, A. Pandit and W. Wang, *Drug Discov Today*, 2013, **18**, 1090-1098.
13. J. Cai, Y. Yue, D. Rui, Y. Zhang, S. Liu and C. Wu, *Macromolecules*, 2011, **44**, 2050-2057.
14. M. Wagner, A. C. Rinkenauer, A. Schallon and U. S. Schubert, *Rsc Adv*, 2013, **3**, 12774-12785.
15. C. V. Synatschke, A. Schallon, V. Jérôme, R. Freitag and A. H. Müller, *Biomacromolecules*, 2011, **12**, 4247-4255.
16. F. Richter, L. Martin, K. Leer, E. Moek, F. Hausig, J. C. Brendel and A. Traeger, *J Mater Chem B*, 2020, **23**, 5026 - 5041.
17. D. Sprouse and T. Reineke, *Biomacromolecules*, 2014, **15**, 2616-2628.
18. H. Li, M. A. Cortez, H. R. Phillips, Y. Wu and T. M. Reineke, *ACS Macro Lett*, 2013, **2**, 230-235.
19. A. K. Trützscher, T. Bus, M. Reifarth, J. C. Brendel, S. Hoeppener, A. Traeger and U. S. Schubert, *Bioconjugate Chem*, 2018, **29**, 2181-2194.
20. S. T. Hemp, M. H. Allen, M. D. Green and T. E. Long, *Biomacromolecules*, 2012, **13**, 231-238.
21. V. Loczenski Rose, F. Mastrotto and G. Mantovani, *Polym Chem*, 2017, **8**, 353-360.
22. D. Zhu, H. Yan, X. Liu, J. Xiang, Z. Zhou, J. Tang, X. Liu and Y. Shen, *Adv Funct Mater*, 2017, **27**, 1606826.
23. R. Kumar, N. Le, Z. Tan, M. E. Brown, S. Jiang and T. M. Reineke, *ACS Nano*, 2020, **14**, 17626-17639.
24. F. Hausig, F. H. Sobotta, F. Richter, D. O. Harz, A. Traeger and J. C. Brendel, *ACS Appl. Mater. Interfaces*, 2021, **13**, 35233-35247.
25. U. Lungwitz, M. Breunig, T. Blunk and A. Göpferich, *Eur. J. Pharm. Biopharm.*, 2005, **60**, 247-266.
26. W. T. Godbey, K. K. Wu and A. G. Mikos, *J. Control Release*, 1999, **60**, 149-160.
27. F. Bollin, V. Dechavanne and L. Chevalet, *Protein Express Purif*, 2011, **78**, 61-68.
28. B. C. Thompson, C. R. J. Segarra, O. L. Mozley, O. Daramola, R. Field, P. R. Levison and D. C. James, *Biotechnol Progr*, 2012, **28**, 179-187.

29. G. Dekevic, L. Tasto, P. Czermak and D. Salzig, *J Biotechnol*, 2022, **346**, 23-34.
30. J. Schindelin, I. Arganda-Carreras, E. Frise, V. Kaynig, M. Longair, T. Pietzsch, S. Preibisch, C. Rueden, S. Saalfeld, B. Schmid, J.-Y. Tinevez, D. J. White, V. Hartenstein, K. Eliceiri, P. Tomancak and A. Cardona, *Nat Methods*, 2012, **9**, 676-682.
31. F. Richter, P. Mapfumo, L. Martin, J. I. Solomun, F. Hausig, J. J. Frietsch, T. Ernst, S. Hoepfner, J. C. Brendel and A. Traeger, *J Nanobiotechnol*, 2021, **19**, 70.
32. F. Salomone, F. Cardarelli, M. Di Luca, C. Boccardi, R. Nifosi, G. Bardi, L. Di Bari, M. Serresi and F. Beltram, *J Control Release*, 2012, **163**, 293-303.
33. S. Brunelli, C. Sciorati, G. D'Antona, A. Innocenzi, D. Covarello, B. G. Galvez, C. Perrotta, A. Monopoli, F. Sanvito, R. Bottinelli, E. Ongini, G. Cossu and E. Clementi, *P Natl Acad Sci USA*, 2007, **104**, 264-269.
34. R. G. Smits, G. J. M. Koper and M. Mandel, *J Phys Chem*, 1993, **97**, 5745-5751.
35. J. D. Ziebarth and Y. Wang, *Biomacromolecules*, 2010, **11**, 29-38.
36. D. Fischer, T. Bieber, Y. Li, H.-P. Elsässer and T. Kissel, *Pharm Res*, 1999, **16**, 1273-1279.
37. Y. Yue, F. Jin, R. Deng, J. Cai, Z. Dai, M. C. M. Lin, H.-F. Kung, M. A. Matthebjerg, T. L. Andresen and C. Wu, *J Control Release*, 2011, **152**, 143-151.
38. G. D. Bowden, B. J. Pichler and A. Maurer, *Sci Rep*, 2019, **9**, 11370.
39. L. Baldi, D. L. Hacker, M. Adam and F. M. Wurm, *Biotechnol Lett*, 2007, **29**, 677-684.
40. P. Kos, U. Lächelt, A. Herrmann, F. M. Mickler, M. Döblinger, D. He, A. Krhač Levačić, S. Morys, C. Bräuchle and E. Wagner, *Nanoscale*, 2015, **7**, 5350-5362.
41. B. Lou, S. De Koker, C. Y. J. Lau, W. E. Hennink and E. Mastrobattista, *Bioconjugate Chem*, 2019, **30**, 461-475.
42. S. Vaidyanathan, J. Chen, B. G. Orr and M. M. Banaszak Holl, *Mol Pharm*, 2016, **13**, 1967-1978.
43. S. Boeckle, K. von Gersdorff, S. van der Piepen, C. Culmsee, E. Wagner and M. Ogris, *J Gene Med*, 2004, **6**, 1102-1111.
44. Z. u. Rehman, D. Hoekstra and I. S. Zuhorn, *ACS Nano*, 2013, **7**, 3767-3777.
45. K. Modra, S. Dai, H. Zhang, B. Shi and J. Bi, *Eng Life Sci*, 2015, **15**, 489-498.
46. Z. Shen, B. Shi, H. Zhang, J. Bi and S. Dai, *Soft matter*, 2012, **8**, 1385-1394.
47. R. N. Cohen, M. A. E. M. van der Aa, N. Macaraeg, A. P. Lee and F. C. Szoka, *J Control Release*, 2009, **135**, 166-174.
48. D. J. Glover, D. L. Leyton, G. W. Moseley and D. A. Jans, *J Gene Med*, 2010, **12**, 77-85.

Supporting Information:

Efficient transfection *via* an unexpected mechanism by near-neutral polypiperazines with tailored response to endosomal pH

*Franziska Hausig-Punke,^a Gregor Dekevic,^b Fabian H. Sobotta,^a Jana I. Solomun,^a Friederike Richter,^a Denise Salzig,^b Anja Traeger,^{*a,c} Johannes C. Brendel,^{*a,c}*

^aLaboratory of Organic and Macromolecular Chemistry (IOMC), Friedrich Schiller University
Jena, Humboldtstrasse 10, 07743 Jena, Germany.

^bInstitute of Bioprocess Engineering and Pharmaceutical Technology, University of Applied
Sciences Mittelhessen, Wiesenstrasse 14, 35390 Giessen, Germany.

^cJena Center for Soft Matter (JCSM), Friedrich Schiller University Jena, Philosophenweg 7,
07743 Jena, Germany.

*Correspondence to A. Traeger (anja.traeger@uni-jena.de)
and J. C. Brendel (johannes.brendel@uni-jena.de)

ADDITIONAL RESULTS

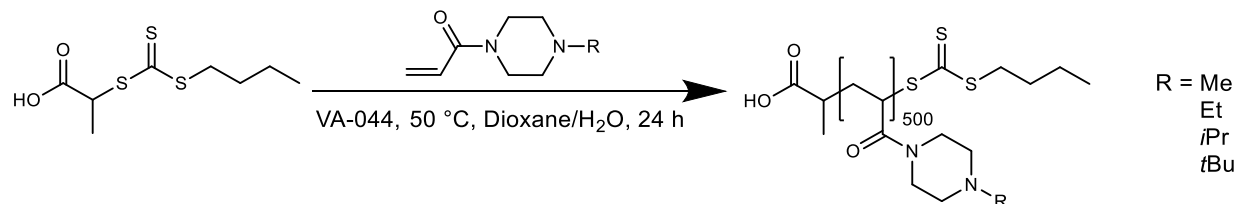


Figure S1. Synthesis of polypiperazines. The piperazine based vinyl monomers were polymerized *via* RAFT polymerization as previously reported.¹

Table S1. Summary of polypiperazines used in this study.

Polymer ID	Polymer abbreviation	Mn, th ^a / g mol ⁻¹	Mn, SEC ^b / g mol ⁻¹	<i>Đ</i> ^b
0C	PNAM ₅₀₀	70 800	47 200*	1.30*
1C	PNAMP ₅₀₀	77 300	53 500*	1.22*
1C'	PNAMP ₅₀₀ -OG	77 800	62 000*	1.31*
2C	PNAEP ₅₀₀	84 400	55 800*	1.29*
2C'	PNAEP ₅₀₀ -OG	84 900	68 200*	1.45*
3C	PNAiPP ₅₀₀	91 400	50 100	1.31
3C_2	PNAiPP ₅₀₀ (2nd batch)	91 400	53 200	1.31
3C'	PNAiPP ₅₀₀ -OG	91 900	67 600*	1.30*
4C	PNAiBP ₅₀₀	98 400	62 500*	1.30*
4C'	PNAiBP ₅₀₀ -OG	98 900	59 000*	1.33*

* These data have already been published and are listed here only for the sake of completeness.¹ a

Calculated based on $[M]_0/[CTA]_0 \times \text{monomer conversion}$. b Determined by SEC (Eluent: DMAc

+ 0.21 wt% LiCl, polystyrene calibration). OG - Oregon green cadavarine 5-isomer.

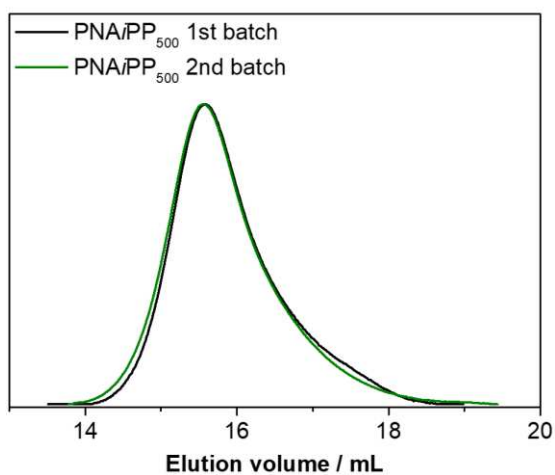


Figure S2. SEC traces of PNAiPP. SEC-traces of both PNAiPP batches utilized in this study. The first batch was used in the classical optimization of the transfection efficiency and for all studies on the transfection mechanism. The second batch was used for the optimization *via* DoE. SEC was measured in DMAc + 0.21 wt% LiCl using refractive index (RI) detection and polystyrene calibration.

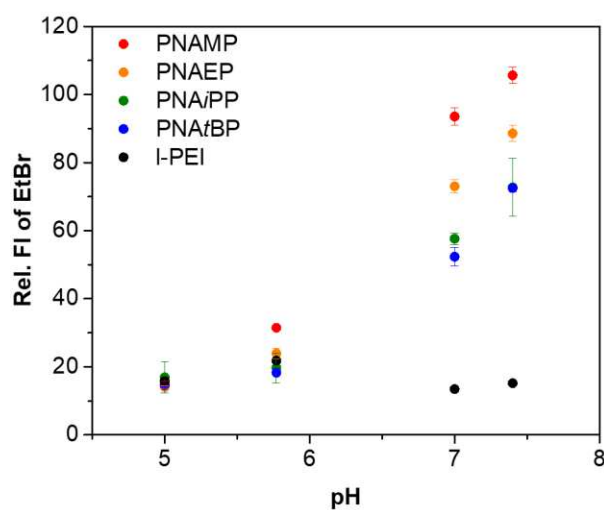


Figure S3. pH-dependent pDNA binding and polyplex stability. The pH-dependent pDNA binding of the polypiperazines was studied at N*/P 30 by an EtBr quenching assay using different buffers in a pH range from 5 to 7.4, representing the physiologically relevant pH range during transfection experiments. l-PEI was investigated for comparison. Data are presented as the mean \pm SD of three independent determinations.

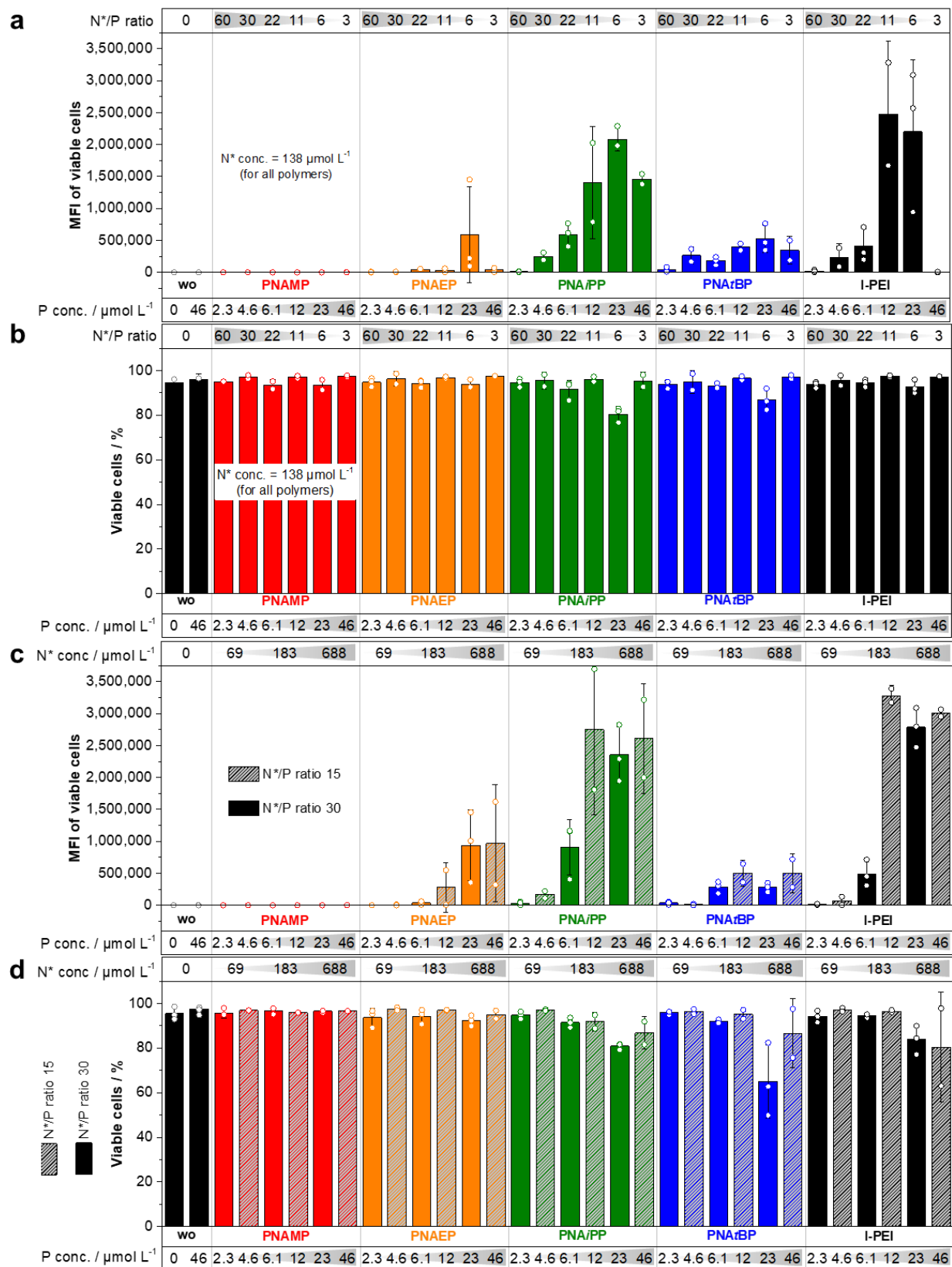


Figure S4. MFI values and viability data of the classical transfection optimization. a, b HEK 293T cells were treated with various polyplex formulations at different pDNA concentrations. The variation of the phosphate concentration (P conc., pDNA) at a constant protonatable amine concentration (N* conc., polymer) of $138 \mu\text{mol L}^{-1}$ resulted in varying N*/P ratios. **c, d** HEK 293T cells in serum-free Opti-MEMTM were treated with various polyplex formulations at varying pDNA concentrations as described in **a, b**. N*/P ratios of 15 (striped) and 30 (solid) were investigated at the resulting concentrations of protonatable amines. **a, c** Transfection efficiency and **b, d** cell viability according to the FSC/SSC plot were investigated by flow cytometry and are represented as the mean \pm SD (bars) and the individual data points (dots). A detailed gating strategy with scatterplots can be found in Figure S5. Corresponding l-PEI polyplexes were investigated for comparison to the polypiperazines.

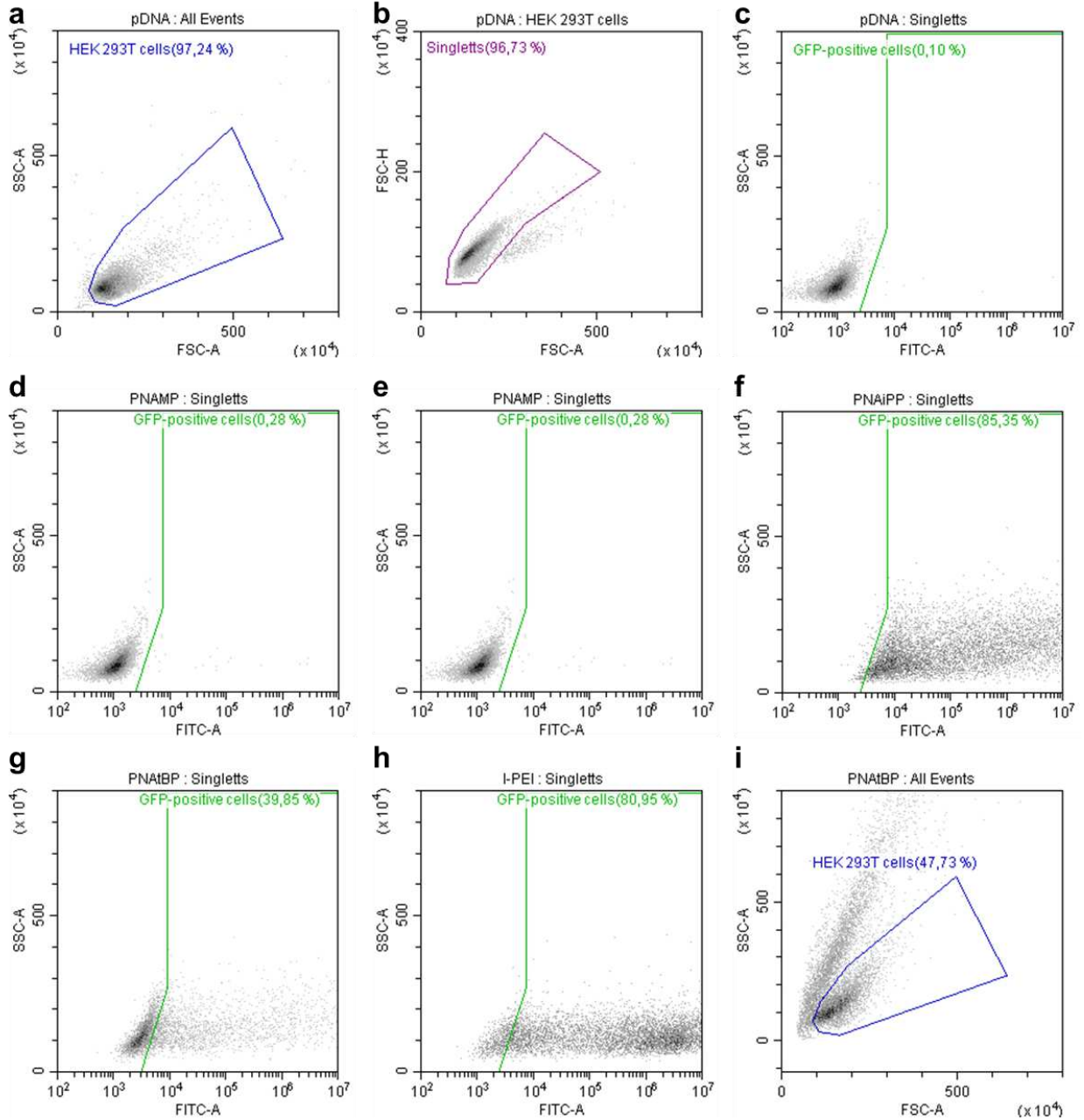


Figure S5. Gating strategy for transfection efficiency experiments. **a** Viable cells were gated according to the FSC/SSC pattern. **b** Subsequently, single cells were discriminated from doublets using the FSC-A/FSC-H dot plot. **c** GFP-fluorescent cells were identified by gating the single cells to the unstained pKMyo control. The FITC/SSC dot plots are shown for **d** PNAMP, **e** PNAEP, **f** PNAiPP, **g** PNAiBP and **h** l-PEI (N* conc. = 688 $\mu\text{mol L}^{-1}$, P conc. = 23 $\mu\text{mol L}^{-1}$, N*/P 30). **i** Cytotoxic side effects were observed for PNAiBP under these conditions (also see figure S4d).

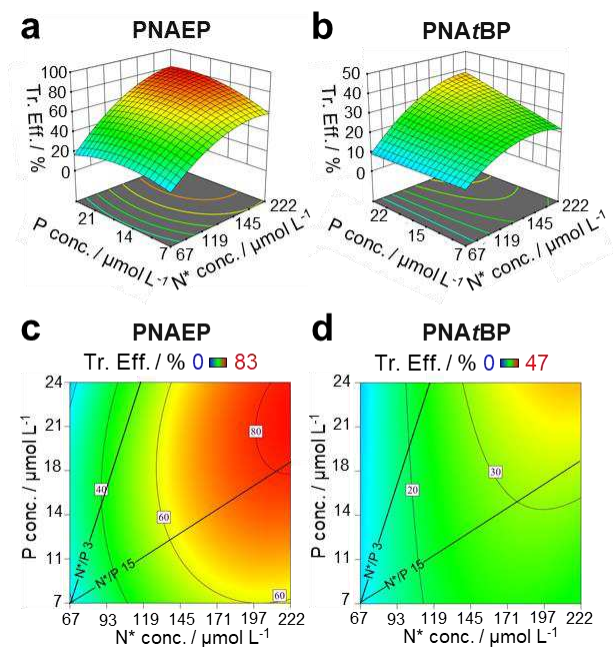


Figure S6. DoE models in narrower range for PNAEP and PNAfBP. a,b 3D plots and c contour plots of models predicting the transfection efficiency (percentage of viable GFP-fluorescent cells) of a,c PNAEP and b,d PNAfBP are shown. a-d HEK 293T cells in serum-free Opti-MEMTM were treated with various polyplex formulations containing pCMV-GFP pDNA for 4 h followed by subsequent incubation in growth medium for 20 h. Transfection efficiency was investigated by flow cytometry.

Factor Coding: Actual

Std Error of Design
 ● Design Points

Std Error Shading
 0.500 1.500
 X1 = A
 X2 = B

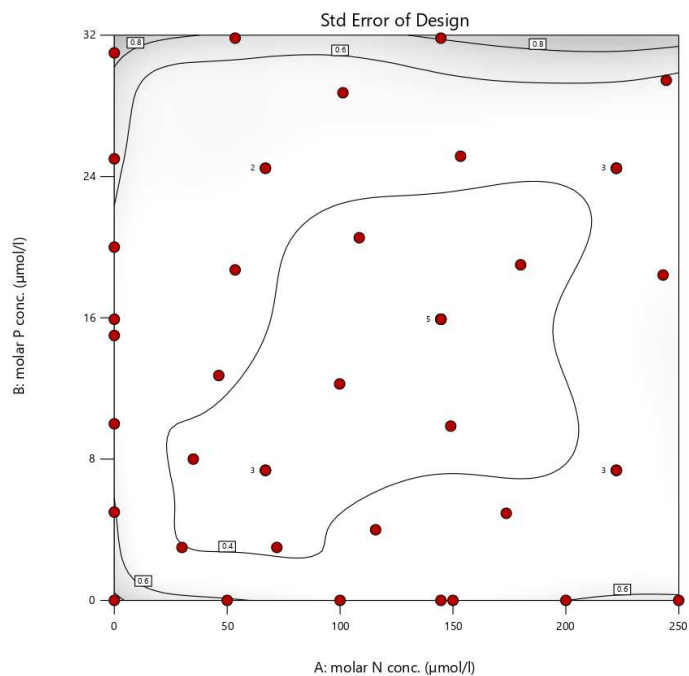


Figure S7. Exemplarily chosen augmented design space of the DoE. Measurement points and the corresponding numbers of repetition are indicated next to the points in the grid.

Table S2. ANOVA applied to the DoE model for PNAiPP in Figure 3b and 3f.

Source	Sum of Squares	df	Mean Square	F-value	p-value	
Block	11.17	1	11.17			
Model	751.29	11	68.30	54.98	< 0.0001	significant
A-molar N conc.	0.5453	1	0.5453	0.4390	0.5115	
B-molar P conc.	0.1800	1	0.1800	0.1449	0.7055	
AB	5.19	1	5.19	4.18	0.0478	
A ²	83.13	1	83.13	66.93	< 0.0001	
B ²	6.26	1	6.26	5.04	0.0305	
A ² B	8.29	1	8.29	6.67	0.0136	
A ³	26.26	1	26.26	21.14	< 0.0001	
B ³	33.69	1	33.69	27.12	< 0.0001	
A ² B ²	9.56	1	9.56	7.69	0.0085	
AB ³	18.69	1	18.69	15.05	0.0004	
B ⁴	38.40	1	38.40	30.92	< 0.0001	
Residual	48.44	39	1.24			
Lack of Fit	47.49	29	1.64	17.17	< 0.0001	significant
Pure Error	0.9537	10	0.0954			
Cor Total	810.91	51				

Table S3. Fit statistics for the DoE model in Figure 3b and 3f.

Std. Dev.	1.11	R²	0.9394
Mean	5.20	Adjusted R²	0.9223
C.V. %	21.44	Predicted R²	0.8388
		Adeq Precision	20.4872

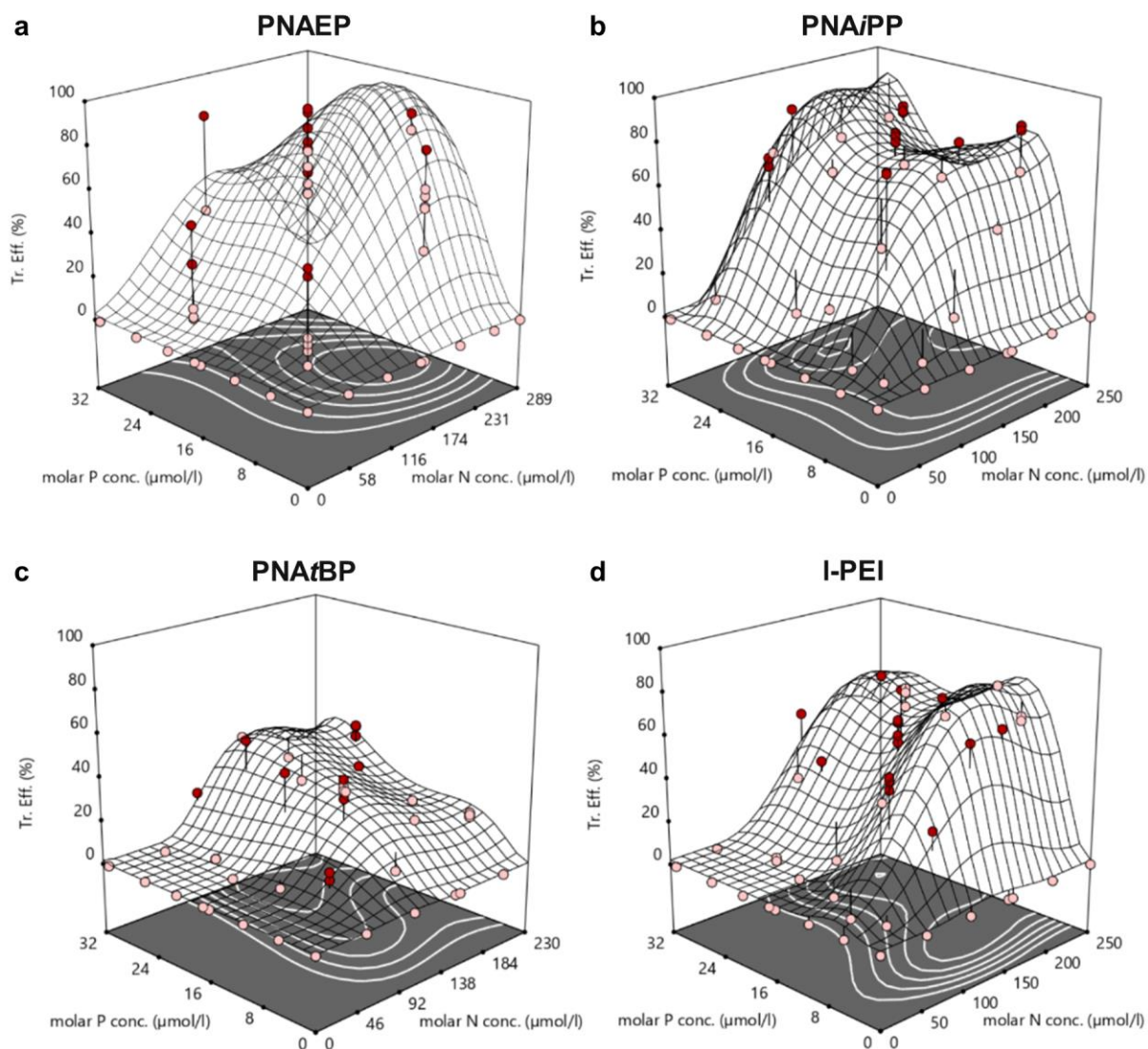


Figure S8. Transparent representation of the 3D surface models in Figure 3. a-d 3D surface models predicting the transfection efficiency (percentage of viable GFP-fluorescent cells) of **a** PNAEP, **b** PNAiPP, **c** PNAfBP, and **d** I-PEI. The measurement points located above the surface of the model are indicated with red dots, while the pink ones represent points below the surface. **a-d** HEK 293T cells were treated with various polyplex formulations. Transfection efficiency was investigated by flow cytometry.

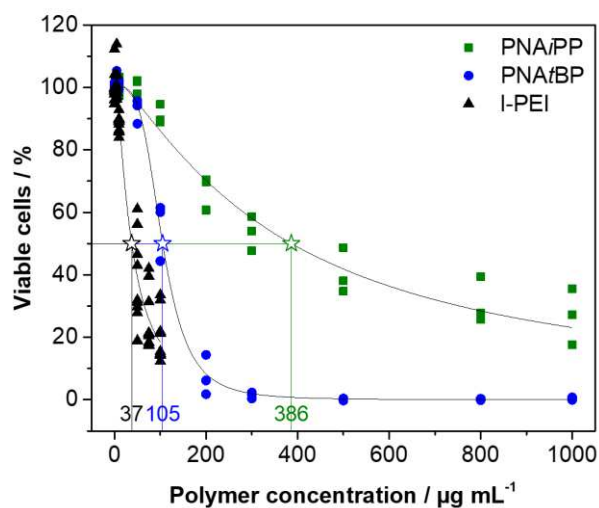


Figure S9. CC₅₀ values of PNAiPP, PNAiBP and commercial l-PEI. As already published, metabolic activity was measured in L929 cells in growth medium using the alamarBlue assay following incubation with PNAiPP (green), PNAiBP (blue) and l-PEI (black) polymers at indicated concentrations for 24 h.¹ Dots represent values of single repetitions and lines represent logistic fit functions calculated *via* OriginPro, version 2020b ($n \geq 3$). The concentration of 50 % toxicity for each polymer is indicated with a star.

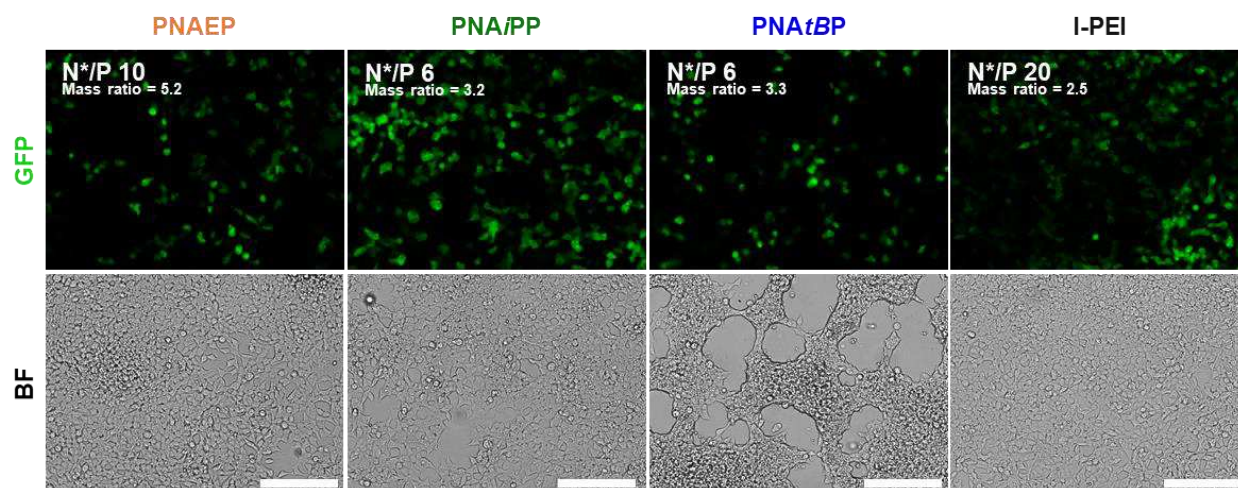


Figure S10. Micrographs of the validation of the augmented design space. The augmented models (see Figure 3) were validated at the predicted optima (see Table 1) by transfecting HEK 293T cells with the respective polyplex formulations. Cells were imaged prior to flow cytometry. Scale bar 200 μ m.

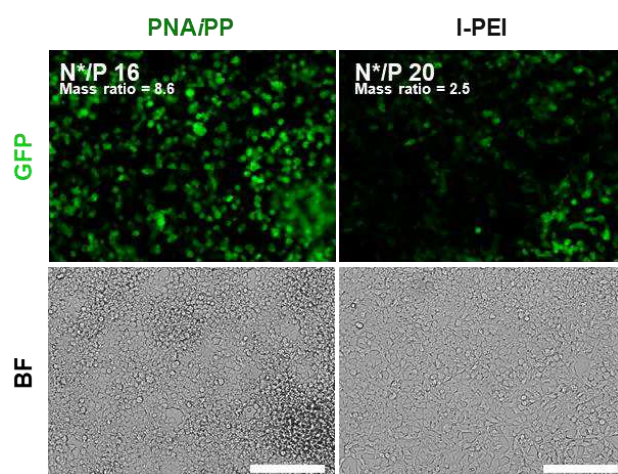


Figure S11. Microscopic images of the validation of PNAiPP and I-PEI at similar N*/P ratios. The augmented models (see Figure 3) were validated at the predicted optima (see Table 1) by transfecting HEK 293T cells with the respective polyplex formulations. Cells were imaged prior to flow cytometry. Scale bar 200 μ m See Figure S10 for flow cytometry results.

Table S4. Polymer and pDNA concentrations in the validation runs.

Polymer	R ² of model	<i>p</i> value of model	Validation runs							
			N* conc.	Polymer conc.	P conc.	pDNA conc.	N*/P	Mass ratios ^d	Viable GFP-fluorescent cells / %	
			$\mu\text{mol L}^{-1}$	$\mu\text{g mL}^{-1}$	$\mu\text{mol L}^{-1}$	$\mu\text{g mL}^{-1}$			Predicted	Mean \pm SD (measured)
PNAEP	88.6	< 0.0001	^a 222	37.3	22	7.2	10	5.2	82.12	80.14 \pm 5.72
			^c 243	40.9	15	4.9	16	8.4	100.59	72.19 \pm 17.53
PNA _i PP	93.9	< 0.0001	^a 176	32.1	12	3.9	14	8.2	80.41	99.96 \pm 0.03
			^b 67	12.2	7	2.3	9	5.3	39.39	99.96 \pm 0.01
			^c 153	27.9	27	8.8	6	3.2	90.63	99.99 \pm 0.01
			^c 165	28.4	10	3.3	16	8.6	76.44	99.97 \pm 0.02
PNA _t BP	92.8	< 0.0001	^c 155	30.4	28	9.2	6	3.3	45.38	56.36 \pm 17.59
l-PEI	87.4	< 0.0001	^a 215	9.0	7	2.3	29	3.9	76.07	99.83 \pm 0.03
			^c 171	7.2	9	2.9	20	2.5	82.62	99.91 \pm 0.06

^a predicted experimental conditions from initial design space for high transfection efficiency.

^b factorial point of the initial design space with lowest N* and P concentration.

^c predicted experimental conditions from augmented design space for high transfection efficiency.

^d polymer/pDNA

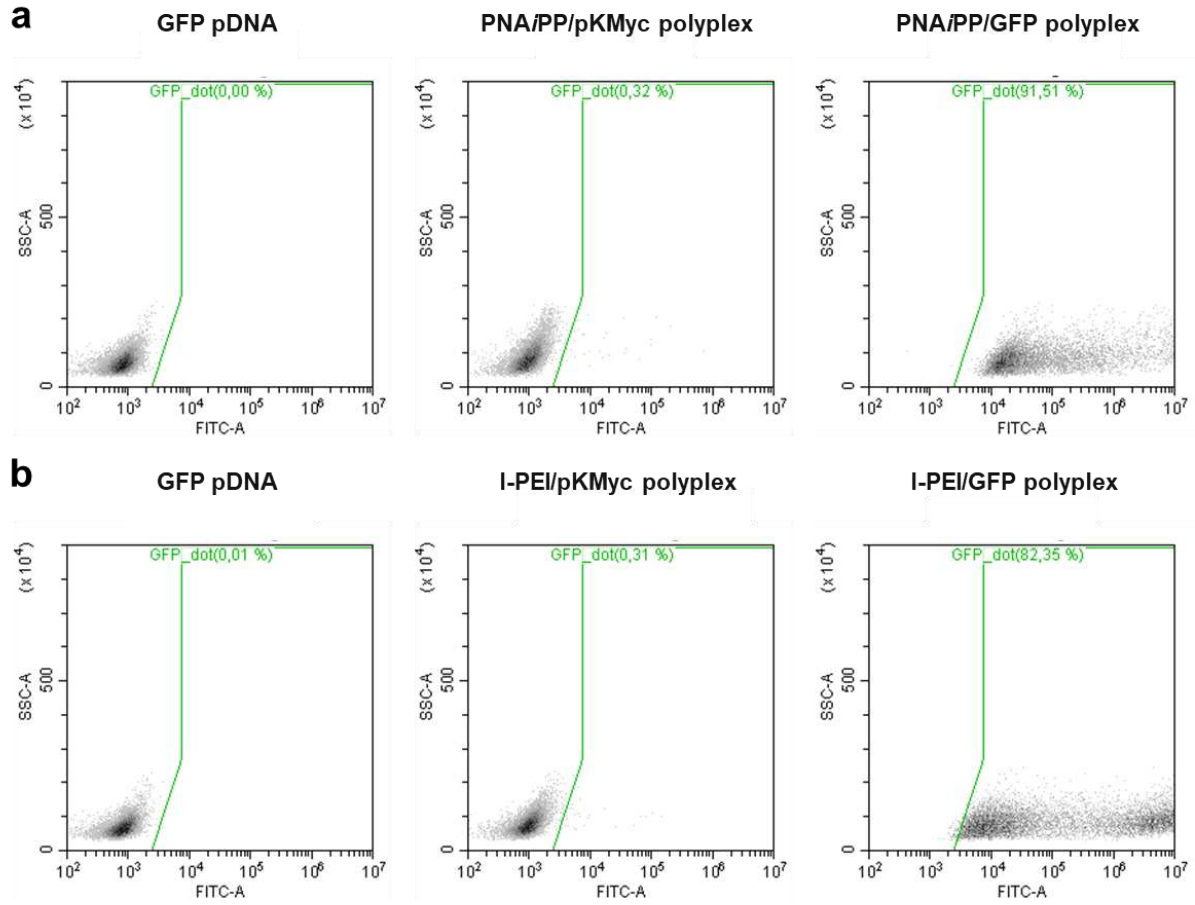


Figure S12. Scatter plots of selected validation experiments. GFP-fluorescent cells were identified by gating the single cells to the unstained pKMyC control. The FITC/SSC dot plots are shown for **a** PNAiPP (N^* conc. = $165 \mu\text{mol L}^{-1}$, P conc. = $10 \mu\text{mol L}^{-1}$, N^*/P 16) and **b** l-PEI (N^* conc. = $171 \mu\text{mol L}^{-1}$, P conc. = $9 \mu\text{mol L}^{-1}$, N^*/P 20).

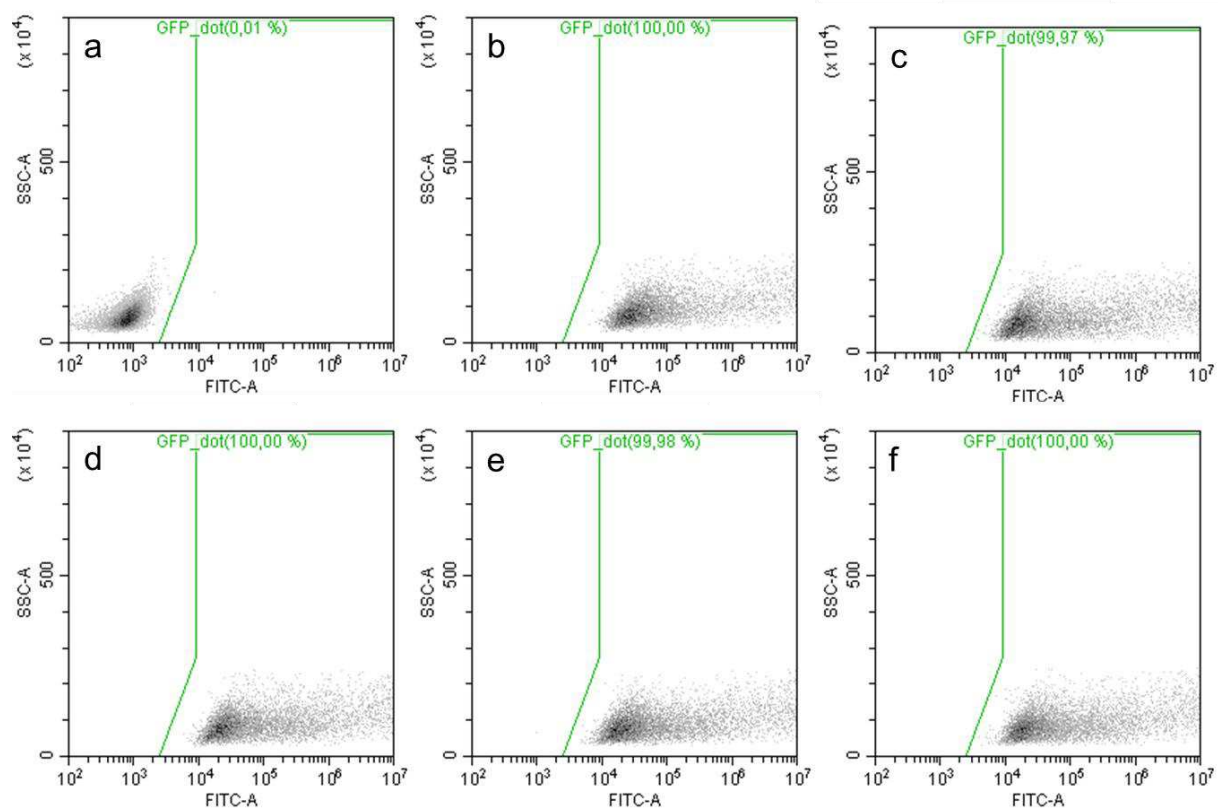


Figure S13 Flow cytometric data of the validation runs for PNAiPP at $176 \mu\text{mol L}^{-1} \text{N}^*$ and $12 \mu\text{mol L}^{-1} \text{P}$. **a** Scatter plots of cells treated with $12 \mu\text{mol L}^{-1}$ pCMV-GFP pDNA for control. **b-f** Scatter plots of cells treated with PNAiPP polyplexes (5 replicates).

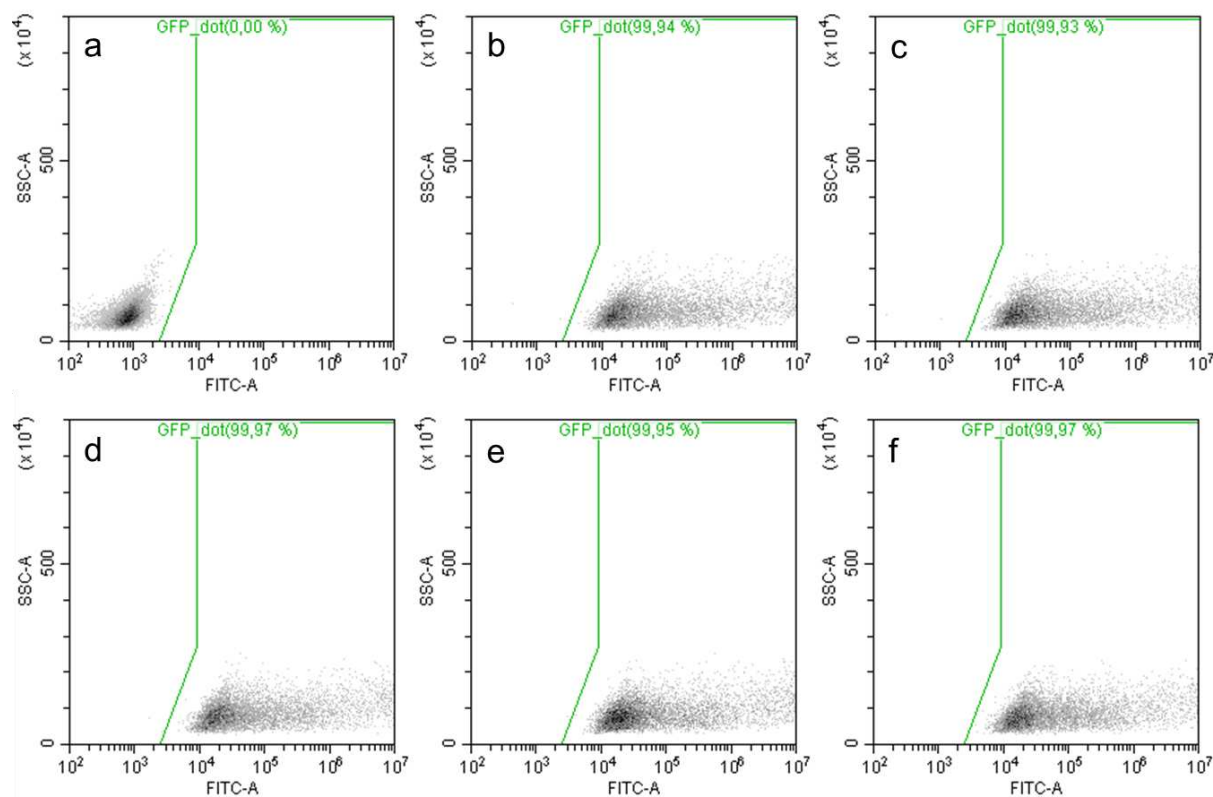


Figure S14. Flow cytometric data of the validation runs for PNAiPP at 67 $\mu\text{mol L}^{-1}$ N* and 7 $\mu\text{mol L}^{-1}$ P. a Scatter plots of cells treated with 7 $\mu\text{mol L}^{-1}$ pCMV-GFP pDNA for control. **b-f** Scatter plots of cells treated with PNAiPP polyplexes (5 replicates).

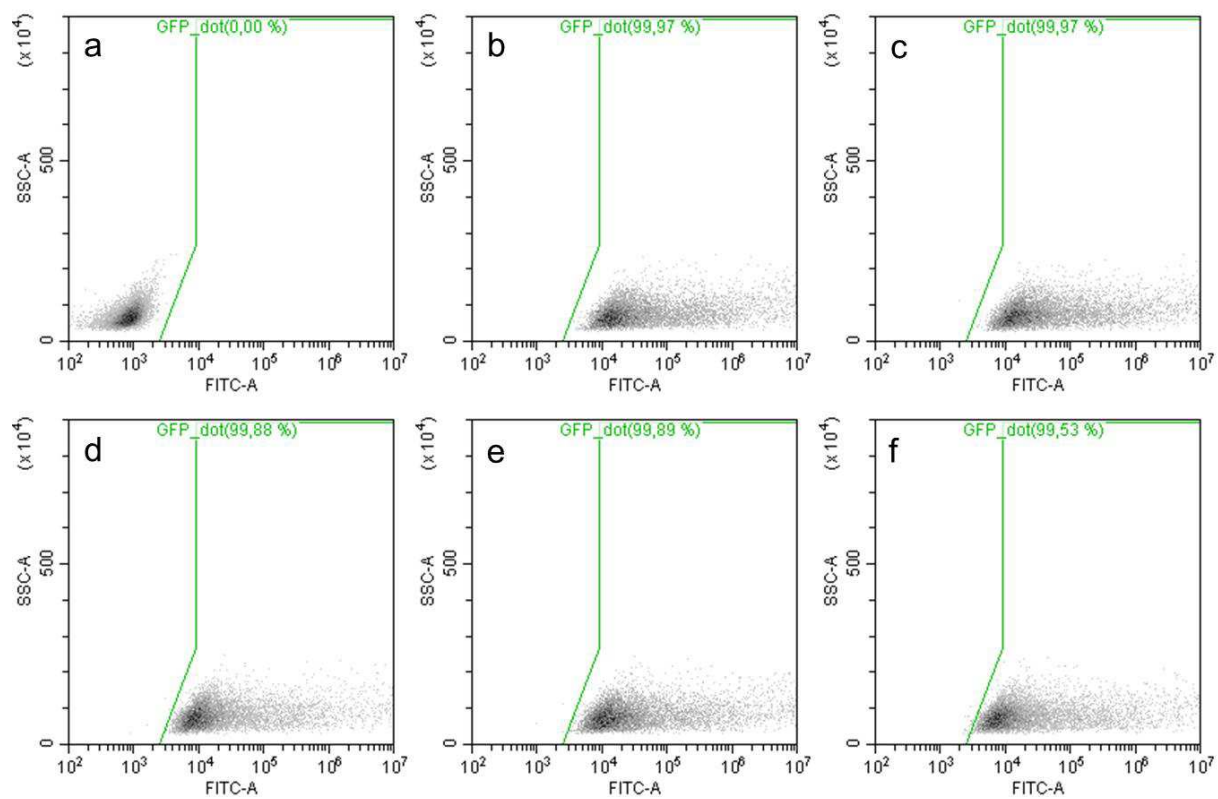


Figure S15. Flow cytometric data of the validation runs for PNAiPP at 153 $\mu\text{mol L}^{-1}$ N* and 27 $\mu\text{mol L}^{-1}$ P. a Scatter plots of cells treated with 27 $\mu\text{mol L}^{-1}$ pCMV-GFP pDNA for control. **b-f** Scatter plots of cells treated with PNAiPP polyplexes (5 replicates).

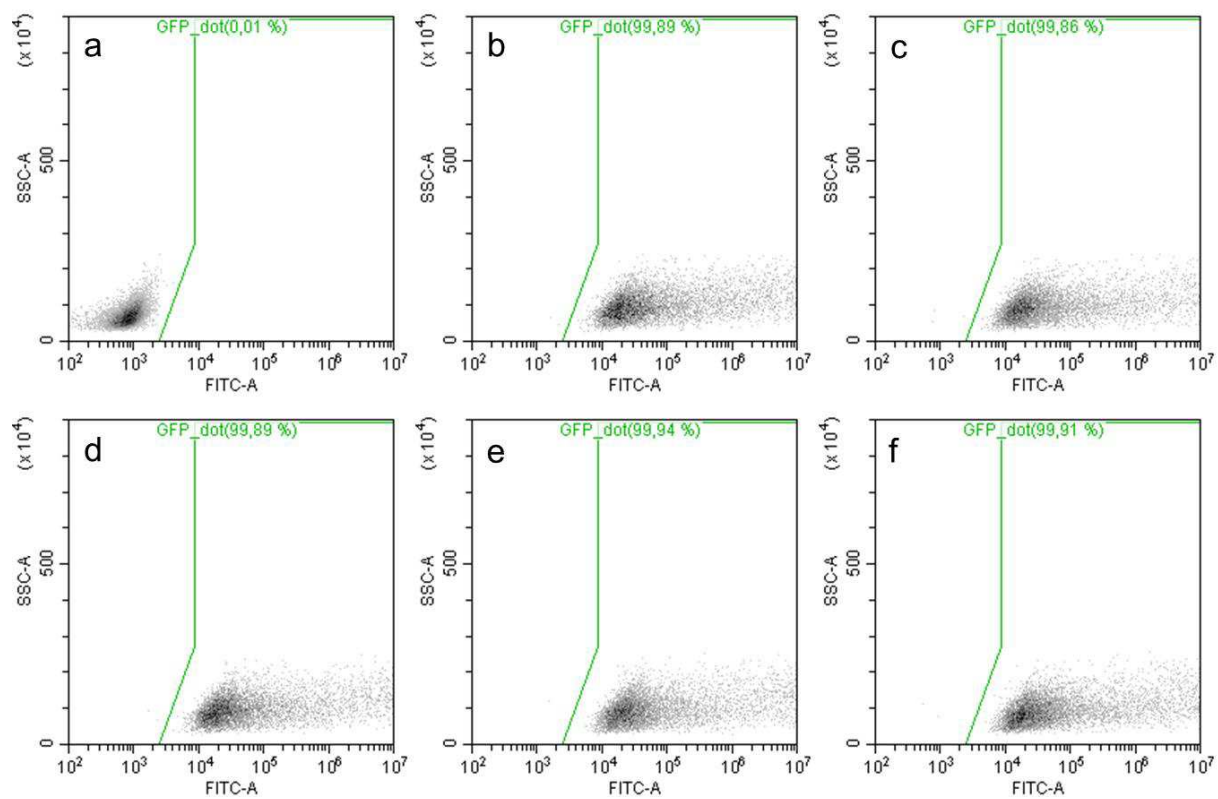


Figure S16. Flow cytometric data of the validation runs for PNAiPP at 165 $\mu\text{mol L}^{-1}$ N* and 10 $\mu\text{mol L}^{-1}$ P. **a** Scatter plots of cells treated with 10 $\mu\text{mol L}^{-1}$ pCMV-GFP pDNA for control. **b-f** Scatter plots of cells treated with PNAiPP polyplexes (5 replicates).

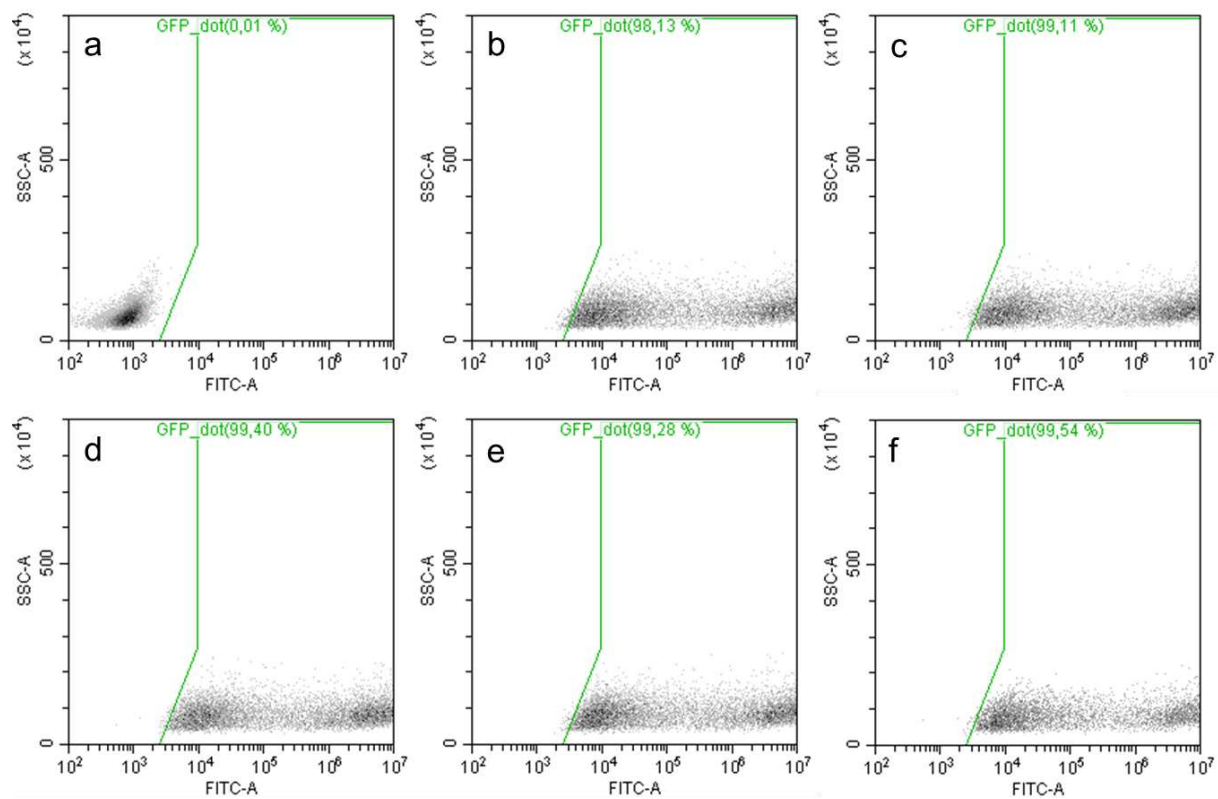


Figure S17. Flow cytometric data of the validation runs for IPEI at 171 $\mu\text{mol L}^{-1}$ N* and 9 $\mu\text{mol L}^{-1}$ P. a Scatter plots of cells treated with 9 $\mu\text{mol L}^{-1}$ pCMV-GFP pDNA for control. **b-f** Scatter plots of cells treated with IPEI polyplexes (5 replicates).

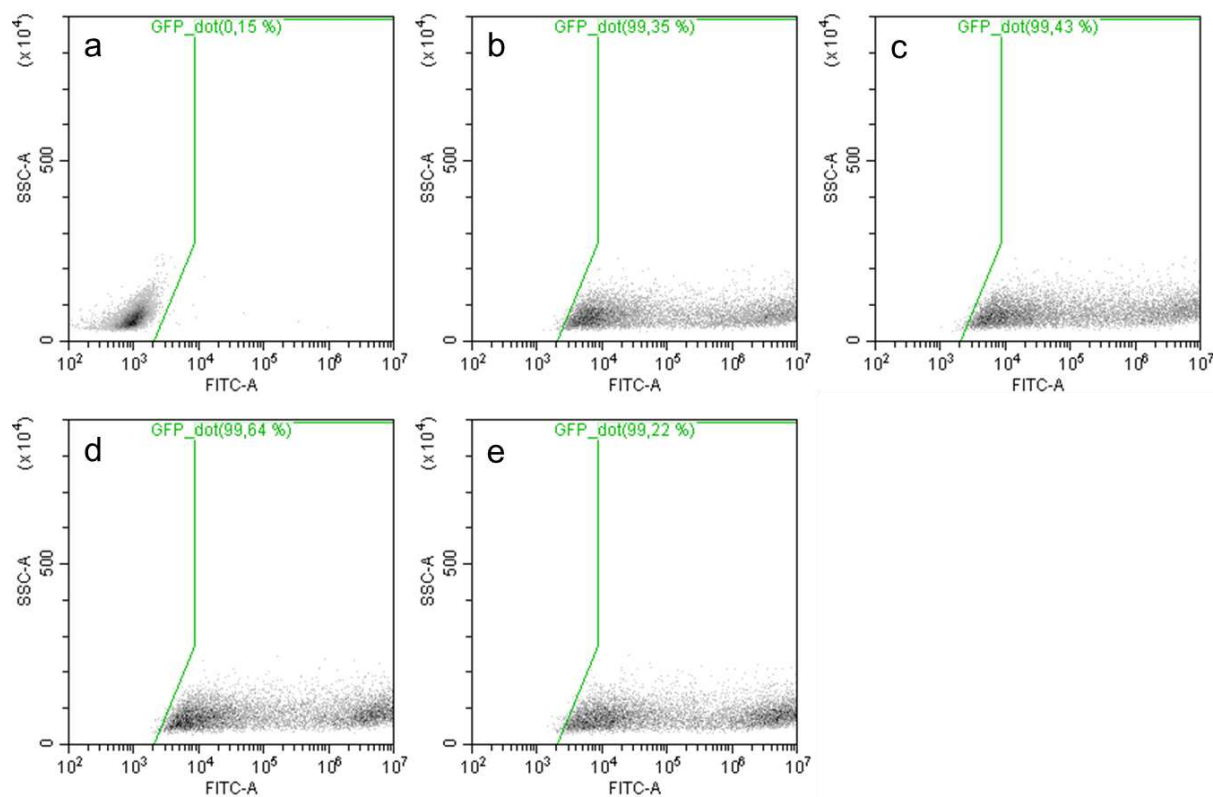


Figure S18. Flow cytometric data of the validation runs for IPEI at 215 $\mu\text{mol L}^{-1}$ N* and 7 $\mu\text{mol L}^{-1}$ P. a Scatter plots of cells treated with 7 $\mu\text{mol L}^{-1}$ pCMV-GFP pDNA for control. **b-f** Scatter plots of cells treated with IPEI polyplexes (5 replicates).

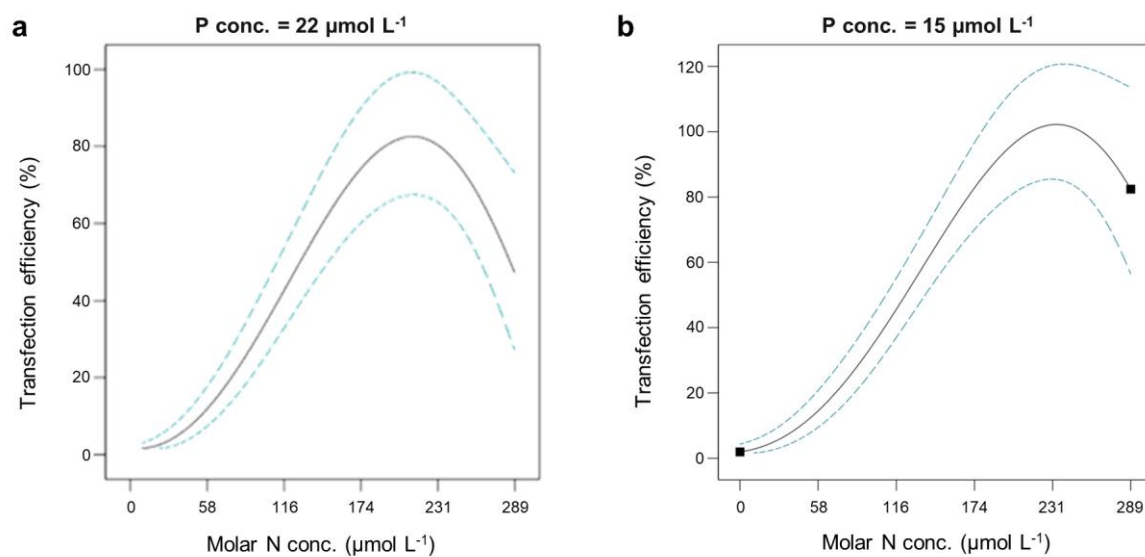


Figure S19. One factor effects plot for PNAEP. 2D plot (solid line) taken from the surface model at fixed concentrations P of 22 $\mu\text{mol L}^{-1}$ (**a**) and 15 $\mu\text{mol L}^{-1}$ (**b**); the dashed lines indicate the 95% confidence interval bands.

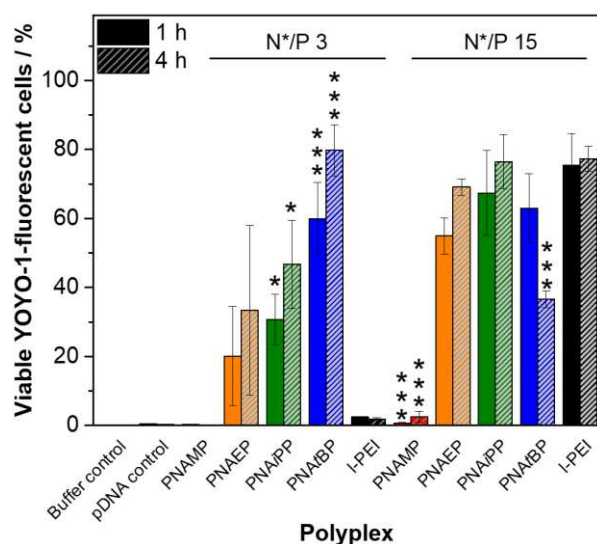


Figure S20. Polyplex uptake in HEK 293T cells. Polyplexes were prepared with YOYO-1 labeled pDNA at N*/P 3 and 15 (final P conc. = 46 $\mu\text{mol L}^{-1}$). The polyplex uptake into HEK 293T cells in serum-free Opti-MEMTM was investigated *via* flow cytometry after 1 h and 4 h, respectively, and is represented as the percentage of viable, single, GFP-fluorescent cells. Fluorescence outside the cells was quenched with 0.04% trypan blue. A detailed gating strategy with scatterplots is provided in Figure S10. Data are represented as the mean \pm SD of three independent measurements. */***Significant difference to the corresponding I-PEI polyplex at respective time point ($p < 0.05/0.001$).

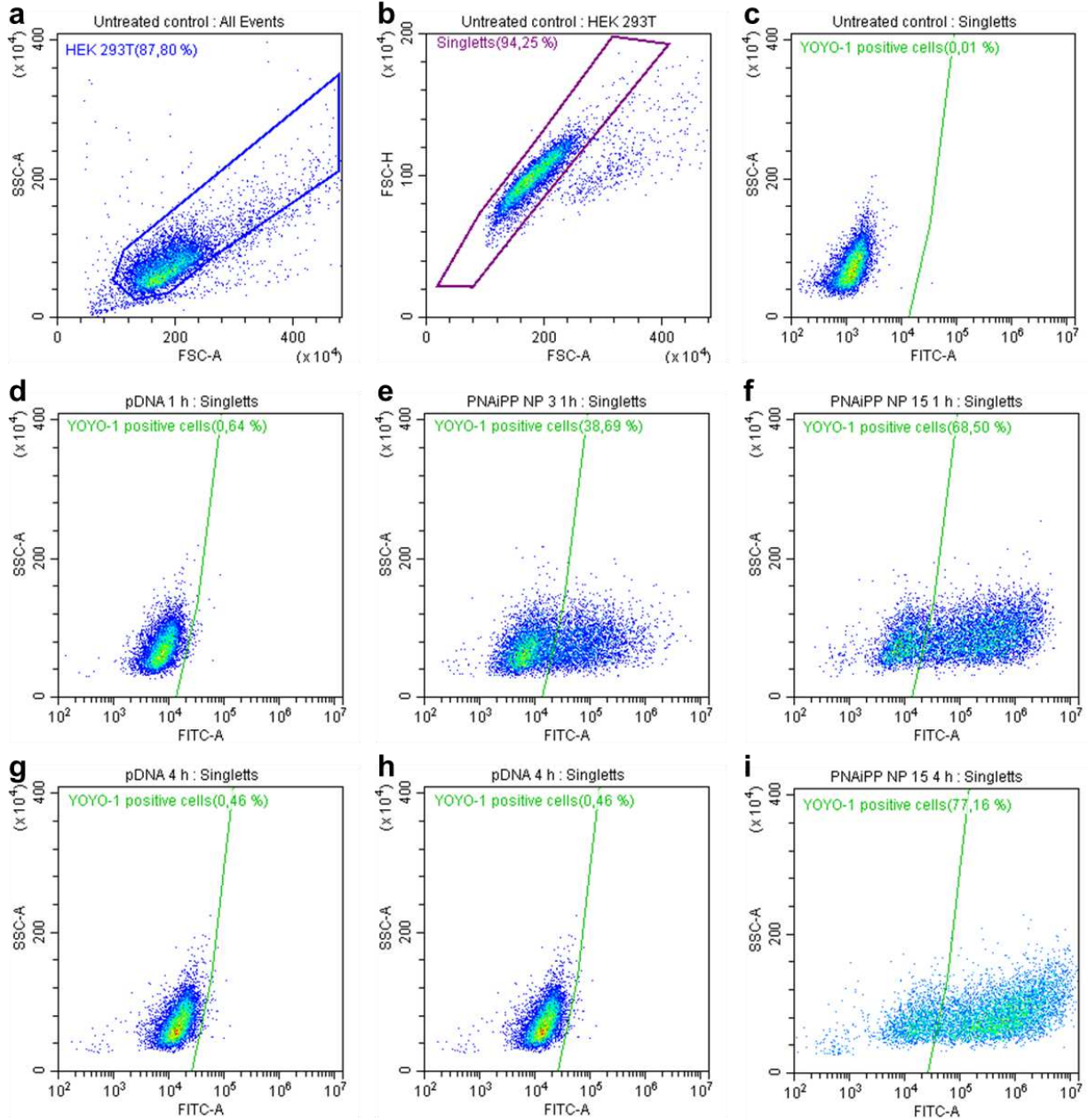


Figure S21. Gating strategy for polyplex uptake experiments. **a** Viable cells were gated according to the FSC/SSC pattern. **b** Subsequently, single cells were discriminated from doublets using the FSC-A/FSC-H dot plot. **c** YOYO-1-fluorescent cells were identified by gating the single cells to the polymer-free control. The FITC/SSC dot plots are shown for **d**, **g** the polymer-free control, **e**, **h** PNAiPP at N*/P 3, **f**, **i** PNAiPP at N*/P 15 **d**, **e**, **h** after 1 h and **g**, **f**, **i** after 4 h (P conc. = 46 $\mu\text{mol L}^{-1}$).

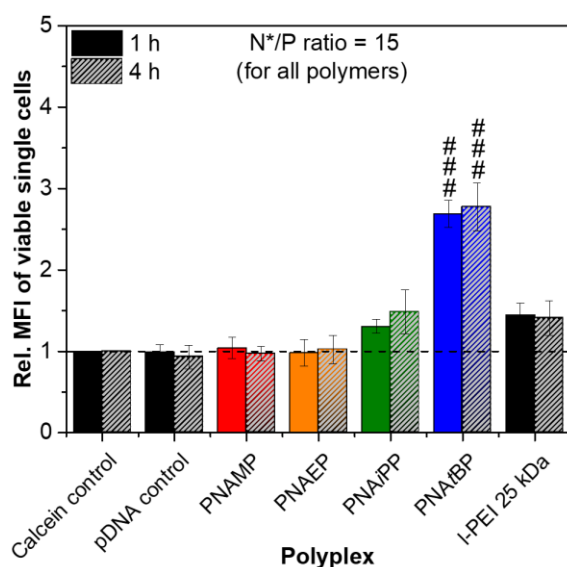


Figure S22. Calcein release at lower pDNA and polymer concentration. The endosomal release of the small molecule calcein was investigated by flow cytometry, whereby higher intensities relative to the calcein control cells (treated with the same calcein concentration, but without endosomal escape-inducing polymers) indicate endosomal escape and membrane interactions. HEK 293T cells in serum-free Opti-MEMTM were treated with polyplexes at N*/P 15 (P conc. = 12 $\mu\text{mol L}^{-1}$) and 25 $\mu\text{g mL}^{-1}$ calcein. Data are reported as the mean \pm SD of three independent experiments. ###Significant difference to the corresponding l-PEI polyplex at the respective time point ($p < 0.001$). Scatter plots illustrating the gating strategy are given in figure S12.

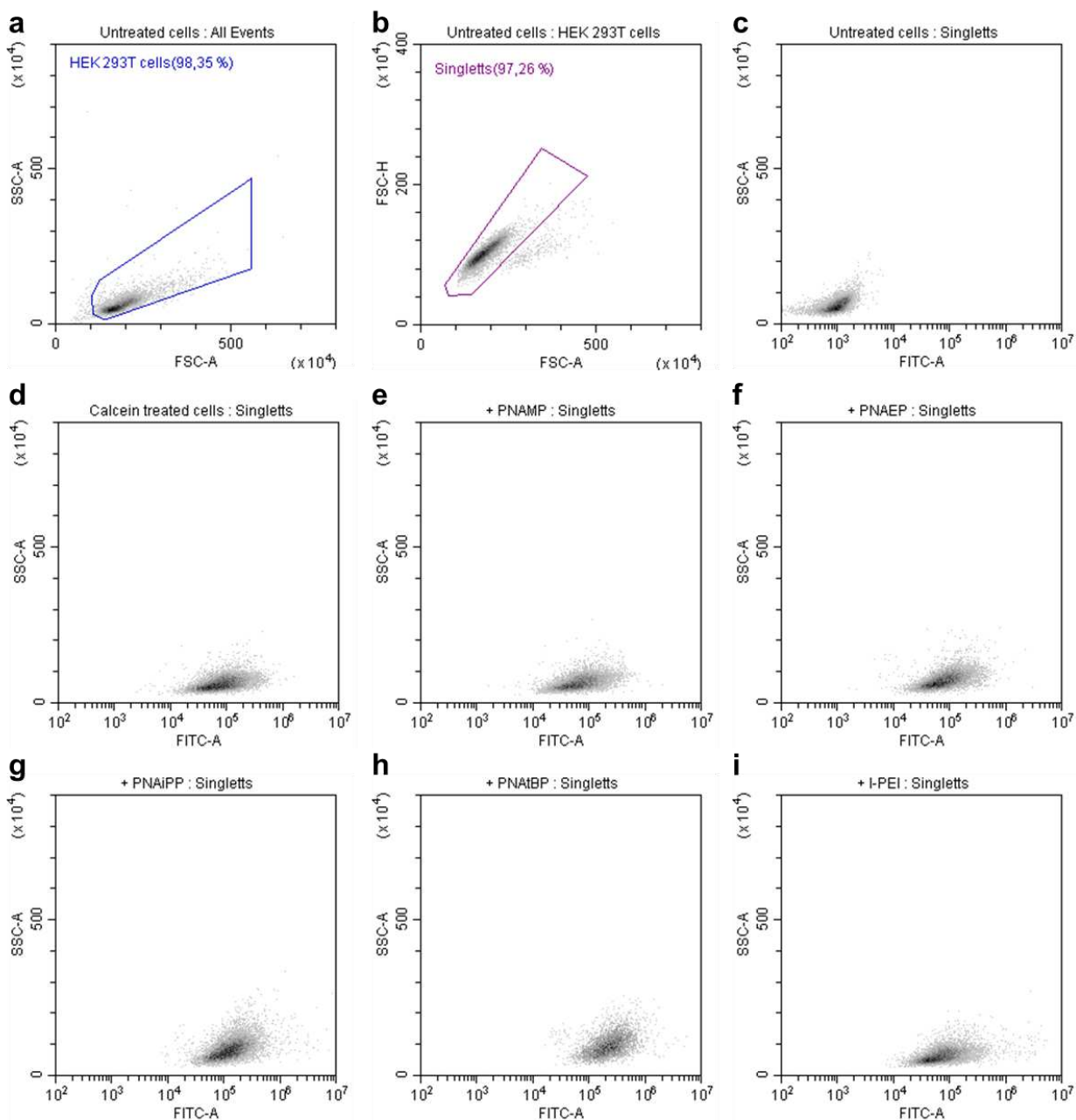


Figure S23. Gating strategy for calcein release experiments. **a** Viable cells were gated according to the FSC/SSC pattern. **b** Subsequently, single cells were discriminated from doublets using the FSC-A/FSC-H dot plot. The FITC/SSC dot plots are shown for **c** untreated cells, **d** calcein treated control cells and cells that were additionally treated with **e** PNAMP, **f** PNAEP, **g** PNAiPP, **h** PNAtBP and **i** l-PEI (P conc. = $46 \mu\text{mol L}^{-1}$).

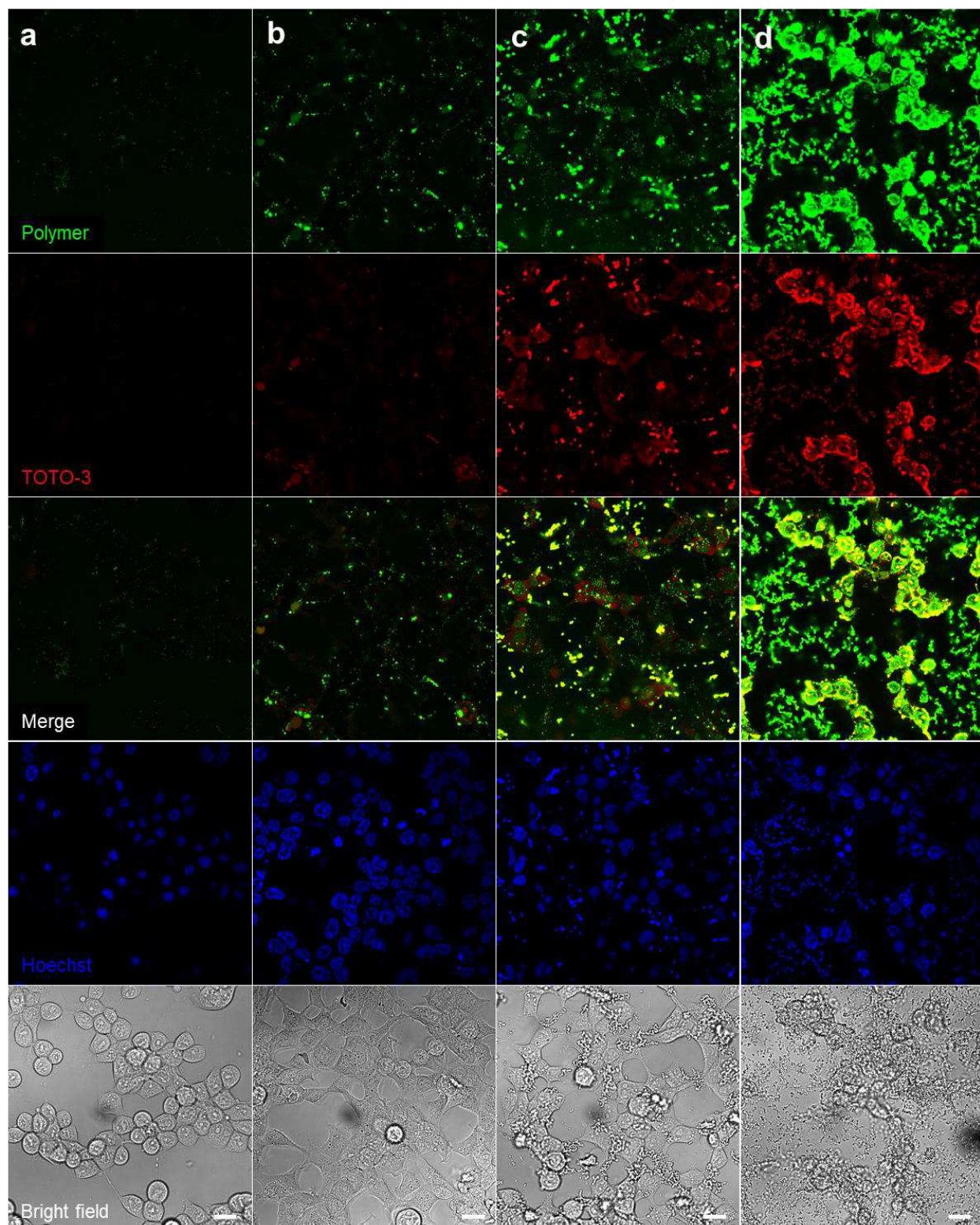


Figure S24. Lower magnification images of HEK 293T cells treated with labeled polyplexes.

HEK 293T cells in serum-free Opti-MEMTM were treated with polyplexes of Oregon Green-labeled polypiperazines (green channel, N* conc. = 183 $\mu\text{mol L}^{-1}$) and TOTO-3 iodide-stained pKMyC pDNA (red channel, P conc.: 12 $\mu\text{mol L}^{-1}$) at N*/P 15 for 4 h. The cells were stained with Hoechst 33342 (blue channel) to visualize the nuclei in live-cell confocal microscopy. Representative images (n = 2) for **a** PNAMP, **b** PNAEP, **c** PNAiPP, and **d** PNAiBP are shown.

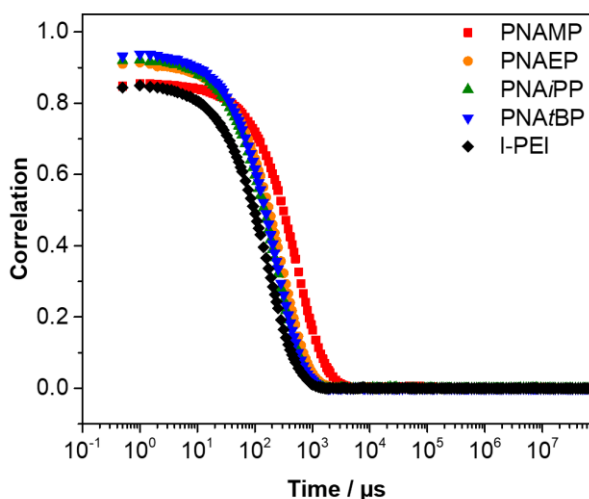


Figure S25. Exemplary exponential decay functions from DLS measurements of polyplexes.

Polyplexes were prepared with 460 $\mu\text{mol L}^{-1}$ pKMyC pDNA at a protonatable amine concentration of 230 $\mu\text{mol L}^{-1}$ (N*/P 6). The exponential decay correlation coefficients of a single measurement are displayed for PNAMP (red), PNAEP (orange), PNAiPP (green), PNAiBP (blue) and I-PEI (black).

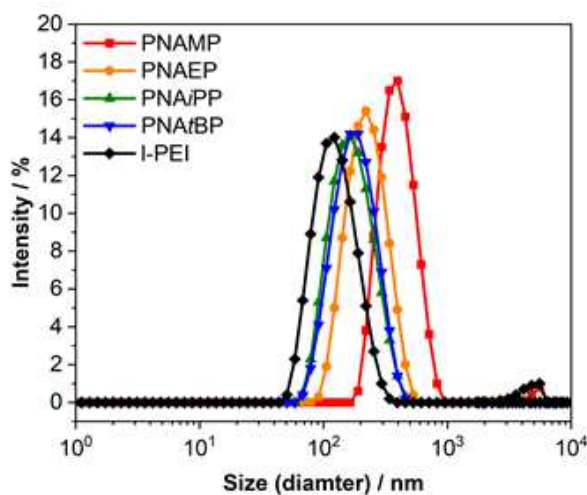


Figure S26. Exemplary histograms from DLS measurements of polyplexes. Polyplexes were prepared with $460 \mu\text{mol L}^{-1}$ pKMyc pDNA at a protonatable amine concentration of $230 \mu\text{mol L}^{-1}$ (N*/P 6). The histograms of a single measurement are displayed for PNAMP (red), PNAEP (orange), PNA/PP (green), PNA/BP (blue) and l-PEI (black).

ADDITIONAL METHODS

Size exclusion chromatography (SEC)

N,N-Dimethylacetamide (DMAc)-SEC was conducted using an 1200 series instrument (Agilent, Santa Clara, United States) equipped with a PSS degasser, a G1310A pump, a G7162A differential refractive index (RI) and an G1315D detector (diode array detector, DAD). The liquid chromatography system used 1 × GRAM 30 Å column and 1 × GRAM 1000 Å column (both 300 × 0.8 mm, 10 µm particle size, PSS, Mainz, Germany) in series. The DMAc eluent contained 0.21% (w/w) LiCl as additive. Samples were run at 1 mL min⁻¹ at 40 °C. Analyte samples were filtered through a polytetrafluoroethylene (PTFE) membrane with 0.45 µm pore size prior to injection. Polystyrene (PS) narrow standards (PSS) were used to calibrate the SEC system.

pH-dependent Ethidium Bromide (EtBr) quenching assay

Adapted from previous reports,² the binding of pDNA to the polymers was measured *via* quenching EtBr fluorescence by the interaction of the polymers with pDNA. Briefly, 46 µmol L⁻¹ pCMV-GFP pDNA were incubated with EtBr (1 µg mL⁻¹) in a total volume of 100 µL buffer at room temperature for 10 min. The buffers used were HBG buffer at pH 7.4 and 7.0 and acetate buffer at pH 5.8 and 5.0. Subsequently, polyplexes at N*/P 30 were prepared in black 96-well plates (Nunc, Thermo Fisher, Waltham, United States) and incubated at 37 °C for 15 min before measuring the fluorescence intensity at $\lambda_{\text{Ex}} = 525 \text{ nm}$ / $\lambda_{\text{Em}} = 605 \text{ nm}$. Samples containing pDNA and EtBr or only EtBr (1 µg mL⁻¹) in the respective buffer were defined as maximum (100 %) and background fluorescence, respectively. The percentage of dye displaced upon polymer-pDNA interaction was calculated using equation S1:

$$\text{Rel. FI} / \% = \frac{\text{FI}_{(\text{sample})} - \text{FI}_{(\text{Blank})}}{\text{FI}_{(\text{pDNA})} - \text{FI}_{(\text{Blank})}} \cdot 100 \quad (\text{S1})$$

Here, rel. FI is the relative fluorescence intensity of EtBr and $\text{FI}_{(\text{sample})}$, $\text{FI}_{(\text{Blank})}$, and $\text{FI}_{(\text{pDNA})}$ are the fluorescence intensities of a given sample, of EtBr in buffer, and the EtBr intercalated into pDNA in buffer, respectively. Data are expressed as mean \pm SD of three independent determinations.

Microscopic investigation of the transfection efficiency

In addition to flow cytometric measurements, transfection efficiency was also examined microscopically. The cells were imaged before flow cytometry analysis employing a Cytation 5 Cell Imaging Multi-Mode Reader (BioTek Instruments, Inc., Winooski, USA) equipped with a 10x objective using brightfield imaging and the GFP channel ($\lambda_{\text{Ex}} = 469/35 \text{ nm}$, $\lambda_{\text{Em}} = 525/39 \text{ nm}$). Images were processed using ImageJ software (Java 8).³

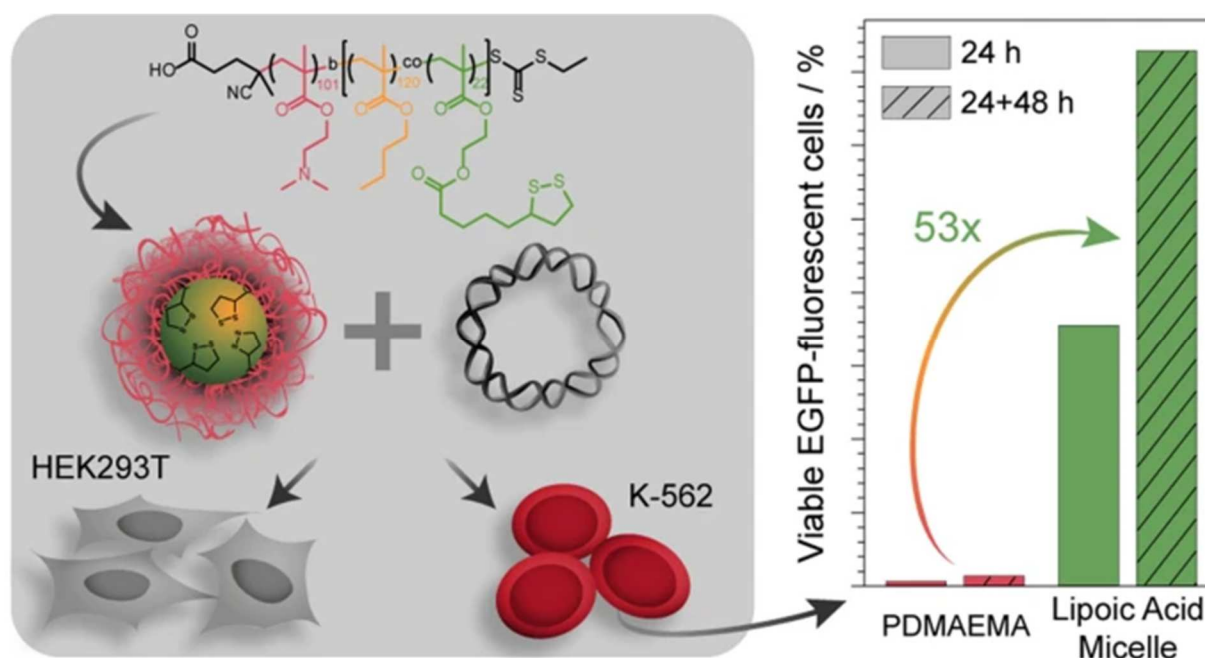
REFERENCES

1. F. Hausig, F. H. Sobotta, F. Richter, D. O. Harz, A. Traeger and J. C. Brendel, *ACS Appl Mater Interfaces*, 2021, **13**, 35233 - 35247.
2. A.-K. Trützscher, T. Bus, M. Reifarth, J. C. Brendel, S. Hoeppener, A. Traeger and U. S. Schubert, *Bioconjugate Chem*, 2018, **29**, 2181-2194.
3. J. Schindelin, I. Arganda-Carreras, E. Frise, V. Kaynig, M. Longair, T. Pietzsch, S. Preibisch, C. Rueden, S. Saalfeld, B. Schmid, J.-Y. Tinevez, D. J. White, V. Hartenstein, K. Eliceiri, P. Tomancak and A. Cardona, *Nat Methods*, 2012, **9**, 676-682.

Publication Pub4

Improved gene delivery to K-562 leukemia cells by lipoic acid modified block copolymer micelles

F. Richter,[‡] P. Mapfumo,[‡] L. Martin, J. I. Solomun, F. Hausig, J. J. Frietsch, T. Ernst, S. Hoepfner, J. C. Brendel, A. Traeger, *J. Nanobiotechnol.*, **2021**, *19*, 70.



RESEARCH

Open Access



Improved gene delivery to K-562 leukemia cells by lipoic acid modified block copolymer micelles

Friederike Richter^{1†}, Prosper Mapfumo^{1†}, Liam Martin¹, Jana I. Solomun¹, Franziska Hausig¹, Jochen J. Frietsch² , Thomas Ernst², Stephanie Hoeppener^{1,3}, Johannes C. Brendel^{1,3} and Anja Traeger^{1,3*}

Abstract

Although there has been substantial progress in the research field of gene delivery, there are some challenges remaining, e.g. there are still cell types such as primary cells and suspension cells (immune cells) known to be difficult to transfect. Cationic polymers have gained increasing attention due to their ability to bind, condense and mask genetic material, being amenable to scale up and highly variable in their composition. In addition, they can be combined with further monomers exhibiting desired biological and chemical properties, such as antioxidative, pH- and redox-responsive or biocompatible features. By introduction of hydrophobic monomers, in particular as block copolymers, cationic micelles can be formed possessing an improved chance of transfection in otherwise challenging cells. In this study, the antioxidant biomolecule lipoic acid, which can also be used as crosslinker, was incorporated into the hydrophobic block of a diblock copolymer, poly{[2-(dimethylamino)ethyl methacrylate]₁₀₁-*b*-[*n*-(butyl methacrylate)₁₂₄-*co*-(lipoic acid methacrylate)₂₂]} (P(DMAEMA₁₀₁-*b*-[*n*BMA₁₂₄-*co*-LAMA₂₂])), synthesized by RAFT polymerization and assembled into micelles (LAMA-mic). These micelles were investigated regarding their pDNA binding, cytotoxicity mechanisms and transfection efficiency in K-562 and HEK293T cells, the former representing a difficult to transfect, suspension leukemia cell line. The LAMA-mic exhibited low cytotoxicity at applied concentrations but demonstrated superior transfection efficiency in HEK293T and especially K-562 cells. In-depth studies on the transfection mechanism revealed that transfection efficiency in K-562 cells does not depend on the specific oncogenic fusion gene *BCR-ABL* alone. It is independent of the cellular uptake of polymer-pDNA complexes but correlates with the endosomal escape of the LAMA-mic. A comparison of the transfection efficiency of the LAMA-mic with structurally comparable micelles without lipoic acid showed that lipoic acid is not solely responsible for the superior transfection efficiency of the LAMA-mic. More likely, a synergistic effect of the antioxidative lipoic acid and the micellar architecture was identified. Therefore, the incorporation of lipoic acid into the core of hydrophobic-cationic micelles represents a promising tailor-made transfer strategy, which can potentially be beneficial for other difficult to transfect cell types.

Keywords: Gene delivery, Cationic polymer, Lipoic acid, Micelle, K-562 cells, Transfection

Introduction

Non-viral gene therapy has become an important research field, with the aim of finding new methods for the treatment of diseases like cancer or genetic disorders or for the development of vaccines [1, 2]. Cationic polymers are of interest due to their ability to form complexes with the genetic material (polyplexes) through

*Correspondence: anja.traeger@uni-jena.de

[†]Friederike Richter, Prosper Mapfumo contributed equally to this work

³ Jena Center for Soft Matter (JCSM), Friedrich Schiller University Jena, Philosophenweg 7, 07743 Jena, Germany

Full list of author information is available at the end of the article



electrostatic interaction, thereby protecting it from degradation, facilitating its cellular uptake, enabling escape from the endolysosomal pathway, and finally releasing it inside the cytosol [3]. Furthermore, polymers are easy and cost-effective to produce on a large scale, show low immunogenicity and can transport high molecular weight genetic materials, such as plasmid DNA (pDNA) [4, 5].

Despite remarkable progress, there are still many challenges encountered for these applications, e.g. not all cell types can be genetically modified (transfected) easily, including primary cells and suspension cells (immune cells) [6–8]. To date, viral infection, electroporation or nucleofection have been successfully applied for these cells. However, this is not suitable for all applications [4, 9, 10]. Alternatively, cationic polymers can be applied to transfect cells. The ability to genetically modify suspension cells is of great interest, not only for vaccinations, inflammation-related diseases or cancer in general, but also for leukemia patients where the immune cells are directly affected. For example, chronic myeloid leukemia (CML) can still only be clinically healed but not cured, with 40% of patients free of treatment after therapy [11–13]. Polymeric nanocarriers could be a promising strategy to interact more efficiently with immune cells and enhance the intracellular concentration of active agents to counteract mechanisms such as drug resistance or poor response to treatment [14, 15]. In this regard, the group of E. Wagner could already show successful transfection of pDNA with poly(ethylene imine) (PEI) only in combination with transferrin [16–18]. Another promising strategy was demonstrated by H. Uludağ and coworkers who statistically incorporated hydrophobic moieties into polymeric nanocarriers that were beneficial for the transfection of siRNA and subsequent knockdown of the BCR-ABL fusion protein in the CML cell line K-562 [19–21].

One key advantage of polymeric gene carriers is their versatility in composition, allowing the introduction of different additional features such as temperature-, pH- or redox-responsiveness, thereby generating nanocarriers tailored for a specific site of action [5, 22]. The advancement of living or controlled polymerization methods resulted in preparation of polymers with various compositions and complex architectures such as, gradient, block, star and comb copolymers [23]. Among reversible deactivation radical polymerization (RDRP) methods, reversible addition fragmentation chain transfer (RAFT) polymerization, a process based on an equilibrium between active and dormant chains achieved by a degenerative transfer system, is promising due to the relative insensitivity towards functional groups of the monomers and can therefore be

applied for a wide range of suitable monomers. However, disulfide bonds are a potential exception since they are susceptible to radicals [23, 24]. Additionally, RAFT polymerization is compatible with a wide range of unprotected monomer functionalities, such as quaternary amino, carboxylic acid, epoxy, hydroxyl (e.g. in hydroxyethyl methacrylate (HEMA)) and tertiary amino (e.g. in 2-dimethylaminoethyl methacrylate (DMAEMA)) groups. This makes the production of polymers with the desired functionalities easier compared to, e.g. the post-modification strategy of polymers to obtain defined polymer architectures [25].

Polymeric micelles with various compositions have already been investigated for gene delivery [26–29]. Due to the amphiphilic nature of the block copolymers, microphase separation occurs during self-assembly, resulting in micellar formation of diverse morphologies [30]. A commonly applied method for polymer assemblies is dispersion of polymers, which involves solvent evaporation, salting-out, dialysis, supercritical fluid technology and nanoprecipitation [31].

In general, polymeric micelles for gene delivery contain a hydrophilic cationic segment, responsible for condensing the genetic material and protecting it from degradation, e.g. PDMAEMA with a pK_a (≈ 7.5) within a physiologically relevant pH range [32, 33]. Besides, micelles also contain a hydrophobic segment responsible for its stability and potentially contributing to efficient transfection as they can facilitate interaction with the lipophilic cell membranes promoting cellular uptake and release from the endosomes [34–36]. Among others, *n*-butyl methacrylate (*n*BMA) has been shown to form a stable hydrophobic core and, as such, been included for hydrophobic modifications of polymers and formation of micelles [36–38].

To stabilize the micelle architecture, crosslinkers such as disulfide linkage have been applied. Disulfide linkages are stable under oxidizing conditions and break down under reductive conditions, which are found inside cells [39]. A stable micelle can therefore be prepared by incorporating sulfur containing moieties, e.g. the antioxidant biomolecule lipoic acid, which is an essential fatty acid, a potential therapeutic [40, 41], and capable of forming disulfide linkages in the micellar core [42]. For drug delivery systems, Zhong and coworkers demonstrated that different lipoic acid conjugated materials possessed superior stability in the extracellular environment and underwent rapid de-crosslinking and disassembly under reductive conditions [39, 43–45]. Moreover, lipoic acid was beneficial for transfection of siRNA or pDNA in different adherent cell lines when incorporated into nanogels [46], as hydrophobic modification of linear poly(ethylene imine) (LPEI) [47], or as amphiphiles

[48, 49]. However, the contribution of lipoic acid within micelles to gene transfer into immune cells is not known.

In the present study, lipoic acid derived micelles were investigated as a potent nanocarrier for genetic material into the CML cell line K-562. The micelles were formulated from a block copolymer synthesized via RAFT polymerization, the first block comprising PDMAEMA and the second lipoic acid methacrylate (LAMA) and *n*BMA. Whereas PDMAEMA forms the shell and contributes to pDNA binding and endosomal escape, *n*BMA forms the micellar core into which lipoic acid-containing monomers were introduced to establish antioxidant and crosslinking potential. Following physicochemical characterization, the pDNA binding properties, cytotoxicity, and transfection efficiency (expression of enhanced green fluorescent protein (EGFP)) in the erythroleukemic suspension cell line K-562 were investigated. The results were compared to the human embryonic kidney cell line HEK293T. The contribution of lipoic acid to the superior transfection efficiency in K-562 cells was investigated in detail by further testing of other leukemia cell lines as well as pDNA uptake and endosomal escape properties. Additionally, the influence of structure and composition was investigated by comparing the potential of the LAMA-micelles with lipoic acid-free precursor micelles.

Main methods

Materials, instruments, further methods and calculations can be found in the Additional file 1.

Synthesis and characterization, general procedure

(4-cyano pentanoic acid)yl ethyl trithiocarbonate (CPAETC) (24.9 mg, 9.47×10^{-5} moles), 2-(dimethylamino)ethyl methacrylate (DMAEMA) (2.25 g, 1.43×10^{-2} moles), 1,4-dioxane (3.0 g), a 1 wt.% solution of 4,4'-azobis(4-cyanovaleric acid) (ACVA) in 1,4-dioxane (318.4 mg, 3.18 mg ACVA, 1.1×10^{-5} moles) and 1,3,5-trioxane (external NMR standard, 25 mg) were introduced to a 8 mL microwave vial equipped with a magnetic stirring bar. The vial was sealed, and the solution deoxygenated by bubbling argon through it for 10 min. The vial was placed in an oil bath at 70 °C and allowed to stir for 7 h. The polymer was precipitated three times from tetrahydrofuran (THF) into cold hexane and dried under reduced pressure to give a yellow solid. A portion of the precursor, macro-chain transfer agent (macro-CTA) of poly[2-(dimethylamino)ethyl methacrylate] (PDMAEMA) (347.0 mg, 2.29×10^{-5} moles), butyl methacrylate (*n*BMA) (557.0 mg, 3.92×10^{-3} moles), lipoic acid methacrylate (LAMA) (220.0 mg, 6.88×10^{-4} moles), THF (4.1 g), a 0.5 wt.% solution of ACVA in THF (250 mg, 4.46×10^{-6} moles) and 1,3,5-trioxane (external NMR standard, 20.0 mg) were introduced

to a 8 mL microwave vial equipped with a magnetic stirring bar. The vial was sealed, and the solution deoxygenated by bubbling argon through it for 10 min. The vial was placed in an oil bath at 70 °C and allowed to stir for 7 h. The polymer was precipitated three times from THF into cold hexane and dried under reduced pressure to give a yellow solid. For further experimental details of all polymerizations refer to Additional file 1.

Assembly procedure for micelle formation

Typical assembly procedure. 30 mg of polymer was dissolved in THF (3 mL) and added to a 20 mL vial. Water (6 mL) was added to this solution through a syringe using a syringe pump (rate: 0.2 mL min^{-1}). Afterwards, (A) the polymer solution was added to a dialysis bag (Standard RC Tubing MWCO: 6–8 kDa) and dialyzed against water over three days, changing the bulk water twice a day or, (B), the polymer solution was left for two days at room temperature until THF was completely evaporated. The final concentration was determined by measuring the mass difference of three freeze dried samples of known volume. The micelles were characterized regarding their critical micelle concentration (CMC), hydrodynamic diameter and morphology using Nile Red as a fluorescent probe, dynamic light scattering (DLS) and cryo transmission electron microscopy, respectively. Experimental details for each analysis are provided in Additional file 1.

Cryo transmission electron microscopy (cryo-TEM)

Cryo-TEM images were acquired with a 200 kV FEI Tecnai G2 20 transmission electron microscope equipped with a $4k \times 4k$ Eagle HS CCD and an Olympus MegaView camera (1379×1024 pixels) for overview images. Sample preparation was performed by plunge-freezing the samples with a Vitrobot Mark IV system. 8.5 μL of the aqueous solutions were blotted (blot force -2 ; blotting time 1 s) on Quantifoil grids (R2/2, Quantifoil, Jena, Germany) and were vitrified in liquid ethane. The grids were rendered hydrophilic by Ar-plasma cleaning for 30 s (Diener Electronics, Germany). Samples were stored in liquid nitrogen until transfer to the cryo holder (Gatan 626). Transfer to the microscope was performed with a Gatan cryo stage and the temperature was maintained below -172 °C at all times after vitrification.

Polyplex preparation

The polyplexes were prepared in HBG buffer (20 mM 4(2hydroxyethyl) piperazine-1-ethanesulfonic acid (HEPES) and 5% (w/v) glucose, pH 7.4). A $30 \mu\text{g mL}^{-1}$ solution of pDNA was mixed 1:2 with different quantities of dissolved polymer to give a final pDNA concentration of $15 \mu\text{g mL}^{-1}$, with varying N*/P ratios (molar ratio of protonatable nitrogen atoms to phosphates of pDNA,

see Additional file 1). Immediately after combination, the mixtures were vortexed for 10 s at maximum speed (3200 rpm) and incubated at room temperature for 15 min to ensure complex formation.

Ethidium bromide quenching assay (EBA) and heparin release assay (HRA)

The formation of polyplexes with pDNA was identified via quenching of ethidium bromide (EtBr) fluorescence by polymers interacting with pDNA as described before. [50] Briefly, 30 $\mu\text{g mL}^{-1}$ pKMyC pDNA in HBG buffer (pH 7.4) were incubated with EtBr (1 $\mu\text{g mL}^{-1}$) at room temperature for 10 min. Different polymer stock solutions were prepared by dilution with HBG buffer (pH 7.4) to give different N*/P ratios. Subsequently, the pDNA-EtBr solution was mixed 1:2 with the different polymer stock solutions in black 96-well plates (Nunc, Thermo Fisher, Germany) and incubated at 37 °C for 15 min before measuring the fluorescence intensity at $\lambda_{\text{Ex}} = 525 \text{ nm}$ / $\lambda_{\text{Em}} = 605 \text{ nm}$. A sample containing only pDNA and EtBr was defined as maximum fluorescence (100%).

For the HRA, heparin was added to the formed polyplex-EtBr mixtures using the dispenser of the microplate reader to obtain the indicated concentrations (Additional file 1: Table S2). After each addition, the plate was shaken, incubated at 37 °C for 10 min and fluorescence intensity was measured.

The percentage of EtBr displaced upon polyplex formation or re-intercalating following pDNA release by heparin was calculated using Eq. (1):

$$\text{rFI}/\% = \frac{F_{\text{Sample}}}{F_{\text{pDNA}}} \cdot 100 \quad (1)$$

Where rFI is the relative fluorescence intensity and F_{Sample} and F_{pDNA} are the fluorescence intensities of a given sample and the EtBr intercalated into pDNA alone (in the case of the HRA with heparin), respectively. Data are expressed as mean \pm SD of three independent determinations.

The heparin concentration needed to release 70% of pDNA was calculated with OriginPro, Version 2018b (OriginLab Corporation, US) and can be found in the Additional file 1.

Cell culture

The mouse fibroblast cell line L-929 and the human embryonic kidney cell line HEK293T were obtained from CLS (Germany). They were maintained as recommended by the supplier and cultured in D10 (low glucose Dulbecco's modified eagle's medium (DMEM) supplemented with 10% (v/v) fetal calf serum (FCS), 100 U mL^{-1}

penicillin and 100 $\mu\text{g mL}^{-1}$ streptomycin) at 37 °C in a humidified 5% (v/v) CO_2 atmosphere. The chronic myeloid leukemia (CML) cell line K-562 was obtained from DSMZ (Germany) and cultured in R10 (Roswell Park Memorial Institute (RPMI) 1640 medium supplemented with 10% (v/v) FCS, 100 U mL^{-1} penicillin and 100 $\mu\text{g mL}^{-1}$ streptomycin) at 37 °C in a humidified 5% (v/v) CO_2 atmosphere. For comparison to other leukemia cell lines and determining the influence of BCR-ABL, the transformed acute myeloid leukemia (AML) cell line M07p210 [51] and the CML blast crisis cell lines LAMA-84 and KCL-22 were analyzed. All cell lines, except for M07p210, were obtained from DSMZ. The cells were cultured as described for the K-562 cells.

For experiments, L-929 and HEK293T cells were seeded at 0.1 or 0.2×10^6 cells mL^{-1} , respectively, in growth medium (D10) containing 10 mM HEPES for stability of the pH value and incubated at 37 °C in a humidified 5% (v/v) CO_2 atmosphere for 24 h. One hour prior to transfection, the medium was changed to fresh growth medium with HEPES. Unless stated otherwise, the K-562 and other leukemia cell lines were seeded at 0.3×10^6 cells mL^{-1} in growth medium (R10) containing 10 mM HEPES and incubated at 37 °C in a humidified 5% (v/v) CO_2 atmosphere for about 3 h before transfection.

Determination of cytotoxicity

For determination of cytotoxicity of the polymers, two different methods were used: The PrestoBlue™ assay for metabolic activity and the CytoTox-ONE™ assay for membrane integrity of the cells. The PrestoBlue™ assay was performed with the L-929 cells based on ISO10993-5. In detail, cells (concentration as indicated above) were seeded in 100 μL per well in a 96-well plate without using the outer wells and treated in sextuplicates with polymers at different concentrations, ranging from 5 $\mu\text{g mL}^{-1}$ to 200 $\mu\text{g mL}^{-1}$ for 24 h. The medium was replaced by a 10% (v/v) PrestoBlue™ solution in fresh culture medium, prepared according to the manufacturer's instructions. Following an incubation at 37 °C for 45 min, the fluorescence was measured at $\lambda_{\text{Ex}} = 570 \text{ nm}$ / $\lambda_{\text{Em}} = 610 \text{ nm}$. Non-treated control cells on the same plate were referred to as 100% viability. Values above 70% were regarded as non-toxic. To assess the toxicity of polyplexes used for transfection, K-562 and HEK293T cells were seeded in 500 μL per well in a 24-well plate and treated with the polyplexes at N*/P 30 for 24 h prior to the PrestoBlue™ assay. The polyplexes were prepared as described above with isolated pKMyC pDNA and added to the cells diluting the polyplexes 1:10 in the cell culture medium. Data are expressed as mean \pm SD of at least three independent determinations.

For determination of the release of lactate dehydrogenase (LDH) due to membrane disruption, the CytoTox-ONE™ assay (LDH-assay) was performed according to the manufacturer's instructions following incubation of the cells with polyplexes as described above in 500 μ L per well of a 24-well plate for 24 h. The supernatant was transferred to a new 96-well plate as a triplicate and allowed to cool down to room temperature for 30 min. Subsequently, the substrate mixture including assay buffer was added and incubated at room temperature for 10 min. The fluorescence intensity was measured at $\lambda_{\text{Ex}} = 560$ nm / $\lambda_{\text{Em}} = 590$ nm following the addition of the stop solution. For the positive control (100% LDH release), cells were incubated with 0.2% Triton X-100 for 30 min prior to analysis. Cells incubated with only pDNA were used as negative control (0% LDH-release). The relative number of viable cells with intact membranes was calculated as follows (2):

$$\text{Viability/\%} = 100 - \frac{F_{\text{Sample}} - F_0}{F_{\text{Positive control}} - F_0} \cdot 100 \quad (2)$$

Where F_{Sample} , F_0 , and $F_{\text{Positive control}}$ represent the fluorescence intensity of a given sample, medium without cells, and of the Triton X-100 treated cells, respectively.

Transfection efficiency

Transfection studies were performed in HEK293T, K-562 and further leukemia cells. The cells were seeded in 500 μ L per well in 24-well plates and treated with polyplexes at N*/P 30. The polyplexes were prepared as described above with isolated mEGFP-N1 pDNA and added to the cells diluting the polyplexes 1:10 in the cell culture medium for an incubation period of 24 h. For analysis via flow cytometry, HEK293T cells were harvested by transferring the supernatant to a 24-well plate, trypsinizing the cells and resuspending them in the respective supernatant again. Subsequently, fresh D10 was added, diluting the cell suspension 1:2. Half of the suspension was transferred to a 96-well plate for measurement, while the remaining cells were incubated for another 48 h. K-562 cells were harvested by resuspension and subsequent transfer of half of the cell suspension to a 96-well plate for measurement. For long-term transfection (72 h), the remaining cell suspension was split 1:2 by adding the same amount of fresh R10 and incubated for further 48 h.

For determination of transfection efficiency, cells were analyzed as described in the instrumentation section (Additional file 1). Viable cells showing EGFP signal higher than the mock control cells incubated with polyplexes of the respective polymer and pKMyC pDNA were gated as percentage of cells expressing EGFP and the

relative mean fluorescence intensity (rMFI) of all viable cells was calculated in relation to the respective mock control. The experiments were performed at least three times and data are expressed as mean \pm SD.

Polyplex uptake

To study the uptake of polymers over time in HEK293T and K-562 cells, the cells were seeded in 500 μ L per well in 24-well plates and treated with polyplexes at N*/P 30 for indicated time periods. The polyplexes were prepared as described above after labelling 1 μ g pKMyC pDNA with 0.027 nmol YOYO-1 iodide. Subsequently, the polymer-pDNA-solutions were added to the cells, diluting the polyplexes 1:10 in cell culture medium. Following incubation, the HEK293T cells were harvested by trypsinization and resuspension in FC-buffer (Hanks' Balanced Salt Solution, supplemented with 2% FCS and 20 mM HEPES), while the K-562 cells were only resuspended. Trypan blue solution (0.4%) was added to a final concentration of 0.04% to quench fluorescence of polyplexes outside the cells. Cells were analyzed via flow cytometry or confocal laser scanning microscopy (CLSM) as described in the instrumentation section (Additional file 1). Viable cells showing YOYO-1 signal higher than the control cells, which were incubated with YOYO-1-pDNA only, were gated as percentage of cells that have taken up pDNA and the rMFI of all viable cells was calculated in relation to the control cells. The experiments were performed at least three times and data are expressed as mean \pm SD.

Calcein release assay

To determine the endosomal escape efficiency of the polymers, a calcein release assay was performed with HEK293T and K-562 cells. The cells were seeded in 500 μ L per well in 24-well plates and treated with polyplexes at N*/P 30. Just before the addition of polyplexes, the non-cell-permeable dye calcein was added to the cells to give a final concentration of 25 μ g mL⁻¹. Following incubation for different time periods, the cells were washed via centrifugation at 250 \times g for 5 min. Prior to the washing step, the HEK293T cells were harvested by trypsinization and resuspension in FC-buffer, whereas the K-562 cells were only resuspended. Via flow cytometry, cells were analyzed as described in the instrumentation section (Additional file 1). Viable cells showing a calcein signal higher than the control cells incubated with calcein only were gated as percentage of cells that show strong calcein signal and the rMFI of all viable cells was calculated in relation to the control cells. The experiments were performed three times.

Statistics

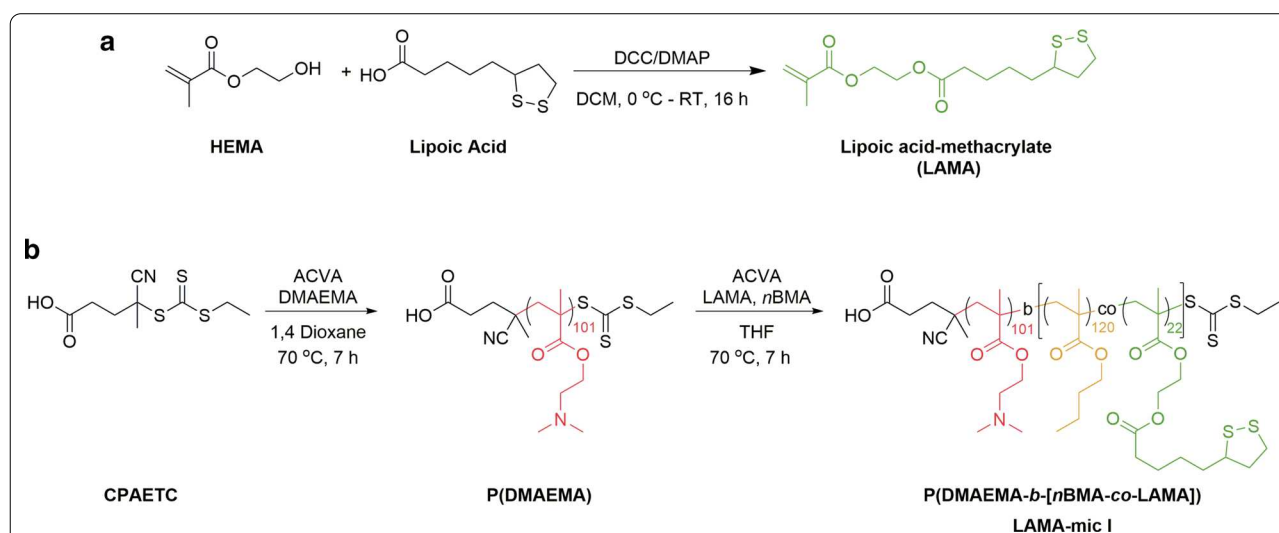
To determine the statistical significance, repeated measures analysis of variance (RM-ANOVA) was performed. If the RM-ANOVA revealed significant differences ($p < 0.05$), post-hoc analyses with a Bonferroni correction were applied. If not stated otherwise, statistically significant differences to the control were indicated with * for $p < 0.05$, ** for $p < 0.01$, and with *** for $p < 0.001$. All statistical analyses were performed with data of $n \geq 3$ in Origin, Version 2018b (OriginLab Corporation, US). Further details can be found in the Additional file 1.

Results and discussion

Polymer synthesis and micelle formation

Lipoic acid has antioxidant potential and has been studied for treatment of different diseases. In addition, studies have shown that lipoic acid exhibits redox properties, thus, they can be used as a crosslinking agent when incorporated in micelles or nanoparticles [52]. Two approaches for incorporating functional groups into polymers include (i) coupling them to a monomer and (ii) post-modification of a polymer. In this study, we opted for the first method due to the advantages for quantification and analysis that are provided by this method. Lipoic acid-methacrylate (2-(methacryloyloxy)ethyl 5-(1,2-dithiolan-3-yl)pentanoate, LAMA), was synthesized by a *N,N'*-dicyclohexylcarbodiimide (DCC)/4-(dimethylamino)pyridine (DMAP) coupling reaction (Scheme 1a), which is a well-established method for esterification reactions [53].

The polymers were synthesized by RAFT polymerization with (4-cyano pentanoic acid)yl ethyl trithiocarbonate (CPAETC) as a chain transfer agent (CTA) and 4,4'-azobis(4-cyanovaleric acid) (ACVA) as the initiator. Firstly, a PDMAEMA homopolymer was synthesized to serve as a macro-CTA for block copolymer synthesis as well as a control polymer for biological studies (Scheme 1b). Previous research had demonstrated that homopolymers of DMAEMA as well as the acrylamide analogue dimethylamino ethyl acrylamide (DMAEAm) were less toxic than LPEI but exhibited decreasing viability of cells with increasing molar mass [50, 54]. For this reason, a target degree of polymerization (DP) of 100 was chosen for the cationic homopolymer and more importantly, to achieve desired spherical micelles of sizes less than 100 nm. The macro-CTA was subsequently chain-extended with LAMA and *n*BMA to form a block copolymer P(DMAEMA-*b*-[*n*BMA-*co*-LAMA]). *n*BMA was chosen because of its biological benefits, i.e. for the interaction with cell membranes [55]. While PDMAEMA was incorporated as the hydrophilic and pH-responsive segment, the LAMA monomer was statistically integrated into the hydrophobic block of *n*BMA. The overall composition (hydrophobic to hydrophilic) was optimized to facilitate the formation of spherical micelles. All polymerizations were carried out at 70 °C and stopped after 7 h to avoid high polydispersity due to dead chain formation. Monomer conversions were typically in the range of 65 to 70% for the homopolymers and 40 to 80% of the subsequently extended block (determined via ^1H NMR, Additional file 1: Table S3, Fig. S2). SEC analysis of the



Scheme 1 Synthetic routes. **a** Synthesis of the LAMA monomer via DCC/DMAP esterification coupling reaction. **b** A chain transfer agent, CPAETC, was used to synthesize a macro-CTA, PDMAEMA, via RAFT polymerization. The macro-CTA was then used to synthesize the block copolymer under same conditions

polymers showed narrow molar mass distributions ($\mathcal{D} = 1.17$ for PDMAEMA and $\mathcal{D} = 1.19$ for P(DMAEMA-*b*-[*n*BMA-*co*-LAMA])), Additional file 1: Fig. S1, S3).

Micelles of the diblock copolymers P(DMAEMA₁₀₁-*b*-[*n*BMA₁₂₀-*co*-LAMA₂₂]) (LAMA-mic), were formed by solvent-exchange followed by dialysis in water. DLS measurements were conducted to determine the hydrodynamic size of the formulated micelles (Fig. 1a, Additional file 1: Table S4). The results showed a monomodal distribution with an average hydrodynamic radius of 47 nm and a polydispersity index of 0.19. It is worth noting that the size below 100 nm is favorable for endocytic uptake [56]. Additionally, cryo-TEM measurements were conducted to investigate the morphology of the particles (Fig. 1b). The images showed micelles featuring a spherical morphology with rather homogeneous particle size distributions ($\bar{\phi} 25.4 \pm 2.9$ nm). The slightly smaller

size measured by cryo-TEM compared to DLS is common due to the micellar shell and the hydrodynamic interactions measured by cryo-TEM showing little or no contrast.

Polyplex formation and characterization

To investigate whether the targeted micelle, LAMA-mic, is able to bind genetic material such as pDNA, fluorescence-based assays as EBA and HRA were performed (Fig. 2). The EBA was conducted at different N*/P ratios (molar ratio of amines of the polymer to phosphates of the genetic material) with a constant amount of pDNA. A decrease in the fluorescence signal of the pDNA-EtBr solution upon addition of the polymers indicated a successful formation of polyplexes due to the displacement of the EtBr from the pDNA. To investigate the stability

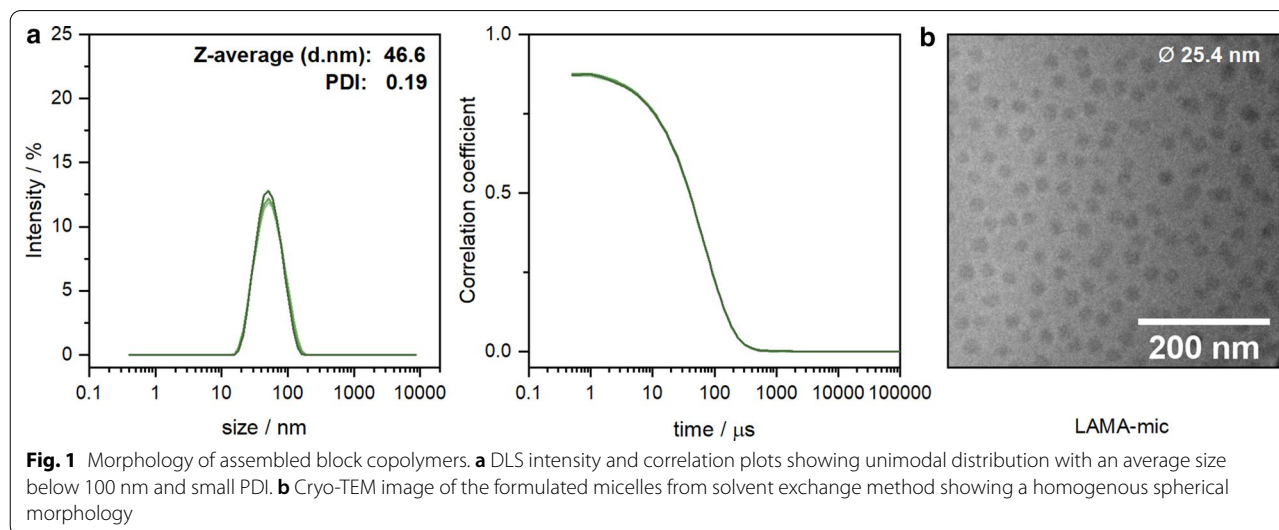


Fig. 1 Morphology of assembled block copolymers. **a** DLS intensity and correlation plots showing unimodal distribution with an average size below 100 nm and small PDI. **b** Cryo-TEM image of the formulated micelles from solvent exchange method showing a homogenous spherical morphology

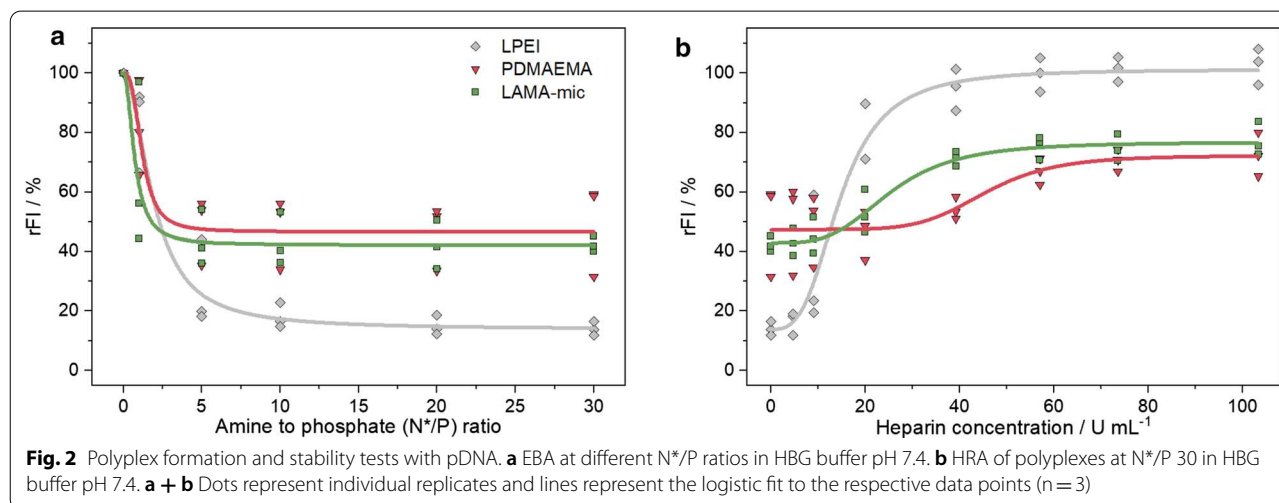


Fig. 2 Polyplex formation and stability tests with pDNA. **a** EBA at different N*/P ratios in HBG buffer pH 7.4. **b** HRA of polyplexes at N*/P 30 in HBG buffer pH 7.4. **a + b** Dots represent individual replicates and lines represent the logistic fit to the respective data points ($n = 3$)

of the polyplex, the polyanionic polysaccharide heparin was added to polyplexes of N*/P 30. Due to its negative charge, heparin can bind to the cationic moiety, replace the pDNA and EtBr can thus intercalate again into the pDNA, resulting in an increasing fluorescence intensity (FI). All tested polymers were shown to decrease the relative FI (rFI) in the EBA but to a different extent. The binding efficiency of the LAMA-mic ($42 \pm 3\%$ rFI) was comparable to that of the PDMAEMA homopolymer ($50 \pm 16\%$ rFI) demonstrating that the architecture has no influence here. However, the EtBr displacement with the LAMA-mic was not as strong as with LPEI ($14 \pm 2\%$ rFI). A gel retardation assay (GRA) indicated a complete retention of the pDNA in polyplexes at N*/P ≥ 10 for all polymers in contrast to the migration of pure pDNA (Additional file 1: Fig. S6). Since the increase in EtBr fluorescence intensity is based on an intercalation between the hydrophobic base pairs of the double helix, [57, 58] the EtBr displacement in case of the LAMA-mic and PDMAEMA may be distorted by the presence of more hydrophobic monomers (for logP values refer to Additional file 1: Table S6) and uncharged cationic moieties at pH 7.4, respectively.

Regarding polyplex stability, the influence of the micellar composition is more pronounced. While LPEI required only 18 U mL^{-1} heparin to release 70% of the pDNA, the LAMA-mic required double and PDMAEMA

nearly four times the amount of heparin, indicating an increased stability of the latter against anionic antagonists, which was also shown for other micellar systems [55]. The PDMAEMA-based systems reached plateaus around 70% rFI. This could be caused by hydrophobic interactions with the pDNA, e.g. by the hydrophobic monomers or uncharged DMAEMA moieties at pH 7.4, which are less influenced by an anionic reagent like heparin. Overall, the LAMA-mic exhibits strong pDNA binding properties required for efficient gene carriers.

Cytotoxicity

Since the presence of cationic charges and hydrophobic side chains in polymers might be problematic for cells, [36, 59] the LAMA-mic was investigated regarding its cytotoxic effects in different cell lines. To assess the metabolic activity of the cells, the PrestoBlue™ assay was performed based on ISO10993-5 with L-929 cells (Fig. 3a). The cells incubated with LAMA-mic and the PDMAEMA homopolymer showed less cytotoxicity at higher concentrations than the commercial LPEI which served as control. At concentrations equal to N*/P 30, which was later used to investigate the transfection efficiency, incubation with polymers resulted in cell viability above 70% in all cases, indicating good viabilities. The metabolic activity was further investigated in HEK293T and K-562 cells applying polyplexes at N*/P

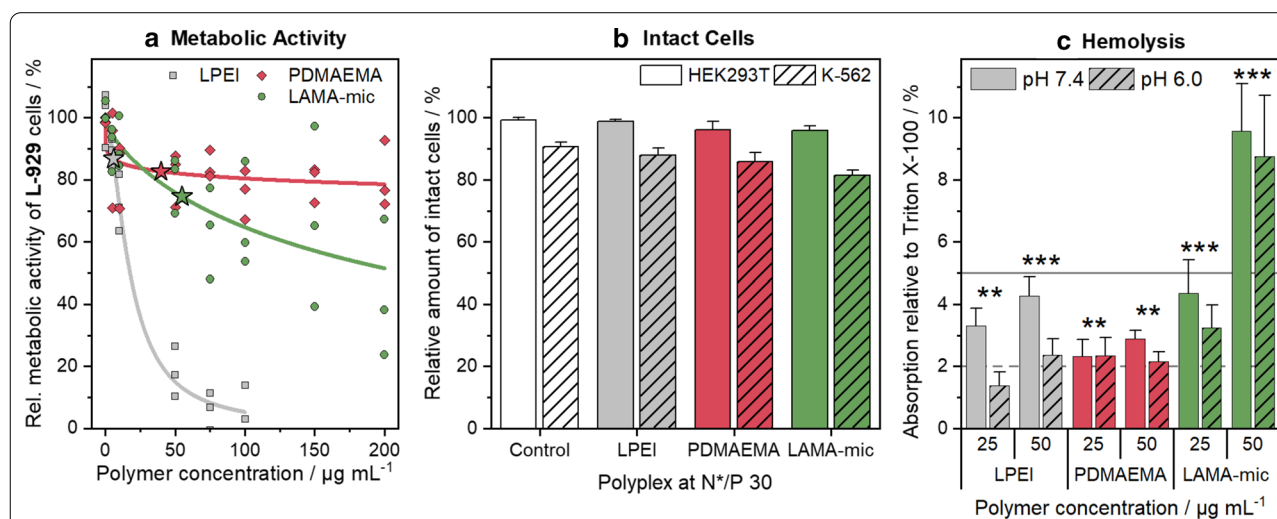


Fig. 3 Toxicity of LAMA-mic in different cell lines. **a** PrestoBlue™ assay in L-929 cells following incubation with respective polymers at indicated concentrations for 24 h. Dots represent values of single repetitions and lines represent logistic fit functions ($n = 3$). Stars indicate polymer concentrations used for N*/P 30 in transfection assays. **b** LDH-assay in HEK293T and K-562 cells following incubation with polyplexes of respective polymers and pDNA at N*/P 30 for 24 h. Values were calculated relative to the positive control Triton X-100 (100% LDH release $\hat{=}$ 0% viability) and represent mean \pm SD ($n = 3$). **c** Hemolysis as the amount of released hemoglobin calculated relative to 1% Triton X-100 as positive control (100% hemolysis). Human erythrocytes were washed and incubated with polymers at indicated concentrations in PBS of different pH values without serum. Values represent mean \pm SD ($n = 3$) and are classified as slightly hemolytic between 2% and 5%, and as non- or hemolytic if lower or higher than 2% or 5%, respectively. Regarding significant differences, the main effects of the treatment were determined since there was no significant interaction of pH value and treatment

30 (Additional file 1: Fig. S7A). Especially in HEK293T cells, the LAMA-mic exhibited lower metabolic activity ($57 \pm 8\%$ viable cells), although the cells did not appear to be dead when observed by light microscopy (Additional file 1: Fig. S8). Upon treatment with the LAMA-mic, HEK293T cells exhibited a rounded shape, formed spheroids, and started to detach. This phenomenon was observed for other polymers as well, [60] but more detailed investigations are required to understand the principle mechanism for this material, which was not the focus of this study.

To ensure that the decreased metabolic activity was not caused by a removal of viable yet detached cells during the washing steps or by the assay reagent not reaching the center of the HEK293T spheroids, other assays employing different cytotoxicity mechanisms were performed. The influence of the polyplexes on the membrane integrity was investigated using the LDH-assay and propidium iodide staining in combination with flow cytometry (Fig. 3b, Additional file 1: Fig. S7B, C). In both assays, an entering of the reagent into the cells is not necessary and the supernatant is measured either pure (LDH-assay) or together with the single cell suspension by re-addition after trypsinization (flow cytometry). The LDH-assay is based on resazurin, measuring the activity of the enzyme LDH after its release into the medium if the membrane integrity of the cells was destroyed. In flow cytometry, on the other hand, dead cells can be identified due to their changes in shape and granularity in the FSC/SSC plot. Propidium iodide staining was used as a further identification of dead cells to adjust the analysis parameters. HEK293T cells treated with the LAMA-mic exhibited viabilities above 90% with both methods, LDH-release and FSC/SSC, whereas K-562 cells showed nearly the same viability as observed in the PrestoBlue™ assay (70 to 80% viable cells). These results indicate that the LAMA-mic is not or only slightly influencing the membrane integrity of HEK293T and K-562 cells, respectively, and that the spheroid formation of the HEK293T cells could be a result of the LAMA-mic's influence on the interaction between HEK293T cells and the surface of the cultivation vessel rather than of toxic effects.

The impact of the polymers on membranes was investigated using human erythrocytes in hemolysis (Fig. 3c) and aggregation assays (Additional file 1: Fig. S9). Following serum removal, the cells were resuspended in PBS of pH values present in blood/cytoplasm (pH 7.4) or endosomal compartments (pH 6) and incubated with the polymers for 1 h, followed by centrifugation and absorption measurement of the released hemoglobin in the supernatant. Whereas LPEI and PDMAEMA were only slightly hemolytic ($\leq 4.4\%$ hemoglobin release), the LAMA-mic showed doubled hemolytic activity at $50 \mu\text{g}$

mL^{-1} , indicating a contribution of the micellar hydrophobic core or the locally increased amount of cationic charges due to micellar architecture to membrane interaction. With the exception of LPEI, there was no significant influence of pH value on hemolysis ($p=0.06$).

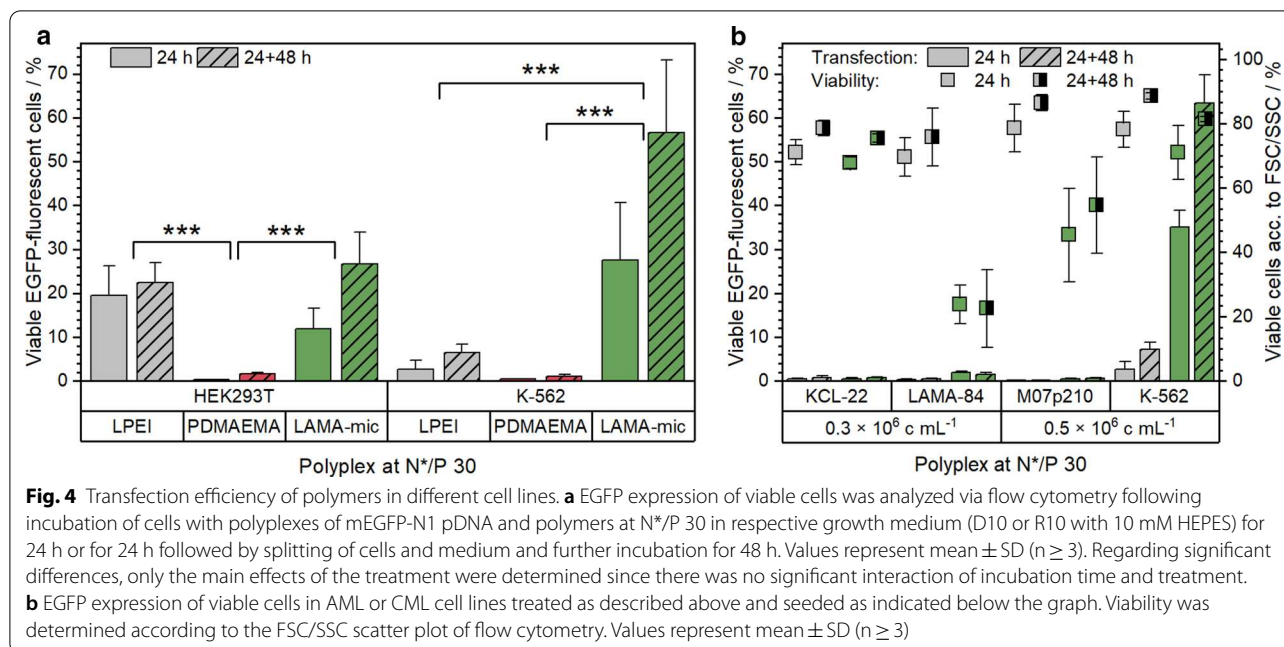
The observed low toxicity for PDMAEMA is consistent with results of previous studies [54, 61]. However, the increased membrane interactions of the LAMA-mic are not too surprising as the integration of hydrophobic moieties (e.g. *n*BMA) is known for this effect [62, 63].

Transfection efficiency

The gene delivery to suspension cells is for unresolved reasons less efficient in comparison to adherent cells [8]. Therefore, the transfection efficiency of the polymers was investigated by treating HEK293T and K-562 cells with polyplexes of polymers and pDNA encoding for EGFP at the optimal N*/P ratio 30. Following incubation (24 h or 24 h with additional 48 h in growth media), cells were analyzed via flow cytometry regarding the amount of viable and EGFP-positive cells (Fig. 4a) and the relative mean fluorescence intensity (rMFI) of all viable single cells (Additional file 1: Fig. S10).

In both cell lines, the LAMA-mic showed an increased number of EGFP-positive cells but with peculiar differences. Whereas in HEK293T cells the transfection efficiency of LAMA-mic and LPEI were comparable after 24 h, the LAMA-mic outperformed LPEI by more than seven times in K-562 cells ($29 \pm 12\%$ vs. $2 \pm 2\%$ viable EGFP-positive cells, $p < 0.001$). Interestingly, the transfection efficiency of the LAMA-mic increased almost twofold in both cell lines following incubation in growth media for further 48 h, although being only significant in K-562 cells ($p(\text{HEK293T})=0.15$, $p(\text{K-562})=0.03$). This could indicate a slower, continuous transfection mechanism (i.e. polyplex uptake and endosomal escape) for the LAMA-mic, whereas LPEI could reach its maximum already after 24 h. In contrast, the homopolymer PDMAEMA showed nearly no transfected cells in both cell lines ($< 2\%$ EGFP-positive cells). This is in accordance to previous studies of PDMAEMA [54, 61, 64]. Successful transfections with PDMAEMA could only be observed at higher molecular weight and/or higher pDNA concentration [65, 66].

Since the LAMA-mic results in a remarkably efficient gene expression in K-562 cells, even without the addition of transferrin and although these cells are considered to be difficult to transfect, the following sections will discuss, which parameter can be responsible for this. One reason could be the altered metabolism of these cells due to the generation of the *BCR-ABL* oncogene encoding for the BCR-ABL fusion protein [67, 68]. Hence,



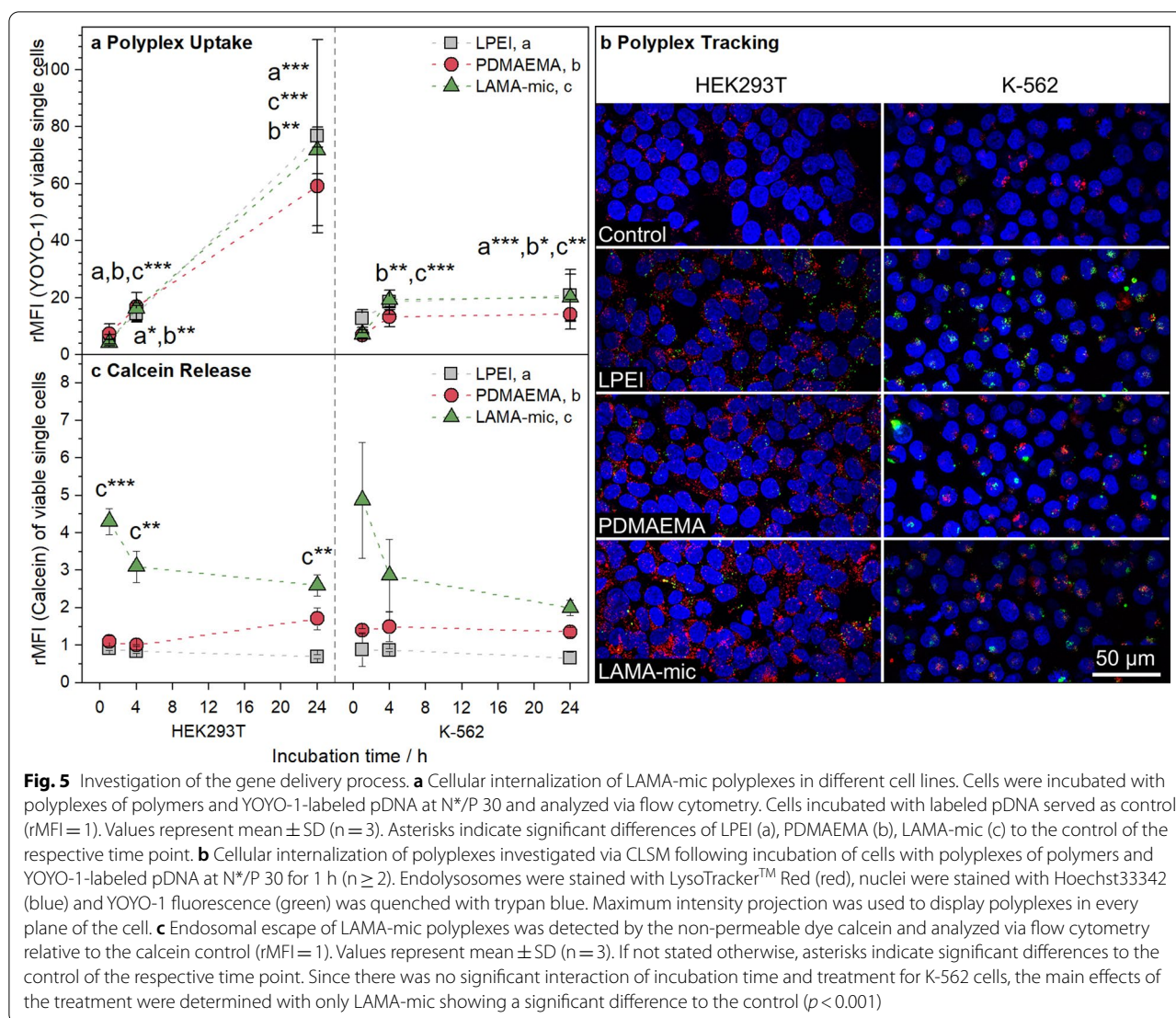
the transfection efficiency of the LAMA-mic was investigated in the additional BCR-ABL positive CML cell lines LAMA-84 and KCL-22, and in the AML cell line M07p210 expressing the fusion protein as well. As shown in Fig. 4b, none of the cell lines could be transfected with the same conditions which were successful in K-562 cells. On the contrary, the LAMA-84 and M07p210 cells showed severe toxicity following incubation with the LAMA-mic implying that BCR-ABL is not the crucial point for the transfection efficiency of the LAMA-mic, and that there must be other/additional parameters whose determination will need more profound investigations, e.g. regarding the influence of differences in signaling and metabolism of the cell lines [69] on the transfection efficiency.

Transfection mechanism of LAMA-mic

For elucidation of the LAMA-mic's high transfection efficiency in the suspension cell line K-562, two crucial cellular issues of gene delivery, namely, the cellular uptake and the endosomal release, were studied in more detail. To assess the polyplex uptake, K-562 and HEK293T cells were incubated with YOYO-1 labelled polyplexes at N*/P 30 for different time periods and analyzed via flow cytometry regarding the amount of YOYO-1 positive cells (Additional file 1: Fig. S12A) and rMFI of all viable single cells or via CLSM regarding the intracellular distribution of the polyplexes (Fig. 5a, b and S15-16). For CLSM studies, the cells were additionally labeled with LysoTrackerTM Red for endolysosomes and Hoechst 33342 for nuclei. Both cell lines show YOYO-1

positive cells after 1 h already with some of the polyplexes located in acidic compartments. It is remarkable that no significant differences between the polymers were observed regarding the rMFI in flow cytometry. To the contrary, the uptake patterns of the cell lines were found to be different. Only PDMAEMA showed slightly lower rMFI values in both cell lines. In HEK293T cells, a time-dependent uptake was found for all polyplexes, whereas in K-562 cells the uptake reached a constant level after 4 h. After 1 h and consistent with the CLSM images, the uptake in K-562 cells was slightly higher than in HEK293T cells, whereas after 24 h, the uptake in HEK293T was almost four times as high as in K-562 cells. A low endocytosis rate by suspension cells was also observed in other studies [20, 70]. This may also be associated with increased exocytosis, where the uptaken polyplexes are removed at a rate comparable to the rate they are taken up. As these results do not correlate to the observed transfection efficiencies, the observed differences of cellular uptake are not a critical aspect for the LAMA-mic in K562 cells.

Moreover, the endosomal escape was investigated using the calcein release assay. Calcein is a non-membrane-permeable dye taken up by endosomes. If a polymer is able to escape the endosome by attacking the endosomal membrane, calcein can be released into the cytoplasm, causing a diffuse fluorescence pattern, which can be detected via flow cytometry, e.g. in an alteration in the pattern of the FITC channel (Additional file 1: Fig. S14). Therefore, the cells were incubated with calcein and polyplexes at N*/P 30 for different periods of time and



were analyzed via flow cytometry (Additional file 1: Fig. S12B and Fig. 5b). In contrast to the pDNA uptake, the endosomal release showed almost no dependence on the cell line but on the polymer used. In both cell lines the LAMA-mic exhibited a significantly better release of calcein ($p < 0.01$), in particular during the first hours (1–4 h), indicating the potential of block copolymers for endosomal release also in difficult to transfect cell lines.

Influence of lipoic acid on stability and transfection efficiency

To investigate the role of lipoic acid for the improved transfection efficiency of the LAMA-mic in detail, an additional set of polymers was prepared comprising two polymers without lipoic acid, P(DMAEMA₈₉-*b*-nBMA₆₈) and P(DMAEMA₈₉-*b*-[nBMA₉₂-*co*-HEMA₁₇]) (see Additional file 1: Table S3). The first resembled an amphiphilic

block copolymer, which lacks the LAMA moiety, while the second was synthesized to mimic a hydrolyzed and cleaved lipoic acid from the original LAMA copolymer. Another version of the LAMA-mic (P(DMAEMA₈₉-*b*-[nBMA₁₀₁-*co*-LAMA₁₉]) copolymer, LAMA-mic II) was synthesized for the comparison of all polymers with the same macro-CTA. The polymeric micelles (BMA-mic, HEMA-mic and LAMA-mic II) were spherical, unimodal and similar in size (Additional file 1: Table S4, Fig. S4, S5).

To investigate the influence of lipoic acid on the micelle stability, the critical micelle concentration (CMC) was determined using Nile Red encapsulation as a fluorescence probe (Additional file 1: Fig. S18) [71]. The results showed comparable CMC values for all micelles below the concentrations used for cell experiments (LAMA-mic II: 29, HEMA-mic: 30, BMA-mic: 26 μ g mL⁻¹) indicating the presence of mainly micelles with comparable

physicochemical properties during transfection (Additional file 1: Table S5). Additionally, the polyplex stability was investigated by DLS following dilution of the respective polyplexes to concentrations used for transfection (Additional file 1: Fig. S17, Table S4). Although the sizes of the micelles hardly changed, the correlation coefficient of lipoic acid free HEMA- and BMA-mic decreased, whereas it remained constant in the case of LAMA-mic

II polyplexes, indicating a synergistic stabilizing effect of lipoic acid and the hydrophobic monomers.

With suitable polymers available, HEK293T and K-562 cells were incubated and analyzed as described before with the corresponding polyplexes at N*/P 15 and 30 (Fig. 6a, b). When comparing the different micelles, the micelles without lipoic acid were also able to transfect HEK293T cells, although to a slightly lesser extent. In K-562 cells, the transfection efficiency of the LAMA-mic

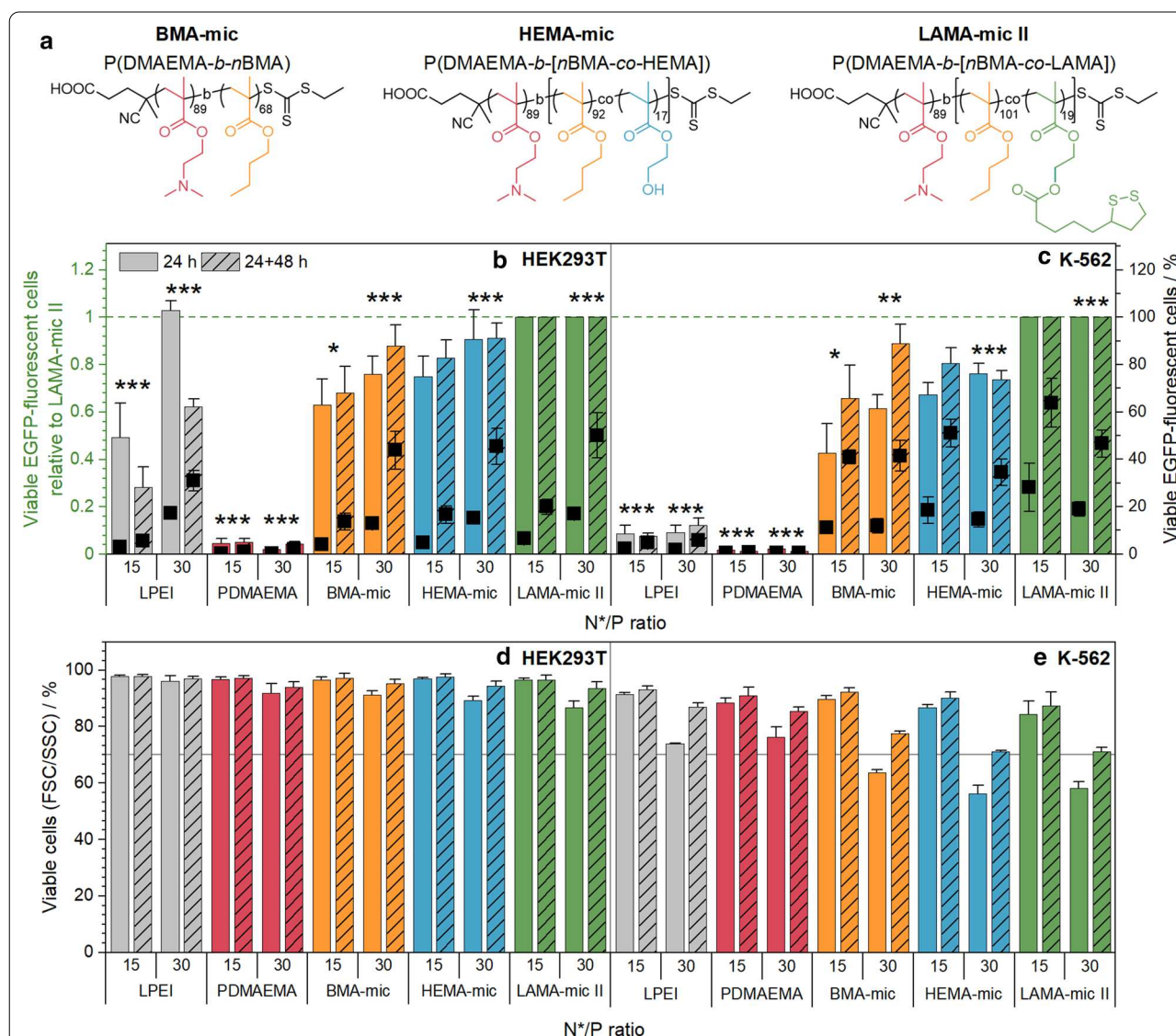


Fig. 6 Transfection efficiency and toxicity of LAMA-mic compared to control micelles. **a** Overview of the structures of the additional polymer set. **b + c** EGFP expression of viable cells was analyzed via flow cytometry following incubation of cells with polyplexes of mEGFP-N1 pDNA and polymers at N*/P 30, in respective growth medium (D10 or R10 with 10 mM HEPES) either for 24 h or for 24 h followed by splitting of cells and medium and further incubation for 48 h. Values represent mean \pm SD (n = 3) of EGFP-positive cells relative (columns) and not relative (squares) to the respective LAMA-mic treatment. **d + e** Viability was determined according to the FSC/SSC scatter plot of flow cytometry. Values represent mean \pm SD (n = 3). **b + d** HEK293T cells. **c + e** K-562 cells. Regarding significant differences, the main effects of the treatment were determined since there was no significant interaction of incubation time and treatment. *: significant difference to LAMA-mic II, N*/P 15 (p < 0.05). **: significant difference to LAMA-mic II, N*/P 15 (p < 0.01). ***: significant difference to LAMA-mic II, N*/P 15 (p < 0.001)

II polyplexes at N*/P 15 was significantly higher than the polyplexes of the other micelles at N*/P 30 (HEMA-mic: $22 \pm 11\%$ points, ppt; $p < 0.001$; BMA-mic: 19 ± 4 ppt, $p = 0.002$) indicating an increase in efficiency by the incorporation of lipoic acid into micelles. The FSC/SSC plot of the flow cytometer was used to investigate the cytotoxicity of the polyplexes at the applied concentrations (Fig. 6c, d). Whereas the HEK293T cells showed no viabilities less than 89% in all cases, the K-562 cells exhibited decreased viability, in particular at N*/P 30 after 24 h (BMA-mic: $64 \pm 1\%$, HEMA-mic: $56 \pm 3\%$, LAMA-mic II: $58 \pm 2\%$ viable cells). Nevertheless, the K-562 cells could recover as indicated by an increase in viability to more than 70% viable cells following splitting and incubation for further 48 h, which is linked to higher transfection efficiency at N*/P 15, especially for LAMA-mic II (black squares in Fig. 6a, b). For HEK293T cells, however, the increase in efficiency was less pronounced compared to the K-562 cells.

In summary, all three micelle systems represent promising candidates for efficient gene delivery to K-562 cells with the higher transfection efficiency of the LAMA-mic II indicating a synergistic effect for the lipoic acid and the architecture.

Conclusions

Since the cells of our immune system and blood are known to be hard to transfect or modulate, diseases like CML still suffer problems like drug resistance or poor treatment response. Polymeric nanocarriers could be a solution to enhance interaction with blood cells and to increase the intracellular concentration of active agents. Therefore, a well-defined lipoic acid containing diblock copolymer, P(DMAEMA₁₀₁-*b*-[*n*BMA₁₂₄-*co*-LAMA₂₂]), was synthesized *via* RAFT polymerization and formulated into defined spherical micelles (LAMA-mic) to investigate its transfection efficiency of pDNA in different cell lines, including the CML cell line K-562. The LAMA-mic is able to bind and release the genetic cargo, caused low toxicity at used concentrations and exhibited transfection efficiencies comparable to that of the commercial control LPEI in HEK293T cells. Remarkably, whereas LPEI showed almost no transfection in K-562 suspension cells, the LAMA-mic exhibited an increase in EGFP-positive cells by more than sevenfold. Compared to the homopolymer PDMAEMA, the 54-fold increase in transfection efficiency was even more impressive and demonstrated the impact of the polymer design and/or architecture. This transfection efficiency does not seem to depend on the BCR-ABL fusion protein as a crucial point, since no other tested CML or AML cell line with this fusion protein could be transfected. Further mechanistic studies were performed regarding endosomal

escape and polyplex uptake kinetics, which however could not be correlated to the performance of the polymers. In contrast to LPEI, the LAMA-mic showed good endosomal escape in both cell lines, pointing to potentially different escape mechanisms. The polymers did not show any effect on cellular uptake, although the cell line itself made a difference.

To investigate the effect of the lipoic acid functionality on transfection efficiency, two precursor polymers without the LAMA monomer, BMA-mic and HEMA-mic, were synthesized and formulated into micelles of comparable sizes and CMCs. It was found that the incorporation of lipoic acid into the core of a hydrophobic-cationic micelle enhances its gene delivery efficacy, especially in the difficult-to-transfect K-562 suspension cells. However, the influence of the architecture in general was more pronounced, as all micelles showed good efficiencies. Therefore, the LAMA-mic represents a promising nanocarrier system for gene delivery in hard-to-transfect blood cells.

Supplementary Information

The online version contains supplementary material available at <https://doi.org/10.1186/s12951-021-00801-y>.

Additional file 1. Description of further methods and results.

Acknowledgements

The authors gratefully acknowledge Carolin Kellner and Bärbel Beringer-Siemers for taking splendid care of the different cell lines and performing toxicity assays. Furthermore, the authors gratefully acknowledge Elisabeth Moek for assistance in transfection assays, and her as well as Elisabeth Preußger, Carolin Kellner and Bärbel Beringer-Siemers for fruitful discussions. The authors gratefully acknowledge Dr. Turgay Yildirim and Daniel Schnoor for preliminary studies. Furthermore, the authors thankfully acknowledge Prof. U. S. Schubert for providing excellent facilities.

Authors' contributions

FR: Conceptualization, Investigation, Methodology, Writing—Preparation of the manuscript, Visualization; PM: Conceptualization, Investigation, Writing—Preparation of the manuscript; LM: Methodology, Writing—Correction of the manuscript; JIS: Methodology, Writing—Correction of the manuscript; FH: Methodology, Writing—Correction of the manuscript; JJF: Writing—Correction of the manuscript, Consulting; TE: Writing—Correction of the manuscript; SH: cryo-TEM investigations, Writing—Correction of the manuscript; JCB: Writing—Correction of the manuscript, Funding acquisition; AT: Conceptualization, Supervision, Writing—Editing of the Manuscript, Project administration, Funding acquisition. All authors read and approved the final manuscript.

Funding

Open Access funding enabled and organized by Projekt DEAL. This work was supported by the Bundesministerium für Bildung und Forschung (BMBF, Germany, #13XP5034A PolyBioMik); the German Research Foundation (DFG, Emmy-Noether Programme, Projekt ID: 358263073); and by the DFG-funded Collaborative Research Centre PolyTarget (SFB 1278, project B01, Z01, project ID: 316213987). Cryo-TEM investigations were performed at the Electron Microscopy facilities of the Jena Center for Soft Matter (JCSM), which was established with grants from the DFG and the European Fund for Regional Development (EFRE). The LSM880 ELYRA PS.1 was further funded with a grant from the DFG.

Availability of data and materials

The datasets used and/or analyzed during the current study are available from the corresponding author on reasonable request. Supporting information available: Material, additional methods and results, Additional file 1: Fig. S1–S18, Tables S1–S6.

Ethics approval and consent to participate

Not applicable.

Consent for publication

Not applicable.

Competing interests

The authors declare that they have no competing interests.

Author details

¹ Laboratory of Organic and Macromolecular Chemistry (IOMC), Friedrich Schiller University Jena, Humboldtstrasse 10, 07743 Jena, Germany. ² Klinik für Innere Medizin II, Abteilung Hämatologie und Internistische Onkologie, Universitätsklinikum Jena, Am Klinikum 1, 07747 Jena, Germany. ³ Jena Center for Soft Matter (JCSM), Friedrich Schiller University Jena, Philosophenweg 7, 07743 Jena, Germany.

Received: 6 October 2020 Accepted: 9 February 2021

Published online: 06 March 2021

References

- Zhang P, Wagner E. History of polymeric gene delivery systems. *Top Curr Chem (Cham)*. 2017;375:26.
- Shim G, Kim D, Le QV, Park GT, Kwon T, Oh YK. Nonviral delivery systems for cancer gene therapy: strategies and challenges. *Curr Gene Ther*. 2018;18:3–20.
- Durymanov M, Reineke J. Non-viral delivery of nucleic acids: insight into mechanisms of overcoming intracellular barriers. *Front Pharmacol*. 2018;9:971.
- Bono N, Ponti F, Mantovani D, Candiani G. Non-viral in vitro gene delivery: it is now time to set the bar! *Pharmaceutics*. 2020;12:183.
- Helal NA, Osami A, Helmy A, McDonald T, Shaaban LA, Nounou MI. Non-viral gene delivery systems: hurdles for bench-to-bedside transformation. *Pharmazie*. 2017;72:627–93.
- Olden BR, Cheng Y, Yu JL, Pun SH. Cationic polymers for non-viral gene delivery to human T cells. *J Control Release*. 2018;282:140–7.
- Gresch O, Engel FB, Nestic D, Tran TT, England HM, Hickman ES, Korner I, Gan L, Chen S, Castro-Obregon S, et al. New non-viral method for gene transfer into primary cells. *Methods*. 2004;33:151–63.
- Basiouni S, Fuhrmann H, Schumann J. High-efficiency transfection of suspension cell lines. *Biotechniques*. 2012;53:1–4.
- Mellott AJ, Forrest ML, Detamore MS. Physical non-viral gene delivery methods for tissue engineering. *Ann Biomed Eng*. 2013;41:446–68.
- Riedl SAB, Kaiser P, Raup A, Synatschke CV, Jerome V, Freitag R. Non-viral transfection of human T lymphocytes. *Processes*. 2018;6:1–17.
- Ross DM, Branford S, Seymour JF, Schwarzer AP, Arthur C, Yeung DT, Dang P, Goynes JM, Slader C, Filshie RJ, et al. Safety and efficacy of imatinib cessation for CML patients with stable undetectable minimal residual disease: results from the TWISTER study. *Blood*. 2013;122:515–22.
- Hochhaus A, Baccarani M, Silver RT, Schiffer C, Apperley JF, Cervantes F, Clark RE, Cortes JE, Deininger MW, Guilhot F, et al. European LeukemiaNet 2020 recommendations for treating chronic myeloid leukemia. *Leukemia*. 2020;34:966–84.
- Mahon FX. Treatment-free remission in CML: who, how, and why? *Hematology Am Soc Hematol Educ Program*. 2017;2017:102–9.
- Hussein Kamareddine M, Ghosn Y, Tawk A, Elia C, Alam W, Makdessi J, Farhat S. Organic nanoparticles as drug delivery systems and their potential role in the treatment of chronic myeloid leukemia. *Technol Cancer Res Treat*. 2019;18:1533033819879902.
- Lin G, Zhang H, Huang L. Smart polymeric nanoparticles for cancer gene delivery. *Mol Pharm*. 2015;12:314–21.
- Kursa M, Walker GF, Roessler V, Ogris M, Roedel W, Kircheis R, Wagner E. Novel shielded transferrin—polyethylene glycol—polyethylenimine/DNA complexes for systemic tumor-targeted gene transfer. *Bioconj Chem*. 2003;14:222–31.
- Ogris M, Steinlein P, Kurs A, Mechtler K, Kircheis R, Wagner E. The size of DNA/transferrin-PEI complexes is an important factor for gene expression in cultured cells. *Gene Ther*. 1998;5:1425–33.
- Ogris M, Steinlein P, Carotta S, Brunner S, Wagner E. DNA/polyethylenimine transfection particles: influence of ligands, polymer size, and PEGylation on internalization and gene expression. *AAPS PharmSci*. 2001;3:E21–1.
- Remant KC, Thapa B, Valencia-Serna J, Domun SS, Dimitroff C, Jiang X, Uludag H. Cholesterol grafted cationic lipopolymers: potential siRNA carriers for selective chronic myeloid leukemia therapy. *J Biomed Mater Res A*. 2020;108:565–80.
- Valencia-Serna J, Gul-Uludag H, Mahdipoor P, Jiang X, Uludag H. Investigating siRNA delivery to chronic myeloid leukemia K562 cells with lipophilic polymers for therapeutic BCR-ABL down-regulation. *J Control Release*. 2013;172:495–503.
- Valencia-Serna J, Aliabadi HM, Manfrin A, Mohseni M, Jiang X, Uludag H. siRNA/lipopolymer nanoparticles to arrest growth of chronic myeloid leukemia cells in vitro and in vivo. *Eur J Pharm Biopharm*. 2018;130:66–70.
- Muhammad K, Zhao J, Gao B, Feng Y. Polymeric nano-carriers for on-demand delivery of genes via specific responses to stimuli. *J Mater Chem B*. 2020;8:9621–41.
- Quinn JF, Davis TP, Barner L, Barner-Kowollik C. The application of ionizing radiation in reversible addition–fragmentation chain transfer (RAFT) polymerization: renaissance of a key synthetic and kinetic tool. *Polymer*. 2007;48:6467–80.
- Sohn CH, Gao J, Thomas DA, Kim TY, Goddard III WA, Beauchamp JL. Mechanisms and energetics of free radical initiated disulfide bond cleavage in model peptides and insulin by mass spectrometry. *Chem Sci*. 2015;6:4550–60.
- Moad G, Rizzardo E, Thang SH. CHAPTER 6. Fundamentals of RAFT polymerization. In: Fundamentals of controlled/living radical polymerization. The Royal Society of Chemistry; 2013, pp 205–249: Polymer Chemistry Series.
- Wang H, Ding S, Zhang Z, Wang L, You Y. Cationic micelle: a promising nanocarrier for gene delivery with high transfection efficiency. *J Gene Med*. 2019;21:e3101.
- Uchida S, Kataoka K. Design concepts of polyplex micelles for in vivo therapeutic delivery of plasmid DNA and messenger RNA. *J Biomed Mater Res A*. 2019;107:978–90.
- Yousefpour Marzbali M, Yari Khosroushahi A. Polymeric micelles as mighty nanocarriers for cancer gene therapy: a review. *Cancer Chemother Pharmacol*. 2017;79:637–49.
- Cabral H, Miyata K, Osada K, Kataoka K. Block copolymer micelles in nanomedicine applications. *Chem Rev*. 2018;118:6844–92.
- Mai Y, Eisenberg A. Self-assembly of block copolymers. *Chem Soc Rev*. 2012;41:5969–85.
- Rao JP, Geckeler KE. Polymer nanoparticles: preparation techniques and size-control parameters. *Prog Polym Sci*. 2011;36:887–913.
- van de Wetering P, Moret EE, Schuurmans-Nieuwenbroek NM, van Steenberg MJ, Hennink WE. Structure-activity relationships of water-soluble cationic methacrylate/methacrylamide polymers for nonviral gene delivery. *Bioconj Chem*. 1999;10:589–97.
- Agarwal S, Zhang Y, Maji S, Greiner A. PDMAEMA based gene delivery materials. *Mater Today*. 2012;15:388–93.
- Wakefield DH, Klein JJ, Wolff JA, Rozema DB. Membrane activity and transfection ability of amphipathic polycations as a function of alkyl group size. *Bioconj Chem*. 2005;16:1204–8.
- Convertine AJ, Benoit DS, Duvall CL, Hoffman AS, Stayton PS. Development of a novel endosomolytic diblock copolymer for siRNA delivery. *J Control Release*. 2009;133:221–9.
- Liu ZH, Zhang ZY, Zhou CR, Jiao YP. Hydrophobic modifications of cationic polymers for gene delivery. *Prog Polym Sci*. 2010;35:1144–62.
- Incani V, Lavasanifar A, Uludag H. Lipid and hydrophobic modification of cationic carriers on route to superior gene vectors. *Soft Matter*. 2010;6:2124–38.
- Sprouse D, Jiang Y, Laaser JE, Lodge TP, Reineke TM. Tuning cationic block copolymer micelle size by pH and ionic strength. *Biomacromol*. 2016;17:2849–59.

39. Li YL, Zhu L, Liu Z, Cheng R, Meng F, Cui JH, Ji SJ, Zhong Z. Reversibly stabilized multifunctional dextran nanoparticles efficiently deliver doxorubicin into the nuclei of cancer cells. *Angew Chem Int Ed Engl*. 2009;48:9914–8.
40. Bast A, Haenen GRMM. The toxicity of antioxidants and their metabolites. *Environ Toxicol Phar*. 2002;11:251–8.
41. Gomes MB, Negrato CA. Alpha-lipoic acid as a pleiotropic compound with potential therapeutic use in diabetes and other chronic diseases. *Diabetol Metab Syndr*. 2014;6:80.
42. Talelli M, Barz M, Rijcken CJ, Kiessling F, Hennink WE, Lammers T. Core-crosslinked polymeric micelles: principles, preparation, biomedical applications and clinical translation. *Nano Today*. 2015;10:93–117.
43. Wei R, Cheng L, Zheng M, Cheng R, Meng F, Deng C, Zhong Z. Reduction-responsive disassemblable core-cross-linked micelles based on poly(ethylene glycol)-b-poly(N-2-hydroxypropyl methacrylamide)-lipoic acid conjugates for triggered intracellular anticancer drug release. *Biomacromol*. 2012;13:2429–38.
44. Wu L, Zou Y, Deng C, Cheng R, Meng F, Zhong Z. Intracellular release of doxorubicin from core-crosslinked polypeptide micelles triggered by both pH and reduction conditions. *Biomaterials*. 2013;34:5262–72.
45. Xu Y, Meng F, Cheng R, Zhong Z. Reduction-sensitive reversibly crosslinked biodegradable micelles for triggered release of doxorubicin. *Macromol Biosci*. 2009;9:1254–61.
46. Li RQ, Wu W, Song HQ, Ren Y, Yang M, Li J, Xu FJ. Well-defined reducible cationic nanogels based on functionalized low-molecular-weight PGMA for effective pDNA and siRNA delivery. *Acta Biomater*. 2016;41:282–92.
47. Zheng M, Zhong Y, Meng F, Peng R, Zhong Z. Lipoic acid modified low molecular weight polyethylenimine mediates nontoxic and highly potent in vitro gene transfection. *Mol Pharm*. 2011;8:2434–43.
48. Tschiche A, Thota BN, Neumann F, Schafer A, Ma N, Haag R. Crosslinked Redox-Responsive Micelles Based on Lipoic Acid-Derived Amphiphiles for Enhanced siRNA Delivery. *Macromol Biosci*. 2016;16:811–23.
49. Balakirev M, Schoehn G, Chroboczek J. Lipoic acid-derived amphiphiles for redox-controlled DNA delivery. *Chem Biol*. 2000;7:813–9.
50. Richter F, Martin L, Leer K, Moek E, Hausig F, Brendel JC, Traeger A. Tuning of endosomal escape and gene expression by functional groups, molecular weight and transfection medium: a structure-activity relationship study. *J Mater Chem B*. 2020;8:5026–41.
51. Matsuguchi T, Salgia R, Hallek M, Eder M, Druker B, Ernst TJ, Griffin JD. Shc phosphorylation in myeloid cells is regulated by granulocyte macrophage colony-stimulating factor, interleukin-3, and steel factor and is constitutively increased by p210BCR/ABL. *J Biol Chem*. 1994;269:5016–21.
52. Cheng R, Feng F, Meng F, Deng C, Feijen J, Zhong Z. Glutathione-responsive nano-vehicles as a promising platform for targeted intracellular drug and gene delivery. *J Control Release*. 2011;152:2–12.
53. Neises B, Steglich W. Simple method for the esterification of carboxylic acids. *Angewandte Chemie International Edition in English*. 1978;17:522–4.
54. Synatschke CV, Schallon A, Jerome V, Freitag R, Muller AH. Influence of polymer architecture and molecular weight of poly(2-(dimethylamino) ethyl methacrylate) polycations on transfection efficiency and cell viability in gene delivery. *Biomacromol*. 2011;12:4247–55.
55. Rinkenauer AC, Schallon A, Gunther U, Wagner M, Betthausen E, Schubert US, Schacher FH. A paradigm change: efficient transfection of human leukemia cells by stimuli-responsive multicompartment micelles. *ACS Nano*. 2013;7:9621–31.
56. Tan Z, Jiang Y, Zhang W, Karls L, Lodge TP, Reineke TM. Polycation architecture and assembly direct successful gene delivery: micelleplexes outperform polyplexes via optimal DNA packaging. *J Am Chem Soc*. 2019;141:15804–17.
57. Lepecq JB, Paoletti C. A fluorescent complex between ethidium bromide and nucleic acids—physical-chemical characterization. *J Mol Biol*. 1967;27:87.
58. Olmsted J, Kearns DR. Mechanism of ethidium bromide fluorescence enhancement on binding to nucleic acids. *Biochemistry*. 1977;16:3647–54.
59. Monnery BD, Wright M, Cavill R, Hoogenboom R, Shaunak S, Steinke JHG, Thanou M. Cytotoxicity of polycations: Relationship of molecular weight and the hydrolytic theory of the mechanism of toxicity. *Int J Pharm*. 2017;521:249–58.
60. Cui X, Hartanto Y, Zhang H. Advances in multicellular spheroids formation. *J R Soc Interface*. 2017;14:20160877.
61. Schallon A, Jerome V, Walther A, Synatschke CV, Muller AHE, Freitag R. Performance of three PDMAEMA-based polycation architectures as gene delivery agents in comparison to linear and branched PEI. *React Funct Polym*. 2010;70:1–10.
62. Kuroda K, Caputo GA, DeGrado WF. The role of hydrophobicity in the antimicrobial and hemolytic activities of polymethacrylate derivatives. *Chemistry*. 2009;15:1123–33.
63. Manganiello MJ, Cheng C, Convertine AJ, Bryers JD, Stayton PS. Diblock copolymers with tunable pH transitions for gene delivery. *Biomaterials*. 2012;33:2301–9.
64. Trutzschler AK, Bus T, Reifarth M, Brendel JC, Hoeppener S, Traeger A, Schubert US. Beyond Gene Transfection with Methacrylate-Based Polyplexes-The Influence of the Amino Substitution Pattern. *Bioconjug Chem*. 2018;29:2181–94.
65. Cherg JY, van de Wetering P, Talsma H, Crommelin DJ, Hennink WE. Effect of size and serum proteins on transfection efficiency of poly((2-dimethylamino)ethyl methacrylate)-plasmid nanoparticles. *Pharm Res*. 1996;13:1038–42.
66. Layman JM, Ramirez SM, Green MD, Long TE. Influence of polycation molecular weight on poly(2-dimethylaminoethyl methacrylate)-mediated DNA delivery in vitro. *Biomacromol*. 2009;10:1244–52.
67. Cilloni D, Saglio G. Molecular pathways: BCR-ABL. *Clin Cancer Res*. 2012;18:930–7.
68. Shinohara H, Kumazaki M, Minami Y, Ito Y, Sugito N, Kuranaga Y, Taniguchi K, Yamada N, Otsuki Y, Naoe T, Akao Y. Perturbation of energy metabolism by fatty-acid derivative AIC-47 and imatinib in BCR-ABL-harboring leukemic cells. *Cancer Lett*. 2016;371:1–11.
69. Fontana S, Alessandro R, Barranca M, Giordano M, Corrado C, Zanella-Cleon I, Becchi M, Kohn EC, De Leo G. Comparative proteome profiling and functional analysis of chronic myelogenous leukemia cell lines. *J Proteome Res*. 2007;6:4330–42.
70. Lorenz MR, Holzapfel V, Musyanovych A, Nothelfer K, Walther P, Frank H, Landfester K, Schrezenmeier H, Mailander V. Uptake of functionalized, fluorescent-labeled polymeric particles in different cell lines and stem cells. *Biomaterials*. 2006;27:2820–8.
71. Knop K, Pretzel D, Urbanek A, Rudolph T, Scharf DH, Schallon A, Wagner M, Schubert S, Kiehnopf M, Brakhage AA, et al. Star-shaped drug carriers for doxorubicin with POEGMA and POEtOxMA brush-like shells: a structural, physical, and biological comparison. *Biomacromol*. 2013;14:2536–48.

Publisher's note

Springer Nature remains neutral with regard to jurisdictional claims in published maps and institutional affiliations.

Ready to submit your research? Choose BMC and benefit from:

- fast, convenient online submission
- thorough peer review by experienced researchers in your field
- rapid publication on acceptance
- support for research data, including large and complex data types
- gold Open Access which fosters wider collaboration and increased citations
- maximum visibility for your research: over 100M website views per year

At BMC, research is always in progress.

Learn more biomedcentral.com/submissions



Supporting Information:

Improved gene delivery to K-562 leukemia cells by lipoic acid modified block copolymer micelles

*Friederike Richter,^{a,†} Prosper Mapfumo,^{a,†} Liam Martin,^a Jana I. Solomun,^a Franziska Hausig,^a
Jochen J. Frietsch,^b Thomas Ernst,^b Stephanie Hoeppener,^{a,c} Johannes C. Brendel,^{a,c} Anja
Traeger^{*a,c}*

^aLaboratory of Organic and Macromolecular Chemistry (IOMC), Friedrich Schiller University
Jena, Humboldtstrasse 10, 07743 Jena, Germany.

^bKlinik für Innere Medizin II, Abteilung Hämatologie und Internistische Onkologie,
Universitätsklinikum Jena, Am Klinikum 1, 07747 Jena, Germany.

^cJena Center for Soft Matter (JCSM), Friedrich Schiller University Jena, Philosophenweg 7,
07743 Jena, Germany.

[†]Authors contributed equally

*Correspondence to A. Traeger (anja.traeger@uni-jena.de)

List of Tables.

Table S1. Amount of different substances used for polymerization of polymers.....	8
Table S2. Kinetic cycle protocol for automated heparin addition by the microplate reader.....	10
Table S3. Summary of polymer characterization.....	17
Table S4. Summary of micelle characterization.	17
Table S5. Polymer concentrations in different assays.....	20
Table S6. Computational analysis of monomer hydrophobicity by Molinspiration.	21

List of Figures.

Figure S1. Characterization of PDMAEMA ₁₀₁ and PDMAEMA ₈₉	14
Figure S2. NMR results.	15
Figure S3. Kinetic results.....	16
Figure S4. DLS measurements of the micelles.	18
Figure S5. Original cryo-TEM images of micelles.....	19
Figure S6. Gel retardation assay.	20
Figure S7. Cytotoxicity of polymers in HEK293T and K-562 cells.....	21
Figure S8. Spheroid formation in different cell lines.....	22
Figure S9. Interaction of polymers with erythrocyte membranes.....	22
Figure S10. Transfection efficiency of LAMA-mic in different cell lines.	23
Figure S11. Gating strategy for pDNA transfection using the example of 24 h incubation.	24
Figure S12. Investigation of the gene delivery process.	25
Figure S13. Gating strategy for polyplex uptake using the example of 4 h incubation.....	26
Figure S14. Gating strategy for calcein release using the example of the 4 h incubation.	27
Figure S15. CLSM study of polyplex uptake in K-562 cells.....	27
Figure S16. CLSM study of polyplex uptake in HEK293T cells.....	28
Figure S17. DLS measurement of the micelles at different concentrations.....	29
Figure S18. CMC determination.	30

ADDITIONAL METHODS

Materials.

2-(Dimethylamino)ethyl methacrylate (DMAEMA) (98%), 2-Hydroxyethyl methacrylate (HEMA) (99%), *n*-Butyl methacrylate (*n*BMA) (99%), N,N'-Dicyclohexylcarbodiimide (DCC) (99%), 4-(Dimethylamino)pyridine (DMAP) (99%) and Nile Red (98%) were obtained from Sigma-Aldrich (Germany) and used as received. α,α' -Azoisobutyronitrile (AIBN) was obtained from Sigma-Aldrich and recrystallized from methanol. (4-cyano pentanoic acid)yl ethyl trithiocarbonate (CPAETC) and 2-(methacryloyloxy)ethyl 5-(1,2-dithiolan-3-yl)pentanoate (LAMA) were synthesized according to previous literature.[1, 2]

For biological studies, following substances were ordered from suppliers in brackets: cell culture media and supplements (Biowest, France), fetal calf serum (FCS, Capricorn Scientific, Germany), PrestoBlue™ solution, YOYO™-1 iodide (Life Technologies, Thermo Fisher, Germany), trypsin-EDTA-solution, Triton X-100, 0.4% trypan blue solution and Hanks' balanced salt solution, calcein (Sigma-Aldrich), 1% ethidium bromide solution (EtBr, Carl Roth, Germany), heparin sodium salt from porcine intestinal mucosa (Alfa Aesar), linear poly(ethyleneimine) (LPEI, $M_w = 25 \text{ kg mol}^{-1}$) and branched PEI (BPEI, $M_w = 10 \text{ kg mol}^{-1}$, Polysciences, Germany), Green Gel Loading Buffer and High Range DNA Ladder (Jena Bioscience, Germany). mEGFP-N1 was a gift from Michael Davidson (Addgene plasmid #54767; <http://n2t.net/addgene:54767>; RRID: Addgene_54767). pKMyc was a gift from Ian Macara (Addgene plasmid #19400; <http://n2t.net/addgene:19400>; RRID: Addgene_19400).

Instruments.

Nuclear magnetic resonance (NMR) spectroscopy. ^1H NMR (300 MHz) and DEPT ^{13}C (75 MHz) spectra were recorded on a Bruker AC 300 MHz spectrometer at 300 K. The delay time (d1) was set at 1 s for ^1H NMR and 2 s for DEPT ^{13}C . Chemical shifts (δ) are reported in ppm.

Size exclusion chromatography (SEC). SEC was conducted on one of two instruments. Dimethylacetamide (DMAc)-SEC was conducted using an Agilent 1200 series instrument equipped with differential refractive index (DRI) and UV/VIS (DAD) detector. The liquid chromatography system used 1 \times PSS GRAM 30 Å column (300 \times 0.8 mm, 10 μm particle size) and 1 \times PSS GRAM 1000 Å column (300 \times 0.8 mm, 10 μm particle size). The DMAc eluent contained 0.21 wt.% LiCl as additive. Samples were run at 1 mL min $^{-1}$ at 40 °C. Analyte samples were filtered through a polytetrafluoroethylene (PTFE) membrane with 0.45 μm pore size prior to injection. Poly(methyl methacrylate) (PMMA) narrow standards (PSS) were used to calibrate the SEC system. The measurements in chloroform were carried out on a Shimadzu system (Shimadzu Corp., Kyoto, Japan) equipped with a SCL-10A VP system controller, a SIL-10AD VP auto sampler, a LC-10AD VP pump, a RID-10A RI detector, a CTO-10A VP oven and a PSS SDVguard/lin S column (5 mm particle size). A mixture of chloroform/iso-propanol/triethylamine (94/2/4 vol%) was used as an eluent at a flow rate of 1 mL min $^{-1}$ and an oven temperature of 40 °C. PMMA standards (400-100,000 g mol $^{-1}$) were used to calibrate the system. Experimental $M_{n,\text{SEC}}$ and D (M_w/M_n) values of synthesized polymers were determined using PSS WinGPC UniChrom GPC software.

Flow cytometry. Flow cytometry was conducted on the CytoFlex S by Beckman Coulter GmbH, Germany. For each experiment, 10 4 cells per sample were analyzed regarding their viability in the

forward and sideward scatter (FSC/SSC) plot and their fluorescence at $\lambda_{\text{Ex}} = 488$ with a 525 nm bandpass filter, since all employed stains (YOYO-1, EGFP, calcein) were green fluorescent.

Microplate reader. Fluorescence intensity measurements for EBA, HRA, PrestoBlue™ and LDH assays as well as absorption measurements for hemolysis and aggregation assays were performed on the Infinite M200 PRO microplate reader (Tecan, Germany) with $\lambda_{\text{Ex}} / \lambda_{\text{Em}}$ used as indicated in the respective method sections and gain set to optimal.

Detailed Monomer/Polymer Synthesis and Characterization.

Synthesis of lipoic acid methacrylate (2-(Methacryloyloxy)ethyl 5-(1,2-dithiolan-3-yl)pentanoate, LAMA). Lipoic acid (2.77 g, 1.34×10^{-2} moles), 2-Hydroxyethyl methacrylate (HEMA) (1.66 g, 1.27×10^{-2} moles) and 4-(Dimethylamino)pyridine (DMAP) (1.02 g, 8.37×10^{-3} moles) were dissolved in Dichloromethane (22 mL) in a round bottom flask and cooled under stirring over ice for approx. 10 min. N,N'-Dicyclohexylcarbodiimide (DCC) (3.36 g, 1.62×10^{-2} moles) dissolved in Dichloromethane (22 mL) was added dropwise to the mixture. The reaction mixture was cooled with ice for 30 min and then left at room temperature overnight. The crude mixture was dried under reduced pressure and then a flash column chromatography was performed to purify the product (hexane 60: ethyl acetate 40). ^1H NMR (300 MHz, Chloroform-*d*) δ 6.14 (s, 1H), 5.61 (s, 1H), 4.35 (s, 4H), 3.64 – 3.47 (m, 1H), 3.26 – 3.05 (m, 2H), 2.55 – 2.41 (m, 1H), 2.36 (t, $J = 7.4$ Hz, 2H), 1.98 – 1.83 (m, 4H), 1.78 – 1.58 (m, 4H), 1.56 – 1.41 (m, 2H). ^{13}C NMR (75 MHz, Chloroform-*d*) δ 173.16, 167.06, 135.93, 126.00, 62.41, 61.98, 56.28, 40.19, 38.47, 34.57, 33.86, 28.67, 24.60, 18.25.

Typical synthesis of P(DMAEMA) via RAFT polymerization. CPAETC (24.9 mg, 9.47×10^{-5} moles), DMAEMA (2.25 g, 1.43×10^{-2} moles), 1,4-dioxane (3.0 g), a 1% (w/w) ACVA in 1,4-dioxane (318,4 mg, 1.1×10^{-5} moles) and 1,3,5-trioxane (external NMR standard, 25 mg) were

introduced to a 8 mL microwave vial equipped with a magnetic stirring bar. The vial was sealed, and the solution deoxygenated by bubbling argon through it for 10 min. The vial was placed in an oil bath at 70 °C and allowed to stir for 7 h. The polymer was precipitated three times from THF into cold hexane and dried under reduced pressure to give a yellow solid.

*Typical synthesis of P(DMAEMA-*b*-[*n*BMA-*st*-LAMA]) via RAFT polymerization.* A portion of the precursor P(DMAEMA) macro-CTA (347.0 mg, 2.29×10^{-5} moles), *n*BMA (557.0 mg, 3.92×10^{-3} moles), LAMA (220.0 mg, 6.88×10^{-4} moles), THF (4.1 g), a 0.5% (w/w) solution of ACVA in THF (250 mg, 4.46×10^{-6} moles) and 1,3,5-trioxane (external NMR standard, 20.0 mg) were introduced to a 8 mL microwave vial equipped with a magnetic stirring bar. The vial was sealed, and the solution deoxygenated by bubbling argon through it for 10 min. The vial was placed in an oil bath at 70 °C and allowed to stir for 7 h. The polymer was precipitated three times from THF into cold hexane and dried under reduced pressure to give a yellow solid.

*Synthesis of P(DMAEMA-*b*-[*n*BMA-*st*-HEMA]) via RAFT polymerization.* A portion of the precursor P(DMAEMA) macro-CTA (200.0 mg, 1.41×10^{-5} moles), *n*BMA (339.9 mg, 2.39×10^{-3} moles), HEMA (54.9 mg, 4.22×10^{-4} moles), THF (3.68 g), a 1.0% (w/w) solution of ACVA in THF (105.0 mg, 3.75×10^{-6} moles) and 1,3,5-trioxane (external NMR standard, 31.0 mg) were introduced to a 8 mL microwave vial equipped with a magnetic stirring bar. The vial was sealed, and the solution deoxygenated by bubbling argon through it for 10 min. The vial was placed in an oil bath set at 70 °C and allowed to stir for 7 h. The polymer was precipitated three times from THF into cold hexane and dried under reduced pressure to give a pale yellow solid.

*Synthesis of P(DMAEMA-*b*-*n*BMA) via RAFT polymerization.* A portion of the precursor P(DMAEMA) macro-CTA (200.0 mg, 1.41×10^{-5} moles), *n*BMA (339.8 mg, 2.39×10^{-3} moles),

THF (3.52 g), a 1.0% (w/w) solution of ACVA in THF (94.0 mg, 3.35×10^{-6} moles) and 1,3,5-trioxane (external NMR standard, 28.0 mg) were introduced to a 8 mL microwave vial equipped with a magnetic stirring bar. The vial was sealed, and the solution deoxygenated by bubbling argon through it for 10 min. The vial was placed in an oil bath set at 70 °C and allowed to stir for 7 h. The polymer was precipitated three times from THF into cold hexane and dried under reduced pressure to give a pale yellow solid.

Calculations for RAFT Polymerization.

Monomer conversion (p) was calculated from ^1H NMR data by comparing the integrals of vinyl peaks (5.5-6.3 ppm) against an external reference (1,3,5-trioxane, 5.14 ppm) before ($t = 0$) and after ($t = \text{final}$) polymerization. The theoretical number-average molar mass ($M_{n,\text{th}}$) was then calculated using equation 3a and b for PDMAEMA and P(DMAEMA-*b*-[*n*BMA-*st*-LAMA]) respectively:

$$M_{n,\text{th}} \left(\frac{\text{g}}{\text{mol}} \right) = (M_{w_{\text{DMAEMA}}} * DP * p) + M_{w_{\text{CTA}}} \quad \dots\dots (3a)$$

$$M_{n,\text{th}} \left(\frac{\text{g}}{\text{mol}} \right) = (M_{w_{\text{LAMA}}} * DP * p) + (M_{w_{n\text{BMA}}} * DP * p) + M_{w_{\text{macroCTA}}} \quad \dots\dots (3b)$$

Where DP is the target degree of polymerization of each monomer and, $M_{w_{\text{DMAEMA}}}$, $M_{w_{n\text{BMA}}}$, $M_{w_{\text{MMA}}}$, $M_{w_{\text{CTA}}}$ and $M_{w_{\text{macroCTA}}}$ are the molecular weight of the monomers, CTA and macro-CTA (PDMAEMA), respectively, and p is the monomer conversion of each monomer. Note: same formula was used for control polymers by substituting variables.

Table S1. Amount of different substances used for polymerization of polymers.

	PDMAEMA	P(DMAEMA- <i>b</i> -[<i>n</i> BMA- <i>st</i> -LAMA])	PDMAEMA	P(DMAEMA- <i>b</i> - <i>n</i> BMA)	P(DMAEMA- <i>b</i> -[<i>n</i> BMA- <i>st</i> -LAMA])	P(DMAEMA- <i>b</i> -[<i>n</i> BMA- <i>st</i> -HEMA])
Monomer	DMAEMA	LAMA, <i>n</i> BMA	DMAEMA	<i>n</i> BMA	LAMA, <i>n</i> BMA	HEMA, <i>n</i> BMA
DP _{<i>n</i>,target}	150	200	150	170	200	200
m _{CTA} added (mg)	50	250.0	50	200	200	200
n _{CTA} added (moles)	1.90×10^{-4}	1.65×10^{-5}	1.9×10^{-4}	1.44×10^{-5}	1.14×10^{-5}	1.14×10^{-5}
m _{monomer} added (mg)	4483	557.7	4483	340	474.2	394.8
n _{monomer} added (moles)	2.85×10^{-2}	3.31×10^{-3}	2.85×10^{-2}	2.39×10^{-3}	2.81×10^{-3}	2.81×10^{-3}
m _{ACVA} added (mg)	4.26	1.24	4.26	0.89	1.05	1.05
n _{ACVA} added (moles)	1.5×10^{-5}	4.4×10^{-6}	1.5×10^{-5}	3.19×10^{-6}	1.41×10^{-6}	3.75×10^{-6}
Dioxane added (μL)	2361	4583	2470	3500	4060	4140
CPAETC/ACVA	12.5	3.8	12.5	4.41	3.75	13.7
T (°C)	70	70	70	70	70	70
Time (min)	420	420	420	420	420	420

From left to right, each PDMAEMA was a precursor of the subsequent block copolymer/s.

Critical Micelle Concentration.

Critical micelle concentrations (CMC) were determined by fluorescence measurements at 25 °C with a Tecan Infinite M200 PRO microplate reader, using Nile Red as the fluorescence dye. A bulk solution of each polymer with concentrations ranging from 3.8-4.6 mg mL⁻¹ were prepared and a solution of Nile Red in THF, 3.14×10^{-4} M (0.01 mg mL⁻¹). Sample concentrations ranging from 1.0 mg mL⁻¹ to 0.001 mg mL⁻¹ of polymer were prepared in a vial by diluting the stock solutions, followed by a solution of Nile Red (0.01 mg mL⁻¹) and incubated for 4 h at room temperature under reduced pressure. Then 100 μL of each sample was transferred to a 96-well plate and equilibrated at each temperature for 30 min. The fluorescence was measured in 96-well plates using an excitation wavelength of 535 nm. The fluorescence emission spectra were measured from 400 to 600 nm in 2 nm steps. For CMC determination the maximum of each fluorescence emission spectra was plotted versus the micelle concentration for each sample,

respectively. The CMC was determined as the intersection point in the plot of the maximum fluorescence emission versus the micelle concentration.

Dynamic Light Scattering (DLS) Measurements.

The hydrodynamic diameters of the nanoassemblies were monitored by DLS using a Zetasizer Nano ZS (Malvern Instruments, Germany) with a He–Ne laser operating at a wavelength of 633 nm. Each sample was measured in triplicates at 25 °C with measurement duration set to automatic (about 10 min) after an equilibration time of 120 s. The counts were detected at an angle of 173°. The mean particle size was approximated as the effective (z-average) diameter and the width of the distribution as the polydispersity index of the particles (PDI) obtained by the cumulants method assuming a spherical shape. Data are expressed as mean \pm SD of three technical repetitions. Each micelle suspension was measured after filtration (0.20 μ m polytetrafluoroethylene (PTFE) membrane) except for P(DMAEMA₁₀₁-*b*-[*n*BMA₁₂₄-*st*-LAMA₂₂]). Filtered bulk polymer solutions were stored at room temperature (RT).

The size (hydrodynamic diameter) of the polyplexes was measured following polyplex preparation at N*/P 30 in 100 μ L HBG buffer as described in the manuscript. Each sample was measured in triplicates with three runs of 30 s at 25 °C after an equilibration time of 30 s. Data are expressed as mean of three technical replicates.

N*/P Ratio Calculations.

The N*/P ratio was defined as the ratio of the total amount of protonatable amines in polymer solution in relation to the total amount of phosphates in the pDNA solution.

The volume of polymer needed to prepare polyplexes with 15 μ g mL⁻¹ pDNA at different N*/P ratios was calculated as described by the following equations:

$$V_{\text{total}} \cdot P = V_{\text{poly}} \cdot N_{\text{poly}}$$

$$V_{\text{poly}} = \frac{V_{\text{total}} \cdot P}{N_{\text{poly}}}$$

$$V_{\text{poly}} = V_{\text{total}} \cdot \frac{n_{\text{pDNA}} \cdot P}{n_{\text{poly}} \cdot N}$$

$$V_{\text{poly}} = V_{\text{total}} \cdot \frac{m_{\text{pDNA}} \cdot P \cdot M_{\text{poly}}}{m_{\text{poly}} \cdot N \cdot M_{\text{pDNA}}}$$

Where V_{total} , P , V_{poly} and N_{poly} are the total required volume, the total number of phosphates of the pDNA, the required volume of polymer and the total number of active amines of the polymer, respectively.

Heparin dissociation assay.

Table S2. Kinetic cycle protocol for automated heparin addition by the microplate reader

Kinetic cycle	Repetitions	Addition of heparin		Orbital shake	Incubation	Measurement
		V / μL	Stock Solution / U mL^{-1}			
1	2	5	100	10 s	10 min, 37°C	$\lambda_{\text{Ex}} = 525 \text{ nm} / \lambda_{\text{Em}} = 605 \text{ nm}$
2	1	15	100	10 s	10 min, 37°C	$\lambda_{\text{Ex}} = 525 \text{ nm} / \lambda_{\text{Em}} = 605 \text{ nm}$
3	3	5	500	10 s	10 min, 37°C	$\lambda_{\text{Ex}} = 525 \text{ nm} / \lambda_{\text{Em}} = 605 \text{ nm}$
4	1	10	500	10 s	10 min, 37°C	$\lambda_{\text{Ex}} = 525 \text{ nm} / \lambda_{\text{Em}} = 605 \text{ nm}$

The heparin concentration needed to release 70% of pDNA was calculated with OriginPro, Version 2018b (OriginLab Corporation, US) using a logistic function fitted to the respective single measurement points ($n = 3$) of each polymer (4).

$$y = \frac{A_1 - A_2}{1 + (x/x_0)^p} + A_2 \quad (4)$$

Where A_1 , A_2 , x_0 and p are the initial value, the final value, the center and the power of the curve, respectively. The HC_{70} -values ($y = 70$) were calculated by substitution of the respective values into the equation.

Gel Retardation Assay (GRA).

The complex formation of the polymers with pDNA was further investigated with the GRA. Briefly, polyplexes were formed at varying N*/P ratios as described in the respective section. Following the 15 min incubation, the samples were diluted 1:6 with Green Gel Loading Buffer and run on a 1% (w/v) agarose gel containing 0.1 $\mu\text{g mL}^{-1}$ ethidium bromide (EtBr) at 80 V for 1 h. The gel was imaged using the Red™ Imaging System (Alpha Innotech, Kasendorf, Germany).

Erythrocyte Aggregation and Hemolysis.

The interaction of polymers with cellular membranes was examined by analyzing the release of hemoglobin from erythrocytes as published before.[3, 4] Blood from human donors, collected in tubes with citrate, was obtained from the Department of Transfusion Medicine of the University Hospital, Jena. The blood was centrifuged without pooling at $4,500 \times g$ for 5 min, and the pellet was washed three times with cold phosphate buffered saline (PBS, pH 7.4). Following a 10 times dilution with PBS (either pH 7.4 or pH 6.0), 500 μL aliquots of erythrocyte suspension were mixed 1:1 with the polymer solutions, which were prepared with PBS pH 7.4 or pH 6.0, and incubated at 37 °C for 60 min. After centrifugation at $2,400 \times g$ for 5 min, the supernatant was transferred to a clear flat bottomed 96-well plate (VWR, Germany) and the hemoglobin release was determined as the hemoglobin absorption at $\lambda = 544 \text{ nm}$. Absorption at $\lambda = 630 \text{ nm}$ was used as reference. Complete hemolysis (100 %) was achieved using 1 % Triton X-100 as positive control. Pure PBS was used as negative control (0 % hemolysis). The hemolytic activity of the polycations was calculated as follows (5):

$$\text{Hemolysis / \%} = \frac{(A_{\text{Sample}} - A_{\text{Negative control}})}{(A_{\text{Positive control}} - A_{\text{Negative control}})} \cdot 100 \quad (5)$$

Where A_{Sample} , $A_{\text{Negative control}}$ and $A_{\text{Positive control}}$ are the absorption values of a given sample, the PBS treatment and the Triton X-100 treatment, respectively. A value less than 2% hemolysis rate was classified as non-hemolytic, 2 to 5% as slightly hemolytic and values $> 5\%$ as hemolytic.

To determine the cell aggregation, erythrocytes were isolated as described above. Subsequently, 100 μL of the erythrocyte-polymer suspension were transferred to a clear flat bottomed 96-well plate (VWR, Germany). The cells were incubated at 37°C for 2 h, and the absorbance was measured at $\lambda = 645\text{ nm}$. Cells treated with PBS served as negative control and cells treated with $50\text{ }\mu\text{g mL}^{-1}$ 10 kDa bPEI were used as positive control. Aggregation potential of the polymers was calculated as follows (6):

$$\text{Aggregation} = \frac{A_{\text{Negative control}}}{A_{\text{Sample}}} \quad (6)$$

Where A_{Sample} and $A_{\text{Negative control}}$ are the absorption values of a given sample and the PBS treatment, respectively. Experiments were run in technical triplicates and were performed with blood from three different blood donors.

Polyplex Uptake with CLSM and Image Processing.

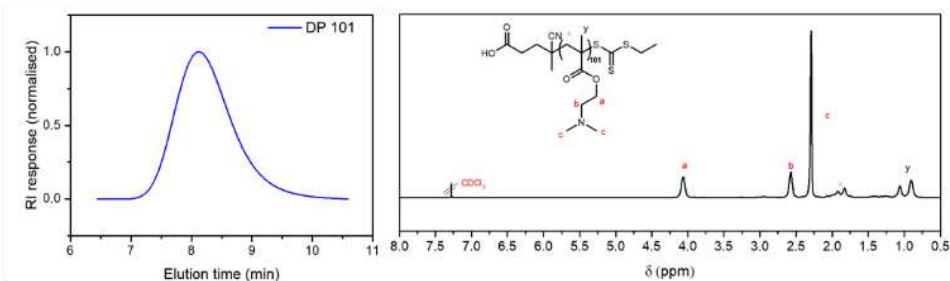
For uptake studies *via* confocal laser scanning microscopy (CLSM), cells were seeded and treated as described for flow cytometry analysis, but in glass-bottomed dishes (CellView cell culture dishes with four compartments, Greiner Bio-One) and analyzed following incubation with polyplexes containing YOYO-1 labeled pDNA (0.027 nmol per 1 μg pDNA) and indicated polymers for 1 h. To image intracellular distribution in living cells, Hoechst 33342 was added for 5 min to stain cell nuclei. To stain acidic compartments inside the cells, 50 nM LysoTrackerTM Red (LTR) were added for 5 min. Prior to imaging, trypan blue was added to a final concentration of 0.04% to quench fluorescence of YOYO-1 outside the cells. Live cell imaging was performed

using a LSM880, Elyra PS.1 system (Zeiss, Germany) applying the argon laser for excitation at 488 nm (2%) and 405 nm (0.5%), emission filters for 410-479 nm (Hoechst) and 508-553 nm (YOYO-1) with a gain of 700, respectively. LTR was excited at 561 nm and detected with an emission filter for 589-690 nm and a gain of 650. To avoid cross talk between the different channels, Hoechst and LTR were imaged simultaneously in one track and YOYO-1 in a second track. For fast imaging, the tracks were switched in every line of the image. The images were acquired as z-stacks of 6 slices around the center of the cells (in total 7 μm for HEK293T and 15 μm for K-562 cells) to image also polyplexes not present in the center of the cells. For magnification, a 40×1.4 NA plan apochromat oil objective was applied. Images were acquired using the ZEN software, version 2.3 SP1 (Zeiss, Germany). The experiments were performed at least twice. All images were processed in batch mode using ImageJ, version 1.52.⁴ At first, the 3D data of the images were turned into 2D images *via* maximum intensity projection of all 6 slices. Subsequently, the lower and upper limits of the grey values were adjusted for each channel to enhance the contrast of the images. Same values were applied to all images within one cell line.

FURTHER RESULTS

Characterization of Polymers.

A



B

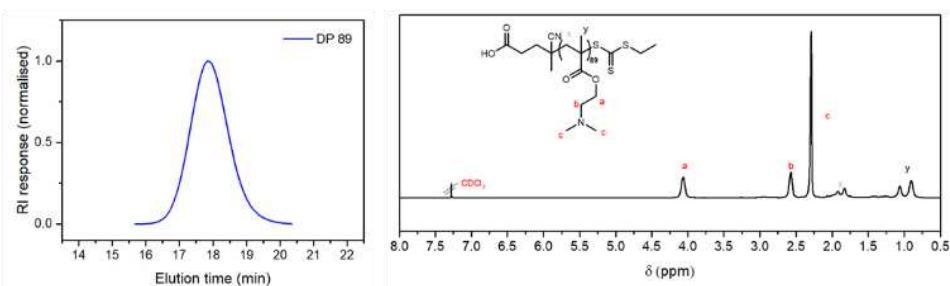


Figure S1. Characterization of PDMAEMA₁₀₁ and PDMAEMA₈₉.

Conversion from ^1H NMR, molar masses determined by (A) ($\text{CHCl}_3/\text{IPA}/\text{NEt}_3$) SEC traces—PMMA calibration and (B) ($\text{DMAc} + 0.21\% \text{ LiCl}$) SEC traces—PMMA calibration.

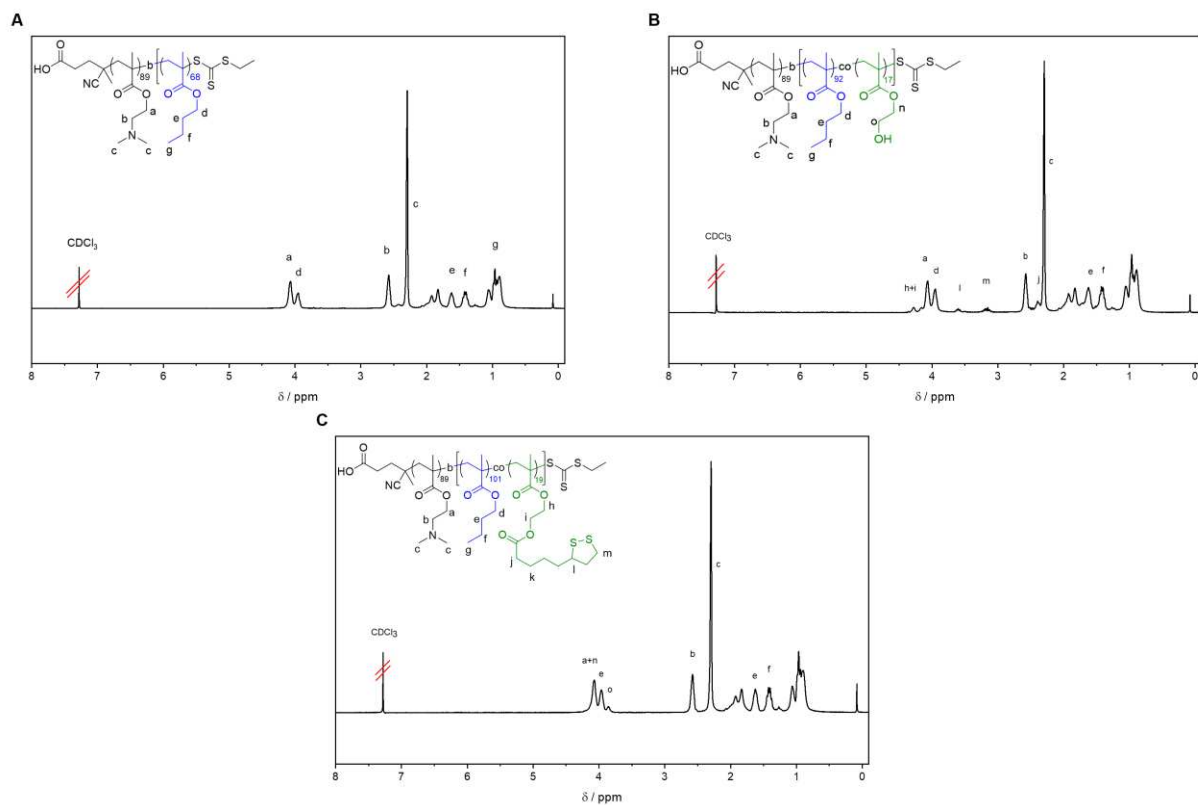


Figure S2. NMR results.

(A) $\text{P(DMAEMA}_{89}\text{-}b\text{-}n\text{BMA}_{68})$, (B) $\text{P(DMAEMA}_{89}\text{-}b\text{-}[\text{nBMA}_{92}\text{-}st\text{-HEMA}_{17}])$, (C) $\text{P(DMAEMA}_{89}\text{-}b\text{-}[\text{nBMA}_{101}\text{-}st\text{-LAMA}_{19}])$.

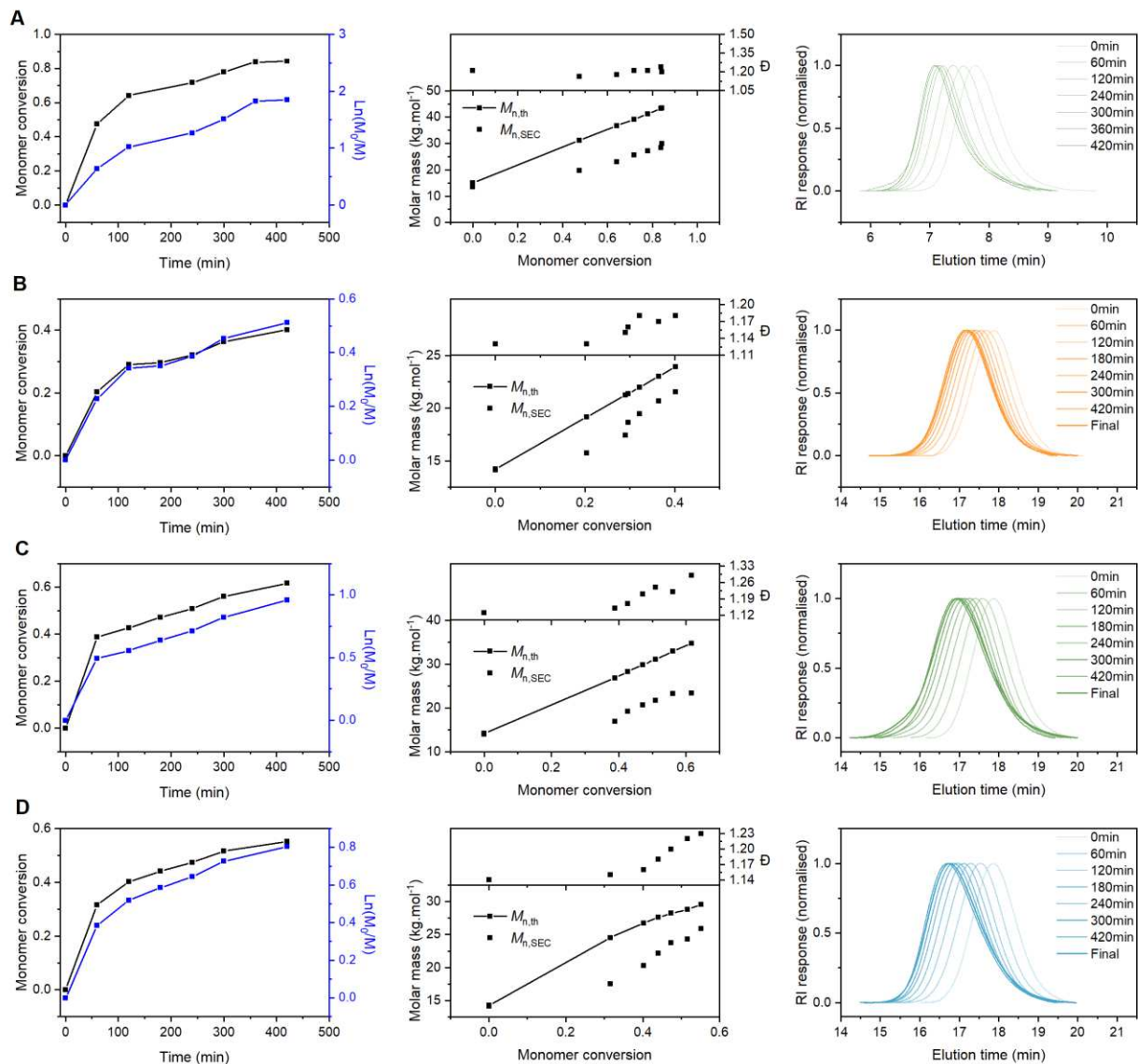


Figure S3. Kinetic results.

(A) P(DMAEMA₁₀₁-*b*-[*n*BMA₁₂₀-*st*-LAMA₂₂]), (B) P(DMAEMA₈₉-*b*-*n*BMA₆₈) (C) P(DMAEMA₈₉-*b*-[*n*BMA₁₀₁-*st*-LAMA₁₉]), (D) P(DMAEMA₈₉-*b*-[*n*BMA₉₂-*st*-HEMA₁₇]). Conversion from ^1H NMR, molar masses determined by ($\text{CHCl}_3/\text{IPA}/\text{NEt}_3$) SEC traces-PMMA calibration (A) and SEC-9: DMAc + 0.21 % LiCl – PMMA calibration (B-D).

Table S3. Summary of polymer characterization.

Polymer-ID [a]	$M_{n,th}$ [b]	$M_{n,SEC}$ [c]	\bar{D} [c]
	kg mol ⁻¹		
PDMAEMA ₁₀₁	16.1	13.8	1.17
P(DMAEMA ₁₀₁ - <i>b</i> -[<i>n</i> BMA ₁₂₀ - <i>co</i> -LAMA ₂₂])	39.2	30.0	1.19
PDMAEMA ₈₉	14.2	14.0	1.15
P(DMAEMA ₈₉ - <i>b</i> - <i>n</i> BMA ₆₈)	23.9	21.0	1.18
P(DMAEMA ₈₉ - <i>b</i> -[<i>n</i> BMA ₉₂ - <i>co</i> -HEMA ₁₇])	29.6	24.7	1.26
P(DMAEMA ₈₉ - <i>b</i> -[<i>n</i> BMA ₁₀₁ - <i>co</i> -LAMA ₁₉])	34.7	23.1	1.32
[a] Degree of Polymerization was determined <i>via</i> ¹ H NMR. [b] Determined using equation 6 of the ESI. [c] Determined <i>via</i> CHCl ₃ -SEC and DMAc-SEC with PMMA standards.			

Table S4. Summary of micelle characterization.

Code	Micelle					Polyplex			
	Stock-solution		370-540 µg mL ⁻¹			370-540 µg mL ⁻¹		37-54 µg mL ⁻¹	
	Size [a]	PDI [b]	Size [a]	PDI [b]	CMC [c]	Size [a]	PDI [b]	Size [a]	PDI [b]
	nm		nm		µg mL ⁻¹	nm		nm	
LAMA-mic	46.6	0.19	53.4	0.15	-	-	-	-	-
BMA-mic	19.5	0.25	46.6	0.10	26	56.8	0.21	73.4	0.38
HEMA-mic	21.7	0.19	51.3	0.08	30	54.1	0.10	63.3	0.26
LAMA-mic II	24.2	0.23	54.2	0.12	29	61.1	0.14	62.4	0.26

[a] Determination of the size as the hydrodynamic diameter *via* DLS (concentrations see Table S3).[b] Determined *via* DLS (concentrations see Table S3).

[c] Determined using Nile Red encapsulation as fluorescence probe.

DLS Measurement of Micelles.

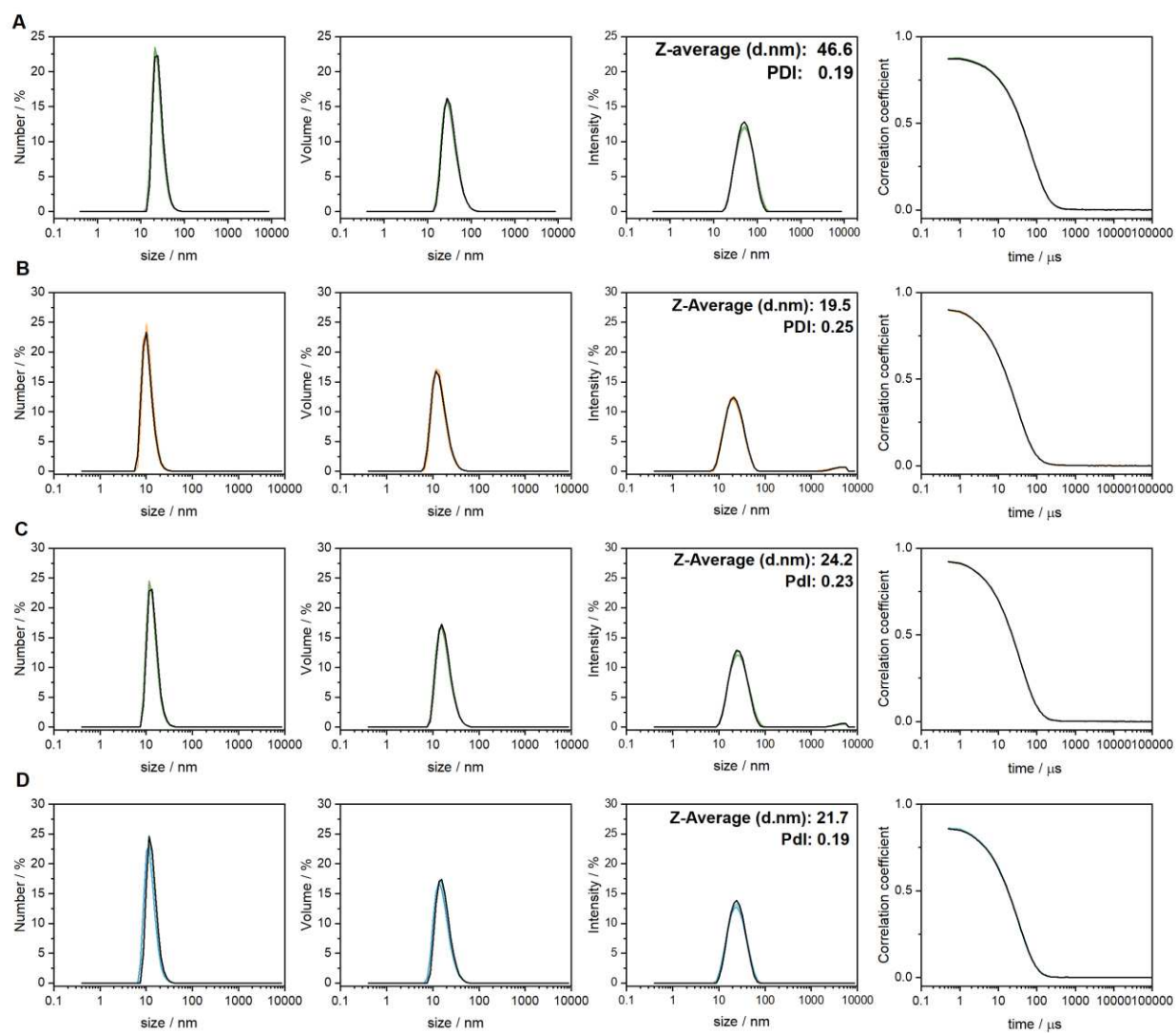


Figure S4. DLS measurements of the micelles.

(A) LAMA-mic, (B) BMA-mic, (C) LAMA-mic II and (D) HEMA-mic; stock solutions.

Original Cryo-TEM images

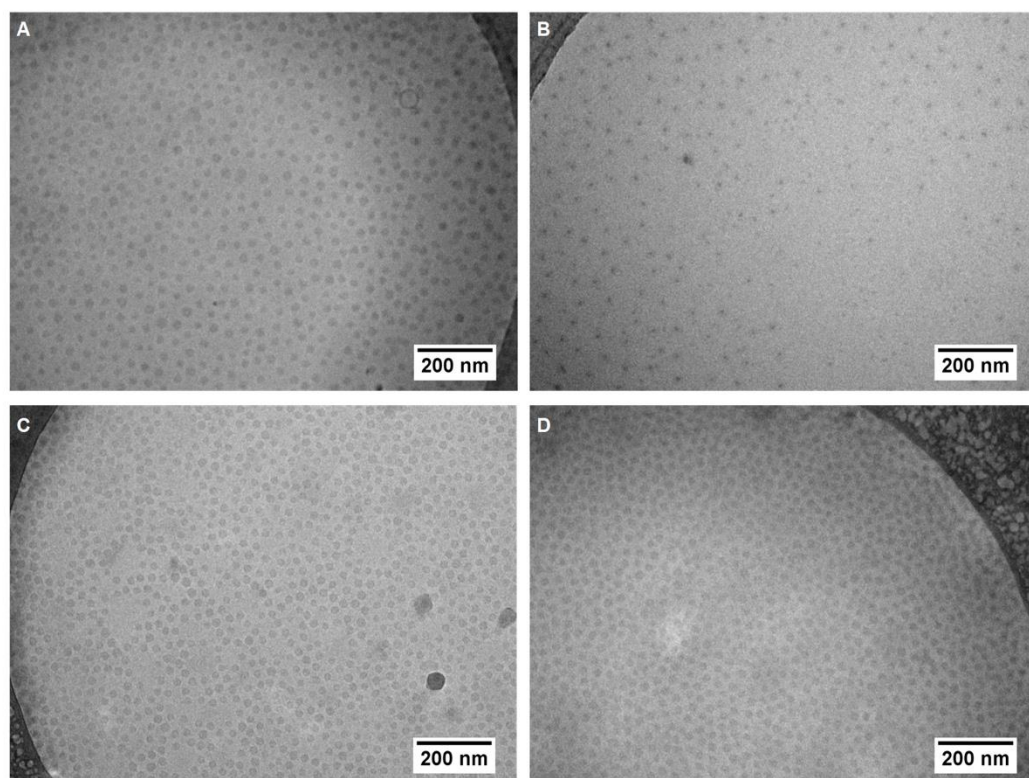


Figure S5. Original cryo-TEM images of micelles.

(A) LAMA-mic, **(B)** BMA-mic, **(C)** LAMA-mic II, **(D)** HEMA-mic.

Further Biological Results.

Table S5. Polymer concentrations in different assays.

	Stock solutions	EBA/HRA, DLS		Cell—based assays		Amount of lipoic acid on cells	
	$\mu\text{g mL}^{-1}$	$\mu\text{g mL}^{-1}$		$\mu\text{g mL}^{-1}$		μM	
	-	N*/P 15	N*/P 30	N*/P 15	N*/P 30	N*/P 15	N*/P 30
pDNA	-	15	15	1.5	1.5	-	-
LPEI	1000	30	59	3.0	5.9	-	-
PDMAEMA	10000	111	221	11.1	22.1	-	-
LAMA-mic	2100	275	549	27.5	54.9	14.8	29.5
PDMAEMA II	10000	111	221	11.1	22.1	-	-
BMA-mic	4940	189	371	18.9	37.1	-	-
HEMA-mic	4600	228	455	22.8	45.5	-	-
LAMA-mic II	4580	269	538	26.9	53.8	14.8	29.5

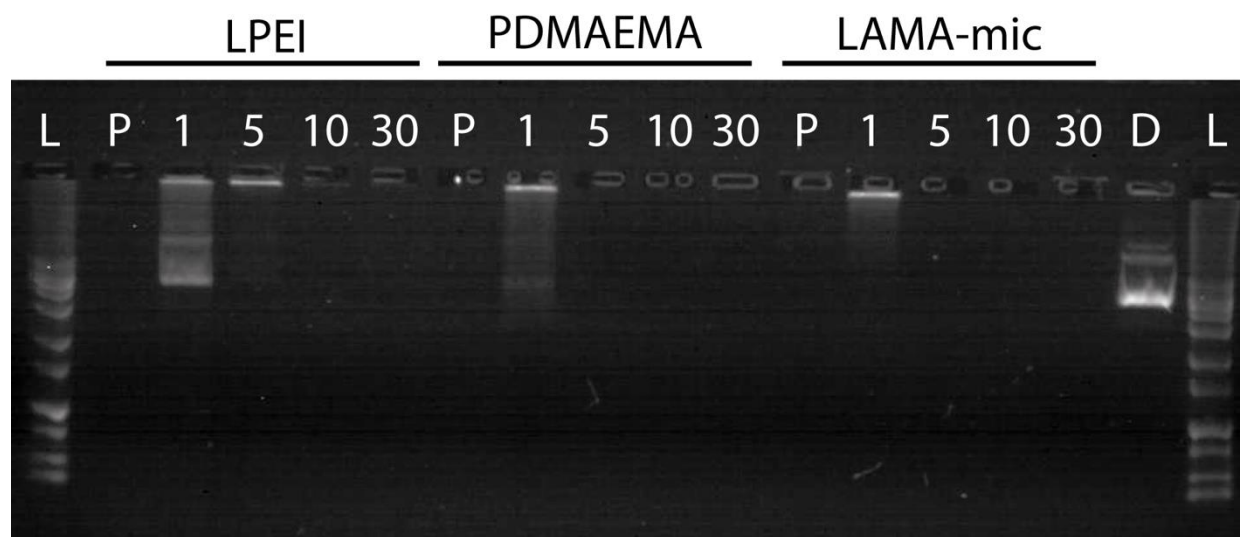


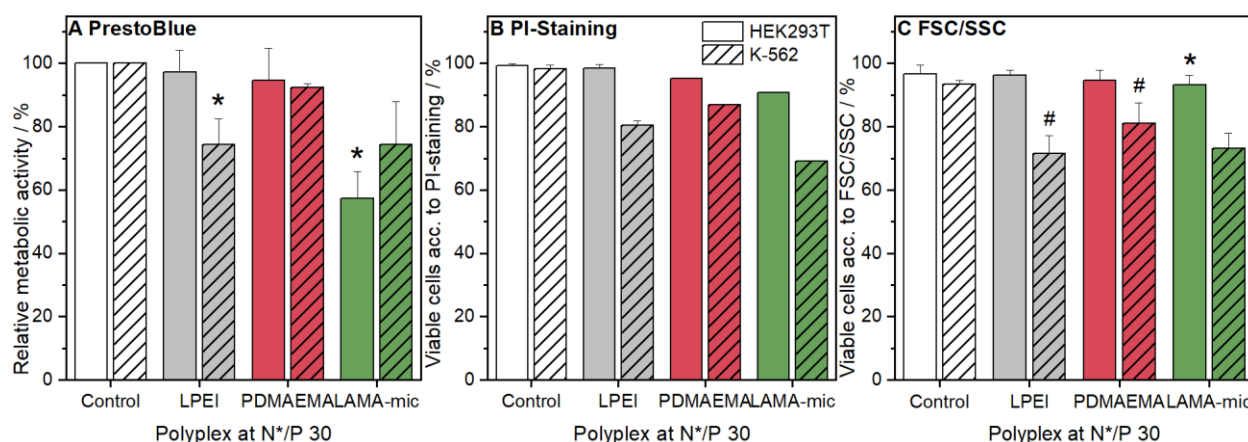
Figure S6. Gel retardation assay.

The agarose gel was loaded with polyplexes prepared as described before. L: High Range DNA Ladder, P: only Polymer at concentrations equal to N*/P 30, numbers indicate the respective N*/P ratios, D: pDNA in HBG buffer at the same concentration used for polyplexes.

Table S6. Computational analysis of monomer hydrophobicity by Molinspiration.

	EI	DMAEMA	<i>n</i> BMA	LAMA
Structure				
MW	45.09	157.21	142.20	318.46
logP ¹	0.1	1.4	2.81	3.43

¹The logP values were calculated using the Molinspiration Property Calculation Service of the Molinspiration Cheminformatics website (<https://www.molinspiration.com/cgi-bin/properties>).

**Figure S7.** Cytotoxicity of polymers in HEK293T and K-562 cells.

(A) Metabolic activity using the PrestoBlue™ assay following incubation of cells with polyplexes of indicated polymers and pDNA at N*/P 30 for 24 h. Values represent mean \pm SD of $n = 3$. (B) Membrane integrity using propidium iodide (PI) staining and flow cytometry following incubation of cells with polyplexes of indicated polymers and pDNA at N*/P 30 for 24 h. Viability was calculated as the difference of 100 and the percentage of PI positive cells gated in the ECD-channel. Values represent mean \pm SD of $n > 1$. (C) Viable cells according to appearance of cells in FSC/SSC plot of flow cytometry. Values represent mean \pm SD of $n > 1$.

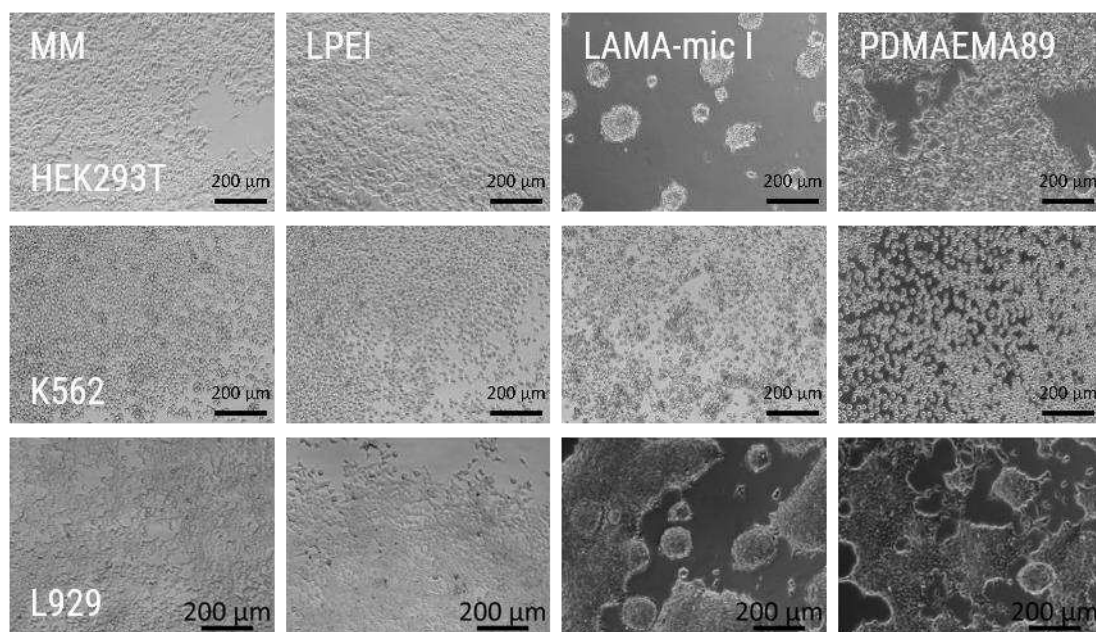


Figure S8. Spheroid formation in different cell lines.

Cells were incubated with polyplexes and pDNA at N*/P 30 for 24 h. Images were acquired *via* light microscopy.

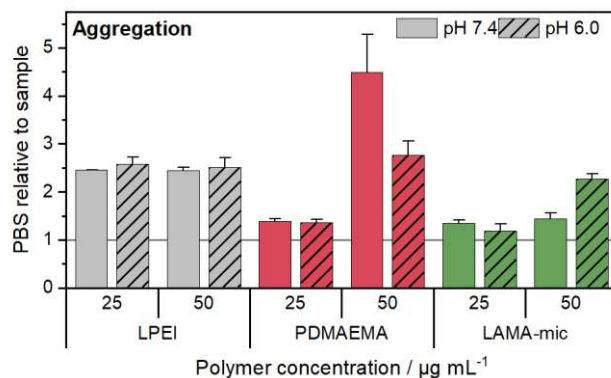


Figure S9. Interaction of polymers with erythrocyte membranes.

Human erythrocytes were washed and incubated with polymers at different concentrations in PBS of different pH values present in blood/cytoplasm (pH 7.4) or endosomal compartments (pH 6). Aggregation of indicated polymers was measured as light absorption by erythrocytes. Values are calculated as the negative control (PBS value) relative to the sample value and represent mean \pm SD (n = 3).

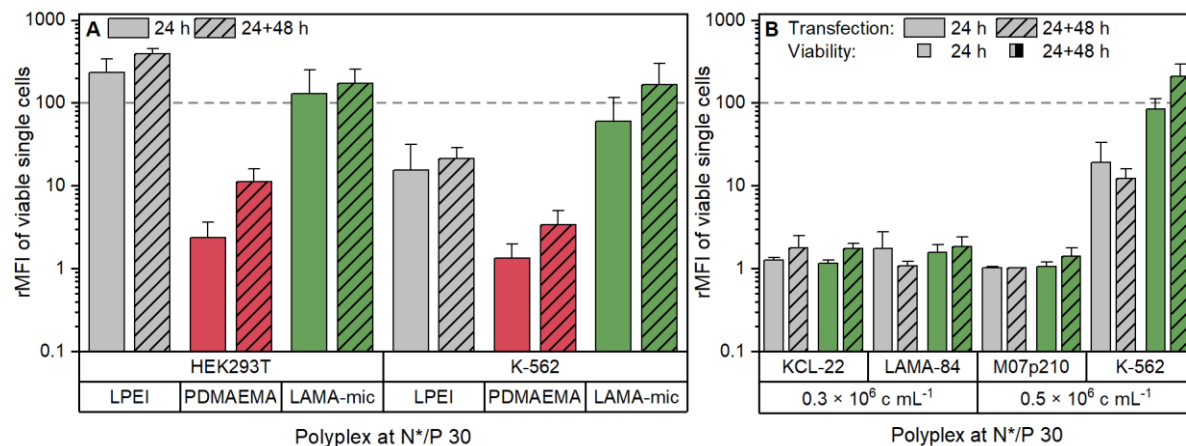


Figure S10. Transfection efficiency of LAMA-mic in different cell lines.

EGFP expression of viable cells was analyzed *via* flow cytometry following incubation of cells with polyplexes of mEGFP-N1 pDNA and polymers at N*/P 30 in respective growth medium (D10 or R10 with 10 mM HEPES) either for 24 h or for 24 h, splitting the cell suspension 1:2 and further incubation for 48 h. Values represent mean \pm SD of rMFI values of viable, single cells ($n \geq 3$).

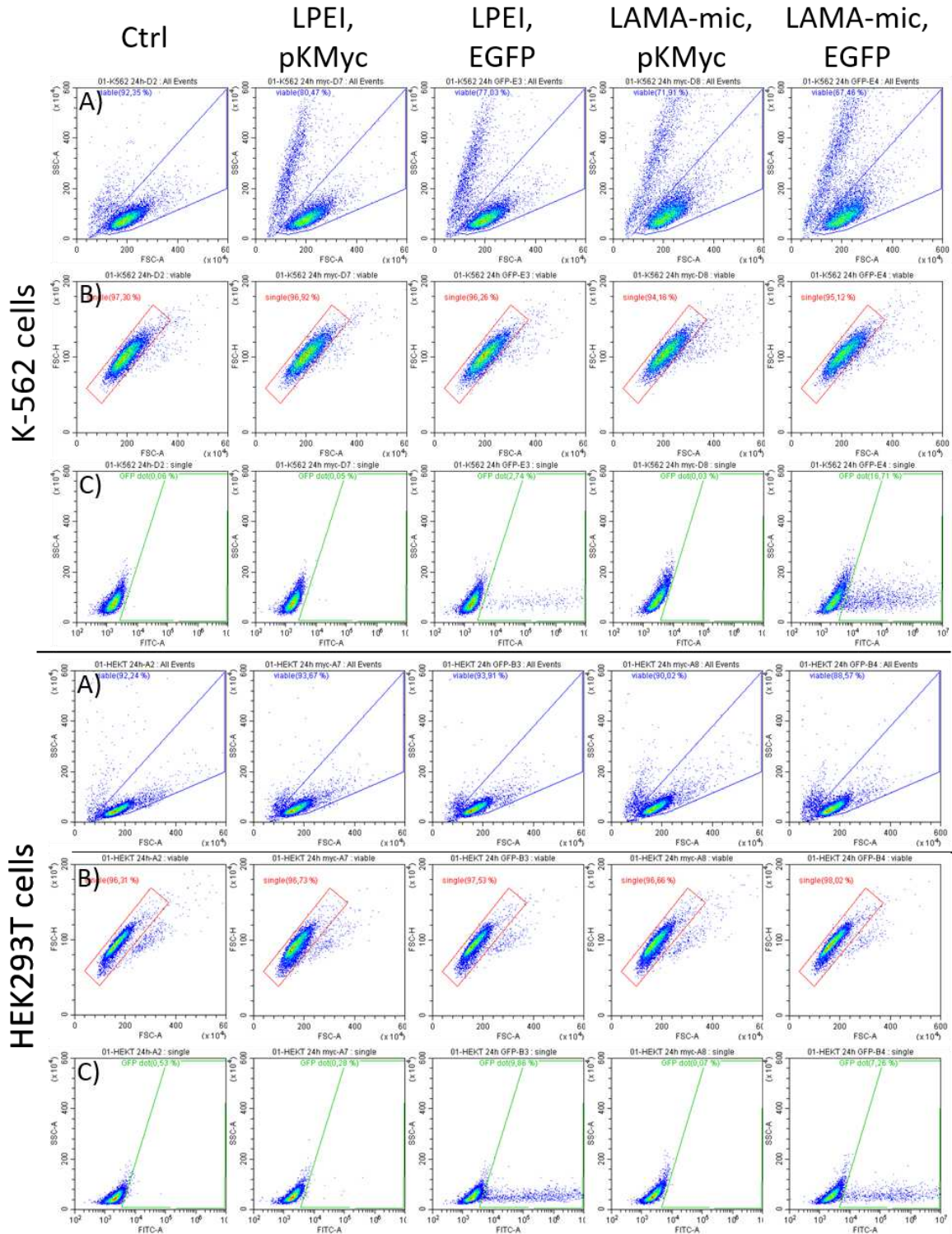


Figure S11. Gating strategy for pDNA transfection using the example of 24 h incubation. Viable single cells were gated in FSC/SSC and FSC-A/FSC-H dot plots (A,B). Subsequently cells with EGFP fluorescence were discriminated by gating to the respective pKMyC control.

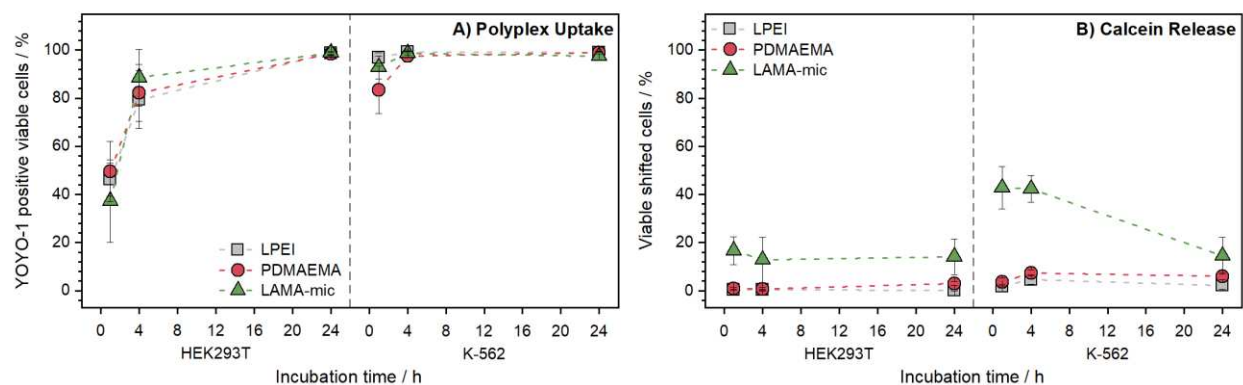


Figure S12. Investigation of the gene delivery process.

(A) Cellular internalization of LAMA-mic polyplexes in different cell lines. Cells were incubated with polyplexes of polymers and YOYO-1-labeled pDNA at N*/P 30 and analyzed *via* flow cytometry. Cells incubated with labeled pDNA served as control. Values represent mean \pm SD of % cells showing YOYO-1 fluorescence higher than the control ($n = 3$). (B) Endosomal escape of LAMA-mic polyplexes detected by the non-permeable dye calcein and analyzed *via* flow cytometry. Values represent mean \pm SD of % cells showing higher fluorescence intensity than the calcein control ($n = 3$).

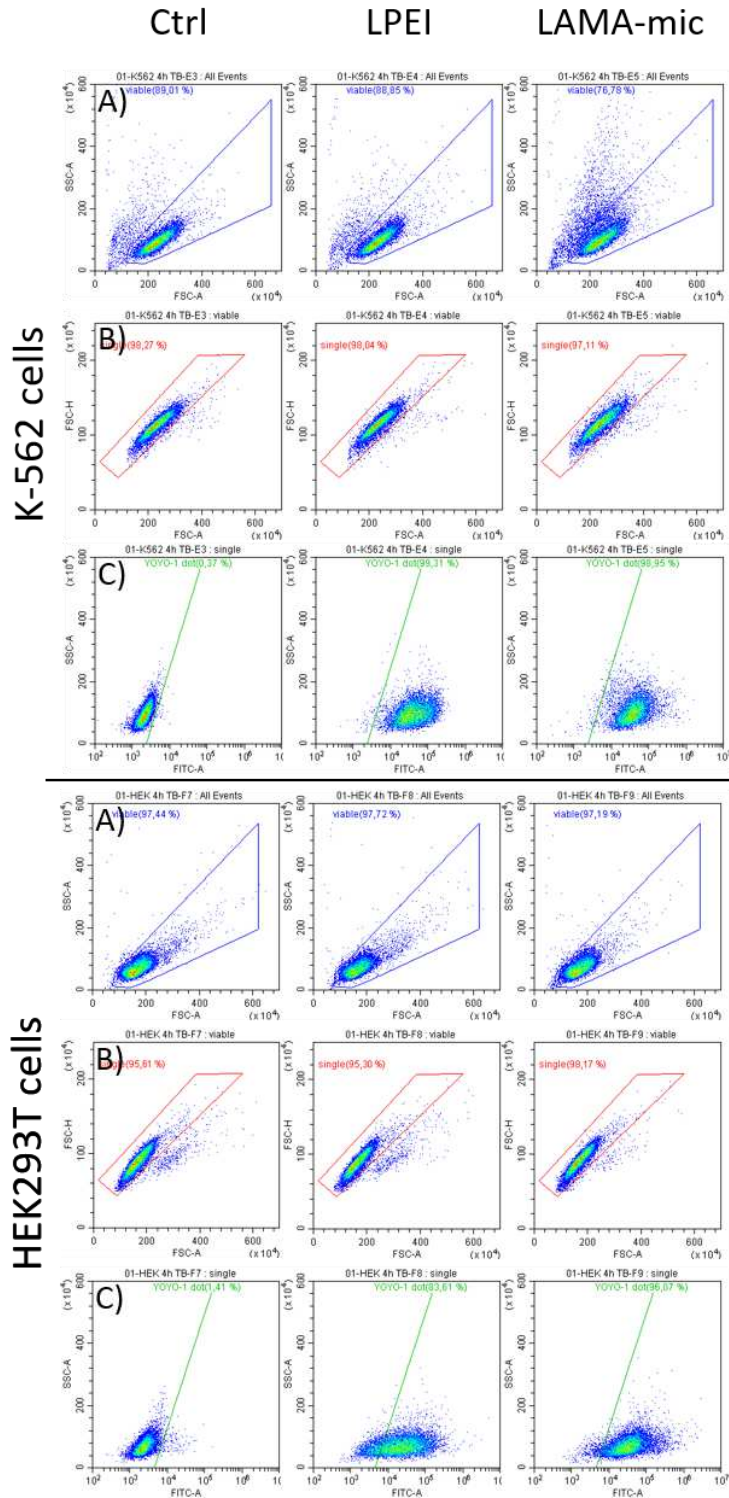


Figure S13. Gating strategy for polyplex uptake using the example of 4 h incubation.

Viable single cells were gated in FSC/SSC and FSC-A/FSC-H dot plots (A,B). Subsequently cells with YOYO-1 fluorescence were discriminated by gating to the pDNA-YOYO-1 control of the respective incubation time.

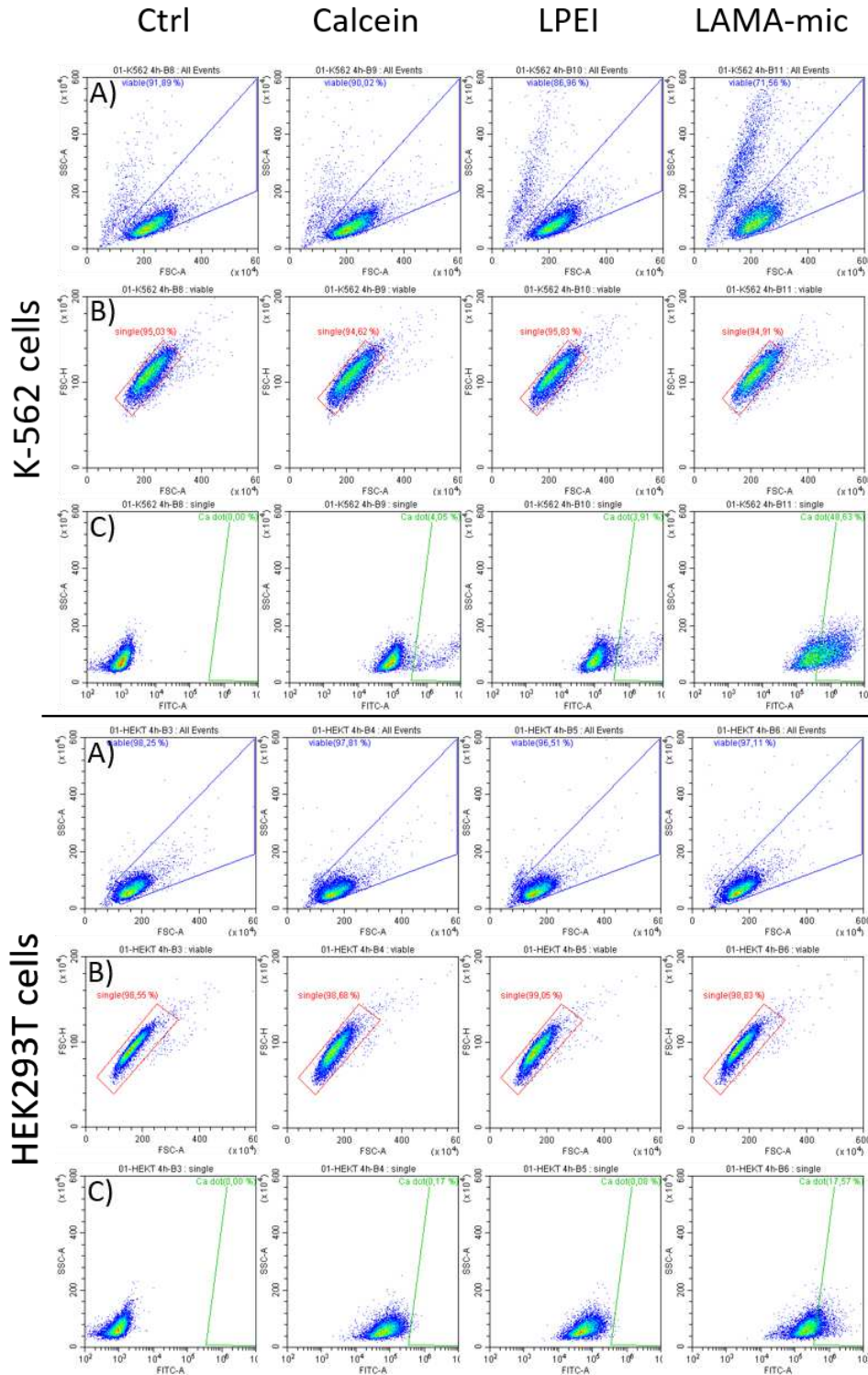


Figure S14. Gating strategy for calcein release using the example of the 4 h incubation.

Viable single cells were gated in FSC/SSC and FSC-A/FSC-H dot plots (A,B). Subsequently cells with calcein fluorescence higher than the control were discriminated by gating to the calcein control of the respective incubation time.

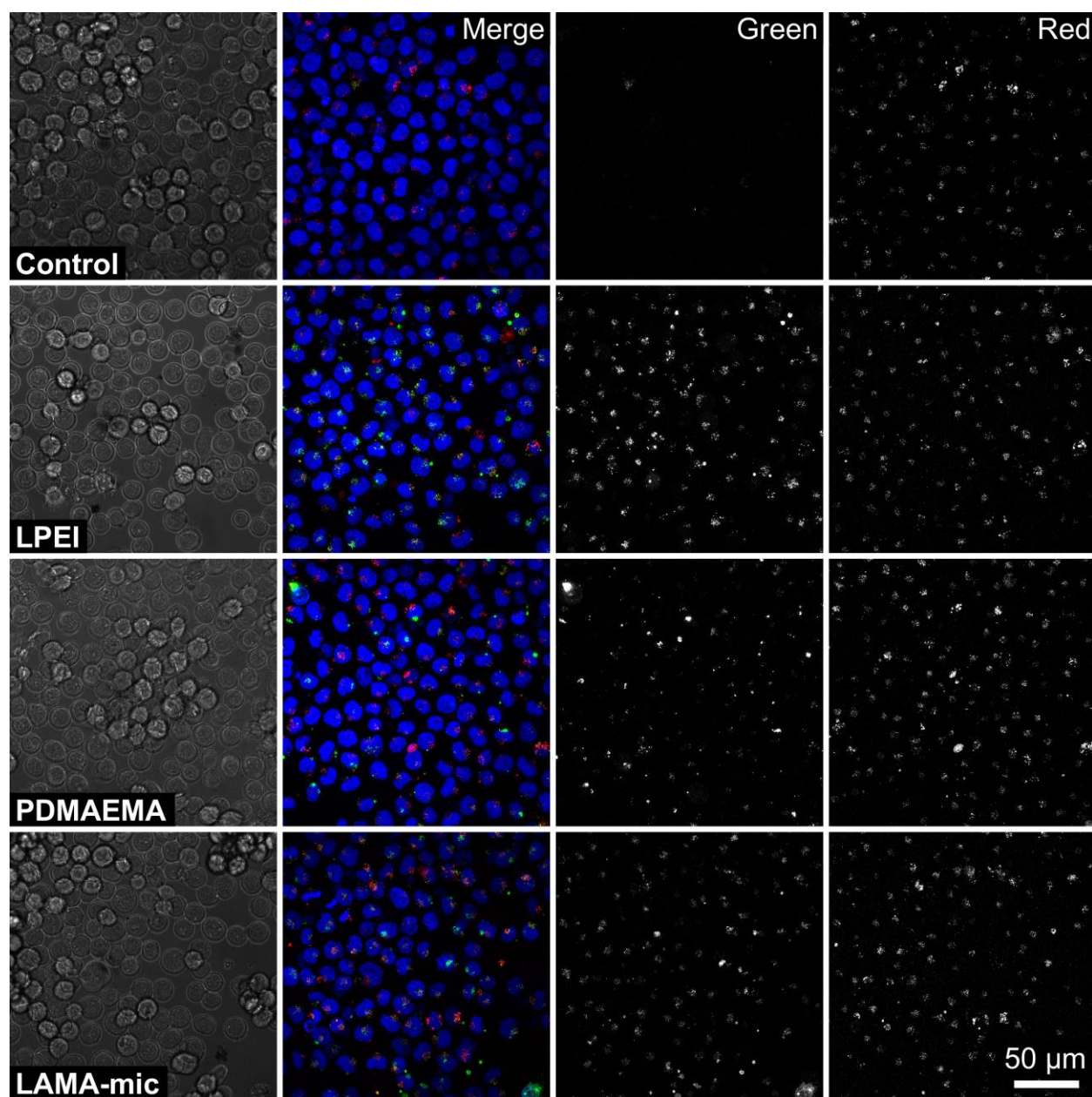


Figure S15. CLSM study of polyplex uptake in K-562 cells.

K-562 cells were incubated with polyplexes of YOYO-1-labeled pDNA and polymers at N*/P 30 in growth medium (R10 with 10 mM HEPES) for 1 h. Endolysosomes were stained with LysoTracker™ Red (red), Nuclei were stained with Hoechst 33342 (blue) and YOYO-1 fluorescence (green) was quenched with trypan blue.

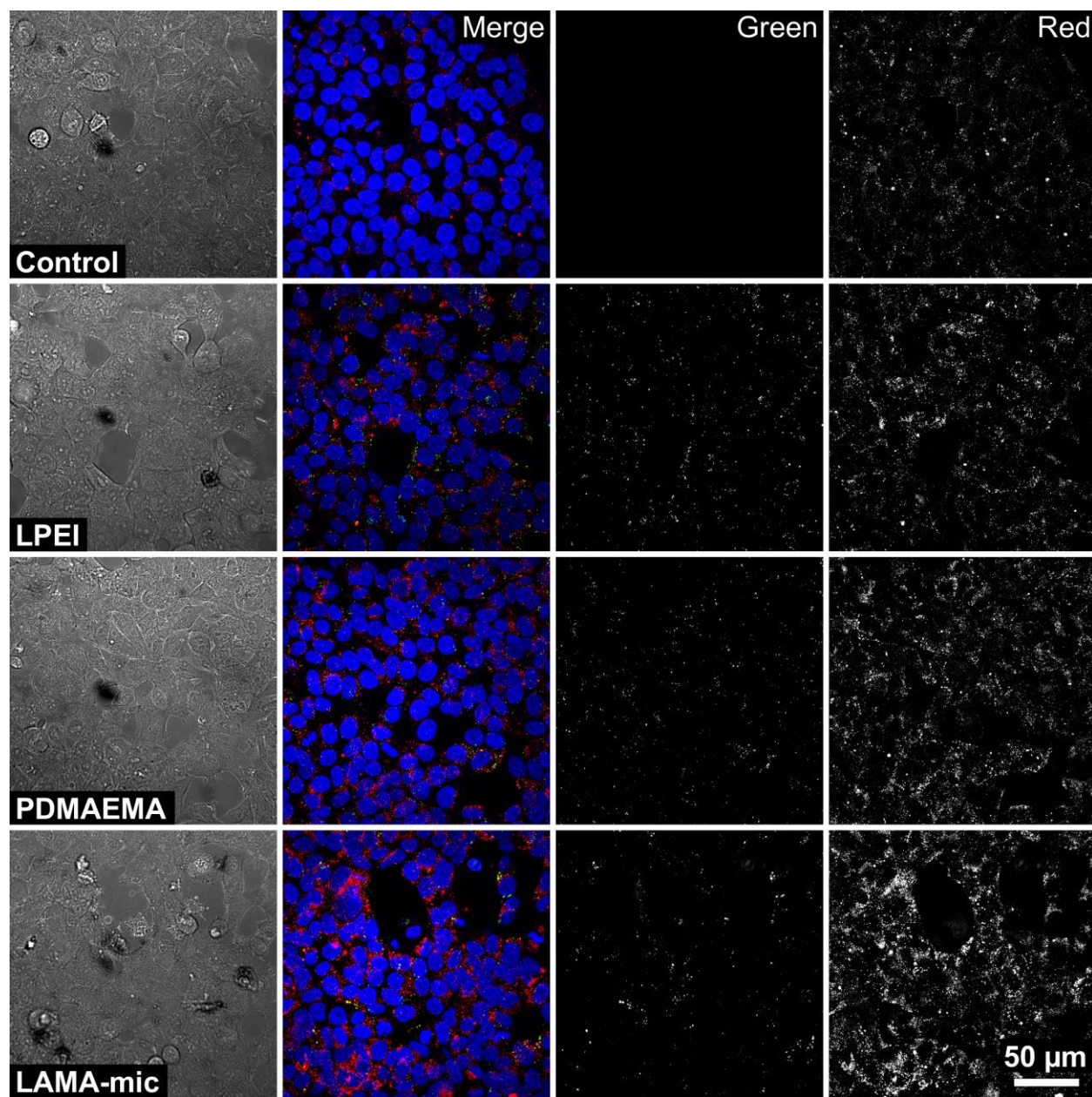


Figure S16. CLSM study of polyplex uptake in HEK293T cells.

HEK293T cells were incubated with polyplexes of YOYO-1-labeled pDNA and polymers at N*/P 30 in growth medium (D10 with 10 mM HEPES) for 1 h. Endolysosomes were stained with LysoTracker™ Red (red), nuclei were stained with Hoechst 33342 (blue) and YOYO-1 fluorescence (green) was quenched with trypan blue.

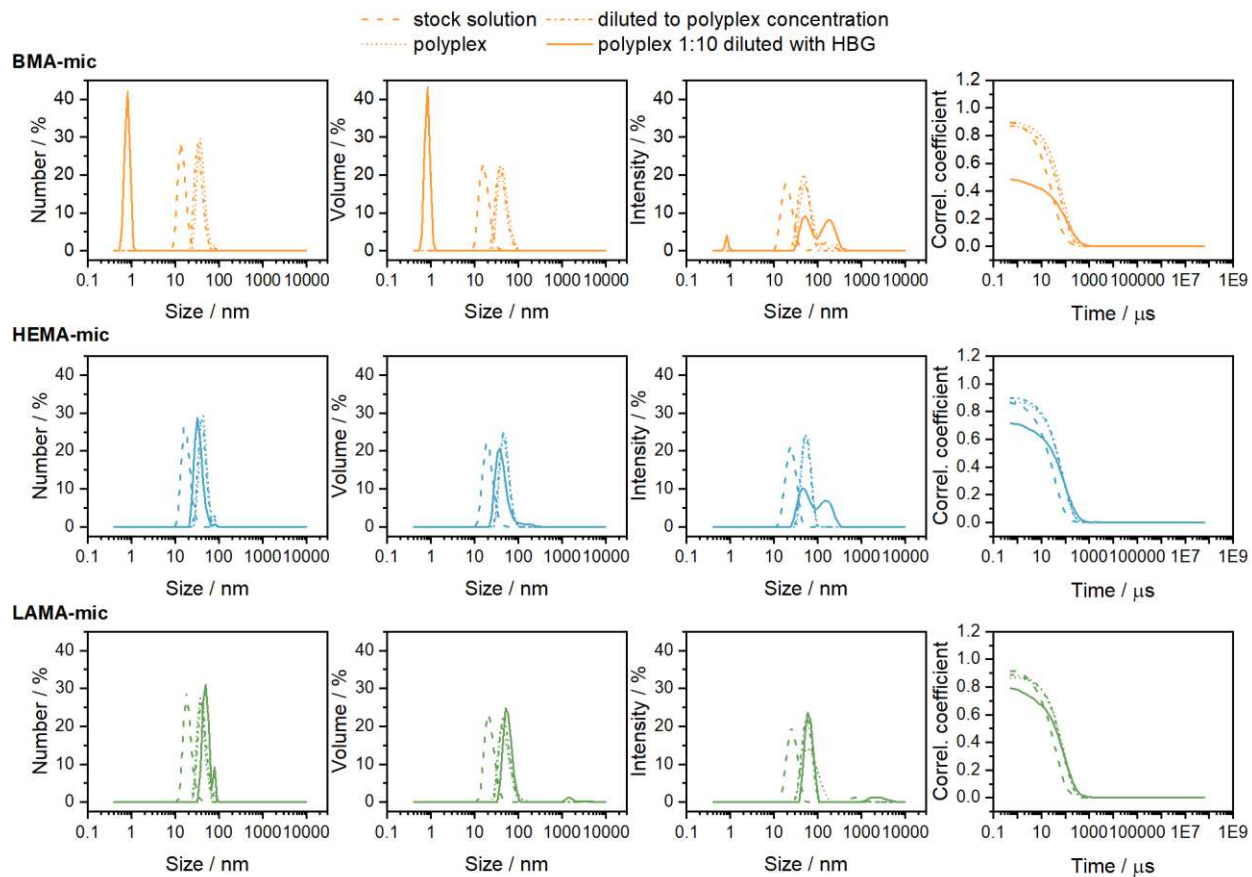


Figure S17. DLS measurement of the micelles at different concentrations.

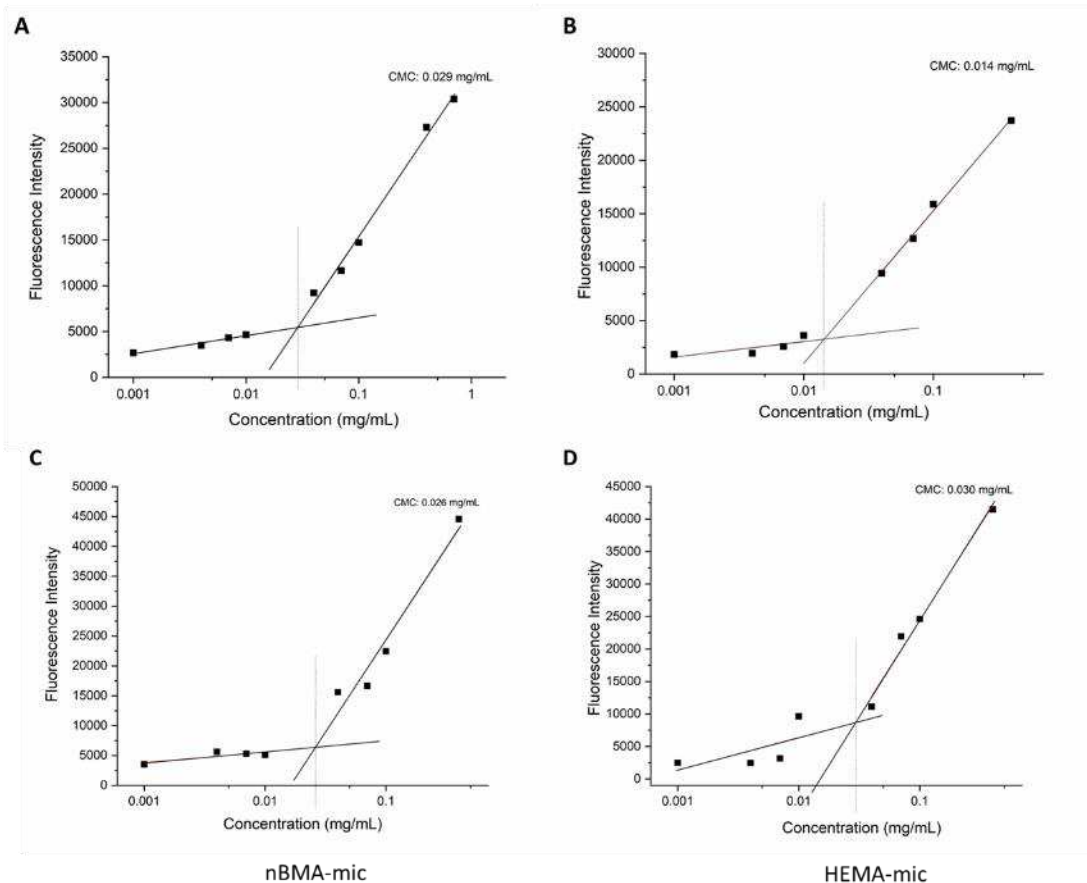


Figure S18. CMC determination.

Maximum of each fluorescence emission spectra was plotted versus the micelle concentration for each sample respectively at 25 °C with a Tecan Infinite M200 PRO microplate reader, using Nile Red as the fluorescence dye as a probe. A) LAMA-mic II, B) LAMA-mic I, C) nBMA-mic, D) HEMA-mic.

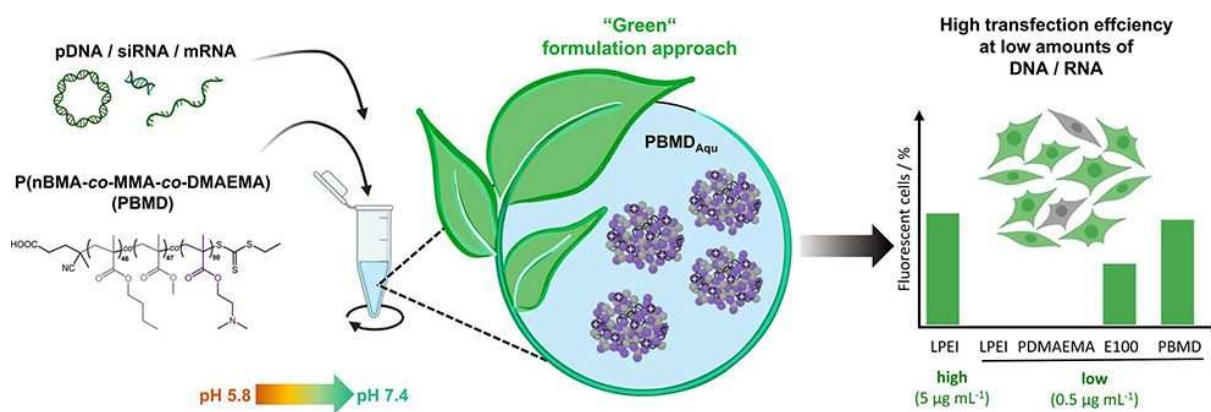
REFERENCES

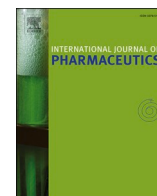
1. McRae Page S, Martorella M, Parelkar S, Kosif I, Emrick T: **Disulfide cross-linked phosphorylcholine micelles for triggered release of camptothecin.** *Molecular pharmaceutics* 2013, **10**:2684-2692.
2. Larnaudie S: **Supramolecular cyclic peptide-polymer nanotubes as drug delivery vectors.** University of Warwick, 2017.
3. Bauer M, Lautenschlaeger C, Kempe K, Tauhardt L, Schubert US, Fischer D: **Poly(2-ethyl-2-oxazoline) as Alternative for the Stealth Polymer Poly(ethylene glycol): Comparison of in vitro Cytotoxicity and Hemocompatibility.** *Macromol Biosci* 2012, **12**:986-998.
4. Richter F, Martin L, Leer K, Moek E, Hausig F, Brendel JC, Traeger A: **Tuning of endosomal escape and gene expression by functional groups, molecular weight and transfection medium: a structure-activity relationship study.** *J Mater Chem B* 2020, **8**:5026-5041.

Publication Pub5

Solely aqueous formulation of hydrophobic cationic polymers for efficient gene delivery

J. I. Solomun, G. Cinar, P. Mapfumo, F. Richter, E. Moek, F. Hausig, L. Martin, S. Hoepfner, I. Nischang, A. Traeger, *Int J. Pharm.*, **2021**, 593, 120080.





Solely aqueous formulation of hydrophobic cationic polymers for efficient gene delivery

Jana I. Solomun^a, Gizem Cinar^a, Prosper Mapfumo^a, Friederike Richter^a, Elisabeth Moek^a, Franziska Hausig^a, Liam Martin^a, Stephanie Hoeppener^{a,b}, Ivo Nischang^{a,b}, Anja Traeger^{a,b,*}

^a Laboratory of Organic Chemistry and Macromolecular Chemistry (IOMC), Friedrich Schiller University Jena, Humboldtstrasse 10, 07743 Jena, Germany

^b Jena Center for Soft Matter (JCSM), Friedrich Schiller University Jena, Philosophenweg 7, 07743 Jena, Germany

ARTICLE INFO

Keywords:

Aqueous formulation
Cationic polymer
Hydrophobicity
mRNA delivery
RAFT polymerization
siRNA delivery

ABSTRACT

Cationic polymers are promising gene delivery vectors due to their ability to bind and protect genetic material. The introduction of hydrophobic moieties into cationic polymers can further improve the vector efficiency, but common formulations of hydrophobic polymers involve harsh conditions such as organic solvents, impairing intactness and loading efficiency of the genetic material. In this study, a mild, aqueous formulation method for the encapsulation of high amounts of genetic material is presented. A well-defined pH-responsive hydrophobic copolymer, *i.e.* poly(*n*-butylmethacrylate)-*co*-(methylmethacrylate)-*co*-(2-(dimethylamino) ethylmethacrylate)), (PBMD) was synthesized by reversible addition fragmentation chain transfer (RAFT) polymerization. Exploiting the pH-dependent solubility behavior of the polymer, stable pDNA loaded nanoparticles were prepared and characterized using analytical ultracentrifugation (AUC), cryo-transmission electron microscopy (cryo-TEM) and dynamic light scattering (DLS). This novel formulation approach showed high transfection efficiencies in HEK293T cells, while requiring 5- to 10-fold less pDNA compared to linear polyethylenimine (LPEI), in particular at short incubation times and in serum-containing media. Furthermore, the formulation was successfully adopted for siRNA and mRNA encapsulation and the commercially approved polymer Eudragit® E(PO/100). Overall, the aqueous formulation approach, accompanied by a tailor-made hydrophobic polymer and detailed physico-chemical and application studies, led to improved gene delivery vectors with high potential for further applications.

1. Introduction

In the past years, it has been shown that several human diseases have a genetic origin and result in symptoms caused by a malfunction in the protein expression. Such malfunctions may be mitigated by the introduction of genetic material into affected cells (Dunbar et al., 2018; Pack et al., 2005). Furthermore, the introduction of nucleic acids such as pDNA and mRNA encoding for antigens is a promising approach for vaccination against infectious diseases and in tumor immunotherapies (Ginn et al., 2018; Hobernik and Bros, 2018; Lopes et al., 2019). Nucleic acids are easily degraded by ubiquitously present nucleases, and their negative net charge also hampers their ability to cross cellular membranes. Therefore, a suitable delivery system is required (Abdelhady et al., 2003; Yin et al., 2014). To date, mostly viral vectors have entered clinical trials for evaluation due to their natural ability to infect cells and

their high delivery efficiency. However, viral vectors are potentially immunogenic and pathogenic, encapsulate only a limited quantity of genetic material per vector, and can be costly to produce (Lundstrom, 2018; Shirley et al., 2020).

Polymer-based, synthetic systems represent a promising area of research to bypass the above-mentioned obstacles. The versatility in architecture, design, and functionalization of cationic polymers offers numerous possibilities to tune the interaction with genetic material, ultimately controlling the size, charge distribution, and stability of the polymer-DNA complexes under physiological conditions (Wong et al., 2007). Additionally, polymers possess the ability to protect negatively charged genetic material from degradation and can facilitate cellular uptake (Bloomfield, 1997). The cationic moieties further contribute to passing intracellular barriers such as the endosomal membrane to avoid lysosomal degradation and to release the intact genetic material at its

* Corresponding author at: Laboratory of Organic and Macromolecular Chemistry (IOMC), Friedrich Schiller University Jena, Humboldtstrasse 10, 07743 Jena, Germany.

E-mail address: anja.traeger@uni-jena.de (A. Traeger).

<https://doi.org/10.1016/j.ijpharm.2020.120080>

Received 26 August 2020; Received in revised form 5 November 2020; Accepted 8 November 2020

Available online 25 November 2020

0378-5173/© 2020 Elsevier B.V. All rights reserved.

desired site of action (Laechelt and Wagner, 2015; Pack et al., 2005). The introduction of hydrophobic moieties into cationic polymers has been found to be beneficial for delivery systems *in vitro* and *in vivo* as this facilitates association and interaction with the lipophilic cell membrane surfaces, thus, promoting cellular uptake and subsequent release from the endosomes (Adolph et al., 2014; Convertine et al., 2009; Incani et al., 2010; Liu et al., 2010; Wakefield et al., 2005). Furthermore, hydrophobicity can induce assembly of polymers in polar environments, improving the complex stability through hydrophobic interactions, particularly under physiological conditions in the presence of proteins and salts (Adolph et al., 2014; Eltoukhy et al., 2013; Rinkenauer et al., 2015a). Optimization of these effects can be facilitated through controlling the hydrophilic-hydrophobic balance within the polymer over the entire physiologically relevant pH range by fine-tuning the combination of cationic pH-responsive and hydrophobic groups (Convertine et al., 2009). The hydrophobic character of the polymers can be introduced in a number of ways, such as functionalization of the cationic polymer with lipophilic moieties such as acetyl groups, lipids, and cholesterol, (Forrest et al., 2004; Han et al., 2001; Schroeder et al., 2012) by the choice of the polymer backbone chemistry, (e.g., norbornenes, methacrylates, acrylates), (Breitenkamp and Emrick, 2008; Rinkenauer et al., 2015b; Smith et al., 2007; van de Wetering et al., 1999) or by introducing monomers in the polymer architecture with hydrophobic side chains such as alkanes, fluorinated, synthetic, or natural aromatic systems (Adolph et al., 2014; Buerkli et al., 2014; Cokca et al., 2020; Eltoukhy et al., 2013; Nelson et al., 2013; Shen et al., 2020; Tan et al., 2018; Wakefield et al., 2005). It was shown that hydrophobic modifications of e.g., poly(2-(dimethylamino)ethyl methacrylate) (PDMAEMA) led to enhancing effects on the gene delivery efficiency (Cheng et al., 2012; Convertine et al., 2009; Manganiello et al., 2012; Nelson et al., 2013). However, most studies were conducted with water-soluble polymers enabling complexation of genetic material in aqueous media. In this case, solubility was maintained by limiting the number of the hydrophobic groups incorporated into the polymer or by designing amphiphilic block copolymers that self-assemble into larger structures in solution (e.g., micelles). However, by a further increase in hydrophobicity, not only water solubility of the polymers is reduced, but also the encapsulation of the genetic material becomes more challenging due to the hydrophilic character of the nucleic acids. Therefore, the formulation method should be carefully designed to ensure sufficient complexation or encapsulation of the genetic material.

Common methods applied for formulation of nanoparticles from water-insoluble, hydrophobic polymers are the emulsion/solvent evaporation and the nanoprecipitation techniques. These methods are applicable to a wide variety of polymers and cargos, and allow to tune nanoparticle size and dispersity (Perevyazko et al., 2012; Yildirim et al., 2015). Genetic material can be encapsulated via different approaches: (i) pre-complexation with cationic polymers followed by encapsulation via emulsion techniques (Press et al., 2014); (ii) addition of the genetic material during the formulation (Cohen et al., 2000; Niu et al., 2009), (iii) complexation to the surface of preformulated cationic particles by electrostatic interactions (Bivas-Benita et al., 2004; Jain et al., 2015), or (iv) complexation of genetic material to the surface of particles coated with cationic surfactants or polymers (Fay et al., 2010). The emulsion method requires the application of ultrasonication or high-speed homogenization, exposing the genetic material to harsh conditions during the formulation process, potentially impairing its integrity and, therefore, its functionality (Lengsfeld and Anchordoquy, 2002). Subsequent addition of genetic material to preformulated nanoparticles is a possibility to avoid exposure to such harsh conditions. However, limitation of pDNA complexation to the nanoparticle surface potentially leads to reduced encapsulation/binding efficiencies compared to encapsulation within the nanoparticle. In comparison to the emulsion technique, nanoprecipitation is a relatively simple and mild method, which does not expose genetic material to high shear forces or temperatures during formulation. It also allows the encapsulation of genetic material during

the formulation process. However, the typical use of organic solvents, which potentially induce cytotoxicity and other adverse effects in biological systems, requires extensive post-formulation purification procedures (evaporation or dialysis) before they can be used as a therapeutic agent (Brayton, 1986; Jamalzadeh et al., 2016).

A well-known example for a hydrophobic cationic polymer used for nanoparticle formulation by the emulsion or nanoprecipitation technique is the commercial polymer Eudragit® E(PO/100) composed of a pH-responsive cationic 2-(dimethylamino)ethyl methacrylate (DMAEMA) unit copolymerized with *n*-butyl methacrylate (*n*BMA) and methyl methacrylate (MMA) as hydrophobic moieties in a typical mass ratio of 2:1:1. This copolymer was approved by the Food and Drug Administration (FDA) and European Medicines Agency (EMA) as a coating material for orally administered drugs and has been used for nanoparticle encapsulation and binding of several drugs (e.g., curcumin, genistein, efavirenz) (Hari et al., 2016; Moorthi et al., 2013; Tang et al., 2011) including genetic material. In a study by Lehr and colleagues, Eudragit® E(PO/100) nanoparticles formulated by the emulsion technique were used to bind siRNA and were shown to induce knock-down of the Bfl1/A1 gene in macrophages (Jain et al., 2015). Another approach by Singh and coworkers used nanoparticles composed of Eudragit® E(PO/100) and PLGA coated with the cationic surfactant cetyltrimethylammonium bromide (CTAB) to transport IL-10 encoding pDNA *in vivo* (Basarkar and Singh, 2009). Both studies demonstrated the potential of the Eudragit® E(PO/100) polymer for efficient gene delivery, but were limited to organic solvent-based formulation methods or surface binding of the genetic material.

The aim of this study was to fully exploit the potential of cationic hydrophobic polymers and to develop a new “green” and organic solvent-free formulation technique that allows the encapsulation of genetic material without the associated cytotoxic effects potentially imposed by the use of organic solvents. Reversible addition fragmentation chain transfer (RAFT) polymerization was used to synthesize a well-defined statistical copolymer P(*n*BMA-*co*-MMA-*co*-DMAEMA) (PBMD) with a monomer composition comparable to the Eudragit® E(PO/100) polymer. Firstly, the PBMD polymer was tested for pDNA binding and release capability in the physiologically relevant pH range (lysosomal to blood pH, pH 5 to pH 7.4). Subsequently, the PBMD polymer was used for encapsulation of pDNA by applying an organic solvent-free, pH-driven formulation technique. The formulated pDNA-polymer complexes (PBMD_{Aqu}(pDNA)) were then characterized by dynamic light scattering (DLS), cryo-transmission electron microscopy (cryo-TEM), and analytical ultracentrifugation (AUC). The transfection efficiency was compared to nanoparticles manufactured by the common nanoprecipitation method with surface-bound pDNA. The PBMD_{Aqu}(pDNA) complexes were further optimized for transfection efficiency in HEK293T cells. The optimized formulation and transfection conditions were then also applied to the commercially available polymer Eudragit® E(PO/100), and compared to other commercially-available and polymer-based transfection agents such as LPEI and Viromer® RED. Furthermore, the new formulation technique was successfully implemented for the complexation and transfection of siRNA and mRNA, thus demonstrating the broad application potential of the polymer and formulation method developed here.

2. Materials and methods

Materials and further methods can be found in the [supporting information](#) (SI).

2.1. Synthesis of P(*n*BMA-*co*-MMA-*co*-DMAEMA) (PBMD) via RAFT polymerization

(4-cyanopentanoic acid)ylethyl trithiocarbonate (CPAETC) (130.7 mg, 4.96×10^{-4} mol), *n*BMA (3.5 g, 2.48×10^{-2} mol), MMA (2.5 g, 2.52×10^{-2} mol), DMAEMA (7.8 g, 4.97×10^{-2} mol), 1,4-dioxane (6.2

g), a 1.0% (w/w) solution of 4,4-azobis(4-cyanovaleric acid) (ACVA) in 1,4-dioxane (1.4 g, 14.4 mg ACVA, 5.12×10^{-5} mol) and 1,3,5-trioxane (external NMR standard, 23.7 mg) were introduced to a 20 mL micro-wave vial equipped with a magnetic stirring bar. The vial was sealed, and the solution deoxygenated by bubbling argon through it for approx. 10 min. The vial was placed in an oil bath set at 70 °C and allowed to stir for 21 h, with samples taken for ^1H NMR and size exclusion chromatography in DMAc (DMAc-SEC) at designated times. The polymer was precipitated three times from THF into cold hexane and dried under reduced pressure to give a yellow solid. DMAc-SEC: $M_{n,SEC} = 25.1 \text{ kg mol}^{-1}$, $D = 1.13$.

2.2. Acid-base titration

Titration of the polymers was conducted using a Metrohm OMNIS integrated titration system (Metrohm, Herisau, Switzerland). For a typical measurement, the polymer was dissolved in 150 mM NaCl (in 0.02 M HCl) at 5 mg mL⁻¹. 9 mL of this solution was taken, and 1 M HCl (50 µL) was added to give an acidic solution (pH < 2). The polymers were titrated against 0.1 M NaOH solution to a pH value of ≈ 12. The pK_a values were estimated from equivalence points determined by the OMNIS titration software, using the Henderson-Hasselbalch equation (1), where [HA] is the concentration of acid and [A⁻] the concentration of the corresponding base:

$$\text{pH} = \text{pK}_a + \log \frac{[\text{A}^-]}{[\text{HA}]} \quad (1)$$

2.3. Gel retardation assay (GRA)

pDNA binding ability of LPEI, PDMAEMA, and the PBMD polymer at varying nitrogen to phosphate (N/P) ratios were determined by agarose gel electrophoresis. PDMAEMA and PBMD polymer were dissolved in 0.2 M sodium acetate buffer (pH 5.8) at a concentration of 2 mg mL⁻¹. LPEI was dissolved in water acidified with HCl at a concentration of 1 mg mL⁻¹. Subsequently, the polymers and the pKMyC pDNA stock solution in water were diluted in HBG buffer (5% (w/v) glucose, 20 mM (4-(2-hydroxyethyl)-1-piperazineethanesulfonic acid) (HEPES), pH 7.4) to the respective concentrations needed for various N/P ratios, mixed 1:2 by vortexing and incubated for 15 min. The samples were diluted 6:1 with green gel loading buffer (Jena Biosciences, Jena, Germany) and were run on a 1% (w/v) agarose gel stained with ethidium bromide (EtBr, 0.1 µg mL⁻¹) at 80 V for 1.5 h. The gels were subsequently imaged by using a gel imager (Red™ Imaging System, Alpha Innotech, Kasendorf, Germany).

2.4. Ethidium bromide binding assay (EBA) and heparin release assay (HRA)

pDNA complexation and complex stability were further investigated by using an EtBr quenching and heparin release assay as described elsewhere (Richter et al., 2020). Briefly, pKMyC-pDNA at a concentration of 15 µg mL⁻¹ was incubated with EtBr in HBG buffer (pH 7.4) for 10 min. The polymer stock solutions (prepared as described above) were diluted with HBG buffer (pH 7.4) in a black 96-well plate (Nunc, Thermo Fisher, Waltham, MA, U.S.) to reach N/P ratios ranging from 1 to 50. Subsequently, pDNA was added and the complexes were incubated at 37 °C for 15 min. EtBr fluorescence intensity was measured at $\lambda_{\text{Ex}} = 525 \text{ nm}$ / $\lambda_{\text{Em}} = 605 \text{ nm}$. pDNA without polymer was defined as 100% free pDNA. The release of complexed pDNA was studied by stepwise addition of heparin and measurement of the resulting changes in EtBr fluorescence intensity. Influence of the pH value on pDNA binding and release was studied by performing the assay at varying pH values in the respective buffers (0.2 M acetate buffer pH 5; 5.8 and HBG buffer pH 6.5; 7; 7.4). The obtained measurement points were fitted using Origin Pro Software (Version 2018b, Origin Lab Corporation, Northampton, MA, U.

S.) using either logistic or exponential functions to represent the apparent experimental results as a guide to the eye.

2.5. Aqueous formulation approach for pDNA encapsulation ((PBMD)_{Aqu}(pDNA))

A stock solution of the PBMD polymer was prepared by dissolution in 0.2 M sodium acetate buffer (pH 5.8). pDNA (pCMV-GFP, mEGFP-N1 or pKMyC) was dissolved in ultrapure water. The solutions were stored at 4 °C prior to use. To prepare PBMD_{Aqu}(pDNA) complexes the PBMD polymer and the pDNA were, accordingly to the GRA and EBA, diluted in HBG buffer (pH 7.4; for DLS and transfection experiments) or 20 mM HEPES buffer (for cryo-TEM and AUC measurements) to reach the respective N/P ratios and mixed in a ratio of 1:2. The mixtures were vortexed immediately for 10 s and incubated for at least 15 min at room temperature (RT) before usage.

2.6. Organic solvent-based formulation of nanoparticles (PBMD)_{Org}(out, pDNA), PBMD)_{Org}(in,pDNA))

For nanoparticle formulation, the polymer was dissolved in 2.5 mL acetone (2 mg mL⁻¹). The polymer solution was dropped manually into 5 mL ultrapure water and the resulting nanoparticle suspension was stirred at 800 rpm overnight to allow the organic solvent to evaporate. Then, the suspensions were stored at 4 °C until usage. To determine the concentration after solvent evaporation, a known volume of the nanoparticle suspension was lyophilized, and the dry residues were weighed afterwards. To reach the respective N/P ratios, pDNA (pCMV-GFP) at varying concentrations was either added during the formulation process to the polymer dissolved in acetone (prior to precipitation in water, PBMD_{Org}(in,pDNA)) or after nanoprecipitation to the final aqueous particle suspension (PBMD_{Org}(out,pDNA)).

2.7. Dynamic light scattering (DLS)

Hydrodynamic diameter and zeta potential of PBMD_{Org}(out,pDNA), PBMD_{Org}(in,pDNA), and PBMD_{Aqu}(pDNA) complexes formulated with pCMV-GFP pDNA at varying N/P ratios were determined by using dynamic and electrophoretic light scattering (DLS/ELS, Zetasizer Nano-ZS, Malvern Instruments, Worcestershire, U.K.). The nanoparticles were diluted in ultrapure water for size and zeta potential determinations. PBMD_{Aqu}(pDNA) complexes were prepared at a pDNA concentration of 15 µg mL⁻¹ in 50 µL HBG buffer for size measurements and were further diluted to 800 µL with ultrapure water for zeta potential determination. The instrument was operated with a 633 nm He-Ne Laser and intensity fluctuations at a backscattering angle of 173° at a temperature of 25 °C were measured. At least three batches were measured per sample. The derived hydrodynamic diameters are presented as mean ± SD. Large aggregates (≥1000 nm) were considered as a fixed value (1000 nm) when calculating the mean and standard deviation. Original data, exemplary decay functions, and derived hydrodynamic diameter distributions are shown in the SI (Table S1 to S4, Fig. S2, S3).

2.8. Cryo-transmission electron microscopy (cryo-TEM) and scanning electron microscopy (SEM) measurements

PBMD_{Aqu}(pDNA) at N/P 20 using mEGFP-N1 pDNA in 20 mM HEPES buffer and PBMD_{Org}(in,pDNA) nanoparticles using pCMV-GFP pDNA were prepared as described above. Electron microscopy imaging was performed with a Sigma VP Field Emission Scanning Electron Microscope (Carl-Zeiss, Jena, Germany) using an InLens detector with an acceleration voltage of 6 kV. The samples were coated with a thin layer of platinum (4 nm) via sputter coating (CCU-010 HV, Safematic, Zizers, Switzerland). Cryo-TEM investigations were performed on a FEI Tecnai G² 20 transmission electron microscope at an acceleration voltage of 200 kV. Samples were blotted onto a Quantifoil grid (R 2/2, Quantifoil,

8.5 μL of solutions with a concentration of 250 $\mu\text{g mL}^{-1}$ utilizing a Vitrobot Mark IV preparation unit (blotting time 1 s, offset -6 mm). Samples were vitrified utilizing liquid ethane as a cryogen. After blotting, the sample temperature was maintained at a temperature below $-165\text{ }^{\circ}\text{C}$ at all times. The grids were loaded into the cryo-holder (Gatan 626) using the Gatan cryo transfer stage. Images were acquired with a CCD camera (MegaView, Olympus Soft Imaging Solutions, Muenster, Germany). Contrast adjustments and image analysis was performed by ImageJ (Version 1.52a, National Institutes of Health, Bethesda, MD, U.S.).

2.9. Sedimentation velocity experiments via analytical ultracentrifugation (AUC)

The PBMD_{Aqu}(pDNA) complexes and PDMAEMA polyplexes at N/P 20 were prepared in 20 mM HEPES buffer using td-tomato-N1 pDNA to obtain concentrations up to 1 mg mL^{-1} . The complexes were investigated via sedimentation velocity AUC experiments at different concentrations (0.1–1 mg mL^{-1}) using the universal refractive index (RI) detection in terms of interference fringes and the absorbance detection in terms of optical density (OD). A rotor speed of 7,500 rpm was used for 24 h, followed by spinning the rotor at a speed of 42,000 rpm for a further 24 h in order to investigate potentially present smaller species. All AUC experiments were performed using an Optima AUC (Beckman Coulter Instruments, Brea, CA, U.S.) with an An-50 Ti eight-hole rotor. The ultracentrifuge cells contained double sector epon centerpieces with a 12 mm optical solution path length. The cells were assembled with sapphire windows. The corresponding sectors were filled with approx. 440 μL pure solvent in the reference sector and approx. 420 μL of diluted sample solution in the sample sector. Rotor position eight was used as the counterbalance and for the optical module calibration. Scans were acquired in six-minute intervals. All experiments were performed at $20\text{ }^{\circ}\text{C}$. The RI detection as well as absorbance detection in terms of OD at the wavelength of the RAFT-agent containing polymer, i.e. at $\lambda = 310\text{ nm}$, and that of the DNA, i.e. at $\lambda = 260\text{ nm}$, were utilized for the observation of sedimentation boundaries in respect to time in the AUC cells. The recorded sedimentation velocity data were numerically analyzed with SEDFIT and the $ls - g^*(s)$ model considering non-diffusing species (Schuck and Rossmanith, 2000).

2.10. Transfection of HEK293T cells with mEGFP-N1 pDNA

The HEK293T cell line was cultured in Dulbecco's modified eagle medium (DMEM, 1 g L^{-1} glucose, 10% (v/v), fetal bovine serum (FBS), 100 U mL^{-1} penicillin and 100 $\mu\text{g mL}^{-1}$ streptomycin) (growth medium) at $37\text{ }^{\circ}\text{C}$ in a humidified 5% (v/v) CO_2 atmosphere. For transfection experiments, 0.2×10^6 cells mL^{-1} were seeded into a 24-well plate in 500 μL growth medium supplemented with 10 mM HEPES and allowed to recover for 24 h. 1 h prior to treatment, medium was changed to 450 μL fresh growth medium (with 10 mM HEPES). PBMD_{Aqu}(pDNA) complexes and LPEI and PDMAEMA polyplexes were freshly prepared as described above using mEGFP-N1 pDNA and pKMyC pDNA (not encoding for green fluorescent protein as negative control). Cells were treated with 50 μL sample solution of the indicated N/P ratio and pDNA concentration or HBG buffer as control and incubated for 1 or 4 h. Subsequently, the supernatant was removed, replaced by fresh growth medium (with 10 mM HEPES) and the cells were further incubated up to 24 h. After incubation, the cells were detached by trypsin-EDTA, resuspended in Hank's Balanced Salt Solution (HBSS) (2% (v/v) FBS, 20 mM HEPES) and measured by flow cytometry (CytoFlex S, Beckmann Coulter, Brea, CA, U.S.). A quantity of 10^4 cells was analyzed by their forward and sideward scatter (FSC/SSC) to determine the viable single cells. The EGFP expression of the viable single cells was analyzed at $\lambda_{\text{Ex}} = 488\text{ nm}$ combined with a 525/40 nm bandpass filter (FITC channel). Fluorescent cells were identified by gating to the negative control not encoding for EGFP (pKMyC-polymer complex). A detailed gating

strategy is shown in the supporting information (SI, Fig. S5). Further, the cells were imaged by using a Cytation5 Cell Imaging Multi-Mode Reader (BioTek Instruments, Inc., Winooski, VT, USA) equipped with a 4x objective using brightfield imaging and the FITC channel ($\lambda_{\text{Ex}} = 469/35\text{ nm}$, $\lambda_{\text{Em}} = 525/39\text{ nm}$). Images were processed using ImageJ software

2.11. Knock-down of GFP in HEK-GFP cells using anti-GFP-siRNA

The HEK-GFP cell line was cultivated in growth medium at $37\text{ }^{\circ}\text{C}$ in a humidified 5% (v/v) CO_2 atmosphere. 24 h prior to transfection experiments, 0.1×10^6 cells mL^{-1} were placed in a 24-well plate in 500 μL growth medium supplemented with 10 mM HEPES and allowed to grow. The growth medium was replaced by 450 μL fresh growth medium (with 10 mM HEPES) 1 h prior to treatment. PBMD_{Aqu}(siRNA) complexes were freshly prepared as described for pDNA-complexes using anti-GFP siRNA (sense: GCAAGCUGACCCUGAAGUUCAU, antisense: GAACUUCAGGGU-CAGCUUGCCG and neg. control siRNA (sense: UUCUCCGAACGUGU-CACGUdTdT, antisense: ACGUGACACGUUCGGAGAAdTdT). The cells were treated with 50 μL of the freshly prepared complexes. Complexes with negative control siRNA and HBG buffer were used as negative controls. Lipofectamine was used as a commercial positive control prepared according to the manufacturers protocol using the same siRNA concentration as for the PBMD_{Aqu}(siRNA) complexes. 24 h after treatment, the samples were removed, replaced by fresh growth medium (with 10 mM HEPES), and incubated up to 72 h. The cells were detached with trypsin-EDTA. After resuspension in HBSS, the cells were analyzed by flow cytometry at an excitation wavelength of 488 nm and a 525/40 nm bandpass filter (OD1; FITC-OD1 channel). The gating strategy is shown in the SI (Fig. S6).

2.12. Transfection of HEK293T cells with GFP-mRNA

The HEK293T cell line was cultivated and seeded into 24-well plates prior to experiments as described above. The medium was replaced by 450 μL fresh growth medium (10 mM HEPES) 1 h prior to treatment. PBMD_{Aqu}(mRNA) complexes with GFP-mRNA were freshly prepared as described for pDNA complexes. Complexes with Viromer® RED were prepared as described by the manufacturers protocol and subsequently diluted to the respective mRNA concentration. 50 μL of the samples was added to the cells and incubated for 4 h. Subsequently, the samples were replaced by fresh growth medium and the cells were incubated for another 20 h. After incubation, the cells were detached by trypsin-EDTA and resuspended in HBSS for analysis by flow cytometry. The fluorescence of the viable single cells was analyzed at $\lambda_{\text{Ex}} = 488\text{ nm}$ using the FITC channel (gating strategy: Fig. S7).

2.13. PrestoBlue™ assay for determination of cytotoxicity in HEK293T and L-929 cells

For cytotoxicity assays, HEK293T cells were seeded into 24-well plates at a density of 0.2×10^6 cells mL^{-1} in 500 μL growth medium (with 10 mM HEPES) and incubated for 24 h to allow cell recovery. After a media change to 450 μL fresh growth medium 1 h prior to treatment, 50 μL of PBMD_{Aqu}(pDNA) complex was added to test a concentration range of 0.25–1.5 $\mu\text{g mL}^{-1}$ pDNA. The cells were incubated with the samples for 1, 4 or 24 h. Subsequently, the supernatant was removed and replaced with 500 μL fresh growth medium (with 10 mM HEPES). 24 h after treatment, the medium was replaced by a 10% (v/v) solution of PrestoBlue™ diluted with growth medium. The cells were incubated for 45 min and the supernatant was transferred to a 96-well plate (100 μL per well) to measure fluorescence intensity ($\lambda_{\text{Ex}} = 560\text{ nm}$, $\lambda_{\text{Em}} = 590\text{ nm}$). Cells treated with HBG buffer were used as a control, and the viability was calculated relative to the buffer control after subtracting the blank (PrestoBlue™ diluted in medium 1:10 without cells). Data were fitted in OriginPro2018b (OriginLab Corporation, Northampton, MA, U.S) with a logistic function. The IC_{50} was calculated as the value

where the samples show 50% viability relative to the control.

For toxicity tests in L-929 cells, the cells were seeded in a 96-well plate format at a density of 0.1×10^6 cells mL⁻¹ and incubated with the dissolved polymers without addition of pDNA for 1, 4 or 24 h. Cell viability was analyzed as described for the HEK293T cells.

2.14. Statistical analysis

Data analysis was conducted using OriginPro2018b software. Multiple groups were analyzed by one-way analysis of variance (one-way ANOVA) followed by Bonferroni's post-hoc test. Normality and homogeneity of variances were assumed. Sample pairs were analyzed by the unpaired t-Test and the Welch-correction was applied when homogeneity of variances was not given. Statistical significance is denoted as follows: * $P < 0.05$, ** $P < 0.01$, and *** $P < 0.001$.

3. Results and discussion

3.1. Polymer synthesis and characterization

The terpolymer P(*n*BMA-co-MMA-co-DMAEMA) (PBMD) was prepared via RAFT polymerization in 1,4-dioxane at 70 °C using (4-cyanopentanoic acid)ylethyl trithiocarbonate (CPAETC) as the chain transfer agent (CTA) and 4,4'-azobis(4-cyanovaleric acid) (ACVA) as the azoinitiator (Fig. 1a). An overall degree of polymerization (DP_n) of 200 was targeted with a 2:1:1 molar ratio of DMAEMA, *n*BMA, and MMA, respectively, at a combined monomer concentration of 62% (w/w) and a [CPAETC]₀/[ACVA]₀ ratio of 10. The polymerization kinetics were followed using ¹H NMR spectroscopy and SEC (Fig. 1b). The Ln([M]₀/

[M]) plot revealed a pseudo first-order polymerization kinetics for all three monomers, each reaching a final conversion of approximately 90% after 21 h. Furthermore, the rate of polymerization for each monomer was found to be very similar, indicating a statistical distribution of moieties throughout the terpolymer backbone and a consistent composition of different molar ratios. The linear evolution of molar mass values with monomer conversion (Fig. 1b) and narrow molar mass distributions ($D = 1.14$) indicate that the RAFT polymerization proceeded in a controlled fashion. The purified polymer possessed a theoretical molar mass ($M_{n,th}$) of 25.4 kg mol⁻¹ and a molar fraction of 0.51, 0.25, and 0.24 for DMAEMA, *n*BMA, and MMA, respectively, as calculated from ¹H NMR (Fig. 1c). A PDMAEMA homopolymer ($DP_n = 101$), containing a similar number of DMAEMA monomers per chain as the PBMD polymer, served as a control polymer (SI, Fig. S1).

To assess the solubility behavior and pH responsiveness of the PBMD polymer at physiological conditions, titration experiments were conducted (Fig. 1d). The PBMD polymer was dissolved under acidic conditions in 150 mM NaCl and titrated against 0.1 M NaOH. It should be noted that precipitation of the PBMD polymer was observed at higher pH values. Using the Henderson-Hasselbalch equation, the pK_a from the resulting titration curve gives a value of $pK_a \sim 6.9$, noticeably lower than the pK_a value reported for PDMAEMA (pK_a 7.4) (van de Wetering et al., 1999). This decreased pK_a value may be attributed to the PBMD polymer chains precipitating out of solution at lower degrees of DMAEMA protonation, due to the incorporation of hydrophobic comonomers. Therefore, the calculated value for the PBMD polymer was only designated as apparent pK_a of the polymer. Above all, the polymer exhibited a pH-dependent behavior as well as pH-dependent solubility, within the physiological pH range.

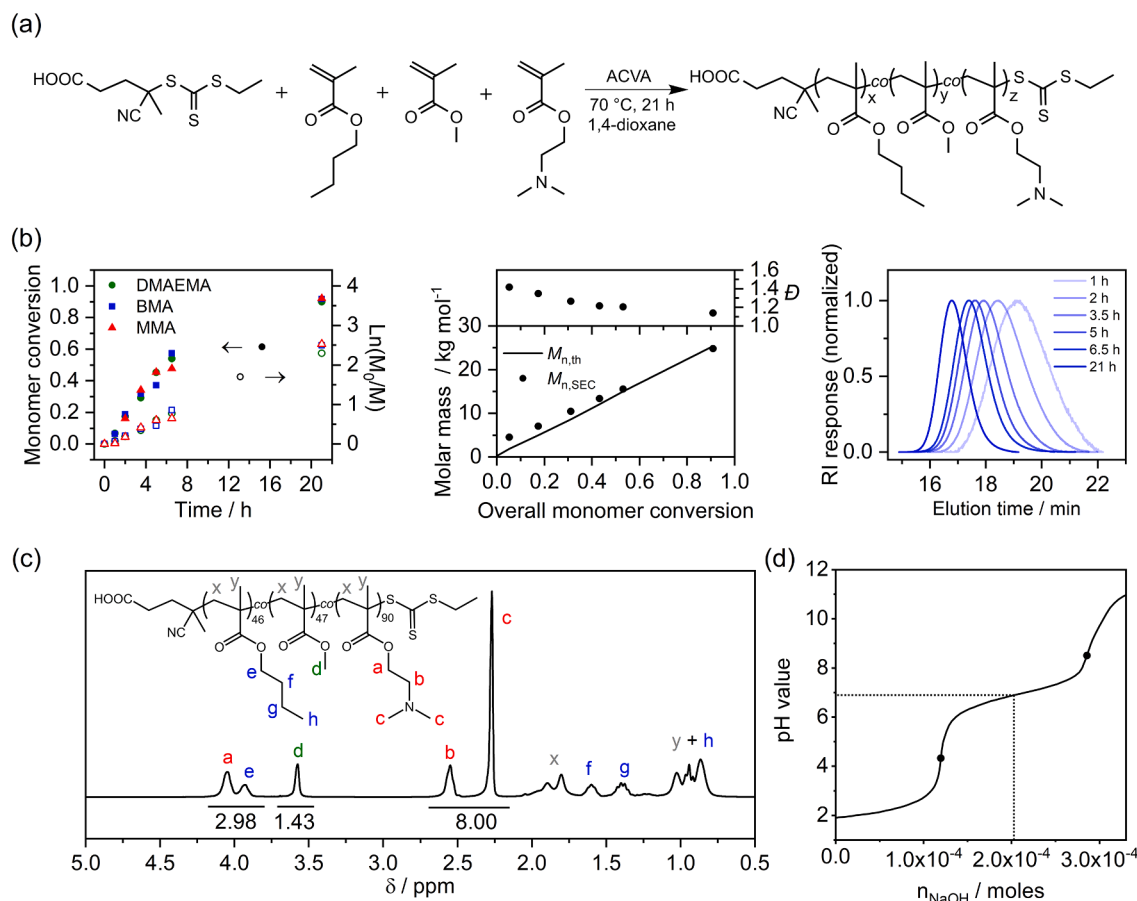


Fig. 1. Synthesis and characterization of P(*n*BMA-co-MMA-co-DMAEMA) (PBMD). (a) Polymerization synthesis scheme of P(*n*BMA-co-MMA-co-DMAEMA) (PBMD) via statistical RAFT polymerization. (b) Polymerization kinetics of the RAFT polymerization of PBMD as determined by ¹H NMR and SEC. (c) ¹H NMR of purified PBMD, and (d) titration curve of PBMD in 150 mM NaCl.

3.2. pDNA binding and release behavior

An efficient binding of pDNA is the first crucial step in the gene delivery process and required for protection and transport of genetic material. To assess the pDNA binding ability of the PBMD polymer under aqueous conditions, agarose gel electrophoresis was performed for different nitrogen (of the polymer) to phosphate (of the pDNA) ratios (N/P ratios), by dissolving the PBMD polymer in acidic sodium acetate buffer. LPEI and a PDMAEMA homopolymer were investigated as controls, the latter composed of the same number of cationic groups as the PBMD polymer. In the so-called gel retardation assay (GRA), non-

complexed pDNA typically appears with multiple bands representing various plasmid conformations, while complex formation with polymers prevents pDNA migration (Meyers et al., 1976). For all polymers, free pDNA was detectable at N/P 1, but at N/P ratios of 5 and higher, PBMD and the other polymers showed efficient complexation (Fig. 2a). To investigate the pDNA-polymer-interaction in more detail, the binding was further characterized by the ethidium bromide binding assay (EBA). The fluorescence of ethidium bromide (EtBr) is reduced in the presence of water, while it is increased by intercalation into the hydrophobic region between DNA base pairs (LePecq and Paoletti, 1967; Olmsted and Kearns, 1977). EtBr can be displaced by complex formation of pDNA

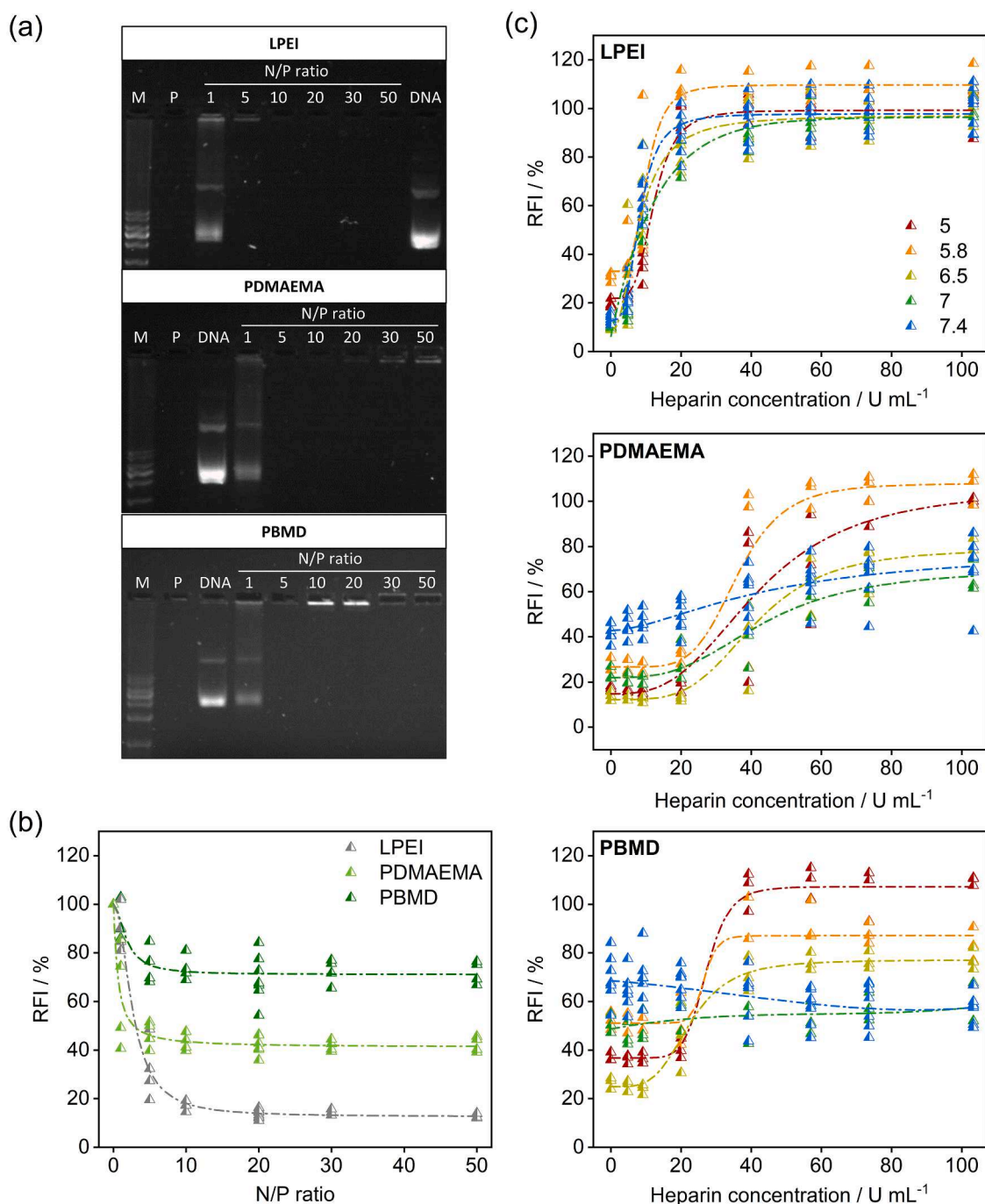


Fig. 2. DNA binding and release behavior of the PBMD polymer, PDMAEMA, and LPEI. pDNA binding ability of the polymers was studied by (a) agarose gel electrophoresis (M: marker; DNA: pDNA; P: polymer without pDNA) and (b) EBA in HBG buffer at pH 7.4 at different N/P ratios (1–50). (c) To investigate the pH dependent stability, DNA binding and release was studied by performing EBA and HRA with complexes formed at N/P 20 in a pH range from 5 to 7.4, representing the physiologically relevant pH range during transfection experiments.

with cationic polymers, which leads to a reduction in fluorescence intensity, used to study polymer interaction (Geall and Blagbrough, 2000; Trutzschler et al., 2018). The EBA was performed with increasing N/P ratios to assess the influence of increasing polymer amount on complex formation. At pH 7.4, all polymers showed a N/P ratio-dependent decrease in relative fluorescence intensity (RFI) reaching a plateau at N/P 10, indicating stable complex formation (Fig. 2b). Interestingly, the binding behavior of the polymers differed considerably, with LPEI showing strong EtBr exclusion (13% free pDNA), followed by PDMAEMA (42% free pDNA) and PBMD (72% free pDNA). The complete complexation of pDNA (GRA) and the different plateaus reached for each polymer indicated differences in the polymer-pDNA interactions. It can be assumed that the low charge density and pronounced hydrophobicity of PBMD causes a lower pDNA condensation compared to PDMAEMA or LPEI, the latter being known for a high charge density. Further, a larger proportion of hydrophobic interactions and therefore a more hydrophobic environment within the complex can be responsible for a reduced displacement of EtBr or even reduced quenching of EtBr by exclusion of water as fluorescence quencher from the complex (LePecq and Paoletti, 1967).

To investigate the stability of pDNA complexation and demonstrate its dynamic release behavior in the relevant physiological pH range, the dissociation of the complexes was studied by incubation with the competing polyanion heparin at pH values ranging from 5 (lysosomal/endosomal pH) to 7.4 (blood/cytosolic pH) (Bertschinger et al., 2006). The resulting release of pDNA from the complex enables the reintercalation of EtBr and increased RFI values.

Interestingly, the observed pDNA release behavior of the investigated polymers differed substantially (Fig. 2c). While 20 U mL⁻¹ heparin was sufficient to release pDNA from LPEI complexes irrespective of the pH, the influence of the pH value increased from PDMAEMA to PBMD (Fig. 2c). The total release of pDNA from PDMAEMA complexes at more acidic pH values required elevated heparin concentrations (~60 to 100 U mL⁻¹), while at higher pH values no complete release could be observed. The PBMD polymer showed an even more pronounced pH-dependent behavior with complete pDNA release only observed at pH 5, whereas with increasing pH values, the RFI values were rather reduced at higher heparin concentrations (>40 U mL⁻¹).

Variation of the pH value is affecting the balance between positive charge and hydrophobicity of the polymers, noticeably more pronounced in the case of the PBMD polymer due to the additional hydrophobic side chains (nBMA and MMA). It can be assumed that the PBMD-complexes are more stable at neutral pH values, since the increasing hydrophobic interactions at neutral pH values seem to prevent interaction with competing polyanions such as glycoproteins or negatively charged amino acids of serum proteins. This stabilizing effect

was shown for water-soluble polymers where hydrophobic modifications increased complex stability and, thus, transfection efficiency (Eltoukhy et al., 2013; Nelson et al., 2013; Wang et al., 2018). Since high stability in the presence of polyanions and the prevention of premature dissociation at neutral pH values are advantageous, the PBMD polymer revealed high potential as gene delivery vector.

3.3. Encapsulation of pDNA

Since the PBMD polymer showed a promising pH-dependent solubility and a promising DNA binding capability, it was used for the development of a nanoparticle formulation aiming for efficient loading of pDNA while maintaining particle sizes below 200 nm with a narrow size distribution. Such size allows controlled cellular uptake by endocytosis (Rejman et al., 2004). However, encapsulation of pDNA by hydrophobic polymers remains challenging due to its large size, charged character, and sensitivity to harsh formulation conditions. To produce stable pDNA-loaded nanoparticles using the PBMD polymer, three formulation strategies were investigated within this study: Two variants of conventional nanoprecipitation (Fig. 3a) were compared with a newly introduced, “green”, aqueous complexation and formulation method (PBMD_{Aqu}(pDNA), Fig. 3b). The former differed in the point of pDNA addition, after the formation of nanoparticles (PBMD_{Org}(out,pDNA)) or during the precipitation process (PBMD_{Org}(in,pDNA)). The aqueous formulation exploited the solubility of the PBMD polymer in aqueous acidic buffer with a pH-driven nanoprecipitation approach at increased pH values.

First, the PBMD polymer was investigated for particle formation by nanoprecipitation from organic solvents without genetic material (PBMD_{Org}), resulting in nanoparticles with a hydrodynamic diameter (z-average, determined by DLS) of approximately 130 nm and an overall positive zeta potential (+51 mV) (Fig. 4). As the positively charged nanoparticles should facilitate the binding and complexation of negatively charged pDNA without the need for an additional cationic surface coating, pDNA was added in different amounts to the preformed nanoparticles (PBMD_{Org}(out,pDNA)). The addition of pDNA led to an increased size and polydispersity (PDI) (Fig. 4a and b, SI Fig. S2), resulting in nanoparticles that are unsuitable for the desired application. Nanoparticles meeting the specifications (sizes below 200 nm and PDI values below 0.250) could only be obtained at very low and high N/P ratios of 5 and 100. Using the coprecipitation of pDNA and polymer from acetone (PBMD_{Org}(in,pDNA)), suitable nanoparticles were formed at high N/P ratios (100), whereas at lower N/P ratios (<N/P 30) only larger nanoparticle populations could be observed by DLS measurements. In addition, an increasing number of particles with larger diameters was observed by scanning electron microscopy (SEM),

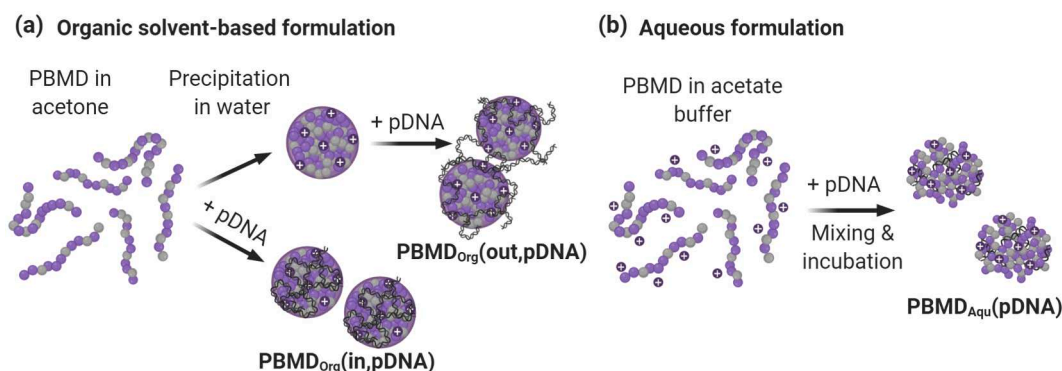


Fig. 3. Schematic overview of applied formulation methods for encapsulation, binding, and complexation of pDNA with the PBMD polymer. (a) Nanoprecipitation using solvent-evaporation techniques was combined with pDNA added at different stages of formulation. pDNA was either added subsequently to nanoprecipitation to the nanoparticle suspension (after-process addition; PBMD_{Org}(out,pDNA)) or to the organic acetone phase during formulation (in-process addition; PBMD_{Org}(in,pDNA)). (b) For the organic solvent-free pH-driven formulation, the PBMD polymer was dissolved under acidic conditions and directly mixed with pDNA for encapsulation (in-process addition; PBMD_{Aqu}(pDNA)). This figure was created with Biorender.com.

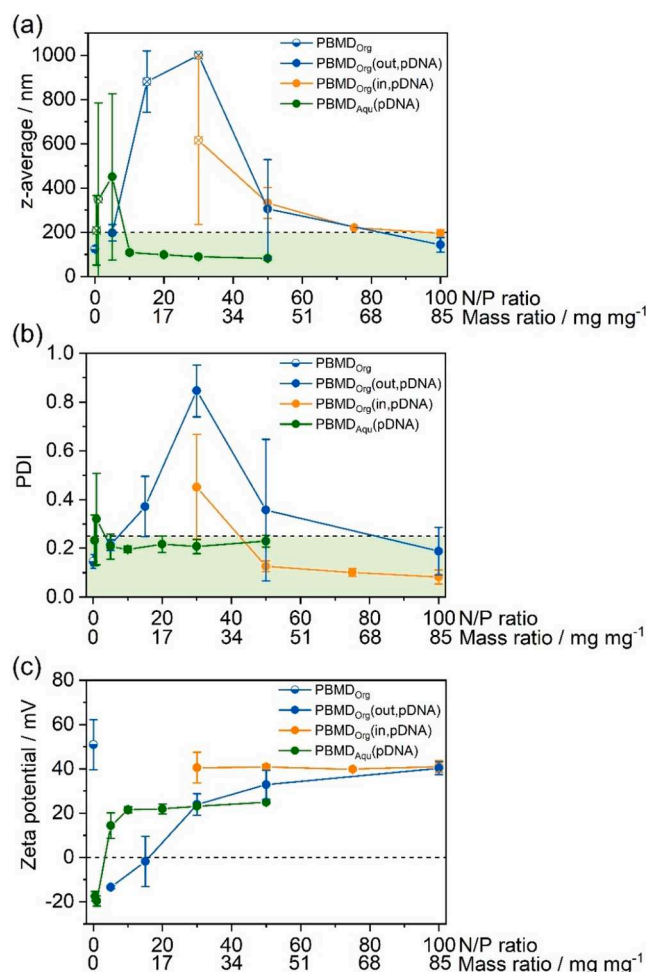


Fig. 4. Comparison of different formulation methods for pDNA-loaded nanoparticles. Formulations were characterized in terms of (a) diameter (z-average) and (b) polydispersity (PDI) by DLS. Empty symbols in panel (a) mark the occurrence of large aggregates (≥ 1000 nm) that were taken into account as 1000 nm during calculation of the mean. The green areas indicate the desired size (≤ 200 nm) and PDI range (≤ 0.250), respectively. (c) The formulations were further characterized in terms of surface charge before (PBMD_{Org}) and after pDNA addition. The measured values are plotted against N/P ratio and mass ratio of polymer to pDNA (mg mg^{-1}) (mean of $n \geq 3 \pm \text{SD}$). (For interpretation of the references to colour in this figure legend, the reader is referred to the web version of this article.)

confirming the increasing size observed by DLS (see SI, Fig. S4). Interestingly, the way in which genetic material was added also had an influence on the apparent surface charge of the nanoparticles. As expected, the positive zeta potential of PBMD_{Org} nanoparticles decreased with increasing amount of pDNA (lower N/P ratios) to the point where an inversion of the zeta potential to negative values occurred (approx. N/P 20, Fig. 4c). In comparison, the zeta potential remained in the positive range when pDNA was added during nanoprecipitation (PBMD_{Org}(in,pDNA)), mainly due to the inability of successful formulation at low N/P ratios (below 30) as this was leading to large visible aggregates during the formulation process. Based on these experiments it can be concluded that the conventional formulation of stable, highly pDNA-loaded nanoparticles cannot be successfully applied for the PBMD polymer by these methods.

Thus, to increase the amount of pDNA encapsulated in stable and defined nanoparticles, a new formulation approach based on the pH-dependent binding and release behavior of the PBMD polymer was developed (Fig. 3b). For this purpose, the pH-dependent solubility of PBMD under acidic conditions ($\text{pH} < 6$, Fig. 1d) was exploited by

dissolving the polymer in sodium acetate buffer ($\text{pH } 5.8$) for nanoparticle formulation without the use of organic solvents. Thereafter, the aqueous polymer solution was mixed 1:2 with pDNA diluted in HBG buffer ($\text{pH } 7.4$) to shift the pH to neutral values during complexation. This formulation approach was tested at N/P ratios ranging from 0.5 to 50, obtaining nanoparticles in the range of 100 nm and low PDI values (around 0.2) at N/P ratios above 5. As the N/P ratio decreased, the positive surface charge changed from $+25$ mV (N/P 50) to -18 mV (N/P 0.5), while being neutral between N/P 1 and 5. This occurred at lower N/P ratios (higher amounts of pDNA) compared to organic-solvent based pre-formulated nanoparticles (PBMD_{Org}(out,pDNA)), with a zeta potential of 0 at \sim N/P 20).

Overall, the pH-dependent PBMD_{Aqu}(pDNA) formulation was successfully applied to form stable nanoparticles in a suitable size range (< 200 nm) with low PDI values at low N/P ratios, which can likely be explained by a high number of charged groups within the polymer dissolved in acetate buffer, interacting with negatively charged pDNA moieties. The use of HBG buffer at $\text{pH } 7.4$ within the formulation process leads to neutralization of the solution and further stabilization of the complex through hydrophobic interactions as already indicated by the EBA/HRA assay (Fig. 2).

There are only a few approaches in the literature reporting water-insoluble cationic polymers such as Eudragit® E(PO/100) for pDNA delivery; all using organic solvents for the formulations. (Basarkar and Singh, 2009; Kanthamneni et al., 2016) The sufficient removal of organic solvents is necessary prior to biological applications and is often a costly and time-consuming additional step. Further, in comparison to the aqueous formulation, during the nanoprecipitation formulation, the cationic hydrophobic polymer can be considered uncharged when dissolved in acetone only, which leads to a reduced electrostatic interaction with genetic material and, in the case of preformed nanoparticles (e.g., PBMD_{Org}(out,pDNA)) to less exposed positively charged moieties on the particle surface. Consequently, this also limits the amount of pDNA that can be bound. On that account, additives such as cationic surfactants (CTAB) or cationic polymers (LPEI) are typically used in both formulation approaches to improve nanoparticle surface charge and thus pDNA binding.

However, the use of organic solvents and additives can be avoided by applying the aqueous, pH-driven nanoprecipitation technique (PBMD_{Aqu}(pDNA)). Moreover, high amounts of pDNA were complexed by the pH-responsive hydrophobic cationic polymer within stable nanoparticles, which turns the method into a simple, straightforward approach for the encapsulation of genetic material.

3.4. Characterization of PBMD_{Aqu}(pDNA) complexes by cryo-TEM and AUC

As the PBMD_{Aqu}(pDNA) complexes obtained by a fully aqueous approach possessed excellent potential for biological applications such as gene delivery, they were further characterized by cryo-TEM and AUC in order to examine particle shape and morphology. Further, the presence of free pDNA and/or polymer chains, and detailed information regarding particle size distributions in dependence of the concentration were evaluated. The PBMD_{Aqu}(pDNA) complexes were studied at N/P 10 and 20, as this led to well-defined particle distributions as evaluated by DLS. Cryo-TEM measurements revealed nanostructures with diameters of approx. 50 nm, clearly smaller than the intensity-weighted hydrodynamic diameters as measured by DLS but closer to the number-weighted distributions (Fig. 5a, Fig. 4a, Fig. S3). Additionally, a few larger structures, although not exceeding the overall 100 nm size range, being favored for biological applications, were observed.

Further, the PBMD_{Aqu}(pDNA) complexes were investigated via sedimentation velocity AUC experiments over a suitable concentration range ($0.1\text{--}1 \text{ mg mL}^{-1}$) using RI and absorbance multidetection. The experiments were conducted at a rotor speed of 7,500 rpm for 24 h, followed by spinning the rotor at a speed of 42,000 rpm for further 24 h

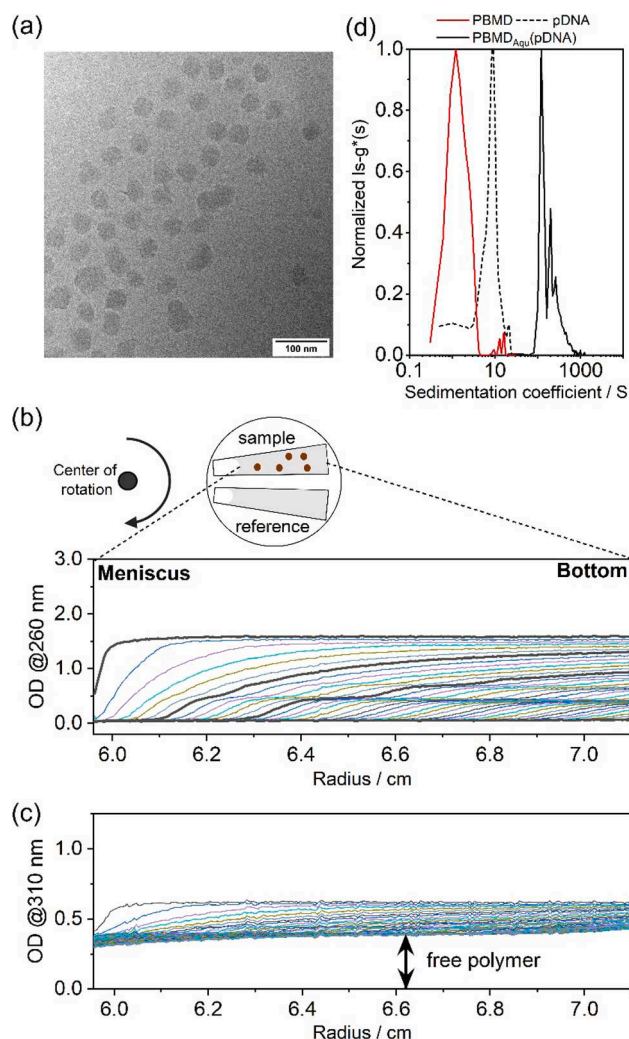


Fig. 5. Characterization of PBMD_{Aqu}(pDNA) complexes at N/P 20 by cryo-TEM and AUC. (a) Cryo-TEM measurements of PBMD_{Aqu}(pDNA) complexes at N/P 20. (b) Sketch of *in situ* sedimentation velocity AUC measurements leading to radially-resolved sedimentation velocity profile scans of the PBMD_{Aqu}(pDNA) complexes at N/P 20, a concentration of 1 mg mL⁻¹, and a rotor speed of 7,500 rpm monitored at $\lambda = 260$ nm. (c) Same as in (b) but monitored at $\lambda = 310$ nm. (d) Normalized differential distributions of sedimentation coefficients of free RAFT-group containing polymer monitored at $\lambda = 310$ nm by acceleration of the rotor speed to 42,000 rpm after the measurement at 7,500 rpm, free DNA at $\lambda = 260$ nm measured separately at a rotor speed of 42,000 rpm, and the PBMD-complexes at N/P 10 at $\lambda = 260$ nm at a rotor speed of 7,500 rpm.

to investigate potentially smaller species present (Cinar et al., 2020). Strikingly, the radially-resolved sedimentation velocity profiles recorded at $\lambda = 260$ nm in terms of optical density (OD) contained several discernable steps (Fig. 6b). However, when the run was finished at 7,500 rpm, a plateau at nearly zero OD was observed. This suggests practically no absorbance at $\lambda = 260$ nm in the supernatant, showing no detectable free pDNA, thereby supporting the results of the GRA (Fig. 2a). When monitoring sedimentation velocity at $\lambda = 310$ nm, a clearly discernable residual OD was observed in the supernatant (Fig. 5c). This could indicate the presence of free polymer in the sample, that is in excess to that bound to the monitored PBMD_{Aqu}(pDNA) complexes. The apparently free polymer, which absorbs at $\lambda = 310$ nm due to the trithiocarbonate RAFT end-group, is too small to efficiently sediment at a rotor speed of 7,500 rpm, and largely remained in the supernatant. Additionally, polymer that is an integral component of the complex apparently sedimented, because it is associated to the pDNA (Fig. 5c).

This situation is also pointed out when comparing the normalized

differential distributions of sedimentation coefficients of the PBMD_{Aqu}(pDNA) complex, free polymer, and free DNA separately (Fig. 5d). The overlap at $\lambda = 260$ nm and $\lambda = 310$ nm and the RI, proved the simultaneous sedimentation of species, respectively the close association of the RAFT group-containing polymer and the pDNA in the form of a complex (Fig. 6a).

By increasing the sample concentration, a third peak in the differential distributions of sedimentation coefficients could be discerned more clearly (dotted line in Fig. 6b). At higher concentrations, the complexes showed a more pronounced tendency to aggregate and/or form larger species, observed by the presence of larger sedimentation coefficients with a discernable peak. In contrast to this observation, the lower sample concentrations featured two major discernable populations (solid black line in Fig. 6b). The differential distributions of sedimentation coefficients (Fig. 6a-c) were also representative for the discernable steps in the sedimentation velocity profiles displayed in, e.g., Fig. 5b. Here, the partial resolution of several species of an increased hydrodynamic size indicated by partly resolved peaks, was more pronounced at higher concentrations.

After sedimentation of all such larger species after 24 h, observation of sedimentation processes in the remaining supernatant revealed sedimentation of the remaining free polymer at a wavelength of $\lambda = 310$ nm (Fig. 5d and Fig. S8). This was also nicely shown by differential distributions of sedimentation coefficients in Fig. 6d. An increase of sample concentrations showed an approximately linear increase of signal intensity of the sedimenting RAFT agent-containing polymer at higher rotor speeds as well (Fig. 6d and 6e). This further represented an increased concentration of free polymer. No free RAFT agent or loss of the RAFT-containing chain-ends of the polymers was observable, indicated by the absence of a remaining plateau of the recorded sedimentation profiles in Fig. S8.

Differences in the N/P ratio of the PBMD_{Aqu}(pDNA) complex were investigated at the lowest sample concentration (0.1 mg mL⁻¹) as this is more close to the experimental implementations in transfection experiments (Fig. 6c). A decrease of the N/P ratio to 10 resulted in the loss of the distinct third population in the differential distributions of sedimentation coefficients, barely indicated at N/P 20 at lower concentrations. Polyplexes formed with the PDMAEMA homopolymer at different N/P ratios were studied in the same manner (Fig. S9). It can be seen in Fig. 6c that N/P 20 revealed a prominent distribution of (lowest) sedimentation coefficients with an apparent shoulder (toward higher sedimentation coefficients). Besides, the differential distribution of sedimentation coefficients at N/P 10 exhibited a clearly discernable further population. Also, an increased amount of free polymer, as already observed for increasing sample concentrations (Fig. 6d) was also observed for higher N/P ratios (Fig. 6f).

When comparing the two N/P ratios, both showed nearly similar distributions in the DLS, with an even slightly larger size and broader distribution for N/P 10 (Fig. 4, Fig. S3). The difference in populations present in the two samples could only be observed by AUC measurements, revealing the importance of detailed characterization of such delivery systems by various techniques. Furthermore, AUC measurements confirmed full pDNA binding within the PBMD complex, which is consistent with results obtained by GRA (Fig. 2a).

3.5. Influence of the formulation approach on transfection of HEK293T cells

After the formation of controlled and stable PBMD_{Aqu}(pDNA) complexes, their transfection performance was investigated, with the PBMD_{Org}(out,pDNA) formulation serving as a control, while the PBMD_{Org}(in,pDNA) formulation was not further investigated since pDNA loaded nanoparticles could only be obtained at high N/P ratios which was not suitable for the intended investigation. For transfection experiments, pDNA encoding for enhanced green fluorescent protein (EGFP) was delivered into HEK293T cells and EGFP expression was

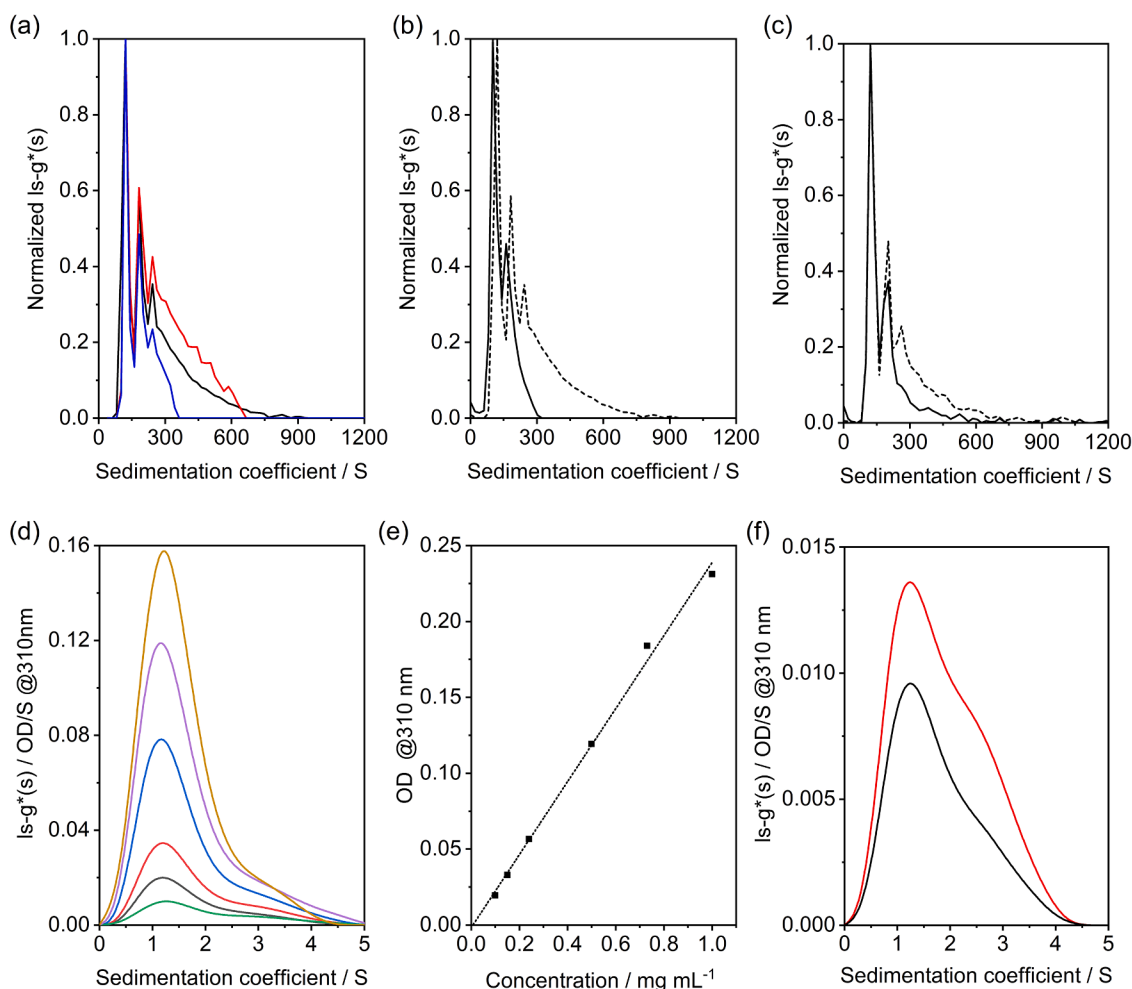


Fig. 6. Normalized differential distributions of sedimentation coefficients of complexes formed with PBMD polymer (PBMD_{Aqu}(pDNA)) at a N/P 20 obtained at a rotor speed of 7,500 rpm. (a) The concentration utilized was 1 mg mL⁻¹ by using RI detection (blue solid line) and the absorbance detection in terms of OD, representative of the DNA at $\lambda = 260$ nm (red solid line) as well as at $\lambda = 310$ nm, being representative of the RAFT agent-containing polymer (black solid line). (b) Same concentration as in (a) using absorbance detection at $\lambda = 260$ nm in terms of OD (black dashed line) and 0.1 mg mL⁻¹ (black solid line), (c) with the PBMD polymer at N/P 10 (black dashed line) and N/P 20 (black solid line). (d) Differential distributions of sedimentation coefficients monitored from data at a subsequent rotor speed of 42,000 rpm and at increasing overall sample concentrations (from bottom to top) at $\lambda = 310$ nm with (e) the obtained linear correlation of integrated ODs of such differential distributions in respect to the overall sample concentration and (f) increased existence of free polymer by comparing (PBMD_{Aqu}(pDNA)) samples at a N/P 10 (black solid line) and at a N/P 20 (red solid line). (For interpretation of the references to colour in this figure legend, the reader is referred to the web version of this article.)

analyzed by flow cytometry and fluorescence microscopy. The transfection efficiency (percentage of viable fluorescent cells) of the formulations were assessed under various conditions by evaluation of (i) two N/P ratios in the lower range (10 and 20), (ii) two media (under serum-free conditions and in the presence of 10% serum), and (iii) varying incubation times (1 and 4 h) followed by analysis at 24 h post transfection. In general, both formulations enabled EGFP expression in HEK293T cells under all tested conditions, with higher expression levels observed under serum-free conditions (Opti-MEMTM) and longer incubation times (Fig. 7). In addition, higher amounts of cationic polymer (higher N/P ratios) further increased expression levels. The PBMD_{Aqu}(pDNA) complex showed significantly higher EGFP expression levels at N/P 20 when compared to the PBMD_{Org}(out,pDNA) formulation, particularly at short incubation times (1 h), in serum-free environment ($61 \pm 9\%$ vs. $27 \pm 15\%$) and even in the presence of serum ($32 \pm 8\%$ vs. $17 \pm 8\%$).

Overall, an EGFP expression of both formulation approaches is in accordance to the literature, reporting the ability of cationic hydrophobic polymers to successfully transfect eukaryotic cells (Basarkar and Singh, 2009; Kanthamneni et al., 2016). The difference in transfection

efficiency could potentially be attributed to the assumed difference in pDNA distribution within the formulation approaches. In one case, the pDNA was present solely on the exterior of the nanoparticles (PBMD_{Org}(out,pDNA)) as opposed to the PBMD_{Aqu}(pDNA) complex where the DNA is expected to be distributed throughout the particle, potentially also effecting pDNA stability. Further, differences in nanoparticle size, PDI, and surface charge might affect cellular uptake, but also endosomal escape ability and, therefore, overall transfection efficiency.

3.6. Optimization of transfection efficiency in HEK293T cells

As the PBMD_{Aqu}(pDNA) complexes resulted in promising efficiencies in the first transfection experiments, and characterization by AUC proved that the pDNA is completely bound to, respectively complexed into the polymer, the transfection protocol was optimized for increasing transfection efficiency while maintaining high cell viability. Therefore, the influence of the polymer itself without the addition of genetic material on the viability of L-929 cells, a standard cell line for cytotoxicity testing recommended by the ISO 10993-5 guideline, was evaluated at

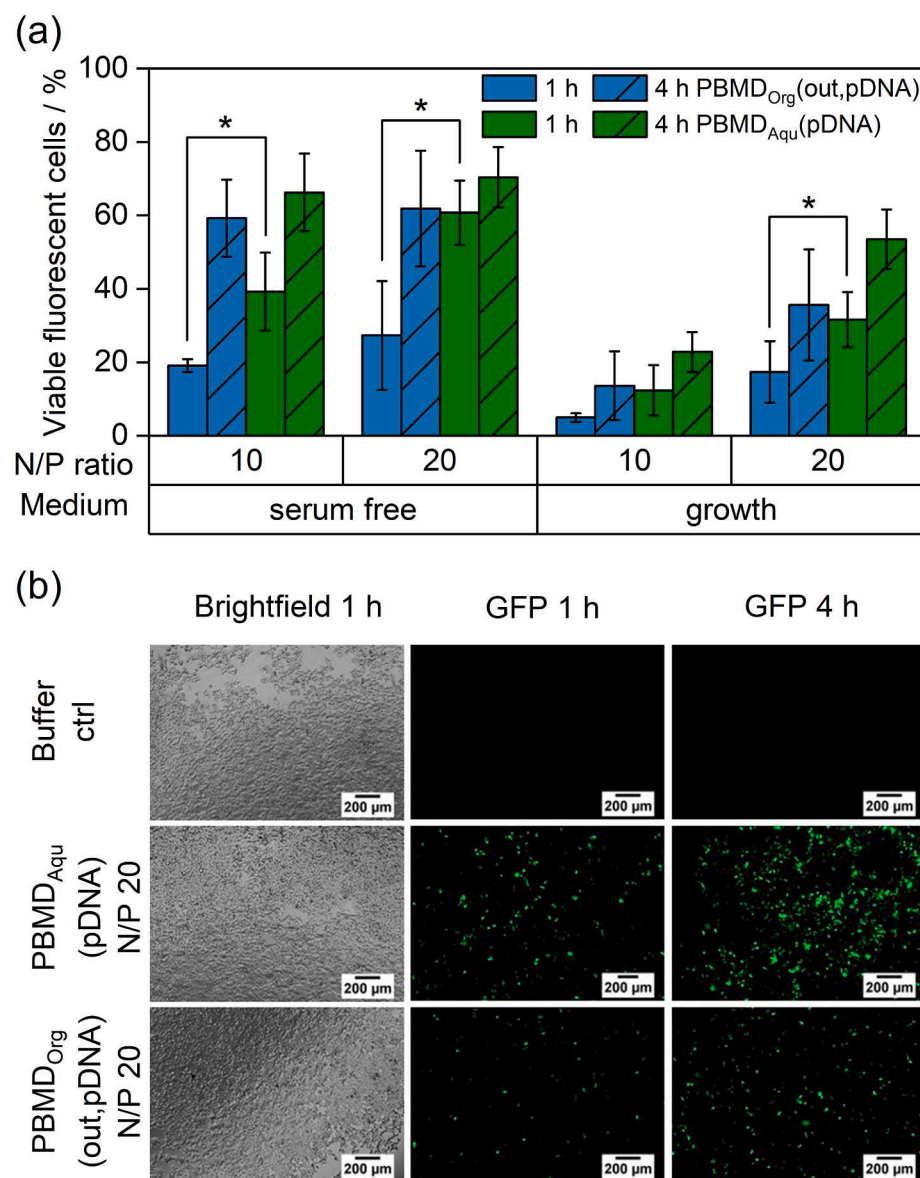


Fig. 7. Influence of the formulation method on the transfection efficiency (percentage of viable fluorescent cells) in HEK293T cells. The pH-dependent formulation (PBMD_{Aqu}(pDNA)) and the nanoprecipitation/after-process addition of pDNA (PBMD_{Org}(out,pDNA)) were tested in growth medium (10% FBS) and under serum free conditions (Opti-MEM™) at varying incubation times. pDNA is encoding for EGFP. Transfection efficiency was investigated by measuring EGFP expression by (a) flow cytometry (mean of $n \geq 3 \pm SD$) and (b) fluorescence microscopy. Statistical significance is denoted as follows: **P* < 0.05, ***P* < 0.01, and ****P* < 0.001.

varying incubation times (Fig. 8a).

The PBMD polymer showed time and concentration dependent cytotoxicity, whereas shorter incubation times and lower concentrations resulted in higher cell viability, and the IC₅₀ values increased from 7.6 μg mL⁻¹ (after 24 h) to 12.2 μg mL⁻¹ (after 4 h) to 15.6 μg mL⁻¹ (after 1 h). Therefore, low polymer concentrations and short incubation times were favored for the optimization of the transfection conditions. To evaluate cell viability at transfection conditions, the cytotoxicity of the PBMD_{Aqu}(pDNA) formulation in HEK293T cells was evaluated additionally (Fig. 8b), revealing a similar concentration dependent trend. Cell viability above 70% was obtained at pDNA concentrations below 0.5 μg mL⁻¹, while an increase in pDNA concentration and N/P ratio reduced cell viability. To optimize transfection conditions, different pDNA concentrations were tested, while keeping the N/P ratio constant at 20 (Fig. 8b). Overall, PBMD_{Aqu}(pDNA) complexes showed high transfection efficiencies already at low pDNA concentrations and short treatment times (Fig. 8b), while longer treatment (4 h) resulted in even higher expression levels over the whole concentration range. The ideal pDNA concentration at N/P 20 was identified as 0.5 mg mL⁻¹ resulting in 41 ± 3% viable EGFP fluorescent cells after 4 h of incubation, while maintaining above 70% viability. Therefore, the N/P ratio was

subsequently optimized by keeping the pDNA concentration at 0.5 μg mL⁻¹. Overall, changes in the N/P ratio did not substantially improved transfection efficiency, but rather resulted in decreased cell viability, and, therefore, a pDNA concentration of 0.5 μg mL⁻¹ with N/P 20 and 4 h treatment were chosen as ideal conditions for pDNA transfection with the PBMD_{Aqu}(pDNA) complex. The results were compared with LPEI polyplexes as a well-known polymer for pDNA transfection and revealed, that very low amounts of pDNA were required to reach high transfection efficiencies with PBMD_{Aqu}(pDNA) complexes at short incubation times (≤4h). To obtain similar expression levels with LPEI, either the pDNA concentration needed to be increased by 5- to 10-fold (2.5–5 μg mL⁻¹) or treatment durations up to 24 h were required (Fig. 8c).

Various studies reported the application of the commercial polymer Eudragit® E(PO/100) with a comparable composition like PBMD for gene or drug delivery. The reported toxicity was typically lower than that observed in this study (Hari et al., 2016; Jain et al., 2015). This could be due to the slightly higher DMAEMA content within the PBMD polymer when compared to Eudragit® E(PO/100). However, the increase of the molar content of DMAEMA is only 10%, which is relatively low to explain these effects. In both previous studies, the nanoparticles

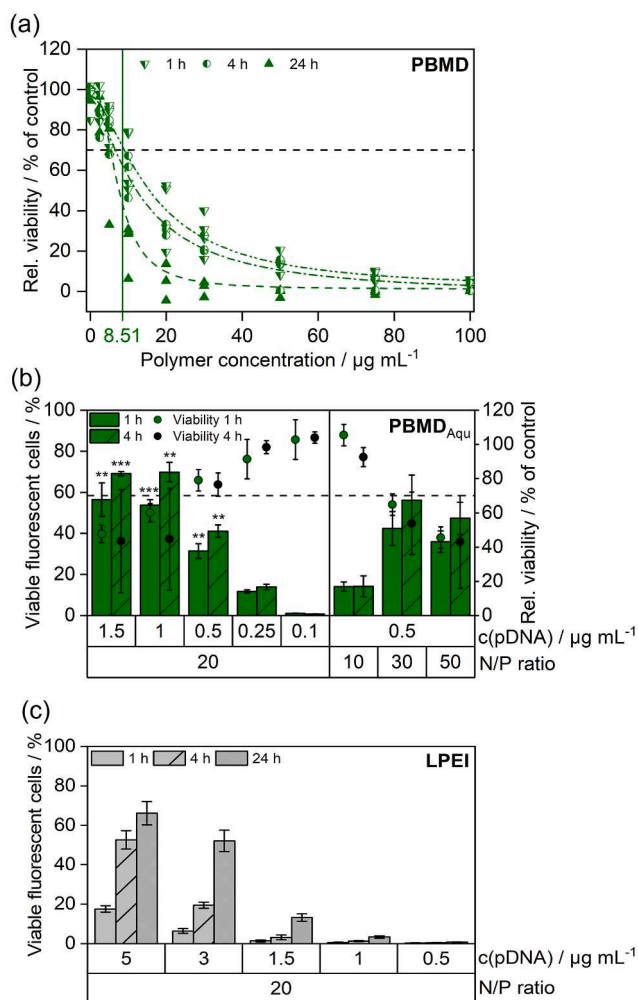


Fig. 8. Optimization of transfection conditions of PBMD_{Aqu}(pDNA) formulated with the pH-dependent method in HEK293T cells. (a) Evaluation of the cytotoxicity of the PBMD polymer dissolved in acetate buffer in L-929 cells. Cells were treated with the polymer for 1, 4 and 24 h and cytotoxicity was determined by the PrestoBlue™ assay after 24 h. The dashed line indicates 70% cell viability and the concentration of PBMD polymer under optimized transfection conditions is indicated by the green line. (b) N/P ratio and pDNA concentrations were optimized to achieve high efficiencies (high number of viable fluorescent cells) while maintaining low cytotoxicity. The expression of EGFP in HEK293T cells after transfection (columns) was measured via flow cytometry (mean of $n = 3 \pm \text{SD}$). Cytotoxicity of the PBMD_{Aqu}(pDNA) complexes (dots) was determined under conditions used for transfection by the PrestoBlue™ assay (mean of $n = 3 \pm \text{SD}$). (c) Transfection efficiency of LPEI-pDNA complexes at varying pDNA concentrations and incubation times was investigated by measuring EGFP expression in HEK293T cells by flow cytometry (mean of $n = 3 \pm \text{SD}$). Statistical significance in comparison to LPEI at the respective pDNA concentration and N/P ratio is denoted as follows: * $P < 0.05$, ** $P < 0.01$, and *** $P < 0.001$. (For interpretation of the references to colour in this figure legend, the reader is referred to the web version of this article.)

were manufactured with the help of surfactants (PVA, Pluronic F-68). Eudragit® E(PO/100) is known for its amphipathic and membrane-destabilizing properties when interacting with lipoproteins, liposomes, and eukaryotic cell membranes. (Alasino et al., 2005, 2012) This is a potential mechanism for cytotoxicity but, on the other hand, if well dosed, useful for application in gene delivery to facilitate cellular uptake, endosomal release, and therefore high transfection efficiencies. Within the PBMD_{Aqu}(pDNA) formulation, no surfactants were present. This could result in stronger interaction with cellular membranes, explaining the high EGFP expression levels already at low complex

concentrations compared to LPEI polyplexes, while maintaining cell viability.

3.7. PBMD vs. commercial controls and for the delivery of siRNA and mRNA

Since the PBMD_{Aqu}(pDNA) complexes showed improved transfection at low pDNA concentrations, the formulation method was applied to the commercial polymer Eudragit® E(PO/100) and tested under optimized transfection conditions (N/P 20, 0.5 μg mL⁻¹ pDNA, 4 h incubation). EGFP expression levels under these conditions were further compared with the PDMAEMA homopolymer and the commercial polymer-based transfection reagent Viromer® RED, which was optimized for pDNA and mRNA transfection (Fig. 9a). Viromer® RED is known for its superior endosomal release mechanism, rendering it a very efficient commercial control (Rao et al., 2015). The pH-dependent formulation applied to the commercial polymer Eudragit® E(PO/100) showed comparable EGFP expression to the PBMD_{Aqu}(pDNA) complexes. Both polymers, PBMD and Eudragit® E(PO/100), were at a comparable level or even outperformed the commercial transfection agents Viromer® RED and LPEI under these optimized conditions. At 4 h incubation time PBMD showed $50 \pm 10\%$ and Eudragit® E(PO/100) $30 \pm 2\%$ fluorescent cells, while Viromer® RED and LPEI resulted in $31 \pm 21\%$ and $0.35 \pm 0.12\%$, respectively. As expected, the PDMAEMA homopolymer, composed of the same number of cationic groups as the PBMD polymer, showed, similarly to LPEI, no transfection under these conditions ($0.48 \pm 0.22\%$). It is known, that the efficiency of PDMAEMA is lower under these conditions, in particular if low molar masses are applied (Layman et al., 2009; Samsonova et al., 2011; Van de Wetering et al., 1998). The high efficiency of the PBMD polymer as well as the commercial control Eudragit® E(PO/100) showed the potential of the novel formulation, which is not only fast and based on a fully aqueous approach, but also increases the transfection efficiency compared to other formulations.

In order to exploit the full potential of the PBMD polymer, the formulation method was applied for complexation and transfection of various genetic materials and was further tested in comparison to commercially available controls more suitable for the respective genetic material than LPEI. siRNA and mRNA are promising candidates for gene delivery offering several advantages over pDNA. Both siRNA and mRNA do not pose the risks accompanied by integration into the genome, since their site of action is within the cytosol. Thus, they avoid the passage of the nuclear membrane, and, importantly, they offer various therapeutic applications such as protein displacement or inhibition of protein expression (Dunbar et al., 2018; Hajj and Whitehead, 2017).

As Eudragit® E(PO/100) has been evaluated for siRNA delivery to macrophages using PVA coated nanoparticles showing significantly reduced protein expression levels, (Jain et al., 2015) PBMD_{Aqu}(siRNA) complexes were tested for knock-down efficiency in HEK-GFP cells, stably expressing GFP. The knock-down efficiency after 72 h incubation was compared to Lipofectamine, which is commonly used for siRNA transfections in the literature, loaded with the same amount of siRNA. A reduction in the percentage of GFP positive cells was observed with Lipofectamine and the PBMD_{Aqu}(siRNA) complexes when compared to the control. PBMD_{Aqu}(siRNA) complexes resulted in $45 \pm 13\%$ GFP negative cells whereas for Lipofectamine $54 \pm 5\%$ GFP negative cells were observed. Thus, the PBMD_{Aqu}(siRNA) complexes showed knock-down efficiencies comparable to Lipofectamine, revealing the high potential for the introduction of siRNA into cells by the PBMD polymer. Furthermore, the transfection efficiency of PBMD_{Aqu}(mRNA) complexes was evaluated by delivering GFP-mRNA into HEK293T cells. The GFP expression was measured after 24 h. The transfection efficiency of the PBMD_{Aqu}(mRNA) formulation was compared with the commercially available Viromer® RED. PBMD_{Aqu}(mRNA) complexes resulted in GFP expression in $73 \pm 12\%$ of cells, while Viromer® RED transfected $87 \pm 1\%$ of cells. Although the percentages of transfected cells were comparable, the polymers exhibited different transfection patterns (SI, Fig. S7),

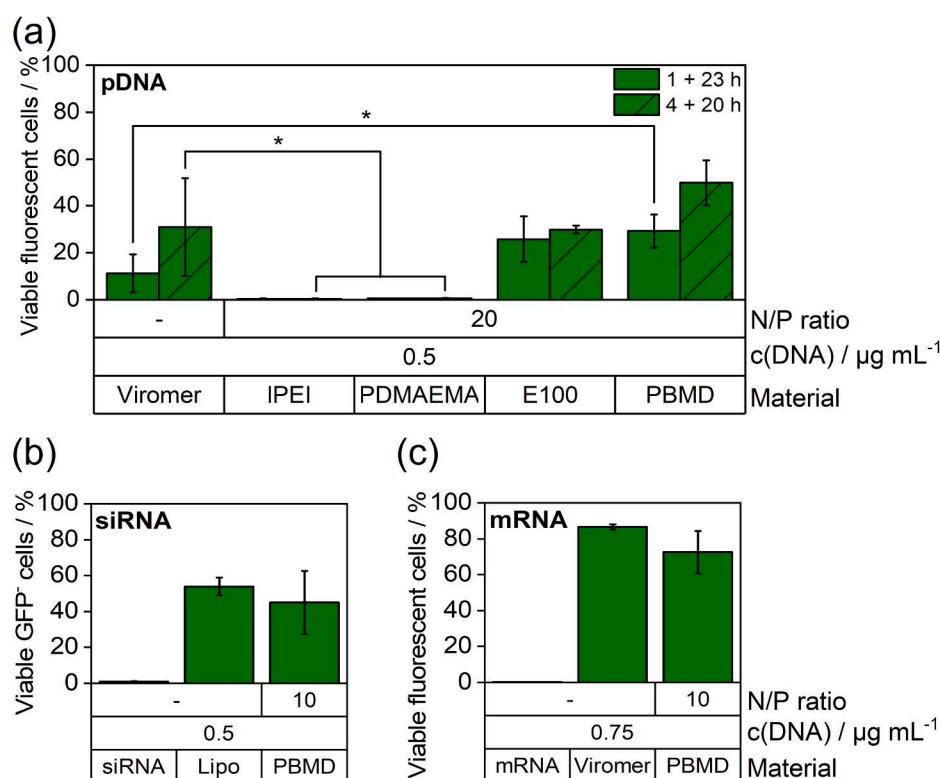


Fig. 9. Transfection efficiency of the aqueous pH-driven formulation (PBMD_{Aqu}(pDNA)) in comparison to commercial transfection agents and its application to siRNA and mRNA encapsulation. (a) Formulation and transfection conditions optimized for the PBMD polymer (N/P ratio 20, 0.5 µg mL⁻¹ pDNA) were applied to Eudragit® E(PO/100) and compared to the PDMAEMA homopolymer in terms of the percentage of viable fluorescent cells. Viomer® RED was used with 0.5 µg mL⁻¹ pDNA for comparison. EGFP expression in HEK293T cells was measured by flow cytometry (mean of $n \geq 3 \pm SD$). The formulation method was further applied for encapsulation of siRNA and mRNA. (b) Knock-down efficiency of anti-GFP siRNA complexed with PBMD (PBMD_{Aqu}(siRNA)) was investigated in HEK-GFP cells at an N/P ratio of 10 (mean of $n \geq 3 \pm SD$). (c) Transfection efficiency of PBMD_{Aqu}(mRNA) complexes was investigated by introducing GFP-mRNA into HEK293T cells. GFP expression was measured by flow cytometry (mean of $n \geq 3 \pm SD$). Statistical significance in comparison to the respective commercial controls (Viomer® RED, Lipofectamine) is denoted as follows: * $P < 0.05$, ** $P < 0.01$, and *** $P < 0.001$. (For interpretation of the references to colour in this figure legend, the reader is referred to the web version of this article.)

which remain to be investigated in further studies. Nevertheless, the PBMD_{Aqu}(mRNA) complex displayed excellent potential for mRNA delivery as the complex is transfecting a high number of cells.

4. Conclusions

In this study, a new, fast, and straightforward formulation strategy for the encapsulation of pDNA without the need of organic solvents into cationic polymer nanoparticles was established. The key requirement for successful encapsulation was the insolubility of the polymer in water under neutral pH conditions. For the development of the utilized pH-dependent formulation method, a well-defined PBMD polymer was synthesized using RAFT polymerization. The PBMD polymer exhibited the desired pH-dependent solubility and pDNA binding behavior under physiological solution conditions, which can be exploited for the assembly of pDNA-polymer complexes, in a fully aqueous scenario. By dissolution of the PBMD polymer in acidic buffer, pDNA binding was facilitated, while shifting the pH to neutral values during the formulation process increased hydrophobic interactions stabilizing the formed nanoparticles. The utilized aqueous pH-driven formulation of cationic hydrophobic polymers showed high pDNA encapsulation efficiencies and desired stability under physiological conditions. In-depth characterization by AUC, cryo-TEM, and DLS/ELS proved a full complexation of the genetic material. The novel formulation resulted in enhanced transfection efficiency at reduced pDNA concentrations compared to commercial controls such as LPEI or Viomer® RED and was successfully applied to the commercially approved Eudragit® E(PO/100) and various types of genetic material, such as siRNA and mRNA. The formulation approach showed a readily high versatility and promising potential to further be optimized and applied to other classes of hydrophobic cationic copolymers for a general delivery vehicle design concerning genetic material.

CRediT authorship contribution statement

Jana I. Solomun: Conceptualization, Investigation, Methodology, Visualization, Writing - original draft. **Gizem Cinar:** Investigation, Methodology, Visualization, Writing - review & editing. **Prosper Mapfumo:** Investigation, Methodology, Writing - review & editing. **Friederike Richter:** Writing - review & editing, Methodology. **Elisabeth Moek:** Investigation, Writing - review & editing. **Franziska Hausig:** Writing - review & editing, Methodology. **Liam Martin:** Investigation, Methodology, Visualization, Writing - review & editing. **Stephanie Hoepfener:** Investigation, Writing - review & editing. **Ivo Nischang:** Methodology, Supervision, Writing - review & editing, Funding acquisition. **Anja Traeger:** Conceptualization, Supervision, Writing - review & editing, Project administration, Funding acquisition.

Declaration of Competing Interest

The authors declare the following financial interests/personal relationships which may be considered as potential competing interests: The Friedrich Schiller University of Jena has applied for a patent based on some data presented here, in which A. Traeger and J. I. Solomun are named as inventors.

Acknowledgements

This work was financially supported by the Collaborative Research Center PolyTarget (SFB 1278 - projects B01/06 and Z01, project ID 316213987) funded by the German Research Foundation (DFG). Further, the authors thank the Bundesministerium für Bildung und Forschung (BMBF, Germany, #13XP5034A PolyBioMik) and the DFG for generous funding within the Emmy-Noether Programme (Projekt ID: 358263073). The authors further acknowledge the support from the Free State of Thuringia and the European Social Fund (2019SD0129). This work was as well supported by the "Thüringer Aufbaubank (TAB)" and the "Europäischer Fonds für regionale Entwicklung (EFRE)"

(2018FGI0025) through funding analytical ultracentrifugation facilities at the Jena Center for Soft Matter (JCSM). The SEM/TEM facilities of the JCSM were established with a grant from the DFG and the EFRE. Further, the authors thank Prof. U. S. Schubert for his continuous support and providing excellent facilities. The authors thankfully acknowledge Carolin Kellner, Bärbel Beringer-Siemers, Elisabeth Preußger, Steffi Stumpf, Maria Strumpf, and Franziska Stanzel for their excellent technical support and helpful discussions.

Appendix A. Supplementary material

Additional methods, materials, synthesis and characterization of PDMAEMA, DLS data of the different formulation methods, DLS measurements with different plasmids, SEM measurements, gating strategy for transfection experiments, AUC measurements of PDMAEMA and additional AUC data for the PBMD polymer and complex solutions can be found in the SI. Supplementary data to this article can be found online at <https://doi.org/10.1016/j.ijpharm.2020.120080>.

References

- Abdelhady, H.G., Allen, S., Davies, M.C., Roberts, C.J., Tendler, S.J., Williams, P.M., 2003. Direct real-time molecular scale visualisation of the degradation of condensed DNA complexes exposed to DNase I. *Nucleic Acids Res.* 31, 4001–4005. <https://doi.org/10.1093/nar/gkg462>.
- Adolph, E.J., Nelson, C.E., Werfel, T.A., Guo, R., Davidson, J.M., Guelcher, S.A., Duvall, C.L., 2014. Enhanced Performance of Plasmid DNA Polyplexes Stabilized by a Combination of Core Hydrophobicity and Surface PEGylation. *J. Mater. Chem. B* 2, 8154–8164. <https://doi.org/10.1039/C4TB00352G>.
- Alasino, R.V., Ausar, S.F., Bianco, I.D., Castagna, L.F., Contigiani, M., Beltramo, D.M., 2005. Amphipathic and membrane-destabilizing properties of the cationic acrylate polymer Eudragit E100. *Macromol. Biosci.* 5, 207–213. <https://doi.org/10.1002/mabi.200400168>.
- Alasino, R.V., Leonhard, V., Bianco, I.D., Beltramo, D.M., 2012. Eudragit E100 surface activity and lipid interactions. *Colloids Surf. B Biointerfaces* 91, 84–89. <https://doi.org/10.1016/j.colsurfb.2011.10.041>.
- Basarkar, A., Singh, J., 2009. Poly (lactide-co-glycolide)-polymethacrylate nanoparticles for intramuscular delivery of plasmid encoding interleukin-10 to prevent autoimmune diabetes in mice. *Pharm. Res.* 26, 72–81. <https://doi.org/10.1007/s11095-008-9710-4>.
- Bertschinger, M., Backliwal, G., Schertenleib, A., Jordan, M., Hacker, D.L., Wurm, F.M., 2006. Disassembly of polyethylenimine-DNA particles in vitro: implications for polyethylenimine-mediated DNA delivery. *J. Control. Release* 116, 96–104. <https://doi.org/10.1016/j.jconrel.2006.09.006>.
- Bivas-Benita, M., Romeijn, S., Junginger, H.E., Borchard, G., 2004. PLGA-PEI nanoparticles for gene delivery to pulmonary epithelium. *Eur. J. Pharm. Biopharm.* 58, 1–6.
- Bloomfield, V.A., 1997. DNA condensation by multivalent cations. *Biopolym.: Original Res. Biomol.* 44, 269–282. <https://doi.org/10.1016/j.ejpb.2004.03.008>.
- Brayton, C.F., 1986. Dimethyl sulfoxide (DMSO): a review. *Cornell Veterinarian* 76, 61–90.
- Breitenkamp, R.B., Emrick, T., 2008. Pentalysine-grafted ROMP polymers for DNA complexation and delivery. *Biomacromolecules* 9, 2495–2500. <https://doi.org/10.1021/bm800511p>.
- Buerkli, C., Lee, S.H., Moroz, E., Stuparu, M.C., Leroux, J.C., Khan, A., 2014. Amphipathic homopolymers for siRNA delivery: probing impact of bifunctional polymer composition on transfection. *Biomacromolecules* 15, 1707–1715. <https://doi.org/10.1021/bm5001197>.
- Cheng, C., Convertine, A.J., Stayton, P.S., Bryers, J.D., 2012. Multifunctional triblock copolymers for intracellular messenger RNA delivery. *Biomaterials* 33, 6868–6876. <https://doi.org/10.1016/j.biomaterials.2012.06.020>.
- Cinar, G., Englert, C., Lehmann, M., Nischang, I., 2020. In situ, quantitative assessment of multifunctional nanoscale drug delivery systems in human serum. *Anal. Chem.* 92 (11), 7932–7939. <https://doi.org/10.1021/acs.analchem.0c01323>.
- Cohen, H., Levy, R., Gao, J., Fishbein, I., Kousaev, V., Sosnowski, S., Slomkowski, S., Golomb, G., 2000. Sustained delivery and expression of DNA encapsulated in polymeric nanoparticles. *Gene Ther.* 7, 1896–1905. <https://doi.org/10.1038/sj.gt.3301318>.
- Cocka, C., Zartner, L., Tabujew, I., Fischer, D., Peneva, K., 2020. Incorporation of Indole Significantly Improves the Transfection Efficiency of Guanidinium-Containing Poly (Methacrylamide)s. *Macromol. Rapid Commun.* 41, 1900668. <https://doi.org/10.1002/marc.201900668>.
- Convertine, A.J., Benoit, D.S., Duvall, C.L., Hoffman, A.S., Stayton, P.S., 2009. Development of a novel endosomal lytic diblock copolymer for siRNA delivery. *J. Control Release* 133, 221–229. <https://doi.org/10.1016/j.jconrel.2008.10.004>.
- Dunbar, C.E., High, K.A., Joung, J.K., Kohn, D.B., Ozawa, K., Sadelain, M., 2018. Gene therapy comes of age. *Science* 359, eaan4672. <https://doi.org/10.1126/science.aan4672>.
- Eltoukhy, A.A., Chen, D., Alabi, C.A., Langer, R., Anderson, D.G., 2013. Degradable terpolymers with alkyl side chains demonstrate enhanced gene delivery potency and nanoparticle stability. *Adv. Mater.* 25, 1487–1493. <https://doi.org/10.1002/adma.201204346>.
- Fay, F., Quinn, D.J., Gilmore, B.F., McCarron, P.A., Scott, C.J., 2010. Gene delivery using dimethyldidodecylammonium bromide-coated PLGA nanoparticles. *Biomaterials* 31, 4214–4222.
- Forrest, M.L., Meister, G.E., Koerber, J.T., Pack, D.W., 2004. Partial acetylation of polyethylenimine enhances in vitro gene delivery. *Pharm. Res.* 21, 365–371. <https://doi.org/10.1016/j.biomaterials.2010.01.143>.
- Geall, A.J., Blagbrough, I.S., 2000. Rapid and sensitive ethidium bromide fluorescence quenching assay of polyamine conjugate-DNA interactions for the analysis of lipoplex formation in gene therapy. *J. Pharm. Biomed. Anal.* 22, 849–859. [https://doi.org/10.1016/S0731-7085\(00\)00250-8](https://doi.org/10.1016/S0731-7085(00)00250-8).
- Ginn, S.L., Amaya, A.K., Alexander, I.E., Edelstein, M., Abedi, M.R., 2018. Gene therapy clinical trials worldwide to 2017: An update. *J. Gene Med.* 20, e3015. <https://doi.org/10.1002/jgm.3015>.
- Hajji, K.A., Whitehead, K.A., 2017. Tools for translation: non-viral materials for therapeutic mRNA delivery. *Nat. Rev. Mater.* 2, 1–17. <https://doi.org/10.1038/natrevmats.2017.56>.
- Han, S.-O., Mahato, R.I., Kim, S.W., 2001. Water-soluble lipopolymer for gene delivery. *Bioconjug. Chem.* 12, 337–345. <https://doi.org/10.1021/bc000120w>.
- Hari, B.N.V., Narayanan, N., Dhevendran, K., Ramyadevi, D., 2016. Engineered nanoparticles of Efavirenz using methacrylate co-polymer (Eudragit-E100) and its biological effects in-vivo. *Mater. Sci. Eng. C Mater. Biol. Appl.* 67, 522–532. <https://doi.org/10.1016/j.msec.2016.05.064>.
- Hobernik, D., Bros, M., 2018. DNA vaccines—how far from clinical use? *Int. J. Mol. Sci.* 19, 3605. <https://doi.org/10.3390/ijms19113605>.
- Incari, V., Lavasanifar, A., Uludağ, H., 2010. Lipid and hydrophobic modification of cationic carriers on route to superior gene vectors. *Soft Matter* 6, 2124–2138. <https://doi.org/10.1039/B916362J>.
- Jain, R., Dandekar, P., Loretz, B., Koch, M., Lehr, C.-M., 2015. Dimethylaminoethyl methacrylate copolymer-siRNA nanoparticles for silencing a therapeutically relevant gene in macrophages. *MedChemComm* 6, 691–701. <https://doi.org/10.1039/C4MD00490F>.
- Jamalzaadeh, L., Ghafouri, H., Sariri, R., Rabuti, H., Nasirzade, J., Hasani, H., Aghamaali, M.R., 2016. Cytotoxic effects of some common organic solvents on MCF-7, RAW-264.7 and human umbilical vein endothelial cells. *Avicenna J. Med. Biochem.* 4, 10–33453. <https://doi.org/10.17795/ajmb-33453>.
- Kanthamneni, N., Yung, B., Lee, R.J., 2016. Effect of Eudragit on In Vitro Transfection Efficiency of PEI-DNA Complexes. *Anticancer Res.* 36, 81–85.
- Laechelt, U., Wagner, E., 2015. Nucleic Acid Therapeutics Using Polyplexes: A Journey of 50 Years (and Beyond). *Chem. Rev.* 115, 11043–11078. <https://doi.org/10.1021/cr5006793>.
- Layman, J.M., Ramirez, S.M., Green, M.D., Long, T.E., 2009. Influence of polycation molecular weight on poly (2-dimethylaminoethyl methacrylate)-mediated DNA delivery in vitro. *Biomacromolecules* 10, 1244–1252. <https://doi.org/10.1021/bm9000124>.
- Lengsfeld, C., Anchordouy, T., 2002. Shear-induced degradation of plasmid DNA. *J. Pharm. Sci.* 91, 1581–1589. <https://doi.org/10.1002/jps.10140>.
- LePecq, J.-B., Paoletti, C., 1967. A fluorescent complex between ethidium bromide and nucleic acids: physical—chemical characterization. *J. Mol. Biol.* 27, 87–106. [https://doi.org/10.1016/0022-2836\(67\)90353-1](https://doi.org/10.1016/0022-2836(67)90353-1).
- Liu, Z., Zhang, Z., Zhou, C., Jiao, Y., 2010. Hydrophobic modifications of cationic polymers for gene delivery. *Prog. Polym. Sci.* 35, 1144–1162. <https://doi.org/10.1016/j.progpolymsci.2010.04.007>.
- Lopes, A., Vandermeulen, G., Préat, V., 2019. Cancer DNA vaccines: current preclinical and clinical developments and future perspectives. *J. Exp. Clin. Cancer Res.* 38, 146.
- Lundstrom, K., 2018. Viral vectors in gene therapy. *Diseases* 6, 42. <https://doi.org/10.1186/s13046-019-1154-7>.
- Manganiello, M.J., Cheng, C., Convertine, A.J., Bryers, J.D., Stayton, P.S., 2012. Diblock copolymers with tunable pH transitions for gene delivery. *Biomaterials* 33, 2301–2309. <https://doi.org/10.1016/j.biomaterials.2011.11.019>.
- Meyers, J.A., Sanchez, D., Elwell, L.P., Falkow, S., 1976. Simple agarose gel electrophoretic method for the identification and characterization of plasmid deoxyribonucleic acid. *J. Bacteriol.* 127, 1529–1537.
- Moorthi, C., Kumar, C.S., Mohan, S., Krishnan, K., Kathiresan, K., 2013. Application of validated RP-HPLC-PDA method for the simultaneous estimation of curcumin and piperine in Eudragit E 100 nanoparticles. *J. Pharm. Res.* 7, 224–229. <https://doi.org/10.1016/j.jopr.2013.03.006>.
- Nelson, C.E., Kintzing, J.R., Hanna, A., Shannon, J.M., Gupta, M.K., Duvall, C.L., 2013. Balancing cationic and hydrophobic content of PEGylated siRNA polyplexes enhances endosome escape, stability, blood circulation time, and bioactivity in vivo. *ACS Nano* 7, 8870–8880. <https://doi.org/10.1021/nn403325f>.
- Niu, X., Zou, W., Liu, C., Zhang, N., Fu, C., 2009. Modified nanoprecipitation method to fabricate DNA-loaded PLGA nanoparticles. *Drug Dev. Ind. Pharm.* 35, 1375–1383.
- Olmsted, J., Kearns, D.R., 1977. Mechanism of ethidium bromide fluorescence enhancement on binding to nucleic acids. *Biochemistry* 16, 3647–3654. <https://doi.org/10.1019/03639040902939221>.
- Pack, D.W., Hoffman, A.S., Pun, S., Stayton, P.S., 2005. Design and development of polymers for gene delivery. *Nat. Rev. Drug Discovery* 4, 581–593. <https://doi.org/10.1038/nrd1775>.
- Perevyazko, I.Y., Vollrath, A., Pietsch, C., Schubert, S., Pavlov, G.M., Schubert, U.S., 2012. Nanoprecipitation of poly (methyl methacrylate)-based nanoparticles: Effect of the molar mass and polymer behavior. *J. Polym. Sci., Part A: Polym. Chem.* 50, 2906–2913. <https://doi.org/10.1002/pola.26071>.
- Press, A.T., Traeger, A., Pietsch, C., Mosig, A., Wagner, M., Clemens, M.G., Jbeily, N., Koch, N., Gottschaldt, M., Beziere, N., Ermolayev, V., Ntziachristos, V., Popp, J.,

- Kessels, M.M., Qualmann, B., Schubert, U.S., Bauer, M., 2014. Cell type-specific delivery of short interfering RNAs by dye-functionalised theranostic nanoparticles. *Nat. Commun.* 5, 5565. <https://doi.org/10.1038/ncomms5565>.
- Rao, S., Morales, A.A., Pearce, D.D., 2015. The comparative utility of viromer RED and lipofectamine for transient gene introduction into glial cells. *Biomed. Res. Int.* 2015 <https://doi.org/10.1155/2015/458624>.
- Rejman, J., Oberle, V., Zuhorn, I.S., Hoekstra, D., 2004. Size-dependent internalization of particles via the pathways of clathrin- and caveolae-mediated endocytosis. *Biochem. J.* 377, 159–169. <https://doi.org/10.1042/bj20031253>.
- Richter, F., Martin, L., Leer, K., Moek, E., Hausig, F., Brendel, J.C., Traeger, A., 2020. Tuning of Endosomal Escape and Gene Expression by Functional Groups, Molecular Weight and Transfection Medium: A Structure-Activity Relationship Study. *J. Mater. Chem. B* 8, 5026–5041. <https://doi.org/10.1039/D0TB00340A>.
- Rinkenauer, A.C., Press, A.T., Raasch, M., Pietsch, C., Schweizer, S., Schworer, S., Rudolph, K.L., Mosig, A., Bauer, M., Traeger, A., Schubert, U.S., 2015a. Comparison of the uptake of methacrylate-based nanoparticles in static and dynamic in vitro systems as well as in vivo. *J. Control Release* 216, 158–168. <https://doi.org/10.1016/j.jconrel.2015.08.008>.
- Rinkenauer, A.C., Tauhardt, L., Wendler, F., Kempe, K., Gottschaldt, M., Traeger, A., Schubert, U.S., 2015b. A Cationic Poly (2-oxazoline) with High In Vitro Transfection Efficiency Identified by a Library Approach. *Macromol. Biosci.* 15, 414–425. <https://doi.org/10.1002/mabi.201400334>.
- Samsonova, O., Pfeiffer, C., Hellmund, M., Merkel, O.M., Kissel, T., 2011. Low molecular weight pDMAEMA-block-pHEMA block-copolymers synthesized via RAFT-polymerization: potential non-viral gene delivery agents? *Polymers* 3, 693–718. <https://doi.org/10.3390/polym3020693>.
- Schroeder, A., Dahlman, J.E., Sahay, G., Love, K.T., Jiang, S., Eltoukhy, A.A., Levins, C. G., Wang, Y., Anderson, D.G., 2012. Alkane-modified short polyethyleneimine for siRNA delivery. *J. Control Release* 160, 172–176. <https://doi.org/10.1016/j.jconrel.2011.11.030>.
- Schuck, P., Rossmanith, P., 2000. Determination of the sedimentation coefficient distribution by least-squares boundary modeling. *Biopolym.: Original Res. Biomol.* 54, 328–341. [https://doi.org/10.1002/1097-0282\(20001015\)54:5<328::AID-BIP40>3.0.CO;2-P](https://doi.org/10.1002/1097-0282(20001015)54:5<328::AID-BIP40>3.0.CO;2-P).
- Shen, W., Wang, R., Fan, Q., Gao, X., Wang, H., Shen, Y., Li, Y., Cheng, Y., 2020. Natural Polyphenol Inspired Polycatechols for Efficient siRNA Delivery. *CCS Chem.* 146–157. <https://doi.org/10.31635/ccschem.020.201900084>.
- Shirley, J.L., de Jong, Y.P., Terhorst, C., Herzog, R.W., 2020. Immune Responses to Viral Gene Therapy Vectors. *Mol. Ther.* 28 (3), 709–722. <https://doi.org/10.1016/j.ymthe.2020.01.001>.
- Smith, D., Pentzer, E.B., Nguyen, S.T., 2007. Bioactive and therapeutic ROMP polymers. *J. Macromol. Sci., Part C: Polym. Rev.* 47, 419–459. <https://doi.org/10.1080/15583720701455186>.
- Tan, E., Lv, J., Hu, J., Shen, W., Wang, H., Cheng, Y., 2018. Statistical versus block fluoropolymers in gene delivery. *J. Mater. Chem. B* 6, 7230–7238. <https://doi.org/10.1039/C8TB01470A>.
- Tang, J., Xu, N., Ji, H., Liu, H., Wang, Z., Wu, L., 2011. Eudragit nanoparticles containing genistein: formulation, development, and bioavailability assessment. *Int. J. Nanomed.* 6, 2429–2435. <https://doi.org/10.2147/IJN.S24185>.
- Trutzschler, A.K., Bus, T., Reifarth, M., Brendel, J.C., Hoepfner, S., Traeger, A., Schubert, U.S., 2018. Beyond Gene Transfection with Methacrylate-Based Polyplexes-The Influence of the Amino Substitution Pattern. *Bioconjug. Chem.* 29, 2181–2194. <https://doi.org/10.1021/acs.bioconjchem.8b00074>.
- Van de Wetering, P., Cherng, J.-Y., Talsma, H., Crommelin, D., Hennink, W., 1998. 2-(Dimethylamino) ethyl methacrylate based (co) polymers as gene transfer agents. *J. Control. Release* 53, 145–153. [https://doi.org/10.1016/S0168-3659\(97\)00248-4](https://doi.org/10.1016/S0168-3659(97)00248-4).
- Van de Wetering, P., Moret, E.E., Schuurmans-Nieuwenbroek, N.M., van Steenberghe, M. J., Hennink, W.E., 1999. Structure– activity relationships of water-soluble cationic methacrylate/methacrylamide polymers for nonviral gene delivery. *Bioconjug. Chem.* 10, 589–597. <https://doi.org/10.1021/bc980148w>.
- Wakefield, D.H., Klein, J.J., Wolff, J.A., Rozema, D.B., 2005. Membrane activity and transfection ability of amphipathic polycations as a function of alkyl group size. *Bioconjug. Chem.* 16, 1204–1208.
- Wang, Y., Ye, M., Xie, R., Gong, S., 2018. Enhancing the in vitro and in vivo stabilities of polymeric nucleic acid delivery nanosystems. *Bioconjug. Chem.* 30, 325–337. <https://doi.org/10.1021/bc050067h>.
- Wong, S.Y., Pelet, J.M., Putnam, D., 2007. Polymer systems for gene delivery—past, present, and future. *Prog. Polym. Sci.* 32, 799–837. <https://doi.org/10.1016/j.progpolymsci.2007.05.007>.
- Yildirim, T., Rinkenauer, A.C., Weber, C., Traeger, A., Schubert, S., Schubert, U.S., 2015. RAFT made methacrylate copolymers for reversible pH-responsive nanoparticles. *J. Polym. Sci., Part A: Polym. Chem.* 53, 2711–2721. <https://doi.org/10.1002/pola.27734>.
- Yin, H., Kanasty, R.L., Eltoukhy, A.A., Vegas, A.J., Dorkin, J.R., Anderson, D.G., 2014. Non-viral vectors for gene-based therapy. *Nat. Rev. Genet.* 15, 541–555. <https://doi.org/10.1038/nrg3763>.

Supporting information

Solely aqueous formulation of hydrophobic cationic polymers for efficient gene delivery

Jana I. Solomun,^a Gizem Cinar,^a Prosper Mapfumo,^a Friederike Richter,^a Elisabeth Moek,^a

Franziska Hausig,^a Liam Martin,^a Stephanie Hoeppener,^{a,b} Ivo Nischang,^{a,b}

Anja Traeger^{a,b}*

^aLaboratory of Organic and Macromolecular Chemistry (IOMC), Friedrich Schiller University
Jena, Humboldtstrasse 10, 07743 Jena, Germany.

^bJena Center for Soft Matter (JCSM), Friedrich Schiller University Jena, Philosophenweg 7,
07743 Jena, Germany.

*Correspondence to A. Traeger (anja.traeger@uni-jena.de)

List of Tables

Table S1. DLS/ELS measurements of the PBMD _{Org} (out,pDNA) formulation.	7
Table S2. DLS/ELS measurements of the PBMD _{Org} (in,pDNA) formulation.	7
Table S3. DLS/ELS measurements of the PBMD _{Aqu} (pDNA) formulation.	8
Table S4. DLS measurements of PBMD _{Aqu} (pDNA) formed with different plasmids used within the study.	10
Table S5. DLS measurements of PBMD _{Aqu} (siRNA) and of PBMD _{Aqu} (mRNA) at N/P 10. ...	17

List of Figures

Fig. S1. Synthesis and characterization of PDMAEMA.	6
Fig. S2. DLS hydrodynamic diameter distributions and example exponential decays from samples of the different formulation methods at N/P 50.	9
Fig. S3. DLS hydrodynamic diameter distributions and example exponential decays of PBMD _{Aqu} (pDNA) complexes at N/P 10 and 20.	10
Fig. S4. Scanning electron microscopy measurements (SEM) of PBMD _{Org} (in,pDNA) and PBMD _{Org}	11
Fig. S5. Gating strategy for pDNA transfection experiments.	12
Fig. S6. Gating strategy for siRNA transfection experiments.	13
Fig. S7. Gating strategy for mRNA transfection experiments.	14
Fig. S8. Sedimentation velocity profiles of free RAFT agent-containing polymer.	15
Fig. S9. AUC measurements of PDMAEMA-polyplexes.	15
Fig. S10. AUC measurements at increasing sample concentrations.	16
Fig. S11. Comparison of AUC measurements of PBMD _{Aqu} (pDNA) and PDMAEMA-polyplexes.	17

1. Additional methods and materials

1.1 Materials

2-(Dimethylamino)ethyl methacrylate (DMAEMA) (98%) was obtained from Sigma-Aldrich (now Merck KGaA, St. Louis, MO, U.S.) and used as received. Butyl methacrylate (*n*BMA) (99%) and methyl methacrylate (MMA) (99%) were obtained from TCI (Tokyo, Japan) and used as received. Bis(ethylsulfanyl thiocarbonyl)disulfide was synthesized according to the literature.[1] α,α' -Azoisobutyronitrile (AIBN) was obtained from Sigma-Aldrich (now Merck KGaA, St. Louis, MO, U.S.) and recrystallized from methanol. Organic solvents for synthesis were obtained from Sigma-Aldrich (now Merck KGaA, St. Louis, MO, U.S.) and re-distilled on-site. All the following materials were ordered from the suppliers stated in brackets: HEK293T cells (DSMZ, Braunschweig, Germany), L-929 cells (CLS Cell Lines Service, Eppelheim, Germany), HEK293-GFP cells (Amsbio LLC, Abington, U.K.), TC treated cell culture flasks (Greiner Bio-One International GmbH, Kremsmünster, Austria), TC treated multiwell cell culture plates (VWR International GmbH, Darmstadt, Germany), Dulbecco's modified eagle medium (DMEM) and 4-(2-hydroxyethyl)-1-piperazineethanesulfonic acid (HEPES) buffer (Biowest SAS, Nuillé, France), fetal bovine serum (FBS, Capricorn Scientific, Ebsdorfergrund, Germany), Opti-MEM™ reduced serum medium, Penicillin-Streptomycin, PrestoBlue™ cell viability reagent (Thermo Fisher Scientific, Waltham, MA, U.S.), trypsin-EDTA, Hanks' balanced salt solution (HBSS) (Sigma-Aldrich, St. Louis, MO, U.S.), ethidiumbromide solution, agarose-HR PLUS (Carl Roth, Karlsruhe, Germany), heparin sodium salt (Alfa Aesar, Haverhill, MA, U.S.), Eudragit® E(PO/E100) (Evonik Industries, Essen, Germany), linear poly(ethylenimine) (25 kDa, Polysciences, Warrington, PA, U.S.), Viomer® RED (Lipocalyx, now BioNTech, Mainz, Germany). Plasmid DNA encoding for enhanced green fluorescent protein (mEGFP-N1, 4.7 kb), td-tomato (td-tomato-N1, 5.4 kb) or Myc (pKMyc, 4.7 kb) was isolated from E. Coli using a Giga plasmid kit (Quiagen, Hilden, Germany). mEGFP-N1 was a gift from Michael Davidson (Addgene plasmid #54767;

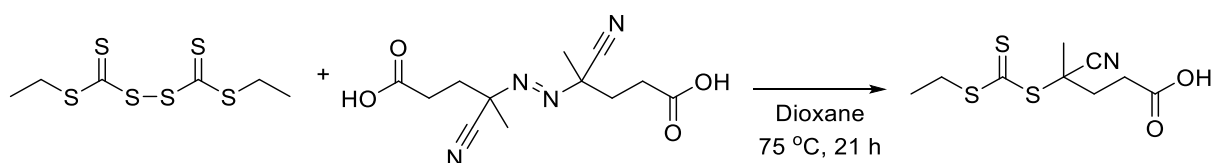
<http://n2t.net/addgene:54767>;RRID: Addgene_54767), tdTomato-N1 was a gift from Michael Davidson & Nathan Shaner & Roger Tsien (Addgene plasmid #54642; <http://n2t.net/addgene:54642>; RRID: Addgene_54642) and pKMyC was a gift from Ian Macara (Addgene plasmid #19400;<http://n2t.net/addgene:19400>;RRID: Addgene_19400). pCMV-GFP plasmid was ordered from Plasmid Factory (Bielefeld, Germany, 3.5 kb). GFP-22 siRNA targeting green fluorescent protein (GFP) and negative control siRNA were ordered from Qiagen (Hilden, Germany). mRNA encoding for GFP was obtained from Oz Biosciences (Marseille, France).

1.2 Synthesis of (4-cyanopentanoic acid)ylethyl trithiocarbonate (CPAETC)

To a solution of bis-(ethylsulfanylthiocarbonyl) disulfide (2.5 g, 9.1 mmol) in 1,4-dioxane (62 mL), 4,4'-azobis(4-cyanovaleric acid) (5.4 g, 2.1 eq., 19.13 mmol) was added and the mixture was stirred for 21 hours at 75 °C. After removal of the solvent under reduced pressure, the crude product was subjected to column chromatography (silica, hexane: ethyl acetate, with a content of ethyl acetate varying from 60 to 30%). The product fractions were collected and dried under vacuum; an orange powder was obtained (81% yield).

¹H NMR (300 MHz, CDCl₃-d) δ [ppm] = 3.36 (q, *J* = 7.4 Hz, 2H, S-CH₂-CH₃), 2.76 – 2.61 (m, 2H, C(O)-CH₂-CH₂-), 2.65 – 2.33 (m, 2H, C(O)-CH₂-CH₂-), 1.90 (s, 3H, C(CN)(CH₃)), 1.37 (t, *J* = 7.4 Hz, 4H, CH₂-CH₃).

¹³C-NMR (75 MHz, CDCl₃) δ [ppm] = 216.66, 177.24, 118.88, 46.37, 77.41, 76.63, 33.47, 31.40, 29.52, 24.84, 12.74.



1.3 Reversible addition fragmentation chain-transfer (RAFT) polymerization

Conversion (p) of each monomer was calculated from ^1H -NMR data by comparing the integrals between vinyl peaks (5.5 - 6.3 ppm) and polymer peaks against an external reference (1,3,5-trioxane, 5.14 ppm) before ($t=0$) and at designated time points throughout the polymerization. The theoretical number-average molar mass ($M_{n,\text{th}}$) was then calculated using equation (1):

$$M_{n,\text{th}} = \frac{[\text{DMAEMA}]_0 p_{\text{DMAEMA}} M_{\text{DMAEMA}} + [\text{BMA}]_0 p_{\text{BMA}} M_{\text{BMA}} + [\text{MMA}]_0 p_{\text{MMA}} M_{\text{MMA}}}{[\text{CTA}]_0} + M_{\text{CTA}} \quad (1)$$

Where $[\text{DMAEMA}]_0$, $[\text{BMA}]_0$, $[\text{MMA}]_0$ and $[\text{CTA}]_0$ are the initial concentrations of the monomers and the chain transfer agent (CTA), respectively, M_{DMAEMA} , M_{BMA} , M_{MMA} , and M_{CTA} are the molar mass of the monomer and CTA, respectively, and p is the monomer conversion of each monomer.

1.4 Synthesis of P(DMAEMA) *via* RAFT polymerization

CPAETC (50.0 mg, 1.9×10^{-4} moles), DMAEMA (4.5 g, 2.9×10^{-2} moles), 1,4-dioxane (2.5 g), 1% (w/w) ACVA in 1,4-dioxane (426.0 mg, 1.5×10^{-5} moles) and 1,3,5-trioxane (external NMR standard, 21 mg) were introduced to a 20 mL microwave vial equipped with a magnetic stirring bar. The vial was sealed, and the solution deoxygenated by bubbling argon through it for approx. 10 min. The vial was placed in an oil bath set at 70 °C and allowed to stir for 7 h, with samples taken for ^1H -NMR and CHCl_3 -SEC analysis at designated times. The polymer was precipitated three times from THF into cold hexane and dried under reduced pressure to give a yellow solid. CHCl_3 -SEC: $M_{n,\text{SEC}} = 14.2 \text{ kg mol}^{-1}$, $D = 1.19$.

2. Further Results

2.1 Characterization of PDMAEMA

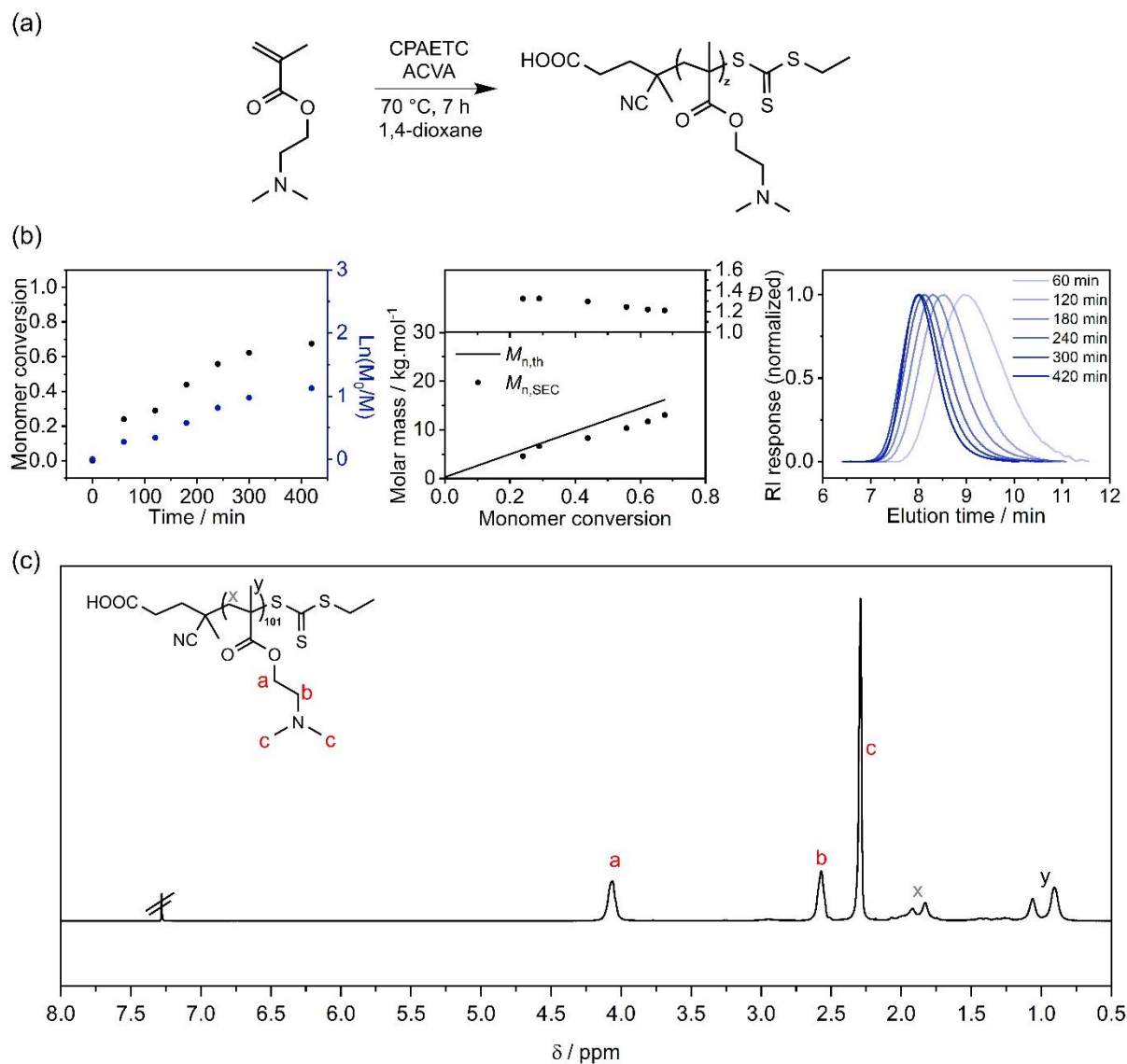


Fig. S1. Synthesis and characterization of PDMAEMA.

(a) Schematic representation of the RAFT polymerization to obtain PDMAEMA. (b) Kinetics of PDMAEMA formation was measured by ^1H -NMR and SEC. (c) ^1H -NMR was measured after precipitation.

2.2 DLS measurements

Table S1. DLS/ELS measurements of the PBMD_{Org}(out,pDNA) formulation.

Size and zeta potential measured by DLS/ELS. Each measurement is displayed as a single value.

Formulation	N/P ratio	z-average / nm	PDI	Zeta potential / mV
PBMD _{Org} (out,pDNA)	0	118.4	0.186	67.1
		144.7	0.141	50.1
		111.9	0.131	44.4
		123.4	0.125	42.1
	5	165.6	0.221	-14.0
		193.6	0.209	-12.9
		248.7	0.237	-14.0
		182.8	0.184	-12.9
	15	764.4	0.376	-7.2
		757.8	0.324	-8.0
		7824.8	0.247	15.4
		1104.3	0.539	-7.3
	30	1168.2	0.699	18.4
		1160.8	0.842	21.6
		7789.0	0.902	29.3
		2673.4	0.943	26.4
	50	608.8	0.489	25.9
		338.7	0.704	32.1
		127.2	0.111	41.6
		148.7	0.123	31.8
	100	188.0	0.329	39.1
		146.0	0.179	42.3
		113.3	0.131	42.9
		126.9	0.111	36.8

Table S2. DLS/ELS measurements of the PBMD_{Org}(in,pDNA) formulation.

Size and zeta potential measured by DLS/ELS. Each measurement is displayed as a single value.

Formulation	N/P ratio	z-average / nm	PDI	Zeta potential / mV
PBMD _{Org} (in,pDNA)	30	1139.8	0.686	45.6
		241.0	0.260	32.6
		605.4	0.405	43.3
	50	4111.0	0.143	42.2
		276.7	0.134	40.3
		311.2	0.102	39.8
	75	214.5	0.117	39.6
		225.5	0.086	40.4
		223.4	0.100	39.6
	100	183.8	0.071	41.9
		188.4	0.115	43.1
		215.4	0.061	38.1

Table S3. DLS/ELS measurements of the PBMD_{Aqu}(pDNA) formulation.

Size and zeta potential measured by DLS/ELS. Each measurement is displayed as a single value.

Formulation	N/P ratio	z-average / nm	PDI	Zeta potential / mV
PBMD _{Aqu} (pDNA)	0.5	113.4	0.236	-19.5
		147.6	0.161	-15.2
		442.8	0.377	-17.7
		129.7	0.155	
	1	2104.0	0.324	-22.3
		73.1	0.582	-18.2
		163.7	0.159	-18.3
		159.7	0.214	
	5	120.4	0.161	8.1
		188.3	0.176	
		101.0	0.150	15.5
		1503.5	0.218	
		535.1	0.269	19.5
		759.4	0.264	
	10	110.1	0.205	23.2
		109.8	0.173	
		98.7	0.190	20.6
		120.5	0.208	
		102.1	0.200	20.8
	20	96.2	0.189	21.9
		98.4	0.179	
		92.7	0.231	24.2
		107.2	0.219	
		100.0	0.263	19.7
	30	89.9	0.176	23.6
		94.4	0.187	
		79.9	0.204	23.4
		93.0	0.221	
		90.6	0.252	22.3
	50	72.2	0.220	24.6
		85.3	0.202	
		75.2	0.238	24.6
		92.7	0.220	
		83.6	0.264	25.5

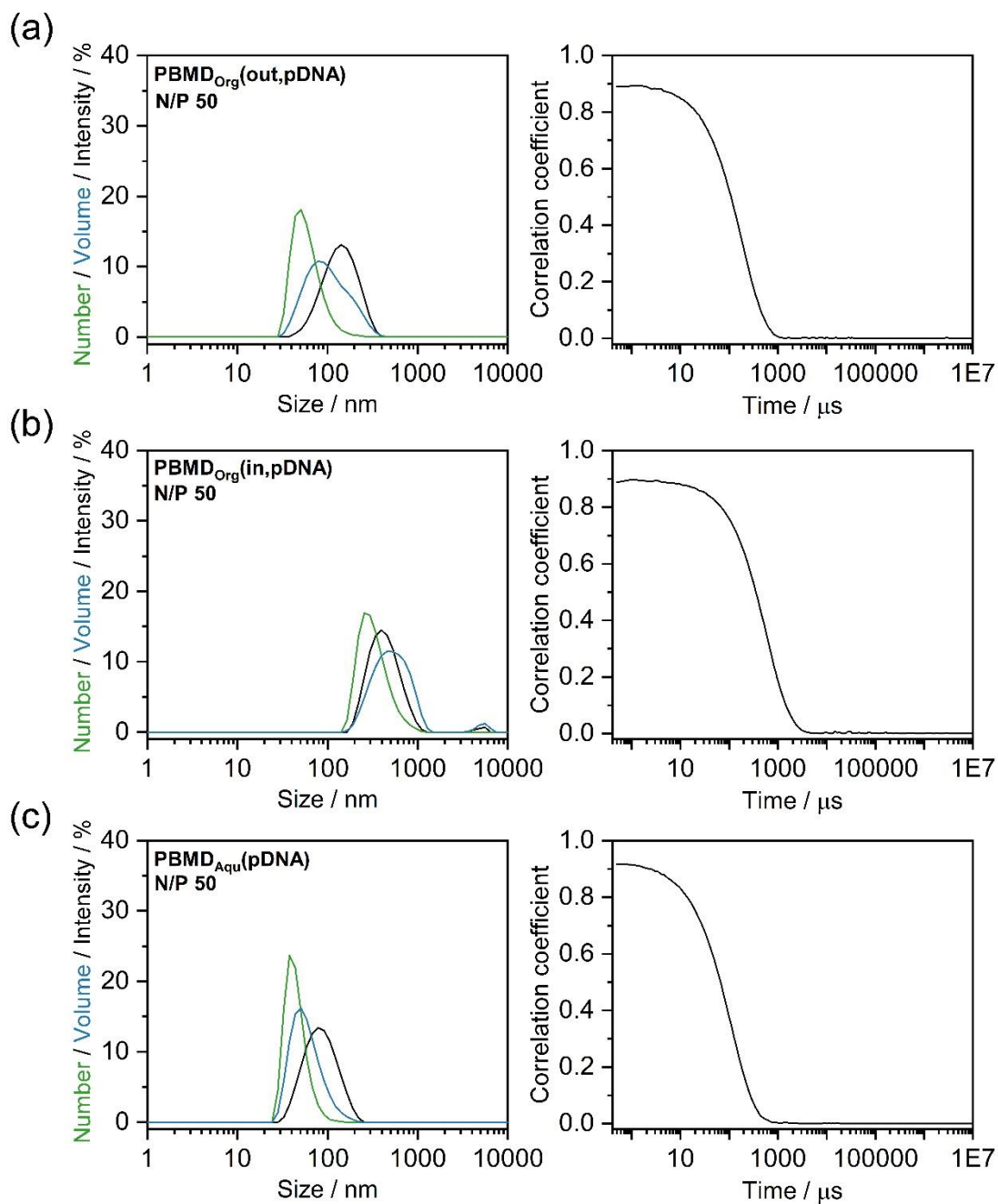


Fig. S2. DLS hydrodynamic diameter distributions and example exponential decays from samples of the different formulation methods at N/P 50.

pDNA-loaded NPs or complexes obtained by different formulation methods at N/P 50 and $15 \mu\text{g mL}^{-1}$ pCMV-GFP plasmid. Exemplary intensity, number, and volume weighted plots and exponential decay correlation coefficients of single measurements are displayed for (a) PBMD_{Org}(out,pDNA), (b) PBMD_{Org}(in,pDNA) and (c) PBMD_{Aqu}(pDNA) formulations.

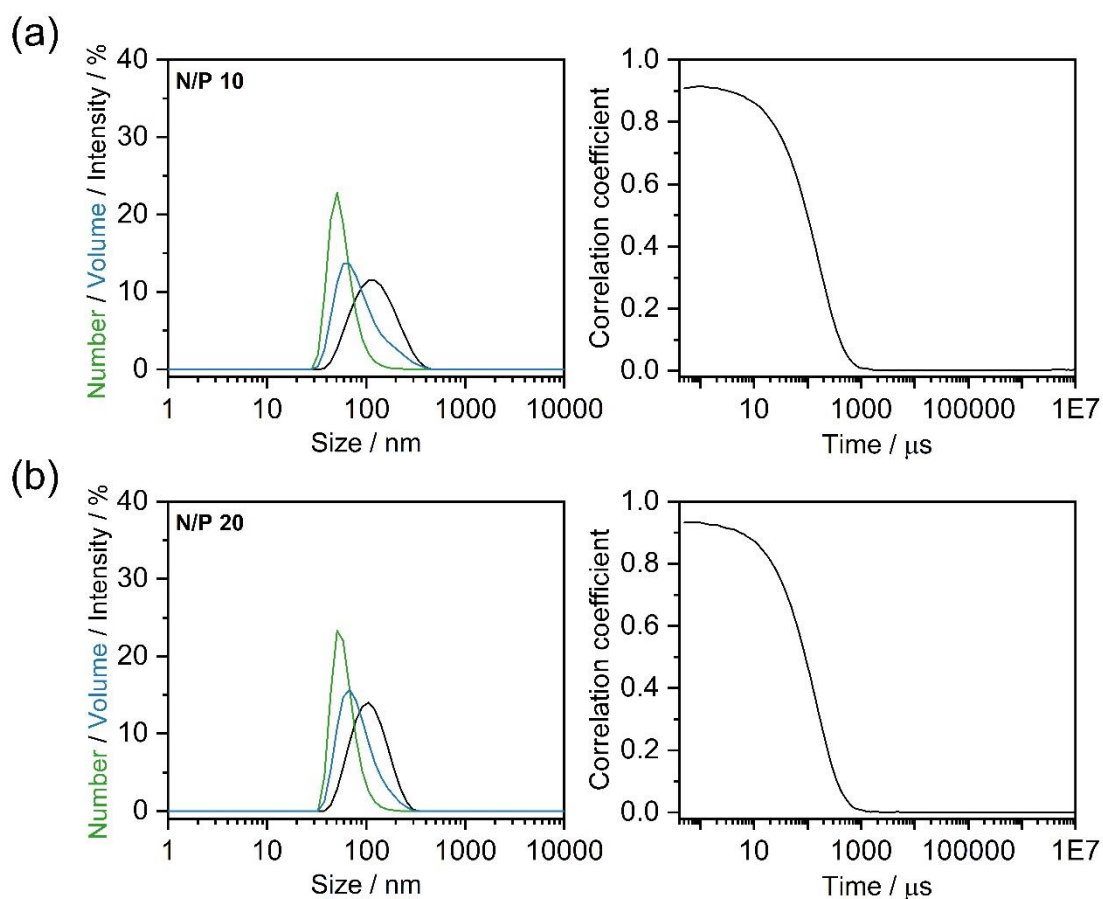


Fig. S3. DLS hydrodynamic diameter distributions and example exponential decays of PBMD_{Aqu}(pDNA) complexes at N/P 10 and 20.

Complexes at (a) N/P 10 and (b) N/P 20 formed using 15 μ g mL⁻¹ pCMV-GFP plasmid.

Table S4. DLS measurements of PBMD_{Aqu}(pDNA) formed with different plasmids used within the study.

Size was measured by DLS (mean of $n=3 \pm$ SD).

pDNA	z-average / nm	PDI
pCMV-GFP	90.9 \pm 1.5	0.182 \pm 0.015
mEGFP-N1	97.3 \pm 2.2	0.175 \pm 0.002
pKmyc	94.6 \pm 1.0	0.180 \pm 0.009
td-tomato-N1	87.2 \pm 1.7	0.164 \pm 0.024

2.3 Scanning electron microscopy measurements (SEM)

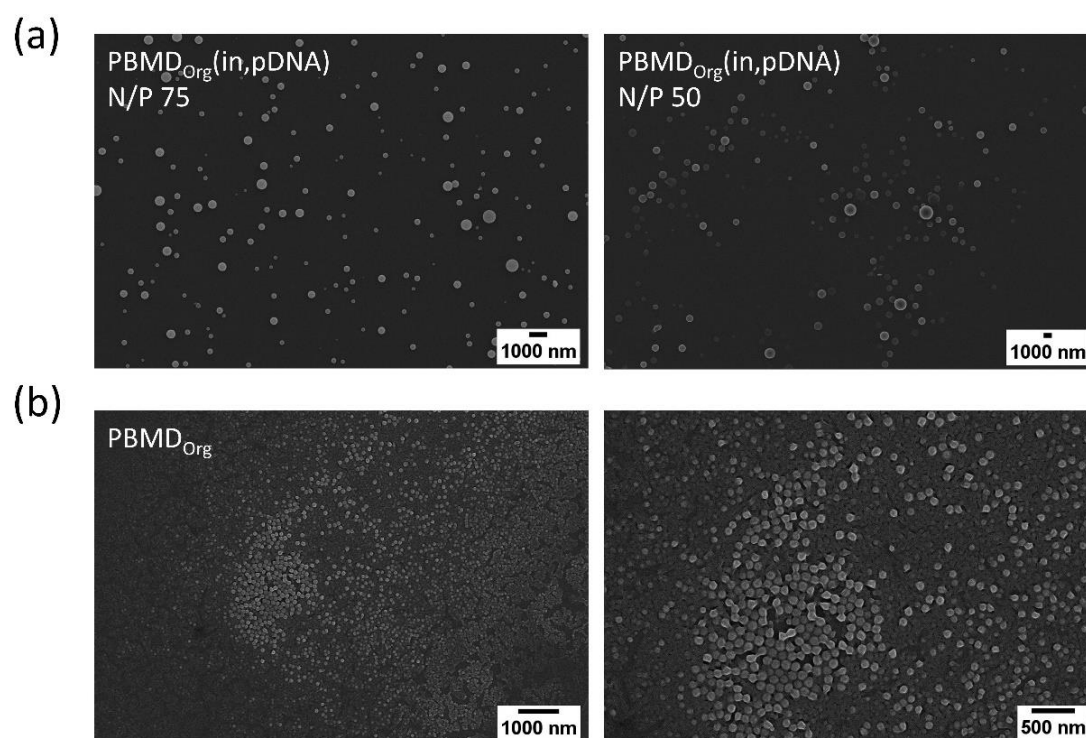


Fig. S4. Scanning electron microscopy measurements (SEM) of PBMD_{Org}(in,pDNA) and PBMD_{Org}.

(a) nanoparticles obtained by the PBMD_{Org}(in,pDNA) formulation at N/P ratios of 75 and 50 and (b) nanoparticles formulated by nanoprecipitation in acetone prior to addition of pDNA (PBMD_{Org}).

2.4 Gating strategy for transfection experiments

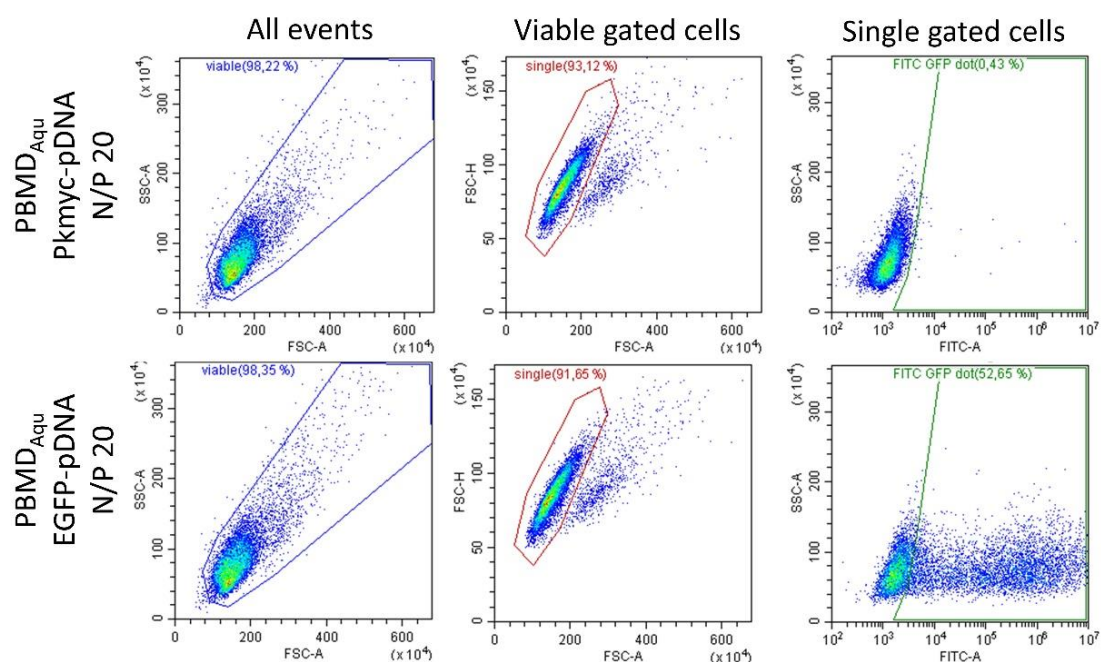


Fig. S5. Gating strategy for pDNA transfection experiments.

Viable cells were gated according to the FSC/SSC pattern. Subsequently the single cells were discriminated from doublets in the sample using the area of FSC signal plotted against the FSC height.

GFP positive cells were identified by gating the single cells to the unstained control (PBMD_{Aqu}(pDNA) complex with pKMyC plasmid).

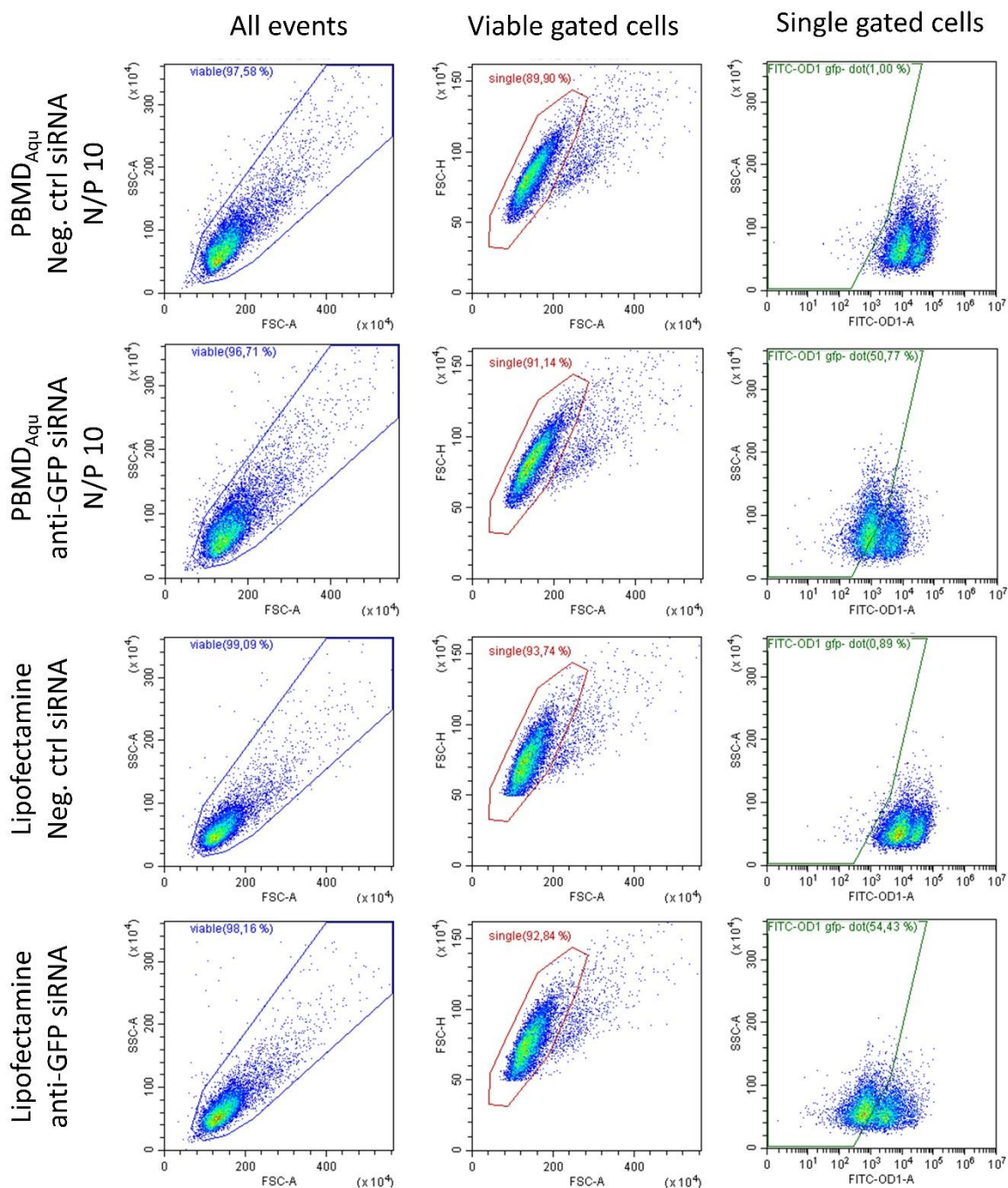


Fig. S6. Gating strategy for siRNA transfection experiments.

Viable single cells were gated as described for pDNA transfection. Subsequently, cells with reduced GFP fluorescence were discriminated by gating to the control (PBMD_{Aqu}(siRNA) complex with neg. ctrl GFP siRNA).

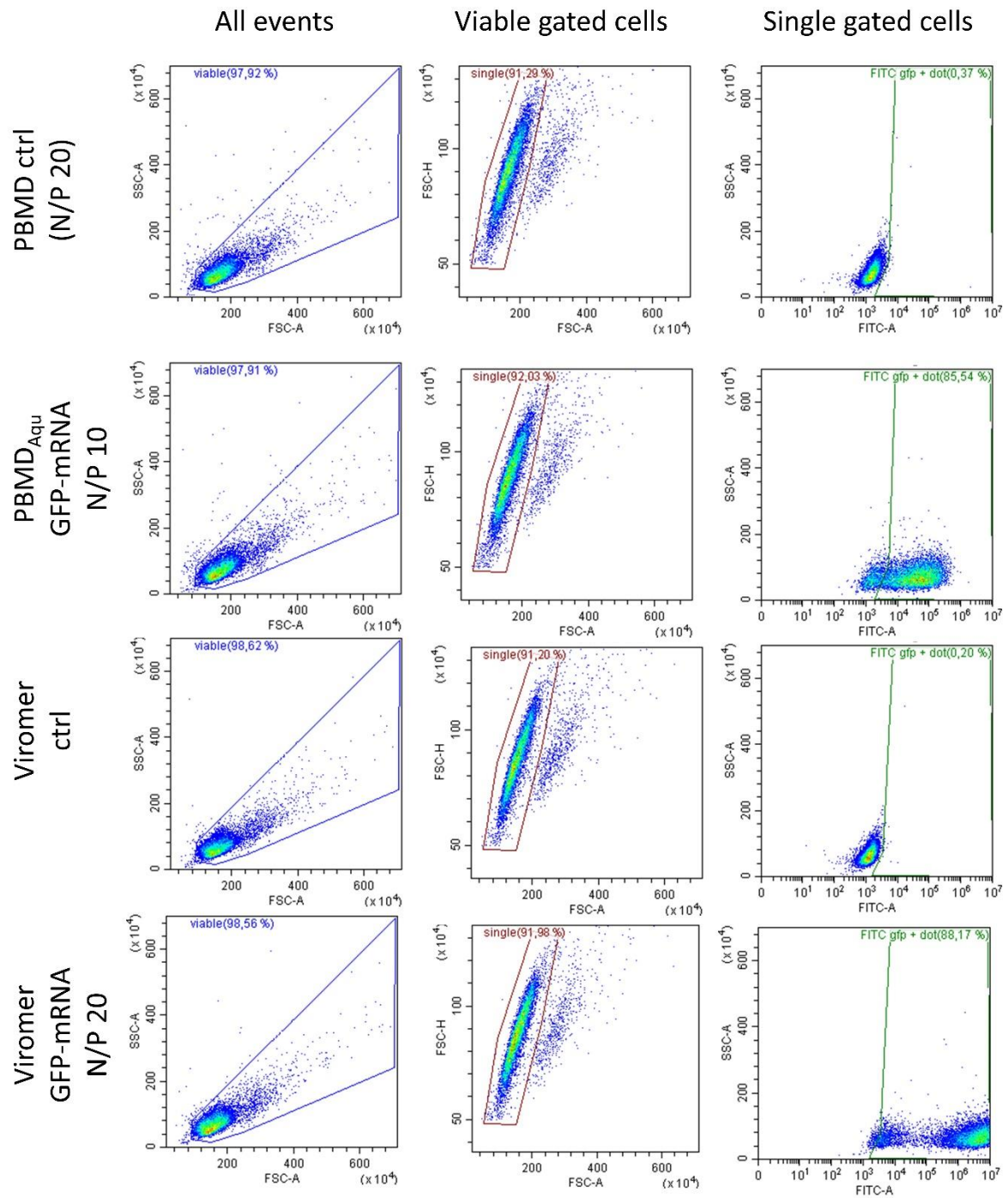


Fig. S7. Gating strategy for mRNA transfection experiments.

Viable single cells were gated as described. Cells expressing GFP were identified by gating to the control (polymer without mRNA).

2.5 Analytical ultracentrifugation (AUC) measurements

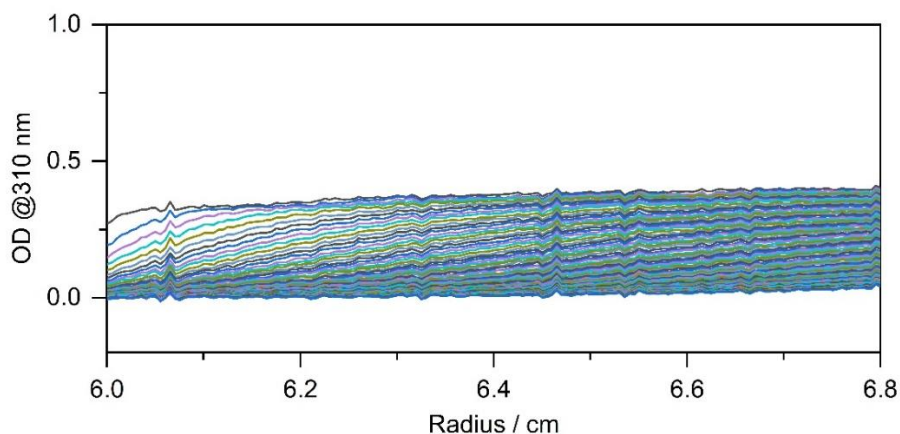


Fig.S8. Sedimentation velocity profiles of free RAFT agent-containing polymer.

Radially resolved sedimentation velocity profiles of free RAFT agent-containing polymer of the PBMD_{Aqu}(pDNA) complex at an N/P ratio of 20 (in terms of OD) at a concentration of $c = 1 \text{ mg mL}^{-1}$ monitored at a wavelength of $\lambda = 310 \text{ nm}$ in terms of OD at a subsequent a rotor speed at 42,000 rpm.

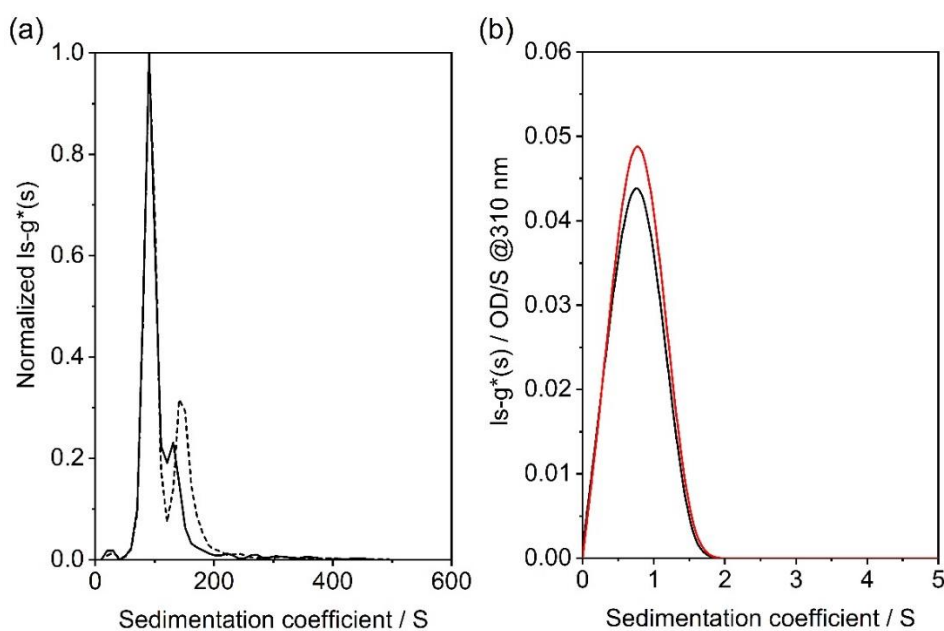


Fig. S9. AUC measurements of PDMAEMA-polyplexes.

(a) Normalized differential distributions of sedimentation coefficients of PDMAEMA complexes at a rotor speed of 7,500 rpm and at $\lambda = 260 \text{ nm}$ in terms of OD formed at N/P 10 (black dashed line) and N/P 20 (black solid line). (b) Differential distributions of sedimentation coefficients at a subsequent

rotor speed of 42,000 rpm and at $\lambda = 310$ nm in terms of OD of the free polymer. Complex formed with PDMAEMA at N/P 10 (black solid line) and N/P 20 (red solid line).

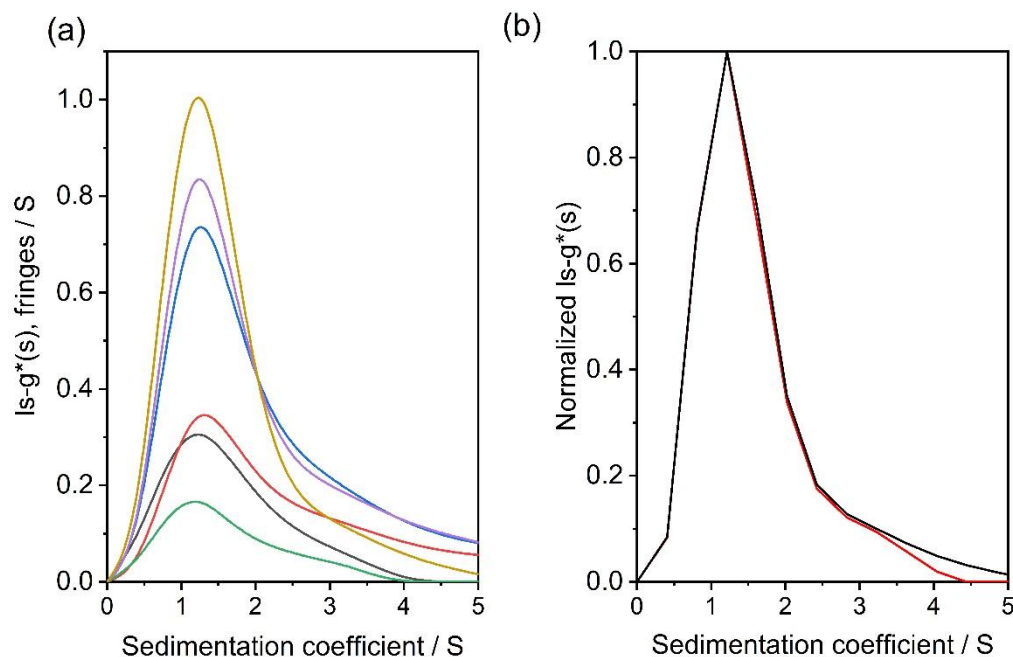


Fig. S10. AUC measurements at increasing sample concentrations.

(a) Differential distributions of sedimentation coefficients obtained at a subsequent rotor speed of 42,000 rpm and at increasing sample concentrations of the PBMD_{Aqu}(pDNA) formulation at N/P 20 (from bottom to top) via RI detection, and (b) overlay of normalized differential distributions of sedimentation coefficients at $\lambda = 310$ nm (red solid line) and RI detection (black solid line) at a rotor speed at 42,000 rpm.

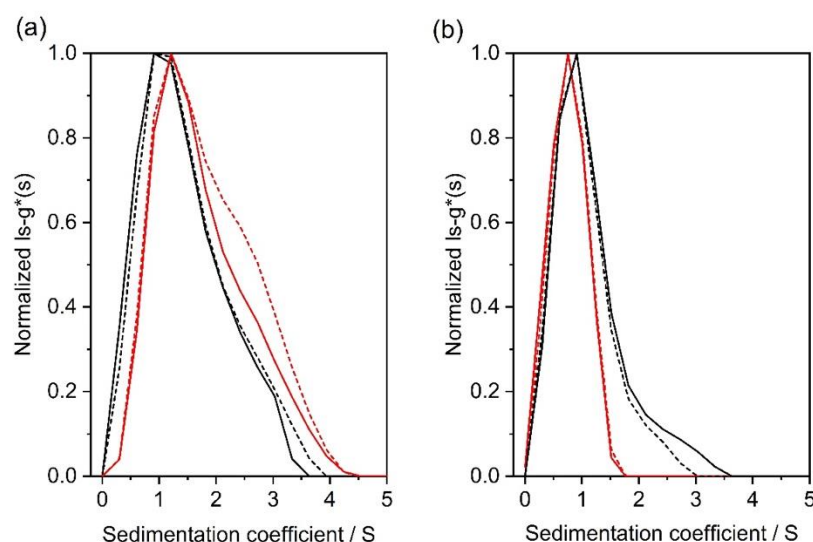


Fig. S11. Comparison of AUC measurements of PBMD_{Aqu}(pDNA) and PDMAEMA-polyplexes.

Normalized differential distributions of sedimentation coefficients at a rotor speed of 42,000 rpm and at $\lambda = 310$ nm of the free polymer. (a) PBMD_{Aqu}(pDNA) complex at an N/P ratio of 10 (solid lines) and N/P20 (dashed lines) at a wavelength of $\lambda = 310$ nm (red lines) and RI detection (black lines). (b) Polyplexes formed with PDMAEMA at an N/P ratio of 10 (solid lines) and N/P 20 (dashed lines) at a wavelength of $\lambda = 310$ nm (red lines) and RI detection (black lines).

Table S5. DLS measurements of PBMD_{Aqu}(siRNA) and of PBMD_{Aqu}(mRNA) at N/P 10.

Size measured by DLS at a RNA concentration of $15 \mu\text{g mL}^{-1}$ ($n = 1$, mean \pm SD of three sub-runs).

Formulation	z-average / nm	PDI
PBMD _{Aqu} (siRNA) N/P10	165.7 ± 4.1	0.229 ± 0.022
PBMD _{Aqu} (mRNA) N/P 10	139.7 ± 2.0	0.174 ± 0.021

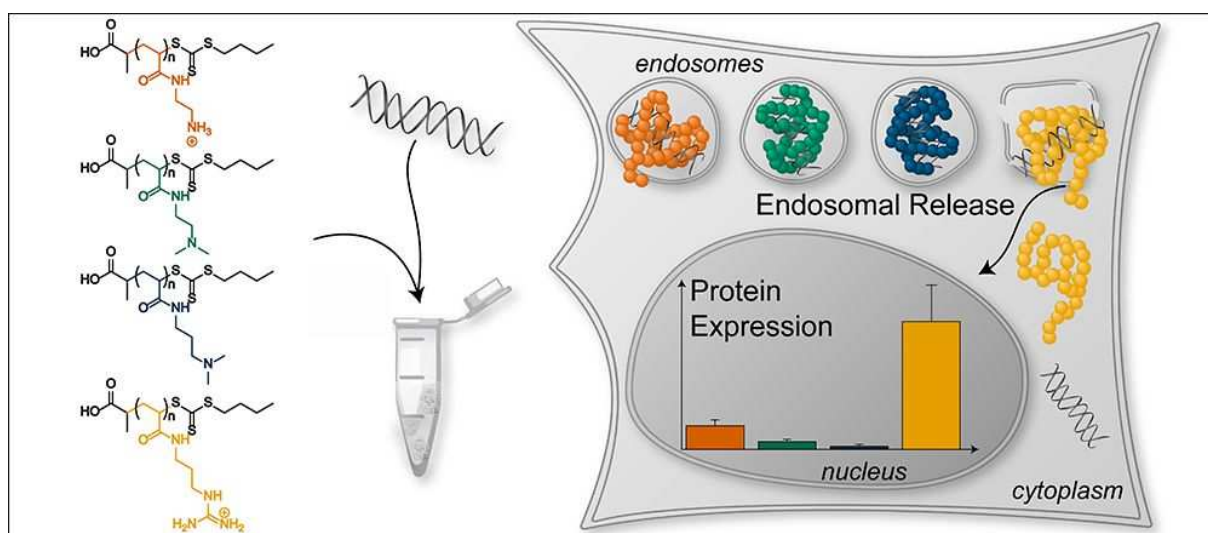
References

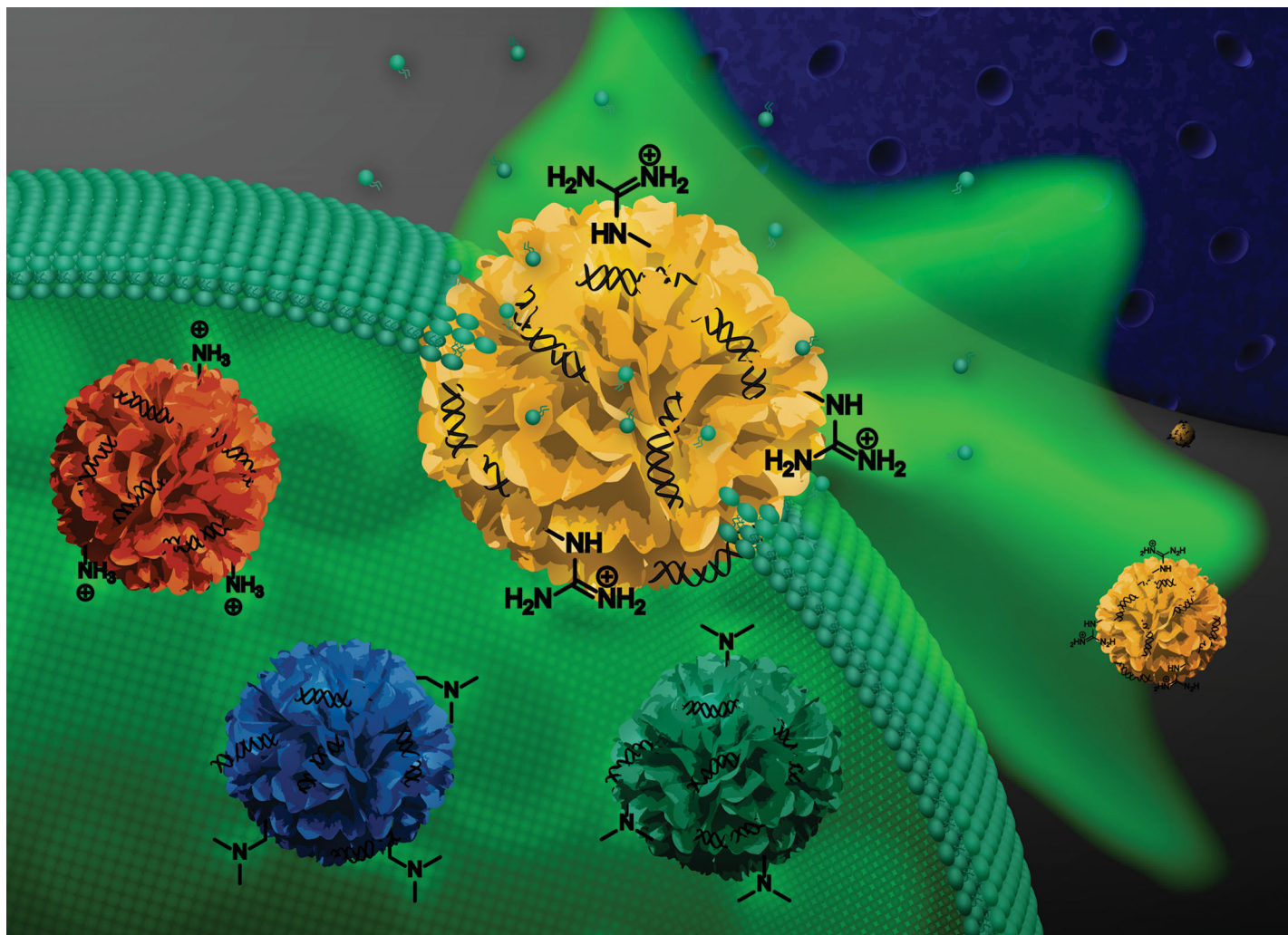
[1] K. Ishitake, K. Satoh, M. Kamigaito, Y. Okamoto, Stereogradient polymers formed by controlled/living radical polymerization of bulky methacrylate monomers, *Angewandte Chemie*, 121 (2009) 2025-2028.

Publication Pub6

Tuning of endosomal escape and gene expression by functional groups, molecular weight and transfection medium: a structure–activity relationship study

F. Richter, L. Martin, K. Leer, E. Moek, F. Hausig, J. C. Brendel, A. Traeger, J.
Mater. Chem. B, **2020**, 8, 5026-5041.



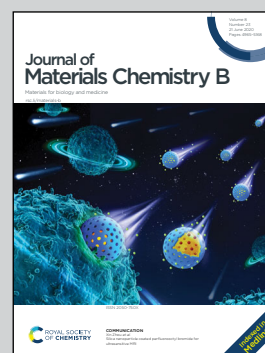


A study on polyacrylamides with different amine moieties for gene delivery by F. Richter and Dr A. Traeger at Friedrich Schiller University Jena

Tuning of endosomal escape and gene expression by functional groups, molecular weight and transfection medium: a structure-activity relationship study

Guanidinium-containing homopolymers showed superior endosomal escape and transfection efficiency, although the degree of protonation does not change during the transfection process.

As featured in:





See Anja Traeger *et al.*,
J. Mater. Chem. B, 2020, **8**, 5026.

PAPER

[View Article Online](#)
[View Journal](#) | [View Issue](#)Cite this: *J. Mater. Chem. B*, 2020, **8**, 5026

Tuning of endosomal escape and gene expression by functional groups, molecular weight and transfection medium: a structure–activity relationship study†

Friederike Richter,^a Liam Martin,^a Katharina Leer,^a Elisabeth Moek,^a Franziska Hausig,^a Johannes C. Brendel ^{ab} and Anja Traeger ^{*ab}

The use of genetic material by non-viral transfer systems is still in its initial stages, but there are high expectations for the development of targeted therapies. However, nucleic acids cannot enter cells without help, they must be well protected to prevent degradation and overcome a variety of biological barriers, the endosomal barrier being one of the greatest cellular challenges. Herein, the structure–property–relationship was investigated in detail, using well-defined polymers. Polyacrylamides were synthesized via RAFT polymerization resulting in a polymer library of (i) different cationic groups as aminoethyl acrylamide (AEAm), dimethylaminoethyl acrylamide (DMAEAm), dimethylaminopropyl acrylamide (DMAPAm) and guanidinopropyl acrylamide (GPAm); (ii) different degree of polymerization; and investigated (iii) in different cell culture settings. The influence of molar mass and cationic moiety on complex formation with pDNA, cytotoxicity and transfection efficiency of the polymers were investigated. The systematic approach identified a pH-independent guanidinium-containing homopolymer (PGPAm₈₉) as the polymer with the highest transfection efficiency and superior endosomal release under optimal conditions. Since PGPAm₈₉ is not further protonated inside endosomes, common escape theories appear unsuitable. Therefore, the interaction with bis(monoacryloylglycerol)phosphate, a lipid specific for endosomal vesicles, was investigated. Our research suggests that the interactions between amines and lipids may be more relevant than anticipated.

Received 7th February 2020,
Accepted 6th April 2020

DOI: 10.1039/d0tb00340a

rsc.li/materials-b

Introduction

Gene therapy is a powerful approach towards treating genetic disorders, cancer and other diseases. Due to an instability against nucleases and reduced uptake ability of naked genetic material, carriers are needed for effective protection and transportation.¹ Carriers designed by nature are known as viruses, some of which have already been approved by different agencies.² However, viruses pose a high risk due to unexpected side-effects, show limitations in modification as well as in the amount of delivered genetic material, and are not amenable to scale-up. Polymers are thus an extremely appealing alternative.^{3,4} To protect their genetic cargo, the polymers form

stable complexes with the negatively charged phosphate groups of the genetic material and are, as such, typically positively charged.⁵ Moreover, the cationic charge aids in overcoming gene delivery barriers like the cellular membrane and lysosomal entrapment. Especially the endosomal escape is important to prevent recycling or enzymatic degradation and to transport the genetic material closer to its site of action.^{6–8} A well-known cationic polymer is linear poly(ethylene imine) (LPEI) which shows high transfection efficiency, but also low biocompatibility, promoting the development of less toxic alternatives.^{9–11}

Beyond PEI, various cationic polymers with a range of backbone chemistries have been studied as non-viral gene delivery vectors. Polymers based on vinyl backbones are of particular interest, since they can possess a broad range of functional pendant groups, and may be readily synthesized by various polymerization techniques, including radical polymerization. For example, poly(2-(dimethylamino)ethyl methacrylate) (PDMAEMA) shows a propensity for gene delivery and is extensively studied. PDMAEMA possesses tertiary amine pendant groups and a pK_a which renders it pH-responsive within a physiologically useful pH window (≈ 7.4).^{12,13} While there are many other examples of

^a Laboratory of Organic and Macromolecular Chemistry (IOMC), Friedrich Schiller University Jena, Humboldtstrasse 10, 07743 Jena, Germany. E-mail: anja.traeger@uni-jena.de

^b Jena Center for Soft Matter (JCSM), Friedrich Schiller University Jena, Philosophenweg 7, 07743 Jena, Germany

† Electronic supplementary information (ESI) available: Material, additional methods and results, Fig. S1–S18, supplementary Tables S1–S8. See DOI: 10.1039/d0tb00340a

vinyl cationic polymers in polymer-based gene delivery, such as polybutylamino vinyl ethers (PBAVE),^{14,15} work has mostly been limited to polymethacrylates or polymethacrylamides. The polyacrylamides (PAMs) represent an interesting alternative since they are hydrolytically stable (unlike many polymethacrylates) and are considered to possess more hydrophilic polymeric backbones than their acrylate, methacrylate and methacrylamide counterparts. Therefore, they are more stable to store and less likely to be modified in the body. Regarding their polymerization, acrylamide monomers possess a comparatively high rate constant of propagation (k_p) and are typically less prone to side reactions of transfer during radical polymerization, which makes them well suited for reversible deactivation radical polymerization (RDRP) techniques such as reversible addition–fragmentation chain transfer (RAFT) polymerization.^{16–19} Concerning gene delivery, Nakayama and co-workers developed cationic star polymers based on poly(*N,N*-dimethylaminopropyl acrylamide) (PDMAAPAM) and showed higher transfection efficiency than PEI in COS-1 cells.^{20–23} The group of Young studied linear PAMs bearing primary amine pendant groups with varying spacer length and also reported promising transfection efficiency with primary amine/imidazole functional polymers, with or without the presence of the stealth polymer poly(ethylene glycol) (PEG).^{24–26} However, to the best of our knowledge, no further systematic studies have been performed with polyacrylamides as cationic homopolymers of linear architecture for gene delivery. In addition to the polymer backbone chemistry, there are a number of other properties which influence gene delivery potential. The molar mass of a given cationic polymer has been demonstrated in several cases to play an important role. Increasing molar masses typically correspond to increased transfection efficiency, but also increased cytotoxicity.^{27–31}

Moreover, the nature of the cationic moiety is of crucial importance, since it is a vital feature for DNA binding, cellular uptake, endosomal escape and DNA release. There are only few systematic studies focusing on the investigation of the correlation between the nature of the cationic moiety and the transfection mechanism; and they were not conducted with polyacrylamides. Reineke and coworkers investigated methacrylamide-based RAFT copolymers bearing primary, secondary, tertiary or ternary amine and carbohydrate pendant groups in different copolymer compositions (block vs. statistical copolymer, monomer ratio).^{32,33} More recently, a library of methacrylate-based homo- and co-polymers (bearing primary, secondary and/or tertiary amines) identified primary amine-based polymers to possess high potential.³⁴ However, the spacing between the cationic moiety and the polymer backbone also had an effect on the physicochemical properties.^{12,29,35}

Most studies focused on pH-responsive polymers that were (partially) protonated at physiological pH values.^{12,34,36} pH-independent polymers with quaternized amines, for example, have rarely been investigated so far. They showed the efficiency–effectiveness dilemma: less toxicity but also less efficiency compared to their pH-dependent analogs. The assumed reasons are an inefficient DNA release and/or a lower endosomal release.^{13,33,37,38} Another interesting cationic moiety is

the guanidinium group, that is not pH-dependent in a physiological context ($pK_a > 12$). Guanidine occurs in many different biomolecules and contributes to protein denaturation, DNA-synthesis inhibition or in the amino acid arginine in active sites of enzymes.³⁹ Many cell penetrating peptides, such as the TAT peptide, are rich in arginine residues.⁴⁰ However, while their proficiency for intracellular trafficking is well known, their mechanism of cellular entry, *i.e.* *via* transduction or endocytosis, remains a topic for debate.^{41–46} Assuming endocytosis, the mechanism of endosomal escape for guanidinium containing cell penetrating peptides (CPP) has to be considered. In studies with membrane lipids of the endolysosomal pathway, arginine containing CPPs were shown to bind bis(monoacryloyl glycerol)phosphate (BMP), a lipid present at the inner side of the membrane of intra late endosomal vesicles (ILEV) and to disrupt BMP-containing liposomes, indicating a possible pathway for the endosomal escape.^{47,48} Since this feature is of great importance in applications such as drug or gene delivery, the guanidinium group is frequently exploited for the development of synthetic vectors.^{46,49–53} Regarding examples possessing vinyl polymeric backbones, Funhoff *et al.* reported promising transfection and uptake in COS-7 cells for poly(3-guanidinopropyl methacrylate) (PGPMA) homopolymers prepared *via* free radical polymerization.³⁸ However, well-defined homopolymers of guanidinium-functional PAMs have not been systematically studied as gene delivery vectors, nor compared with other cationic moieties. Still, they are of vital importance for the potential utilization of nature-inspired specific cation–lipid-interactions.

In this work, we synthesized a library of well-defined cationic PAM homopolymers of varying molar mass bearing either primary amine, tertiary amine or guanidinium pendant groups *via* RAFT polymerization in order to assess their potential for gene delivery. The influence of the different properties on the transfection efficiency of the polymers was investigated and they were further characterized regarding the media influence, their pDNA binding capability, uptake and different types of toxicity. Due to the outstanding performance of the guanidinium functionalized polymer, the underlying endosomal escape mechanism was investigated in more detail using calcein release and lipid–polymer binding assays.

Material and methods

Materials, instruments, further methods and calculations can be found in the ESI.†

RAFT polymerization

Typical synthesis of P(GPAm^{diBoc}) *via* RAFT polymerization. A 5.0 wt% solution of 2-(Butylthiocarbonothioylthio) propanoic acid (PABTC) in DMAc (89.6 mg, 4.48 mg PABTC, 1.88×10^{-2} mmol), GPAm^{diBoc} (700.6 mg, 1.89 mmol), a 1.0 wt% solution of V65B in 1,4-dioxane (301.1 mg, 3.01 mg V65B, 1.17×10^{-2} mmol), DMAc (316.4 mg), 1,4-dioxane (731.3 mg) and 1,3,5-trioxane (external NMR standard, 8.4 mg) were introduced to a 4 mL microwave vial

equipped with a magnetic stirring bar. The vial was sealed, and the solution deoxygenated by bubbling argon through it for *ca.* 10 min. The vial was placed in an oil bath set at 45 °C and allowed to stir for 5 h. The polymer was precipitated three times (from THF) into cold hexane, and then dried under vacuum to give a yellow solid.

Typical synthesis of P(AEAmBoc) *via* RAFT polymerization.

PABTC (27.0 mg, 0.113 mmol), AEAm^{Boc} (602.4 mg, 2.81 mmol), a 1.0 wt% solution of V65B in 1,4-dioxane (290.0 mg, 2.90 mg V65B, 1.12×10^{-2} mmol), DMAc (394.4 mg), 1,4-dioxane (695.4 mg) and 1,3,5-trioxane (external NMR standard, 9.2 mg) were introduced to a 4 mL microwave vial equipped with a magnetic stirring bar. The vial was sealed, and the solution deoxygenated by bubbling argon through it for *ca.* 10 min. The vial was placed in an oil bath set at 50 °C and allowed to stir for 5 h. The polymer was precipitated three times from THF into cold hexane, and then dried under vacuum to give a yellow solid.

Typical synthesis of P(DMAPAm) *via* RAFT polymerization.

PABTC (19.9 mg, 8.35×10^{-2} mmol), DMAPAm (383.3 mg, 2.95 mmol), a 1.5 wt% solution of V65B in 1,4-dioxane (140.7 mg, 2.11 mg V65B, 8.17×10^{-3} mmol), DMAc (193.0 mg), 1,4-dioxane (70.6 mg) and 1,3,5-trioxane (external NMR standard, 3.3 mg) were introduced to a 2 mL vial equipped with a magnetic stirring bar. The vial was sealed, and the solution deoxygenated by bubbling argon through it for *ca.* 10 min. The vial was placed in an oil bath set at 60 °C and allowed to stir for 4 h. The polymer was precipitated three times from THF into cold hexane, and then dried under vacuum to give a yellow solid. The polymer was then dissolved in distilled H₂O and dried by lyophilization.

Typical synthesis of P(DMAEAm) *via* RAFT polymerization.

PABTC (25.1 mg, 0.105 mmol), DMAEAm (371.8 mg, 2.62 mmol), a 1.5 wt% solution of V65B in 1,4-dioxane (203.5 mg, 3.05 mg V65B, 1.18×10^{-2} mmol), DMAc (218.8 mg), 1,4-dioxane (36.1 mg) and 1,3,5-trioxane (external NMR standard, 5.9 mg) were introduced to a 2 mL vial equipped with a magnetic stirring bar. The vial was sealed, and the solution deoxygenated by bubbling argon through it for *ca.* 10 min. The vial was placed in an oil bath set at 60 °C and allowed to stir for 4 h. The polymer was precipitated three times from THF into cold hexane, and then dried under vacuum to give a yellow solid. The polymer was then dissolved in distilled H₂O and dried by lyophilization.

Deprotection of P(diBocGPAm) and P(BocAEAm). Polymers were dissolved at 50 mg mL⁻¹ in TFA/H₂O (97/3 v/v) and allowed to stir for 4 h. The TFA was then blown off using compressed air, the polymers were precipitated three times into diethyl ether from methanol and dried under reduced pressure to give a yellow solid.

Experimental details of all polymerizations are provided in the Tables S1 and S2 (ESI[†]).

Polyplex preparation

For the preparation of polyplexes, plasmid DNA (pDNA) and different amounts of polymer dissolved in water were mixed in HBG buffer (20 mM 4-(2-hydroxyethyl)piperazine-1-ethanesulfonic acid (HEPES) and 5% (w/v) glucose, pH 7.2) to give a final pDNA concentration of 15 µg mL⁻¹, with varying N*/P ratios

(molar ratio of protonatable nitrogen atoms to phosphates of pDNA, see ESI[†]). Immediately after combination, the mixtures were vortexed for 10 s at maximum speed (3200 rpm) and incubated at room temperature for 15 min to ensure complex formation.

Ethidium bromide quenching (EBA) and heparin dissociation assays (HRA)

The formation of polyplexes with pDNA was identified *via* quenching of ethidium bromide (EtBr) fluorescence by polymers interacting with pDNA. Briefly, 15 µg mL⁻¹ pCMV-GFP pDNA in a total volume of 100 µL HBG buffer were incubated with EtBr (1 µg mL⁻¹) at room temperature for 10 min. Subsequently, polyplexes with different quantities of polymer stock solutions (various N*/P ratios) were prepared in black 96-well plates (Nunc, Thermo Fisher, Germany) and incubated at 37 °C for 15 min before measuring the fluorescence intensity at $\lambda_{\text{Ex}} = 525$ nm/ $\lambda_{\text{Em}} = 605$ nm. A sample containing only pDNA and EtBr was defined as maximum fluorescence (100%).

For the heparin dissociation assay, heparin was added to the formed polyplex-EtBr mixtures using the dispenser of the microplate reader to obtain the indicated concentrations (Table S4, ESI[†]). After each addition, the plate was shaken, incubated at 37 °C for 10 min and fluorescence intensity was measured.

The percentage of EtBr displaced upon polyplex formation or re-intercalating following pDNA release by heparin was calculated using eqn (1):

$$\text{rFI}/\% = \frac{F_{\text{Sample}}}{F_{\text{pDNA}}} \times 100 \quad (1)$$

where rFI is the relative fluorescence intensity and F_{Sample} , and F_{pDNA} are the fluorescence intensities of a given sample and the EtBr intercalated into pDNA alone (in the case of the HRA with heparin), respectively. Data are expressed as mean \pm SD of three independent determinations.

For a summarized depiction of the EBA results, the % of bound pDNA was calculated as 100% – rFI%. The heparin concentration needed to release the maximum of pDNA was calculated with OriginPro, Version 2018b (OriginLab Corporation, US) which can be found in the ESI[†].

Determination of cytotoxicity

Cytotoxicity studies were performed with the mouse fibroblast cell line L929 (CLS, Germany), as recommended by ISO10993-5. For cytotoxicity of the polymers in HEK293T cells, refer to ESI[†]. The L929 cells were cultured in low glucose Dulbecco's modified eagle's medium (DMEM) supplemented with 10% fetal calf serum (FCS, Capricorn), 100 U mL⁻¹ penicillin and 100 µg mL⁻¹ streptomycin at 37 °C in a humidified 5% (v/v) CO₂ atmosphere. In detail, cells were seeded at 10⁴ cells per well in a 96-well plate without using the outer wells and incubated in medium containing 10 mM HEPES for 24 h. 1 h after medium change, cells were treated in sextuplicates with polymers at different concentrations, ranging from 5 µg mL⁻¹ to 500 µg mL⁻¹, and incubated for additional 24 h. The medium was replaced

by a 10% (v/v) alamarBlue solution in fresh culture medium, prepared according to the manufacturer's instructions. Following an incubation for 4 h at 37 °C, the fluorescence was measured at $\lambda_{\text{Ex}} = 570/\lambda_{\text{Em}} = 610$ nm. Non-treated control cells on the same plate were referred to as 100% viability. Values below 70% were regarded as cytotoxicity. Data are expressed as mean \pm SD of at least three independent determinations or as CC_{50} values \pm 95% confidence interval (CI). Information regarding CC_{50} calculations can be found in the ESI.^{††}

Transfection of adherent cells

Transfection studies were performed with the human embryonic kidney cell line HEK293T (CLS, Germany). The cells were routinely cultured in DMEM medium (1 g L⁻¹ glucose) supplemented with 10% FCS, 100 $\mu\text{g mL}^{-1}$ streptomycin and 100 U mL⁻¹ penicillin at 37 °C in a humidified 5% (v/v) CO₂ atmosphere.

For transfection studies, HEK293T cells were seeded at a density of 10⁵ cells per well in 24-well plates and incubated at 37 °C (5% CO₂) for 24 h. One hour prior to transfection, the medium was replaced by 450 μL serum reduced Opti-MEM[™] or fresh growth medium (DMEM + 10% FCS + 10 mM HEPES) to reduce pH variance during the experiments. Polyplexes were prepared as described above with isolated pEGFP-N1 pDNA and added to the cells diluting the polyplexes 1:10 in the cell culture medium. If incubated in Opti-MEM[™], the supernatant was replaced by fresh growth medium after 4 h and incubated for further 20 h. When transfections were performed in growth medium, the cells were incubated with polyplexes for 24 h. For analysis *via* flow cytometry, cells were harvested by trypsinization and resuspension in Hanks' Balanced Salt Solution, supplemented with 2% FCS and 20 mM HEPES (FC-buffer). For determination of transfection efficiency, cells were analyzed as described in the instrumentation section (see ESI[†]). Viable cells showing EGFP signal higher than the control cells incubated with pDNA only were gated as % of cells expressing EGFP and the relative mean fluorescence intensity (rMFI) of all viable cells was calculated in relation to the control. The experiments were performed at least three times and data are expressed as mean \pm SD.

Polyplex uptake

To study the uptake of polymers over time, cells were seeded at a density of 10⁵ cells per well in 24-well plates and cultured for 24 h in growth medium. One hour prior to the addition of the polyplexes, the medium was changed to serum reduced Opti-MEM[™] or fresh growth medium. Polyplexes were prepared as described above after labelling 1 μg pCMV-GFP pDNA with 0.027 nmol YOYO-1 iodide. Subsequently, the polymer-pDNA-solutions were added to the cells, diluting the polyplexes 1:10 in cell culture medium. Following incubation for 4 h, cells were harvested by trypsinization and resuspension in FC-buffer. Trypan blue solution (0.4%) was added to a final concentration of 0.04% to quench fluorescence of polyplexes outside the cells. Cells were analyzed *via* flow cytometry as described in the instrumentation section (see ESI[†]). Viable cells showing YOYO-1 signal higher than the control cells, which were

incubated with YOYO-1-pDNA only, were gated as % of cells that have taken up pDNA and the relative mean fluorescence intensity (rMFI) of all viable cells was calculated in relation to the control cells. The experiments were performed at least three times.

Hemolysis assay

The interaction of polymers with cellular membranes was examined by analyzing the release of hemoglobin from erythrocytes as published before.^{36,54} Blood from human donors, collected in tubes with citrate, was obtained from the Department of Transfusion Medicine of the University Hospital, Jena. The blood was centrifuged at 4500 $\times g$ for 5 min, and the pellet was washed three times with cold phosphate buffered saline (PBS, pH 7.4). Following a 10 times dilution with PBS (either pH 7.4 or pH 6.0), 500 μL aliquots of erythrocyte suspension were mixed 1:1 with the polymer solutions, which were prepared with PBS pH 7.4 or pH 6.0, and incubated at 37 °C for 60 min. After centrifugation at 2400 $\times g$ for 5 min, the supernatant was transferred to a clear flat bottomed 96-well plate (VWR, Germany) and the hemoglobin release was determined as the hemoglobin absorption at $\lambda = 544$ nm. Absorption at $\lambda = 630$ nm was used as reference. Complete hemolysis (100%) was achieved using 1% Triton X-100 as positive control. Pure PBS was used as negative control (0% hemolysis). The hemolytic activity of the polycations was calculated as follows (2):

$$\text{Hemolysis}/\% = \frac{(A_{\text{Sample}} - A_{\text{Negative control}})}{(A_{\text{Positive control}} - A_{\text{Negative control}})} \times 100 \quad (2)$$

where A_{Sample} , $A_{\text{Negative control}}$ and $A_{\text{Positive control}}$ are the absorption values of a given sample, the PBS treatment and the Triton X-100 treatment, respectively. A value less than 2% hemolysis rate was classified as non-hemolytic, 2 to 5% as slightly hemolytic and values >5% as hemolytic. Experiments were run in technical duplicates and were performed with three different blood donors.

Erythrocyte aggregation

Erythrocytes were isolated as described above. For determining the aggregation, 100 μL of the erythrocyte-polymer suspension were transferred to a clear flat bottomed 96-well plate (VWR, Germany). The cells were incubated at 37 °C for 2 h, and the absorbance was measured at $\lambda = 645$ nm. Cells treated with PBS served as negative control and cells treated with 50 $\mu\text{g mL}^{-1}$ 10 kDa BPEI were used as positive control. Aggregation potential of the polymers was calculated as follows (3):

$$\text{Aggregation} = \frac{A_{\text{Negative control}}}{A_{\text{Sample}}} \quad (3)$$

where A_{Sample} and $A_{\text{Negative control}}$ are the absorption values of a given sample and the PBS treatment, respectively. Experiments were run in technical duplicates and were performed with blood from three different blood donors.

Calcein release assay

To determine the endosomal escape efficiency of the polymers, a calcein release assay was performed. HEK293T cells were

seeded at a density of 10^5 cells per well in 24-well plates and cultured for 24 h in growth medium. They were treated with polyplexes as described for transfection studies. Just before the addition of polyplexes, the non-cell-permeable dye calcein was added to the cells to give a final concentration of $25 \mu\text{g mL}^{-1}$. Following incubation for 4 h, cells were carefully washed twice with cold PBS and harvested by trypsinization and resuspension in FC-buffer. *Via* flow cytometry, cells were analyzed as described in the instrumentation section (ESI†). Viable cells showing a calcein signal higher than the control cells incubated with calcein only were gated as % of cells that show strong calcein signal and the relative mean fluorescence intensity (rMFI) of all viable cells was calculated in relation to the control cells. The experiments were performed three times.

Lipid–polymer binding assay

To investigate the polymer–membrane-interaction in more detail, the binding of the polymers to several lipids specific for different membrane stages along the endolysosomal pathway was determined using a lipid–polymer binding assay which was modified according to Erazo-Olivereas *et al.* 2016.⁴⁷ The lipids were dissolved in hexane and the DY635-labeled polymers (see ESI†) were diluted in acetate buffer (0.1 M, pH 5.7) at equal amine concentrations (\approx N*/P 30, 1.2–1.4 mM). The lipid and polymer solutions were vigorously mixed at a ratio of 1 : 1 in 200 μL for one minute. Following incubation at -20°C for 10 min, all samples were centrifuged in a microcentrifuge at 6000 rpm (Carl Roth, Germany) to allow phase separation. To determine the amount of polymer binding to the lipids, 50 μL of the aqueous phase were diluted 1 : 2 with acetate buffer, transferred to a black 96-well plate (Nunc, Thermo Fisher, Germany) and fluorescence intensity of DY635 was measured at $\lambda_{\text{Ex}} = 633/\lambda_{\text{Em}} = 680 \text{ nm}$ in a plate reader. The mixture of pure hexane and the respective labeled polymer in the aqueous phase was used as the negative control (0% lipid binding). The polymer–lipid interaction was calculated as follows (4):

$$\text{rFI} = \frac{F_{\text{Sample}} - F_0}{F_{\text{Negative control}} - F_0} \quad (4)$$

where F_{Sample} , $F_{\text{Negative control}}$ and F_0 represent the fluorescence intensity of the aqueous phase following lipid incubation, the fluorescence intensity of the aqueous phase following pure hexane incubation and the fluorescence intensity of pure buffer, respectively.

Statistics

To determine the statistical significance, analysis of variance (ANOVA) was performed. If the ANOVA revealed significant differences ($p < 0.05$), *post hoc* analyses with a Bonferroni correction were applied. All statistical analyses with data of $n \geq 3$ and the determination of the Pearson's correlation coefficient were performed with Origin, Version 2018b (OriginLab Corporation, US). Further details can be found in the ESI.†

Results and discussion

Monomer synthesis and characterization

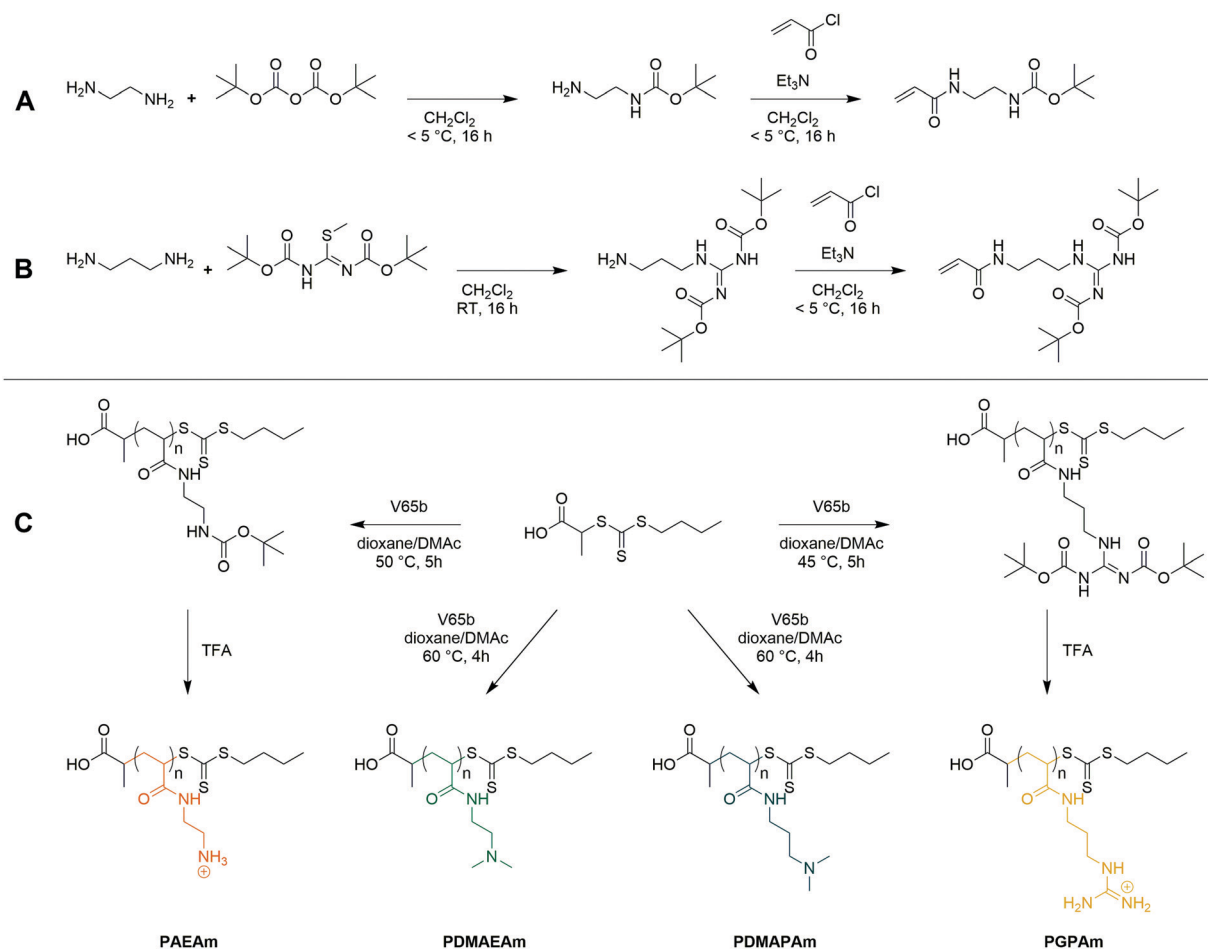
Four acrylamide-based monomers were selected to prepare the cationic polymer library. Dimethylamino ethyl acrylamide (DMAEm) is the acrylamide analogue of widely studied DMAEMA, while dimethylamino propyl acrylamide (DMPAm) is a pertinent addition since PDMPAm is a promising instance of cationic polyacrylamides used in gene delivery.^{20–23} While both monomers bear the same cationic moiety, the different length of the alkyl chain should influence the hydrophobicity and the pK_{a} of the resulting polymers, which in turn influences their interactions with DNA and cells, and ultimately their propensity for transfection.¹² Boc-protected forms of the primary amine- and guanidinium-functional monomers were used in this work since it permits the use of typical RAFT polymerization conditions, circumventing the need to conduct polymerizations in aqueous buffer. The Boc-protected primary amine-functional monomer, Boc-aminoethyl acrylamide (AEAm^{Boc}), was synthesized according to literature (A),⁵⁵ while a newly reported di-Boc-protected guanidinium-functional monomer, di-Boc-Guanidine propyl acrylamide (GPAm^{Boc}), was synthesized in a two-step synthesis adapted from literature (Scheme 1B).⁵⁶ Characterization of the monomers may be found in the ESI.†

Polymer synthesis and characterization

For each monomer, homopolymers with average degrees of polymerization (DP) ranging from 10 to 100 were targeted, in order to assess the influence of the polymer molar mass on biological activity. The library of cationic polymers was synthesized by RAFT polymerization using PABTC or its NHS activated ester derivative NHS-PABTC as CTA, with 1,4-dioxane/DMAc as a solvent system and V65B as azoinitiator (Scheme 1C). PABTC has been extensively used for the controlled polymerization of acrylamide and acrylate monomers.^{17,19} Moreover, the COOH R-group may be used to functionalize the polymers at the α -chain end. The solvent system was found to be suitable for the polymerization of all four monomers, while V65B (10 h half-life temperature of 51°C in toluene) offers a reasonable rate of radical generation across the range of polymerization temperatures employed ($45\text{--}60^\circ\text{C}$) in this solvent system.

Polymerizations of DMAPAm were stopped at monomer conversions of 70–80% in order to reduce the occurrence of side reactions, while for the other monomers, polymerizations were able to reach higher conversions (typically 85–95% as determined *via* ^1H NMR). SEC analysis of the polymers revealed monomodal populations with narrow molar mass distributions ($D \leq 1.3$) in most cases (Table 1, Fig. 1E–H and Table S2, ESI†). The experimental molar masses ($M_{\text{n,SEC}}$) were slightly different to the theoretically determined values in most cases, which may be attributed to differences in the hydrodynamic radii of the polymers and the standards used to calibrate the respective SEC systems (PMMA for DMAc-SEC and P2VP for Aq.-SEC).

Deprotection of the $\text{PGPAm}^{\text{diBoc}}$ and $\text{PAEAm}^{\text{Boc}}$ polymers to give well-defined guanidinium and primary amine polymers, respectively, was performed using TFA. Quantitative removal of



Scheme 1 Synthesis of the AEAmBoc (A) and GPAmBoc (B) monomers used in this work and synthetic route towards cationic polyacrylamide library (C).

the Boc-protecting groups was confirmed using ^1H NMR (Fig. 1A and D), while Aq.-SEC of the resulting polymers revealed monomodal populations with narrow molar mass distributions in all cases ($D \leq 1.3$) (Fig. 1E and H).

To better understand the behavior of these cationic homopolymers at different pH values, the pK_a values of the highest and lowest molar mass polymers from each set were determined. Acidified solutions ($\sim\text{pH } 2$) of the polymers in 125 mM NaCl were titrated with 0.1 mol L^{-1} NaOH (0.5 mol L^{-1} in the case of PGPAm polymers) and pK_a values were determined using the Henderson–Hasselbalch equation ((S5) and Fig. S4–S6, ESI†). Fig. S8 (ESI†) shows the calculated degree of protonation of the polymers at different pH values. All measured polymers possessed a pK_a of 7.8 or above, while for the PGPAm polymers the pK_a could not be determined with the available system (assumed to be 12 or above, Fig. S7, ESI†). All polymers are mainly positively charged under physiological conditions (pH 7.4) promoting the complexation with nucleic acids. A small molar mass dependence on pK_a value was observed for each cationic polymer type, with the lowest molar mass polymer possessing the higher pK_a in each case. This trend is consistent with simulations conducted by Nová and co-workers, where the difference in pK_a showed little variation after a DP of ~ 50 .⁵⁷

However, it was also observed that the titration curves become increasingly non-ideal with increasing polymer length (again up to a DP of ~ 50), due to local effects of the neighboring monomers. There is a clear trend in the pK_a of the different cationic moieties, with PDMAEAm (7.8–8.0) < PAEAm (8.3–8.5) < PDMApAm (8.7–8.9) < PGPAm (assumed ≈ 12). The values for PDMAEAm and PDMApAm are comparable to those obtained for methacrylamide-based systems.^{12,58} The significant difference between PDMAEAm and PDMApAm can likely be attributed to the distance between protonatable groups, where increasing distance would reduce electrostatic repulsion between charged groups, leading to higher pK_a values.⁵⁹

Transfection efficiency and cytotoxicity

Since all polymers contain positively charged amines suitable for gene delivery, the polymer library was investigated regarding their potential for protein expression (Fig. 2A). HEK293T cells were incubated with polyplexes at N*/P 30 of pDNA encoding the EGFP protein using different transfection protocols: (i) adding polyplex to growth medium for 24 h or (ii) adding polyplex to serum-reduced Opti-MEM™ for 4 h and further incubation in growth medium for 20 h. For the different types of cationic polymer an increased EGFP-expression was observed with

Table 1 Summary of cationic homopolymers prepared via RAFT polymerization

Polymer	DP ^a	$M_{n,th}$ ^b	$M_{n,th}$ ^c	$M_{n,SEC}$ ^d	D^d
		(kg mol ⁻¹)			
PGPAm ₈	8	2.0	1.7	1.8	1.12
PGPAm ₂₂	22	4.8	4.0	3.4	1.12
PGPAm ₄₃	43	9.1	7.6	5.0	1.18
PGPAm ₉₄	94	19.6	16.3	8.5	1.27
PAEAm ₉	9	2.3	1.3	2.6	1.09
PAEAm ₂₄	24	5.7	3.0	4.5	1.08
PAEAm ₄₅	45	7.0	5.4	7.0	1.15
PAEAm ₉₆	96	14.6	11.3	10.0	1.17
PDMAEAm ₈	8	1.4	—	3.3	1.13
PDMAEAm ₂₂	22	3.4	—	4.2	1.13
PDMAEAm ₄₅	45	6.6	—	5.6	1.50
PDMAEAm ₈₈	88	12.7	—	10.0	1.48
PDMAPAm ₁₁	11	2.0	—	3.5	1.19
PDMAPAm ₂₄	24	4.0	—	5.1	1.13
PDMAPAm ₃₈	38	6.2	—	6.2	1.41
PDMAPAm ₇₁	71	11.3	—	9.7	1.26

^a Determined via ¹H NMR. ^b Determined using eqn (6), ESI. ^c Excluding mass of counter-ion. ^d Determined via Aq.-SEC with P2VP standards.

increasing molar mass, but to different extents for each type of cationic polymer. The transfection efficiency in Opti-MEM™ was increased compared to growth medium for LPEI (28% vs. 12% EGFP-positive cells) and PGPAm (30% vs. 3% EGFP-positive cells) with the highest increase of about ten-fold by PGPAm₈₉ ($p < 0.001$). The highest transfection efficiency was achieved with the PGPAm₈₉-based polyplex using Opti-MEM™ (30% EGFP-positive cells), which showed no significant difference to the positive control LPEI ($p = 1.000$). Taking the different DP of these polymers into account (89 for PGPAm vs. 600 for LPEI) the observed transfection efficiency showed the potential of the PGPAm polymers. All other polymers in the PAm library revealed less transfection efficiency compared to commercial LPEI ($p < 0.05$). Moderate transfection efficiency of PAEAm₉₆ (7% EGFP-positive cells) was observed in serum-reduced medium. In growth medium, PAEAm₉₆ showed the highest transfection efficiency among the PAm polymers (7% EGFP-positive cells, $p = 1.000$ compared to LPEI). Enhanced transfection efficiency in Opti-MEM™ is well-known and was also found for other polymer-based transfection agents.^{34,36,60} The lower transfection efficiency in growth medium could indicate interaction with serum proteins.

Polymers for gene delivery, in particular homopolymers, are known to reduce the viability of cells due to their cationic charges affecting the integrity of the cellular membrane.²⁹ Therefore, the alamarBlue assay was performed in L929 cells according to ISO10993-5 (Fig. S9 and S10, ESI†) and of the interesting polymers with longer DP values in HEK293T cells (B). All tested acrylamide-based cationic polymers were found to be less toxic than the commercial gold standard LPEI (CC₅₀ = 26 µg mL⁻¹; see ESI†) and showed a reduced viability with increasing molar mass and concentration. The type of the cationic group influenced the viability and the following trend

of cytotoxicity was observed: PDMAEAm < PDMAEAm < PAEAm = PGPAm, indicating the polymers with tertiary amines as least cytotoxic. The length of the side chain (propyl vs. ethyl) appeared to have a slight influence on the cytotoxic profile of the dimethylamino functional polymers. However, the concentrations used for further biological investigations (N*/P 30; 19–24 µg mL⁻¹) showed high viability ($\geq 90\%$) for all polymers (Table S6, ESI†). Regarding the cytotoxicity of N*/P 30 polyplexes in HEK293T cells, a similar trend was observed but with slightly less viability of PAEAm and PGPAm polymers (65–85%; Fig. 2B).

To the best of our knowledge, this is the first systematic study of PAm homopolymers of different molar mass, cationic moiety and hydrophobicity for gene delivery. However, some structure–property-relationships were already described in literature. The molar mass dependency of transfection efficiency and cytotoxicity has been shown for a variety of polymers such as PEI, PDMAEMA or lysine-functionalized methacrylamides.^{28,29,31,61–66} This dependency on molar mass could be attributed to the charge distribution in relation to the cell membrane by the polymers: in high molar mass polymers the positive charge is present in one large coiled molecule focusing the charge at one spot of the cellular membrane which could lead to its disruption. In low molar mass polymers, the same amount of charges is distributed within several small molecules and therefore spread over a larger membrane area. Regarding different cationic moieties, an increased toxicity for polymers with primary amines compared to the tertiary analogs was also shown for poly(2-oxazolines).⁶⁷ In our study, the polymers with tertiary amines showed slight differences in toxicity and in protein expression with the ethyl spacer polymers performing slightly better than polymers with propyl spacer. This was also observed in studies of other vinyl polymers and could be due to increased interactions between propyl spacer polymers and DNA leading to a slow release of the genetic material inside the cytosol.^{12,24}

Guanidinium-containing polymers are inspired by nature, more precisely by the amino acid arginine, which is abundant in well-known CPPs such as TAT or R8.^{68,69} However, the known polymer backbones differ to the polymers investigated herein and the guanidinium group is often used in combination with other functional moieties. Relatively low molar mass guanidinium-bearing poly(methacrylamides) (DP of 20) offered transfection efficiency of about 50% of that of jetPEI in HEK293T cells in serum free medium and 48 h post transfection.⁷⁰ On the other hand, a guanidinium-bearing polymethacrylate with an approximately twofold higher number average molar mass (25 kg mol⁻¹) compared to PGPAm₈₉ and a 42.4 kDa poly-arginine exhibited lower transfection efficiency than PDMAEMA in COS-7 cells and serum-free medium.³⁸ In another study a similar poly-arginine showed transfection efficiency comparable to lipofectamine in mixed cortical cells.⁷¹ The observed toxicity was also described with comparable guanidinium functional polymers of different backbone chemistry and spacer length.^{38,56,72}

In the case of PGPAm polymers with low molecular weight, comparisons are only possible with oligo-arginines. Oligo-arginines ranging from 5 to 11 residues in length showed



Fig. 1 ^1H NMR of (A) PAEAm₂₄, (B) PDMAEAm₂₂, (C) PDMAPAm₂₄, (D) PGPAm₂₂ in D₂O. Aqueous (0.1% TFA + 0.1 mol L⁻¹ NaCl) SEC traces of (E) PAEAm, (F) PDMAEAm, (G) PDMAPAm, (H) PGPAm polymers synthesized via RAFT polymerization.

transfection of about 50% of that of BPEI (25 kDa) in A549 cells in serum free medium.⁷³

All in all, the high molar mass guanidinium functional polyacrylamide PGPAm₈₉ led to promising transfection results, comparable to commercial LPEI, which nicely demonstrates the potential of the controlled synthesis of this polymer class. However, the mechanism for the pDNA delivery of PGPAm₈₉

remains to be investigated, as the guanidinium functionality was used to support gene delivery in random studies before, but successful protein expression was not shown with a homopolymer. The common design of polymers for gene delivery is based on the pH-sensitive character of the polymers, which changes the protonation and thus partly also the hydrophilicity in the endosome.^{74,75} However, the influence of the buffer



Fig. 2 Transfection efficiency and toxicity of PAm homopolymers in HEK293T cells. (A) Transfection efficiency: cells were incubated with polyplexes of pEGFP-N1 pDNA and polymers at N*/P 30 (Table S6, ESI†). EGFP expression of viable cells was analyzed via flow cytometry. Two different transfection protocols were applied; either 24 h in growth medium (DMEM + 10% FCS + 10 mM HEPES) or 4 h in serum-reduced Opti-MEM™ followed by medium change to growth medium and further incubation for 20 h. Values represent mean \pm SD ($n \geq 3$). a: no significant difference ($p > 0.05$) to LPEI in growth medium, b: no significant difference ($p > 0.05$) to LPEI in Opti-MEM™, *: significant difference ($p < 0.001$) to same polymer in growth medium. (B) Cytotoxicity of PAm homopolymers in HEK293T cells. Metabolic activity was measured in HEK293T cells using the alamarBlue assay following incubation with indicated polymers at equal amine concentrations (\approx N*/P 30) for 4 h. Values represent mean \pm SD ($n = 3$).

capacity of the polymer was also discussed contrarily.⁷⁶ Since the protonation of PGPAm₈₉ does not change at endosomal pH (Fig. S8, ESI†), more detailed investigations of the transfection mechanism can help to design more efficient polymers.

Polyplex formation and characterization

To investigate the transfection mechanism, different bottle necks were investigated, starting at the formation of polyplexes. Therefore, the interaction between polymer and pDNA was investigated using the ethidium bromide quenching assay (EBA, Fig. 3A). The formation of polyplexes is indicated by displacement of intercalated ethidium bromide from the pDNA due to hydrophobic and electrostatic interactions of pDNA with the polymer, resulting in a decrease of ethidium bromide fluorescence. Various N*/P ratios were analyzed to determine

the optimal conditions for sufficient pDNA binding (Fig. S11A, ESI†). In the EBA, all polymers reduced the fluorescence intensity of the pDNA-ethidium bromide solution with increasing N*/P ratios, plateauing at values of N*/P 5 or above. However, while the molar mass of the polymer within each cation set had no impact on the value of the plateaus, the nature of the cationic group showed an influence. At N*/P 30, PDMAAm polymers led to a binding of about 75% of the pDNA, whereas all other polymer groups, including LPEI, bound about 85–90% of the pDNA.

Subsequently, the HRA and pH dependent EBA were used to further investigate the influence of cationic moiety, side chain length and DP on polyplex properties. In the case of the HRA, the formed polyplexes were incubated with heparin, a competing polyanion disrupting the electrostatic interaction between pDNA and polymer, which leads to re-intercalation of ethidium

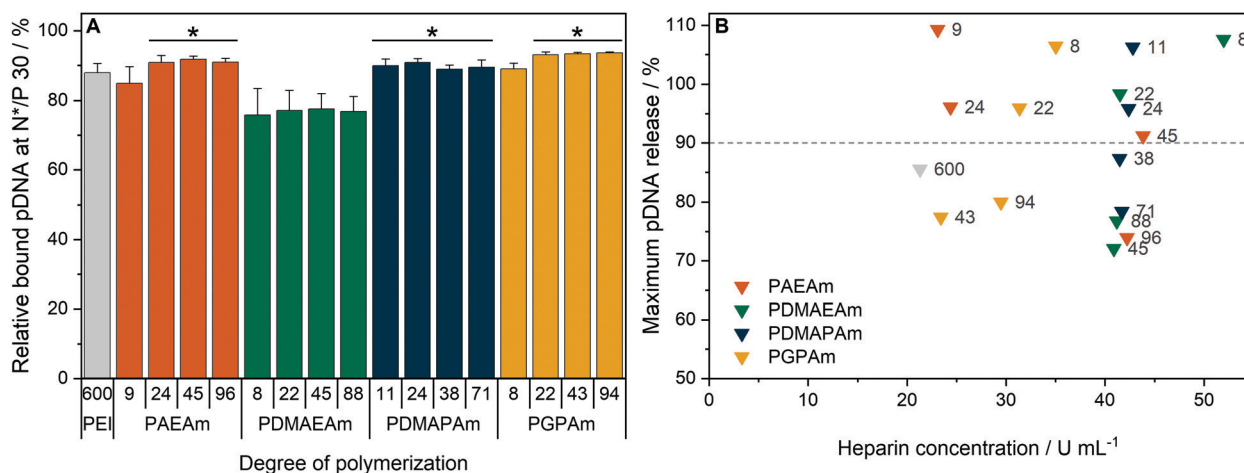


Fig. 3 Polyplex formation and stability tests with pDNA and PAm homopolymers. (A) EBA of all polymers at N*/P 30 in HBG buffer. Values represent mean \pm SD ($n \geq 3$). *: significant difference to all PDMAAm polymers ($p < 0.05$). (B) HRA of polymers at N*/P 30. Values were calculated as the heparin concentration needed to release the maximum amount of pDNA (defined as the beginning of the plateau, see Fig. S1 and S11B, ESI†) following fitting of a piecewise equation to the respective data ($n = 3$) for each polymer. Numbers in plot represent the degree of polymerization.

bromide and therefore increased rFI. The release of genetic material was observed with all investigated polymers, albeit with different release profiles and plateaus. At N*/P 30, only the polymers with lower molar mass ($DP < 50$) were able to release the pDNA completely, as indicated by an increase of the rFI above 90% (B). Interestingly at $DP < 25$, the PAEAm and PGPAm polymers required less heparin ($20\text{--}35\text{ U mL}^{-1}$) to release the same amount of pDNA than PDMAEAm and PDMA-PAm polymers with tertiary amines ($40\text{--}50\text{ U mL}^{-1}$). Regarding the higher molar mass polymers with $DP > 50$, only PGPAm₉₄ (30 U mL^{-1}) released the pDNA at low heparin concentrations comparable to LPEI (21 U mL^{-1}). This molar mass dependency was not observed for PDMAEAm and PDMA-PAm polymers. In contrast to the EBA, these results showed a dependency on the polymer length for PAEAm and PGPAm and on the property of the side chain (Fig. S11B, ESI†). Furthermore, the results identify the polyplexes with PGPAm₄₃ and PGPAm₉₄ to be promising polymers, showing strong binding but no full release of pDNA by electrostatic competitors.

Additionally, a pH-dependent EBA (pH value 5 to 9) was performed and differences between PGPAm and the other PAm were observed (Fig. S12, ESI†). The PGPAm polyplexes showed a strong and pH-independent polyplex formation, whereas the other polymers showed less pDNA binding at higher pH values.

The investigation of polyplex formation and stability indicated that PAEAm and PGPAm polymers bind pDNA very well (Fig. 3A), complexing pDNA to a slightly greater extent than LPEI and releasing it at moderate heparin concentrations (B). The good binding of PGPAm polymers could be attributed to the nature of the bidentate binding of guanidinium to the phosphate of the pDNA displacing EtBr more efficiently than the other polymers.⁷⁷ On the other hand, the low heparin concentration needed to partially release the PGPAm could indicate a high affinity of guanidinium for the sulphate groups of heparin compared to the phosphate groups of the pDNA.^{78,79} In the case of the longer PGPAm, the inefficient release of pDNA by heparin may also be due to further, non-electrostatic interactions of the polymers with the DNA. In contrast, pDNA binding with PDMAEAm appeared to be weaker despite higher concentration of heparin being required for release of the genetic material (Fig. 3). The other tertiary amine-based system, PDMA-PAm, showed the same strong pDNA-polymer interaction once the polyplex was formed. This difference in pDNA binding affinity between primary and tertiary amine moieties has been observed previously with polymers comprising methacrylate backbones.³⁴ The higher pDNA complexation by PDMA-PAm polymers compared to PDMAEAm could be due to the increased hydrophobicity conferred by the propyl spacer of the side chain.^{80,81} Moreover, Van de Wetering *et al.* explained this reduced affinity for the phosphates of the pDNA with the reduced steric availability of the tertiary amines of ethyl spacer polymers.¹² In the end, the complexation of less pDNA by PDMAEAm compared to the other PAm polymers could also be explained by the partial protonation of the PDMAEAm polymers, which possess the lowest pK_a of this library, at pH 7.4 leading to a decrease in protonated amines available for pDNA binding (see Fig. S8 and S12, ESI†).

To further characterize the formed polyplexes, their size (hydrodynamic diameter) was investigated (Table S7 and Fig. S13, S14, ESI†). Indeed, several studies have reported that polyplex sizes below 100 nm offer increased transfection efficiency.^{74,82} The size of polyplexes formed at N*/P 30 was assessed *via* dynamic light scattering (DLS). The Z-average diameter of all polyplexes ranged from 32 to 69 nm with only PAEAm₅ and PDMAEAm₂₂ showing polyplex sizes of 127 and 115 nm, respectively. Therefore, the main size-population was in the favored size range for all polyplexes.

In summary, no significant influence of hydrophobicity or type of cationic moiety on the polyplex size was found. The molar mass of the polymers showed only a slight influence on the size of the polyplexes. These results correspond very well to conclusions of other research groups using various cationic polymeric materials.^{12,29,62,83} So far, the only difference that corresponds to high transfection efficiency is the low heparin concentration required to release a high amount of the pDNA. Hydrophobic interactions might be a reason for the incomplete release by heparin. They were also promoted for other gene carrier systems.⁸⁴

Cellular internalization of PAm homopolymers

To further investigate the difference in transfection efficiency between the PAm polymers, pDNA uptake properties were studied using flow cytometry or confocal laser scanning microscopy (CLSM) with HEK293T cells following incubation of the cells with polyplexes of YOYO-1 iodide labeled pDNA and polymers at N*/P 30 for 4 h. This method was used to assess the influence of temperature, media and molar mass of the polymers.

To visualize the uptake, HEK293T cells were incubated with YOYO-1-labeled polyplexes containing the highest molar mass polymers or LPEI at N*/P 30 in Opti-MEM™ for 4 h and imaged with CLSM (Fig. 4A). Hoechst 33342 was added 10 min before imaging to stain the nuclei and trypan blue was used to quench the fluorescence of YOYO-1-labeled pDNA outside the cells. All tested polymers led to a punctate pattern of green fluorescence within the cells, whereas the control with YOYO-1 labeled pDNA and no polymer did not show green fluorescence. These results indicate an efficient uptake of YOYO-1-labeled pDNA by the PAm polymers or LPEI.

The uptake was investigated in more detail by flow cytometry (Fig. 4B). First, the common method of incubating cells at low temperature was used to find out whether the polyplexes were taken up *via* energy-dependent processes like clathrin-mediated endocytosis, often proposed for nanoparticles below 200 nm, or by translocation across the membrane.⁸² Therefore, HEK293T cells were incubated with the polyplexes in growth medium at 4 °C for 4 h, to inhibit all energy-dependent processes. All tested polymers showed a significant decrease of pDNA uptake compared to that observed in growth medium at 37 °C ($p < 0.001$). Furthermore, no difference in pDNA uptake was observed between the different polyplexes at 4 °C ($p = 0.937$).

Subsequently, the influence of the used transfection media on cellular uptake was studied. All polymers showed increased rMFI in both media. When incubated in Opti-MEM™, the quantity of internalized pDNA was slightly increased compared

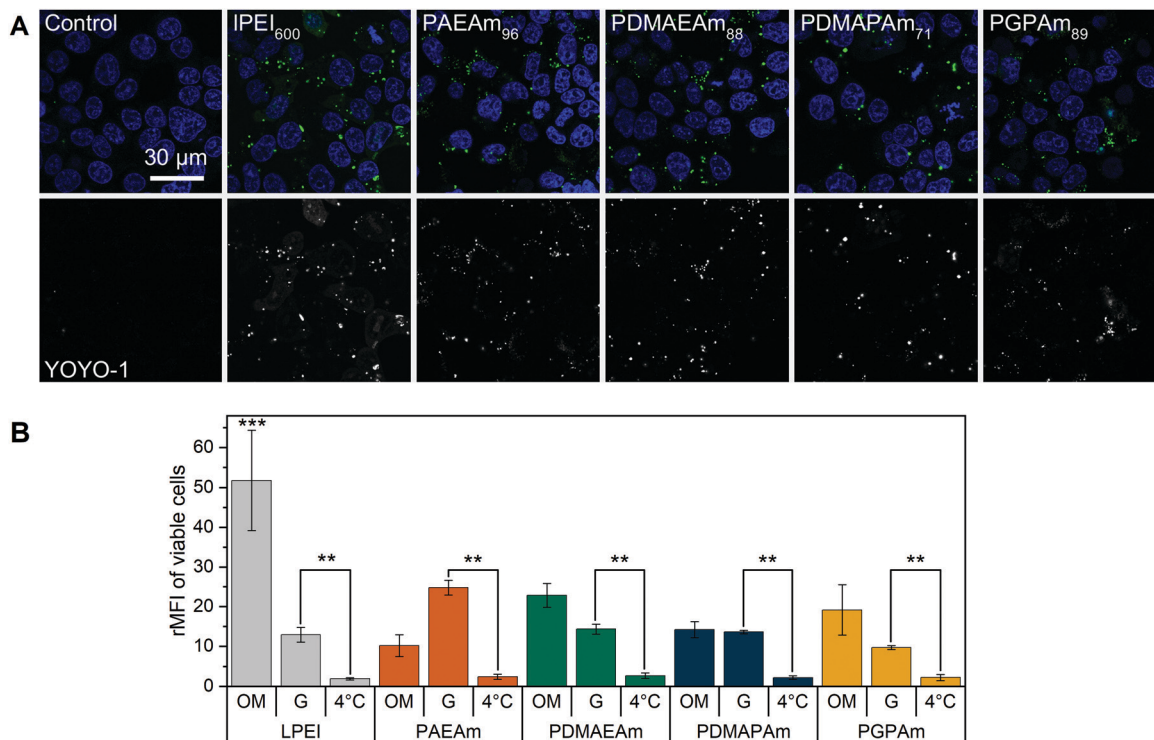


Fig. 4 Polyplex uptake with PAM polymers (A) CLSM: HEK293T cells were incubated with polyplexes of YOYO-1-labeled pDNA and polymers at N*/P 30 (Table S6, ESI†) in Opti-MEM™ for 4 h. Nuclei were stained with Hoechst33342 and YOYO-1 fluorescence was quenched with trypan blue. (B) Flow cytometry: HEK293T cells were incubated with polyplexes of YOYO-1-labeled pDNA and LPEI, PAEAm₉₆, PDMAEAm₈₈, PDMAPAm₇₁ or PGPAm₈₉ at N*/P 30. Incubation was in growth medium at 37 °C for 4 h (G), in serum-reduced Opti-MEM™ at 37 °C for 4 h (OM) or in growth medium at 4 °C for 4 h (4 °C). Cells incubated with labeled pDNA served as control (rMFI = 1). Values represent mean ± SD (n ≥ 3). **: significant difference to indicated sample (p < 0.001). ***: significant difference to all other samples (p < 0.001).

to growth medium, but only for LPEI significance ($p < 0.001$) was found. The highest increase in uptake of pDNA in Opti-MEM™ was observed for all PDMAEAm polymers and LPEI with rMFI of up to 25 and 51.8, respectively. However, LPEI-polyplexes showed a threefold higher pDNA uptake compared to all PAM homopolymers ($p < 0.001$). In growth medium, the highest increase in rMFI was observed for PAEAm₉₆, indicating a possible explanation for the higher transfection efficiency of the polymer in the presence of serum. Interestingly, molar mass dependence was only observed for the PAEAm polymers in growth medium (Fig. S15, ESI†).

The temperature dependent uptake and a punctuate uptake pattern in CLSM studies, demonstrate that polyplexes (pDNA) were taken up *via* an energy-dependent mechanism. Although this was not previously investigated for PAM homopolymers, it is known for other cationic polymers used for gene delivery.^{34,36,85} Regarding the guanidinium functional polymers, previous studies of other research groups showed contradictory results of temperature-independent and temperature-dependent uptake, respectively.^{38,70} This inconsistency is also known for guanidinium-containing peptides,⁸⁶ indicating that there are other factors additional to the type of functional group determining the way of internalization and should therefore be considered for novel polymers.

A reduced uptake of pDNA in the presence of growth medium was also observed by other groups.^{87,88} In the presence

of serum, the cationic charged polyplexes tend to interact with negatively charged proteins, leading to aggregation and therefore reduced uptake.^{6,89,90} It could also be assumed that the interaction with extracellular matrix components such as heparan sulfate proteoglycans is less pronounced due to competition with serum proteins, so that less pDNA can be uptaken.^{91–94} However, in our study, the uptake of pDNA did not correlate well to the observed EGFP expression, where PGPAm₉₆ showed the best performance in Opti-MEM™ whereas the other PAM polymers exhibited only slight EGFP expression. This was also observed in previous studies using methacrylate-based polymers.³⁴ Therefore, further mechanistic assays were performed to find out, why PDMAEAm delivered as much pDNA into the cells as PGPAm, but showed nearly no transfection efficiency.

Interaction of polymers with cellular membranes

To further investigate the structure–property relationship of polymers for efficient gene delivery, the interaction with membranes, representing the main biological barriers, was analyzed. The influence of the polymers on the membrane integrity was tested *via* hemolysis and aggregation assays using human erythrocytes, which are well known for studies regarding membrane–polymer-interaction. The cells were washed with PBS and incubated with the polymers at equal amine concentrations

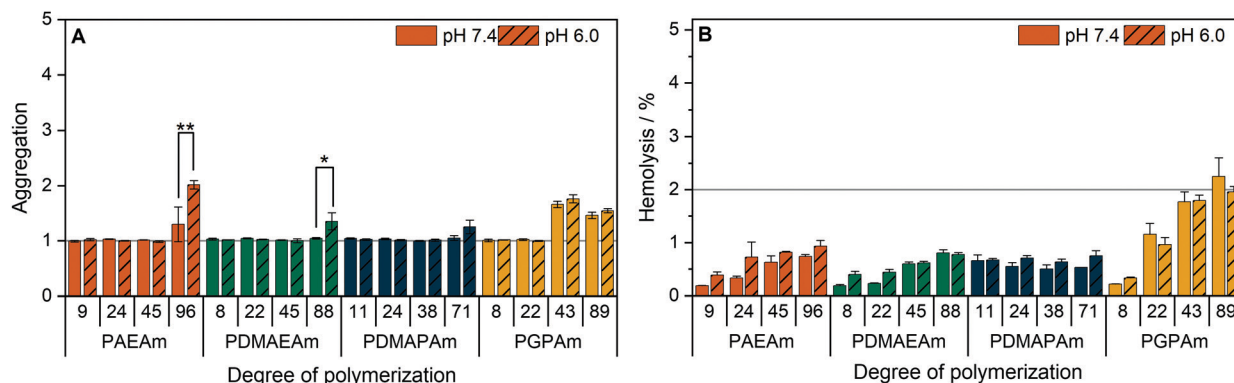


Fig. 5 Interaction of PAMs with erythrocyte membranes. Human erythrocytes were washed and incubated with polymers at equal amine concentrations ($\approx N^*/P$ 30, Table S6, ESI†) in PBS of different pH values present in blood/cytoplasm (pH 7.4) or endosomal compartments (pH 6). (A) Aggregation of indicated polymers measured as light absorption by erythrocytes. Values are calculated as the negative control (PBS value) relative to the sample value and represent mean \pm SD ($n = 3$). *: significant difference ($p < 0.05$), **: significant difference to indicated sample ($p < 0.001$). (B) Hemolysis as the amount of released hemoglobin calculated relative to 1% Triton X-100 as positive control (100% hemolysis). Values represent mean \pm SD ($n = 3$) and are classified as slightly hemolytic between 2% and 5%, as non- or hemolytic if lower or higher than 2% or 5%, respectively.

($\approx N^*/P$ 30) before either the release of hemoglobin from the cells as indicator for cell lysis or the absorption of light by the cells as indicator for cell aggregation was measured.

The low molar mass polymers can be considered as non-aggregating at the tested conditions (Fig. 5A). Meanwhile, the highest molar mass polymers (additionally PGPAm₄₃) exhibited a potential for aggregation of erythrocytes ($p < 0.001$). The influence of the pH value was dependent on the type of cationic polymer, whereby only PAEAm₉₆ ($p < 0.001$) and PDMAEAm₈₈ ($p = 0.02$) showed significant dependence.

Beside the aggregation of erythrocytes, the potential of the polymers to induce membrane leakage was tested (Fig. 5B). It was found that all polymers were non-hemolytic (values below 2%). Moreover, the pH value had no significant influence on the hemolytic activity.

The increased aggregation of the red blood cells by the high DP polymers does not necessarily relate to membrane destruction but rather to membrane interaction *via* the high positive charge density of cationic polymers.⁹⁵ The findings of this study indicate that, at concentrations equal to N^*/P 30, no severe lysis of the erythrocyte membrane occurred in the presence of any of the polymers and also the pH values showed no influence on the membrane leakage potential of the polymers.

Since the membrane composition of erythrocytes differs from that of the cells used for transfection, the influence of polyplexes on membranes of HEK293T cells was studied (Fig. S16, ESI†).^{96,97} Therefore, a LDH assay was performed following incubation of the cells with polyplexes of the highest DP polymers at N^*/P 30 in growth medium or in Opti-MEM™ for 4 h. If the polyplex or polymer decreases the integrity of the cellular membrane, the enzyme LDH will be released to the medium, which can be measured indirectly *via* the conversion of its substrates into fluorescent molecules. All polymers showed higher LDH release profiles in Opti-MEM™ compared to growth medium with only PAEAm₉₆ and PGPAm₈₉ showing significant differences ($p < 0.001$). The tertiary amine polymers and LPEI caused minor increases in both media (up to 5% relative to Triton X-100),

whereas PAEAm₉₆ and PGPAm₈₉ in Opti-MEM™ showed an increase of about 26 and 31%, respectively ($p < 0.001$), indicating membrane-lytic activity. In growth medium, the LDH release by PGPAm₈₉ was comparable to that of the tertiary amine polymers (2% relative to Triton X-100), whereas PAEAm₉₆ exhibited the highest LDH-release of 14% ($p = 1.000$). This correlates well with the results for transfection efficiency and could again point out a medium dependency of PGPAm.

Endosomal release of polymers

To elucidate the mechanism of transfection for the polymer library, in particular for PGPAm, further investigations were required. The PGPAm polymers showed high transfection and only slight membrane destruction, while being pH unresponsive. The common hypotheses for endosomal release “proton sponge” as well as the “membrane permeability and pore formation” are based on the concept of pH-dependent increased protonation of the polymers during endosomal maturation.⁷⁴ These hypotheses do not fit for polymers such as PGPAm exhibiting very high pK_a values (≈ 12). To study the endosomal release of the polymer library, a calcein release assay was performed. Calcein is a non-cell-permeable, fluorescent dye taken up *via* endocytic pathways resulting in the formation of a punctuated pattern inside the cytoplasm. If polymers are able to destabilize the endosomal membrane, calcein is released into the cytoplasm giving a diffused fluorescence pattern.^{98,99} This effect can be detected by flow cytometry as an increase in fluorescence intensity as well as in an altered histogram (see Fig. S18, ESI†). Based on the previous results, only the polymers with the highest molar masses were screened using HEK293T cells following incubation with the polyplexes at N^*/P 30 and calcein ($25 \mu\text{g mL}^{-1}$) for 4 h (Fig. 6A).

A significant increase in calcein fluorescence was observed following incubation with PGPAm₈₉-containing polyplexes ($p < 0.001$). All other tested polyplexes caused only a slight increase in rMFI. Interestingly, the endosomal release of PGPAm₈₉-polyplexes was again influenced by the medium. The calcein fluorescence in growth medium was about 80% lower than in Opti-MEM™

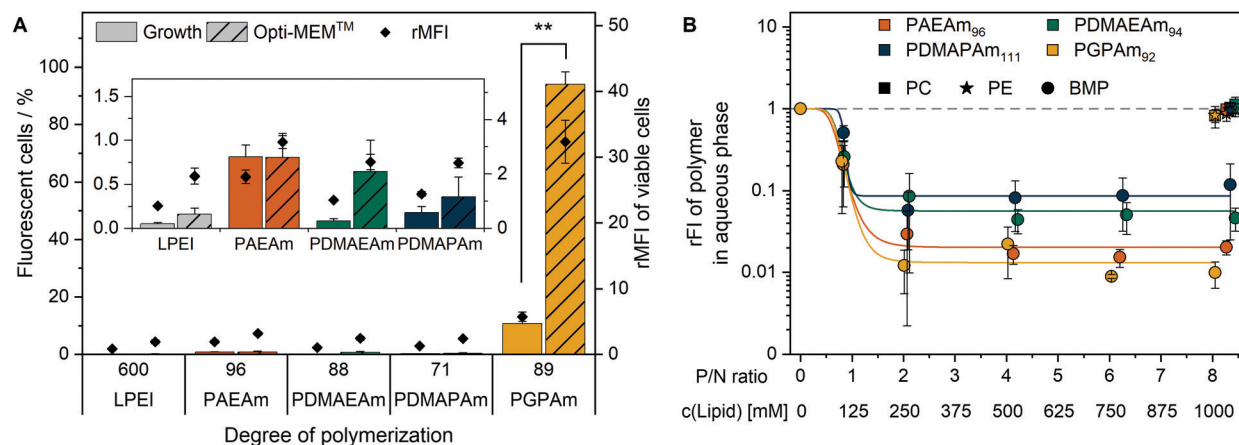


Fig. 6 Endosomal escape of PAm homopolymers. (A) Calcein release assay: HEK293T cells were incubated with indicated polymers at N*/P 30 (Table S6, ESI†) for 4 h at 37 °C and the mean fluorescence intensity relative to the calcein control as well as the number of viable cells with higher fluorescence than the calcein control (%) were analyzed via flow cytometry. Values represent mean \pm SD ($n = 3$). **: significant difference to indicated sample ($p < 0.001$). (B) Lipid binding assay: DY635-labeled PAm polymers in acetate buffer (pH 5.7) were incubated with different lipids in hexane at indicated concentrations and P/N ratios (lipid-phosphate to polymer-amine). Following phase separation, FI of the aqueous phase was measured and rFI calculated relative to the control with no lipids in the hexane phase. A decrease in rFI indicated partitioning of the DY635-labeled polymer into the hexane phase. Dots represent mean \pm SD ($n = 3$). Lines represent a logistic equation fitted to the values of each replicate.

and only 10.7% of cells showed higher fluorescence than the calcein control ($p < 0.001$).

The results of the calcein release assay demonstrate the potential of PGPAm₈₉-polyplexes to escape the endosome. In serum-reduced and growth medium, the endosomal release of polyplexes with PGPAm₈₉ outperformed all other tested polyplexes including those with LPEI. The difference between transfection and calcein release of LPEI-polyplexes could be explained with the higher pDNA uptake with LPEI compared to all other polymers, so that few calcein release from a higher number of endosomes was sufficient to yield a high transfection efficiency. The endosomal release potential for PDMAEMA, the methacrylate analog to PDMAEAm and PDMAPAm, was also found to be low.¹⁰⁰ However, for guanidinium-containing CPPs an efficient endosomal release is known.⁴¹ To our knowledge, the high level of calcein release achieved with polyplexes of PGPAm₈₉ homopolymers in this study was not shown for guanidinium functional polymers before. The results indicate an efficient and pH-independent endosomal release for PGPAm₈₉.

Since the PGPAm polymers were not pH-sensitive but able to escape the endosome, the endosomal escape mechanism of those polymers was investigated in more detail. For guanidinium-containing CPPs, the endosomal release was proposed to occur via binding to BMP, a lipid present in the membranes of ILEV, but not in the limiting membrane of late endosomes or lysosomes.^{47,101,102} Therefore, the lipid-polymer binding assay was conducted to investigate the interaction of the PAm homopolymers with this lipid (Fig. 6B). DY635-labeled PAm polymers were diluted in acetate buffer (pH 5.7) to equal amine concentrations and mixed thoroughly with different concentrations of BMP in hexane. For comparison to other phosphate-containing but neutral lipids, PC and PE were used in the hexane phase. Following phase separation and isolation of the aqueous phase, the fluorescence of the aqueous phase was measured.

A decrease in fluorescence intensity indicated the removal of the polymer from the aqueous phase and therefore lipid binding.

The incubation of the polymers with PC or PE in the hexane phase caused a negligible decrease in relative fluorescence intensity (rFI) by all tested polymers. When incubated with BMP, all tested polymers showed a decrease in fluorescence intensity with increasing P/N ratio (lipid-phosphate to polymer-amine). PGPAm exhibited the highest decrease in rFI indicating a slightly stronger binding than PAEAm and the tertiary amine analogues. The results are comparable to those for dTTAT of Erazo-Oliveras *et al.*, who propose BMP-binding as the mechanism for endosomal escape of this peptide.⁴⁷ In our study however, the non-calcein-releasing polymers also showed BMP-binding properties, albeit not as strong as PGPAm. This might be due to the higher density of cationic moieties in the PAm homopolymers compared to the density in dTTAT. The investigations indicate a multifactorial endosomal escape of PGPAm.

Conclusions

In this study, a library of cationic PAm homopolymers was synthesized and investigated for their transfection efficiency. RAFT polymerization was used to yield a series of well-defined polymers with narrow dispersity and narrow molar mass distributions. The polymers differ in their properties regarding (i) molar mass (DP10-100), (ii) cationic moiety (primary, tertiary, guanidinium) and (iii) length of alkyl spacer in the side chain (ethyl, propyl). The primary and tertiary amine functional polymers possessed pK_a values slightly above physiological pH, whereas for PGPAm the pK_a value could not be determined. Therefore, all PAm polymers in principle possess a high degree of protonation ($\geq 70\%$) at physiological

pH values and exhibited good pDNA binding ($\geq 80\%$) as determined *via* EBA.

Toxicity and efficiency are the main characteristics of transfection polymers. Therefore, the polymer library was investigated to identify interesting candidates. All PAM homopolymers were found to be less cytotoxic than LPEI in L929 cells, but only the highest molar mass guanidinium polymer, PGPAm₉₄, was able to achieve a transfection efficiency as high as LPEI. The primary amine functional PAEm₉₆ polymers also resulted in notable transfection efficiency. For a better understanding of the transfection mechanism of the polymers, further investigations were performed, in detail: polyplex uptake, membrane interaction and endosomal release. The results showed beneficial effects of increasing molar mass and the presence of guanidinium- as well as primary amine-functional groups on transfection relevant aspects.

There was evidence for an endocytic uptake with a punctuate pattern of YOYO-1-labeled pDNA in CLSM studies and no uptake of all PAM polymers at 4 °C (inhibition of ATP-dependent uptake). Furthermore, there was a strong correlation with increased lysis of cytoplasmic membranes (erythrocyte, HEK293T) and efficient endosomal release (Fig. 7).

Interestingly, PGPAm₈₉ exhibited superior endosomal release properties, although it is not pH responsive. Therefore, we postulate a strong interaction of the polymer with the endolysosomal membrane as a mechanism for endosomal escape. However, the lipid-polymer binding assay investigating the binding of the PAMs to BMP revealed that all tested polymers were able to bind BMP, albeit PGPAm was the most efficient. A possible explanation could be the difference to the composition of natural ILEV consisting of more than just one lipid or a more effective mechanism of guanidinium polymers to leave the endolysosome once the polymers escaped the ILEV. Further aspects should also be considered. The pDNA release could be a further crucial step in the delivery process, since the results showed a strong correlation between the amount of

heparin needed to achieve an incomplete pDNA release and transfection efficiency (Fig. 7).

Finally, with a transfection efficiency as high as that of LPEI and superior calcein release properties, the guanidinium functional PAM polymers present a promising class of polymers for gene delivery.

Conflicts of interest

The authors declare that the research was conducted in the absence of any commercial or financial relationships that could be construed as a potential conflict of interest.

Acknowledgements

The authors gratefully acknowledge the Bundesministerium für Bildung und Forschung (BMBF, Germany, #13XP5034A PolyBioMik), the German Research Foundation (DFG) for generous funding within the Emmy-Noether Programme (Projekt ID: 358263073), and the support by the DFG-funded Collaborative Research Centre PolyTarget (SFB 1278, project B06, project ID: 316213987). The authors thankfully acknowledge Karina Rost for performing toxicity assays and Prof. U. S. Schubert for providing excellent facilities. Furthermore, the authors acknowledge Bärbel Beringer-Siemers, Carolin Kellner, Elisabeth Preußger and Jana Solomun for their excellent technical assistance and discussions.

References

- 1 D. Lechardeur, K. Sohn, M. Haardt, P. Joshi, M. Monck, R. Graham, B. Beatty, J. Squire, H. O'brodovich and G. Lukacs, *Gene Ther.*, 1999, **6**, 482.
- 2 K. Lundstrom, *Diseases*, 2018, **6**, 42.
- 3 R. Gardlik, R. Palfy, J. Hodossy, J. Lukacs, J. Turna and P. Celec, *Med. Sci. Monit.*, 2005, **11**, Ra110–Ra121.
- 4 B. Kealy, A. Liew, J. M. McMahon, T. Ritter, A. O'Doherty, M. Hoare, U. Greiser, E. E. Vaughan, M. Maenz and C. O'Shea, *Tissue Eng., Part C*, 2009, **15**, 223–231.
- 5 D. He and E. Wagner, *Macromol. Biosci.*, 2015, **15**, 600–612.
- 6 R. J. Christie, N. Nishiyama and K. Kataoka, *Endocrinology*, 2010, **151**, 466–473.
- 7 U. Lächelt and E. Wagner, *Chem. Rev.*, 2015, **115**, 11043–11078.
- 8 Z. Zhou, X. Liu, D. Zhu, Y. Wang, Z. Zhang, X. Zhou, N. Qiu, X. Chen and Y. Shen, *Adv. Drug Delivery Rev.*, 2017, **115**, 115–154.
- 9 D. Fischer, Y. Li, B. Ahlemeyer, J. Kriegelstein and T. Kissel, *Biomaterials*, 2003, **24**, 1121–1131.
- 10 H. K. de Wolf, J. Luten, C. J. Snel, G. Storm and W. E. Hennink, *Mol. Pharmaceutics*, 2008, **5**, 349–357.
- 11 M. Neu, D. Fischer and T. Kissel, *J. Gene Med.*, 2005, **7**, 992–1009.
- 12 P. van de Wetering, E. E. Moret, N. M. E. Schuurmans-Nieuwenbroek, M. J. van Steenberg and W. E. Hennink, *Bioconjugate Chem.*, 1999, **10**, 589–597.

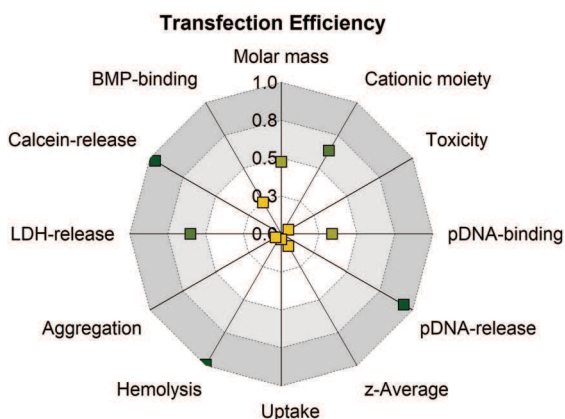


Fig. 7 Analysis of structure–property–correlations for PAMs using the squared Pearson's correlation coefficient (R^2) to determine linearity of the correlation. Values around 1.0 indicate strong positive (green) and values around 0 indicate no correlation (yellow). For a detailed overview which data were used for correlation see Table S8 (ESI†).

- 13 S. Agarwal, Y. Zhang, S. Maji and A. Greiner, *Mater. Today*, 2012, **15**, 388–393.
- 14 D. B. Rozema, D. L. Lewis, D. H. Wakefield, S. C. Wong, J. J. Klein, P. L. Roesch, S. L. Bertin, T. W. Reppen, Q. Chu, A. V. Blokhin, J. E. Hagstrom and J. A. Wolff, *Proc. Natl. Acad. Sci. U. S. A.*, 2007, **104**, 12982–12987.
- 15 D. H. Wakefield, J. J. Klein, J. A. Wolff and D. B. Rozema, *Bioconjugate Chem.*, 2005, **16**, 1204–1208.
- 16 J. Schrooten, I. Lacík, M. Stach, P. Hesse and M. Buback, *Macromol. Chem. Phys.*, 2013, **214**, 2283–2294.
- 17 G. Gody, T. Maschmeyer, P. B. Zetterlund and S. Perrier, *Nat. Commun.*, 2013, **4**, 2505.
- 18 G. Gody, T. Maschmeyer, P. B. Zetterlund and S. Perrier, *Macromolecules*, 2014, **47**, 639–649.
- 19 L. Martin, G. Gody and S. Perrier, *Polym. Chem.*, 2015, **6**, 4875–4886.
- 20 I. Mizoguchi, Y. Ooe, S. Hoshino, M. Shimura, T. Kasahara, S. Kano, T. Ohta, F. Takaku, Y. Nakayama and Y. Ishizaka, *Biochem. Biophys. Res. Commun.*, 2005, **338**, 1499–1506.
- 21 Y. Nakayama, C. Kakei, A. Ishikawa, Y.-M. Zhou, Y. Nemoto and K. Uchida, *Bioconjugate Chem.*, 2007, **18**, 2037–2044.
- 22 Y. Nemoto, A. Borovkov, Y.-M. Zhou, Y. Takewa, E. Tatsumi and Y. Nakayama, *Bioconjugate Chem.*, 2009, **20**, 2293–2299.
- 23 N. Yasuhide, M. Takeshi, N. Makoto, H. Michiko, O. Moto and H.-S. Mariko, *Curr. Drug Delivery*, 2005, **2**, 53–57.
- 24 J.-H. Ke, M.-F. Wei, M.-J. Shieh and T.-H. Young, *J. Biomater. Sci., Polym. Ed.*, 2011, **22**, 1215–1236.
- 25 J.-H. Ke, M.-F. Wei, M.-J. Shieh and T.-H. Young, *J. Biomater. Sci., Polym. Ed.*, 2011, **22**, 1753–1775.
- 26 J.-H. Ke and T.-H. Young, *Biomaterials*, 2010, **31**, 9366–9372.
- 27 A. Aied, U. Greiser, A. Pandit and W. Wang, *Drug Discovery Today*, 2013, **18**, 1090–1098.
- 28 J. Cai, Y. Yue, D. Rui, Y. Zhang, S. Liu and C. Wu, *Macromolecules*, 2011, **44**, 2050–2057.
- 29 A. C. Rinkenauer, S. Schubert, A. Traeger and U. S. Schubert, *J. Mater. Chem. B*, 2015, **3**, 7477–7493.
- 30 M. Wagner, A. C. Rinkenauer, A. Schallon and U. S. Schubert, *RSC Adv.*, 2013, **3**, 12774–12785.
- 31 C. V. Synatschke, A. Schallon, V. Jérôme, R. Freitag and A. H. E. Müller, *Biomacromolecules*, 2011, **12**, 4247–4255.
- 32 D. Sprouse and T. M. Reineke, *Biomacromolecules*, 2014, **15**, 2616–2628.
- 33 H. Li, M. A. Cortez, H. R. Phillips, Y. Wu and T. M. Reineke, *ACS Macro Lett.*, 2013, **2**, 230–235.
- 34 A. K. Trutzschler, T. Bus, M. Reifarh, J. C. Brendel, S. Hoeppener, A. Traeger and U. S. Schubert, *Bioconjugate Chem.*, 2018, **29**, 2181–2194.
- 35 C. Zhu, S. Jung, G. Si, R. Cheng, F. Meng, X. Zhu, T. G. Park and Z. Zhong, *J. Polym. Sci., Part A: Polym. Chem.*, 2010, **48**, 2869–2877.
- 36 T. Bus, C. Englert, M. Reifarh, P. Borchers, M. Hartlieb, A. Vollrath, S. Hoeppener, A. Traeger and U. S. Schubert, *J. Mater. Chem. B*, 2017, **5**, 1258–1274.
- 37 C. Arigita, N. J. Zuidam, D. J. A. Crommelin and W. E. Hennink, *Pharm. Res.*, 1999, **16**, 1534–1541.
- 38 A. M. Funhoff, C. F. van Nostrum, M. C. Lok, M. M. Fretz, D. J. A. Crommelin and W. E. Hennink, *Bioconjugate Chem.*, 2004, **15**, 1212–1220.
- 39 E. D. Raczynska, M. K. Cyrański, M. Gutowski, J. Rak, J. F. Gal, P. C. Maria, M. Darowska and K. Duczmal, *J. Phys. Org. Chem.*, 2003, **16**, 91–106.
- 40 C. Bechara and S. Sagan, *FEBS Lett.*, 2013, **587**, 1693–1702.
- 41 J. K. Allen, D. J. Brock, H. M. Kondow-McConaghy and J.-P. Pellois, *Biomolecules*, 2018, **8**, 50.
- 42 F. Madani, S. Lindberg, Ü. Langel, S. Futaki and A. Gräslund, *J. Biophys.*, 2011, 414729.
- 43 A. Pantos, I. Tsogas and C. M. Paleos, *Biochim. Biophys. Acta, Biomembr.*, 2008, **1778**, 811–823.
- 44 M. Silhol, M. Tyagi, M. Giacca, B. Lebleu and E. Vivès, *Eur. J. Biochem.*, 2002, **269**, 494–501.
- 45 S. Futaki and I. Nakase, *Acc. Chem. Res.*, 2017, **50**, 2449–2456.
- 46 J. D. Ramsey and N. H. Flynn, *Pharmacol. Ther.*, 2015, **154**, 78–86.
- 47 A. Erazo-Oliveras, K. Najjar, D. Truong, T. Y. Wang, D. J. Brock, A. R. Prater and J. P. Pellois, *Cell Chem. Biol.*, 2016, **23**, 598–607.
- 48 S.-T. Yang, E. Zaitseva, L. V. Chernomordik and K. Melikov, *Biophys. J.*, 2010, **99**, 2525–2533.
- 49 Y. Kim, S. Binauld and M. H. Stenzel, *Biomacromolecules*, 2012, **13**, 3418–3426.
- 50 N. Schmidt, A. Mishra, G. H. Lai and G. C. Wong, *FEBS Lett.*, 2010, **584**, 1806–1813.
- 51 M. Ahmed, *Biomater. Sci.*, 2017, **5**, 2188–2211.
- 52 K. J. Abd Karim, R. H. Utama, H. Lu and M. H. Stenzel, *Polym. Chem.*, 2014, **5**, 6600–6610.
- 53 C. Cokca, L. Zartner, I. Tabujew, D. Fischer and K. Peneva, *Macromol. Rapid Commun.*, 2020, **41**, 1900668.
- 54 M. Bauer, C. Lautenschlaeger, K. Kempe, L. Tauhardt, U. S. Schubert and D. Fischer, *Macromol. Biosci.*, 2012, **12**, 986–998.
- 55 A. Kuroki, P. Sangwan, Y. Qu, R. Peltier, C. Sanchez-Cano, J. Moat, C. G. Dowson, E. G. L. Williams, K. E. S. Locock, M. Hartlieb and S. Perrier, *ACS Appl. Mater. Interfaces*, 2017, **9**, 40117–40126.
- 56 L. Martin, R. Peltier, A. Kuroki, J. S. Town and S. Perrier, *Biomacromolecules*, 2018, **19**, 3190–3200.
- 57 L. Nová, F. Uhlík and P. Košovan, *Phys. Chem. Chem. Phys.*, 2017, **19**, 14376–14387.
- 58 A. Kuroki, P. Sangwan, Y. Qu, R. Peltier, C. Sanchez-Cano, J. Moat, C. G. Dowson, E. G. L. Williams, K. E. S. Locock, M. Hartlieb and S. Perrier, *ACS Appl. Mater. Interfaces*, 2017, **9**, 40117–40126.
- 59 M. Ullner, B. Jönsson, B. Söderberg and C. Peterson, *J. Chem. Phys.*, 1996, **104**, 3048–3057.
- 60 D. M. Drake, R. K. Keswani and D. W. Pack, *Pharm. Res.*, 2010, **27**, 2457–2465.
- 61 J. M. Layman, S. M. Ramirez, M. D. Green and T. E. Long, *Biomacromolecules*, 2009, **10**, 1244–1252.
- 62 A. C. Rinkenauer, A. Vollrath, A. Schallon, L. Tauhardt, K. Kempe, S. Schubert, D. Fischer and U. S. Schubert, *ACS Comb. Sci.*, 2013, **15**, 475–482.

- 63 W. T. Godbey, K. K. Wu and A. G. Mikos, *J. Biomed. Mater. Res.*, 1999, **45**, 268–275.
- 64 R. N. Johnson, D. S. H. Chu, J. Shi, J. G. Schellinger, P. M. Carlson and S. H. Pun, *J. Controlled Release*, 2011, **155**, 303–311.
- 65 B. D. Monnery, M. Wright, R. Cavill, R. Hoogenboom, S. Shaunak, J. H. G. Steinke and M. Thanou, *Int. J. Pharm.*, 2017, **521**, 249–258.
- 66 C. J. Bishop, K. L. Kozielski and J. J. Green, *J. Controlled Release*, 2015, **219**, 488–499.
- 67 A. C. Rinkenauer, L. Tauhardt, F. Wendler, K. Kempe, M. Gottschaldt, A. Traeger and U. S. Schubert, *Macromol. Biosci.*, 2015, **15**, 414–425.
- 68 D. M. Copolovici, K. Langel, E. Eriste and U. Langel, *ACS Nano*, 2014, **8**, 1972–1994.
- 69 S. Deshayes, M. C. Morris, G. Divita and F. Heitz, *Cell. Mol. Life Sci.*, 2005, **62**, 1839–1849.
- 70 Z. Tan, Y. K. Dhande and T. M. Reineke, *Bioconjugate Chem.*, 2017, **28**, 2985–2997.
- 71 J.-B. Kim, J. S. Choi, K. Nam, M. Lee, J.-S. Park and J.-K. Lee, *J. Controlled Release*, 2006, **114**, 110–117.
- 72 A. Kuroki, A. Kengmo Tchoupa, M. Hartlieb, R. Peltier, K. E. S. Locock, M. Unnikrishnan and S. Perrier, *Biomaterials*, 2019, **217**, 119249.
- 73 N. A. Alhakamy and C. J. Berkland, *Mol. Pharmaceutics*, 2013, **10**, 1940–1948.
- 74 T. Bus, A. Traeger and U. S. Schubert, *J. Mater. Chem. B*, 2018, **6**, 6904–6918.
- 75 D. W. Pack, A. S. Hoffman, S. Pun and P. S. Stayton, *Nat. Rev. Drug Discovery*, 2005, **4**, 581–593.
- 76 A. M. Funhoff, C. F. van Nostrum, G. A. Koning, N. M. E. Schuurmans-Nieuwenbroek, D. J. A. Crommelin and W. E. Hennink, *Biomacromolecules*, 2004, **5**, 32–39.
- 77 D. M. Perreault, L. A. Cabell and E. V. Anslyn, *Bioorg. Med. Chem.*, 1997, **5**, 1209–1220.
- 78 P. Juhasz and K. Biemann, *Proc. Natl. Acad. Sci. U. S. A.*, 1994, **91**, 4333–4337.
- 79 K. A. Schug and W. Lindner, *Chem. Rev.*, 2005, **105**, 67–114.
- 80 Z. Liu, Z. Zhang, C. Zhou and Y. Jiao, *Prog. Polym. Sci.*, 2010, **35**, 1144–1162.
- 81 A. Alshamsan, A. Haddadi, V. Incani, J. Samuel, A. Lavasanifar and H. Uludag, *Mol. Pharming*, 2009, **6**, 121–133.
- 82 S. Prabha, G. Arya, R. Chandra, B. Ahmed and S. Nimesh, *Artif. Cells, Nanomed., Biotechnol.*, 2016, **44**, 83–91.
- 83 I. Tabujew, C. Cokca, L. Zartner, U. S. Schubert, I. Nischang, D. Fischer and K. Peneva, *J. Mater. Chem. B*, 2019, **7**, 5920–5929.
- 84 E. Mastrobattista and W. E. Hennink, *Nat. Mater.*, 2012, **11**, 10–12.
- 85 T. Lühmann, M. Rimann, A. G. Bittermann and H. Hall, *Bioconjugate Chem.*, 2008, **19**, 1907–1916.
- 86 E. Wexselblatt, J. D. Esko and Y. Tor, *J. Org. Chem.*, 2014, **79**, 6766–6774.
- 87 A. K. Trutzschler, T. Bus, M. Sahn, A. Traeger, C. Weber and U. S. Schubert, *Biomacromolecules*, 2018, **19**, 2759–2771.
- 88 S. Pan, D. Cao, R. Fang, W. Yi, H. Huang, S. Tian and M. Feng, *J. Mater. Chem. B*, 2013, **1**, 5114–5127.
- 89 R. Kircheis, S. Schüller, S. Brunner, M. Ogris, K. H. Heider, W. Zauner and E. Wagner, *J. Gene Med.*, 1999, **1**, 111–120.
- 90 M. Ogris, P. Steinlein, M. Kurs, K. Mechtler, R. Kircheis and E. Wagner, *Gene Ther.*, 1998, **5**, 1425–1433.
- 91 I. Kopatz, J.-S. Remy and J.-P. Behr, *J. Gene Med.*, 2004, **6**, 769–776.
- 92 K. A. Mislick and J. D. Baldeschwieler, *Proc. Natl. Acad. Sci. U. S. A.*, 1996, **93**, 12349–12354.
- 93 P. C. Billings and M. Pacifici, *Connect. Tissue Res.*, 2015, **56**, 272–280.
- 94 G. W. Doorley and C. K. Payne, *Chem. Commun.*, 2011, **47**, 466–468.
- 95 E. Moreau, M. Domurado, P. Chapon, M. Vert and D. Domurado, *J. Drug Targeting*, 2002, **10**, 161–173.
- 96 A. A. Spector and M. A. Yorek, *J. Lipid Res.*, 1985, **26**, 1015–1035.
- 97 T. Harayama and H. Riezman, *Nat. Rev. Mol. Cell Biol.*, 2018, **19**, 281–296.
- 98 S. A. Smith, L. I. Selby, A. P. R. Johnston and G. K. Such, *Bioconjugate Chem.*, 2019, **30**, 263–272.
- 99 Y. Hu, T. Litwin, A. R. Nagaraja, B. Kwong, J. Katz, N. Watson and D. J. Irvine, *Nano Lett.*, 2007, **7**, 3056–3064.
- 100 R. A. Jones, M. H. Poniris and M. R. Wilson, *J. Controlled Release*, 2004, **96**, 379–391.
- 101 T. Kobayashi, M.-H. Beuchat, J. Chevallier, A. Makino, N. Mayran, J.-M. Escola, C. Lebrand, P. Cosson, T. Kobayashi and J. Gruenberg, *J. Biol. Chem.*, 2002, **277**, 32157–32164.
- 102 W. Mobius, E. van Donselaar, Y. Ohno-Iwashita, Y. Shimada, H. F. Heijnen, J. W. Slot and H. J. Geuze, *Traffic*, 2003, **4**, 222–231.

Supporting Information:

Tuning of Endosomal Escape and Gene Expression by Functional Groups, Molecular Weight and Transfection Medium: A Structure-Activity Relationship Study

*Friederike Richter^a, Liam Martin^a, Katharina Leer^a, Elisabeth Moek^a, Franziska Hausig^a,
Johannes C. Brendel^{a,b}, Anja Traeger^{*a,b}*

^aLaboratory of Organic and Macromolecular Chemistry (IOMC), Friedrich Schiller University
Jena, Humboldtstrasse 10, 07743 Jena, Germany.

^bJena Center for Soft Matter (JCSM), Friedrich Schiller University Jena, Philosophenweg 7,
07743 Jena, Germany.

*Correspondence to A. Traeger (anja.traeger@uni-jena.de)

List of Tables.

Table S1. Amount of different substances used for polymerization of PGPAms and PAEAms.	10
Table S2. Amount of different substances used for polymerization of PDMAEAms and PDMAPAms.	11
Table S3. Amount of different substances used for attachment to DY-635 amine to PAm	12
Table S4. Kinetic cycle protocol for automated heparin addition by the microplate reader.	13
Table S5. Summary of (protected) cationic homopolymers prepared <i>via</i> RAFT polymerization.	20
Table S6. Toxicity and concentration at N*/P 30 and CC ₅₀ values calculated <i>via</i> non-linear fit.	25
Table S7. Size determination of formed polyplexes via DLS.	27
Table S8. Data used for determination of the squared Pearson's correlation coefficient (R ²).	31

List of Figures.

Figure S1. Equations used by OriginPro, Version 2018b to provide the piecewise linear fit functions for the polymers. Screenshots taken from the software.	14
Figure S2. NMR spectra of GPAm ^{diBoc} .	18
Figure S3. NMR spectra of AEAm ^{Boc} .	19
Figure S4. Titration curves and equivalence point recognition criterion for titrations of PAEAm polymers.	21
Figure S5. Titration curves and equivalence point recognition criterion for titrations of PDMAEAm polymers.	21
Figure S6. Titration curves and equivalence point recognition criterion for titrations of PDMAPAm polymers.	22
Figure S7. Titration curves and equivalence point recognition criterion for titrations of PGPAm polymers.	22
Figure S8. Theoretical determination of the degree of protonation.	23
Figure S9. Cytotoxicity of PAm homopolymers in L929 cells.	24
Figure S10. Cytotoxicity of PAm homopolymers. Metabolic activity was measured in L929 cells after 24 h incubation with PAm polymers at indicated concentrations (Figure S8) using the alamarBlue™ assay. Values represent CC ₅₀ values calculated after fitting the resulting toxicity values to a logistic function ± 95% CI (n = 3). Upwards pointing arrows and striped columns indicate CC ₅₀ values above 500 µg mL ⁻¹ .	25
Figure S11. Polyplex formation and stability tests with pCMV-GFP pDNA and PAm homopolymers.	26
Figure S12. Polyplex formation with pCMV-GFP pDNA and polyacrylamide-homopolymers at different pH values.	26
Figure S13. Size determination of formed polyplexes <i>via</i> DLS.	27
Figure S14. DLS traces of polyplexes formed with PAm polymers and 15 µg mL ⁻¹ DNA at N*/P 30 in HBG buffer.	28
Figure S15. Influence of degree of polymerization on polyplex uptake in HEK293T cells.	29

Figure S16. LDH release assay with PAm polyplexes in HEK293T cells.	29
Figure S17. LDH release assay with HEK293T cells.	30
Figure S18. Flow Cytometry Analysis of Calcein Release Assay.	30

ADDITIONAL METHODS

Materials.

All chemicals were used as received unless stated otherwise. BocAEAm was prepared according to a previously described procedure.^{1,2} The chain transfer agents 2-(Butylthiocarbonothioylthio)propanoic acid (PABTC) and 2-(Butylthiocarbonothioylthio)propanoic acid-*N*-hydroxysuccinimide (NHS-PABTC) were prepared following previously reported procedures.³ Dimethylamino propyl acrylamide (DMAPAm) was obtained from ABCR (Germany). Dimethylamino ethyl acrylamide (DMAEAm) was obtained from ABCR and purified by column chromatography (silica, ethyl acetate). Sodium hydrogen carbonate (NaHCO_3) and sodium chloride (NaCl) was obtained from Fisher (Germany). Acryloyl chloride (97%), 1,3-bis-(*tert*-butoxycarbonyl)-2-methyl-2-thiopseudourea (98%), ethylene diamine and 1,3-diaminopropane ($\geq 99\%$) were obtained from Sigma (Germany). Trimethylamine ($\geq 99.5\%$) was obtained from Carl Roth (Germany). Di-*tert*-butyl dicarbonate and trifluoroacetic acid (TFA) were obtained from TCI (Germany). 2,2'-Azobis(2,4-dimethylvaleronitrile) (V65B) was obtained from FUJIFILM Wako Chemicals (Germany). HPLC grade dimethylformamide (DMF) (HiPerSolv CHROMANORM) was obtained from VWR (Germany). Anhydrous *N,N*-dimethylacetamide (99.8%, DMAc) was obtained from Sigma. 1,4-dioxane ($>99.5\%$) was obtained from Carl Roth and purified over inhibitor remover beads (for hydroquinone and monomethyl ether hydroquinone) at 4 °C. Dichloromethane (DCM) was obtained from a solvent purification system (SPS) on site, tetrahydrofuran (THF), methanol, hexane and ethyl acetate were distilled on site. DY-635 amine and DY-635 NHS ester were obtained from Dyomics (Germany). 2-(1H-Benzotriazol-1-yl)-1,1,3,3-tetramethyluronium hexafluorophosphate (HBTU) was obtained from Iris Biotech (Germany). 4-methylmorpholine (99%) was obtained from Alfa Aesar (Germany). For biological studies, following substances were ordered from suppliers in brackets: cell culture media and

supplements (Biochrom, Merck Millipore, Germany), Opti-MEM™ reduced serum medium (Gibco, Thermo Fisher, Germany), fetal calf serum (FCS, Capricorn Scientific, Germany), alamarBlue™ solution, YOYO™-1 iodide (Life Technologies, Thermo Fisher, Germany), trypsin-EDTA-solution, Triton X-100, 0.4% trypan blue solution and Hanks' balanced salt solution, calcein, L- α -phosphatidylcholine (PC), L- α -phosphatidylethanolamine, dioleoyl (PE, Sigma-Aldrich), Bis(monomyristoyl-glycero)phosphate (BMP, Avanti Polar Lipids, US), 1% ethidium bromide solution (EtBr, Carl Roth), heparin sodium salt from porcine intestinal mucosa (Alfa Aesar) and linear poly(ethyleneimine) (LPEI, $M_w = 25 \text{ kg mol}^{-1}$) and branched PEI (BPEI, $M_w = 10 \text{ kg mol}^{-1}$, Polysciences, Germany). Plasmid DNA (pDNA) encoding the enhanced green fluorescent protein (EGFP) for transfection studies was isolated with the Giga Plasmid Kit (Qiagen, Germany) from *E. coli* containing pEGFP-N1 (4.7 kb, Clontech, USA). For all other studies, like pDNA binding or uptake, the ready-to-use plasmid pCMV-GFP (PlasmidFactory, Germany) was used.

Instruments.

Nuclear magnetic resonance (NMR) spectroscopy. ^1H NMR (300 MHz) and DEPT ^{13}C (75 MHz) spectra were recorded on a Bruker AC 300 MHz spectrometer at 300 K. The delay time (d1) was set at 1 s for ^1H NMR and 2 s for DEPT ^{13}C . Chemical shifts (δ) are reported in ppm.

Size exclusion chromatography (SEC). SEC was conducted on one of two instruments. Dimethylacetamide (DMAc)-SEC was conducted using an Agilent 1200 series instrument equipped with differential refractive index (DRI) and UV/vis (DAD) detector. The liquid chromatography system used 1 \times PSS GRAM 30 Å column (300 \times 0.8 mm, 10 μm particle size) and 1 \times PSS GRAM 1000 Å column (300 \times 0.8 mm, 10 μm particle size). The DMAc eluent contained 0.21 wt.% LiCl as additive. Samples were run at 1 mL min $^{-1}$ at 40 °C. Analyte samples

were filtered through a polytetrafluoroethylene (PTFE) membrane with 0.45 μm pore size prior to injection. Poly(methyl methacrylate) (PMMA) narrow standards (PSS) were used to calibrate the SEC system. Aq.-SEC was conducted using a Jasco instrument equipped with DRI and UV (DAD) detector. The liquid chromatography system used 2 \times PSS NOVEMA-MAX column (300 \times 0.8 mm, 10 μm particle size). The aqueous eluent contained 0.1% TFA + 0.1 mol L⁻¹ NaCl as additive. Samples were run at 1 mL min⁻¹ at 30 °C. Analyte samples were filtered through a nylon membrane with 0.45 μm pore size prior to injection. Poly(2-vinylpyridine) (P2VP) narrow standards (Polymer Source Inc. Dorval, Quebec, Canada) were used to calibrate the SEC system. Experimental $M_{n,SEC}$ and \bar{D} (M_w/M_n) values of synthesized polymers were determined using PSS WinGPC UniChrom GPC software.

Titration. Titration of the polymers was conducted using a Metrohm OMNIS integrated titration system. For a typical measurement, the polymer was dissolved in 125 mM NaCl (in ultrapure water) (1.0 mg mL⁻¹), which was acidified with addition of 1 M hydrochloric acid (pH \sim 2). The polymers were titrated (with dynamic flow rate adjustment) against 0.1 M NaOH solution up to a pH value of 12. The PGPAm polymers were titrated against 0.5 M NaOH. The pK_a values were estimated using the Henderson-Hasselbalch equation (5) from equivalence points determined by the OMNIS titration software.

$$\text{pH} = \text{p}K_a + \log \frac{[\text{A}^-]}{[\text{HA}]} \quad (5)$$

Flow cytometry. Flow cytometry was conducted on either the Cytomics FC 500 or the CytoFlex S by Beckman Coulter. With both instruments 10⁴ cells were analyzed regarding their forward and sideward scattering (FSC, SSC) and their fluorescence at $\lambda_{\text{ex}} = 488$ with a 525 nm bandpass filter, since all employed stains (YOYO-1, EGFP, calcein) were green fluorescent.

Microplate reader. Fluorescence intensity measurements for EBA, HRA, alamarBlue™, LDH and BMP assays as well as absorption measurements for hemolysis and aggregation assays were performed on the Infinite M200 PRO microplate reader (Tecan, Germany) with λ_{Ex} / λ_{Em} used as indicated in the respective method sections and gain set to optimal.

Monomer Synthesis.

Synthesis of 1,3-Di-Boc-guanidinopropyl acrylamide, GPAm^{diBoc}. 1,3-Bis(*tert*-butoxycarbonyl)-2-methyl-2-thiopseudourea (10.34 g, 3.56×10^{-2} moles) in dry DCM (85 mL) was added dropwise *via* a pressure-equalizing dropping funnel to a solution of 1,3-diaminopropane (7.99 g, 9.0 mL, 1.08×10^{-1} moles) in DCM (85 mL) in a 250 mL round-bottomed flask equipped with a magnetic stirring bar. Following complete addition, the reaction was left to stir at room temperature overnight. A white precipitate formed. Dry DCM (40 mL) was added, and the solution was filtered to remove the precipitate. The solution was washed with deionized H₂O (3 × 200 mL) and brine (2 × 200 mL), the organic layer was dried over MgSO₄ and the DCM was removed under vacuum to yield crude 2-[1,3- Bis(*tert*-butoxycarbonyl)guanidine]ethylamine as a colourless, slightly turbid oil (12.40 g, 3.92×10^{-2} moles). The crude product was dissolved in dry DCM (200 mL) and transferred to a 500 mL two-necked round-bottomed-flask equipped with a magnetic stirring bar. Et₃N (6.6 mL, 4.74×10^{-2} moles) was added, the flask was fitted with a pressure-equalising dropping funnel, sealed, purged with argon, and cooled in an ice bath. Acryloyl chloride (2.84 g, 3.20 mL, 3.94×10^{-2} moles) in dry DCM (40 mL) was added dropwise and the reaction was left to stir at room temperature overnight, to give a clear pale-yellow solution. Dry DCM (100 mL) was added, then saturated NaHCO₃ (400 mL) was added and the aqueous layer was extracted with DCM (3 × 3400 mL). The organic layers were dried over MgSO₄ and the solvent was removed under vacuum to give a viscous yellow oil, which was subjected to flash column chromatography

(silica, hexane/ethyl acetate) to afford 2-[1,3-Bis(*tert*-butoxycarbonyl)guanidine]propyl acrylamide as a white solid. ^1H NMR (300 MHz, 300 K, CDCl_3 , δ): 11.44 (s, 1 H, $-\text{NH}(-\text{N}=\text{C})-\text{NH}-$), 8.47 (t, 6.1 Hz, 1 H, $-\text{CH}_2-\text{NH}-(\text{C}=\text{N}-)\text{NH}-$), 7.91 (t, 1 H, $-\text{CH}_2-\text{NH}-(\text{C}=\text{O})-$), 6.30 (1 H, $-(\text{C}=\text{O})-\text{CH}=\text{CH}_2$), 6.28 (d, 1 H, $-(\text{C}=\text{O})-\text{CH}=\text{CH}_2$), 5.55 – 5.59 (dd, 1 H, $-(\text{C}=\text{O})\text{CH}=\text{CH}_2$), 3.46 – 3.52 (m, 2 H, $-\text{CH}_2-\text{NH}-(\text{C}=\text{N}-)\text{NH}-$), 3.30 – 3.36 (m, 2 H, $-\text{CH}_2-\text{NH}-(\text{C}=\text{O})-$), 1.69 (m, 2 H, $-\text{CH}_2-\text{CH}_2-\text{CH}_2-$), 1.49 (2 \times s, 18 H, $-\text{O}-\text{C}((\text{CH}_3)_3)$). ^{13}C NMR (75 MHz, 300 K, CDCl_3 , δ): 131.8 ($\text{CH}_2=\text{CH}-(\text{C}=\text{O})-$), 125.4 ($\text{CH}_2=\text{C}-$), 37.1 ($-\text{CH}_2-\text{NH}-(\text{C}=\text{O})-$), 34.8 ($-\text{CH}_2-\text{NH}-(\text{C}=\text{N}-)\text{NH}-$), 29.7 ($-\text{CH}_2-\text{CH}_2-\text{CH}_2-$), 28.3 ($-\text{O}-\text{C}((\text{CH}_3)_3)$), 28.0 ($-\text{O}-\text{C}((\text{CH}_3)_3)$). MS: $[\text{M} + \text{H}]^+$ 371.22 (calculated), 371.23 (found).

Synthesis of N-tert-butoxycarbonyl-N'-acryloyl-1,2-diaminoethane (AEAm^{Boc}). Ethylene diamine (30.02 g, 5.00×10^{-1} moles) was dissolved in dry DCM (280 mL) in a 500 mL round-bottomed flask equipped with a magnetic stirring bar. The flask was fitted with a pressure-equalising dropping funnel, sealed, purged with argon, and cooled in an ice bath. Di-*tert*-butyl dicarbonate (27.6 g, 1.25×10^{-1} moles) in dry DCM (120 mL) added dropwise with stirring over 1 h. The reaction was allowed to reach room temperature and left to stir overnight. The resulting solution was filtered to remove precipitate, and concentrated under vacuum. Deionized H_2O (350 mL) added, and the solution was filtered to remove the resulting precipitate (*N,N'*-(bis-*tert*-butoxycarbonyl)-1,2-diaminoethane). The aqueous solution was saturated with NaCl, and extracted with EtOAc (3 \times 300 mL), the organic layers combined, dried over MgSO_4 and concentrated under vacuum to yield *N-tert*-butoxycarbonyl-1,2-diaminoethane as a clear oil (14.39 g, 8.985×10^{-2} moles), which was dissolved in dry DCM (300 mL) and transferred to a 500 mL two-necked round-bottomed flask equipped with a magnetic stirring bar. Et_3N (15.0 mL, 1.08×10^{-1} moles) was added, the flask was fitted with a pressure-equalizing dropping funnel, sealed,

purged with argon, and cooled in an ice bath. Acryloyl chloride (7.30 mL, 8.96×10^{-2} moles) in dry DCM (100 mL) was added dropwise and the reaction was left to stir at room temperature overnight. The solution was concentrated under vacuum, dissolved in deionized H₂O (300 mL), and extracted with CHCl₃ (3 \times 300 mL). The organic layers were combined, dried over MgSO₄ and concentrated under vacuum to give a white solid, which was subjected to flash column chromatography (silica, hexane/ethyl acetate) to afford *N*-*tert*-butoxycarbonyl-*N'*-acryloyl-1,2- as a white solid. ¹H NMR (300 MHz, 300 K, CDCl₃, δ): 6.65 (br, 1 H, $-\text{NH}-(\text{C}=\text{O})\text{CH}=\text{CH}_2$), 6.22 – 6.28 (dd, 17.1 Hz, 1.4 Hz, 1 H, $-\text{NH}-(\text{C}=\text{O})\text{CH}=\text{CH}_2$), 6.05 – 6.14 (dd, 17.1 Hz, 10.1 Hz, 1 H, $-\text{NH}-(\text{C}=\text{O})\text{CH}=\text{CH}_2$), 5.60 – 6.64 (dd, 10.1 Hz, 1.6 Hz, 1 H, $-\text{NH}-(\text{C}=\text{O})\text{CH}=\text{CH}_2$), 5.11 (br, 1 H, $-\text{NH}-(\text{C}=\text{O})\text{O}-$), 3.40 – 3.45 (m, 2 H, $-\text{CH}_2-\text{NH}-(\text{C}=\text{O})\text{CH}=\text{CH}_2$), 3.27 – 3.32 (m, 2 H, $-\text{CH}_2-\text{NH}-(\text{C}=\text{O})\text{O}-$), 1.42 (s, 9 H, $-\text{O}-\text{C}((\text{CH}_3)_3)$). ¹³C NMR (75 MHz, 300 K, CDCl₃, δ): 130.9 ($\text{CH}_2=\text{CH}-(\text{C}=\text{O})-$), 126.3 ($\text{CH}_2=\text{C}-$), 41.0 ($-\text{CH}_2-\text{NH}-(\text{C}=\text{O})\text{CH}=\text{CH}_2$), 40.1 ($-\text{CH}_2-\text{NH}-(\text{C}=\text{O})\text{O}-$), 28.3 ($-\text{O}-\text{C}((\text{CH}_3)_3)$). MS: [M + H]⁺ 237.13 (calculated), 237.12 (found).

Calculations for RAFT Polymerization.

Monomer conversion (p) was calculated from ¹H NMR data by comparing the integrals of vinyl peaks (5.5-6.3 ppm) against an external reference (1,3,5-trioxane, 5.14 ppm) before ($t=0$) and after ($t=\text{final}$) polymerization. The theoretical number-average molar mass ($M_{n,\text{th}}$) was then calculated using equation (6):

$$M_{n,\text{th}} = \frac{[\text{M}]_0 p M_M}{[\text{CTA}]_0} + M_{\text{CTA}} \quad (6)$$

Where $[\text{M}]_0$ and $[\text{M}]_0$ are the initial concentrations of monomer and chain transfer agent (CTA), respectively, M_M and M_{CTA} are the molecular weight of the monomer and CTA, respectively, and p is the monomer conversion.

Table S1. Amount of different substances used for polymerization of PGPAms and PAEAms.

	PGPAm ₈	PGPAm ₂₂	PGPAm ₄₃	PGPAm ₈₉	PGPAm ₉₄	PAEAm ₉	PAEAm ₂₄	PAEAm ₄₅	PAEAm ₉₆
Monomer	diBocGPAm	diBocGPAm	diBocGPAm	diBocGPAm	diBocGPAm	BocAEAm	BocAEAm	BocAEAm	BocAEAm
DP _{n,target}	10	25	50	100	100	10	25	50	100
m _{CTA} added (mg)	38.2	15.41	4.13*[a]	4.48	3.25[a]	68.4	27.0	6.12[a]	5.44[a]
n _{CTA} added (moles)	1.60×10^{-4}	6.46×10^{-5}	1.24×10^{-5}	1.88×10^{-5}	9.74×10^{-6}	2.87×10^{-4}	1.13×10^{-4}	1.83×10^{-5}	1.63×10^{-5}
m _{monomer} added (mg)	597.7	599.9	230.7	700.6	362.7	600.2	602.4	194.2	348.6
n _{monomer} added (moles)	1.61×10^{-3}	1.61×10^{-3}	6.20×10^{-4}	1.89×10^{-3}	9.74×10^{-4}	2.80×10^{-3}	2.81×10^{-3}	9.07×10^{-4}	1.63×10^{-3}
m _{V65b} added (mg)	3.18	3.23	0.65	3.01	0.515	5.40	2.90	0.63	0.42
n _{V65b} added (moles)	1.23×10^{-5}	1.25×10^{-5}	2.51×10^{-6}	1.17×10^{-5}	1.99×10^{-6}	2.09×10^{-5}	1.12×10^{-5}	2.43×10^{-6}	1.63×10^{-6}
Dioxane added (uL)	835.6	841.9	185.5	1029.4	540.9	949.9	951.1	283.4	563.7
DMAc added (uL)	375.9	365.8	430.6	428.5	222.3	420.8	369.6	297.8	269.8
PABTC/V65b	13.0	5.2	4.9	1.6	4.9	13.7	10.1	7.6	10.0
T (°C)	45	45	50	45	45	50	50	50	60
Time (min)	540	540	360	300	300	300	300	360	240

Table S2. Amount of different substances used for polymerization of PDMAEAm_s and PDMApAm_s.

	PDMAEAm ₈	PDMAEAm ₂₂	PDMAEAm ₄₅	PDMAEAm ₈₈	PDMApAm ₁₁	PDMApAm ₂₄	PDMApAm ₃₈	PDMApAm ₇₁
Monomer	DMAEAm	DMAEAm	DMAEAm ^[a]	DMAEAm ^[a]	DMApAm ^[a]	DMApAm ^[a]	DMApAm ^[a]	DMApAm ^[a]
DP _{n,target}	10	25	49	99	14	30	50	99
m _{CTA} added (mg)	67.1	25.1	8.25 ^[b]	5.97 ^[b]	50.3	19.9	7.49 ^[b]	5.33 ^[b]
n _{CTA} added (moles)	2.81×10^{-4}	1.05×10^{-4}	2.47×10^{-5}	1.79×10^{-5}	2.11×10^{-4}	8.35×10^{-5}	2.24×10^{-5}	1.60×10^{-5}
m _{monomer} added (mg)	400.7	371.8	174.0	252.2	461.0	383.3	175.5	248.9
n _{monomer} added (moles)	2.82×10^{-3}	2.62×10^{-3}	1.22×10^{-3}	1.77×10^{-3}	2.95×10^{-3}	2.46×10^{-3}	1.12×10^{-3}	1.59×10^{-3}
m _{V65b} added (mg)	5.77	3.05	1.21	0.93	5.07	2.11	1.16	0.85
n _{V65b} added (moles)	2.23×10^{-5}	1.18×10^{-5}	4.67×10^{-6}	3.60×10^{-6}	1.96×10^{-5}	8.17×10^{-6}	4.49×10^{-6}	3.27×10^{-6}
Dioxane added (uL)	461.4	229.0	514.4	574.1	242.3	202.5	483.5	577.0
DMAc added (uL)	209.6	233.5	141.9	140.9	249.7	206.0	136.8	34.5
PABTC/V65b	12.6	8.9	5.3	5.0	10.8	10.2	5.0	4.9
T (°C)	60	60	50	60	60	60	50	60
Time (min)	240	240	420	240	240	240	420	240

[a] Monomer was not purified

[a] Polymerization using PBTC-NHS

Typical Attachment of DY-635 to PAm Polymers.

New batches of polymers were used in each instance (Aq.-SEC, P2VP standards): PAEAm₉₆, $M_{n,SEC} = 12.8 \text{ kg mol}^{-1}$, $\bar{D} = 1.16$; PGPA_{m94}, $M_{n,SEC} = 9.2 \text{ kg mol}^{-1}$, $\bar{D} = 1.25$; PDMAEAm₉₄, $M_{n,SEC} = 10.3 \text{ kg mol}^{-1}$, $\bar{D} = 1.26$; PDMA_{PAm111}, $M_{n,SEC} = 11.9 \text{ kg mol}^{-1}$, $\bar{D} = 1.51$. The respective polymer, a 2 mg mL⁻¹ solution of DY-635 amine in HPLC grade DMF, a 2 mg mL⁻¹ solution of HBTU in HPLC grade DMF and a 2 mg mL⁻¹ solution of NMM in HPLC grade DMF were added to a screw-cap vial equipped with a magnetic stirring bar (Table S3). The reaction was left to stir in the dark for 24 h. The solution was diluted in ultrapure water and dialyzed against first H₂O/MeOH (4/1) for 2 days and then against H₂O for 3 days. The polymer was obtained as a blue solid following lyophilization. For PDMAEAm₉₄, a 5 mg mL⁻¹ solution of DY-635 amine and a 1 mg mL⁻¹ solution of NMM were used. Regarding dye attachment to PAEAm₉₆, the DY-635 NHS-ester was used.

Table S3. Amount of different substances used for attachment to DY-635 amine to PAm

Substance	Mass mg	Amount of substance mol
PGPA _{m94}	39.6	1.35×10^{-6}
DY-635-Amine	0.99	1.39×10^{-6}
HBTU	0.84	2.02×10^{-6}
NMM	0.41	4.04×10^{-6}
PAEAm ₉₆	29.0	1.31×10^{-6}
DY-635-NHS	0.99	1.35×10^{-6}
NMM	0.40	3.93×10^{-6}
PDMAEAm ₉₄	21.3	1.57×10^{-6}
DY-635-Amine	1.16	1.57×10^{-6}
HBTU	0.97	2.35×10^{-6}
NMM	0.48	4.7×10^{-6}
PDMA _{PAm111}	22.7	1.34×10^{-6}
DY-635-Amine	0.99	1.34×10^{-6}
HBTU	0.83	2.02×10^{-6}
NMM	0.41	4.03×10^{-6}

N*/P Ratio Calculations.

The N*/P ratio was defined as the ratio of the total amount of protonatable amines in polymer solution in relation to the total amount of phosphates in the pDNA solution.

The volume of polymer needed to prepare polyplexes with 15 $\mu\text{g mL}^{-1}$ pDNA at different N*/P ratios was calculated as described by the following equations:

$$V_{\text{total}} \cdot P = V_{\text{poly}} \cdot N_{\text{poly}}$$

$$V_{\text{poly}} = \frac{V_{\text{total}} \cdot P}{N_{\text{poly}}}$$

$$V_{\text{poly}} = V_{\text{total}} \cdot \frac{n_{\text{pDNA}} \cdot P}{n_{\text{poly}} \cdot N}$$

$$V_{\text{poly}} = V_{\text{total}} \cdot \frac{m_{\text{pDNA}} \cdot P \cdot M_{\text{poly}}}{m_{\text{poly}} \cdot N \cdot M_{\text{pDNA}}}$$

Where V_{total} , P , V_{poly} and N_{poly} are the total required volume, the total number of phosphates of the pDNA, the required volume of polymer and the total number of active amines of the polymer, respectively.

Heparin dissociation assay.

Table S4. Kinetic cycle protocol for automated heparin addition by the microplate reader

Kinetic cycle	Repetitions	Addition of heparin		Orbital shake	Incubation	Measurement
		V / μL	Stock Solution / U mL^{-1}			
1	2	5	100	10 s	10 min, 37°C	$\lambda_{\text{Ex}} = 525 \text{ nm} / \lambda_{\text{Em}} = 605 \text{ nm}$
2	1	15	100	10 s	10 min, 37°C	$\lambda_{\text{Ex}} = 525 \text{ nm} / \lambda_{\text{Em}} = 605 \text{ nm}$
3	3	5	500	10 s	10 min, 37°C	$\lambda_{\text{Ex}} = 525 \text{ nm} / \lambda_{\text{Em}} = 605 \text{ nm}$
4	1	10	500	10 s	10 min, 37°C	$\lambda_{\text{Ex}} = 525 \text{ nm} / \lambda_{\text{Em}} = 605 \text{ nm}$

The heparin concentration needed to release the maximum of pDNA was calculated with OriginPro, Version 2018b (OriginLab Corporation, US) using a piecewise linear function with three segments fitted to the respective data ($n \geq 3$) of each polymer, keeping the value of the first and third slopes constant at 0 (Figure S1). The values for the heparin concentration (x_{i2}) required to release maximum pDNA ($a3$) were read off the equation.

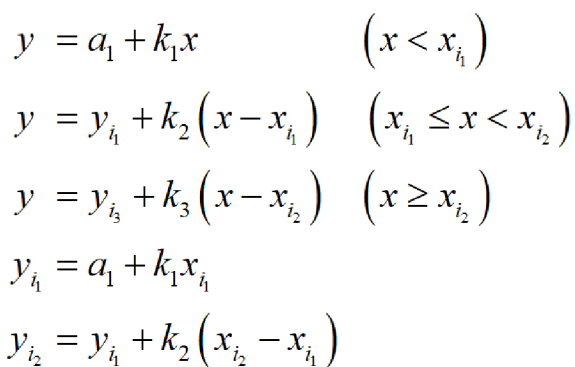


Figure S1. Equations used by OriginPro, Version 2018b to provide the piecewise linear fit functions for the polymers. Screenshots taken from the software.

Dynamic Light Scattering.

The size (diameter) of the polyplexes was investigated by dynamic light scattering (DLS). The polyplexes were prepared at N*/P 30 in 100 μ L HBG buffer as described above. Measurements were conducted on a Zetasizer Nano ZS (Malvern Instruments, Germany) with a He–Ne laser operating at a wavelength of 633 nm. Each sample was measured in quintuplicates with three runs of 30 s at 25 °C after an equilibration time of 30 s. The counts were detected at an angle of 173°. The mean particle size was approximated as the effective (z-average) diameter and the width of the distribution as the polydispersity index of the particles (PDI) obtained by the cumulants method assuming a spherical shape. Data are expressed as mean \pm SD of two independent determinations.

Determination of Cytotoxicity in HEK293T Cells.

The HEK293T cells were seeded at 10^5 cells per well in a 24-well plate and incubated in medium containing 10 mM HEPES for 24 h. 1 h after medium change, cells were treated with polymers at concentrations equal to N*/P 30 and incubated for additional 4 h. Cells on the same plate incubated with 10% (v/v) in growth medium served as non-treated controls. The medium was replaced by a 10% (v/v) alamarBlue™ solution in fresh culture medium, prepared according to the manufacturer's instructions. Following an incubation for 4 h at 37 °C, the fluorescence was

measured at $\lambda_{\text{Ex}} = 570$ / $\lambda_{\text{Em}} = 610$ nm. The non-treated control cells were referred to as 100 % viability. Values below 70 % were regarded as cytotoxic. Data are expressed as mean \pm SD of at least three independent determinations.

Determination of CC₅₀ and Cell Viability at N*/P 30.

With OriginPro, version 2018b a logistic function was fitted to the data of each polymer with the following equation (7):

$$y = \frac{A_1 - A_2}{1 + (x/x_0)^p} + A_2 \quad (7)$$

Where A_1 and A_2 are the initial and the final values, respectively, x_0 is the center and p is the power of the curve. For polymers reaching $\geq 50\%$ toxicity, A_1 and A_2 were kept constant at 1 and 0, respectively. For polymers not reaching 50% toxicity, A_2 and p were kept constant at 0 and 1.5, respectively. With the obtained equations, the “polymer concentration needed to kill 50% of the cells” (CC₅₀) or the “cell viability at N*/P 30” were calculated by substituting y with 50 or x with the concentration of the respective polymer at N*/P 30, respectively.

Polyplex Uptake with CLSM and Image Processing.

For uptake studies *via* confocal laser scanning microscopy (CLSM), HEK293T cells were seeded and cultured as described above in glass-bottomed dishes (CellView cell culture dishes with four compartments, Greiner Bio-One) and analyzed following incubation with polyplexes containing YOYO-1 labeled pDNA (0.31 nmol per 1 μ g pDNA) and indicated polymers for 4 h. To image intracellular distribution in living cells, Hoechst 33342 was added for 10 min to stain cell nuclei. Prior to imaging, trypan blue was added to a final concentration of 0.04% to quench fluorescence of YOYO-1 outside the cells. Live cell imaging was performed using a LSM880, Elyra PS.1 system (Zeiss, Germany) applying the argon laser for excitation at 488 nm (0.2%) and 405 nm

(0.5%), emission filters for 410-479 nm (Hoechst) and 508-553 nm (YOYO-1) with gains of 750 and 800, respectively. For magnification, a 40×1.4 NA plan apochromat oil objective was applied. Images were acquired using the ZEN software, version 2.3 SP1 (Zeiss, Germany). The experiments were performed at least twice. All images were processed in batch mode using ImageJ, version 1.52.⁴ They were resized with a scaling factor of 2 in x- and y-dimension and bicubic interpolation. Regarding the Hoechst-channel, the images were processed as follows: The background was corrected using the rolling ball background subtraction tool applying a sliding paraboloid with a radius of 23.5 pixels without previous image smoothing. The contrast was enhanced automatically with a normalization of 0.01% saturation. For YOYO-1 fluorescence, only the background was corrected applying a sliding paraboloid with a radius of 7 pixels following image smoothing. For the overlay image, both channels were merged.

Lactate Dehydrogenase Release (LDH) Assay.

To analyze membrane interactions of the polymers with HEK293T cells, the LDH release assay was performed using the CytoTox-ONE™ assay (Promega, Germany) according to the manufacturer's instructions. Briefly, cells were seeded at a density of 10^5 cells per well in 24-well plates and treated with polyplexes as described for uptake studies (including YOYO-1 for pDNA staining, having no influence on the performed assay, see Figure S16). Following incubation for 4 h, while cells were used to analyze uptake efficiency *via* flow cytometry, the supernatant was transferred to a new 96-well plate as a triplicate and allowed to cool down to room temperature. Subsequently, the substrate mixture including assay buffer was added and incubated at room temperature for 10 min. After the addition of the stop solution fluorescence intensity was measured at $\lambda_{\text{Ex}} = 560 \text{ nm}$ / $\lambda_{\text{Em}} = 590 \text{ nm}$. For the positive control (100 % LDH release), cells were incubated with 0.2% Triton X-100 for 30 min prior to analysis. Cells incubated with only pDNA

and YOYO-1 were used as negative control (0% LDH release). The LDH release of the polymers was calculated as follows (8):

$$\text{LDH release} / \% = \frac{F_{\text{Sample}} - F_0}{F_{\text{Positive control}} - F_0} \cdot 100 \quad (8)$$

Where F_{sample} , F_0 , and $F_{\text{Positive control}}$ represent the fluorescence intensity of a given sample, medium without cells, and of the Triton X-100 treated cells, respectively.

FURTHER RESULTS

Characterization of Polymers.

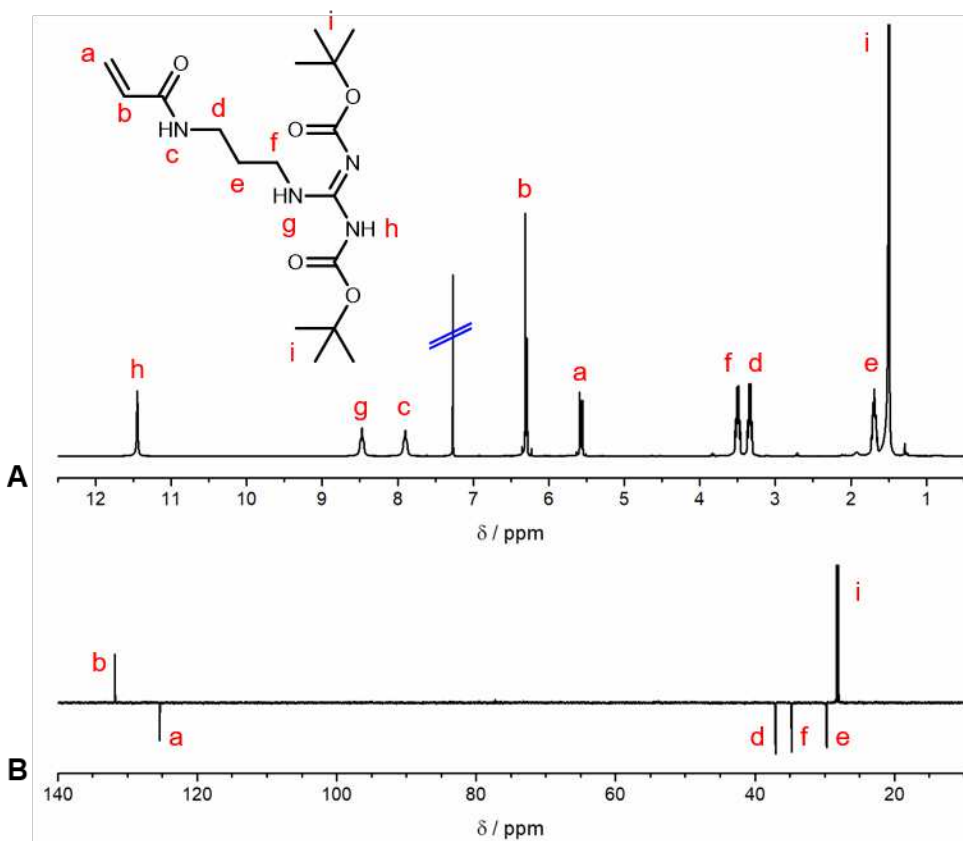


Figure S2. NMR spectra of GPAm^{diBoc}.

¹H (A) and DEPT ¹³C (B) NMR spectra of GPAm^{diBoc} in CDCl₃.

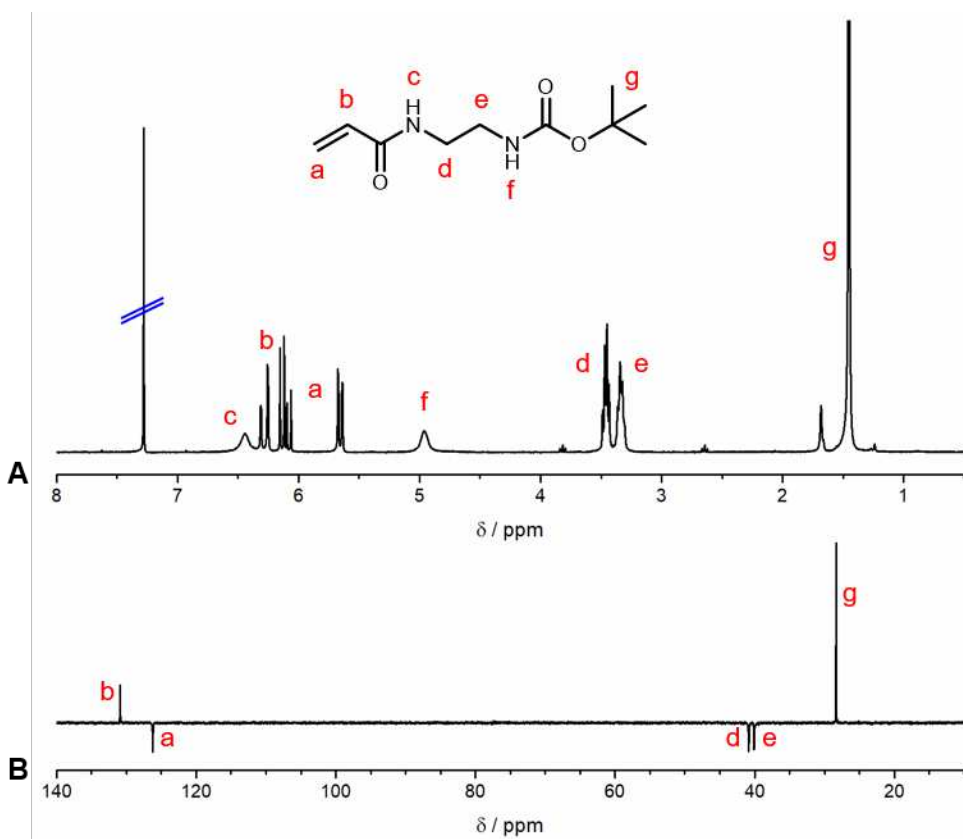


Figure S3. NMR spectra of AEAm^{Boc}.

¹H (A) and DEPT ¹³C (B) NMR spectra of AEAm^{Boc} in CDCl₃.

Table S5. Summary of (protected) cationic homopolymers prepared *via* RAFT polymerization.

Polymer	DP _n [a]	Protected polymers		
		M _{n,th} [b]	M _{n,SEC} [c]	Đ [c]
		(kg mol ⁻¹)		
PGPAm ₈	8	3.3	5.1	1.11
PGPAm ₂₂	22	8.4	9.9	1.11
PGPAm ₄₃	43	16.2	14.7	1.22
PGPAm ₉₄	94	35.0	27.4	1.31
PAEAm ₉	9	2.2	4.3	1.11
PAEAm ₂₄	24	5.4	8.3	1.11
PAEAm ₄₅	45	9.9	16.1	1.09
PAEAm ₉₆	96	20.8	26.3	1.15
PDMAEAm ₈	8	-	-	-
PDMAEAm ₂₂	22	-	-	-
PDMAEAm ₄₅	45	-	-	-
PDMAEAm ₈₈	88	-	-	-
PDMAPAm ₁₁	11	-	-	-
PDMAPAm ₂₄	24	-	-	-
PDMAPAm ₃₈	38	-	-	-
PDMAPAm ₇₁	71	-	-	-

[a] Determined *via* ¹H NMR.

[b] Determined using equation 6.

[c] Determined *via* DMAc-SEC with PMMA standards.

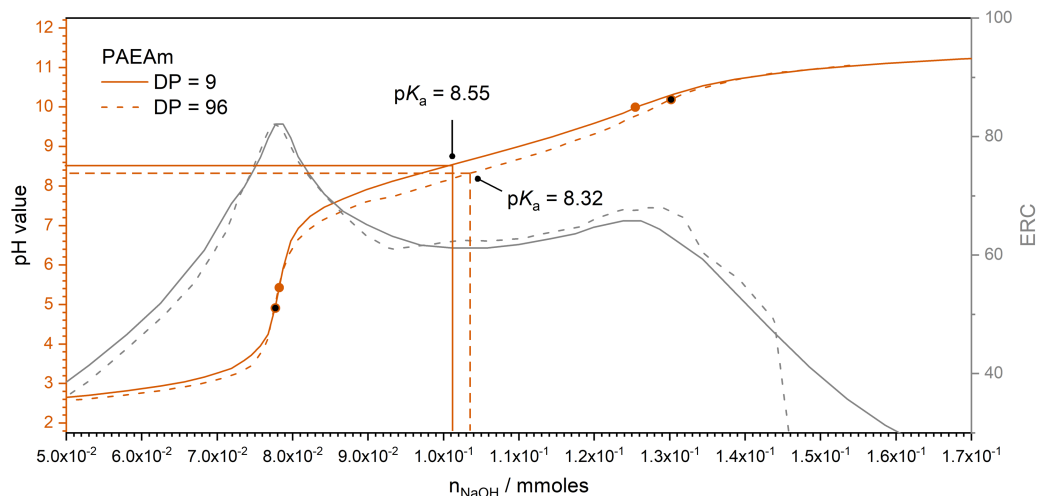


Figure S4. Titration curves and equivalence point recognition criterion for titrations of PAEAm polymers.

Polymers were dissolved at 1 mg mL^{-1} in 125 mM NaCl and titrated against 0.1 M NaOH up to pH 11. A new batch of PAEAm (PAEAm₉₆, Aq.-SEC, P2VP standards: $M_{n,SEC} = 12.8 \text{ kg mol}^{-1}$, $\bar{D} = 1.16$) was used in this case.

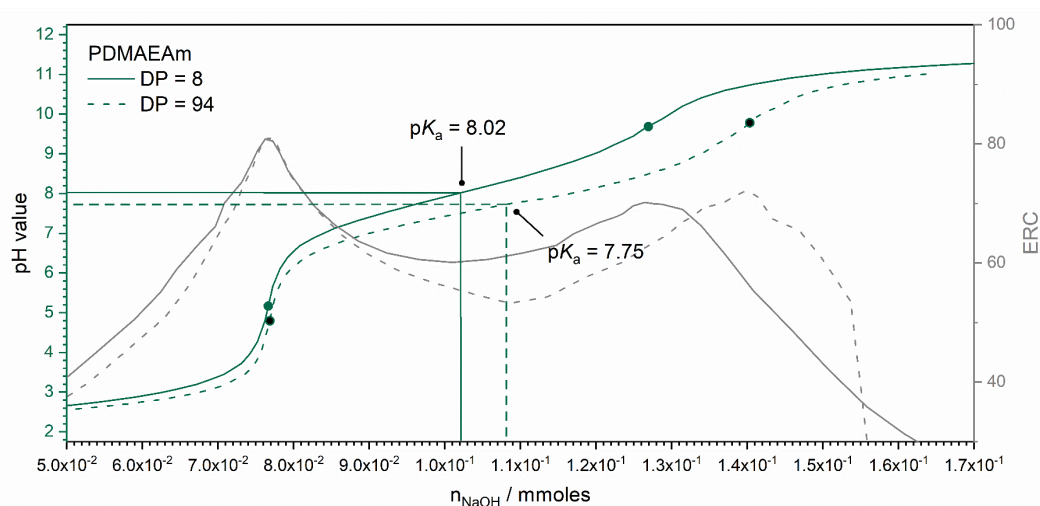


Figure S5. Titration curves and equivalence point recognition criterion for titrations of PDMAEm polymers.

Polymers were dissolved at 1 mg mL^{-1} in 125 mM NaCl and titrated against 0.1 M NaOH up to pH 11. A new batch of PDMAEm (PDMAEm₉₄, Aq.-SEC, P2VP standards: $M_{n,SEC} = 10.3 \text{ kg mol}^{-1}$, $\bar{D} = 1.26$) was used in this case.

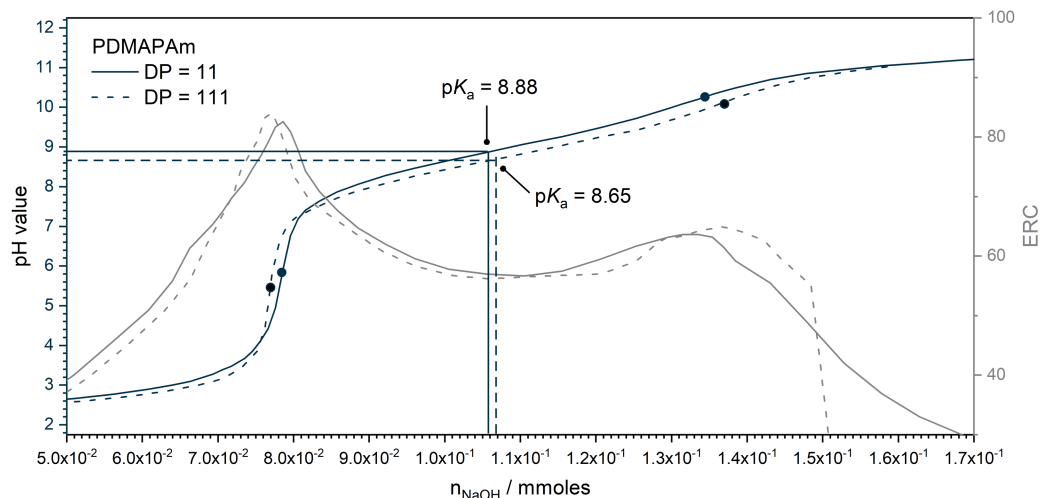


Figure S6. Titration curves and equivalence point recognition criterion for titrations of PDMAPAm polymers.

Polymers were dissolved at 1 mg mL^{-1} in 125 mM NaCl and titrated against 0.1 M NaOH up to pH 11. A new batch of PDMAPAm (PDMAPAm₁₁₁, Aq.-SEC, P2VP standards: $M_{n,SEC} = 11.9 \text{ kg mol}^{-1}$, $\bar{D} = 1.51$) was used in this case.

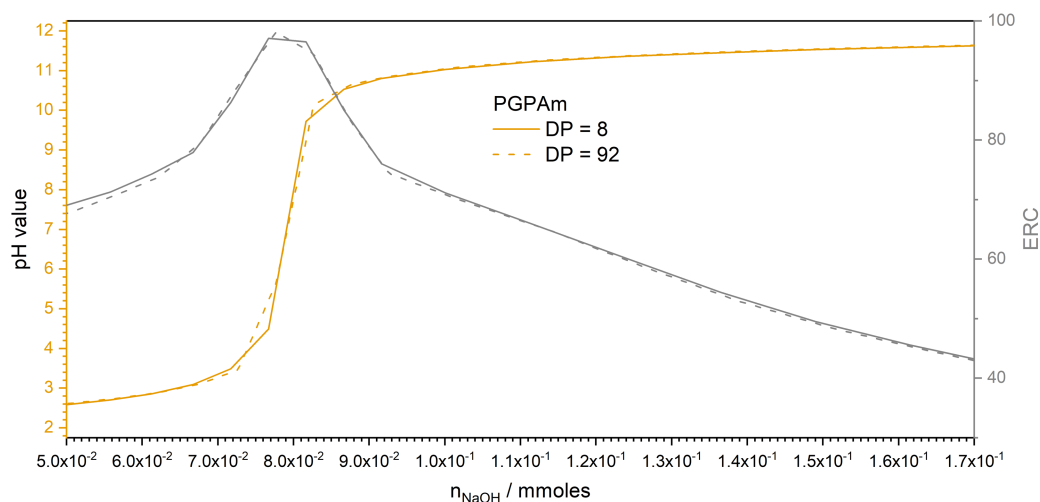


Figure S7. Titration curves and equivalence point recognition criterion for titrations of PGPAAm polymers.

Polymers were dissolved at 1 mg mL^{-1} in 125 mM NaCl and titrated against 0.5 M NaOH up to pH 12. A new batch of PGPAAm (PGPAAm₉₂, Aq.-SEC, P2VP standards: $M_{n,SEC} = 10.6 \text{ kg mol}^{-1}$, $\bar{D} = 1.24$) was used in this case.

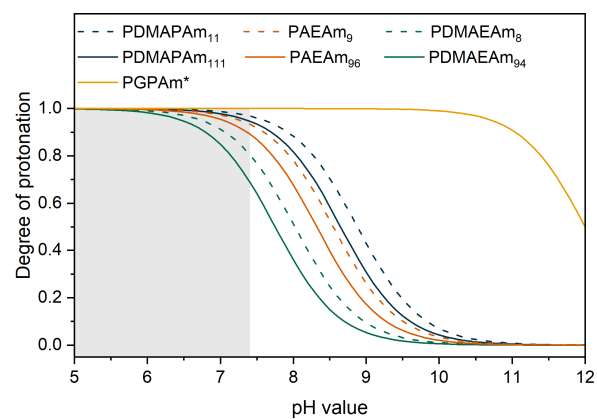


Figure S8. Theoretical determination of the degree of protonation.

The pH for the cationic polymer library based on their pK_a values calculated using the Henderson–Hasselbalch equation (1). Since the pK_a of PGPAm could not be determined the curve is generated assuming a pK_a of 12. The grey region designates the physiologically relevant pH window.

Biological Results.

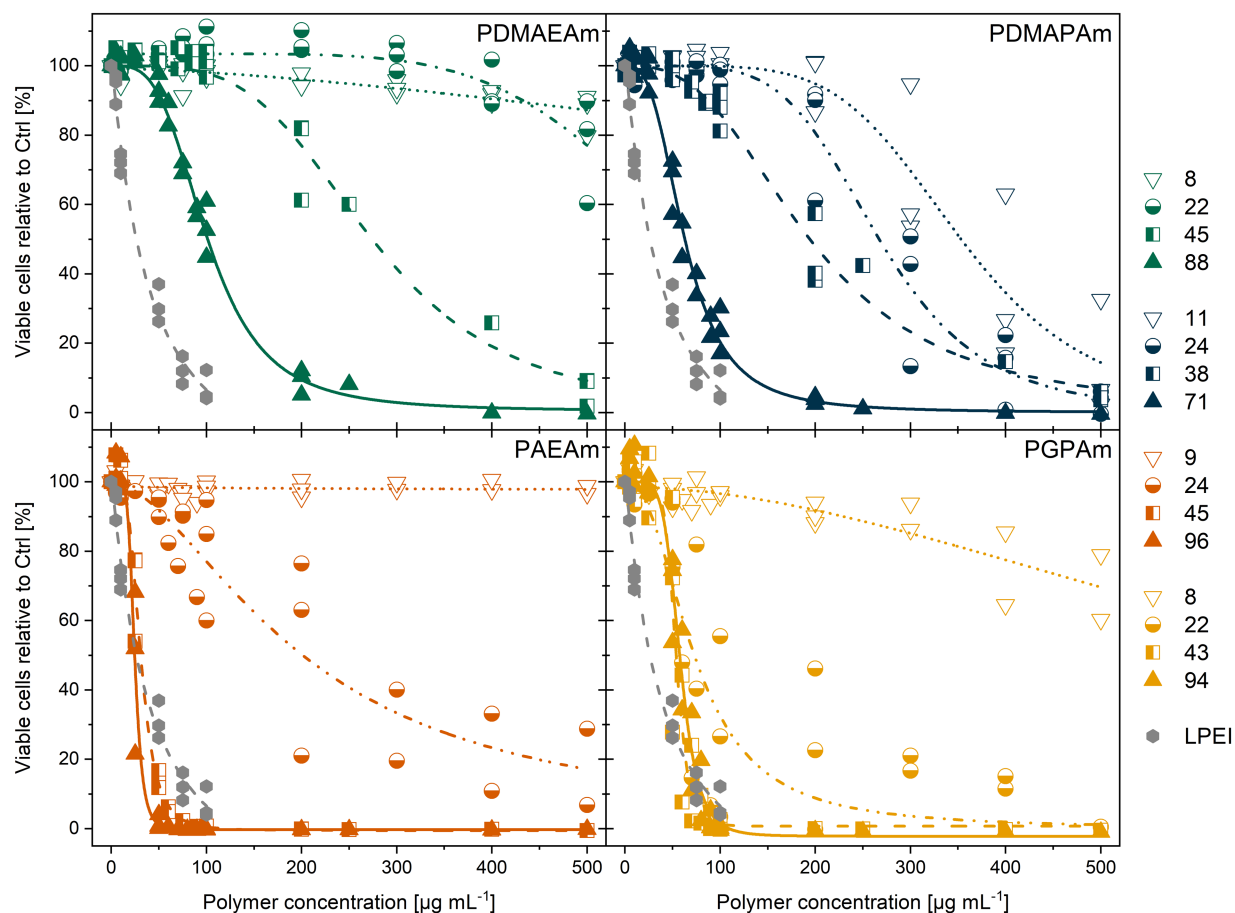
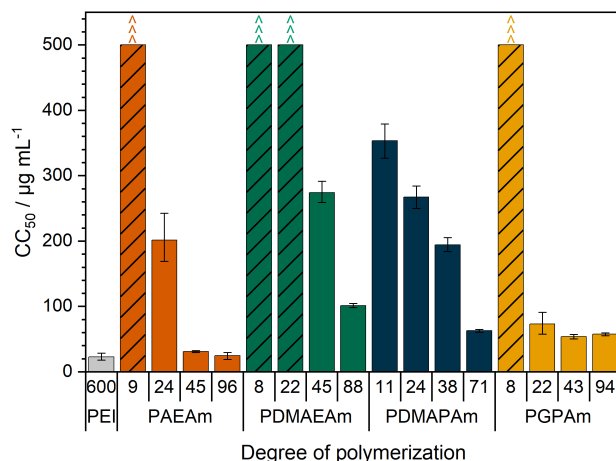


Figure S9. Cytotoxicity of PAm homopolymers in L929 cells.

Metabolic activity was measured in L929 cells using the alamarBlue™ assay following incubation with (A) PDMAEAm, (B) PDMAPAm, (C) PAEAm, (D) PGPAm polymers at indicated concentrations for 24 h. Dots represent values of single repetitions and lines represent logistic fit functions calculated via OriginPro ($n = 3$).

Table S6. Toxicity and concentration at N*/P 30 and CC₅₀ values calculated *via* non-linear fit.

ID	DP	Viability at N*/P 30 / % (c in $\mu\text{g mL}^{-1}$)	CC ₅₀ / $\mu\text{g mL}^{-1}$
PAEAm	9	99 (19)	> 500
	24	99 (17)	201.27
	45	93 (16)	30.92
	96	95 (16)	24.59
PDMAEAm	8	99 (23)	> 500
	22	105 (21)	> 500
	45	100 (20)	274.26
	88	100 (20)	101.22
PDMAPAm	11	100 (24)	353.24
	24	100 (22)	267.26
	38	100 (22)	194.31
	71	96 (22)	62.80
PGPAm	8	99 (27)	> 500
	22	92 (25)	72.93
	43	100 (24)	53.72
	94	99 (24)	57.41
PEI	600	88 (6)	22.73

**Figure S10.** Cytotoxicity of PAm homopolymers of different DP and amino group. Metabolic activity was measured in L929 cells after 24 h incubation with PAm polymers at indicated concentrations (Figure S8) using the alamarBlue™ assay. Values represent CC₅₀ values calculated after fitting the resulting toxicity values to a logistic function \pm 95% CI (n = 3). Upwards pointing arrows and striped columns indicate CC₅₀ values above 500 $\mu\text{g mL}^{-1}$.

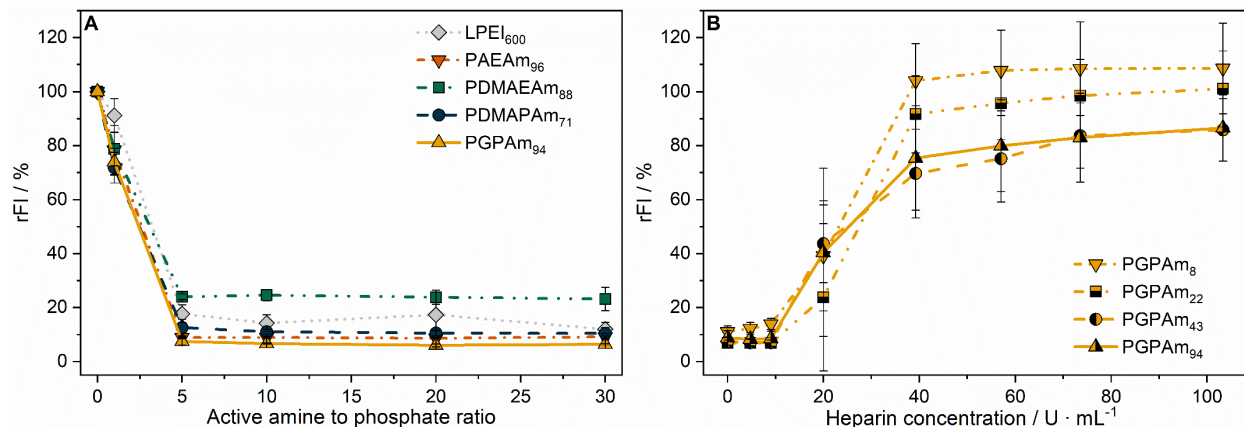


Figure S11. Polyplex formation and stability tests with pCMV-GFP pDNA and PAM homopolymers.

(A) EBA of polymers with highest DP at different N*/P ratios in HBG buffer showing strong pDNA binding of all polymers. Values represent mean \pm SD ($n \geq 3$). (B) HRA of polyplexes formed with P(GPAm) polymers at N*/P 30 using heparin as a competing polyanion showing the reversible binding of the polyplex. Values represent mean \pm SD ($n \geq 3$).

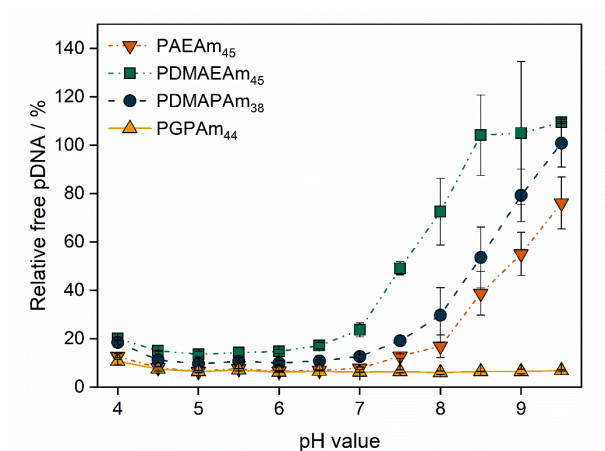


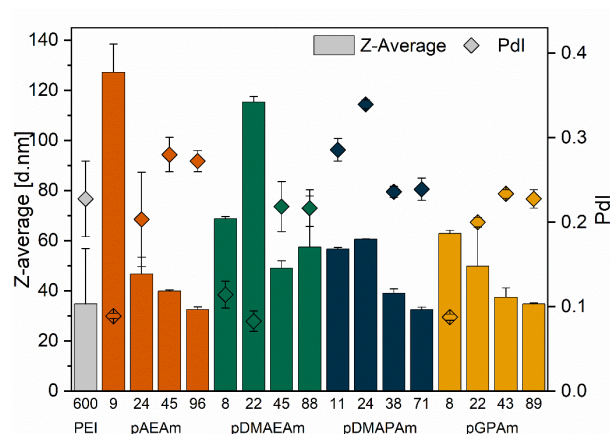
Figure S12. Polyplex formation with pCMV-GFP pDNA and polyacrylamide-homopolymers at different pH values.

EBA of polymers with second highest DP at N*/P 30 in HBG buffer of different pH showing a good pDNA binding of all polymers from pH 4 to pH 7 but differences between the polymers at pH > 7. Values represent mean \pm SD ($n \geq 2$).

Table S7. Size determination of formed polyplexes via DLS.

Polyplexes were formed using $15 \mu\text{g mL}^{-1}$ DNA at N*/P ratio of 30 in HBG buffer.

Polymer	DP	Z-Average (d / nm)	PdI	Main peak (d / nm)	Intensity-weighted % of main peak
PAEAm	9	127 ± 11	0.09 ± 0.00	135 ± 13	100 ± 0
	24	47 ± 7	0.20 ± 0.06	54 ± 6	98 ± 2
	45	40 ± 0	0.28 ± 0.02	43 ± 1	92 ± 3
	96	33 ± 1	0.27 ± 0.01	44 ± 1	92 ± 8
PDMAEAm	8	69 ± 1	0.11 ± 0.02	73 ± 2	100 ± 0
	22	115 ± 2	0.08 ± 0.01	123 ± 5	100 ± 0
	45	49 ± 3	0.22 ± 0.03	58 ± 3	100 ± 0
	88	58 ± 20	0.22 ± 0.02	66 ± 23	96 ± 3
PDMApAm	11	57 ± 1	0.29 ± 0.01	61 ± 2	89 ± 4
	24	61 ± 0	0.34 ± 0.01	71 ± 7	54 ± 3
	38	39 ± 2	0.24 ± 0.01	51 ± 0	87 ± 1
	71	32 ± 1	0.24 ± 0.01	39 ± 1	87 ± 1
PGPAm	8	63 ± 1	0.09 ± 0.00	68 ± 2	100 ± 0
	22	50 ± 18	0.20 ± 0.01	58 ± 19	100 ± 0
	43	37 ± 4	0.23 ± 0.01	46 ± 6	100 ± 0
	89	35 ± 0	0.23 ± 0.01	42 ± 1	99 ± 1
PEI	600	59 ± 22	0.25 ± 0.04	60 ± 11	82 ± 1

**Figure S13.** Size determination of formed polyplexes of PAm library of different DP *via* DLS.

Polyplexes were formed using $15 \mu\text{g mL}^{-1}$ DNA at N*/P ratio of 30 in HBG buffer.

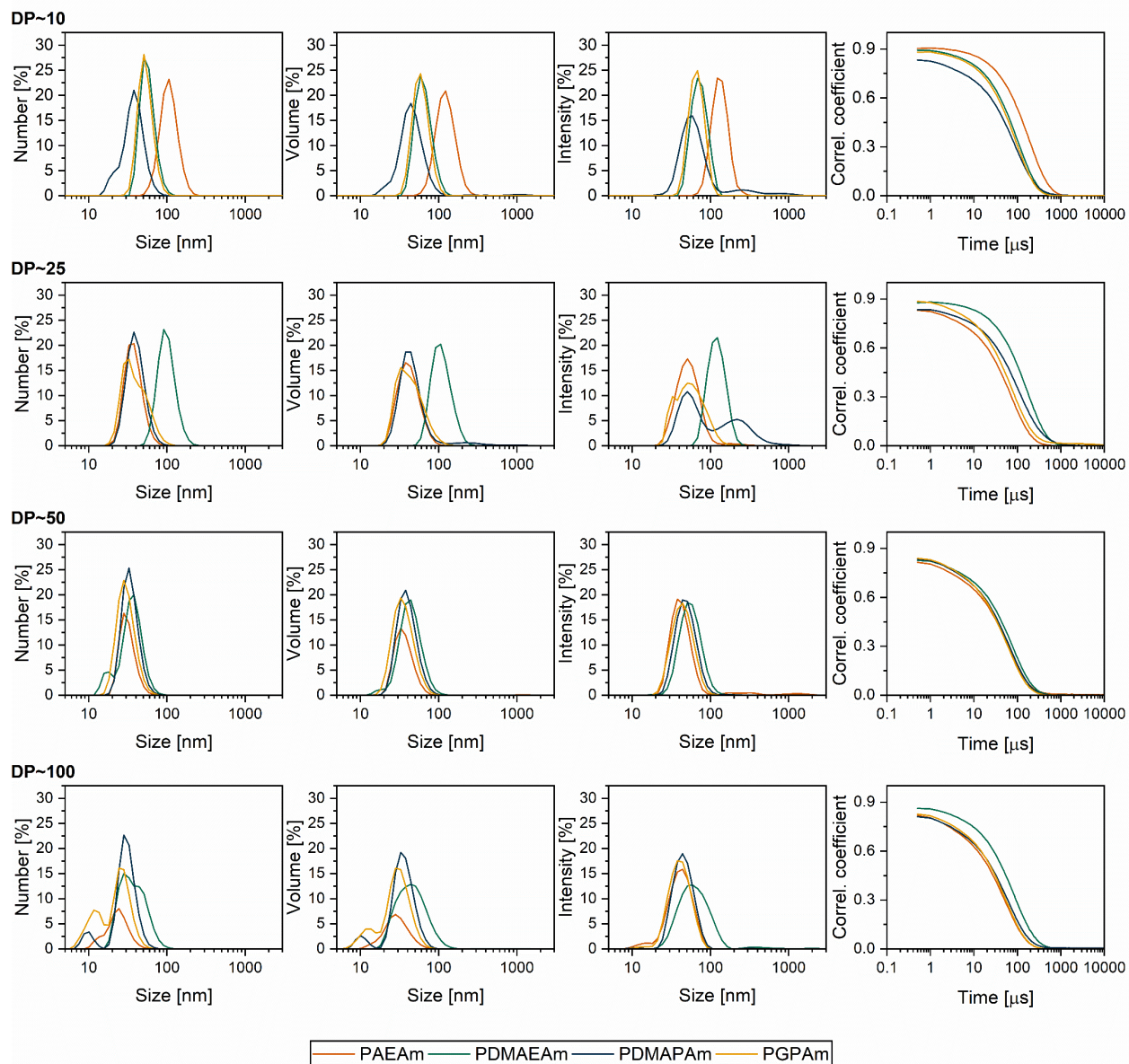


Figure S14. DLS traces of polyplexes formed with PAM polymers and 15 $\mu\text{g mL}^{-1}$ DNA at N*/P 30 in HBG buffer.

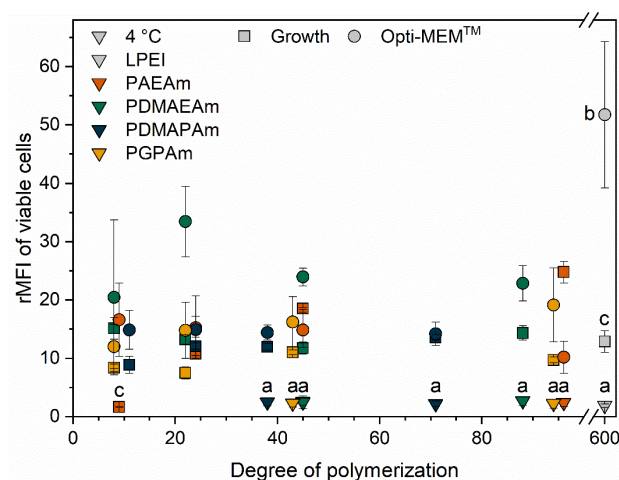


Figure S15. Influence of degree of polymerization on polyplex uptake in HEK293T cells.

Flow cytometry following incubation with polyplexes of YOYO-1-labeled pDNA and polymers at N*/P 30. Incubation was in growth medium at 37°C for 4 h (G), in serum-reduced Opti-MEM™ at 37 °C for 4 h (OM) or in growth medium at 4 °C for 4 h (4 °C). Cells incubated with labeled pDNA served as control (rMFI = 1). Values represent mean \pm SD ($n \geq 3$). a: significant difference to the same polymer in G, b: significant difference to all polymers in OM, c: significant difference to same polymer in OM ($p < 0.001$)

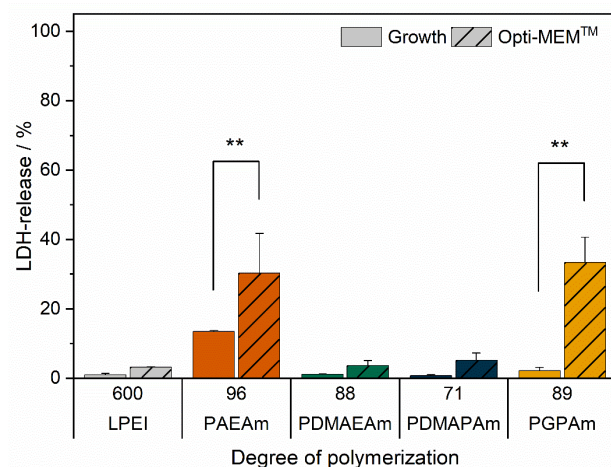


Figure S16. LDH release assay with PAm polyplexes in HEK293T cells.

Cells were incubated with YOYO-1 labeled polyplexes at N*/P 30 in growth medium or Opti-MEM™ for 4 h. Values represent mean \pm SD ($n \geq 1$). **: significant difference ($p < 0.001$).

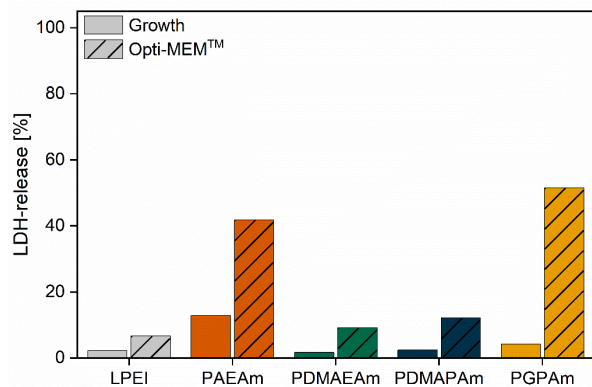


Figure S17. LDH release assay with HEK293T cells.

Cells were incubated with polyplexes (not labeled) at N*/P 30 in growth medium or Opti-MEM™ for 4 h and showed no difference to the results with YOYO-1 labeled polyplexes. Determination was performed once.

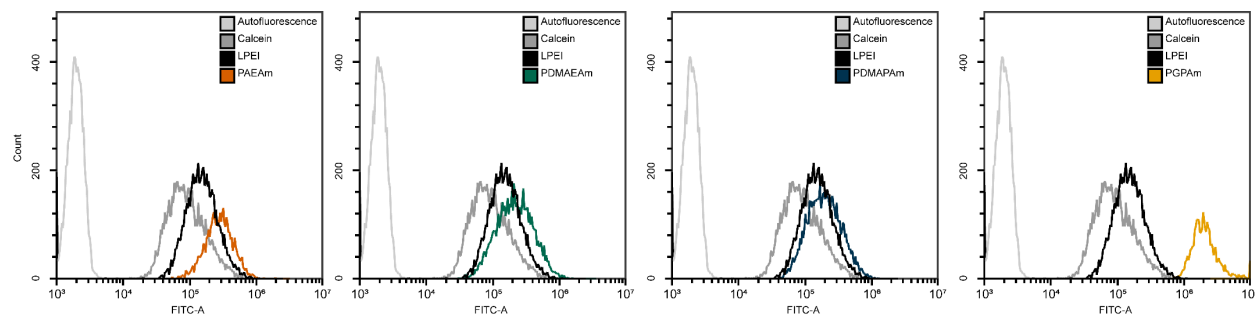


Figure S18. Flow cytometry analysis of calcein release assay.

Representative plots of the calcein channel following flow cytometry of HEK293T cells incubated with the respective polymers at equal amine concentrations (\triangleq N*/P 30) in Opti-MEM™ for 4 h.

Table S8. Data used for determination of the squared Pearson's correlation coefficient (R^2).

Title of factor in correlation graph	Data
Transfection	Viable EGFP-fluorescent HEK293T cells in Opti-MEM in %
Molar mass ^a	Theoretical molar mass without counter ion in g mol ⁻¹
Cationic moiety ^b	C/N ratio of the different amine moieties (3 for tertiary amines, 1 for primary amines, 0.6 for guanidinium)
Toxicity ^b	CC ₅₀ values in µg mL ⁻¹ polymer following 24 h incubation in L929 cells
pDNA-binding ^b	Results of EBA as rFI at N*/P 30
pDNA-release ^b	Heparin concentration needed to release maximum amount of DNA at N*/P 30 in U/mL
Uptake ^b	rMFI values of viable HEK293T cells following 4 h incubation in Opti-MEM
Hemolysis ^b	Hemolysis in % of positive control Triton X-100 at pH 6
Aggregation ^b	Negative control PBS relative to respective polymer at pH 6
LDH release ^b	Mean of LDH release in Opti-MEM in % of positive control Triton X-100
Calcein-release ^b	Viable calcein-fluorescent HEK293T cells in Opti-MEM in %
pDNA-binding ^b	Results of EBA as rFI at N*/P 30
BMP-binding ^b	rFI values of lipid-polymer-binding assay at BMP-concentration of 1 mM

[a] Data of all PAM polymers were considered

[b] Only data of longest PAM polymers were considered.

REFERENCES

1. L. J. Hobson and W. J. Feast, *Polymer*, 1999, **40**, 1279-1297.
2. A. Kuroki, P. Sangwan, Y. Qu, R. Peltier, C. Sanchez-Cano, J. Moat, C. G. Dowson, E. G. L. Williams, K. E. S. Locock, M. Hartlieb and S. Perrier, *ACS Appl. Mater. Interfaces*, 2017, **9**, 40117-40126.
3. S. C. Larnaudie, J. C. Brendel, K. A. Jolliffe and S. Perrier, *J. Polym. Sci., Part A: Polym. Chem.*, 2016, **54**, 1003-1011.
4. J. Schindelin, I. Arganda-Carreras, E. Frise, V. Kaynig, M. Longair, T. Pietzsch, S. Preibisch, C. Rueden, S. Saalfeld, B. Schmid, J.-Y. Tinevez, D. J. White, V. Hartenstein, K. Eliceiri, P. Tomancak and A. Cardona, *Nat. Methods*, 2012, **9**, 676.